

THE MECHANICAL BEHAVIOR OF NORMALLY CONSOLIDATED SOILS AS A FUNCTION OF PORE FLUID SALINITY

by

AIDEN JAMES HORAN

National Certificate in Civil Engineering
Galway-Mayo Institute of Technology, Galway, Ireland (2004)

Bachelor of Engineering (Ord.) in Civil Engineering
Galway-Mayo Institute of Technology, Galway, Ireland (2005)

Bachelor of Engineering (Hon.) in Civil Engineering
National University of Ireland Galway, Galway, Ireland (2007)

Submitted to the Department of Civil and Environmental Engineering
in Partial Fulfillment of the Requirements for the Degree of

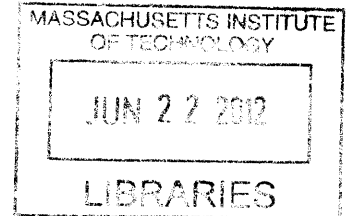
Masters of Science in Civil and Environmental Engineering

at the

MASSACHUSETTS INSTITUTE OF TECHNOLOGY

June 2012

ARCHIVES



© 2012 Massachusetts Institute of Technology. All rights reserved.

SIGNATURE OF AUTHOR.....
Department of Civil and Environmental Engineering
May 11, 2012

CERTIFIED BY.....
John T. Germaine
Senior Research Associate and Senior Lecturer of Civil and Environmental Engineering
Thesis Supervisor

ACCEPTED BY.....
Heidi M. Nepf
Chair, Departmental Committee for Graduate Students

1000

MECHANICAL BEHAVIOR OF NORMALLY CONSOLIDATED SOILS AS A FUNCTION OF PORE FLUID SALINITY

BY

AIDEN JAMES HORAN

SUBMITTED TO THE DEPARTMENT OF CIVIL AND ENVIRONMENTAL ENGINEERING ON MAY 11TH, 2012 IN PARTIAL FULFILLMENT OF THE REQUIREMENT FOR THE DEGREE OF MASTERS OF SCIENCE IN CIVIL AND ENVIRONMENTAL ENGINEERING

ABSTRACT

Pore fluid salinities in the Gulf of Mexico area can reach levels of 250 grams of salt per liter of pore fluid (g/l). It is now necessary to determine the effect that this salinity level can play on the mechanical behaviors of marine sediments.

An extensive laboratory testing program involving Constant Rate of Strain (CRS) and K_0 consolidated undrained shear in compression triaxial testing (CK_0UC) was undertaken. Soil specimens reached axial effective stresses of 10 MPa with a select few reaching 40 MPa in a modified CRS device. All triaxial tests were performed in a low pressure triaxial apparatus. The shear behavior of all soils was obtained in the normally consolidated region. Several reverse leaching tests were performed in the CRS cell whereby high salinity pore water was flushed through a low salinity soil while consolidation was halted.

The majority of testing was performed on resedimented specimens using several different soils from around the world. These include Boston Blue Clay (BBC), London Clay, Gulf of Mexico soil and sodium montmorillonite. Several derivatives of BBC were resedimented including BBC which had some of its natural salt removed via leaching, and also BBC which had its fabric completely dispersed using sodium hexametaphosphate. Pore fluid salinities ranging from 0 (distilled water) to 256 g/l were used when resedimenting these soils. The resedimented BBC test results were compared to intact BBC soil which was recovered from below the MIT campus.

The results show that BBC and London Clay are relatively insensitive to increases in pore fluid salinities up to 256 g/l. This sensitivity can be increased by leaching some of the natural salt from the soil and then resedimenting to different pore fluid salinities. The strength characteristics of BBC over this large salinity range also remain fairly constant with the only differences being observed in leached BBC. It was also seen that the strain to failure for resedimented BBC is half that which is required for intact soil with all other measured parameters being similar.

Interesting observations were seen in relation to how the fabric of BBC evolves with an increase in stress level and a theory of how floc breakage occurs at a given stress level is proposed. A potential crude method of quantifying the contribution of electro-chemical forces to a soils strength is also suggested.

Thesis Supervisor: John T. Germaine

Title: Senior Research Associate and Senior Lecturer of Civil and Environmental Engineering

ACKNOWLEDGEMENTS

It has been my great privilege to work with Dr. John Germaine during my time at MIT as my thesis, research and academic advisor. I would like to pay my sincere gratitude and heartfelt appreciation for his help, advice, wisdom and immeasurable patience which he has shown to me during my time here. His attention to detail, technical knowledgebase, attitude towards work and ability to recall information at the drop of a hat are a benchmark we should all aim to achieve someday.

My time at MIT was made possible thanks to Ward and Burke Construction Ltd. who sponsored this research. I would particularly like to thank Michael Ward and Robert Ward (MIT SM 89') who displayed belief in my abilities and taught me to have the confidence to believe in them myself. It is indeed a great experience and education to work alongside them.

I would like to extend thanks my other teachers in Geotechnical Engineering namely Professor Andrew Whittle and Professor Herbert Einstein. Their understanding and passion for Geotechnical Engineering is admirable and encouraging. I would also like to extend a special thanks to Dr. Lucy Jen P.E. whom I had the pleasure of studying under, in addition to serving as teaching assistant for. Her balance of technical and practical knowledge makes her one of the best in the business.

I consider myself extremely fortunate to have met so many interesting people from so many different backgrounds while at MIT. I have made some great friends during my time and can't possibly name them all but a special mention must go to my immediate lab group, namely Amy Adams whose cheerful spirit and willingness to help makes her a joy to work with, Brendan Casey who kept me grounded in my Irish ways and was always a good man to go to if you needed an alternative view on issues and Jana Marjanovic with whom I shared manys an office banter and joke with. I would also like to extent my thanks to Rory Clune for his friendship, advice and sense of humor during my two years at MIT.

It is fair to say that I have been working alongside an extremely talented and gifted bunch of engineers while at MIT – I wish every one of you all the best in the future and hope that we cross paths very often.

A special thanks must also go to my friends and family at home in Ireland whose calls, cards and visits meant the world to me.

To my fiancée Tasha LaMarca. You more often than not added that element of perspective to life that I sometimes failed to see. Your patience and understanding during this demanding period meant so much, you truly are an inspirational person to me. As we leave Cambridge behind, I'm looking forward to whatever the future brings our way.

To my parents, Sean & Helen Horan, who always supported me at every juncture and showed faith in the decisions I made for myself.

I dedicate this thesis to you.

TABLE OF CONTENTS

Abstract	3
Acknowledgements	5
Table of Contents	9
List of Tables	13
List of Figures	15
List of Symbols	35
1 INTRODUCTION	39
1.1 Research Statement	39
1.2 Objectives of the Research.....	39
1.3 Organization of the Thesis	40
2 BACKGROUND	43
2.1 Introduction	43
2.2 Electro-Chemical Effects on Soil Behavior	44
2.2.1 Introduction.....	44
2.2.2 Specific Surface	45
2.2.3 Soil Formation	46
2.3 Literature Review	47
2.3.1 Introduction.....	47
2.3.2 Traditional Leaching of Soil	48
2.3.3 Adding Salt to Soils	49
2.3.4 Results From In-Tact Material.....	50
2.4 Normalized Behavior of Boston Blue Clay.....	51
2.4.1 Effect of Stress Level on Normalized Strength	52

3	MATERIALS USED IN TESTING PROGRAM.....	61
3.1	Introduction	61
3.2	Boston Blue Clay	61
3.2.1	Resedimented Boston Blue Clay	61
3.2.2	Batch Data.....	62
3.2.3	Consolidation Behavior During Resedimentation	63
3.2.4	Engineering Behavior of RBBC	64
3.2.5	Terminology of BBC Series IV Derivatives Used.....	67
3.2.6	Killian Court in-situ BBC	68
3.2.7	Scanning Electron Microscope Images.....	69
3.3	London Clay.....	70
3.3.1	Introduction.....	70
3.3.2	London Clay Characteristics.....	71
3.3.3	Engineering Behavior of Resedimented London Clay	75
3.4	Gulf of Mexico Soil.....	76
3.4.1	Gulf of Mexico – Ursa	76
3.5	Sodium Montmorillonite.....	77
3.5.1	Engineering Behavior of Sodium Montmorillonite.....	78
3.5.2	Scanning Electron Microscope Images.....	80
4	MATERIAL PROCESSING, EQUIPMENT AND TESTING PROCEDURES	137
4.1	Introduction	137
4.2	Material Processing.....	138
4.2.1	Introduction.....	138
4.2.2	Processing of London Clay.....	138
4.2.3	Processing of Leached Boston Blue Clay.....	141
4.3	RESEDIMENTATION	143

4.3.1	Introduction.....	143
4.3.2	Resedimentation Procedure	144
4.3.3	Resedimenting Boston Blue Clay	149
4.3.4	Resedimenting London Clay.....	152
4.3.5	Resedimenting Gulf of Mexico Soil	152
4.3.6	Resedimenting Sodium Montmorillonite.....	152
4.3.7	Resedimentation Issues.....	153
4.3.8	Measuring Pore Pressures During Resedimentation.....	155
4.4	EQUIPMENT.....	156
4.4.1	Introduction.....	156
4.4.2	Measurement Instrumentation	157
4.4.3	Data Acquisition	159
4.4.4	Computer Control System for Triaxial Testing	161
4.4.5	Constant Rate of Strain Testing Equipment.....	162
4.4.6	Triaxial Testing Equipment	164
4.5	TESTING PROCEDURES	165
4.5.1	Introduction.....	165
4.5.2	Characterization	166
4.5.3	Constant Rate of Strain Tests.....	169
4.5.4	Triaxial Testing.....	177
5	RESULTS.....	215
5.1	Introduction	215
5.2	Constant Rate of Strain Testing	216
5.2.1	Introduction.....	216
5.2.2	Boston Blue Clay	216
5.2.3	Natural London Clay.....	233

5.2.4	Resedimented Gulf of Mexico – Ursa Clay.....	236
5.2.5	Sodium Montmorillonite.....	237
5.2.6	Comparison of Different Soil Types.....	239
5.2.7	Evaluation of CRS Testing Program.....	240
5.3	Triaxial Tests.....	241
5.3.1	Introduction.....	241
5.3.2	Triaxial Results.....	242
6	REVIEW & CONCLUSIONS.....	331
6.1	Introduction.....	331
6.2	Review of Research Undertaken.....	331
6.3	Results and Conclusions.....	332
6.3.1	Observed Effects on Mechanical Properties.....	332
6.4	Recommendations for Future Research.....	336
	References.....	339
	Appendix A.....	345
	Appendix B.....	351

LIST OF TABLES

Table 3-1 Index properties of RBBC from Series I - III (after Cauble, 1996).....	79
Table 3-2 Overview of previous studies performed using RBBC	80
Table 3-3 Index properties of BBC Series IV (extended from Santagata, 1998).....	81
Table 3-4 London Clay properties determined from laboratory testing from West Hendon development (West Hendon development, SI document)	82
Table 3-5 Summary of results from chemical tests performed on London Clay from West Hendon development (West Hendon development, SI document).....	83
Table 4-1 Details of soils tested in CRS testing program	179
Table 4-7 List of all resedimentation batches produced for this research.....	180
Table 4-2 List of soils resedimented during the course of this research and the required mass of fluid required to bring the soil to a stable slurry at the salt concentrations indicated.....	181
Table 4-3 Characteristics of instruments used in CRS TR4 apparatus Note: Resolution and stability based on central data acquisition system, calculations based on specific dimensions .	182
Table 4-4 Characteristics of instruments used in triaxial MIT01 apparatus Note: Resolution and stability based on central data acquisition system, calculations based on specific dimensions .	182
Table 4-5 Characteristics of instruments used in triaxial MIT02 apparatus Note: Resolution and stability based on central data acquisition system, calculations based on specific dimensions .	183
Table 4-6 Characteristics of instruments used in triaxial MIT02 apparatus Note: Resolution and stability based on central data acquisition system, calculations based on specific dimensions .	183
Table 5-1 List of Constant Rate of Strain (CRS) tests performed on several derivatives of Boston Blue Clay	253
Table 5-2 List of Constant Rate of Strain (CRS) tests performed on other soils in testing program	254
Table 5-3 List of triaxial tests (CK ₀ UC) performed on Boston Blue Clay soils in the testing program	255
Table 5-4 List of c _c values for all soils tested in the CRS device	256

LIST OF FIGURES

Figure 2.1 Average values of relative sizes, thicknesses and specific surface area of the most common clay minerals (Yong & Warkentin, 1975).....	53
Figure 2.2 Sodium montmorillonite at different pore fluid salinities. Saltwater content L-R: 1, 4, 16, 64, 128 & 256 g/l NaCl. (1 g of soil used in each tube)	53
Figure 2.3 Modes of particle association in clay suspensions and terminology (a) dispersed and deflocculated (b) aggregated but deflocculated (c) edge to face flocculated but dispersed (d) edge to edge flocculated but dispersed (e) edge to face flocculated and aggregated (f) edge to edge flocculated and aggregated (g) edge to face and edge to edge flocculated and aggregated (Van Olphen, 1977)	54
Figure 2.4 Graph of attractive forces acting on illite soil particles in a low salinity environment (Ladd & Kinner, 1967)	55
Figure 2.5 Comparison of the undrained shear strength of salt, leached and fresh-water clays (Bjerrum & Rosenqvist, 1956).....	55
Figure 2.6 Soil profiles from the Caspian Sea: Atterberg limits on the left and measured preconsolidation pressures on the right (van Paassen. et. al., 2004).....	56
Figure 2.7 Oedometer test results from Caspian Sea recovered from two different depths run at different cell fluid salinities (van Paassen. et al., 2004)	56
Figure 2.8 Consolidation procedure for CK_0U testing (Ladd, 1991).....	57
Figure 2.9 Normalized undrained shear strength versus OCR for AGS Plastic Marine Clay via SHANSEP (Koutsoftas & Ladd, 1985)	57
Figure 2.10 Normalized undrained shear strength versus OCR for RBBC from selected CK_0UC triaxial tests indicating the effect of stress level (Abdulhadi, 2009).....	58
Figure 2.11 Friction angle at peak and maximum obliquity versus stress level for NC RBBC from CK_0UC triaxial tests (Abdulhadi, 2009).....	58
Figure 3.1 Results of grain size analysis for series IV BBC powder (Abdulhadi, 2009)	84

Figure 3.2 Results of grain size analysis for series IV BBC powder (Force, 1998).....	84
Figure 3.3 Plasticity chart for 5 determinations on natural and leached BBC (corrected for salt)	85
Figure 3.4 Plasticity chart showing data for RBBC Series IV (Abdulhadi, 2009).....	85
Figure 3.5 Mineralogy of Boston Blue Clay – bulk sample on left, <2 micron on right (Reference Required).....	86
Figure 3.6 Axial displacement versus root time for RBBC Series IV at different stress levels (data from RS175, RBBC at 64 g/l, consolidometer diameter 4.4 cm, initial height 12.9 cm, final height 7.8 cm).....	86
Figure 3.7 Axial displacement versus log time for RBBC Series IV at different stress levels (data from RS175, RBBC at 64 g/l).....	87
Figure 3.8 1-D compression behavior in e-log space for NC and OC RBBC from triaxial testing	88
Figure 3.9 Coefficient of consolidation versus stress level for RBBC from CRS testing (Abdulhadi, 2009).....	89
Figure 3.10 Coefficient of consolidation versus stress level for RBBC from CRS testing – Note: 10 ksc ~ 1 MPa (Force, 1998).....	89
Figure 3.11 Void ratio versus hydraulic conductivity for RBBC Series IV from CRS tests referenced to batch data (Abdulhadi, 2009).....	90
Figure 3.12 Void ratio versus hydraulic conductivity for RBBC Series IV from CRS tests (Force, 1998).....	90
Figure 3.13 Variation in lateral stress ratio K versus stress level measured during consolidation phase of triaxial test (Abdulhadi, 2009).....	91
Figure 3.14 Variation in lateral stress ratio K versus stress level measured during consolidation phase of triaxial test (Casey, 2011).....	91

Figure 3.15 Normalized shear stress-strain behavior of RBBC Series III at different OCR values in undrained triaxial compression (Santagata, 1994).....	92
Figure 3.16 Normalized effective stress path for RBBC Series III at different OCR values in undrained triaxial compression (Santagata, 1994).....	92
Figure 3.17 Normalized excess pore pressure of RBBC Series III at varying OCR values in undrained triaxial compression (Santagata, 1994).....	93
Figure 3.18 Normalized shear induced pore pressures of RBBC Series III at varying OCR values in undrained triaxial compression (Santagata, 1994).....	93
Figure 3.19 Normalized undrained secant modulus versus axial strain for RBBC Series III in triaxial compression (Santagata, 1994).....	94
Figure 3.20 Sedimentation test performed on natural BBC Series IV powder. Salinities from L-R: 1, 4, 16, 64, 128 & 256 g/l NaCl. 5 grams of soil used in each tube	94
Figure 3.21 Sedimentation test performed on leached BBC powder. Salinities from L-R: 0 (distilled water) 1, 4, 16, 64, 128 & 256 g/l NaCl. 5 grams of soil used in each tube.....	95
Figure 3.22 Location from where undisturbed samples were obtained on MIT campus (Google Earth).....	95
Figure 3.23 Site plan identifying actual location of boreholes (The T2P Project)	96
Figure 3.24 Borehole log for B10-T2PA in Killian Court (The T2P Project).....	97
Figure 3.25 Orientation of all imaging presented	98
Figure 3.26 SEM image of natural RBBC Series IV at a pore fluid salinity of 4 g/l and a stress level of 100 kPa	99
Figure 3.27 SEM image of natural RBBC Series IV at a pore fluid salinity of 256 g/l and a stress level of 100 kPa	100
Figure 3.28 Analysis of RBBC Series IV at 2 different salinities but same stress level (100 kPa).	101

Figure 3.29 SEM image of leached RBBC at a pore fluid salinity of 1 g/l and a stress level of 100 kPa.....	102
Figure 3.30 SEM image of leached RBBC at a pore fluid salinity of 1 g/l and a stress level of 1,000 kPa.....	103
Figure 3.31 Analysis of leached RBBC at same salinity (1 g/l) but different stress level.....	104
Figure 3.32 SEM image of sodium hex. RBBC at a pore fluid salinity of 0 g/l and a stress level of 100 kPa. Note: different magnifications (corresponding void ratio = 1.01).....	105
Figure 3.33 SEM image of sodium hex. RBBC at a pore fluid salinity of 0 g/l and a stress level of 10,000 kPa. Note: different magnifications (corresponding void ratio = 0.48).....	106
Figure 3.34 SEM image of sodium hex. RBBC at a pore fluid salinity of 0 g/l and a stress level of 100 kPa (top) and 10,000 kPa (bottom) at same magnification. Note: void ratio top image – 1.01, void ratio bottom image - 0.48.....	107
Figure 3.35 SEM image of sodium hex. RBBC at a pore fluid salinity of 0 g/l and a stress level of 100 kPa (top) and 10,000 kPa (bottom) at same magnification. Note: void ratio top image – 1.01, void ratio bottom image - 0.48.....	108
Figure 3.36 SEM image of sodium hex. RBBC at a pore fluid salinity of 0 g/l and a stress level of 100 kPa on top, and natural RBBC Series IV at a salinity of 4 g/l and a stress of 100 kPa on bottom (corresponding void ratios, 1.01 on top, 1.26 on bottom)	109
Figure 3.37 Location of London (Google Earth).....	110
Figure 3.38 Location of Hendon relative to Greater London (Google Earth)	111
Figure 3.39 Location of source in Hendon, actual site identified with red circle, site coordinates: Latitude - 51°34'31.94"N Longitude - 0°14'30.83"W (Google Earth)	111
Figure 3.40 Brown firm weathered London Clay as recovered from the ground at project location (West Hendon development, SI document)	112
Figure 3.41 Stratigraphic sequence for central London (after King, 1981).....	113

Figure 3.42 Photograph of a typical chunk of London Clay with inclusions visible on a surface cut with a razor blade.....	114
Figure 3.43 Quartz inclusions visible in London Clay as received to MIT Geotechnical Laboratory (magnification x2).....	115
Figure 3.44 White quartz inclusions in London Clay as received to MIT Geotechnical Laboratory (magnification x1, bottom right x2).....	115
Figure 3.45 Blue staining visible as veins on the surface of London Clay received to the MIT Geotechnical Laboratory (magnification x1).....	116
Figure 3.46 Whole rock mineralogy and corresponding surface area for London Clay from multiple locations - location closest to Hendon has been identified (British Geological Survey, 2006).....	116
Figure 3.47 Particle size distribution by sedimentation test performed on London Clay at a similar depth to soil which was shipped to MIT (West Hendon development, SI document) ...	117
Figure 3.48 Particle size distribution performed on ground London Clay powder in the MIT Geotechnical Laboratory (tested by Brendan Casey)	118
Figure 3.49 Atterberg limits performed on London Clay from project location. Note: testing depth uncertain (West Hendon development, SI document)	118
Figure 3.50 Atterberg limits performed at MIT on London Clay from Hendon	119
Figure 3.51 Plasticity results for specimens from multiple locations in London (Pantelidou & Simpson, 2007)	119
Figure 3.52 Moisture content versus depth for London Clay at project location (West Hendon development, SI document)	120
Figure 3.53 Mineralogy of London Clay - location closest to Hendon has been identified (British Geological Survey, 2006)	121
Figure 3.54 Sedimentation test performed on natural London Clay powder. Salinities from L-R: 0 (distilled water), 1, 4, 16, 64 & 256 g/l NaCl. 5 grams of soil used in each tube.....	121

Figure 3.55 Axial displacement versus root time for London Clay at different stress levels (data from RS232, London Clay at 44 g/l, consolidometer diameter 4.1 cm).....	122
Figure 3.56 Axial displacement versus log time for London Clay at different stress levels (data from RS232, London Clay at 4 g/l)	122
Figure 3.57 Oedometer test results on intact London Clay from West Hendon development recovered at 5.04 m depth (West Hendon development, SI document)	123
Figure 3.58 Oedometer test results on intact London Clay from West Hendon development recovered at 9.53 m depth (West Hendon development, SI document)	124
Figure 3.59 Compression data from natural in-tact specimens of London Clay tested in the oedometer. Specimen A ₃ recovered between 45-48 m deep, specimen A ₂ recovered between 48-52 m deep (Gasparre, 2005).....	125
Figure 3.60 Compression data from reconstituted specimens of London Clay tested in the oedometer (Gasparre, 2005).....	125
Figure 3.61 Location map of Ursa Basin where IODP Leg 308 performed exploratory borings. Small box represents exploration area (IODP Expedition 308 Report, 2006).....	126
Figure 3.62 Map showing borings performed as part of IODP - Leg 308. Soil tested obtained from Site U1322 (IODP Expedition 308 Report, 2006)	127
Figure 3.63 Sedimentation test performed on RGOM - Ursa. Salinities from L-R 1, 4, 16, 64, 128 & 256 g/l NaCl. Note: 5 g of soil used in each tube	127
Figure 3.64 Plasticity chart showing where GOM - Ursa soil plots	128
Figure 3.65 Particle size distribution for GOM - Ursa performed by Brendan Casey	128
Figure 3.66 Sedimentation test performed on sodium montmorillonite. Salinities from L-R 1, 4, 16, 64, 128 & 256 g/l NaCl. Note: 1 g of soil used in each tube	129
Figure 3.67 One dimensional consolidation curves for sodium montmorillonite Note: 10 lb/ft ² = 0.479 kPa (Mesri & Olsen, 1971 _a).....	129

Figure 3.68 Hydraulic Conductivity versus void ratio curves for sodium montmorillonite (Mesri & Olsen, 1971 _a).....	130
Figure 3.69 Hydraulic conductivity versus void ratio for all three sodium clays in water (Mesri & Olsen, 1971 _b)	130
Figure 3.70 Variation in coefficient of consolidation, c_v with axial consolidation pressure for clay minerals with water as the pore fluid on left, and with CCl_4 (carbon tetrachloride, which negates the double layer) on the right (Robinson & Allam, 1998).....	131
Figure 3.71 Square root of time versus axial displacement for 1 g/l montmorillonite (data from RS245 - target stress level 50 kPa)	131
Figure 3.72 Log of time versus axial displacement for 1 g/l montmorillonite (data from RS245 - target stress level 50 kPa)	132
Figure 3.73 Images of sodium montmorillonite resedimented with 256 g/l pore water at a stress level of 200 kPa. Note: different magnification. Corresponding void ratio 1.58	133
Figure 3.74 Comparison between sodium motmorillonite and natural RBBC Series IV at similar stress levels and at the same pore fluid salinity. Sodium montmorillonite (top) at 200 kPa BBC (bottom) at 100 kPa. Corresponding void ratios 1.58 (SM) and 1.16 (RBBC).	134
Figure 3.75 Comparison between sodium motmorillonite and sodium hex BBC at similar stress levels at the same magnification. Sodium montmorillonite (top) at 200 kPa sodium hex BBC (bottom) at 100 kPa. Corresponding void ratios 1.58 (SM) and 0.98 (RBBC)	135
Figure 4.1 Bulk London Clay as received to the MIT Geotechnical Laboratory	184
Figure 4.2 Close up of bulk London Clay soil with blue flow channel areas and pockets of quartz visible.....	184
Figure 4.3 Air Drying of London Clay using industrial fan (performed in MIT basement, building 1).....	185
Figure 4.4 GPX Disc Grinder Used in Processing London Clay and Leached BBC	186
Figure 4.5 Quartz crystals visible in bulk London Clay visible at X2 magnification.....	187

Figure 4.6 Schematic of the blending procedure for large samples (Germaine & Germaine, 2009)	188
Figure 4.7 Schematic of the sequential quartering procedure (Germaine & Germaine, 2009) .	188
Figure 4.8 Finely ground London Clay being prepared for storage in 10 gallon plastic containers	189
Figure 4.9 Test for determining ideal water content for resedimenting an unfamiliar soil. Top: test tubes showing water contents which were tested Bottom: close up showing free water existing on top of tubes containing too much water (soil being tested BBC which has been leached twice)	190
Figure 4.10 Consolidometers used for this research. Left: consolidometer for triaxial testing, Middle: consolidometer for CRS testing, Right: consolidometer for CRS testing when very small quantities of soil were resedimented.....	191
Figure 4.11 Kitchen Aid mixer which is used in the laboratory to mechanically agitate slurry	191
Figure 4.12 Vacuuming arrangement for slurry. Process starts on left with mixed slurry then proceeds into vacuum flask. Vacuum pump on right creates vacuum which de-airs slurry.....	192
Figure 4.13 Vacuum flask ready to de-air soil on left, and de-airing soil on right where soil is allowed to free fall into the vacuum flask.....	192
Figure 4.14 Pouring slurry into consolidometer with funnel and flexible tube. Note the discharge is kept slightly over the rising soil surface (soil being poured is BBC leached twice which was resedimented with distilled water).....	193
Figure 4.15 Consolidometer which is set up ready to receive slurry. Note that the water bath has been filled with the required fluid half way up the porous stone.....	194
Figure 4.16 Resedimentation set-up at high stress with hanger weights applying stress for safety	194
Figure 4.17 Top: Root time method for determining time to end of primary consolidation. Bottom: The same data plotted in log time to determine the time to end of primary (graph for London Clay resedimented to 4 g/l – the stress level at EOP is 100 kPa).....	195

Figure 4.18 Extruding London Clay soil from consolidometer. Approximately 2 cm of soil is required per CRS test with careful trimming (soil being extruded is London Clay at 256 g/l).. 196

Figure 4.19 Sedimentation test showing the variation in sedimentation height with different quantities of pore fluid salinity (1 g of sodium montmorillonite in each tube. Pore fluid salinities L-R: 1, 4, 16, 64, 128 & 256 g/l NaCl)..... 196

Figure 4.20 Issue of salt precipitating out of solution in high salinity resedimentation (soil shown is sodium montmorillonite being resedimented to 256 g/l)..... 197

Figure 4.21 New method of wrapping porous stone in PTFE tape to help prevent extrusion, close-up shown on right (soil being consolidated is sodium montmorillonite at 1 g/l)..... 198

Figure 4.22 Method to help reduce extrusion from base stone in thin slurries (internal porous stone placed flush with the base of the consolidometer; this in turn is placed on top of a larger diameter porous stone and filter screen as shown) 199

Figure 4.23 Basic method of measuring pore pressures during resedimentation (soil is sodium montmorillonite at 1 g/l) 199

Figure 4.24 Plot of axial deformation and normalized pore pressures versus the square root of time (soil is sodium montmorillonite at 1 g/l - target stress level is 100 kPa)..... 200

Figure 4.25 Plot of axial deformation and normalized pore pressures versus the log of time (soil is sodium montmorillonite at 1 g/l - target stress level is 100 kPa)..... 200

Figure 4.26 Plot of axial deformation and normalized pore pressures versus time (soil is sodium montmorillonite at 1 g/l - target stress level is 100 kPa) 201

Figure 4.27 Electronic transducers used throughout the testing program. Top Left: Trans-Tek LVDTs, 0243-0000 D-90 LVDT (large LVDT), 0240-0000 H-8 (small LVDT), Top Right: Pressure Transducer, Bottom Left: 500 lb Load Cell, Bottom Left: Close up of pressure transducer and also a section through a pressure transducer to help demonstrate its operation. 202

Figure 4.28 Pressure Volume Actuator for CRS testing (calibration factor on tag)..... 203

Figure 4.29 Pressure Volume Actuators for pore pressures (left), and cell pressure (right) used in triaxial testing. Copper tubing exiting from top is plumbed into triaxial cell..... 203

Figure 4.30 10,000 lb capacity load cell used for CRS testing..... 204

Figure 4.31 Schematic diagram of a central data acquisition system (Germaine & Germaine, 2009) 204

Figure 4.32 Schematic diagram of the control system hardware components..... 205

Figure 4.33 CRS trimming ring used for research on right, and standard CRS Trimming ring on left 205

Figure 4.34 Items required for CRS testing. Items include porous stones kept saturated in distilled water, cutting ring with square seal, recess tool and data sheet 206

Figure 4.35 CRS Cell TR4 set-up and running a test..... 206

Figure 4.36 Schematic diagram of Trautwein CRS cell (TR4)..... 207

Figure 4.37 Trautwein CRS cell showing overflow hole which allows any water passing the seal to exit the apparatus before it damages the roller bearings housed further up in the column 208

Figure 4.38 Wykeham Farrance load frame used for CRS testing 208

Figure 4.39 Schematic of low pressure triaxial cell (Santagata 1998)..... 209

Figure 4.40 MIT04 triaxial cell..... 209

Figure 4.41 Low pressure triaxial pedestal & topcap O-ring sealing arrangement with 2 rubber membranes (spacing's exaggerated for clarity) 210

Figure 4.42 MIT04 triaxial cell in 1 Tonne (9.8 kN) Wykeham Farrance screw driven loading frame with adjustable gears 210

Figure 4.43 Entire triaxial testing apparatus. Cell, load frame and PVA's on right of photo; computer control on left (PVA's are masked behind cell, PC controlling testing is visible on bottom left of photo under the table) 211

Figure 4.44 Plot of cell pressure stability for a typical CRS test..... 212

Figure 4.45 Apparatus compressibility for CRS cell TR4 - determined from 2 loadings (obtained January 2011).....	212
Figure 4.46 Positioning cutting edge of CRS ring onto London Clay sample taking care to ensure there is soil available to be cut all the way around (soil being trimmed is London Clay at 256 g/l).....	213
Figure 4.47 Trimming London Clay sample into small diameter CRS ring (soil being trimmed is London Clay at 256 g/l).....	213
Figure 4.48 Small diameter CRS ring with perfectly squared end of London Clay soil (soil being trimmed is London Clay at 256 g/l).....	214
Figure 4.49 Opposite side of cutting ring to Figure 4.48 where soil has been pushed through with recess tool to leave correct height of soil inside ring for testing (soil in ring is London Clay at 256 g/l).....	214
Figure 5.1 Compression behavior in ϵ_a - $\log\sigma'_{ac}$ space for RBBC Series IV at various pore fluid salt concentrations.....	214
Figure 5.2 Compression behavior in e - $\log\sigma'_{ac}$ space for RBBC Series IV at various pore fluid salt concentrations.....	214
Figure 5.3 Hydraulic conductivity in void ratio space for RBBC Series IV at various pore fluid salt concentrations.....	214
Figure 5.4 Coefficient of consolidation versus axial effective stress for RBBC Series IV at various pore fluid salinities.....	214
Figure 5.5 Plot of hydraulic conductivity and coefficient of consolidation data versus stress level for CRS1219 (RBBC Series IV @ 16 g/l). Note that changes in behavior for both datasets occur at same stress levels	214
Figure 5.6 Relationship between pore fluid salinity and required axial strain to achieve an axial effective stress (σ'_{ac}) of 10 MPa for RBBC Series IV.....	261
Figure 5.7 Relationship between pore fluid salinity and initial void ratio for RBBC Series IV.....	261

Figure 5.8 Relationship between pore fluid salinity and void ratio at an axial effective stress (σ'_{ac}) of 10 MPa for RBBC Series IV.....	262
Figure 5.9 Compression behavior in ϵ_a - $\log\sigma'_{ac}$ space for leached BBC at various pore fluid salt concentrations	263
Figure 5.10 Compression behavior in e - $\log\sigma'_{ac}$ space for leached BBC at various pore fluid salt concentrations	264
Figure 5.11 Hydraulic conductivity in void ratio space for leached BBC at various pore fluid salt concentrations	265
Figure 5.12 Coefficient of consolidation versus axial effective stress for leached BBC at various pore fluid salinities.....	265
Figure 5.13 Relationship between pore fluid salinity and required axial strain to achieve an axial effective stress (σ'_{ac}) of 10 MPa for leached RBBC.....	266
Figure 5.14 Relationship between pore fluid salinity and initial void ratio for leached RBBC	266
Figure 5.15 Relationship between pore fluid salinity and void ratio at an axial effective stress (σ'_{ac}) of 10 MPa for leached RBBC.....	267
Figure 5.16 Compression behavior in ϵ_a - $\log\sigma'_{ac}$ space for Killian Court in-situ BBC	268
Figure 5.17 Compression behavior in e - $\log\sigma'_{ac}$ space for Killian Court in-situ BBC	269
Figure 5.18 Hydraulic conductivity in void ratio space for Killian Court in-situ BBC.....	270
Figure 5.19 Coefficient of consolidation versus axial effective stress for Killian Court in-situ BBC.....	270
Figure 5.20 Compression behavior in ϵ_a - $\log\sigma'_{ac}$ space for BBC dispersed with sodium hexametaphosphate.....	271
Figure 5.21 Compression behavior in e - $\log\sigma'_{ac}$ space for BBC dispersed with sodium hexametaphosphate.....	271

Figure 5.22 Hydraulic conductivity in void ratio space for BBC dispersed with sodium hexametaphosphate	272
Figure 5.23 Coefficient of consolidation versus axial effective stress for BBC dispersed with sodium hexametaphosphate	272
Figure 5.24 Compression behavior in $\epsilon_a\text{-log}\sigma'_{ac}$ space reverse leaching test performed on previously leached BBC	273
Figure 5.25 Compression behavior in $e\text{-log}\sigma'_{ac}$ space for reverse leaching test performed on previously leached BBC	273
Figure 5.26 Compression behavior in $e\text{-log}\sigma'_{ac}$ space for reverse leaching test performed on previously leached BBC, close up of point where preconsolidation pressure increases	274
Figure 5.27 Hydraulic conductivity in void ratio space for reverse leaching test performed on previously leached BBC	274
Figure 5.28 Coefficient of consolidation versus axial effective stress for reverse leaching test performed on previously leached BBC.....	275
Figure 5.29 Compression behavior in $\epsilon_a\text{-log}\sigma'_{ac}$ space reverse leaching test performed on previously leached BBC	275
Figure 5.30 Compression behavior in $e\text{-log}\sigma'_{ac}$ space for reverse leaching test performed on previously leached BBC	276
Figure 5.31 Compression behavior in $e\text{-log}\sigma'_{ac}$ space for reverse leaching test performed on previously leached BBC, close up of point where preconsolidation pressure increases	276
Figure 5.32 Hydraulic conductivity in void ratio space for reverse leaching test performed on previously leached BBC	277
Figure 5.33 Coefficient of consolidation versus axial effective stress for reverse leaching test performed on previously leached BBC.....	277
Figure 5.34 Compression behavior synthesis plot in $\epsilon_a\text{-log}\sigma'_{ac}$ space for all Boston Blue Clay derivatives in the testing program.....	278

Figure 5.35 Compression behavior synthesis plot in $e\text{-log}\sigma'_{ac}$ space for all Boston Blue Clay derivatives in the testing program.....	279
Figure 5.36 Hydraulic conductivity synthesis plot in void ratio space for all soils in testing program.....	280
Figure 5.37 Coefficient of consolidation versus axial effective stress synthesis plot for Boston Blue Clay derivatives in the testing program.....	280
Figure 5.38 Relationship between pore fluid salinity and required axial strain to achieve an axial effective stress (σ'_{ac}) of 10 MPa for RBBC (3 types) and in-situ Killian Court BBC.....	281
Figure 5.39 Relationship between pore fluid salinity and void ratio at an axial effective stress (σ'_{ac}) of 10 MPa for RBBC (3 types) and in-situ Killian Court BBC	281
Figure 5.40 Relationship between pore fluid salinity and wet density for RBBC (3 types) and in-situ Killian Court BBC.....	282
Figure 5.41 Relationship between pore fluid salinity and dry density for RBBC (3 types) and in-situ Killian Court BBC.....	282
Figure 5.42 Compression behavior in $\epsilon_a\text{-log}\sigma'_{ac}$ space for R.London Clay at various pore fluid salinities	283
Figure 5.43 Compression behavior in $e\text{-log}\sigma'_{ac}$ space for R.London Clay at various pore fluid salinities	284
Figure 5.44 Hydraulic conductivity in void ratio space for R.London Clay at various pore fluid salinities	285
Figure 5.45 Coefficient of consolidation versus axial effective stress (up to 10,000 kPa) for R.London Clay at various pore fluid salinities	285
Figure 5.46 Coefficient of consolidation versus axial effective stress (up to 40,000 kPa) for R.London Clay at various pore fluid salinities	286
Figure 5.47 Required Axial Strain to $\sigma'_{ac} = 10$ MPa, ϵ_a (%) for R.London Clay.....	286
Figure 5.48 Relationship between pore fluid salinity and initial void ratio for R.London Clay	287

Figure 5.49 Relationship between pore fluid salinity and void ratio at an axial effective stress (σ'_{ac}) of 10 MPa for R.London Clay.....	287
Figure 5.50 One dimensional test from consolidation phase of triaxial testing on RGOM - Ursa soil performed by Brendan Casey.....	288
Figure 5.51 Compression behavior in ϵ_a - $\log\sigma'_{ac}$ space for RGOM - Ursa	288
Figure 5.52 Compression behavior in e - $\log\sigma'_{ac}$ space for RGOM – Ursa.....	289
Figure 5.53 Hydraulic conductivity in void ratio space for RGOM - Ursa	289
Figure 5.54 Coefficient of consolidation versus axial effective stress (up to 40,000 kPa) for RGOM – Ursa.....	290
Figure 5.55 Coefficient of consolidation versus axial effective stress (up to 10,000 kPa) for RGOM – Ursa.....	290
Figure 5.56 Compression behavior in ϵ_a - $\log\sigma'_{ac}$ space for sodium montmorillonite with 256 g/l pore fluid.....	291
Figure 5.57 Compression behavior in e - $\log\sigma'_{ac}$ space for sodium montmorillonite with 256 g/l pore fluid.....	291
Figure 5.58 Hydraulic conductivity in void ratio space for sodium montmorillonite with 256 g/l pore fluid.....	292
Figure 5.59 Coefficient of consolidation versus axial effective stress for sodium montmorillonite with 256 g/l pore fluid.....	292
Figure 5.60 Compression behavior synthesis plot in ϵ_a - $\log\sigma'_{ac}$ space for all soils in testing program.....	293
Figure 5.61 Compression behavior synthesis plot in e - $\log\sigma'_{ac}$ space for all soils in testing program.....	294
Figure 5.62 Hydraulic conductivity synthesis plot in void ratio space for all soils in testing program.....	295

Figure 5.63 Coefficient of consolidation versus axial effective stress synthesis plot (up to 40,000 kPa) for all soils in testing program	296
Figure 5.64 Coefficient of consolidation versus axial effective stress synthesis plot (up to 10,000 kPa) for all soils in testing program	297
Figure 5.65 Normalized stress-strain curve for NC natural RBBC Series IV at different pore fluid salinities from CK ₀ UC triaxial tests	298
Figure 5.66 Normalized stress-strain curves (small strains) for NC RBBC Series IV at different pore fluid salinities from CK ₀ UC triaxial tests	298
Figure 5.67 Normalized stress-(log) strain curves for NC natural RBBC Series IV from CK ₀ UC triaxial tests	299
Figure 5.68 Normalized undrained secant modulus versus axial strain for NC RBBC Series IV at different pore fluid salinities from CK ₀ UC triaxial tests	299
Figure 5.69 Normalized effective stress path for NC natural RBBC Series IV at different pore fluid salinities from CK ₀ UC triaxial testing.....	300
Figure 5.70 Normalized effective stress path (close up view) for NC natural RBBC Series IV at different pore fluid salinities from CK ₀ UC triaxial testing.....	300
Figure 5.71 Friction angle versus axial strain for NC RBBC Series IV at different pore fluid salinities from CK ₀ UC triaxial tests.....	301
Figure 5.72 Normalized excess pore pressure versus axial strain for NC natural RBBC Series IV from CK ₀ UC triaxial tests.....	301
Figure 5.73 Normalized shear induced pore pressure versus axial strain for NC natural RBBC Series IV from CK ₀ UC triaxial tests.....	302
Figure 5.74 A parameter versus axial strain (small strains) for NC RBBC Series IV at different pore fluid salinities from CK ₀ UC triaxial testing	302
Figure 5.75 Relationship between axial strain to failure and salt concentration for natural RBBC Series IV from CK ₀ UC triaxial testing	303

Figure 5.76 Relationship between normalized shear stress and axial strain failure for natural RBBC Series IV from CK₀UC triaxial testing..... 303

Figure 5.77 Plot of soil brittleness at an axial strain of 10 % as a function of pore fluid salinity for natural RBBC Series IV 304

Figure 5.78 Relationship between salinity and friction angle at failure for RBBC Series IV from CK₀UC triaxial testing..... 304

Figure 5.79 Relationship between salinity and friction angle at maximum obliquity for RBBC Series IV from CK₀UC triaxial testing 305

Figure 5.80 Relationship between salinity and axial strain at maximum obliquity for RBBC Series IV from CK₀UC triaxial testing 305

Figure 5.81 Relationship between A parameter at failure and salt concentration for natural RBBC Series IV from CK₀UC testing..... 306

Figure 5.82 Normalized stress-strain curve for NC leached BBC at different pore fluid salinities from CK₀UC triaxial tests..... 306

Figure 5.83 Normalized stress-strain curves (small strains) for NC leached BBC at different pore fluid salinities from CK₀UC triaxial tests 307

Figure 5.84 Normalized stress-(log)strain curves for NC leached BBC at different pore fluid salinities from CK₀UC triaxial tests..... 307

Figure 5.85 Normalized undrained secant modulus versus axial strain for NC leached BBC at different pore fluid salinities from CK₀UC triaxial tests 308

Figure 5.86 Normalized effective stress path for NC leached BBC at different pore fluid salinities from CK₀UC triaxial testing 308

Figure 5.87 Normalized effective stress path (close up view) for NC leached BBC at different pore fluid salinities from CK₀UC triaxial testing 309

Figure 5.88 Friction angle versus axial strain for NC leached BBC at different pore fluid salinities from CK₀UC triaxial tests..... 309

Figure 5.89 Normalized excess pore pressure versus axial strain for NC leached RBBC from CK ₀ UC triaxial tests.....	310
Figure 5.90 Normalized shear induced pore pressure versus axial strain for NC leached RBBC from CK ₀ UC triaxial tests.....	310
Figure 5.91 A parameter versus axial strain (small strains) for NC leached BBC at different pore fluid salinities from CK ₀ UC triaxial testing.....	311
Figure 5.92 Relationship between axial strain to failure and salt concentration for natural leached BBC from CK ₀ UC triaxial testing.....	311
Figure 5.93 Relationship between normalized shear stress and axial strain failure for leached BBC from CK ₀ UC triaxial testing	312
Figure 5.94 Plot of soil brittleness at an axial strain of 10 % as a function of pore fluid salinity for leached RBBC.....	312
Figure 5.95 Relationship between salinity and friction angle at failure for leached BBC from CK ₀ UC triaxial testing.....	313
Figure 5.96 Relationship between salinity and friction angle at maximum obliquity for leached BBC from CK ₀ UC triaxial testing	313
Figure 5.97 Relationship between salinity and axial strain at maximum obliquity for leached BBC from CK ₀ UC triaxial testing	314
Figure 5.98 Relationship between A parameter at failure and salt concentration for leached BBC from CK ₀ UC testing.....	314
Figure 5.99 Normalized stress-strain curve for NC Killian Court in-situ BBC from CK ₀ UC triaxial tests.....	315
Figure 5.100 Normalized stress-strain curves (small strains) for NC Killian Court in-situ BBC from CK ₀ UC triaxial tests.....	315
Figure 5.101 Normalized stress-strain curves (log strain) for NC Killian Court in-situ BBC from CK ₀ UC triaxial tests.....	316

Figure 5.102 Normalized undrained secant modulus versus axial strain for NC Killian Court in-situ BBC from CK ₀ UC triaxial tests	316
Figure 5.103 Normalized effective stress path for NC Killian Court in-situ BBC from CK ₀ UC triaxial testing.....	317
Figure 5.104 Normalized effective stress path (close up view) for Killian Court in-situ BBC from CK ₀ UC triaxial testing	317
Figure 5.105 Friction angle versus axial strain for NC Killian Court in-situ BBC from CK ₀ UC triaxial tests	318
Figure 5.106 Normalized excess pore pressure versus axial strain for Killian Court in-situ BBC from CK ₀ UC triaxial tests.....	318
Figure 5.107 Normalized shear induced pore pressure versus axial strain for Killian Court in-situ BBC from CK ₀ UC triaxial tests.....	319
Figure 5.108 A parameter versus axial strain (small strains) for NC Killian Court in-situ BBC from CK ₀ UC triaxial testing	319
Figure 5.109 Normalized stress-strain curve synthesis plot for all types of NC BBC from CK ₀ UC triaxial tests.....	320
Figure 5.110 Normalized stress-strain curves (small strains) synthesis plot all types of NC BBC from CK ₀ UC triaxial tests.....	321
Figure 5.111 Normalized stress-strain curves (log strains) synthesis plot all types of NC BBC from CK ₀ UC triaxial tests.....	322
Figure 5.112 Normalized undrained secant modulus versus axial strain synthesis plot for all types of NC BBC from CK ₀ UC triaxial tests	323
Figure 5.113 Normalized effective stress path synthesis plot for all types of NC BBC from CK ₀ UC triaxial testing (legend can be seen in Figure 5.111).....	324
Figure 5.114 Normalized effective stress path synthesis plot (close up view) for all types of NC BBC from CK ₀ UC triaxial testing (legend can be seen in Figure 5.111).....	324

Figure 5.115 Friction angle versus axial strain synthesis plot for all types of NC BBC from CK ₀ UC triaxial tests.....	325
Figure 5.116 Friction angle at peak and maximum obliquity versus stress level for NC RBBC from CK ₀ UC triaxial tests (Abdulhadi, 2009).....	326
Figure 5.117 Normalized excess pore pressure versus axial strain synthesis plot for all types of NC BBC from CK ₀ UC triaxial tests	326
Figure 5.118 Normalized shear induced pore pressure versus axial strain synthesis plot for all types of NC BBC from CK ₀ UC triaxial tests	327
Figure 5.119 A parameter versus axial strain synthesis plot for all types of NC BBC from CK ₀ UC triaxial tests.....	327
Figure 5.120 Relationship between K ₀ value and normalized shear stress for all types of BBC in testing program from CK ₀ UC triaxial testing	328
Figure 5.121 Relationship between axial strain to failure and normalized shear stress for all types of BBC in the testing program from CK ₀ UC triaxial testing	328
Figure 5.122 Relationship between friction angle at failure and axial strain for all types of BBC in testing program from CK ₀ UC triaxial testing.....	329
Figure 5.123 Relationship between friction angle at maximum obliquity and axial strain for all types of BBC in testing program from CK ₀ UC triaxial testing	329

LIST OF SYMBOLS

AC	Alternating Current
A/D	Analog-to-Digital Converter
BBC	Boston Blue Clay
CF	Clay Fraction
CK ₀ U	K ₀ -Consolidated Undrained Shear Test
CK ₀ UC	K ₀ -Consolidated Undrained Compression Test
CK ₀ UE	K ₀ -Consolidated Undrained Extension Test
CL	Low Plasticity Clay
CR	Virgin Compression Ratio
CRS	Constant Rate of Strain
D/A	Digital-to-Analog Converter
DC	Direct Current
DCDT	Direct Current Displacement Transducer
ESP	Effective Stress Path
GOM	Gulf of Mexico
LIR	Load Increment Ratio
LVDT	Linear Variable Differential Transformer
MIT	Massachusetts Institute of Technology
NC	Normally Consolidated
NSP	Normalized Soil Parameter
OC	Overconsolidated
OCR	Overconsolidation Ratio
PC	Personal Computer
PID	Proportional-Integral-Derivative
PVC	Pressure-Volume Controller
QBASIC	Quick Beginners All-purpose Symbolic Instruction Code
RBBC	Resedimented Boston Blue Clay
RGOM	Resedimented Gulf of Mexico Soil
SR	Swelling Ratio
TC	Triaxial Compression Shear Test

TE	Triaxial Extension Shear Test
TX	Triaxial
USR	Undrained Strength Ratio (s_u/σ'_{ac})
SHANSEP	Stress History and Normalized Soil Engineering Properties
TSP	Total Stress Path
USCS	Unified Soil Classification System
VCL	Virgin Compression Line
A (A _f)	Skempton's pore pressure parameter (at failure)
B	Skempton's pore pressure parameter
CCB	Cambridge City Base (datum)
C _c	Compression index
C _s	Swelling index
C _α	Secondary compression index
c _v	Coefficient of consolidation in the vertical direction
c'	Cohesion intercept
E	Young's modulus
E _u	Undrained secant Young's modulus
E _{u (MAX)}	Undrained secant Young's modulus (maximum)
e	Void ratio
e ₀	Initial void ratio
G _s	Specific gravity
G _i	Initial shear modulus
H	Height
H _d	Drainage height
I _p	Plasticity index
K	Lateral coefficient of earth pressure
K ₀	Coefficient of lateral earth pressure at rest
K _{0NC}	Coefficient of lateral earth pressure at rest for NC soil
k _v	Vertical hydraulic conductivity
L	Length

M	Exponent in the SHANSEP equation describing the change in normalized strength with OCR
m_v	Coefficient of volume change
p, p'	Average effective stress, $(\sigma_1 + \sigma_3) / 2$, $(\sigma'_1 + \sigma'_3) / 2$
q	Shear stress, $(\sigma_1 - \sigma_3) / 2$
S	Undrained strength ratio for NC soil in SHANSEP equation
S_i	Initial Saturation
s_u	Undrained shear strength
t	Time
t_p	Time to end of primary
$u,$	Δu Pore pressure, change in pore pressure
u_e	Excess pore pressure
u_s	Shear induced pore pressure
u_0	Pore (back) pressure at start of shearing
$V, \Delta V$	Current volume, change in volume
V_0	Initial volume
w	Water content
w_L	Liquid limit
w_p	Plastic limit
ϵ	Strain
ϵ_a	Axial strain
ϵ_{af}	Strain at peak shear stress
ϵ_v	Specimen volume strain
$\dot{\epsilon}$	Strain rate
ϕ, ϕ'	Friction angle, effective friction angle
ϕ'_p	Effective friction angle at peak
ϕ'_{mo}	Effective friction angle at maximum obliquity
γ_w	Unit weight of water
ν	Poisson's ratio
ρ	Density
σ_v, σ'_v	Vertical stress, vertical effective stress

σ_h, σ'_h	Horizontal stress, horizontal effective stress
σ'_p	Preconsolidation pressure
σ'_{ac}	Axial effective stress
σ'_{ac}	Axial consolidation effective stress
σ'_{am}	Maximum axial vertical consolidation effective stress
σ'_{vc}	Vertical consolidation effective stress
$\sigma_1, \sigma_2, \sigma_3$	Principal stresses
σ_{oct}	Mean octahedral stress
τ	Shear stress

1 INTRODUCTION

1.1 RESEARCH STATEMENT

Traditional Geotechnical Engineering pays very little attention to the effect of pore fluid salinity on the behavior of a given soil. The only real acknowledgement that salt exists as part of a soil matrix occurs when allowances are made for it in phase relation calculations. When estimating the behavioral aspects of a soil mass consideration is usually not given to the salinity of the soil in its present state, as opposed to when it was deposited. The exception to this occurs when leaching of the soil has potentially occurred. Given that the pore fluid salinity may have changed over time, it is wise to anticipate that the soil behavior will have changed also.

The Geotechnical Engineer frequently encounters marine deposited soils which were formed in saline or brackish environments with pore fluid salinities in the order of 30 – 35 grams of salt per liter of water (g/l). These soils exist today in coastal regions where the original sea bed has undergone uplift and now provides a location for construction activities. The effects of how the changes in soil salinity due to a reduction in pore fluid salinity have been well studied.

In the Gulf of Mexico, the reverse process to that previously described occurs whereby a marine sediment deposited in a saltwater environment (~35 g/l), can undergo an increase in salinity. Pore fluid salinities of up to 250 g/l are possible around salt domes (structures) which exist on the sea floor in the Gulf Region. These salt domes are often located in areas of interest for hydrocarbon exploration. It is therefore now necessary to study the effects, if any, which this increase in salinity will produce in a given soil.

1.2 OBJECTIVES OF THE RESEARCH

Boston Blue Clay was chosen as the main testing material for this research because it is relatively plentiful. It is desirable to study the effects on such an abundant source before moving onto more relevant materials which have far greater retrieval costs and processing requirements. The majority of specimens tested were derived from resedimented materials in which the pore fluid salinity has been varied. Other soils were tested in order to see if some trends apply as to what effects these variations in pore fluid salinity bring about.

An extensive laboratory testing program was established in the form of a suite of Constant Rate of Strain (CRS) and K_0 consolidated, undrained shear in compression (CK_0UC) triaxial testing. These tests will help identify any changes in one dimensional and shear behavior between soils at different pore fluid salinities.

1.3 ORGANIZATION OF THE THESIS

This thesis is organized into six chapters with the intention of conveying a complete and thorough picture into the research performed, the results obtained and any observations noted.

Chapter 2 presents the background information on the research. Previous researchers findings in relation to altering the salinity of a given soil are examined. This is done so in three parts: i) research involving the leaching of salt from a soil; ii) research involving the addition of salt to a soil (whereby the salinity is increased beyond depositional levels), and iii) research on intact specimens of very high salinity soils. A background is also given into the normalized shear behavior of RBBC, a method which has been utilized in this research.

Chapter 3 presents all of the different type of soils used in testing. A total of four derivatives of BBC were used and these are described in detail. London Clay was resedimented at MIT for the first time as part of this research and a description of how it was processed is given. Gulf of Mexico soil from the Ursa Basin was resedimented as well as sodium montmorillonite at different pore fluid salinities. Scanning Electron Microscope (SEM) images taken on oven dried specimens are presented for various derivatives of BBC at different stress levels and at different pore fluid salinities. Images are also shown for sodium montmorillonite.

Chapter 4 identifies the equipment, methods and procedures used throughout the research. Thorough descriptions are given of the equipment as well as the ways in which this equipment was used. This includes the Constant Rate of Strain (CRS) cell, the low pressure triaxial apparatus and the control hardware and software and measurement instrumentation associated with successful laboratory testing. Variations to traditional testing methodology are also explained here.

Chapter 5 presents the results from all laboratory testing performed. A large bank of CRS results are presented which include one dimensional compression data, hydraulic conductivity

data and coefficient of consolidation data. These results are appraised against each other and their behaviors compared for similar materials. Conclusions are drawn in relation to some observed anomalies in the behavior of RBBC, and all RBBC specimens are compared against in-situ BBC soil which was also tested as part of the research. A synthesis analysis is provided for all soils used.

The results from K_0 consolidated undrained shear tests are presented in detail for all types of BBC tested. The specimens were generally consolidated to different stress levels and then sheared in axial compression on normally consolidated soil. As with the CRS results, a synthesis analysis of the triaxial data is given and conclusions drawn as to the observed behaviors.

Chapter 6 summarizes the results and conclusions from the research and presents recommendations for future research.

Appendix A presents pore pressure ratio plots for all soils tested in the CRS device and Appendix B gives example phase relation calculations to allow for the presence of such large salt quantities in some of the soils tested.

2 BACKGROUND

2.1 INTRODUCTION

This chapter presents the background information on how altering the salinity of a soil affects its behavior as both a soil mass and as an individual soil particle. Although much research has been performed into the effect of removing natural salt from a soil fabric, only a handful of researchers have performed tests on what happens when additional salt is introduced to a soil matrix.

Section 2.2 describes how either introducing or removing salt from the pore fluid changes the behavior of individual soil particles. Depending on the type of minerals present in a soil, different levels of behavioral change will be observed. More often than not, natural soils contain a mixture of minerals, it is therefore not readily obvious what impact the introduction or removal of salt to a soil-water system will have. The known effect of how changes in pore fluid salinity can affect a pure clay mineral may be different to how the same changes in pore fluid salinity will affect a soil mass containing a fraction of that same mineral.

Section 2.3 identifies previous research which has been performed in this area. It breaks previous research into three areas: research where leaching salt from the soil was performed, research where adding salt to soil was performed and finally research which was performed on in-tact soil samples containing very high pore fluid salinities.

Section 2.4 reviews fundamental soil behavior aspects during undrained shear deformation that are related to this research. It also discusses the concept of normalized behavior and its application to the results presented in this research.

2.2 ELECTRO-CHEMICAL EFFECTS ON SOIL BEHAVIOR

2.2.1 INTRODUCTION

The way in which the pore fluid salinity affects the soil behavior will be described for a homogeneous mass. The discrete particles that make up soil are not strongly bonded in the way that crystals of metal are, and hence they are relatively free to move with respect to one another. The deformation of a soil mass is controlled by interactions between individual particles, especially by sliding between particles. Because sliding is a nonlinear and irreversible deformation, the stress-strain behavior of the soil is strongly nonlinear and irreversible. This process describes the mechanical contact between particles (Lambe & Whitman, 1969).

There is also a chemical interaction between particles. The space between particles are called pore spaces and they are usually filled with air and/or water. The nature of the pore fluid will influence the magnitude of the shear resistance existing between two particles by introducing chemical matter to the surface of contact. In the case of very tiny soil particles, the pore fluid may intrude between the particles meaning there is no mechanical contact and that physio-chemical forces dominate the behavior of the soil mass. The spacing of these particles will increase or decrease as the transmitted compressive forces decreases or increases. Therefore soil is an inherently multiphase system consisting of a mineral phase called the mineral skeleton and a fluid phase called the pore fluid. The constituents of the pore phase will influence the nature of the mineral surfaces and hence affect the process of force transmission at the particle contacts. This interaction between the phases is called chemical interaction (Lambe & Whitman, 1969).

The way in which a soil behaves in a given environment is a function of what the soil is made of. Differences in particle size and shape are mainly due to differences in the types and arrangements of elements in the crystalline structure which in effect defines the mineralogy of a soil. A clay particle is a colloid, which is a term used to describe a particle whose behavior is controlled by surface derived forces rather than mass derived forces. The size range of colloids has been more or less arbitrarily set as $1 \text{ m}\mu$ to 1μ ($10^{-9} - 10^{-6} \text{ m}$), (Lambe & Whitman, 1969).

2.2.2 SPECIFIC SURFACE

The smaller the particle size, the larger its specific surface. The specific surface is the ratio of the surface area of a material to either its mass or its volume. In terms of mass:-

$$\text{Specific surface} = \text{surface area} / \text{mass} \quad (2.1)$$

It is a common fact that larger particles, regardless of shape, have smaller surface areas per unit of mass and therefore smaller specific surfaces than small particles. Specific surface is inversely proportional to the grain size of a soil. A soil mass made up of many small particles will have, on average, a larger specific surface than the same mass made up of larger particles. From the concept of specific surface, a larger moisture content should be expected from a fine-grained soil than a coarse grained soil and all other things such as void ratio and soil structure to be equal. Figure 2.1 shows the average values of relative sizes, thicknesses and specific surface areas for the most common clay minerals. It can be seen from this Figure that montmorillonite is the smallest clay mineral that is encountered and it is also the most sensitive to water. Kaolinite on the other hand, is one of the larger and less sensitive minerals to water encountered in clay (Holtz & Kovacs, 1981).

For a typical sodium soil, a montmorillonite particle would carry 1.4×10^4 ions while the kaolinite has 4×10^6 ions. If the individual clay particles are now dropped into water, both the mineral surfaces and the exchangeable ions pick up water i.e. hydrate. Upon hydration, the sodium ion grows about sevenfold. These hydrated ions are too large to fit into a monoionic layer on a mineral particle even if they wanted to, and the exchangeable ions with their shells of water move away from the mineral surface to positions of equilibrium. The ions are attracted to the mineral surface to satisfy the negative charge existing on the surface but they also desire to move away from each other because of their thermal energies. In actual fact, the position which they occupy is a compromise between these two types of forces. Therefore when the particles are dropped into water, the ions move away from the surface to form what is termed the double layer (Lambe & Whitman, 1969). It is at this juncture it should be noted that development of the double layer on a clay particle will be controlled by the salinity of the pore fluid. Because an increase in ionic concentration is noted with an increase in salinity, double layer growth will be hindered with an increase in pore fluid ionic concentration (salinity). The maximum distance to

which the double layer of a given soil will develop beyond the soil particle will only be realized in distilled water. In saltwater, the double layer of a given soil will extend away from the particle until the concentration of sodium ions in the double layer is equal to that of the pore water. It is therefore stated that at some salinity there will be no double layer growth as the ionic concentration of the pore fluid will be able to satisfy the ionic demand of the particle at the particle surface. The double layer thickness is therefore the distance from the surface of a soil particle over which there is an electric potential. This is best demonstrated in Figure 2.2 where a simple sedimentation test is performed on hydrated sodium montmorillonite. Each tube contains the same quantity of soil (1 g), but the pore fluid salinity increases from 1 g/l on the left to 256 g/l on the right. It can be seen that the ionic demand of the double layer for this soil is satisfied in between salinities of 16 & 64 g/l as after 64 g/l there is no change in sedimentation height with an increase in salinity. The Figure also shows proof that between the 1 & 16 g/l pore fluid contents, when an increase in salinity is observed there is a corresponding decrease in double layer growth – this is evident by the lower sedimentation height.

2.2.3 SOIL FORMATION

If two fully hydrated clay particles which exist in water are brought closer together, they will reach an interparticle spacing at which they begin to exert forces on each other. Because each particle carries a net negative charge, they tend to repel each other. Since this negative charge on clay particles is balanced by the cations in the double layer, the two particles begin to repel each other when their double layers overlap one another. This represents the repulsive force which exists between soil particles and it is directly related to the size of the double layer (Lambe & Whitman, 1969). By changing the pore water chemistry of a soil-water system, double layer development will be either hindered or encouraged. Generally, as the pore fluid salinity increases, the size of the double layer decreases.

An attractive force also exists between two soil particles. This attractive force is the van der Waals' force, or secondary bonding force which acts between all adjacent pieces of matter and it is essentially independent of the characteristics of the fluid between the particles. If the net force between two clay particles is attractive then the two particles will move towards each other and become attached – this is known as flocculation. If the net force between the two particles is

repulsive then they will move away or disperse. When a suspension of clay particles flocculates, three different modes of particle association may occur: face-to-face, edge-to-face and edge-to-edge. Face-to-face association leads to thicker and possibly larger flakes whereas edge-to-face and edge-to-edge associations will lead to three dimensional voluminous card house structures (Van Olphen, 1977). The various modes of particle association are shown in Figure 2.3.

The structure of a soil once formed consists of interparticle forces and the fabric. The interparticle forces describe how the shear and normal stresses are transmitted between soil particles while the fabric of a soil is defined by the orientation and distribution of particles. The clay mineral illite is distinguished from montmorillonite primarily by the absence of interlayer swelling in the presence of water. Illite is also not as active as montmorillonite and therefore will not be as susceptible to changes in pore fluid salinity as montmorillonite. Figure 2.4 shows a graph of the forces which act on an illite particle in a low salinity environment. As the particles move further away from each other, different repulsive and attractive forces act to cause either flocculation or dispersion. It can also be seen from this Figure that illitic particles have very little repulsive forces associated with them, even in a low salinity environment. This repulsive force is present at a relatively short distance from the particle and can be easily overcome by the stronger attractive forces. It is therefore very likely that marine deposits which contain illite as one of its main minerals, will contain flocs as part of its structure.

2.3 LITERATURE REVIEW

2.3.1 INTRODUCTION

The research presented in this thesis involves both the addition and removal of salt from soil. Although the effect of salt on soil behavior has been previously studied, the results from this previous research will be described in three different Sections.

Firstly, the effect of leaching the salt from a soil fabric will be presented. This research focuses on what happens to a soil in which the natural salts are removed thereby reducing the electrolyte content of the soil. Extensive research has been performed in this area as it is a more common issue which confronts Geotechnical Engineers. The issue arises in areas where a marine soil has been uplifted and is undergoing the process described. The second Section will cover

what happens when a soil undergoes the addition of a salt to the fabric after the soil has been deposited. This is a less common scenario and exists in regions where the marine deposit has undergone further or prolonged burial and now exist in regions where the salinity of the water is higher than when the soil was deposited. The Gulf of Mexico is one such area and soils at the sea floor in this location commonly encounter salinities much higher than those that existed when the soil was originally deposited. Pore fluid salinities of 80 g/l are common but salinity can reach levels of up to 250 g/l. The third and final section looks at in-situ soil which is naturally high in salinity. Laboratory testing which was performed on recovered specimens will be examined and information which is relevant to this research will be identified.

2.3.2 TRADITIONAL LEACHING OF SOIL

The effect of salt on a soil mass has been well studied and researched. This involves removing (leaching) the existing salt from a marine soil to determine how the soil behavior changes. One example is a marine clay which has been laid down in a marine environment with a typical salinity of 35 g/l or less. Marine deposits frequently undergo uplift so that they rise above the level of the sea. The result of fresh groundwater percolating through the clay serves to gradually remove this natural salt from the clay. This process occurs over many thousands of years. The pore fluid at which a soil exists today can be much different from that at the time of deposition. This process also happens when artesian pressure is present in the groundwater such as is the case in areas of Boston. This reduction in the electrolyte content of the water around the soil particles can reduce the net attraction between them – in other words, leaching of the salt from the pore fluid can cause a reduction in shear strength (Lambe & Whitman, 1969). Laboratory experiments such as those described in Lambe & Whitman (1969) had previously been performed by Bjerrum & Rosenqvist (1956) on artificially sedimented clays. Their experiments proved that if a soil is sedimented in salt water and the soil is then later subjected to a hydraulic gradient resulting in the leaching of salt, the undrained shear strength will be reduced and its sensitivity increased. They also found that if the same clay is deposited in a fresh water, the shear strength is two to three times as high as the one sedimented in the salt water. The clay used in this research was an Asrum clay in which the salt had been leached from the soil naturally in-situ. The clay fraction of the soil was approximately 60 % illite with the remainder composed of quartz and feldspar. The soil is of very low plasticity and with a liquid limit (w_l) of

28 % and a plastic limit (w_p) of 18.8 %. Some of the results from this research can be seen in Figure 2.5. Their work shows that for an illitic clay, the addition of salt increases the undrained shear strength whereby at a given stress, an increase in the shear strength is observed for an increase in salt content.

Skempton & Northey (1952) also showed that a reduction in the salt concentration in the pore fluid, caused by leaching clays of marine or estuarine origin, can result in high sensitivities (or lower shear strength).

2.3.3 ADDING SALT TO SOILS

At MIT in 1961, William Bailey conducted research into the effects of salt on the shear strength of Boston Blue Clay. He ran isotropically consolidated undrained triaxial tests on resedimented Boston Blue Clay ranging in salt content from 3 – 35 g/l. As part of his research, he also leached some Boston Blue Clay and strength tested this soil. In general, he found that soil which contained more salt (35 g/l as opposed to 3 g/l) had a higher effective stress envelope at maximum principle stress difference, and that leaching the salt from a normally consolidated salt samples decreased the shear strength and the strain to failure and increased the excess Δu at maximum obliquity. He also found a 6.5° reduction in the effective stress envelope at maximum principle stress difference for the leached soil. Again, for an illitic clay, the addition of salt has been shown to increase the undrained shear strength.

Also in 1961 at MIT, Anwar Wissa performed research on the environmental changes on the stress-strain properties of kaolinite. He ran a series of triaxial compression tests on resedimented sodium kaolinite. In contrast to illitic soils, he showed that with an increase in salinity, a corresponding reduction in undrained strength is observed. He links this change in behavior with an increase in salinity to the fact that the positive and negative charge on the clay particle will be reduced meaning that the degree of flocculation decreases as the pore fluid salinity increases. In fact, Wissa found that kaolinite soils resedimented with distilled water as the pore fluid were stronger than those resedimented with salt water as the pore fluid.

In 1985, A.S. Stipho conducted research on salt bearing soils from Saudi Arabia. He conducted laboratory testing on sands and clays using various salt types, up to pore fluid

concentrations of 200 g/l. Among his findings he found that the compressibility of a salt bearing clay increased with an increase with salt content and also that with an increase in salt content, a decrease in void ratio at a given stress was recorded. The salt used for the results quoted was NaCl. The mineralogy of the soil being tested is not available, however, it has a low plasticity index ($w_L = 29\%$ and $w_p = 22.5\%$) indicating that the clay fraction consists mostly of silt and large clay sized particles. The liquid limit was also found to drop with an increase in salt content for all salt types but it is not described how the salt was accounted for in the phase relation calculations. Another interesting finding of the research is that an increase in cohesion is noted with an increase in salt contents.

2.3.4 RESULTS FROM IN-TACT MATERIAL

Laboratory tests were run on in-tact marine clay recovered at depths of up to 180 m below the Caspian Sea in 1996 (Leon A. et. al, 2004). The salinity of the soil at the recovery depths was around 250 g/l and the soil was described as high to extremely high plasticity clay. They found the preconsolidation pressures of the soil they tested to be less than the calculated overburden stress meaning that the soil is not normally consolidated, but is in fact underconsolidated. Their results can be seen in Figure 2.6 and show clearly that the measured preconsolidation pressure is much lower than the calculated overburden stress. Interestingly, these low preconsolidation pressures were attributed to using fresh water as the surrounding fluid in the oedometer cell. They believe that this in effect caused leaching of the salt from the soil during the test. To prove this theory, several more oedometer tests were run on recovered material with different cell fluid salinities and the results show that when the cell fluid salinity closely matches the pore fluid salinity, a higher preconsolidation pressure is recorded than when fresh water is used. The results of these tests are shown in Figure 2.7.

This is an important finding in relation to the research performed in this thesis as all one-dimensional compression testing will be performed on soils with a large range of pore fluid salinities. It is therefore essential to use cell fluid which matches the pore fluid salinity of the soil being tested in order to ascertain the correct compression behavior.

2.4 NORMALIZED BEHAVIOR OF BOSTON BLUE CLAY

The normalized soil parameter concept is based on the empirical observation that the results of laboratory tests on clay samples having the same overconsolidation ratio, but different consolidation stresses, and therefore different preconsolidation pressures, exhibit similar properties (i.e. strength, stress-strain, pore pressure parameters, moduli etc.) when normalized with respect to the consolidation stress (Ladd & Foott, 1974). This concept has a significant practical value as it provides a useful framework for comparing and relating the behavioral characteristics of different cohesive soils and has led to the development of the Stress History and Normalized Soil Engineering Properties (SHANSEP) design method (Ladd & Foott, 1974). Moreover, the normalized soil parameter is also the basis of other frameworks of soil behavior such as Critical State Soil Mechanics (Schofield & Wroth, 1968) and the “simple” clay (Ladd, 1960) as well as analytical soil models such as the Modified Cam Clay (Roscoe & Burland, 1968) and MIT-E3 (Whittle & Kavvas, 1994).

The SHANSEP method is applicable to uniform cohesive soils that have been mechanically overconsolidated or are truly normally consolidated and maintain the same basic structure during loading beyond the in-situ stresses and therefore exhibit behavior that can be normalized by the preshear consolidation stress level. The method is not intended for use in cemented, highly sensitive clays or in the drying crust of a soil deposit. The technique can be used in either drained or undrained conditions but is more usually used to describe the undrained shear in triaxial compression and extension, and in the direct simple shear tests. The premise of this method is that the in-situ stress history can be simulated in the laboratory that will provide accurate predictions of the in-situ soil behavior at different overconsolidation ratios. Therefore while the actual stresses are different between the laboratory and the field, the SHANSEP method is able to predict identical behavior for a given overconsolidation ratio. The new stress history is achieved by one dimensional (K_0) consolidation well past the preconsolidation pressure into the normally consolidated range to some new maximum state of stress – this is shown by points A or B in Figure 2.8. For overconsolidation ratios greater than unity, the soil is mechanically overconsolidated by K_0 swelling (points C or D). It is assumed that regardless of the physical mechanisms causing the in-situ overconsolidation, all overconsolidated soil will behave in the same way.

Figure 2.9 shows typical results of a SHANSEP test program for AGS plastic marine clay with three modes of shearing (triaxial compression and extension and direct simple shear). The results of this data can be represented by the equation:

$$\frac{S_u}{\sigma'_{vc}} = S(OCR)^m \quad (2.2)$$

where S is the undrained strength ratio for the normally consolidated clay, and m is the slope of the regression line. The difference in behavior for the three modes of shearing is a reflection of the anisotropic nature of soil. Given that all the strength testing performed for this research was done on normally consolidated clay, the OCR value from Equation 2.2 will remain as 1. Note that the axial stress in triaxial space now corresponds to vertical stress in the SHANSEP design procedure.

2.4.1 EFFECT OF STRESS LEVEL ON NORMALIZED STRENGTH

The underlying assumption of the SHANSEP method is that the normalized behavior is dependent only on the overconsolidation ratio. Therefore, while the preshear stresses used in the laboratory testing program may be different to the field stresses, the method predicts identical behavior for a given OCR. The results of work performed by Abdulhadi (2009) indicate that the normalized properties can have a stress level dependence, at least for resedimented Boston Blue Clay. Figure 2.10 illustrates the effect of stress level on the SHANSEP parameters S and m for resedimented BBC in triaxial compression. It is shown that the S parameter decreases consistently with increasing consolidation stress while the m parameter varies only slightly. A corresponding decrease in the friction angle is observed with an increase in the consolidation stress and this is shown in Figure 2.11.




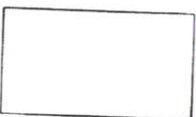
Edge View	Typical Thickness (nm)	Typical Diameter (nm)	Specific Surface (km ² /kg)
 Montmorillonite	3	100-1000	0.8
 Illite	30	10 000	0.08
 Chlorite	30	10 000	0.08
 Kaolinite	50-2000	300-4000	0.015

Figure 2.1 Average values of relative sizes, thicknesses and specific surface area of the most common clay minerals (Yong & Warkentin, 1975)

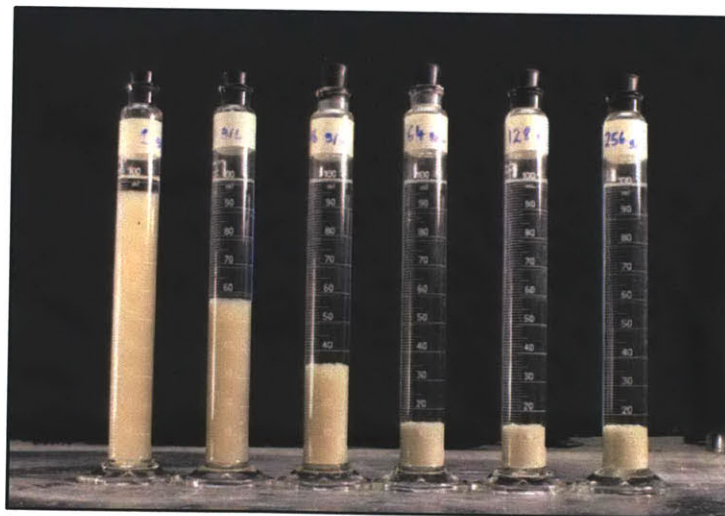


Figure 2.2 Sodium montmorillonite at different pore fluid salinities. Saltwater content L-R: 1, 4, 16, 64, 128 & 256 g/l NaCl. (1 g of soil used in each tube)

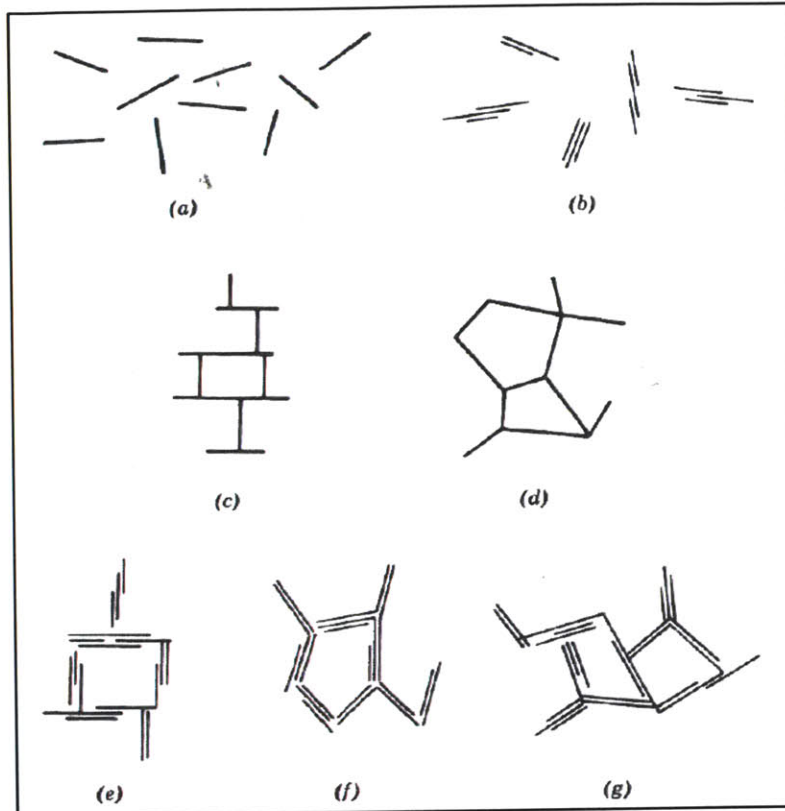


Figure 2.3 Modes of particle association in clay suspensions and terminology (a) dispersed and deflocculated (b) aggregated but deflocculated (c) edge to face flocculated but dispersed (d) edge to edge flocculated but dispersed (e) edge to face flocculated and aggregated (f) edge to edge flocculated and aggregated (g) edge to face and edge to edge flocculated and aggregated (Van Olphen, 1977)

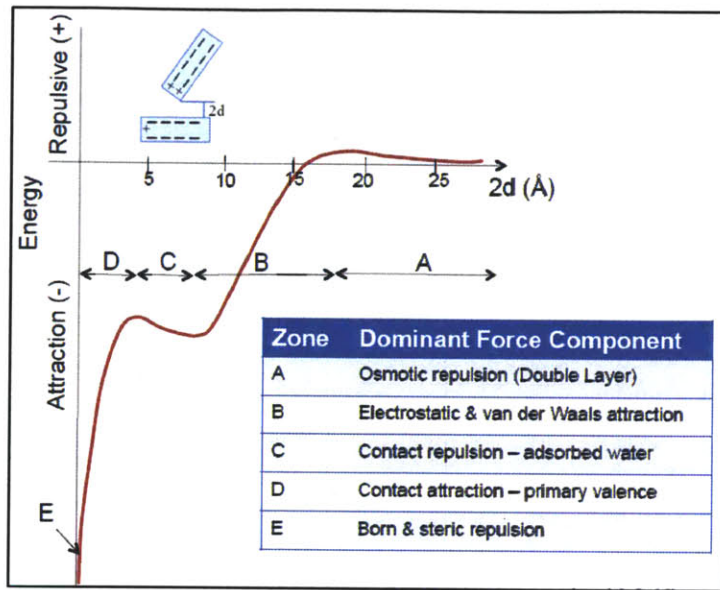


Figure 2.4 Graph of attractive forces acting on illite soil particles in a low salinity environment (Ladd & Kinner, 1967)

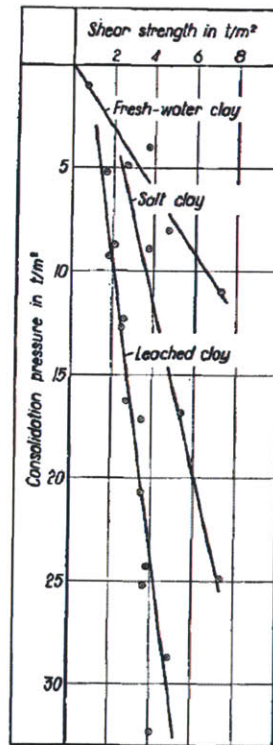


Figure 2.5 Comparison of the undrained shear strength of salt, leached and fresh-water clays (Bjerrum & Rosenqvist, 1956)

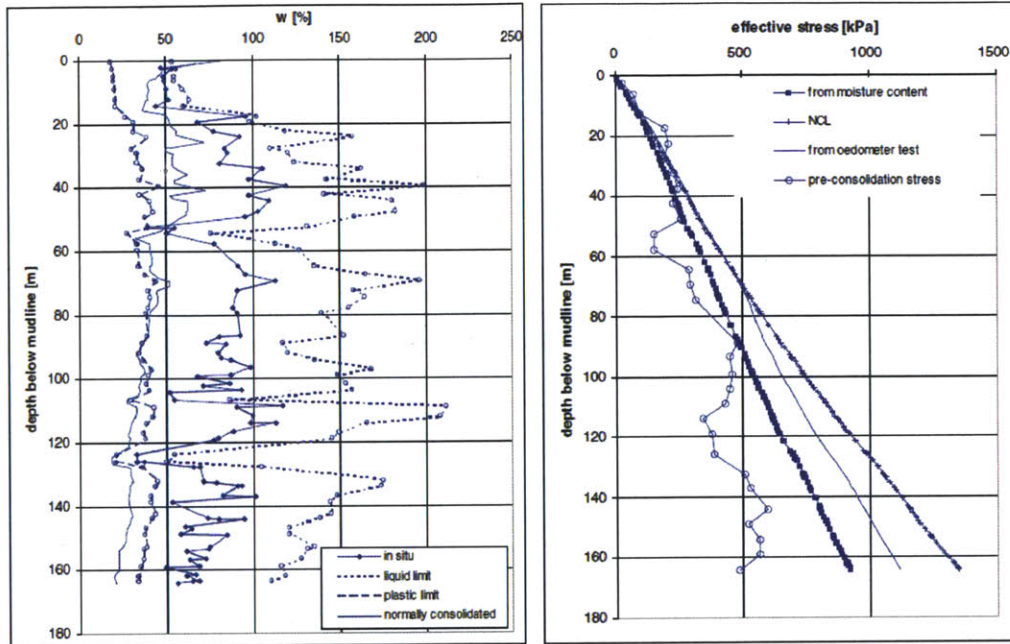


Figure 2.6 Soil profiles from the Caspian Sea: Atterberg limits on the left and measured preconsolidation pressures on the right (van Paassen. et. al., 2004)

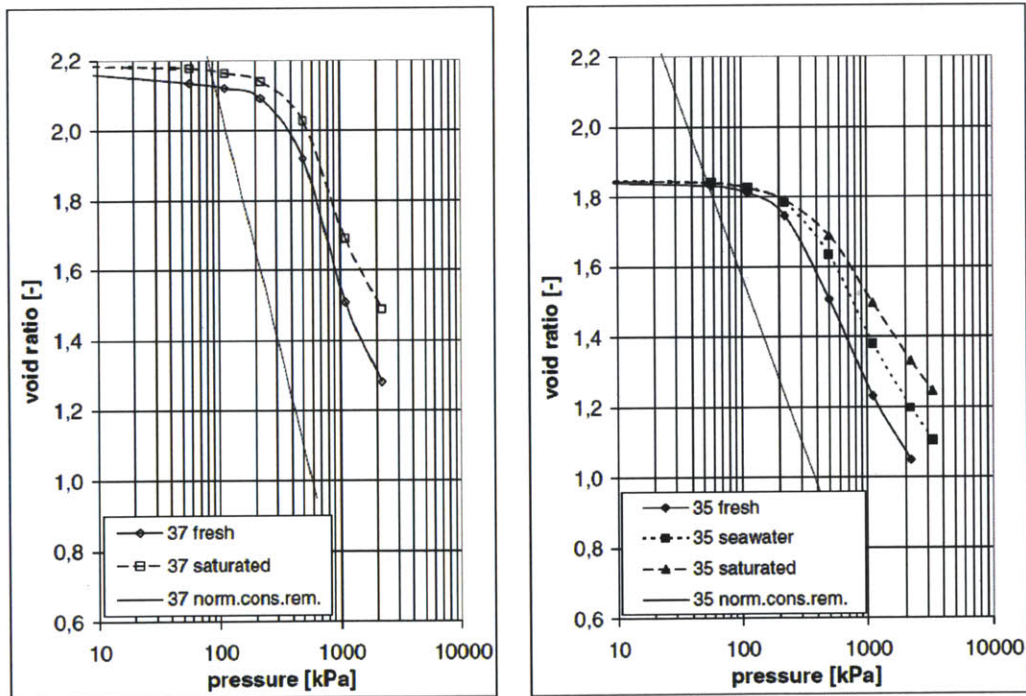


Figure 2.7 Oedometer test results from Caspian Sea recovered from two different depths run at different cell fluid salinities (van Paassen. et al., 2004)

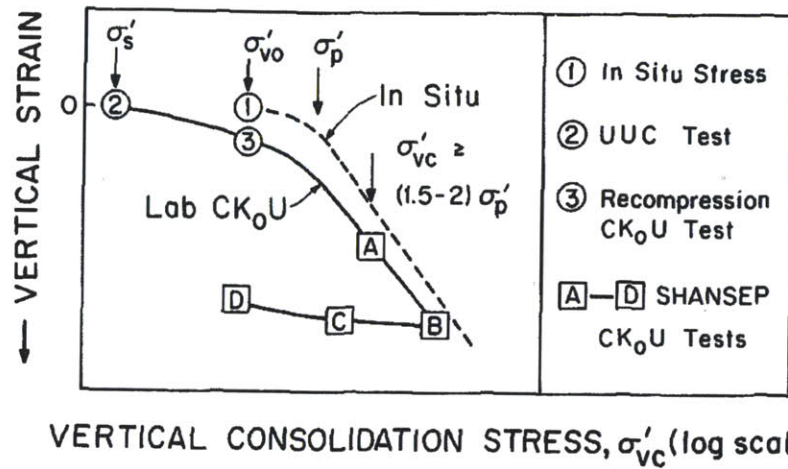


Figure 2.8 Consolidation procedure for CK₀U testing (Ladd, 1991)

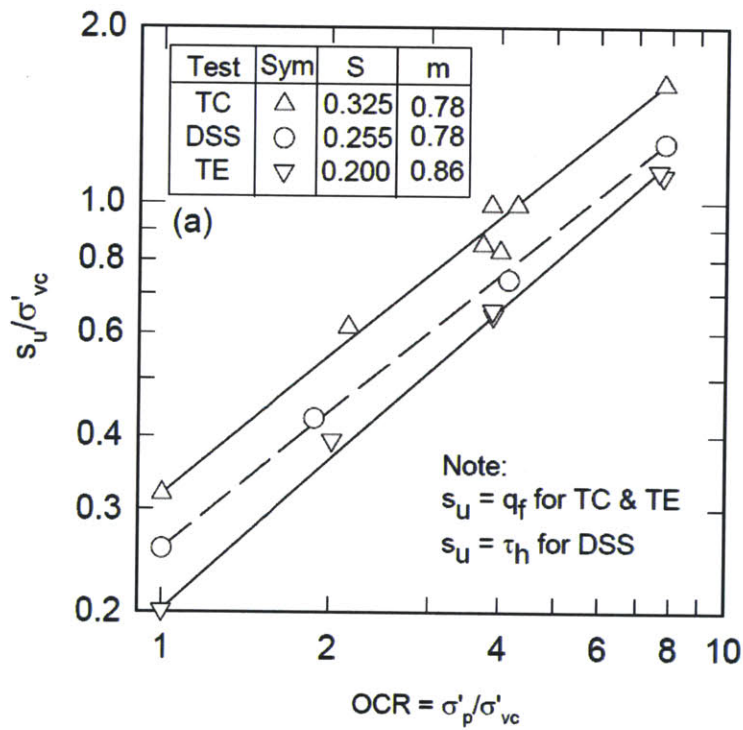


Figure 2.9 Normalized undrained shear strength versus OCR for AGS Plastic Marine Clay via SHANSEP (Koutsoftas & Ladd, 1985)

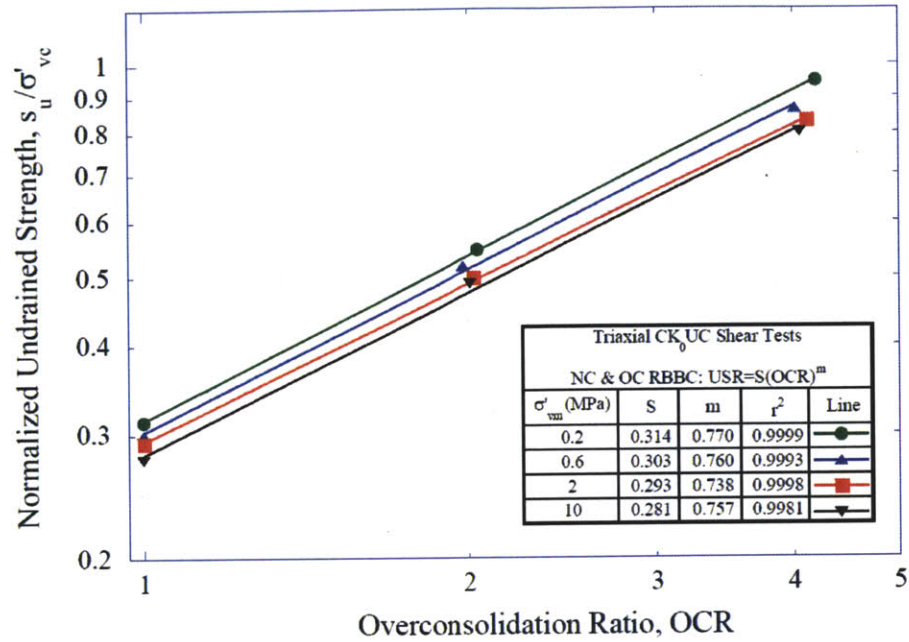


Figure 2.10 Normalized undrained shear strength versus OCR for RBBC from selected CK0UC triaxial tests indicating the effect of stress level (Abdulhadi, 2009)

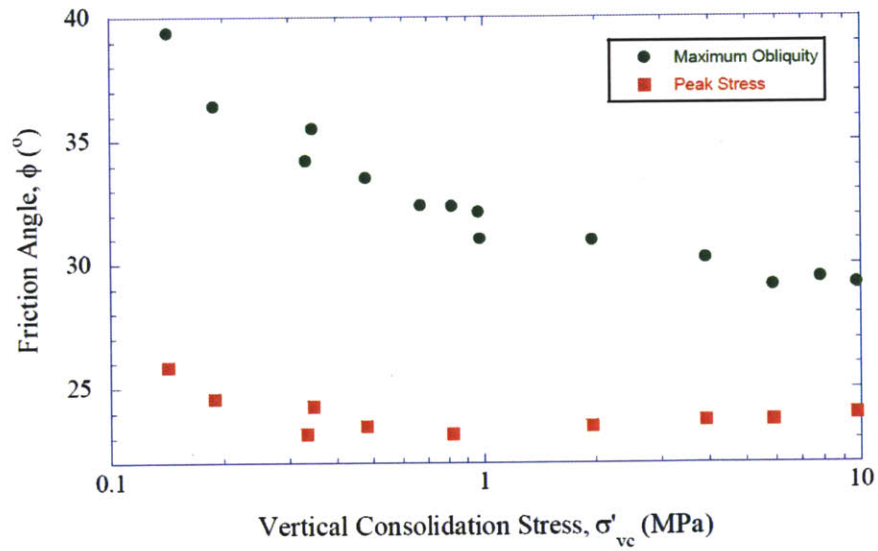


Figure 2.11 Friction angle at peak and maximum obliquity versus stress level for NC RBBC from CK0UC triaxial tests (Abdulhadi, 2009)

3 MATERIALS USED IN TESTING PROGRAM

3.1 INTRODUCTION

During the course of this research, a number of different soils were tested. These included Boston Blue Clay (BBC), London Clay, several variations of Gulf of Mexico Clay and pure sodium montmorillonite. Several derivatives of BBC were used and these will be described later in this Chapter. Perhaps the most important distinction to be made in terms of the soils used is the fact that BBC has been altered in several different ways for this research, therefore each derivative has been given a different title and as such, will be treated as a different soil.

3.2 BOSTON BLUE CLAY

3.2.1 RESEDIMENTED BOSTON BLUE CLAY

Boston Blue Clay (BBC) is an illitic glacio-marine clay of low plasticity (CL) and medium sensitivity. BBC was deposited in the Boston basin about 12,000 to 14,000 years ago following the Wisconsin glacial period (Kenney, 1964). Natural BBC is present throughout the Boston area and varies in thickness from 20 – 40 m. While the depositional history and general characteristics of BBC are similar throughout the Boston area, some variability can be expected in soil from different locations, and thus in the resedimented BBC specimens derived from these natural sources. The properties of the clay depends on several factors, for example, the particle size distribution, the chemistry of the pore fluid and the mineralogy.

The material used in this research is from Series IV which was obtained in 1992 from the base of an excavation for MIT's Biology Building (Building #68). Approximately 2,500 kg of soil was obtained at a depth of about 12 m. This soil had an OCR which varied between 1.3 & 4.3 (Berman, 1993). The processing of this soil is described in Cauble (1996).

Resedimentation of BBC at MIT has produced some 70 recorded batches of testing material for a variety of projects. Table 3-1 summarizes the index properties reported for these

batches used in research since 1961 (Series I, II and III). Table 3-2 summarizes research which ha

was performed on RBBC at MIT since the 1960's.

3.2.2 BATCH DATA

The properties of BBC vary over the Boston area even though the basic mineralogy of the clay is thought to be the same. Therefore, each time new material is obtained for resedimentation, it is necessary to perform several index and engineering tests to verify that the soil is reasonably similar to all prior source material. Another purpose of this testing is to obtain basic engineering properties which are needed to characterize any cohesive soil. Table 3-3 lists the index data for Series IV RBBC used in this research. In general, the index testing performed is in agreement with previous determinations. The specific gravity, clay fraction and salinity of the soil are all in agreement with previous researchers, however, in all determinations of the Atterberg limits for this research, they were found to be consistently higher than previous values.

Figure 3.1 and Figure 3.2 shows the grain size distribution for Series IV BBC powder obtained from the hydrometer test after Abdulhadi (2009) and Force (1998) respectively. In both datasets, the soil has a fine fraction greater than 98 % passing the US #200. Abdulhadi determined the clay fraction to be approximately 56 % while Force found it to be around 58 %. In general, both distribution curves are in good agreement.

The Atterberg limits were determined a total of 5 times for this research; 3 times on natural RBBC and twice on leached RBBC. The liquid limit for all soils tested was determined using the fall cone in accordance with BS 1377-3. The plastic limit for all soils was determined in accordance with ASTM D4318. The Atterberg limits tests were conducted with distilled water, 1 g/l and 256 g/l pore fluid in order to ascertain whether the salinity would affect the plastic or liquid limit. It was found that, despite the vast change in pore fluid salinity, the limit values were not noticeably altered once allowance was made for the salt content. When allowing for the salt content, it was assumed that salt has a specific gravity of 2.3 and that the mass of water evaporated after oven drying is proportional to the mass of salt which remains –for instance, if 10 g of water evaporates after oven drying in a 256 g/l determination, it is assumed

that 2.56 g of salt remains as a solid in the soil. This mass of salt would then be converted to a volume which would then be added to the volume of water. An example of this calculation is shown in Appendix B. A plot of the plasticity chart showing the results of these five determinations can be seen in Figure 3.3. The limits recorded are slightly higher than those observed by previous researchers. Figure 3.4 shows results obtained by Abdulhadi (2009) for RBBC Series IV for comparison.

Measurement of the specific gravity G_s for series IV RBBC yielded an average value of 2.78 which is the same value obtained by Zriek (1994) and very similar to that obtained by Sinfield (1994). The specific gravity value for Boston Blue Clay which was used in this research was 2.78.

The natural salt content of RBBC Series IV was measured as described in Chapter 4 and was found to be 10.7 grams of salt (NaCl) per liter (g/l) of pore fluid.

The test for organic content by loss on ignition was performed in accordance with ASTM D2974 and was found to be 1.37 % after constant mass was achieved. This is lower than the value obtained by Cauble (1996).

3.2.3 CONSOLIDATION BEHAVIOR DURING RESEDIMENTATION

When resedimenting BBC Series IV, the end of primary consolidation varies with the drainage length of the soil in question. Given that drainage is provided at the top and bottom of the consolidometer, the maximum drainage length will be half the axial length of the soil column in question. In general, the time to reach end of primary is longer for the first few increments while the soil still resembles a slurry. As the stress level increases and therefore the water content of the soil decreases, the time to reach end of primary also drops. The axial displacement also reduces as the stress increases and these observations are true for RBBC at all salinities. Figure 3.6 and Figure 3.7 show these changes for a 64 g/l RBBC soil. These figures show that the time to reach end of primary varies from around 24 hours when the soil is still a slurry to just over 3 hours for the final increment. The decrease in time is due to both a reduction in the drainage height and the coefficient of consolidation c_v .

3.2.4 ENGINEERING BEHAVIOR OF RBBC

This section presents a brief summary of the most important engineering properties of RBBC available from previous research studies. The purpose of this section is to provide a clear picture into the behavior of RBBC derived from previous laboratory testing. Only in previous years has the consolidation behavior up to 10,000 kPa been investigated by Abdulhadi (2009) and Casey (2011). Before this, previous studies were confined to relatively low stresses up to 1,000 kPa due to mechanical limitations of the testing equipment. This section will therefore focus on the results from these two researchers for one-dimensional compression behavior, and from other sources for lower stress triaxial testing.

3.2.4.1 ONE DIMENSIONAL CONSOLIDATION BEHAVIOR

Figure 3.8 from Abdulhadi (2009) shows compression curves for RBBC Series IV for σ'_{ac} up to 10,000 kPa in conventional e - $\log\sigma'_{ac}$ space. These curves also demonstrate the excellent repeatability which is available with RBBC when meticulous testing methods are employed. The curves in this figure were obtained from the K_0 consolidation phase of triaxial testing. The K_0 algorithm used for the consolidation stage of triaxial testing at the MIT Geotechnical Engineering Laboratory works by continually adjusting the cell pressure in order to ensure zero radial strain as the specimen is being strained axially at a constant rate. The compression curves are characterized by a well-defined yield close to the batch preconsolidation pressure where the soil changes from overconsolidated to normally consolidated. In the unloading portion, the slope of the curve is much steeper and becomes even steeper with increasing OCR (reduction in axial effective stress).

The virgin consolidation line for RBBC is approximately linear with a somewhat constant slope in the range of stress 200 – 10,000 kPa. At higher stresses the curve displays more of an S-shape. The value of CR at low pressures is consistent with prior studies on RBBC, e.g. Ahmed (1990), Sheahan (1991), Seah (1990) and Santagata (1994). The value of CR reported by Abdulhadi at higher stresses is lower than any value previously quoted. The swelling ratio which is defined as the average slope of the swelling line in ϵ_a - $\log\sigma'_{ac}$ space, is approximately an order of magnitude smaller than the CR value. As OCR increases from 1 to 4, the SR increases from 0.012 to 0.015.

Figure 3.9 and Figure 3.10 show the variation in coefficient of consolidation reported by two separate researchers. Although Force (1998) did not go to the same high stress levels as Abdulhadi (2009), at low axial effective stresses the data compare well. The results in Figure 3.9 and Figure 3.10 were interpreted using the standard linear theory after Wissa et al., (1971). The value of c_v was computed from $c_v = k_v/m_v\gamma_w$ where k_v and m_v are directly measured from test data. In general, c_v decreases with an increase in axial effective stress in the recompression or overconsolidated range and then drops abruptly at σ'_p . In the normally consolidated region, c_v tends to increase with an increase in axial consolidation stress. Both datasets show c_v increasing from a minimum of about $c_v = 20 \times 10^{-4}$ cm²/sec at $\sigma'_{ac} = 200$ kPa (2 ksc) to $c_v = 40 \times 10^{-4}$ cm²/sec at $\sigma'_{ac} = 900$ kPa (9 ksc).

Figure 3.11 and Figure 3.12 show the variation in axial hydraulic conductivity with void ratio. The axial hydraulic conductivity decreases with a decrease in void ratio which represents an increase in axial effective stress. Both researchers used Series IV RBBC and the testing was performed more than a decade apart. The hydraulic conductivity curves presented by Force are linear whereas the curves shown by Abdulhadi display a distinct change slope at a void ratio of about 0.80. The reason these kinks are not present in Forces data is because she did not achieve high enough stresses to realize such void ratios. There is, however, good agreement between the data in the overlay range. The axial hydraulic conductivity reduces from approximately $k_v = 2 \times 10^{-7}$ cm/sec at $\sigma'_{ac} = 200$ kPa (2 ksc) to approximately 3×10^{-8} cm/sec at $\sigma'_{ac} = 1,000$ kPa.

The values of the coefficient of earth pressure at rest (K_0) can be obtained from feedback-controlled 1-D consolidation in the triaxial shear cell. Figure 3.13 and Figure 3.14 both show the typical trend of K_0 with axial effective stress during consolidation from two previous researchers. These results show that the K_0 value decreases during re-loading to the preconsolidation pressure σ'_p and then increases slightly. Once the soil is consolidated well into the virgin compression region, $K_0 = K_{0nc}$ remains fairly stable but there is a definite trend whereby the value increases with an increase in stress level.

3.2.4.2 UNDRAINED SHEAR BEHAVIOR IN TRIAXIAL COMPRESSION

The undrained shear behavior of RBBC has been well studied by researchers at MIT (refer to Table 3-2 Overview of previous studies performed using RBBC). The following

Sections provide a brief overview into the general undrained shear behavior of the material in one dimensional consolidated-undrained triaxial compression (CK_0UC). The results are presented in normalized form as this provides a very convenient format for presenting and evaluating clay behavioral characteristics. The background into normalizing data has been covered in Chapter 2. The following Figures will demonstrate the behavior of NC RBBC during a CK_0UC test and all plots are normalized. The results from these Figures have been verified by many researchers such as Santagata (1998), Abdulhadi (2009) and Casey (2011).

Figure 3.15 shows the normalized shear stress-strain behavior for both normally consolidated and overconsolidated RBBC (Series III) after Santagata (1994). It can be seen that for a normally consolidated soil, there is a distinct peak corresponding to soil failure at very small strains. A axial strain rate of 0.50 %/hr is used to produce the results in Figure 3.15 which is the same rate that was used in this research.

The corresponding normalized effective stress paths using MIT stress space are shown in Figure 3.16. The Figure shows the change in pore pressure development during a test. There is little pore pressure generation up to a yield point, followed by much greater development thereafter. Peak shear conditions coincide with a yield condition but the peak point moves further down the stress path as the consolidation stress increases.

The excess pore pressure and shear induced pore pressures which are generated during a test are shown in Figure 3.17 and Figure 3.18. The plots show that for a normally consolidated soil, both the excess pore pressures and shear induced pore pressures continually rise from a zero value with an increase in axial strain. This indicates fully contractive behavior for an $OCR = 1$ soil.

Figure 3.19 shows curves of the undrained secant Young's modulus versus axial strain for RBBC at various OCR values. As the measurements were performed using external LVDT's, the estimates are considered reliable only above 0.01 % axial strain. This figure shows that the soil exhibits strong non-linearity from the very beginning of shear and that the decrease in stiffness is particularly marked once the soil reaches failure due to the large amount of post peak strain softening.

Because the purpose of this research is aimed at investigating the effect of pore fluid salinity on the mechanical behavior of soil, a simple sedimentation test was performed on all soils in the testing program whereby a specific quantity of soil was placed in a test tube with pore fluids of different salinities. This was done to see how the soil would behave in different pore fluid environments and to give an indication as to where the greatest effects lay in terms of behavioral changes. Several methods of agitating the soil in the tubes were attempted but the best results in terms of reaction to variations in salinity were produced when the tubes were mixed in an ultrasonic bath. This method was employed for all subsequent sedimentation tests. The results from once such test for natural BBC Series IV can be seen in Figure 3.20. The test shows that for a wide range of pore fluid salinities, natural BBC Series IV displays little if any visible change in behavior. The same amount of soil has been used in each tube (5 g) and the soil sediments to almost the same height for all salinities. This simple test was also performed on leached BBC and can be seen in Figure 3.21. In this test, an additional tube containing 0 g/l (distilled water) was used. Again, 5 g of soil was used in all tubes but this time the sedimentation height is roughly twice that which was observed for the natural BBC Series IV soil. With an increase in pore fluid salinity, a very slight increase in sedimentation height is observed indicating a larger void ratio with an increasing salt content. An interesting observation is that a portion of the fine fraction in the distilled water tube has not settled out and continues to remain in suspension occupying all the free water space in the tube. The coarse element of the leached BBC can be seen at the bottom of the 0 g/l tube. It is believed that this fine fraction which has not settled, was produced when the soil was leached, which in turn deflocculated the soil. With the addition of just 1 g of salt (per liter) to the pore fluid, the effect is no longer visible.

3.2.5 TERMINOLOGY OF BBC SERIES IV DERIVATIVES USED

Several derivatives of RBBC were used for testing purposes. The RBBC Series IV was altered in numerous ways in order to derive changes in behavior. These alterations involved removing the natural salt from RBBC Series IV powder in an attempt to deflocculate the natural fabric, and also adding a dispersing chemical called sodium hexametaphosphate to a quantity of RBBC Series IV. These alteration processes are described in Chapter 4. Because of this work, it is necessary to establish terminology relating to each soil for clarity.

The BBC powder contained in BBC Series IV will be called natural RBBC Series IV. It still contains all the same elements as a powder, as it would if it were buried in the ground. The only processing of this soil has been to air dry and grind it to a powder passing a US#100 sieve.

It was thought advantageous to remove as much of the natural salt from a quantity of BBC Series IV powder to determine if the mechanical behavior would be altered. This was performed by washing about 3.5 kg (dry mass) of soil with distilled water in a centrifuge. Each run of the centrifuge could process 120 g of soil. It was therefore a laborious and time consuming activity. After the soil was washed once, it was air dried and ground to a powder in order to pass a US#100 sieve and then processed through the centrifuge a second time. After the second run, the soil was once again air dried and ground to pass a US#100 sieve. The resulting powder was then used for resedimentation. This soil will be termed leached RBBC.

Following on from the idea that leaching BBC Series IV powder would disperse the fabric and structure of the soil, it was decided to completely obliterate any residual flocs for 300g of BBC Series IV powder using sodium hexametaphosphate. This chemical is used in Geotechnical laboratory testing as a dispersing agent when performing the particle size distribution test by sedimentation. It is an established fact that the chemical completely disperses all existing soil fabric and structure thereby reducing a soil to its rudimentary individual elements. Because this chemical is detrimental to the behavior of all soils, it is to be used with extreme caution in a Geotechnical laboratory. Particular care must be taken when testing a soil which contains the chemical in its pore fluid, such was the case with this soil because of the process used to create it. Because the name of the chemical is so long, the soil will be referred to as sodium hex RBBC (sodium hexametaphosphate BBC).

3.2.6 KILLIAN COURT IN-SITU BBC

In June of 2010, samples of in-situ BBC were recovered from the MIT campus under the Killian Court area. Figure 3.22 and Figure 3.23 identify this location relative to the MIT main building. The samples were recovered in 7.2 cm (internal diameter) brass Shelby tubes. These tubes were subsequently x-rayed by Dr. John Germaine at MIT prior to testing in order to determine if any impurities were present and also to ensure uniform soil specimens are obtained once the tubes are cut. A total of two tubes were used for this research and were identified as

B10-T2PA S3 (51 - 53 ft deep) and B10-T2PA S2 (48 – 50 ft deep). A log of the borehole which these samples were obtained from can be seen in Figure 3.24. This material will be referred to as in-situ Killian Court BBC.

3.2.7 SCANNING ELECTRON MICROSCOPE IMAGES

Scanning Electron Microscope (SEM) images were taken of natural RBBC Series IV at different salinities and at different stress levels. The images presented are done with thanks to the Bureau of Economic Geology at the University of Texas at Austin. All images were taken on oven dried specimens in the vertical plane – for clarity, this orientation is shown in Figure 3.25.

Figure 3.26 presents two images of natural RBBC Series IV at 4 g/l and at a maximum confining stress of 100 kPa. The stress represents the soil after resedimentation in a consolidometer which has been unloaded to an OCR of 4. Figure 3.27 shows natural RBBC Series IV at the same stress level which was resedimented with 256 g/l pore fluid. At first glance, it is not apparent what differences, if any exist between the structure or fabric of both specimens. For this reason, a side by side analysis is conducted in Figure 3.28. In this figure, the 4 g/l images are placed on the extreme left and extreme right of the page and are overlain by a 256 g/l image. The images are demarked by a black border on the 256 g/l image. It can be seen from these images that both fabrics are very similar despite the large difference in pore fluid salinity. It is hypothesized that the fabric which is being observed at both salinities is not a function of their resedimentation pore fluid salinity, but rather as a function of the remaining flocs in the soil after processing. The fabric of both salinities is therefore said to be the same. This hypothesis will be further developed in Chapter 5.

Figure 3.29 shows two images of leached RBBC at a pore fluid salinity of 1 g/l and at a stress of 100 kPa. Figure 3.30 shows two images of the same salinity soil but this time at a stress of 1,000 kPa. Despite the order of magnitude change in stress level, very little difference can be seen in the fabric of the soil. Given that both sets of images are at different stress levels, the keen reader would expect a denser packing of particles (given the associated reduction in void ratio), as well as more particle orientation. Upon visual examination of both sets of images, this is not the case. Figure 3.31 shows a side-by-side analysis of both sets of images. 1 g/l images at 100 kPa are placed on the extreme left and right and both are overlain by another image; 1 g/l at a

stress level of 1,000 kPa. Without demarcation by the central image border, distinction between all three photos would be very difficult. It is further hypothesized that despite the difference in stress of one order of magnitude between both image sets, very little if any rearrangement of particles has occurred. It is proposed that the flocs which are visible in both image sets are accepting stress and deforming very little – similar to a steel truss and like a steel truss, failure will occur at some load whereby particles will start rearranging. This stress level for failure to occur at has been identified in Chapter 5.

Images of BBC which has been dispersed with sodium hexametaphosphate and subsequently resedimented are shown at different stress levels in Figure 3.32 & Figure 3.33. Both of these Figures contain images at two different magnifications so a comparison is drawn between both stress levels in Figure 3.34 & Figure 3.35 at the same magnification. It is apparent that there is now more of a reduction in void space between different stress levels, however, images displaying such difference in stress level (100 vs. 10,000 kPa) have not been compared up to now. Further analysis is performed on images of sodium hex BBC and natural RBBC series IV in Figure 3.36. It is now evident that dispersion of the fabric has occurred as intended and that a much denser (lower void ratio) soil is produced at the same stress level in the sodium hex BBC.

3.3 LONDON CLAY

3.3.1 INTRODUCTION

During this research, access was obtained to a batch of London Clay via a Civil Engineering contractor whom the author previously worked with. Ward & Burke Construction Ltd. were constructing a 1.20 m internal diameter open face tunnel in the Hendon area of London, England during the summer of 2011. Approximately 300 kg of the material they excavated during this work was shipped to the MIT Geotechnical laboratory for research purposes. Because of the methods used to excavate this soil, it is not possible to test intact samples and therefore the soil received at MIT was processed and used for resedimentation. This is the first instance of London Clay being resedimented and tested at MIT. London Clay in a similar fashion to Boston Blue Clay is a heavily researched soil insofar as both soil deposits are home to leading Geotechnical research institutions. For this reason a large bank of data exists on the properties of the soil. London Clay is, however, notorious for its variability from location to

location. Although it is often treated as a uniform material, significant variations in strength, stiffness and consolidation behavior within the London Clay formation are directly linked to a variable depositional history (Pantelidou & Simpson, 2007). It is fortunate that an extensive and relatively thorough site investigation program was undertaken for the project from which the soil was received. Laboratory testing of intact samples was also performed. The results from this report will be referenced as well as the already existing database of information on London Clay. Figure 3.37, Figure 3.38 and Figure 3.39 identify the location of the project site. The site is located off Rosemead and Cool Oak Lane, West Hendon, NW9 7QS. Figure 3.39 give GPS coordinates which will pinpoint the site exactly.

3.3.2 LONDON CLAY CHARACTERISTICS

London Clay is a stiff heavily overconsolidated marine clay, deposited across the London and Hampshire Basins of South-East England. It was deposited in the Eocene period around 30 million years ago. The soil is the principal geological formation in the London district and is of considerable engineering importance to the area. London Clay provides the stratum on which many large buildings and bridges are founded, and through which a great deal of the local underground railways are driven. The commonly referenced point for this sedimentary deposit is its base, the material was deposited from the base upwards, with erosion, re-deposition and other events continually changing the top of the formation. In some localities the full thickness of the bed is present and is found to be between 100 and 145 m thick. Under London itself, the formation has undergone considerable erosion and is now only between 28 & 43 m thick. It belongs to a type known as “stiff fissured” clay and is slightly laminated. Normally it has a dark bluish-grey color but in the surface layers, oxidation of ferrous to ferric salts changes its color from blue to brown. In some regions, this zone of oxidation has been proved to a depth of 13 m (Cooling & Skempton, 1942). The London Clay retrieved from Hendon was of the oxidized type and a photo showing the clay as extracted from the ground can be seen in Figure 3.40.

According to King (1981), five sedimentary cycles have been recognized within the London Clay formation representing an initial marine transgression followed by a gradual reduction in sea level. At the boundaries between subdivisions, there are abrupt changes in the coarse-grained content and mineralogy. A typical cycle starts with a bed containing scattered

glauconitic grains and, in some cases, rounded flint pebbles. This is followed by a sequence of clays which become progressively more silty and sandy upwards (Pantelidou & Simpson, 2007). A stratigraphic diagram of what has been described is shown in Figure 3.41. The soil from the Hendon project was excavated at a depth below ground surface of approximately 6 m. Although the boreholes from this particular development did not reach bedrock, in a borehole obtained from the British Geological Survey website which was drilled close by, chalk was encountered at a depth of 63.1 m below ground surface. Assuming the ground level for this borehole is at a similar level to the ground level at the tunnel location, this places the soil received to MIT in Division C from Figure 3.41.

While handling the London Clay in the laboratory, pockets of “clear” sand, pockets of white sandy areas as well as blue veins were visible to the naked eye. Upon further investigation, it was determined that these inclusions were quartz¹ while the blue veiny areas were believed to be flow channels for ground water through the soil. Figure 3.42, Figure 3.43, Figure 3.44 and Figure 3.45 show the pictures of the London Clay in its natural state as received to the MIT Geotechnical Laboratory. The mineralogy of the in-tact soil is shown in Figure 3.46. These data are not available for the project location at Hendon. The figure shows that London Clay is composed mostly of quartz and has a large clay fraction. The specific surface area of the London Clay closest to the Hendon location is roughly 175 m²/g of soil. The particle size distribution shown in Figure 3.47 is from site investigation (SI) information from the project and shows that 4 % of the soil is above sand size, with the largest particle recorded being 3.35 mm. The coefficient of curvature and coefficient of uniformity are not available because the D₁₀ and D₃₀ particle sizes are not available. The site investigation curve shows that the soil has a 56 % clay fraction and this agrees well with a particle size distribution by sedimentation performed at MIT by Brendan Casey which is shown in figure Figure 3.48. Particle size analysis performed at MIT does not show the sand fraction which was identified in the SI information because the soil used at MIT had been ground prior to testing.

The Atterberg limits for London Clay were determined several times for the site investigation and are shown in Figure 3.49. A plot of the Atterberg limits determined at the MIT Geotechnical laboratory is shown in Figure 3.50. The liquid limit (w_l) was found to be 73.8 % while the plastic limit (w_p) is 30.5 %. This gives a plasticity index of 43.3 %. The soil is classed

as a clay of high plasticity (CH) using the Unified Soil Classification System (USCS). The soil plots just above the A line as can be seen in Figure 3.49. As the soil was shipped to MIT in sealed durable plastic bags, a water content determination was performed. The natural water content was found to be 31.6 % and although it is acknowledged that this water content may differ from the natural water content in the, it is in fact slightly higher than water content determinations shown in Figure 3.52 performed on freshly excavated soil. Upon further examination of the Atterberg limit data from several locations in London which are shown in Figure 3.51, it can be seen that the soil received to the MIT Geotechnical laboratory is very representative of the mechanical behavior exhibited by London Clay. The water content is just above the plastic limit for the soil and gives a liquidity index (I_L) of 0.03. The activity of the soil (A) is defined by Skempton (1953) as the plasticity index divided by the clay fraction (less than 2 μm). The activity for London Clay is therefore $A = 0.77$. Clays with an activity of $0.75 < A < 1.25$ are classified as normal. $A < 0.75$ are inactive clays and $A > 1.25$ are active clays. It is believed that the activity of a soil is only at best, a crude estimate of likeliness of a soil to prove troublesome. It is more advantageous to determine the mineralogy of the clay fraction to determine how a soil is likely to behave. Although a detailed mineralogy of the London Clay from Hendon is not available, Figure 3.53 presents the mineralogy of London Clay from multiple locations throughout the London Basin. In general, the dominant mineral is smectite followed by an almost equal portion of illite and kaolinite with chlorite making up the smallest fraction.

The specific gravity, G_s , of the soil was found to have an average value of 2.80 from three determinations performed at MIT. This value was used in all phase relation calculations for London Clay. This value is higher than those obtained in the literature from previous studies on London Clay such as Cooling & Skempton (1942), and Ward (1959).

The method in which the natural salt content of the soil is measured will be described in Chapter 4 and was found to be 12 grams of salt (NaCl) per liter (g/l) of pore fluid at a water content of 31 %.

The test for organic content by combustion was performed in accordance with ASTM D2974 and was found to be 4.12 %. This is much lower than the loss on ignition tests performed for the SI document. For the SI, the loss on ignition was found to be 7.9 – 9.2 %, however, after

examining the appropriate British Standard (BS1377-3) which the SI tests were performed in accordance with, it was found that the soil is to be initially dried at a temperature of 50°C as opposed to 105°C for the ASTM standard. For a highly plastic soil such as London Clay, there may still be moisture present in the fabric of the soil after oven drying to this temperature. It is believed that remaining moisture has produced the higher numbers quoted in the SI document.

The effect of varying the pore fluid salinity for London Clay can be seen in Figure 3.54. In this determination, the 128 g/l tube has been replaced with a 0 g/l (distilled water) tube. This distilled water was used in an attempt to see the full potential of any double layer growth in the natural soil. Unlike what was observed for the natural BBC Series IV, there is now a clear difference in sedimentation heights dependent on the pore fluid salinity present. The 16 g/l tube produces the largest sedimentation height of all salinities which is counter intuitive. One would expect to see a higher sedimentation height as the salinity decreases. This is not so in the case of the London Clay under scrutiny. The test was repeated several times changing out the soil and pore fluid each time in order to eliminate the possibility of experimental error, and the same results were obtained each time. It is believed that this is the actual response of the soil to changes in salinity. If we examine the tubes on either side of the 16 g/l tube, it can be seen there is a trend whereby as you move away from this salinity in either direction, a drop in sedimentation height is observed. This is attributed to floc interaction. The distilled water tube does not harbor full double layer development for this soil which indicates that with an increasing ionic supply (up to a certain level), double layer development is promoted. It is believed that processing some leached London Clay would indicate if this trend can be altered, thereby indicating that flocs are indeed responsible for the observed behavior.

Previous published work on London Clay in the Hendon area include Marsland (1974), Marsland (1977), Skempton (1959) and Tchalenko (1968).

3.3.2.1 CONSOLIDATION BEHAVIOR DURING RESEDIMENTATION

In a similar fashion to RBBC, the time to reach end of primary takes longer for the first few increments while the soil still resembles a slurry. As the stress level increases and therefore the water content of the soil decreases, the time to reach end of primary drops. In contrast to RBBC, the axial displacement increases with increasing stress level as can be seen from Figure

3.55 and Figure 3.56. These figures show that the time to reach end of primary varies from around 38 hours when the soil is still a slurry to just over 23 hours for the final increment. It is worth reiterating that these figures depend on the drainage length. The increase in deformation with increase in stress level would suggest that there is not yet full particle to particle contact at the given stress and that a strong double layer or some other chemical effect is partially supporting the applied load. The fact that this is accompanied by a reduction in time to EOP also suggests that less pore water is available to initially support the applied load. A theory can be extracted from these data that even though particle to particle contact is not present, the double layer of the soil is occupying an increasing volume of the void area thereby reducing the pore fluid available to support load. It can therefore be assumed that the bound water in the double layer is not contributing to the flow of water in the pore space. This assumption is in line with what is stated in Robinson & Allam (1998).

3.3.3 ENGINEERING BEHAVIOR OF RESEDIMENTED LONDON CLAY

This section provides a brief summary of previous work on both intact and resedimented London Clay. Because the research in this thesis examines the one dimensional behavior of resedimented London Clay, reference to previous work will only include oedometer test results. No instances of London Clay being tested via the CRS device were found during the literature review.

3.3.3.1 ONE DIMENSIONAL CONSOLIDATION BEHAVIOR

The one dimensional consolidation behavior of London Clay has been studied by various researchers in the past (Ward, 1959; Cooling & Skempton, 1942; Gasparre, 2005). All previous one dimensional testing has been performed in an oedometer (with the exception of one dimensional consolidation performed during triaxial testing). It is a typical trait of stiff intact specimens tested in the oedometer that the preconsolidation pressure is hard to define. This is because the slope of the reload and VCL are more similar than what is observed in other soils. This leads to a more gradual change from overconsolidated to normally consolidated behavior. This transition can span a large axial stress range despite extreme care being taken in sample recovery. Such examples of this are shown in Figure 3.57, Figure 3.58 and Figure 3.59. Two of these Figures are from the SI document from the Hendon development and show that the

preconsolidation pressures for both tests will fall in the 200 – 500 kPa range. Both specimens were recovered less than 10 m below ground level and are taken from an area which has undergone extensive weathering and erosion. The soil tested in Figure 3.59 is from the Heathrow Airport location where it is known that a greater thickness of the natural London Clay formation still exists. This means the soil recovered will invariably have a larger preconsolidation pressure given that it would have been closer to the applied load during glaciation of the area. This is reflected in the preconsolidation pressure seen for the test – approximately 3,000 kPa. The void ratios at a given stress are relatively small which is understandable given the millions of years of secondary compression which the soil has undergone.

Figure 3.60 shows compression data from a resedimented London Clay specimen for research performed at Imperial College in London. For tests performed on resedimented material, there is a relatively large scatter in void ratio at a given stress level and there is no apparent batch preconsolidation pressure. The results from Figure 3.60 give larger void ratios at a given stress than in-tact material. Reasons for these variations are not immediately apparent, however, the cause could be attributed to different soil mineralogy, different resedimentation techniques or different testing procedures.

3.4 GULF OF MEXICO SOIL

3.4.1 GULF OF MEXICO – URSA

Resedimented Gulf of Mexico - Ursa (RGOM – Ursa) soil was recovered during the Integrated Ocean Drilling Program (IODP) Expedition Leg 308. This expedition involved drilling three cores in the Ursa Basin. The Ursa Basin is located approximately 100 miles south-east of New Orleans. It is located on a continental slope. A location map of the Ursa Basin is shown in Figure 3.62 while Figure 3.64 shows a more detailed map of the area where the borings were performed. The soil used for this research was obtained from core U1322 which is identified in the Figure. The main reasoning behind the exploration were to analyze slope stability in the region which could trigger tsunamis and also to explore energy resources in the area.

Atterberg limits were performed in the MIT Geotechnical Laboratory by Brendan Casey. The liquid limit (w_l) was found to be 51.7 % and the plastic limit (w_p) 23.7 % - the corresponding plasticity index is therefore 28 %. The location where GOM-Ursa soil plots on the plasticity chart is shown in Figure 3.64. The soil is classified as a clay of high plasticity (CH). Figure 3.65 shows a particle size distribution curve for GOM-Ursa soil performed in the MIT Geotechnical laboratory. It can be seen that the soil has a clay content of approximately 43 %. The activity of GOM-Ursa is 0.65 rating it as an inactive clay. Compression data for RGOM-Ursa were presented by Mazzei, (2007) but are not referenced here because it is believed they produced abnormally high void ratios at a given stress value. A specific gravity (G_s) value of 2.667 was used in the phase relation calculations for GOM-Ursa soil.

3.5 SODIUM MONTMORILLONITE

Montmorillonite is an ideal medium for the theoretical investigation of how clay minerals react to a change in salinity of the pore fluid. This fact can be seen in Figure 3.66. This Figure demonstrates the effect of the pore fluid salinity on double layer growth. At low salinities such as 1 g/l, the ionic concentration in the pore fluid is low and therefore a large double layer develops around the clay particle; there is very little if any particle to particle contact in the low salinity tubes. With an increase in salt content, a corresponding reduction in sedimentation height is seen. This demonstrates that double layer growth is reducing as the salinity increases. In high salinity water, double layer growth is inhibited and the soil sediments to a much lower height given that there is more particle to particle contact. At a salinity of 64 g/l, the double layer effect has been eradicated and all salinities higher than this produce the same sedimentation heights regardless of salt concentration. For this research, montmorillonite was resedimented to two pore fluid salinities. These were 1 & 256 g/l. It is now acknowledged that the same results would most likely have been obtained from a 64 g/l batch as a 256 g/l batch. Large differences in water content were required for resedimentation at the two extremes. 1 g/l sodium montmorillonite required a water content of 1,050 % while the 256 g/l soil required 100 % water content. This represents more than an order of magnitude difference in required pore fluid based on how much the double layer is allowed to develop.

3.5.1 ENGINEERING BEHAVIOR OF SODIUM MONTMORILLONITE

This section gives a brief description of the established engineering characteristics of sodium montmorillonite. Several authors have previously studied the one dimensional behavior of several types of montmorillonite and other pure clay minerals, however, only results relevant to sodium montmorillonite tests will be shown here. The Atterberg limits were determined for this soil. Both the Casagrande Cup (ASTM D2487) and Fall Cone (BS 1377 - 3) method were used to determine the liquid limit. They gave a liquid limit of 634 % and 505 % respectively. This is consistent with the trend that a higher liquid limit is observed with the Casagrande Cup for soils of higher plasticity. Both methods typically agree well for soils with liquid limit values between 10 and 100 % (Germaine & Germaine, 2009). The plastic limit was found to be 76 %.

3.5.1.1 ONE DIMENSIONAL CONSOLIDATION BEHAVIOR

Figure 3.67 shows one dimensional compression data obtained from previous tests by Mesri & Olsen (1971_a). They show that for tests with very low electrolyte concentration (low salinity), the void ratios can be very large – up to 34 or 35. With an increase in electrolyte concentration, a corresponding decrease in void ratio at a given stress is seen. As expected, for an increase in axial consolidation stress, a decrease in void ratio is recorded. The compression curves for all electrolyte concentrations reach a common void ratio at a stress level of around 2,800 kPa (60,000 lb/ft²). The void ratio quoted at this stress is approximately 1.0. The curves display a definite yield point corresponding to a preconsolidation pressure which indicates that the soil remembers its stress history upon unloading. There is a change of slope in the normally consolidated range with an increase in stress, and this change is more pronounced for the lower electrolyte soils. Upon unloading of the soil, the higher electrolyte soils exhibit less of a recovery in void space than the lower electrolyte tests.

Previous authors who have studied the compression behavior of clay minerals and the effect of clay mineralogy on compression characteristics have noted that for clays such as montmorillonite, a decrease in c_v is recorded with an increase in stress level. This is contrary to kaolinite and illite whose c_v values rise with an increase in stress level. Since this research involved testing montmorillonite at two very different salinities, it is worth noting that the compressibility of clays is influenced by mechanical and physicochemical effects depending on

the type of pore fluid. The term mechanical is used to denote short range particle interactions controlled by the physical properties of the mineral particles namely their strength, flexibility and surface friction. The term physico-chemical signifies comparatively long-range interactions between particles, especially through double layer interaction. The virgin compressibility of the majority of minerals is primarily controlled by mechanical effects, whereas physicochemical effects control the compressibility of montmorillonite. In very high salinity environments, the double layer around the particles are suppressed and the compressibility of all clay minerals, including montmorillonite will be influenced mainly by mechanical effects (Olson & Mesri, 1970_a; Sridharan & Rao, 1976; Robinson and Allam, 1998).

As this research tests montmorillonite at salinities in which the double layer is no longer present, and where it is almost fully present (ref Figure 3.66), it is anticipated that a large difference will be observed in one dimensional compression behavior based on the differences of mechanical compression of the grains and physicochemical compression of the matrix. This was observed during the resedimentation process for montmorillonite at both salinities. High salinity montmorillonite reached the end of primary consolidation very quickly. This time was very comparable to most other soils being resedimented. Although the compression data obtained during resedimentation was poor because of sidewall friction associated with the porous stones, it was seen that the time to the end of primary consolidation did not change with an increase in stress level and was almost constant at between 10-15 hours for every increment with no trend versus stress level. This is further evidence that there was mechanical contact from a very low stress and that any deformation of the soil is down to mechanical bending and breaking of the particles. The low salinity montmorillonite provides a glaring contrast to this. The low salinity montmorillonite was resedimented on the 20th of December 2011, and end of primary consolidation was not recorded until the middle of May 2012. Even though the end of primary consolidation was not reached for each load increment, the next load was applied in an attempt to keep the consolidation process moving. No end of primary event was recorded for any load increment save the last one. A typical time displacement curve for one such increment can be seen in Figure 3.71 and Figure 3.72. Figure 3.71 which is plotted in square root of time space shows the line curving downward with increasing time (square root of time), this indicates a reduction in the c_v value and is consistent with the findings of Robinson & Allam (1998).

Although data from previous one dimensional testing on montmorillonite was obtained from oedometer testing, it is believed that the soil has not been tested in the Constant Rate of Strain device previously as no data could be found in the literature to suggest so.

3.5.2 SCANNING ELECTRON MICROSCOPE IMAGES

Scanning Electron Microscope (SEM) images were taken of sodium montmorillonite at a stress level of 200 kPa (after resedimentation). As with the BBC images presented in Section 3.2.7, all images were taken on oven dried specimens in the vertical plane.

Figure 3.73 presents images of sodium montmorillonite resedimented to a stress of 200 kPa with a pore fluid salinity of 256 g/l. At this pore fluid salinity it is thought that any double layer effect has been eradicated by the ionic concentration, therefore purely mechanical contact between soil grains dominate the soil behavior. Shrinkage cracking is evident in both images presented in Figure 3.73. Even though the soil has had any double layer effect killed off and can exist as a relatively stable soil while saturated (as a slurry), issues can still arise upon drying of the soil. Figure 3.74 & Figure 3.75 show comparisons between the fabric of sodium montmorillonite and RBBC at similar stress levels. Figure 3.74 presents a comparison with natural RBBC Series IV while Figure 3.75 compares sodium montmorillonite with sodium hex BBC. Both comparisons are made at the same magnification and despite what looks like a more open fabric in both BBC soils, they exist at a lower void ratio than the sodium montmorillonite.

Year	Researcher	Series	Source Batch	G _s	w _l	w _p	I _p	Clay Frac. <2 μ m (%)	Salt (g/l)	
1961	Bailey	Ia	MIT	2.77	30.0	17.5	12.5	40	2-3	
			1139		34.7	17.7	17.0		35	
1963	Jackson				36.2	19.5	16.7		16.7	
1964	Varallyay		S4		32.6	19.5	13.1	35	16.8	
			S5		33.3	20.4	12.9			
			S6		32.8	20.3	12.5			
1965	Ladd, R.S.	Ib		2.77	45	22	23		16	
1965	Preston		S1	2.77	45.6	23.4	22.2	35	24	
1966	Braathen		S2	2.77	45.4	23.1	22.3		22	
1967	Dickey				34.5	23.9	19.6			
1970	Kinner		100	2.78	43.5	19.6	23.9	50		
			150		43.5	19.6	23.9			
		200	38.1		17.8	20.3				
		300	39.7		21.6	18.1	52	8		
		400	39.4		21.3	18.1	52	10		
		800	41.5		19.5	22.0	48	16		
		900	41.2		18.7	22.5	54	16		
		1000	41.1		19.5	22.6	58	16		
		1100	42.0		20.6	21.4		16		
		1200	40.2		18.6	21.6	48	16		
		M101	40.7		19.6	21.1	52			
		M104	40.3		19.6	20.7				
		M107	41.3		19.6	21.7				
		M200	42.3		18.5	23.8	52			
M400	39.8	18.9	20.9	47						
1971	Ladd et al.	160	2.78	38.1	17.8	20.3		8		
		1300		42.1	22.1	20.0		16		
		1500		43.8	20.6	23.2		16		
1984	Bensari	II	105	2.75	47.6	23.3	24.3		16	
			111	2.75	47.1	24.9	22.2		16	
1985	O'Neill		105-112	2.78	41.3	22.1	19.2	52	16	
1989	Seah		III	200-207	2.78	45.2	21.7	23.5	58	16
1991	Sheahan			210,214, 216		45.6	21.4	24.2		
				217-218	2.78	37.0	21.3	15.7		
1994	Santagata	219-220			40.4	20.9	19.5			

Table 3-1 Index properties of RBBC from Series I - III (after Cauble, 1996)

Series	Year	Researcher	Topic	Testing Performed
I	1961	Bailey	Effect of salt concentration on undrained shear strength	-
	1963	Jackson	Thixotropy	Triaxial
	1964	Varallyay	Influence of stress system on undrained strength	Triaxial
	1965	Ladd	Use of pressure transducers to measure soil pressure	
	1965	Preston	Sample disturbance	Triaxial
	1966	Braathen	Disturbance effects on undrained strength	Triaxial
	1967	Dickey	Development of plane strain device	Plane strain device
	1967	Rixner	Behavior in plane strain at OCR 1, 2 & 4	Plane strain device
	1968	Bovee	Behavior in plane strain at OCR 1, 2 & 4	Plane strain device
	1970	Kinner	Behavior of strip footings during undrained loading	Model footing tests
II	1982	Germaine	Cross-anisotropic behavior at OCR 4	DSC, Triaxial
	1984	Bensari	Stress-strain and yielding behavior	Triaxial
	1985	O'Neill	Anisotropy of thixotropic clay	DSC, Triaxial
	1986	Fayad	Volumetric and undrained behavior	Triaxial
	1987	Malek	Behavior under cyclic loading	DSS
III	1988	Walbaum	Investigation of sample disturbance	DSS
	1988	Sheahan	Modification of computer controlled triaxial apparatus	Triaxial
	1989	DeGroot	Behavior in undrained multidirectional DSS at OCR 1	DSS
	1990	Ahmed	Normalized behavior in DSS	DSS
	1990	Seah	Anisotropy at OCR 1	DSC
	1991	Ting	Performance of sand drains	Model Testing
	1991	Sheahan	Time dependent materials	Triaxial
	1992	Ortega	Computer automation of DSS	DSS
	1993	Cauble	Cyclic and post cyclic behavior in simple shear	DSS
	1994	Santagata	Simulation of sampling disturbance in soft clays using triaxial tests	Triaxial
IV	1994	Sinfield	Simulation of sampling and effects on compression and shear	CRS, Triaxial
	1996	Cauble	Behavior of model suction caisson	Model Caisson
	1998	Santagata	Pre-failure behavior	Triaxial
	1998	Force	Strain rate selection in triaxial tests	CRS
	2000	Gonzalez	Investigation of CRS consolidation	CRS
	2009	Abdulhadi	Stability of Boreholes	Triaxial, Model BH
	2009	Moniz	Normalized behavior in triaxial extension	Triaxial
	2011	Casey	Significance of end restraint in triaxial testing	Triaxial
	2011	Adams	Measurement of hydraulic conductivity in CRS	CRS
	2012	Marjanovic	Shear wave velocity	Bender Element Apparatus
	2012	Horan	Effect of salt on normally consolidated behavior	CRS, Triaxial

Table 3-2 Overview of previous studies performed using RBBC

Year	Researcher	Batch	wl (%)	wp (%)	Ip (%)	Gs	Clay Fraction (%)	Salt (g/l)
1994	Zriek	powder	46.4	22.5	23.9	2.78	60.1	
1994	Sinfield	powder	47	23.8	23.2	2.79		
		402	46.8	22.4	24.4			
		403	47.2	23.3	23.9			
1996	Cauble	powder				2.81		
		401	46.7	21.8	24.9			
		404	47.4	21.9	25.5			10.4
		405	45.2	22.1	23.1			10
		406	45	22.6	22.4		57.6	12.5
		407	44.6	23	21.6		57.8	13.1
		408	44.7	23.9	20.8		58.7	10.1
		409	45.4	24	21.4		56.8	13
		410	46.6	25	21.6			13.4
		411	46.7	24.5	22.2		56.9	10.2
		413	45.5	24.3	21.2			9.7
		414	46.3	24.3	22			12
		415	46.1	24.7	21.4			10.5
		416	46.7	24	22.7			12.9
		417	47.2	24.5	22.7			13.2
1998	Santagata	418						
		419	47.8	23.3	24.5			
1998	Force	420	45.2	23.3	21.9			
2009	Abdulhadi	powder	46.5	23.5	23	2.81	56	11.1
2012	Horan	powder ¹	49.6	25.4	24.2	2.78	56	10.7
		1 g/l pore water *	50.16	23.6	26.56			
		256 g/l pore water *	46.8	24.4	22.4			
		1 g/l pore water #	49.3	24.7	24.6			
		256 g/l pore water #	47.4	25.6	21.8			

1 - Atterberg limits performed with distilled water

* - Atterberg limits performed on Series IV BBC powder with pore fluid at the salinity shown

- Atterberg limits performed on Series IV BBC which had been leached twice in a centrifuge, with pore fluid at the salinity shown

Table 3-3 Index properties of BBC Series IV (extended from Santagata, 1998)

Borehole Number	Sample Number	Depth (m)	Wet Density Mg/m ³	Moisture Content %	Dry Density Mg/m ³	Saturated Moisture Content %	Porosity %	
BH1	D3	1.50 - 1.95	1.99	24.39	1.60	25.4	40.7	
BH1	D8	7.50 - 7.95	1.95	29.09	1.51	29.2	44.1	
BH2	D4	3.00 - 3.45	1.93	31.33	1.47	31.1	45.6	
BH2	D9	7.50 - 7.95	1.95	27.79	1.52	28.5	43.5	
BH2	D16	16.45 - 16.55	1.95	27.23	1.53	28.3	43.3	
BH2	D20	22.45 - 22.55	2.01	25.37	1.61	25.3	40.5	
BH3	B1	0.50	Test Cancelled - Unsuitable material					
BH3	D8	4.50 - 4.95	1.90	28.68	1.48	30.6	45.2	
BH3	D12	10.50 - 10.95	1.98	27.82	1.55	27.6	42.7	
BH3	D13	12.00 - 12.45	1.94	30.00	1.49	30.0	44.7	
BH4	D3	1.50 - 1.95	1.95	28.85	1.51	29.2	44.1	
BH4	D7	6.00 - 6.45	1.98	27.47	1.55	27.4	42.5	

Table 3-4 London Clay properties determined from laboratory testing from West Hendon development (West Hendon development, SI document)

GEOLABS											
PROJECT NAME :			LAKESIDE DEVELOPMENT, WEST HENDON Project Number: 49319110								
PROJECT NO:			GEO / 15939								
BH	Sample No.	Depth (m)	pH	Total (Acid-soluble) SO ₄ (%)	Water-soluble (2:1 extract) SO ₄ (g/l)	Total Sulphur (%)	Water Soluble Chloride (mg/l)	Water Soluble Nitrate (mg/l)	Magnesium (mg/l)	Organic Content (%)	Loss on ignition (%)
BH1	B2	1.00	7.7	0.036	0.240	0.018	<5.0	<2.0	-	-	-
BH1	D3	1.50 - 1.95	-	-	-	-	-	-	-	1.0	7.0
BH1	D4	3.00 - 3.45	-	-	-	-	-	-	-	0.2	7.9
BH1	D5	4.50 - 4.95	7.3	0.59	5.8	0.29	60	3.6	770	-	-
BH1	D11	10.95 - 11.05	7.9	0.34	2.3	0.57	<5.0	<2.0	-	-	-
BH1	D13	14.00 - 14.45	7.6	0.19	1.8	0.86	<5.0	<2.0	-	-	-
BH1	D17	20.00 - 20.45	7.5	0.17	1.7	0.37	<5.0	<2.0	-	-	-
BH1	D19	24.00 - 24.45	7.9	0.14	1.4	0.43	<5.0	<2.0	-	-	-
BH1	D22	27.00 - 27.45	7.3	0.15	1.3	0.76	<5.0	<2.0	-	-	-
BH1	-	29.50 - 30.00	7.5	0.17	1.5	0.60	<5.0	<2.0	-	-	-
BH2	D17	18.00 - 18.45	7.3	0.17	1.3	0.40	<5.0	<2.0	-	-	-
BH3	B1	0.50	-	-	-	-	-	-	-	3.4	10
BH3	D6	3.50 - 3.95	-	-	-	-	-	-	-	0.2	7.9
BH4	B1	0.50	7.9	0.074	0.078	0.037	<5.0	<2.0	-	-	-
BH4	B2	1.00	-	-	-	-	-	-	-	1.9	6.9
BH4	D6	4.95 - 5.05	7.6	1.2	5.8	0.41	64	2.3	680	-	-
BH4	D11	9.95 - 10.05	7.6	1.2	6.2	1.1	5.9	<2.0	700	-	-
TP8	-	0.40 - 0.50	7.6	0.054	0.11	0.023	<5.0	<2.0	-	-	-
TP8	-	1.00 - 1.20	-	-	-	-	-	-	-	0.6	9.2
TP10	-	0.40 - 0.45	7.9	0.027	0.083	0.012	<5.0	<2.0	-	-	-
TP12	-	1.00 - 1.20	7.8	0.041	0.35	0.014	17	<2.0	-	-	-
Checked and approved:											
Initials: JS											
Date: 30/07/2010											
SUMMARY OF CHEMICAL TESTS ON SOIL											

Table 3-5 Summary of results from chemical tests performed on London Clay from West Hendon development (West Hendon development, SI document)

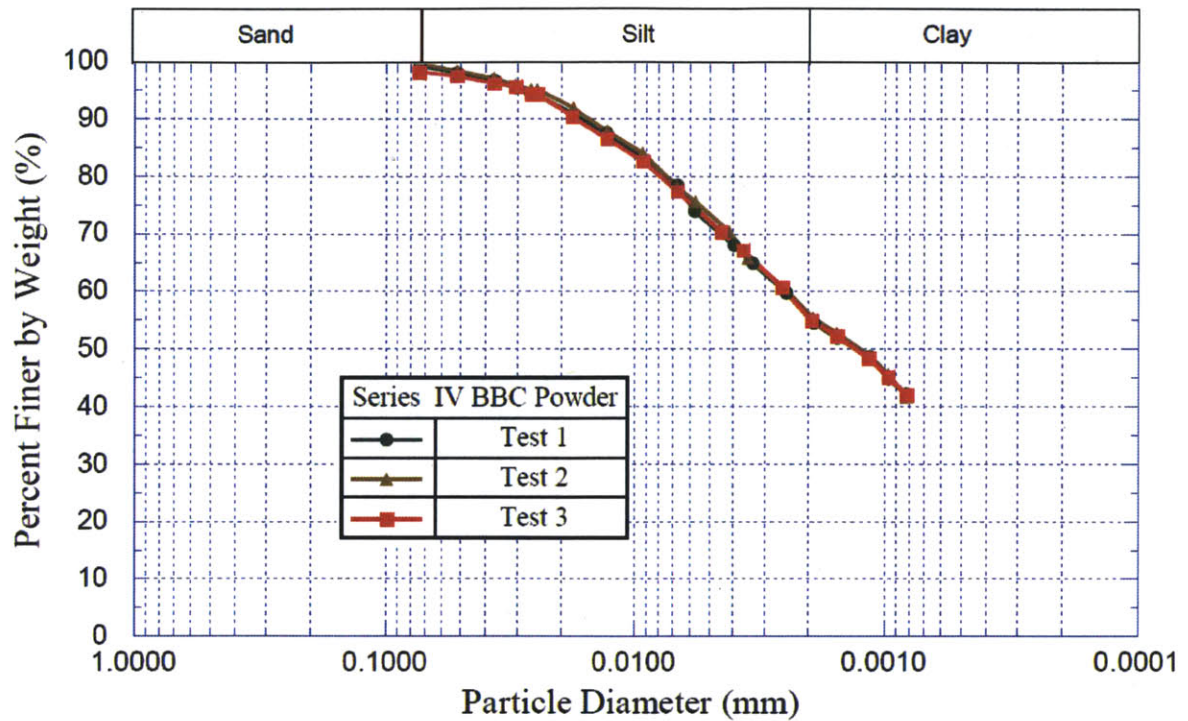


Figure 3.1 Results of grain size analysis for series IV BBC powder (Abdulhadi, 2009)

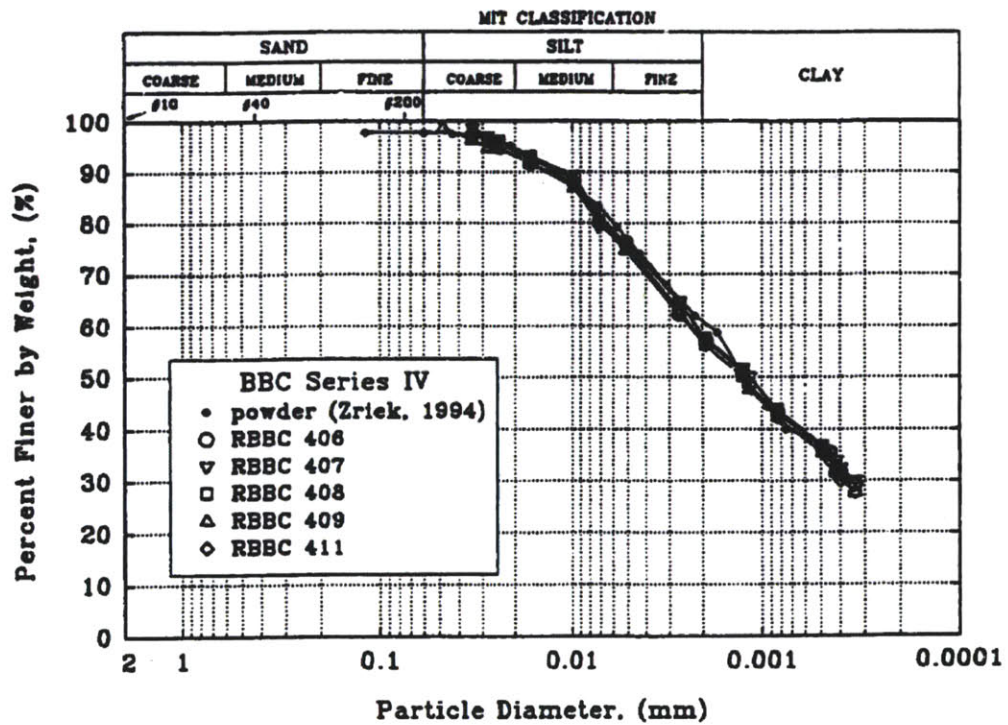


Figure 3.2 Results of grain size analysis for series IV BBC powder (Force, 1998)

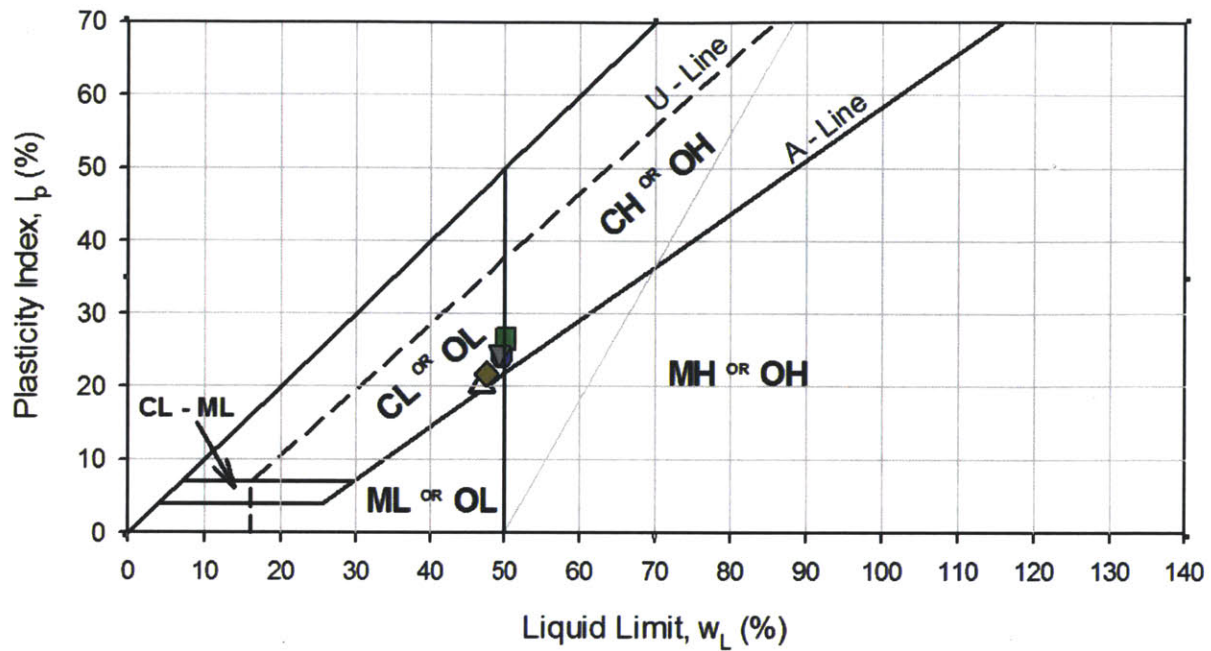


Figure 3.3 Plasticity chart for 5 determinations on natural and leached BBC (corrected for salt)

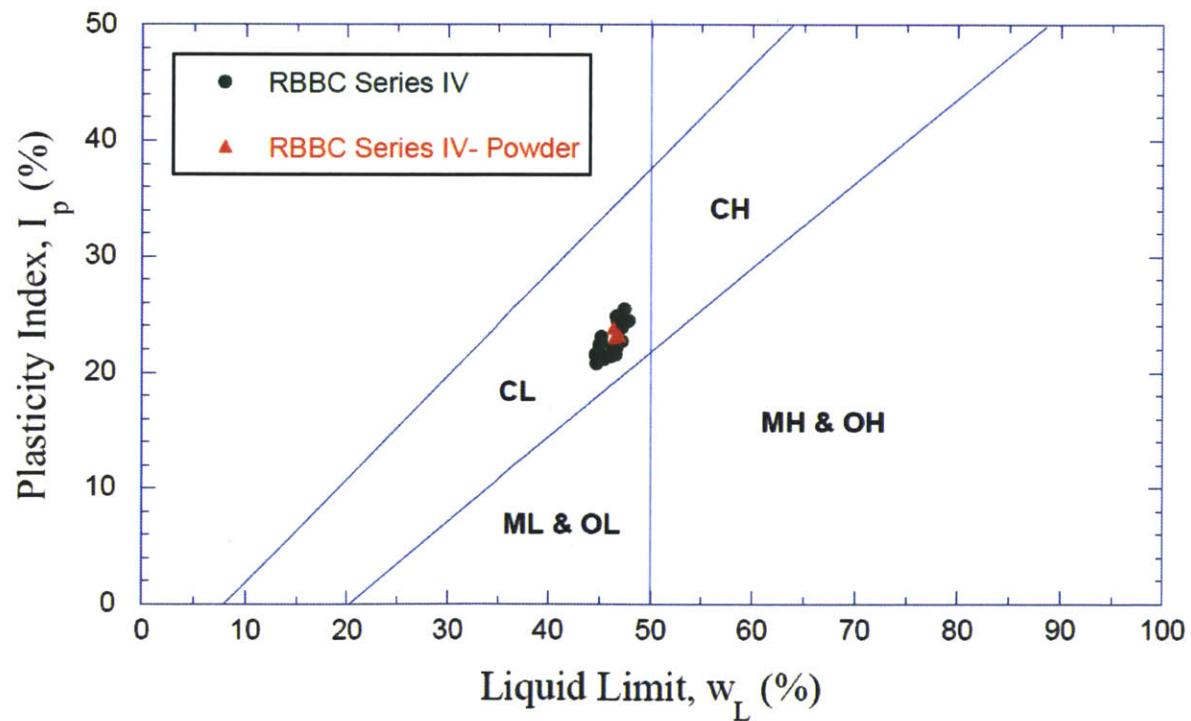


Figure 3.4 Plasticity chart showing data for RBBC Series IV (Abdulhadi, 2009)

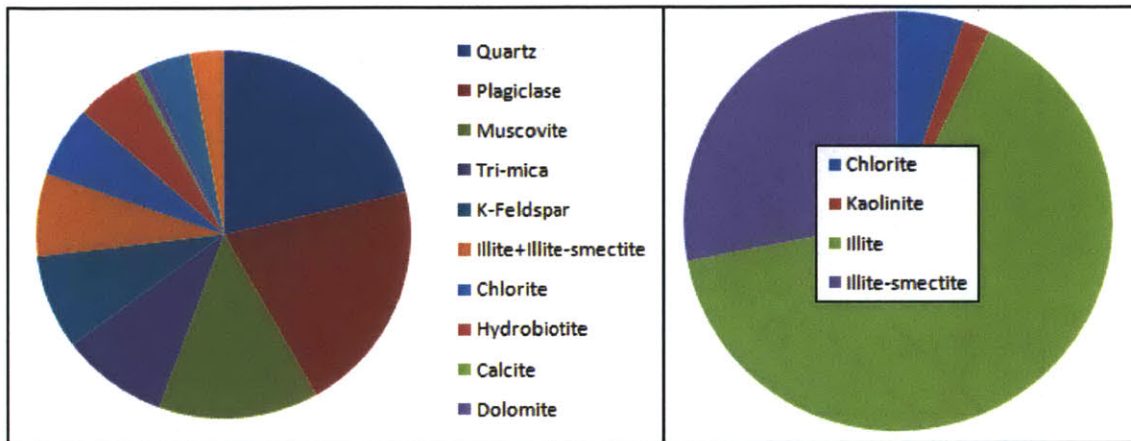


Figure 3.5 Mineralogy of Boston Blue Clay – bulk sample on left, < 2 micron on right

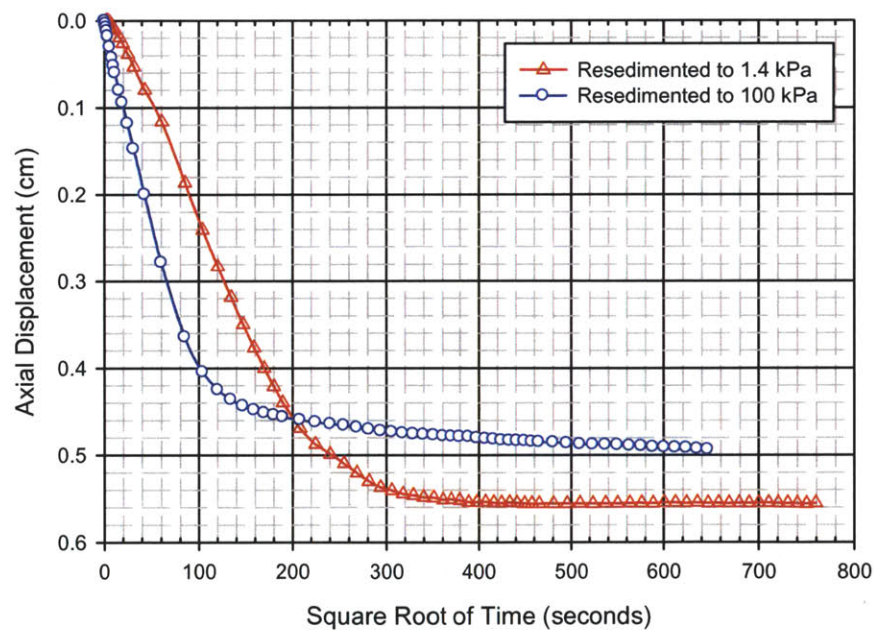


Figure 3.6 Axial displacement versus root time for RBBC Series IV at different stress levels (data from RS175, RBBC at 64 g/l, consolidometer diameter 4.4 cm, initial height 12.9 cm, final height 7.8 cm)

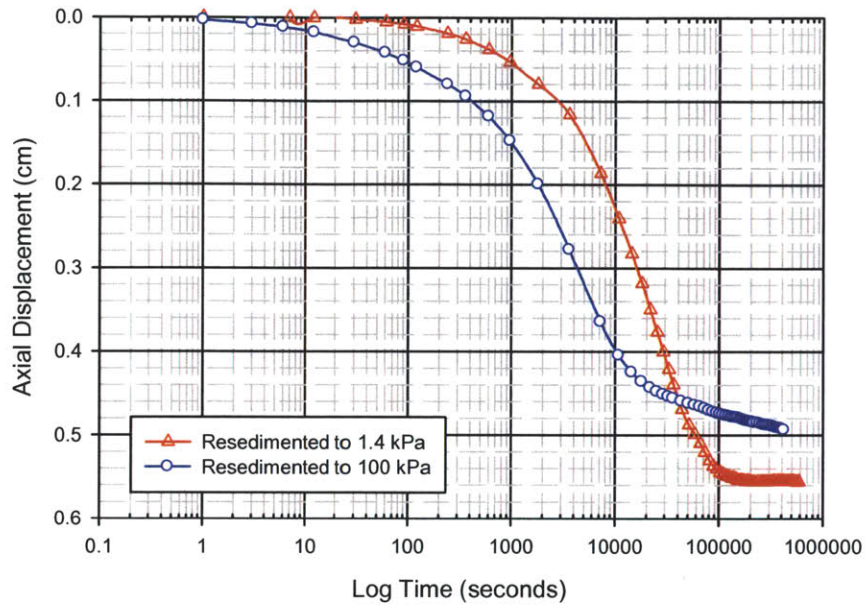


Figure 3.7 Axial displacement versus log time for RBBC Series IV at different stress levels (data from RS175, RBBC at 64 g/l)

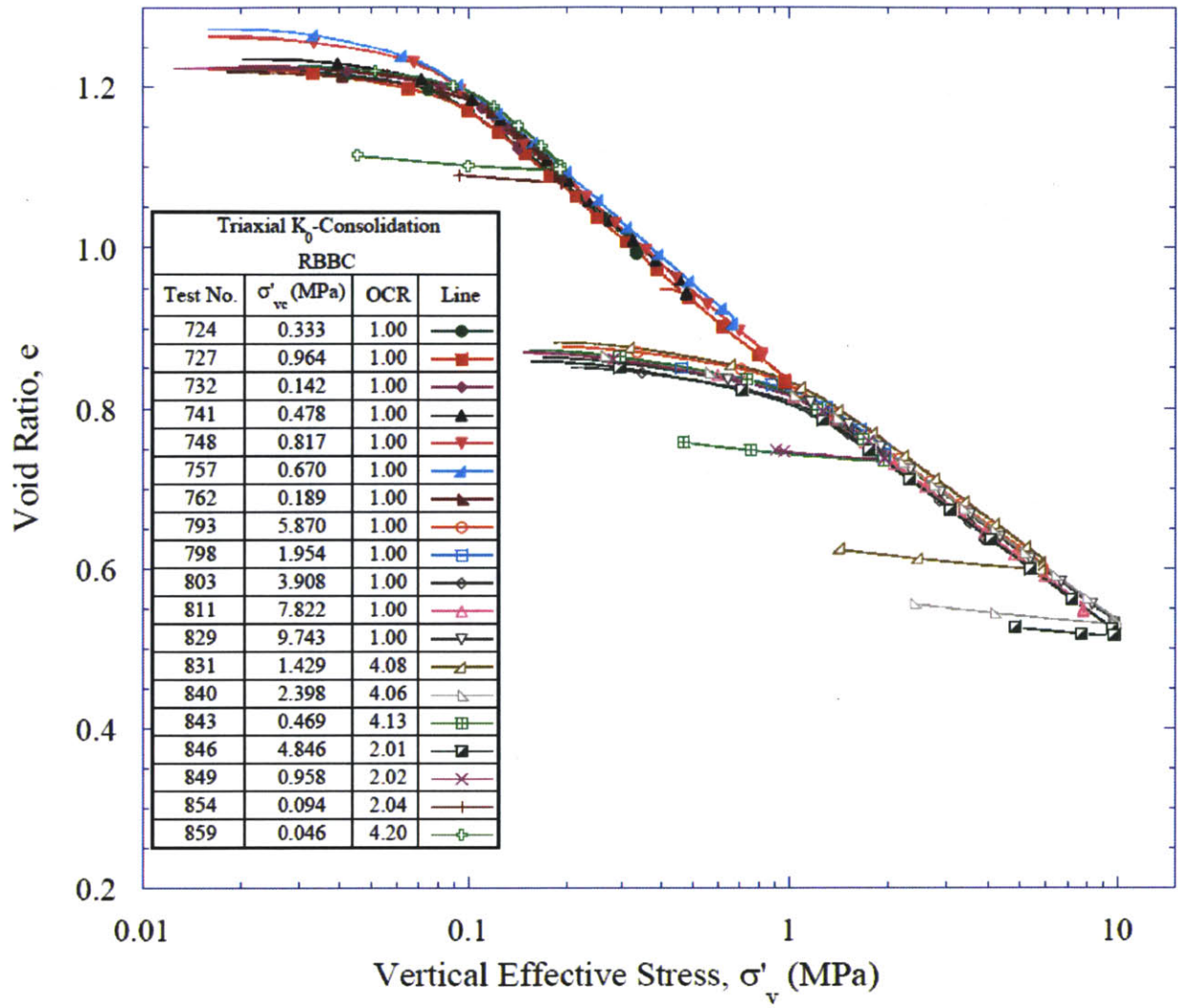


Figure 3.8 1-D compression behavior in e-log space for NC and OC RBBC from triaxial testing

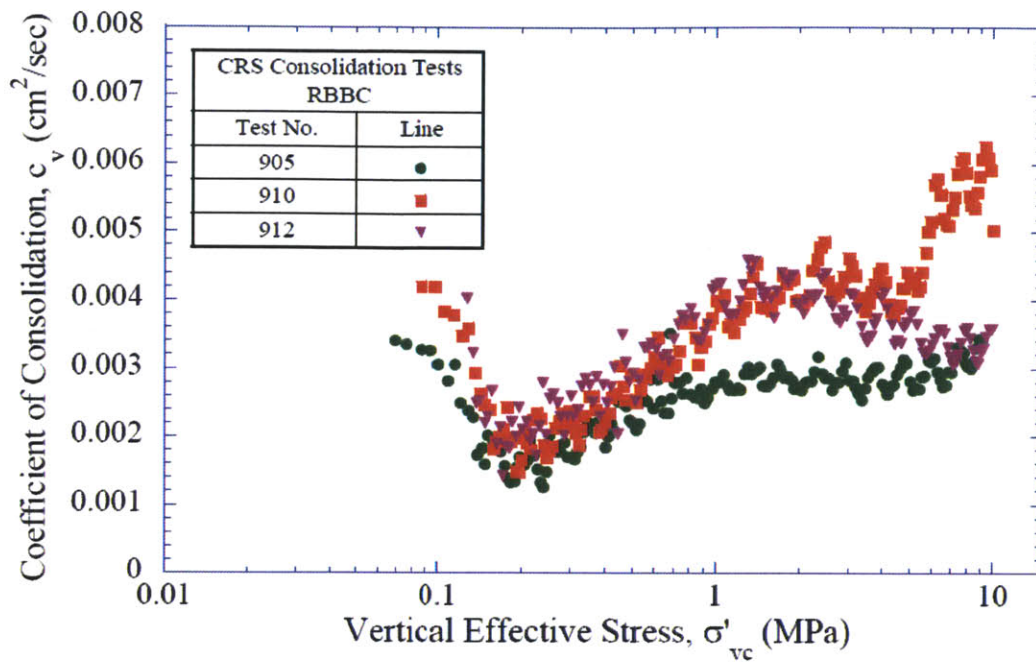


Figure 3.9 Coefficient of consolidation versus stress level for RBBC from CRS testing (Abdulhadi, 2009)

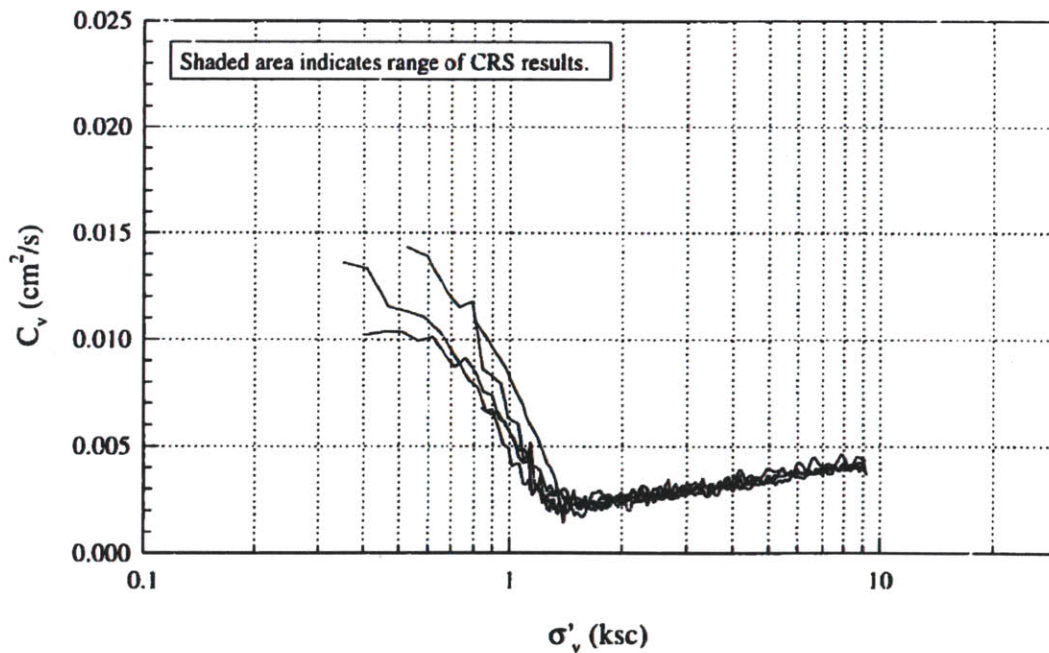


Figure 3.10 Coefficient of consolidation versus stress level for RBBC from CRS testing – Note: 10 ksc ~ 1 MPa (Force, 1998)

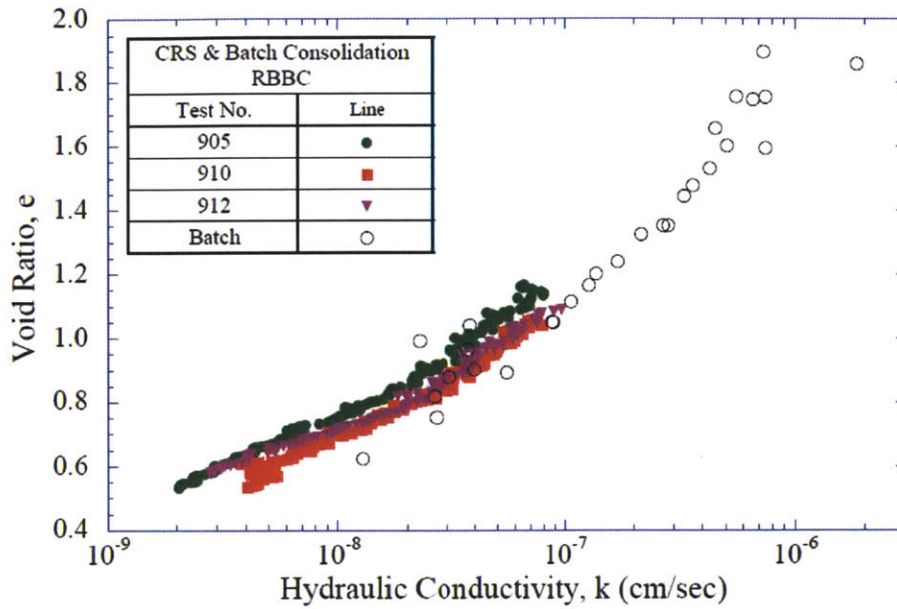


Figure 3.11 Void ratio versus hydraulic conductivity for RBBC Series IV from CRS tests referenced to batch data (Abdulhadi, 2009)

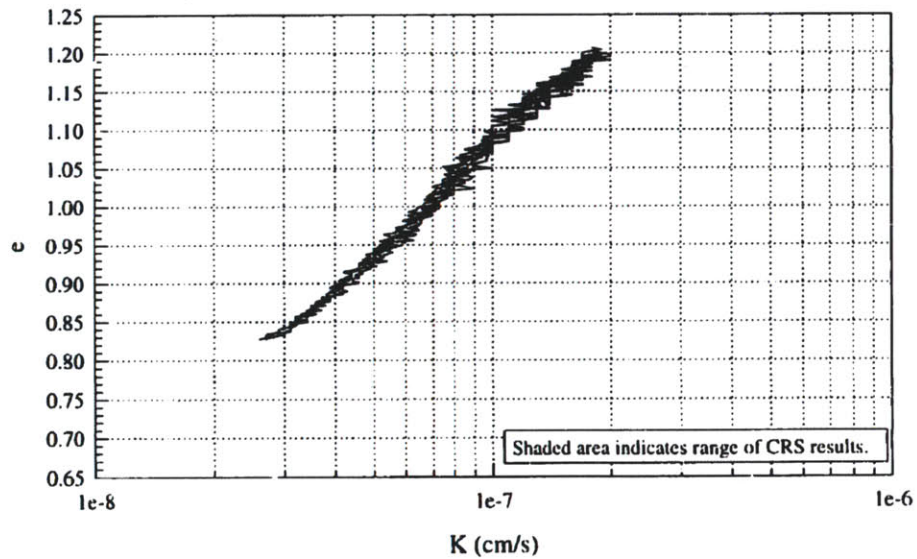


Figure 3.12 Void ratio versus hydraulic conductivity for RBBC Series IV from CRS tests (Force, 1998)

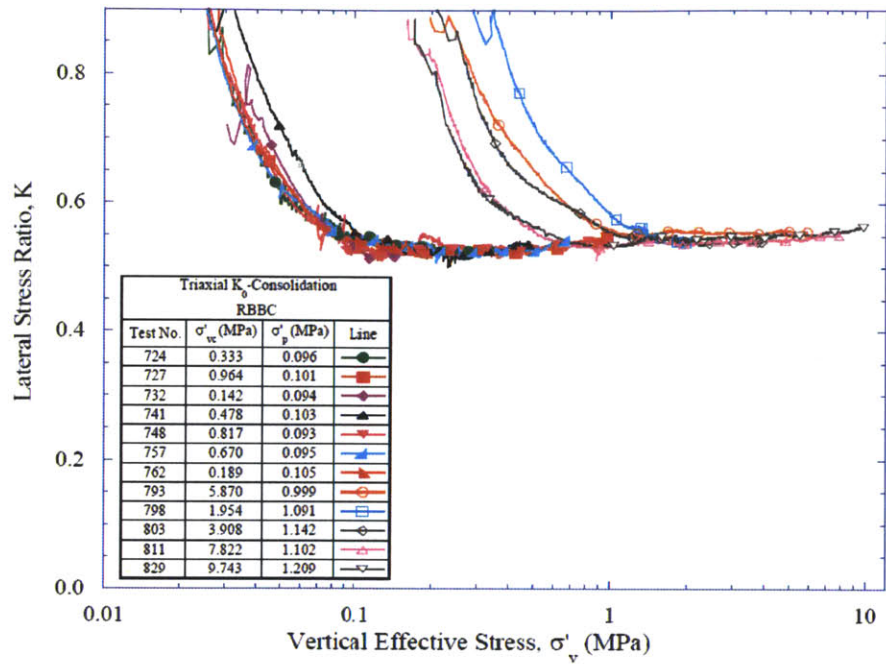


Figure 3.13 Variation in lateral stress ratio K versus stress level measured during consolidation phase of triaxial test (Abdulhadi, 2009)

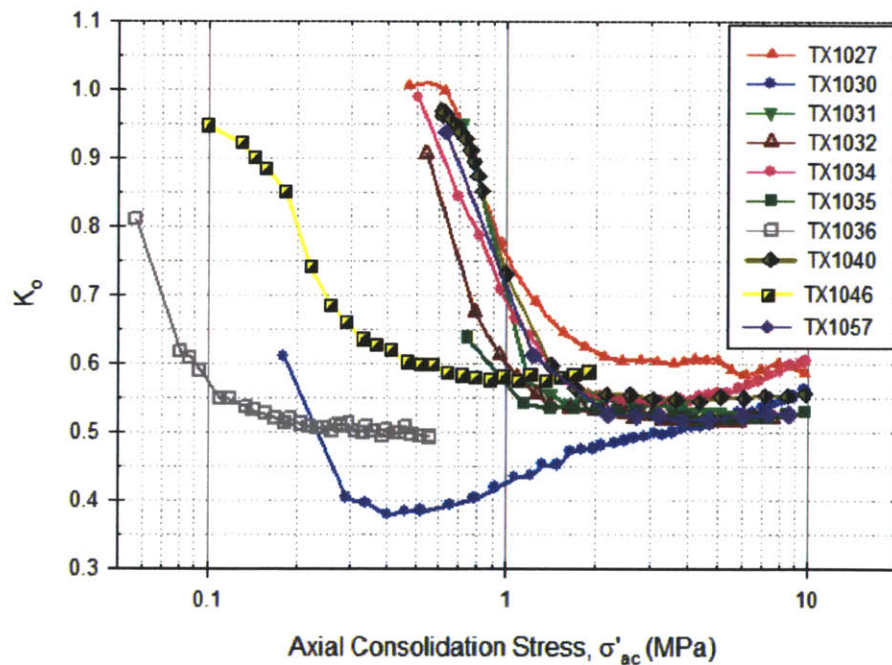


Figure 3.14 Variation in lateral stress ratio K versus stress level measured during consolidation phase of triaxial test (Casey, 2011)

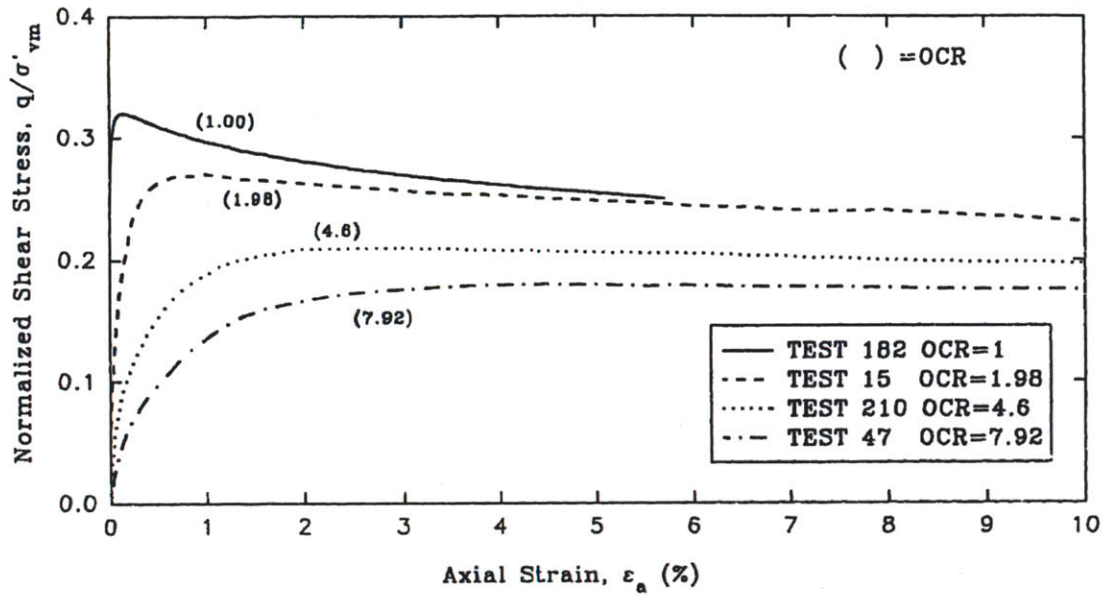


Figure 3.15 Normalized shear stress-strain behavior of RBBC Series III at different OCR values in undrained triaxial compression (Santagata, 1994)

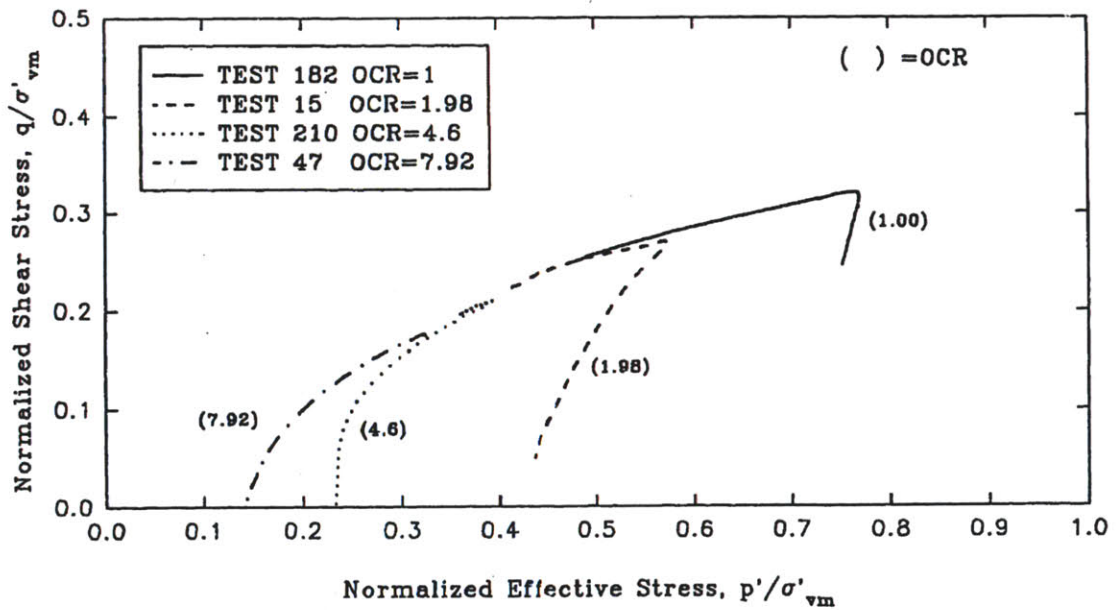


Figure 3.16 Normalized effective stress path for RBBC Series III at different OCR values in undrained triaxial compression (Santagata, 1994)

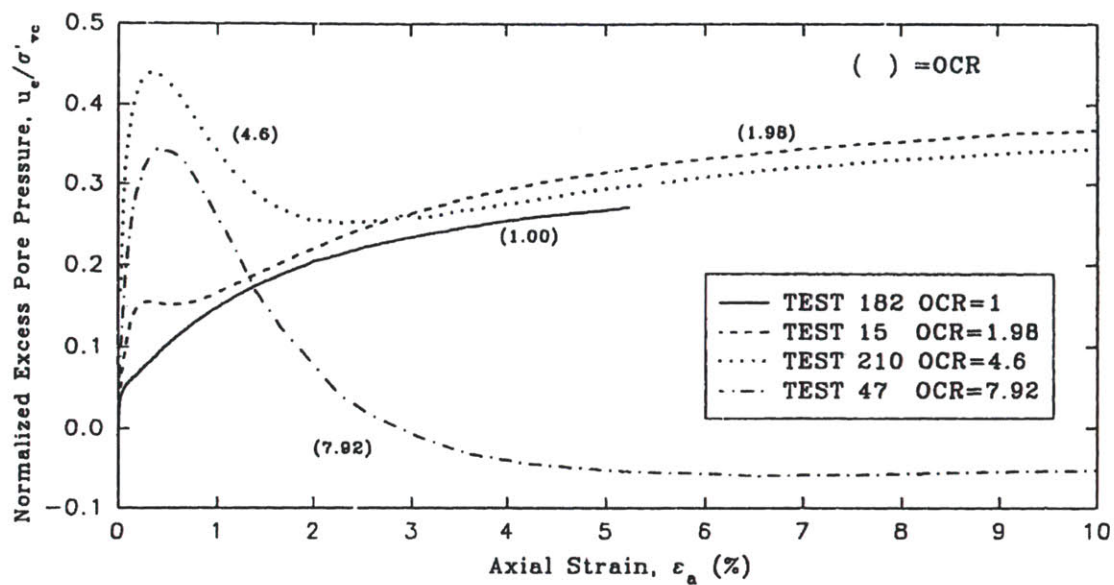


Figure 3.17 Normalized excess pore pressure of RBBC Series III at varying OCR values in undrained triaxial compression (Santagata, 1994)

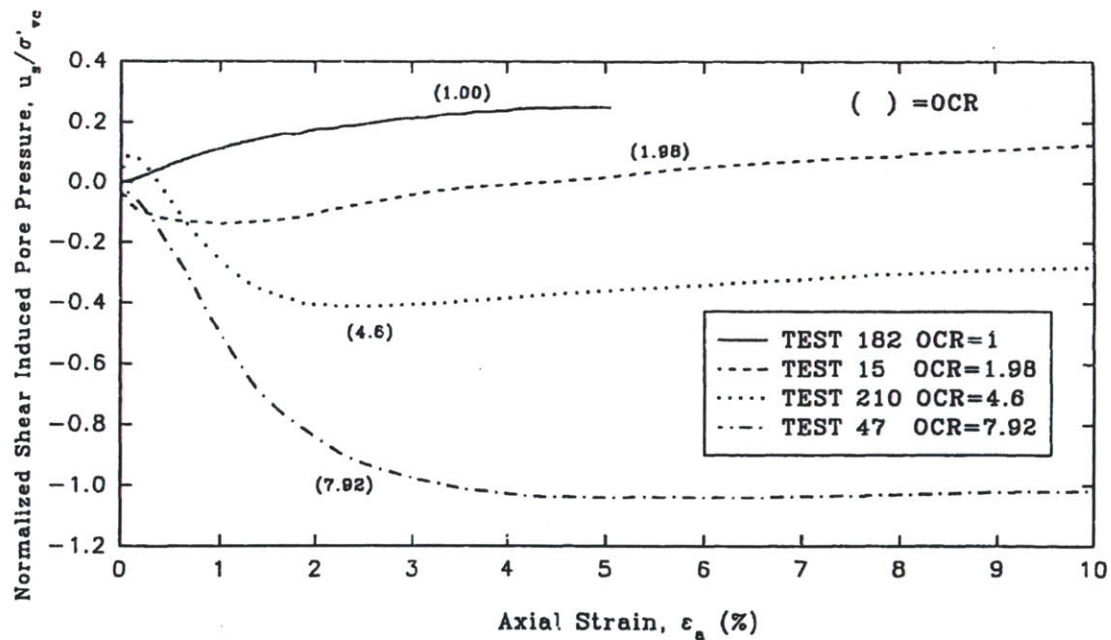


Figure 3.18 Normalized shear induced pore pressures of RBBC Series III at varying OCR values in undrained triaxial compression (Santagata, 1994)

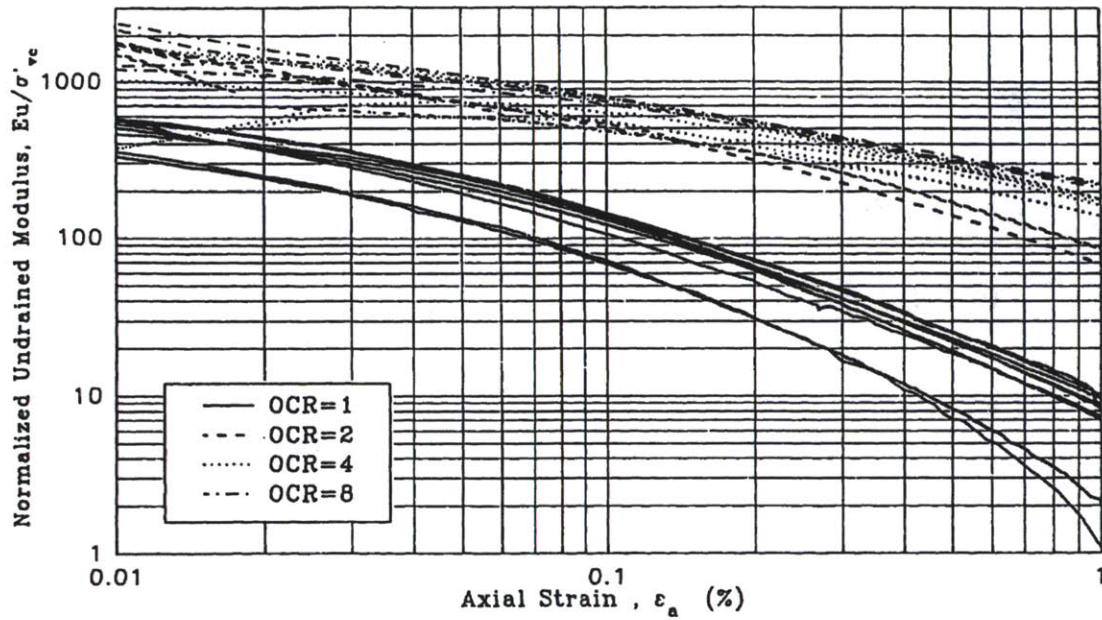


Figure 3.19 Normalized undrained secant modulus versus axial strain for RBBC Series III in triaxial compression (Santagata, 1994)

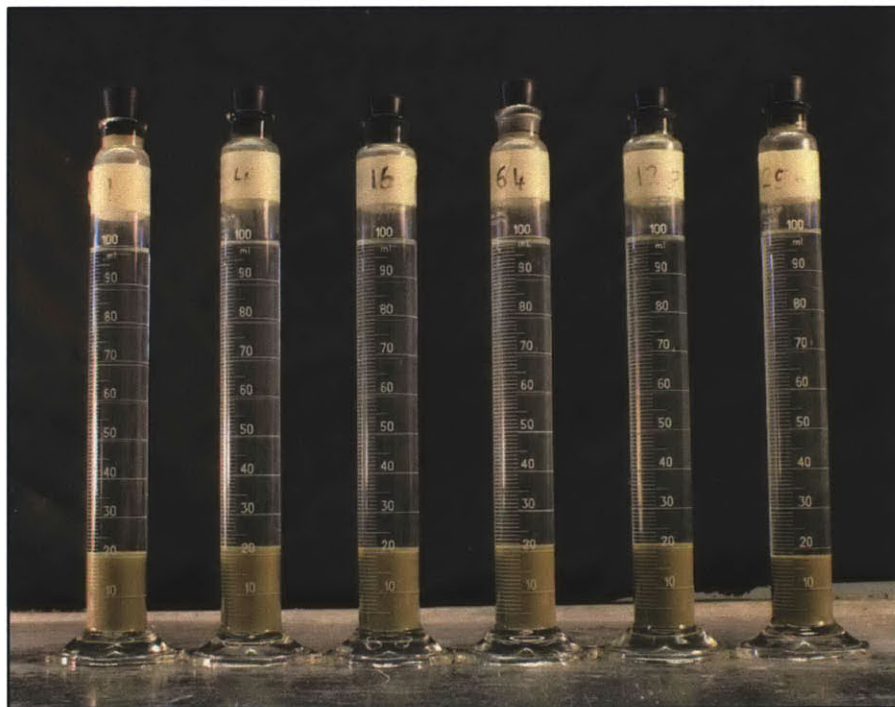


Figure 3.20 Sedimentation test performed on natural BBC Series IV powder. Salinities from L-R: 1, 4, 16, 64, 128 & 256 g/l NaCl. 5 grams of soil used in each tube

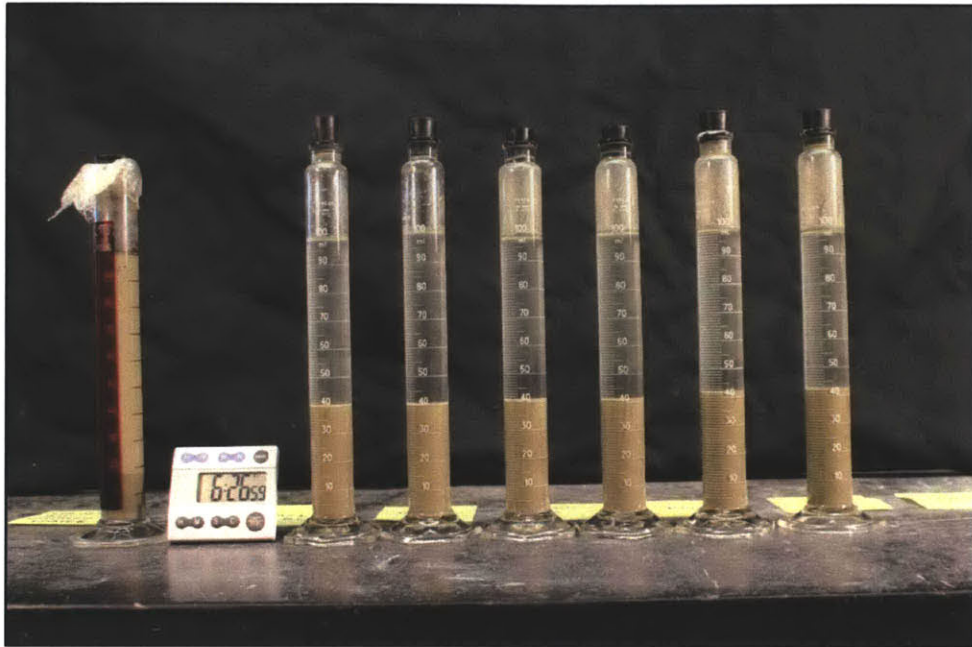


Figure 3.21 Sedimentation test performed on leached BBC powder. Salinities from L-R: 0 (distilled water) 1, 4, 16, 64, 128 & 256 g/l NaCl. 5 grams of soil used in each tube

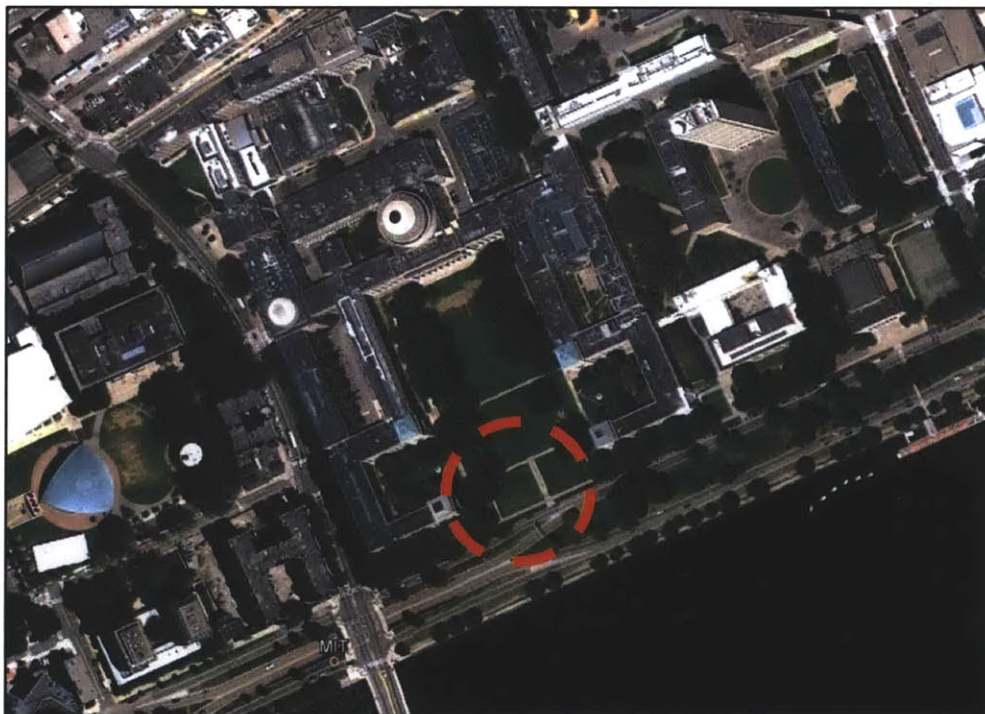


Figure 3.22 Location from where undisturbed samples were obtained on MIT campus (Google Earth)

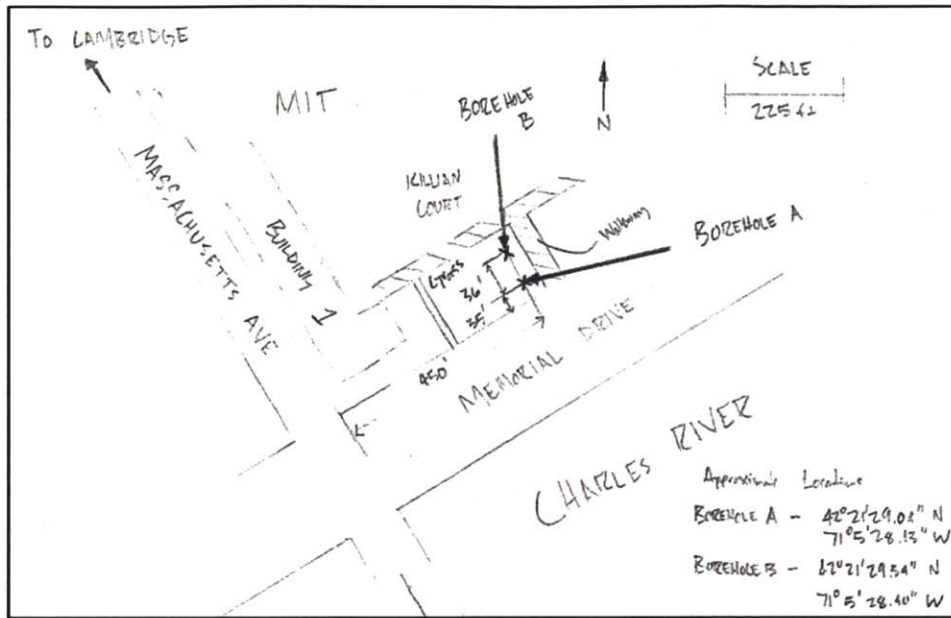


Figure 3.23 Site plan identifying actual location of boreholes (The T2P Project)

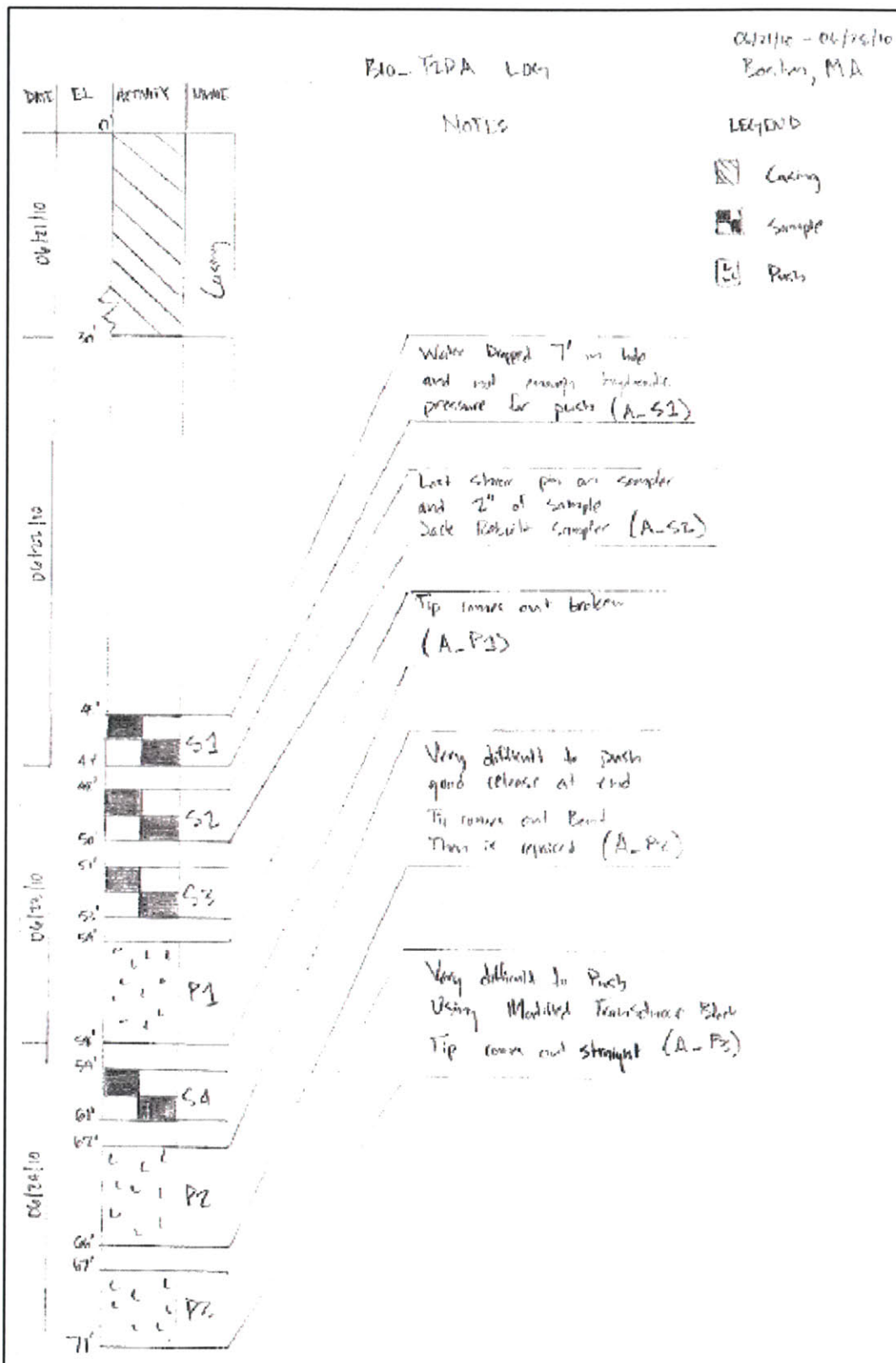


Figure 3.24 Borehole log for B10-T2PA in Killian Court (The T2P Project)

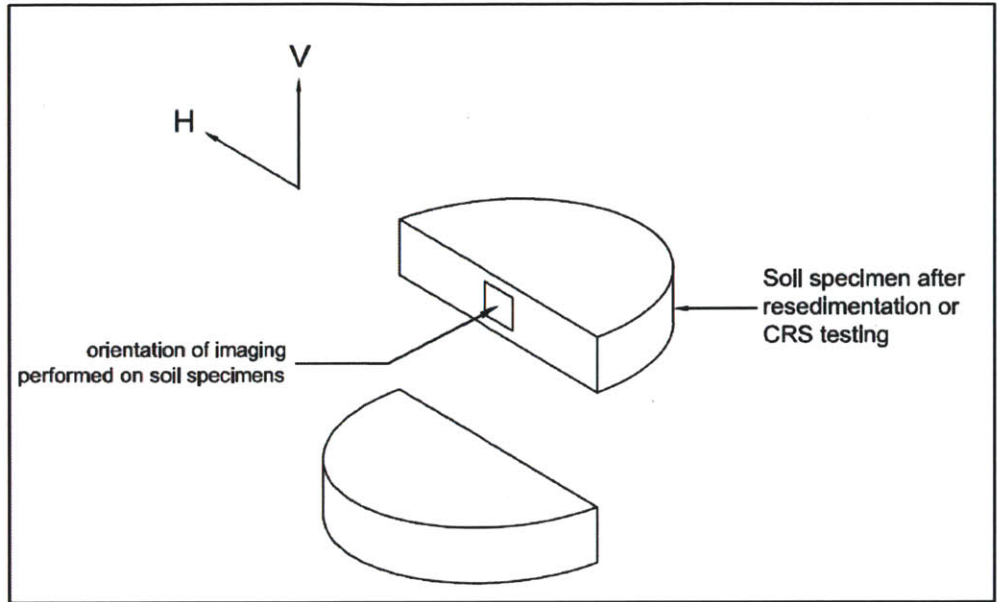


Figure 3.25 Orientation of all imaging presented

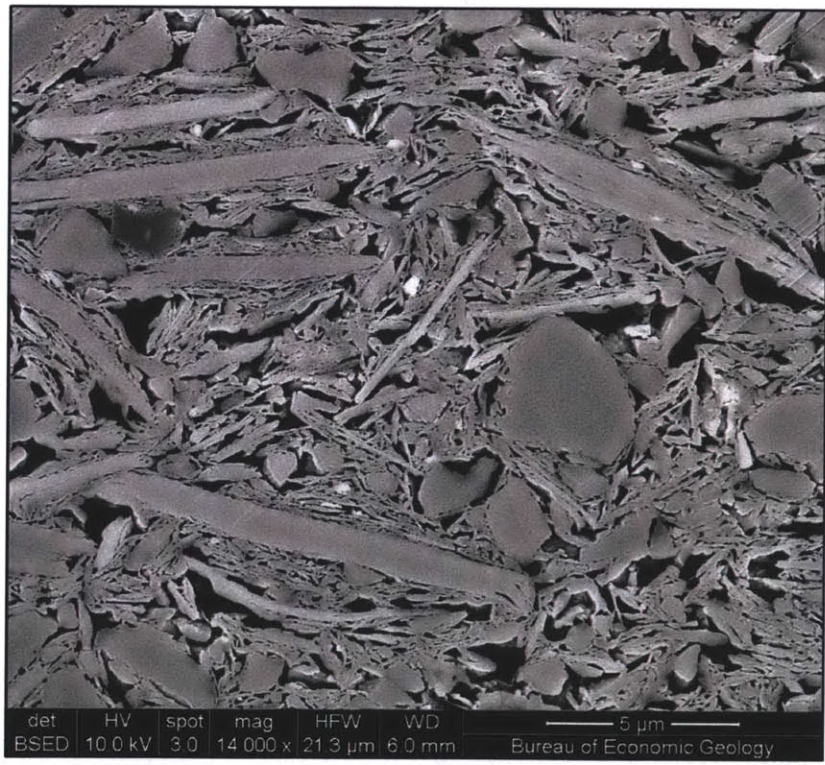


Figure 3.26 SEM images of natural RBBC Series IV at a pore fluid salinity of 4 g/l and a stress level of 100 kPa (corresponding void ratio ~ 1.22)

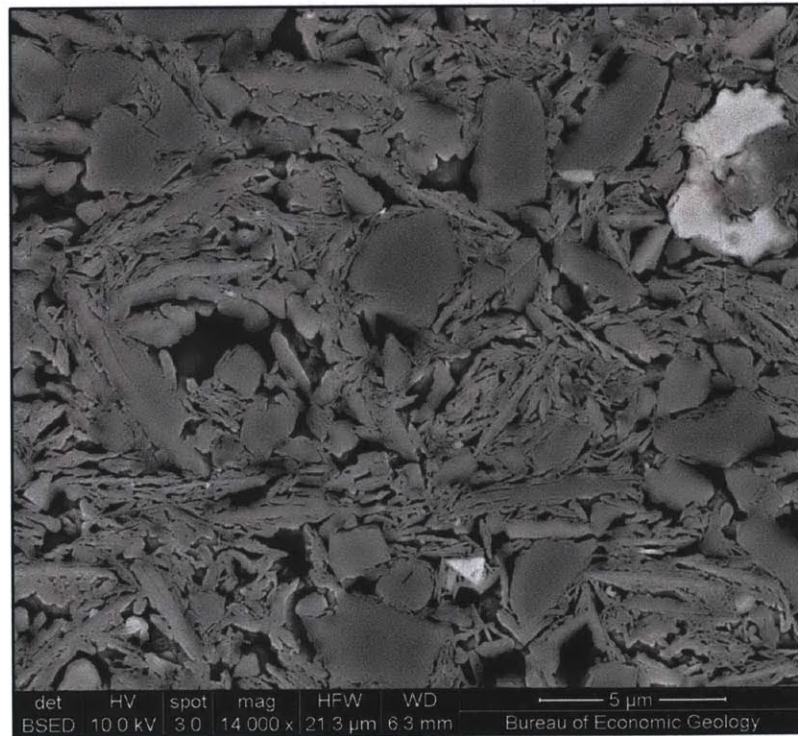
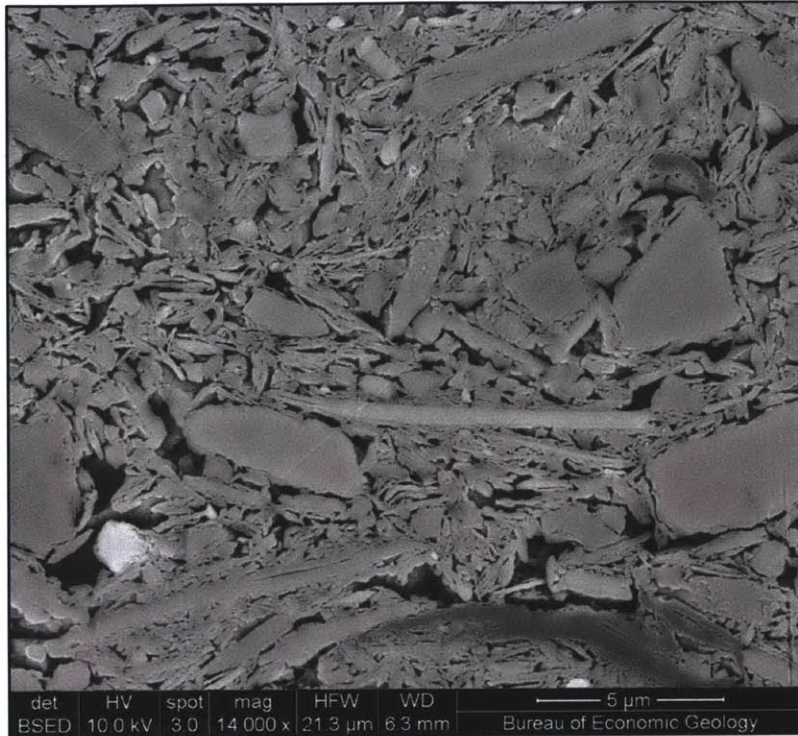


Figure 3.27 SEM images of natural RBBC Series IV at a pore fluid salinity of 256 g/l and a stress level of 100 kPa (corresponding void ratio ~ 1.22)

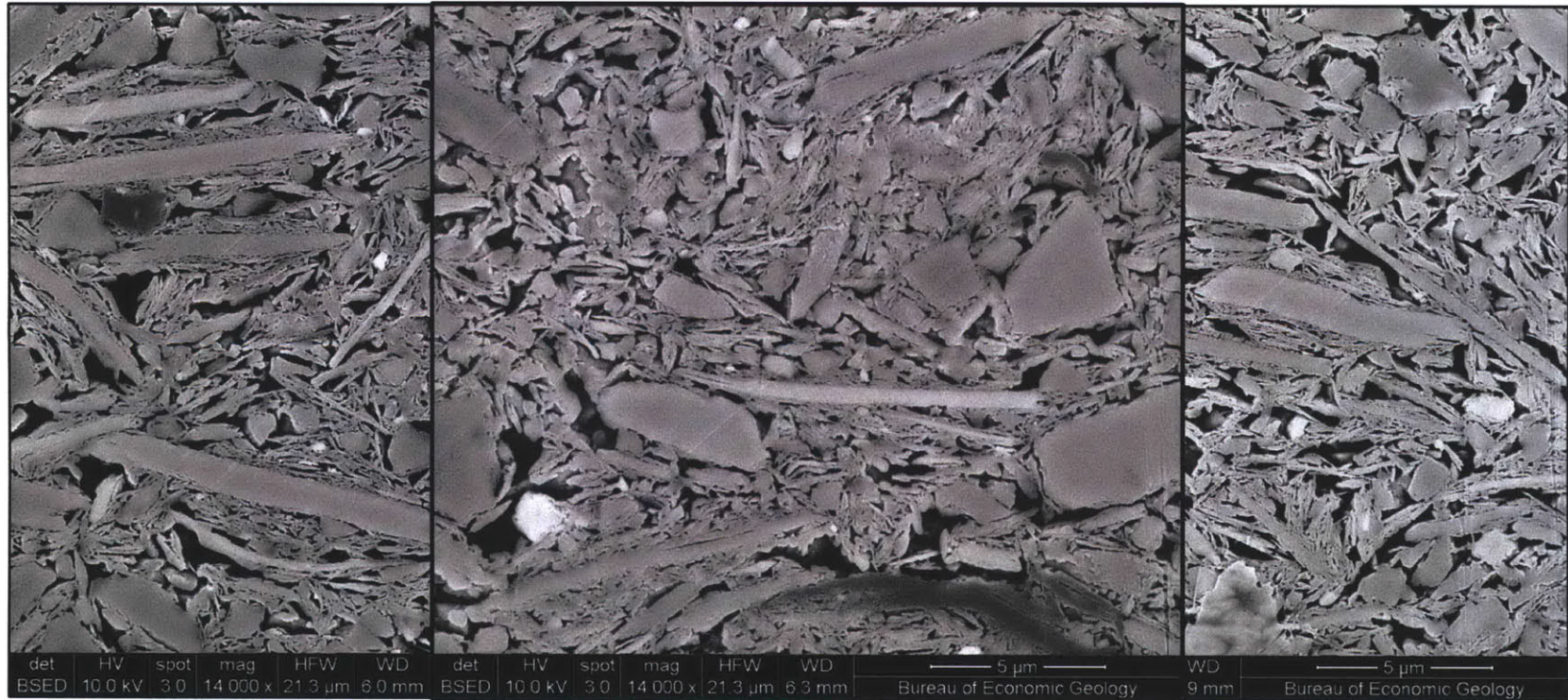


Figure 3.28 Analysis of RBBC Series IV at 2 different salinities but same stress level (100 kPa).

Image on outer left and outer right are 4 g/l, image in the center is at 256 g/l (void ratio for all images ~ 1.22)

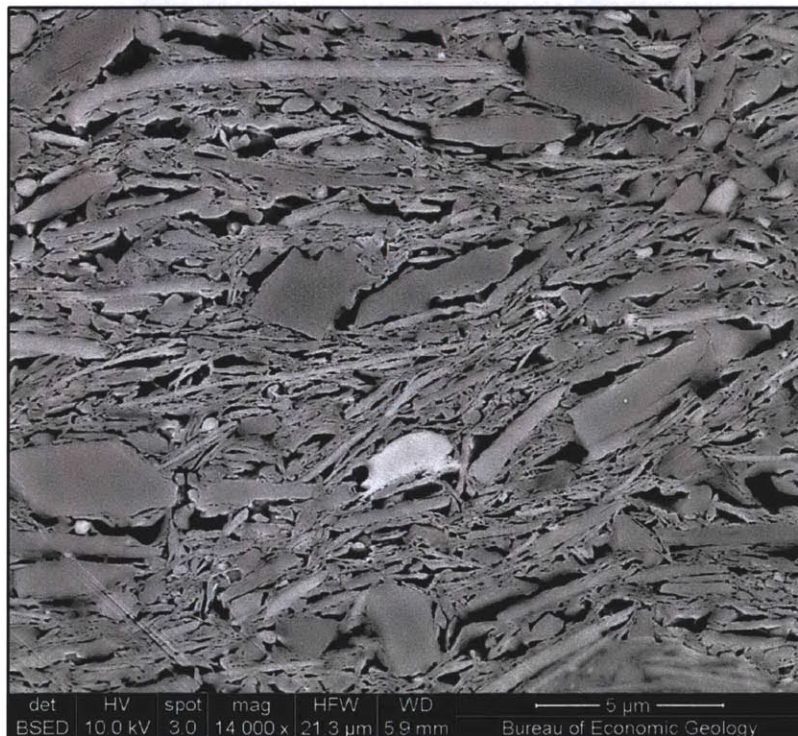
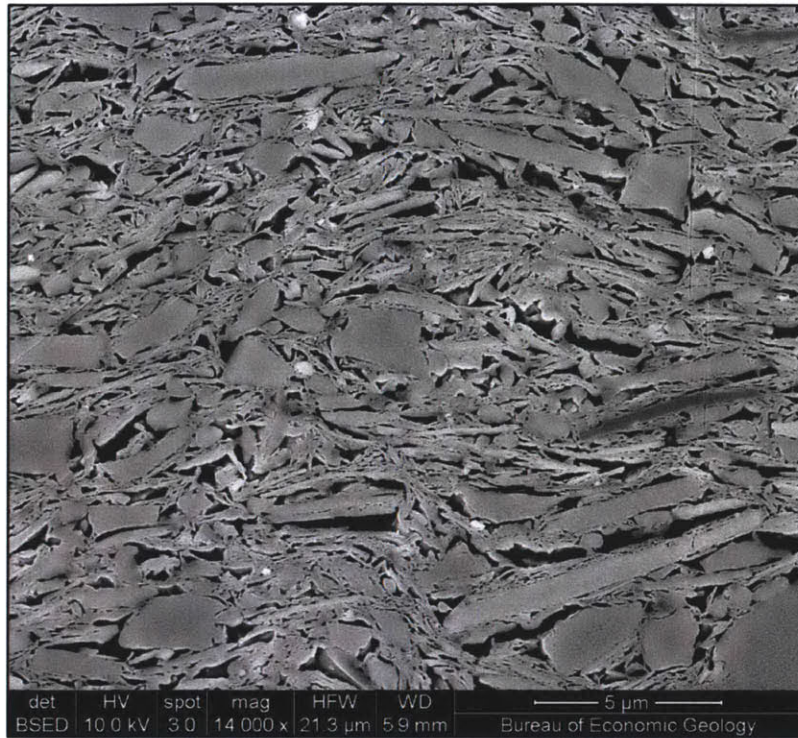


Figure 3.29 SEM images of leached RBBC at a pore fluid salinity of 1 g/l and a stress level of 100 kPa (corresponding void ratio ~ 1.14)

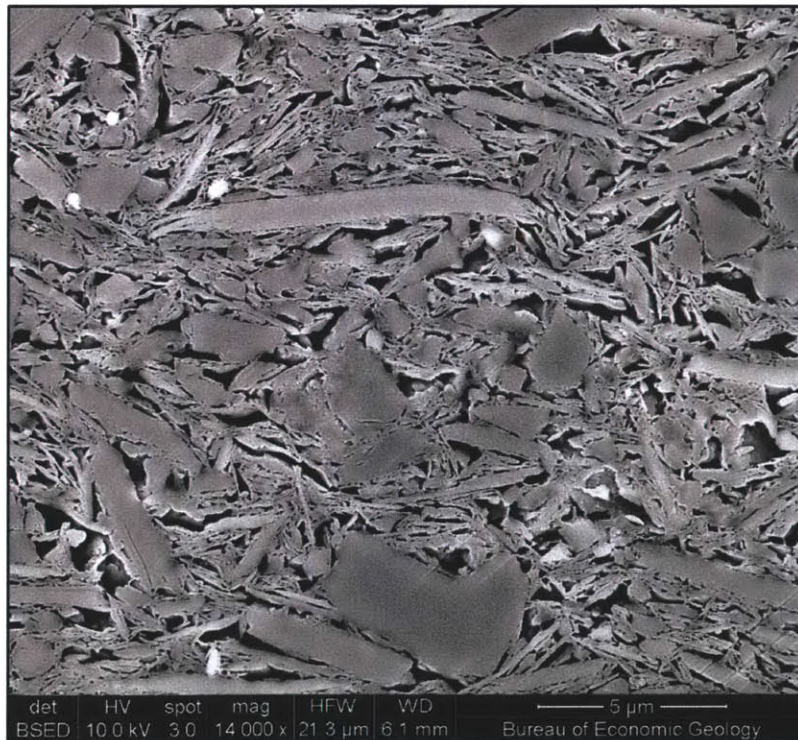
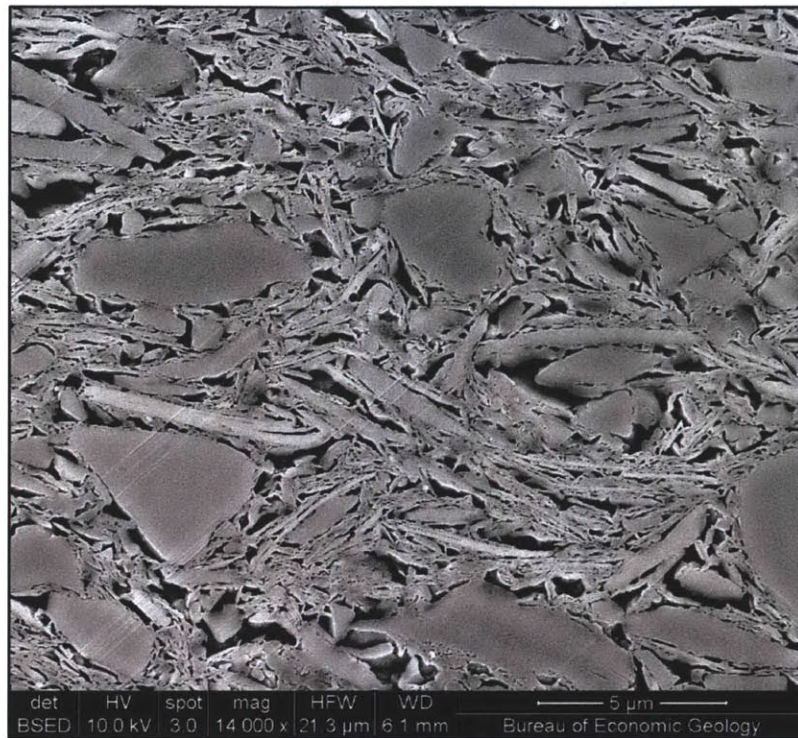


Figure 3.30 SEM images of leached RBBC at a pore fluid salinity of 1 g/l and a stress level of 1,000 kPa (corresponding void ratio ~ 0.775)

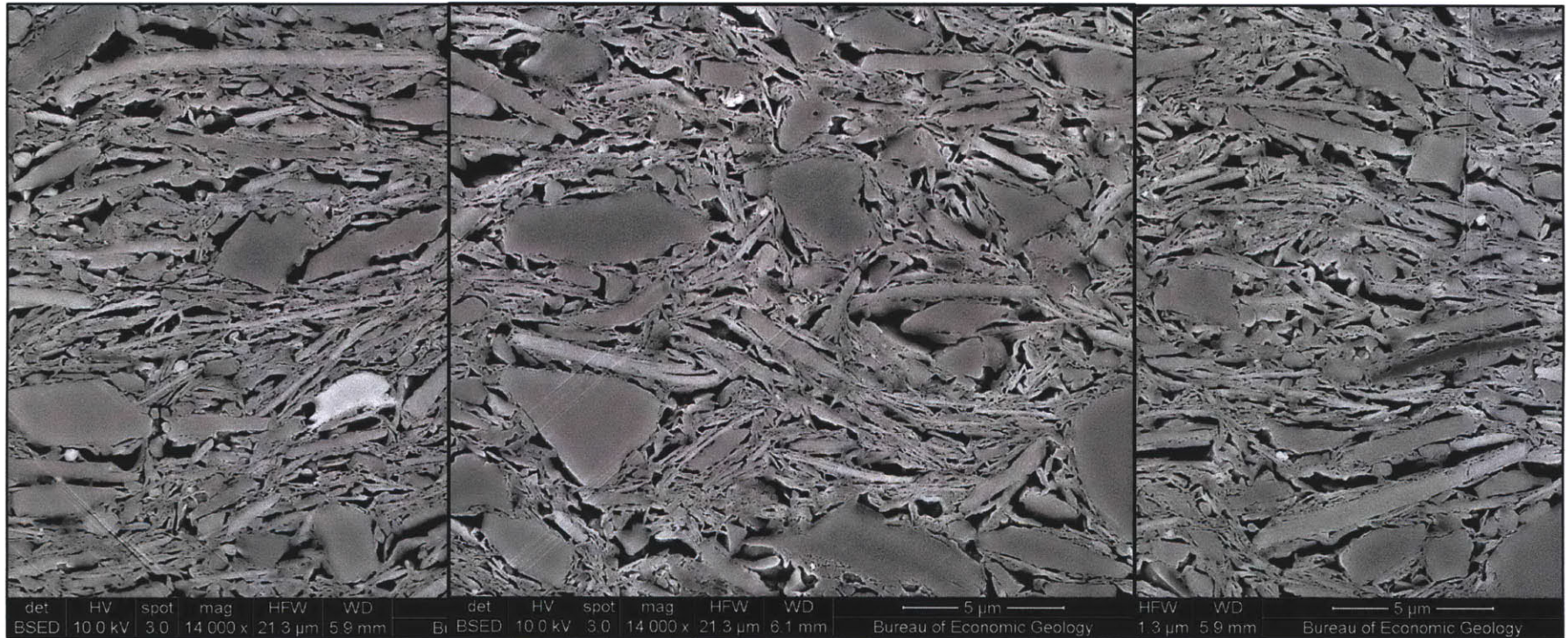


Figure 3.31 Analysis of leached RBBC at the same salinity (1 g/l) but different stress level.

Image on outer left and outer right are 100 kPa (corresponding void ratio ~ 1.14), image in the center is at 1,000 kPa (corresponding void ratio ~ 0.775)

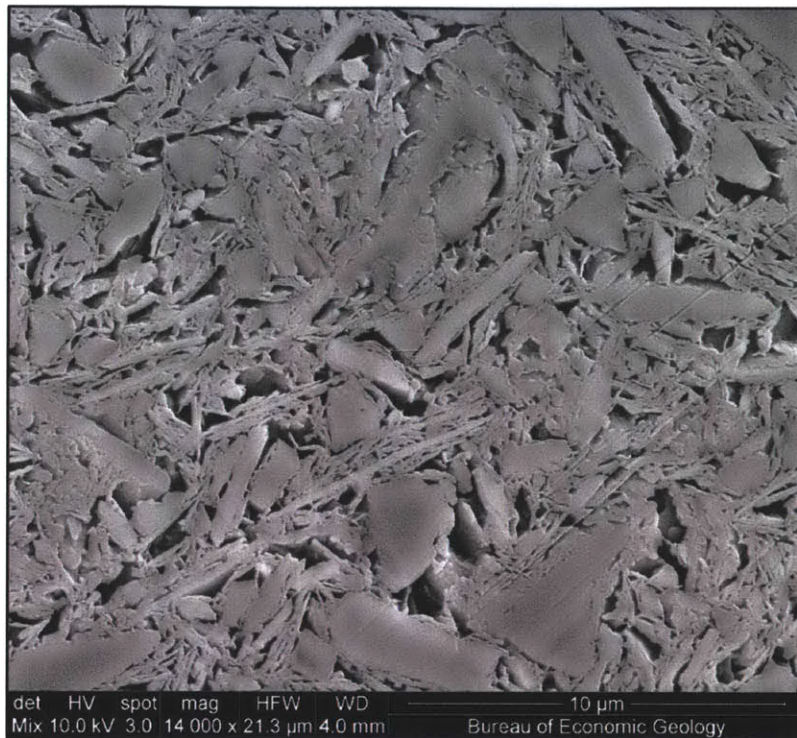


Figure 3.32 SEM images of sodium hex RBBC at a pore fluid salinity of 0 g/l and a stress level of 100 kPa. Note: different magnifications (corresponding void ratio = 1.01)

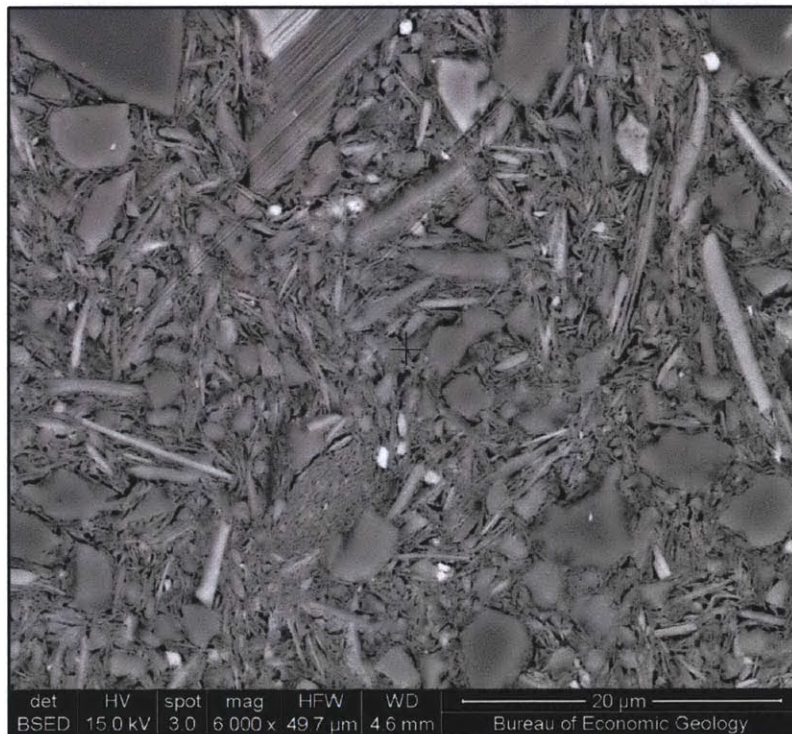
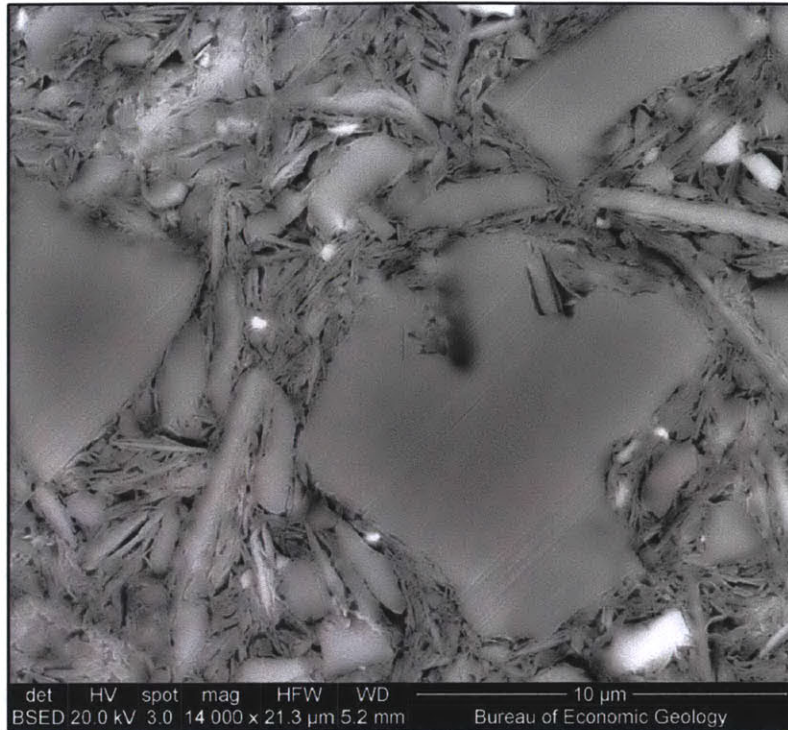


Figure 3.33 SEM images of sodium hex RBBC at a pore fluid salinity of 0 g/l and a stress level of 10,000 kPa. Note: different magnifications (corresponding void ratio = 0.48)

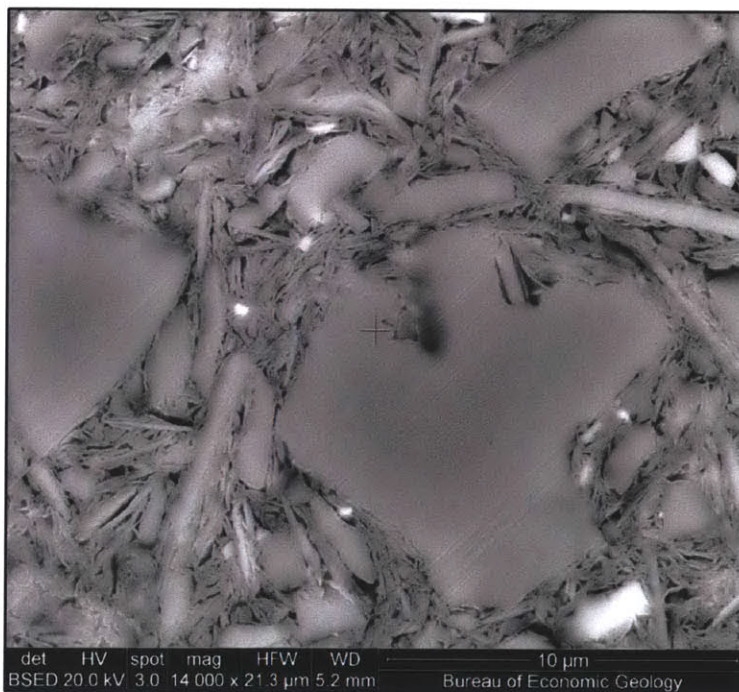
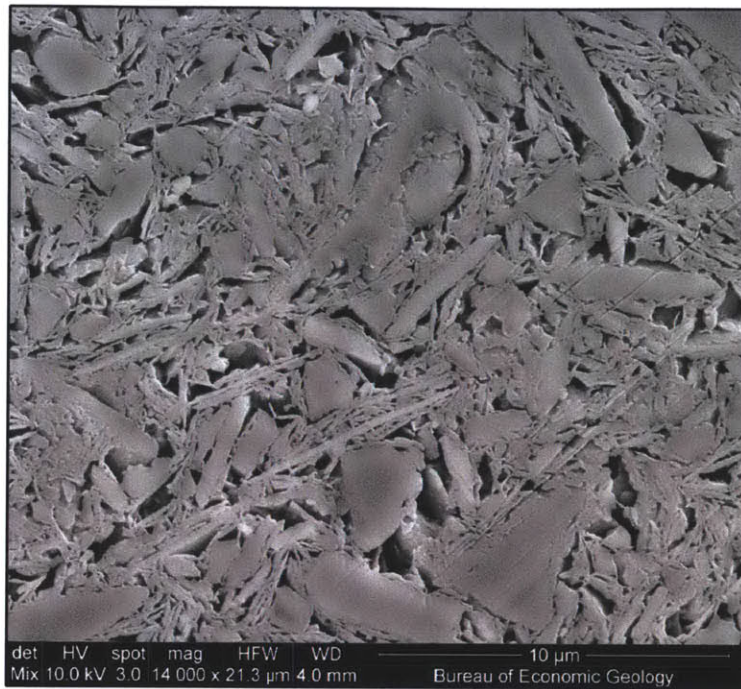


Figure 3.34 SEM images of sodium hex RBBC at a pore fluid salinity of 0 g/l and a stress level of 100 kPa (top) and 10,000 kPa (bottom) at same magnification. (corresponding void ratio top image ~ 1.01, bottom image ~ 0.48)

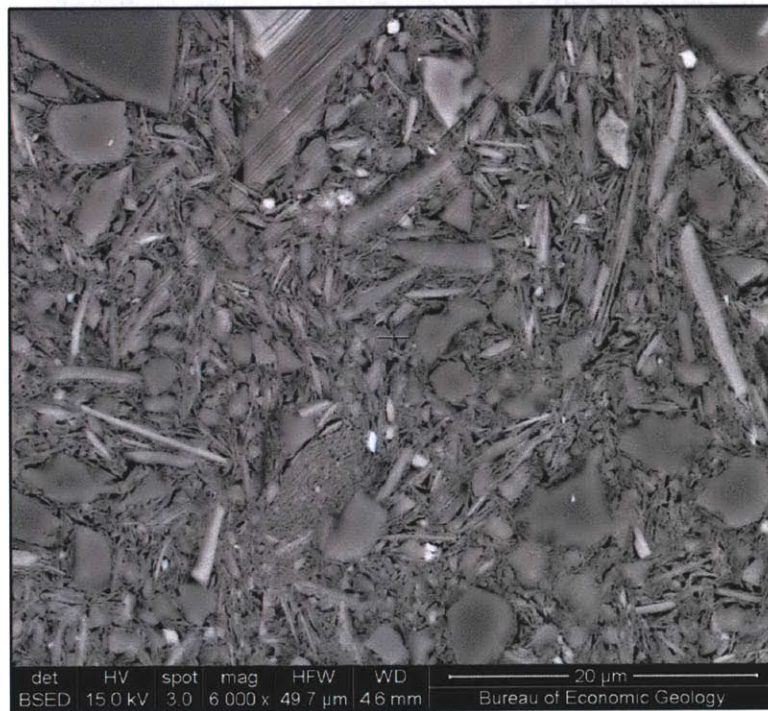
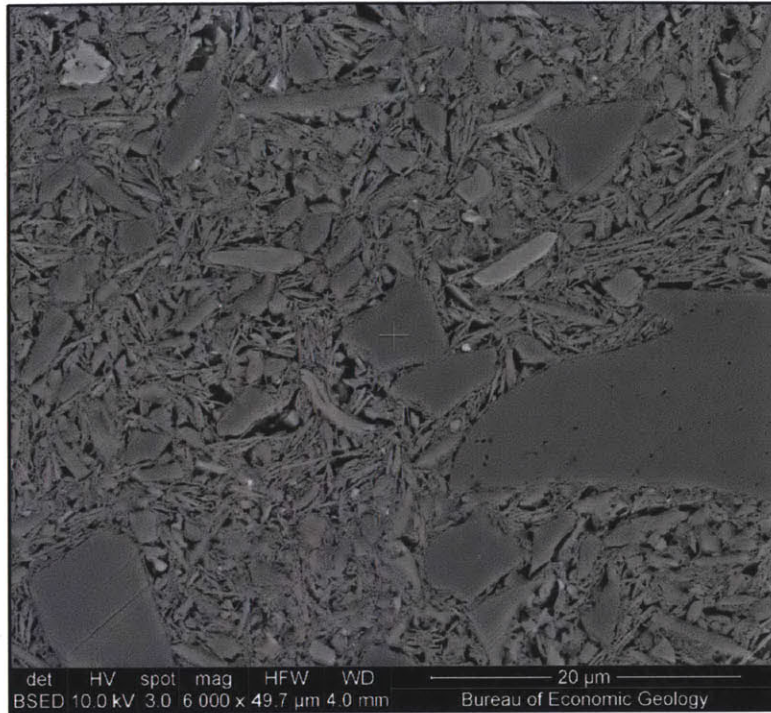


Figure 3.35 SEM images of sodium hex RBBC at a pore fluid salinity of 0 g/l and a stress level of 100 kPa (top) and 10,000 kPa (bottom) at same magnification. (corresponding void ratio top image ~ 1.01, bottom image ~ 0.48)

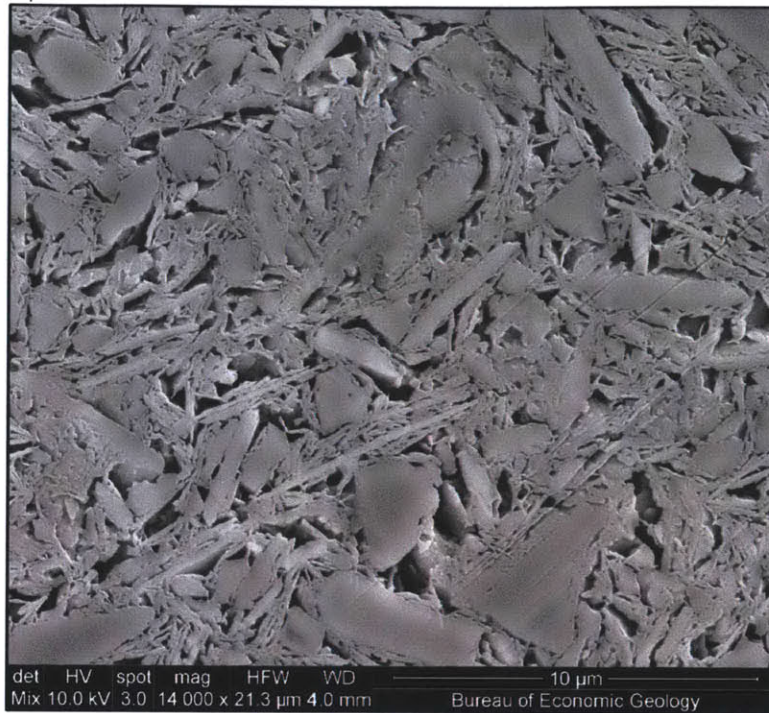


Figure 3.36 SEM images of sodium hex RBBC at a pore fluid salinity of 0 g/l and a stress level of 100 kPa on top, and natural RBBC Series IV at a salinity of 4 g/l and a stress of 100 kPa on bottom (corresponding void ratios, ~ 1.01 top image, ~ 1.26 on bottom)



Figure 3.37 Location of London (Google Earth)

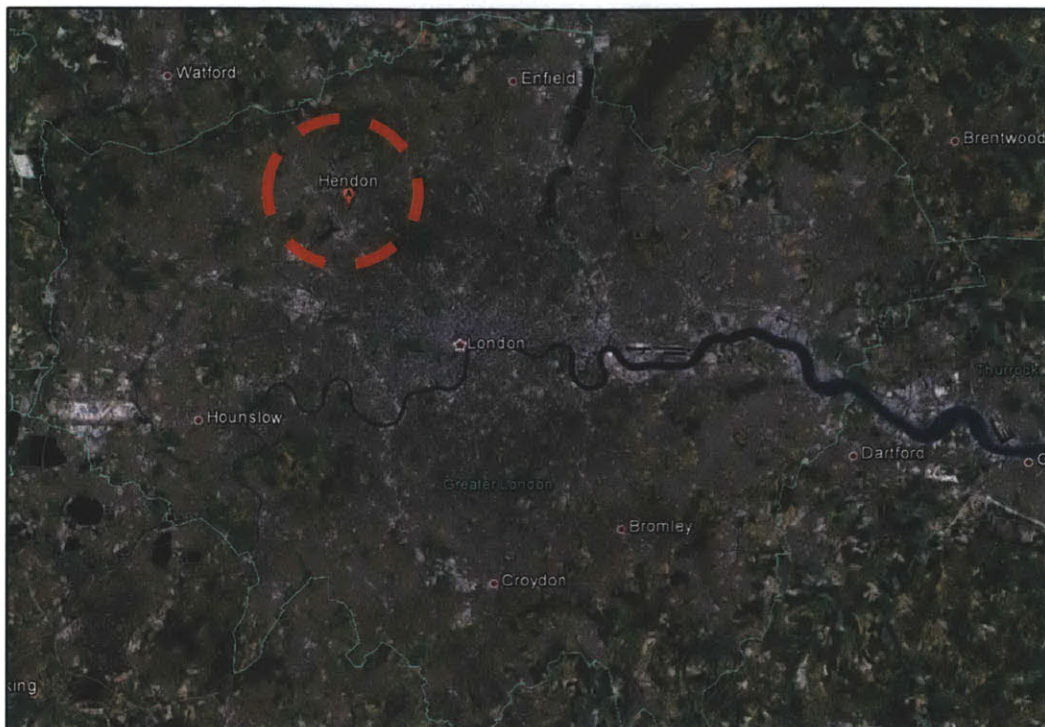


Figure 3.38 Location of Hendon relative to Greater London (Google Earth)

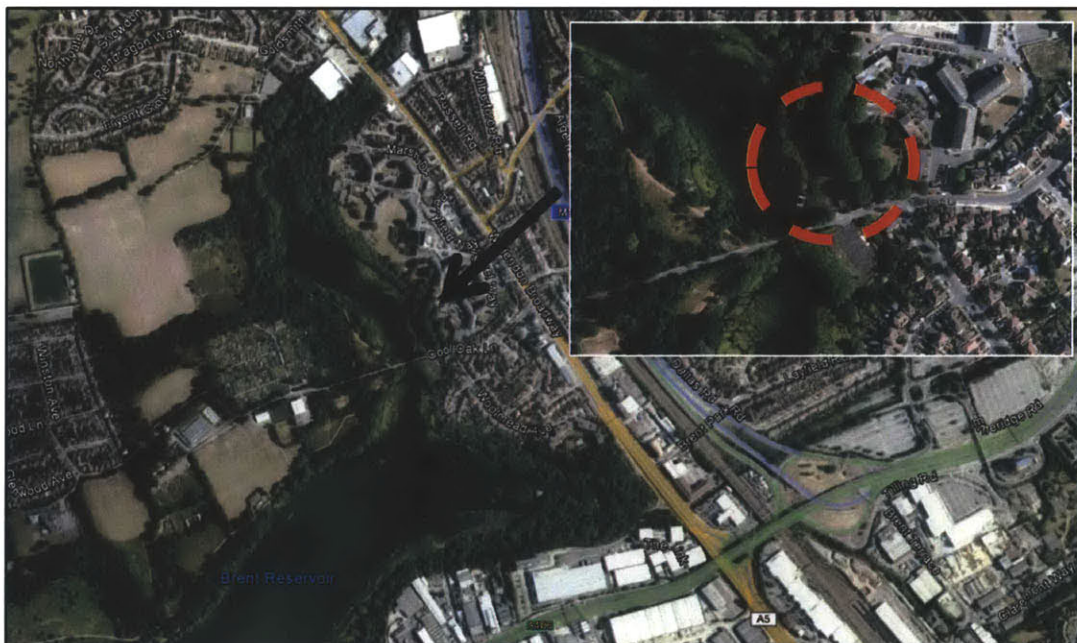


Figure 3.39 Location of source in Hendon, actual site identified with red circle, site coordinates:
Latitude - 51°34'31.94"N Longitude - 0°14'30.83"W (Google Earth)



Figure 3.40 Brown firm weathered London Clay as recovered from the ground at project location (West Hendon development, SI document)

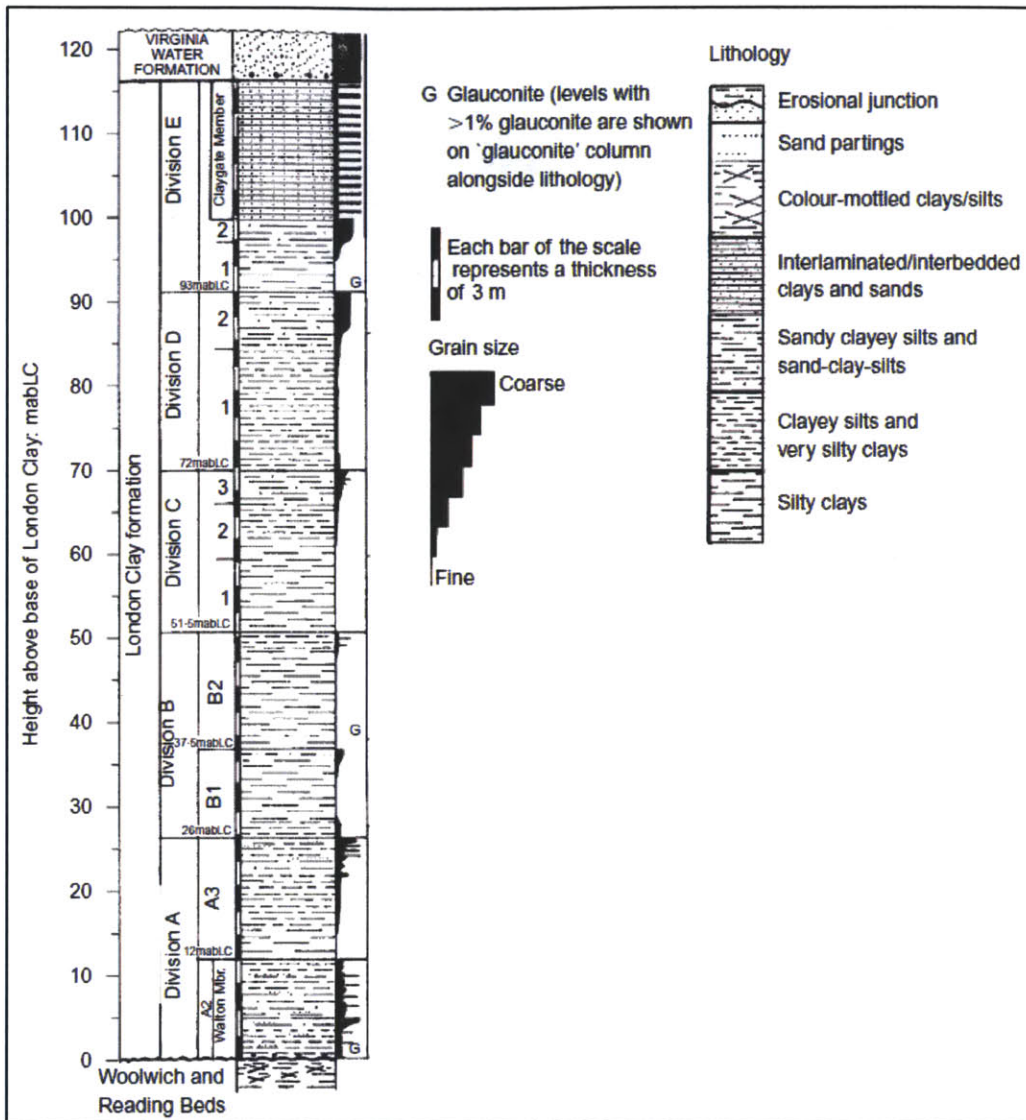


Figure 3.41 Stratigraphic sequence for central London (after King, 1981)



Figure 3.42 Photograph of a typical chunk of London Clay with inclusions visible on a surface cut with a razor blade



Figure 3.43 Quartz inclusions visible in London Clay as received to MIT Geotechnical Laboratory (magnification x2)

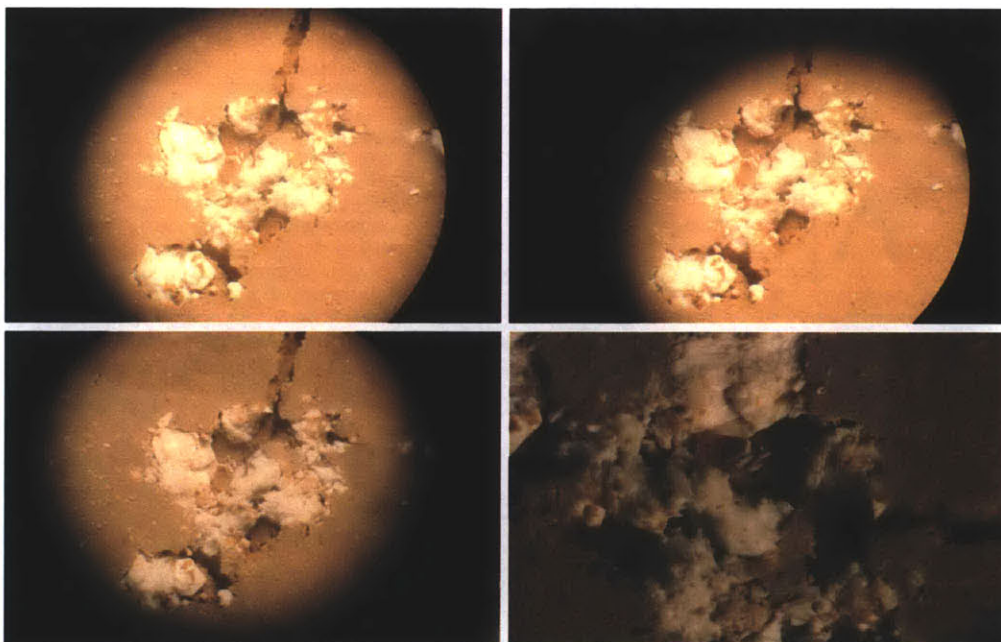


Figure 3.44 White quartz inclusions in London Clay as received to MIT Geotechnical Laboratory (magnification x1, bottom right x2)

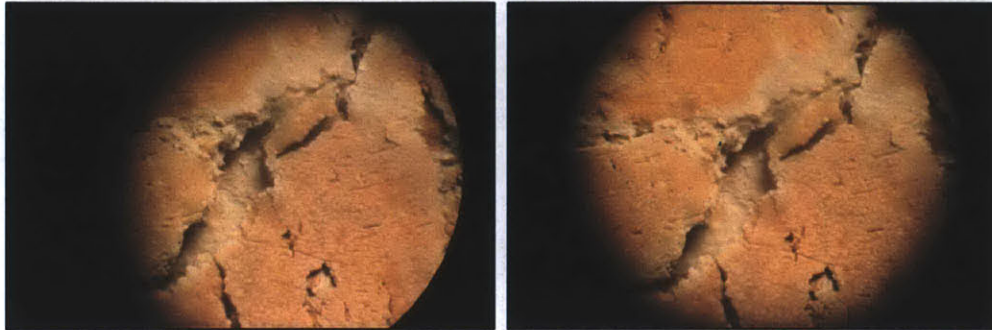


Figure 3.45 Blue staining visible as veins on the surface of London Clay received to the MIT Geotechnical Laboratory (magnification x1)

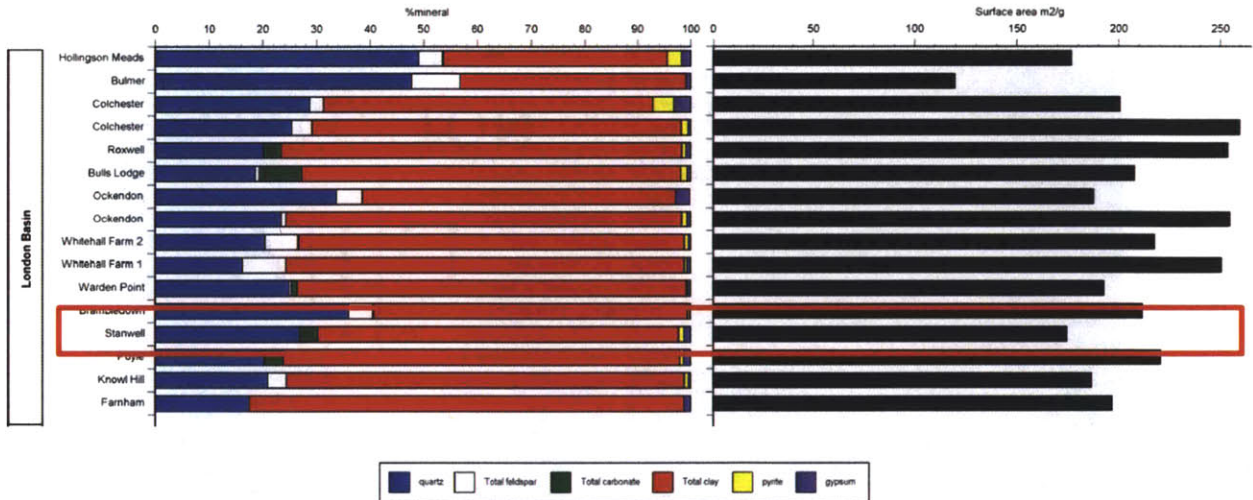


Figure 3.46 Whole rock mineralogy and corresponding surface area for London Clay from multiple locations - location closest to Hendon has been identified (British Geological Survey, 2006)

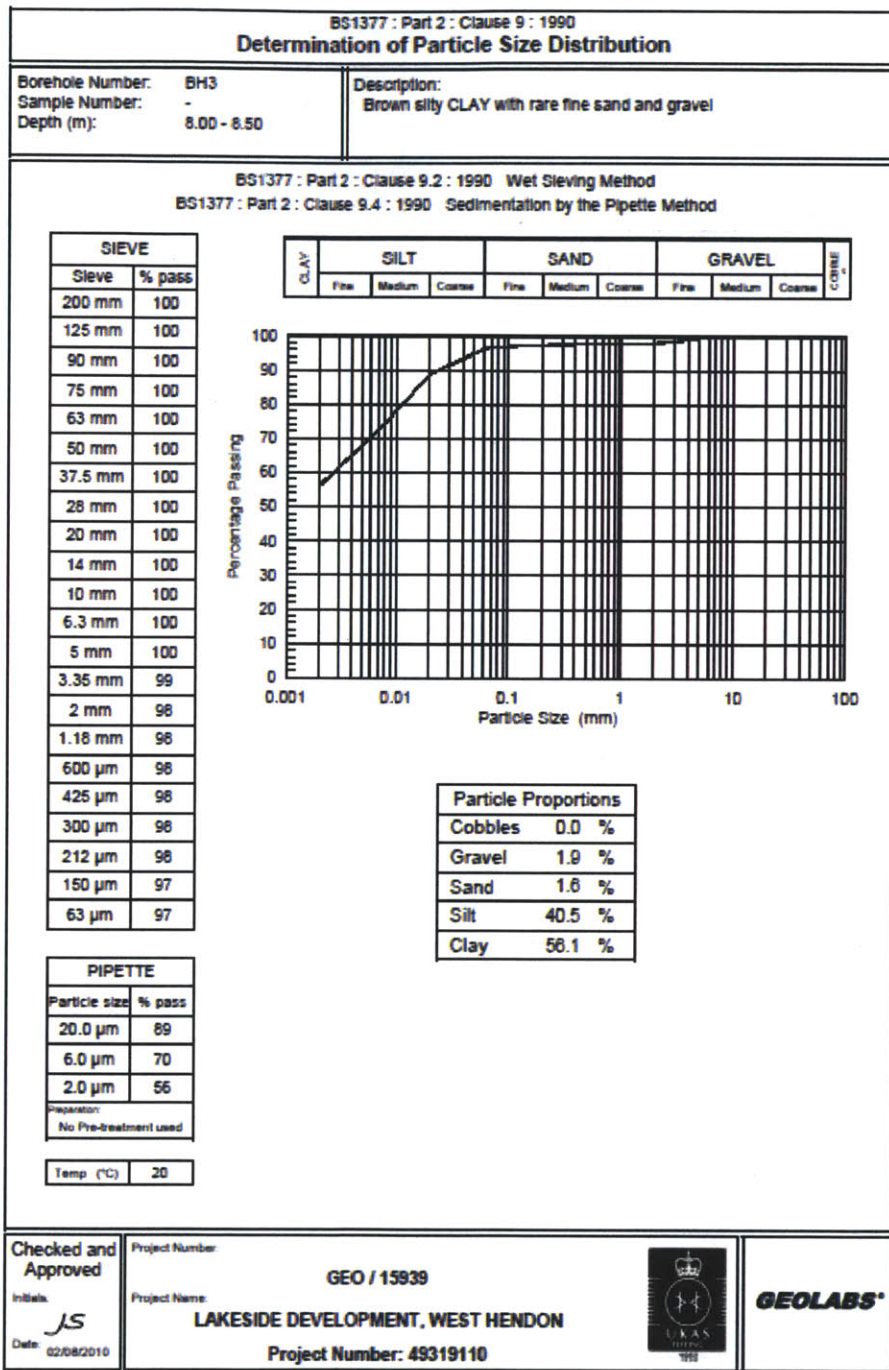


Figure 3.47 Particle size distribution by sedimentation test performed on London Clay at a similar depth to soil which was shipped to MIT (West Hendon development, SI document)

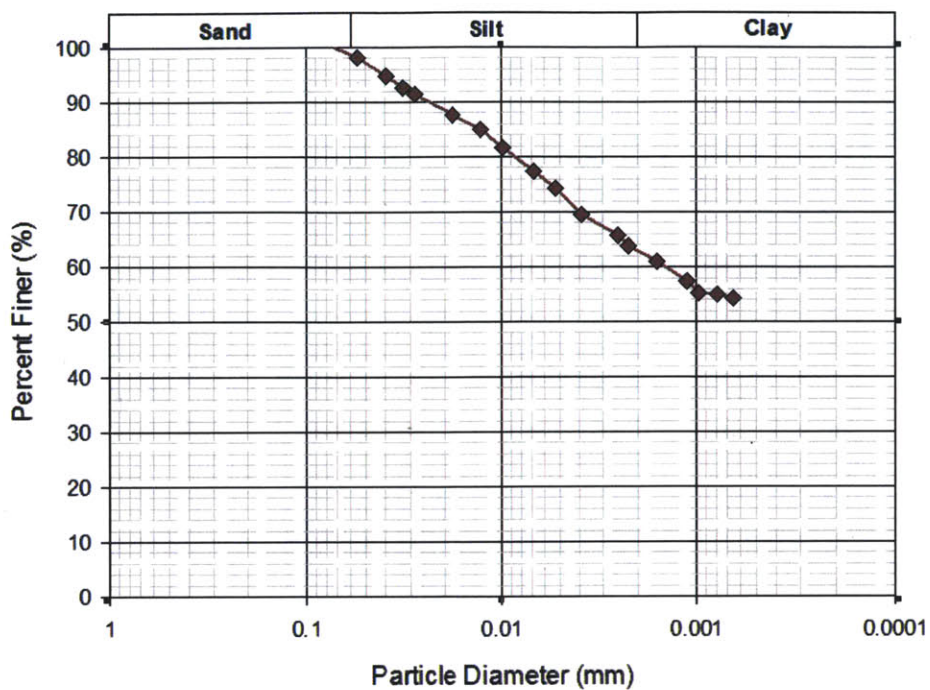


Figure 3.48 Particle size distribution performed on ground London Clay powder in the MIT Geotechnical Laboratory (tested by Brendan Casey)

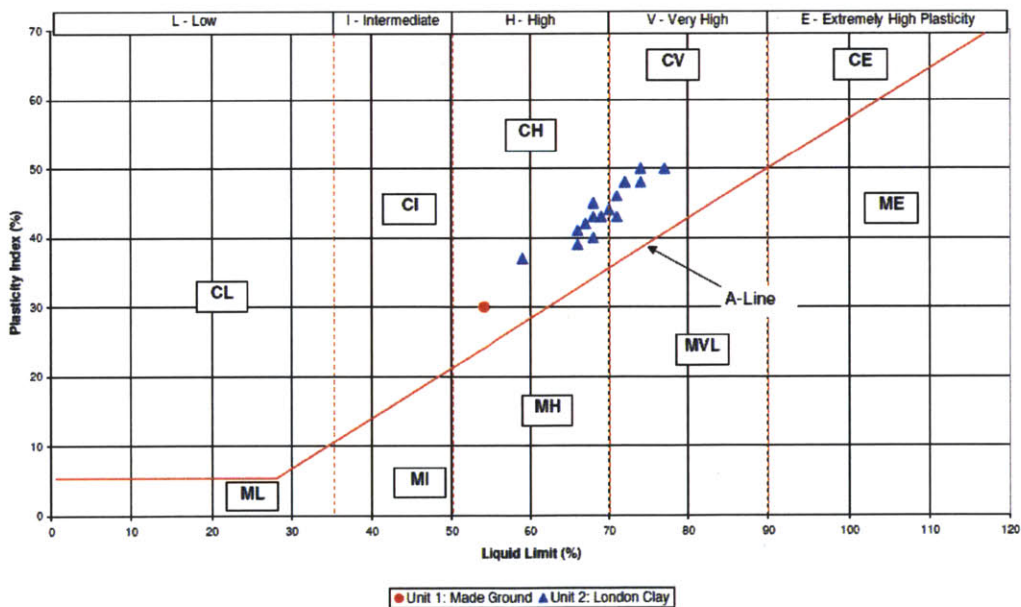


Figure 3.49 Atterberg limits performed on London Clay from project location. Note: testing depths uncertain (West Hendon development, SI document)

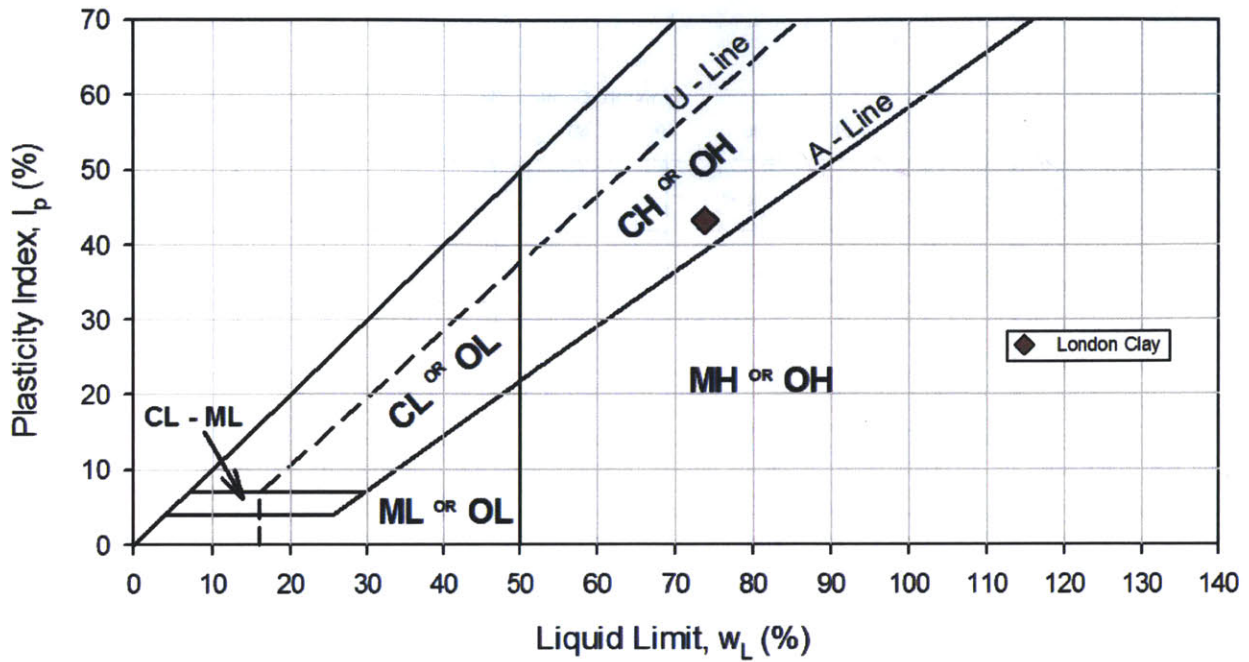


Figure 3.50 Atterberg limits performed at MIT on London Clay from Hendon

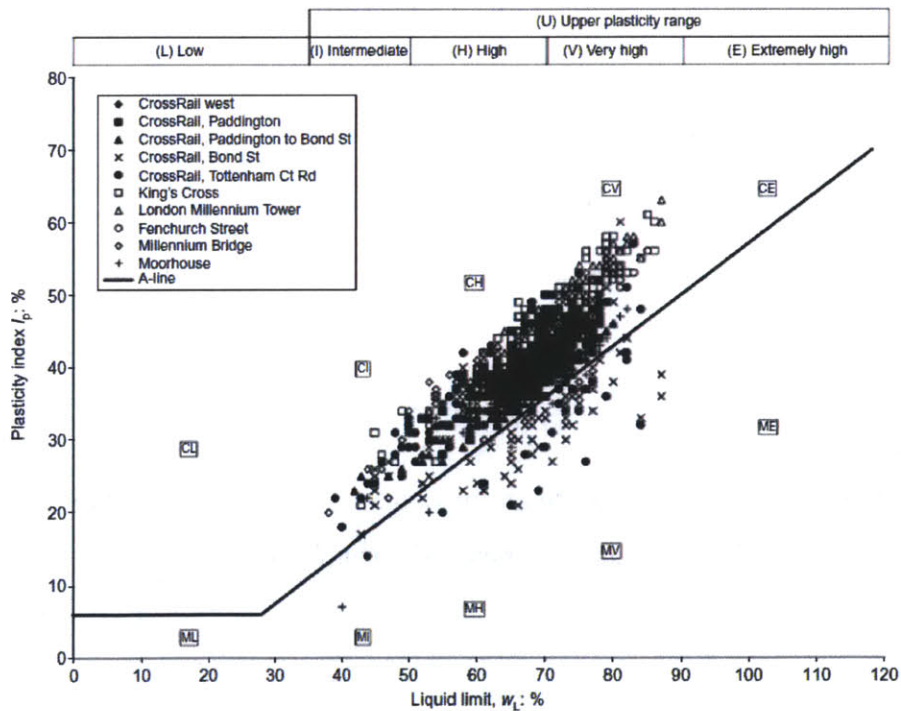


Figure 3.51 Plasticity results for specimens from multiple locations in London (Pantelidou & Simpson, 2007)

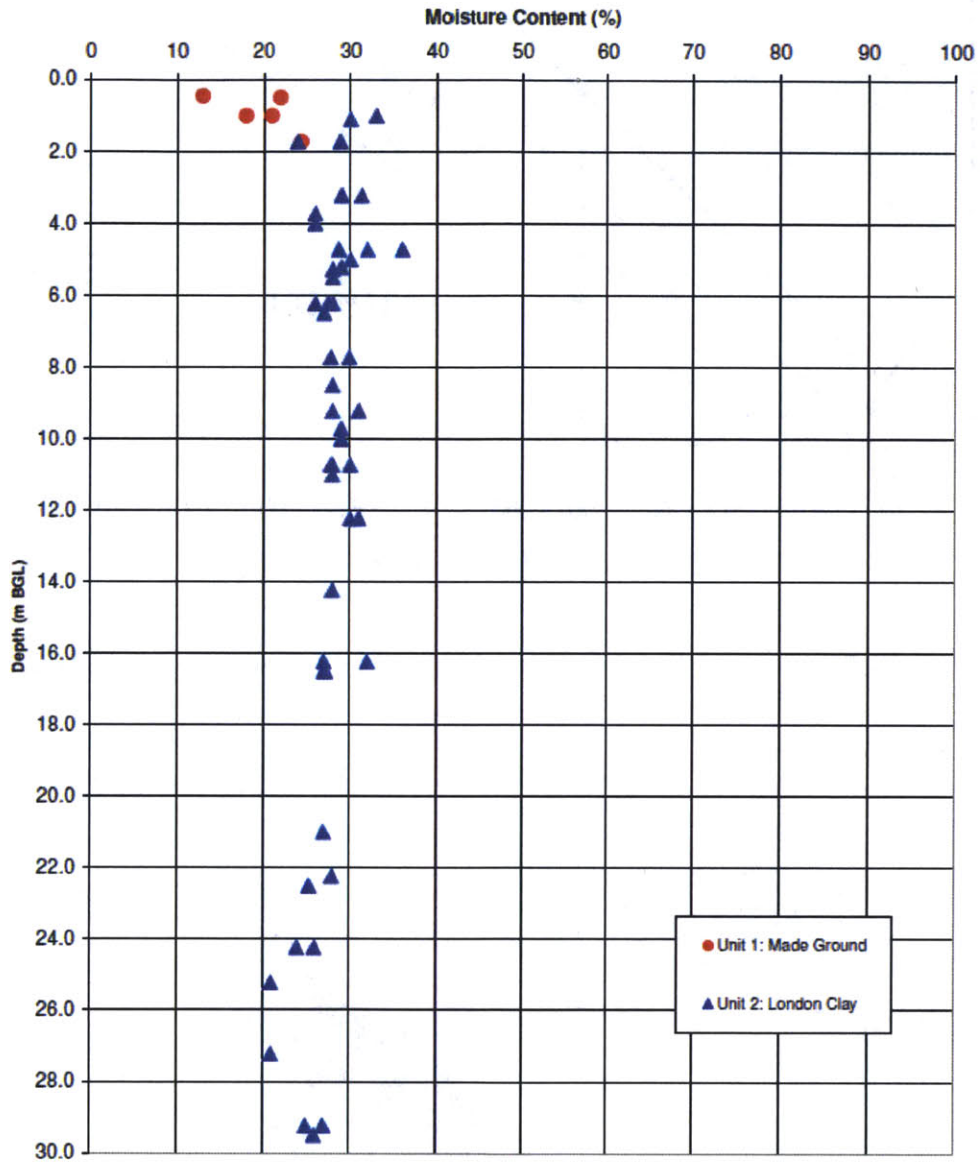


Figure 3.52 Moisture content versus depth for London Clay at project location (West Hendon development, SI document)

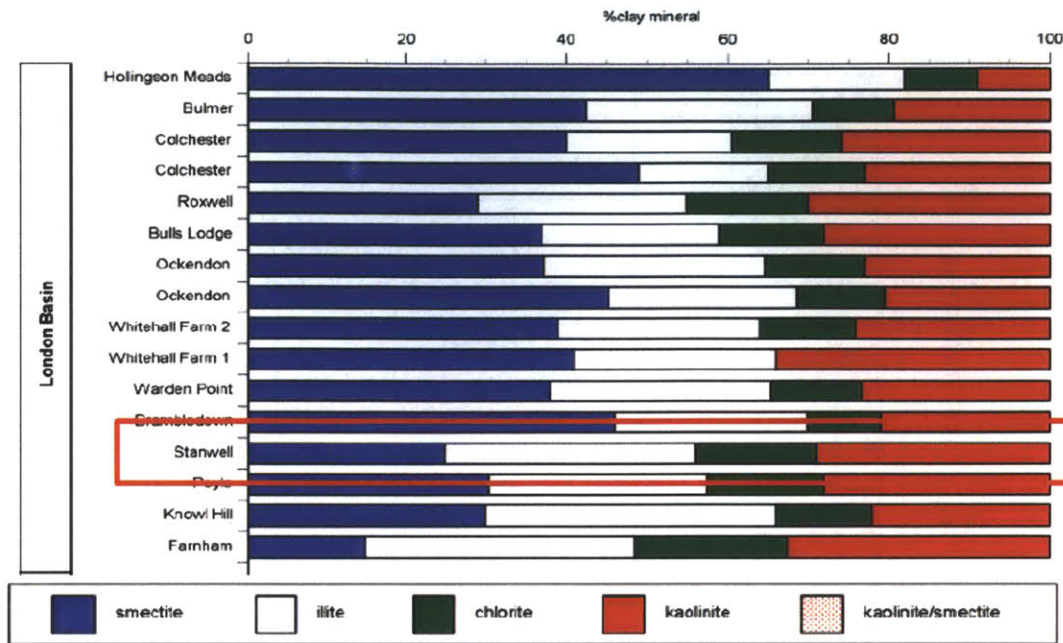


Figure 3.53 Mineralogy of London Clay - location closest to Hendon has been identified (British Geological Survey, 2006)

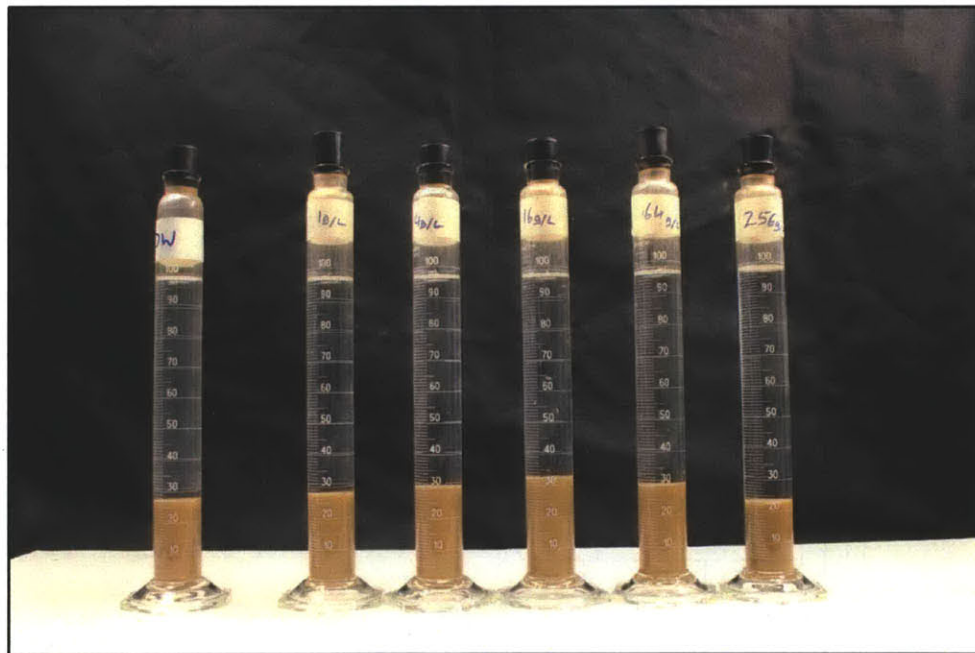


Figure 3.54 Sedimentation test performed on natural London Clay powder. Salinities from L-R: 0 (distilled water), 1, 4, 16, 64 & 256 g/l NaCl. 5 grams of soil used in each tube

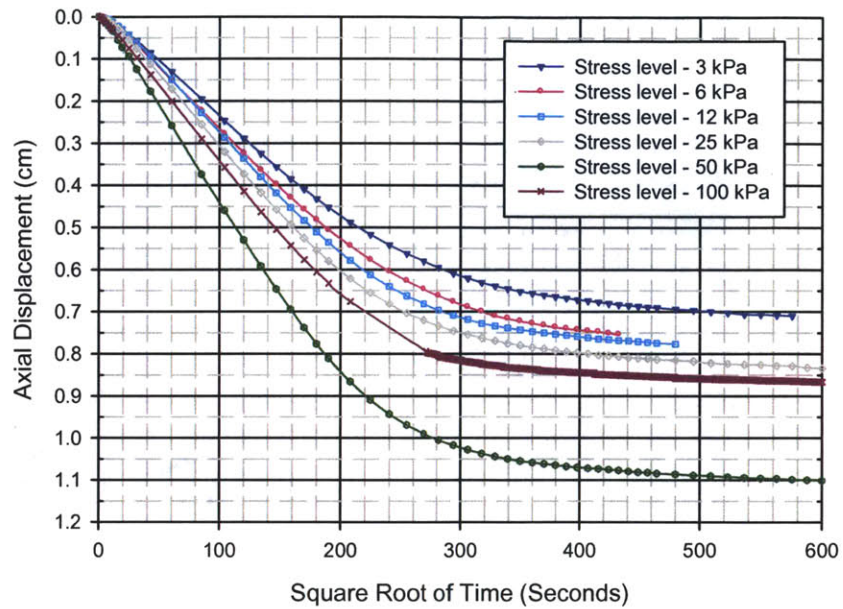


Figure 3.55 Axial displacement versus root time for London Clay at different stress levels (data from RS232, London Clay at 44 g/l)

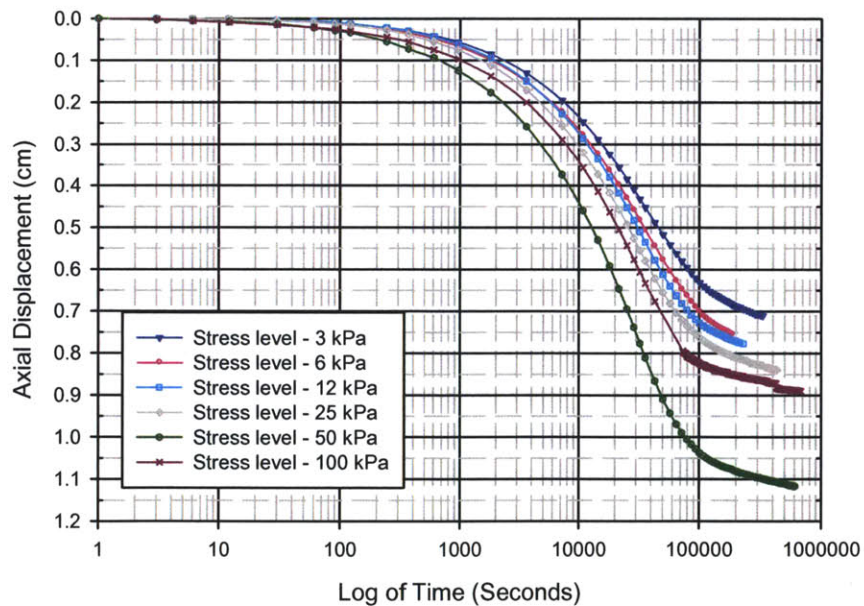


Figure 3.56 Axial displacement versus log time for London Clay at different stress levels (data from RS232, London Clay at 4 g/l)

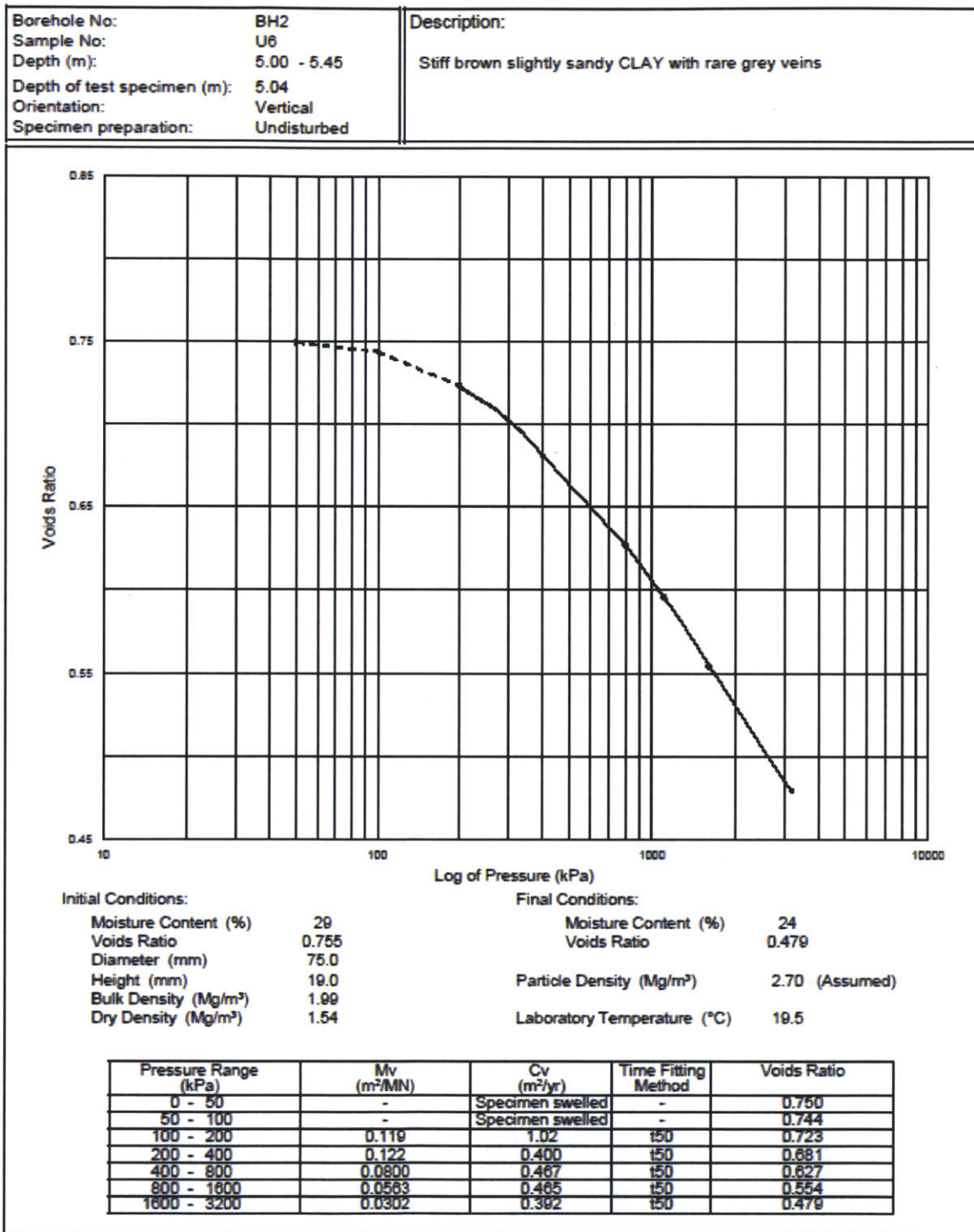


Figure 3.57 Oedometer test results on intact London Clay from West Hendon development recovered at 5.04 m depth (West Hendon development, SI document)

Borehole No:	BH4	Description: Stiff brown slightly sandy CLAY
Sample No:	U10	
Depth (m):	9.50 - 9.95	
Depth of test specimen (m):	9.53	
Orientation:	Vertical	
Specimen preparation:	Undisturbed	

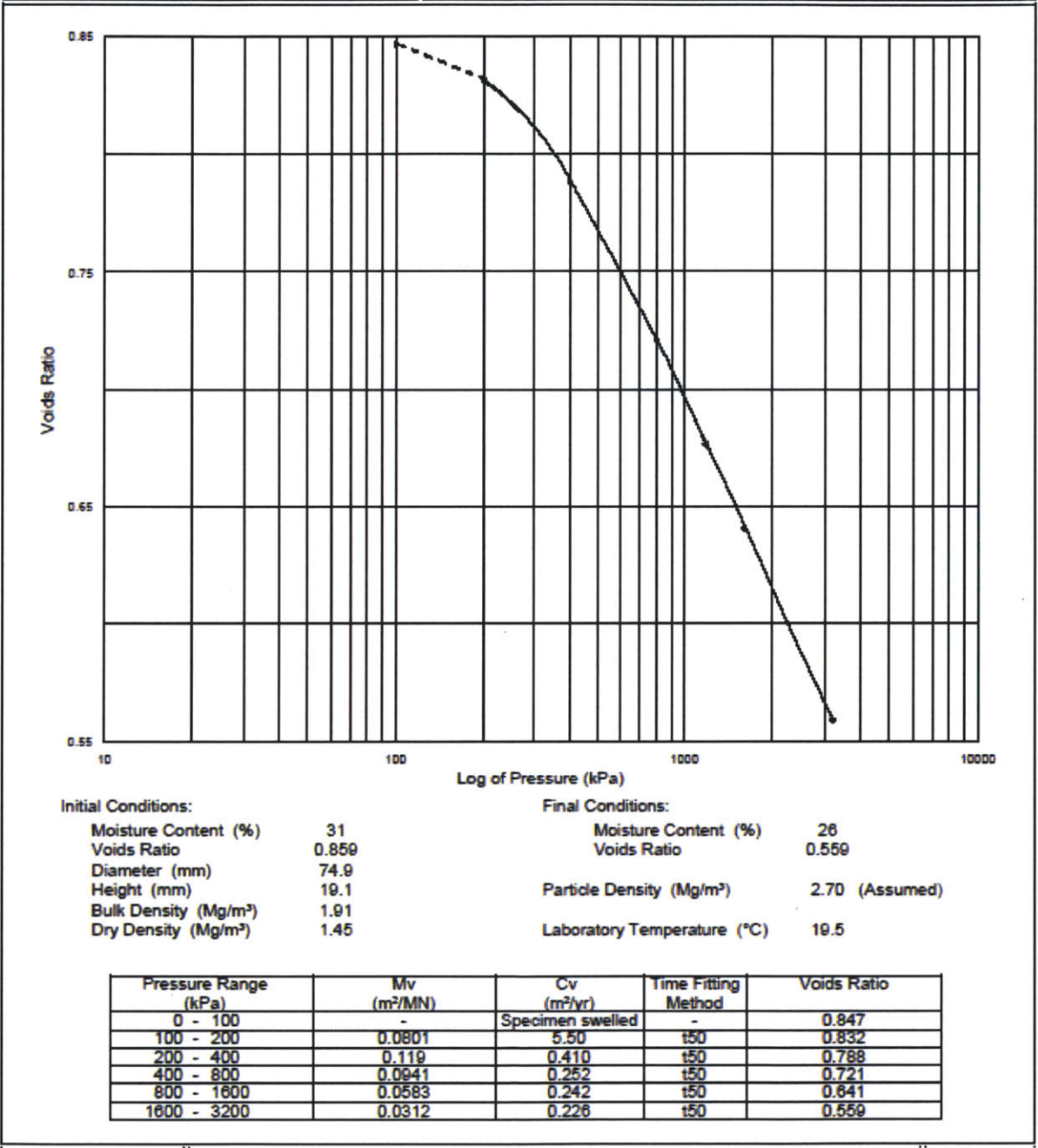


Figure 3.58 Oedometer test results on intact London Clay from West Hendon development recovered at 9.53 m depth (West Hendon development, SI document)

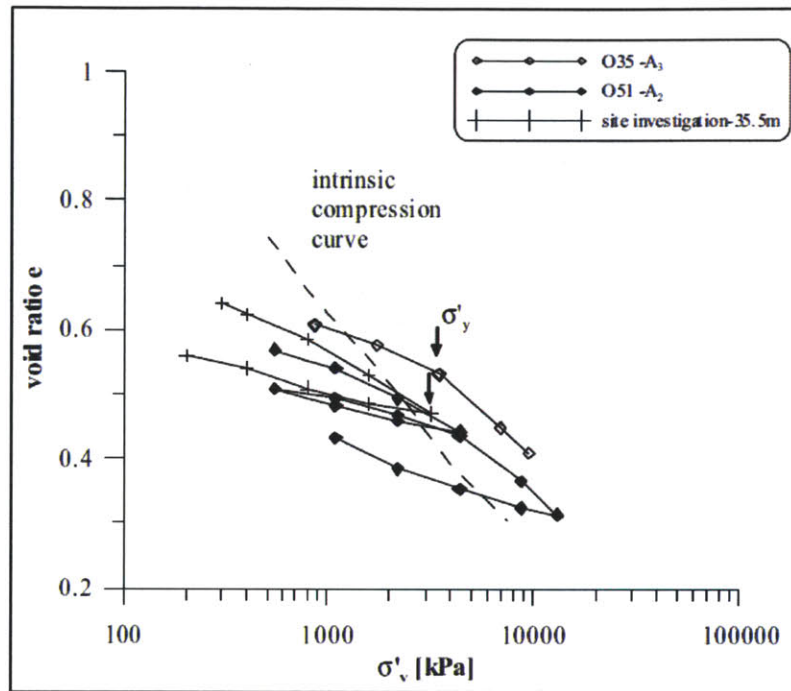


Figure 3.59 Compression data from natural in-tact specimens of London Clay tested in the oedometer. Specimen A₃ recovered between 45-48 m deep, specimen A₂ recovered between 48-52 m deep (Gasparre, 2005)

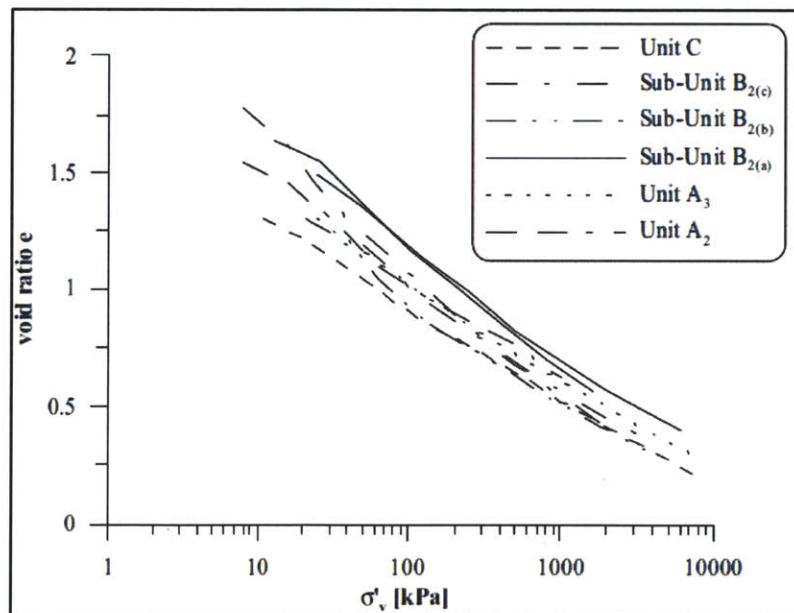


Figure 3.60 Compression data from reconstituted specimens of London Clay tested in the oedometer (Gasparre, 2005)

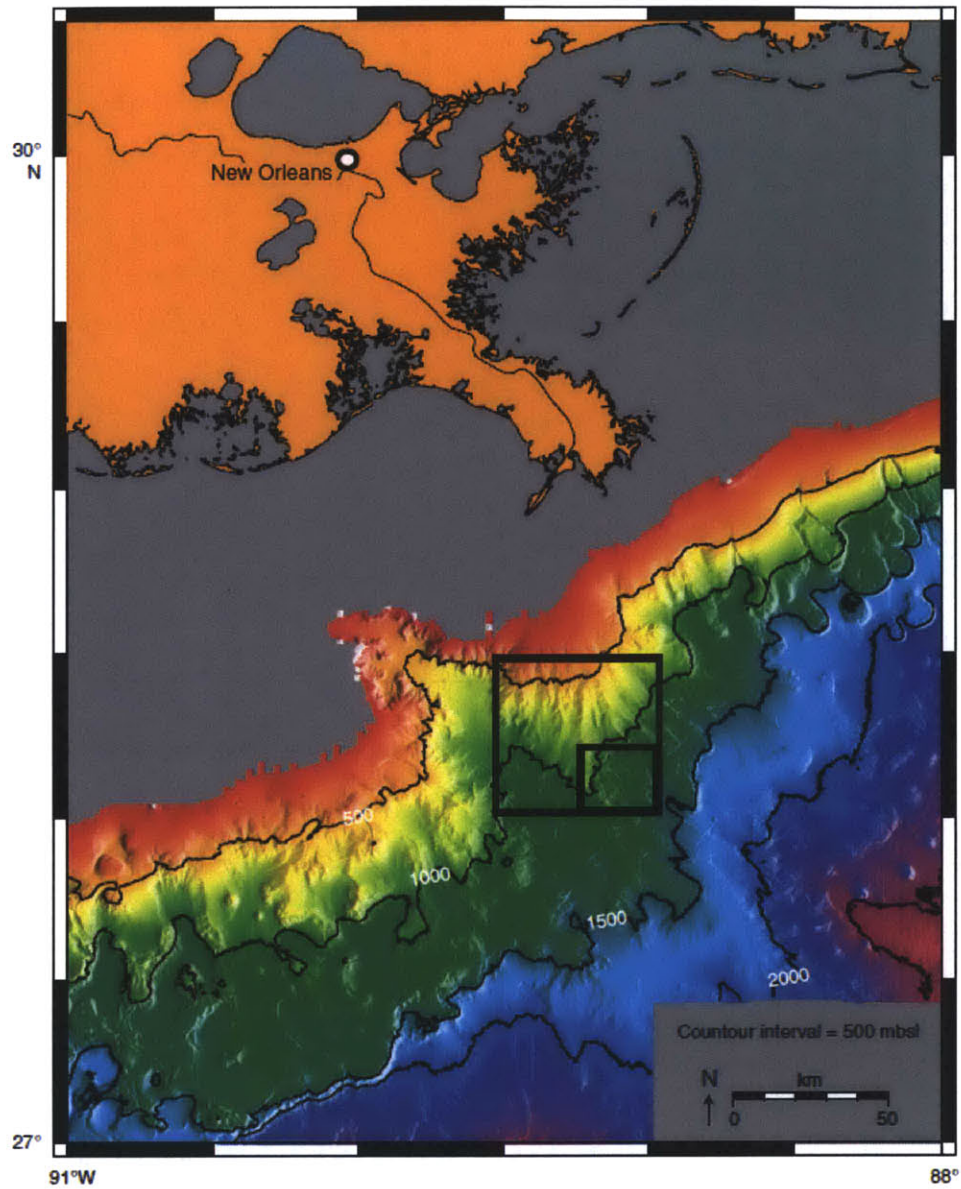


Figure 3.61 Location map of Ursa Basin where IODP Leg 308 performed exploratory borings. Small box represents exploration area (IODP Expedition 308 Report, 2006)

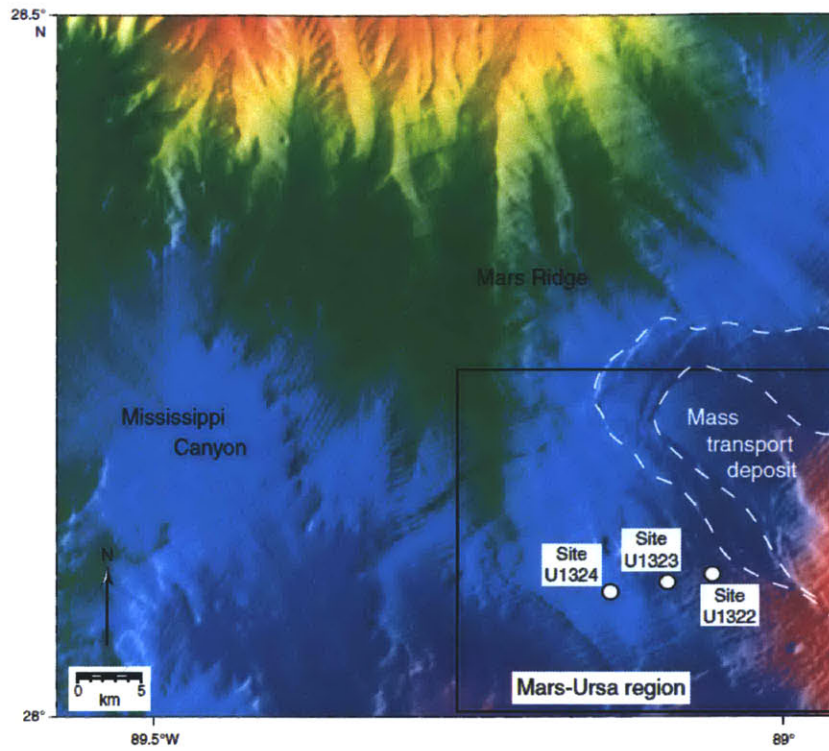


Figure 3.62 Map showing borings performed as part of IODP - Leg 308. Soil tested obtained from Site U1322 (IODP Expedition 308 Report, 2006)

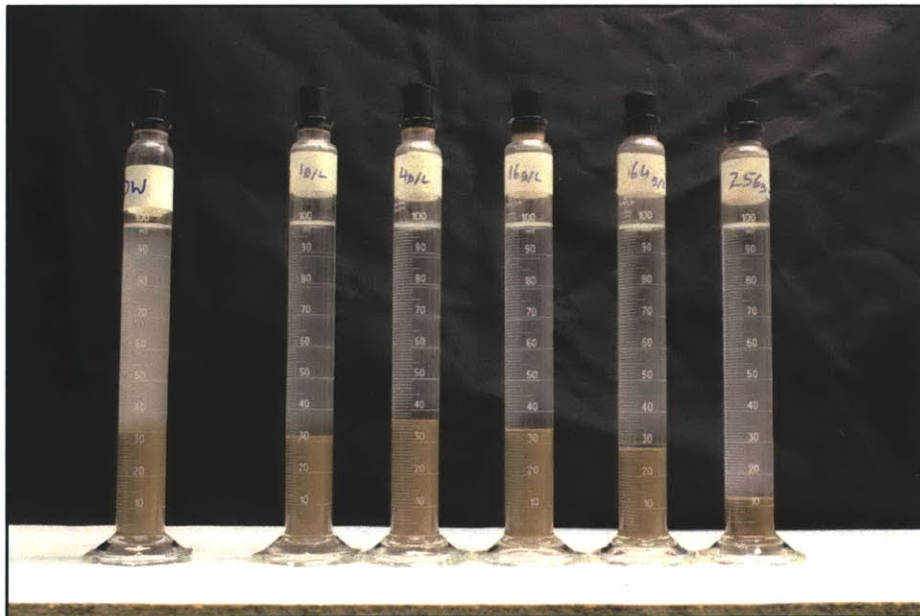


Figure 3.63 Sedimentation test performed on RGOM - Ursa. Salinities from L-R 0, 1, 4, 16, 64 & 256 g/l NaCl. Note: 5 g of soil used in each tube

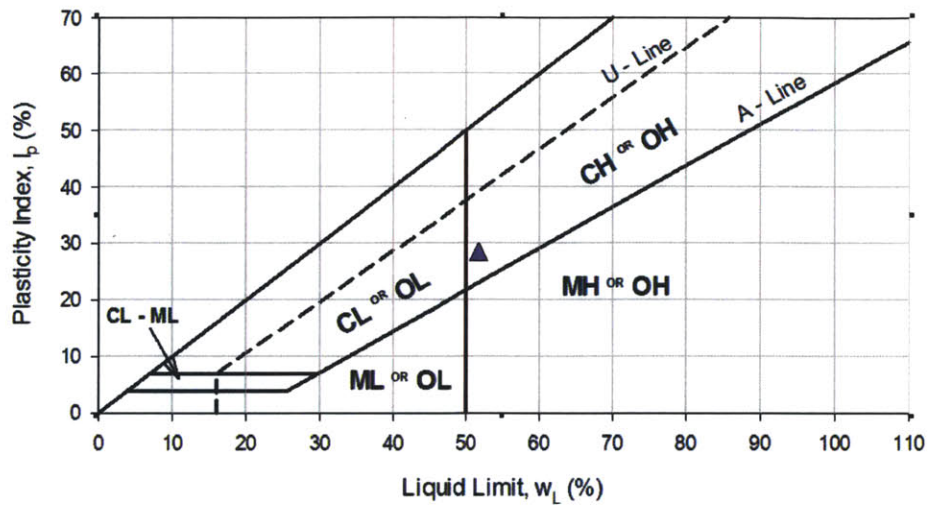


Figure 3.64 Plasticity chart showing where GOM-Ursa soil plots

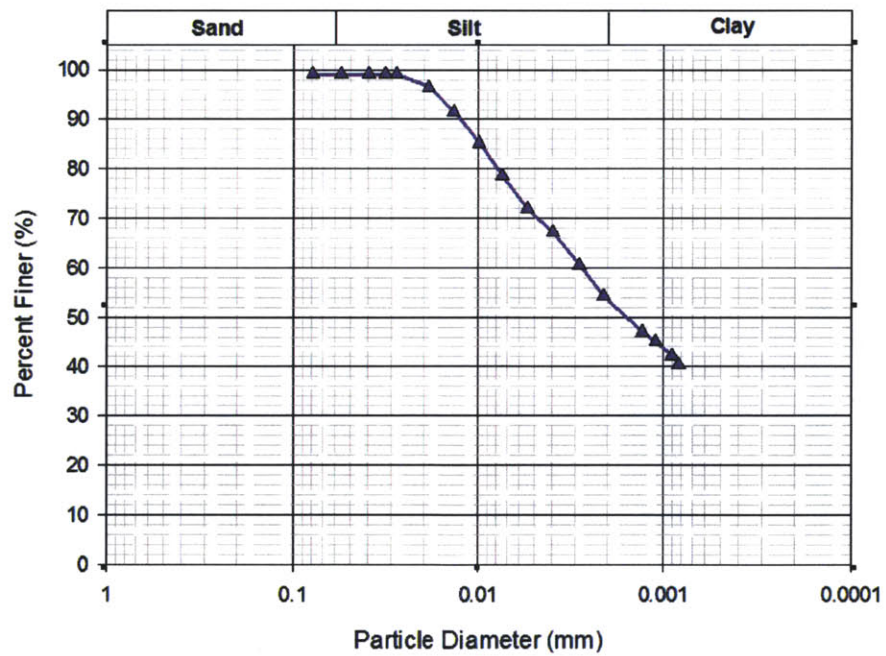


Figure 3.65 Particle size distribution for GOM-Ursa performed by Brendan Casey

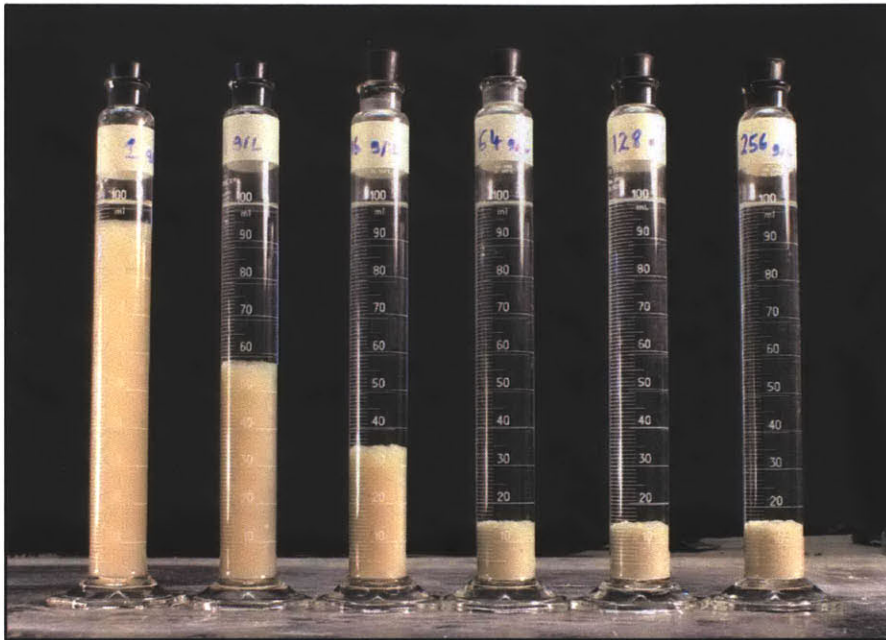


Figure 3.66 Sedimentation test performed on sodium montmorillonite. Salinities from L-R 1, 4, 16, 64, 128 & 256 g/l NaCl. Note: 1 g of soil used in each tube

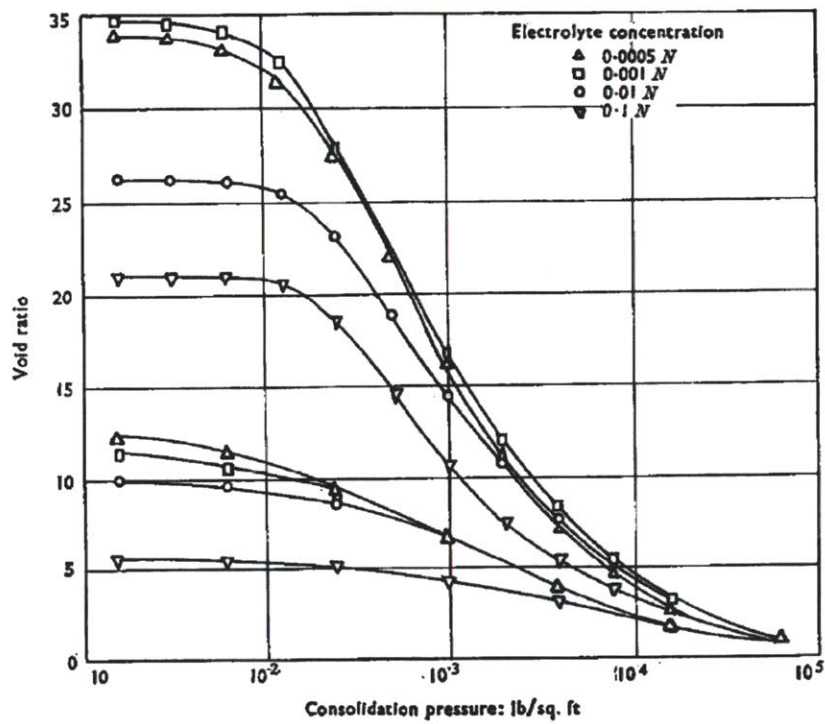


Figure 3.67 One dimensional consolidation curves for sodium montmorillonite

Note: 10 lb/ft² = 0.479 kPa (Mesri & Olsen, 1971_a)

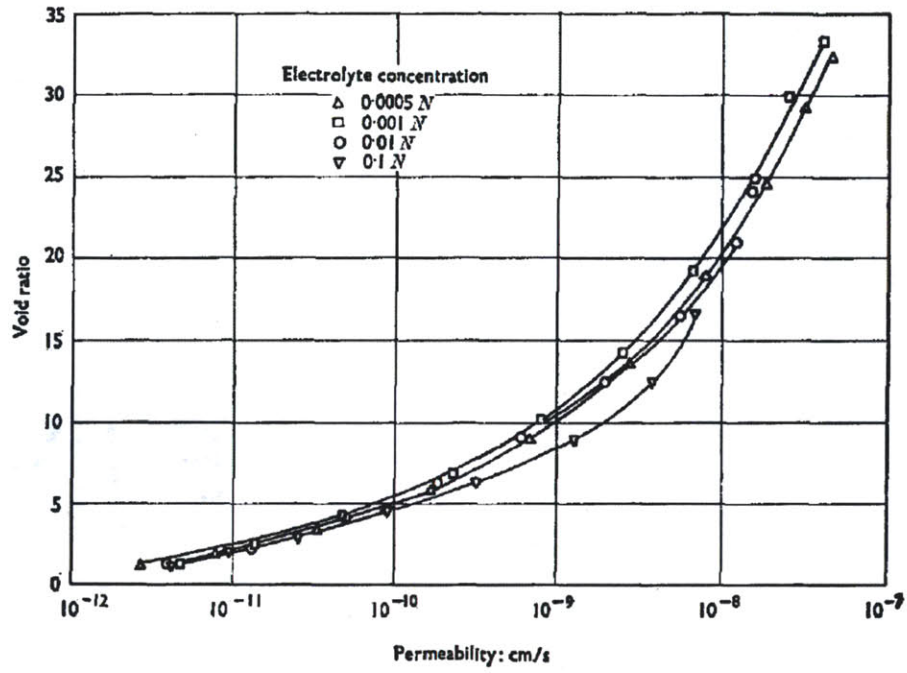


Figure 3.68 Hydraulic Conductivity versus void ratio curves for sodium montmorillonite (Mesri & Olsen, 1971_a)

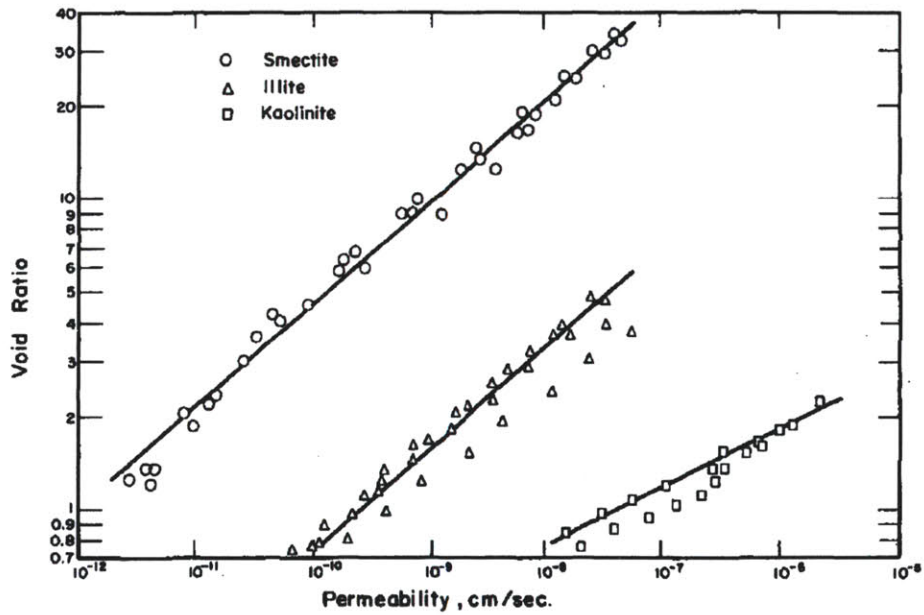


Figure 3.69 Hydraulic conductivity versus void ratio for all three sodium clays in water (Mesri & Olsen, 1971_b)

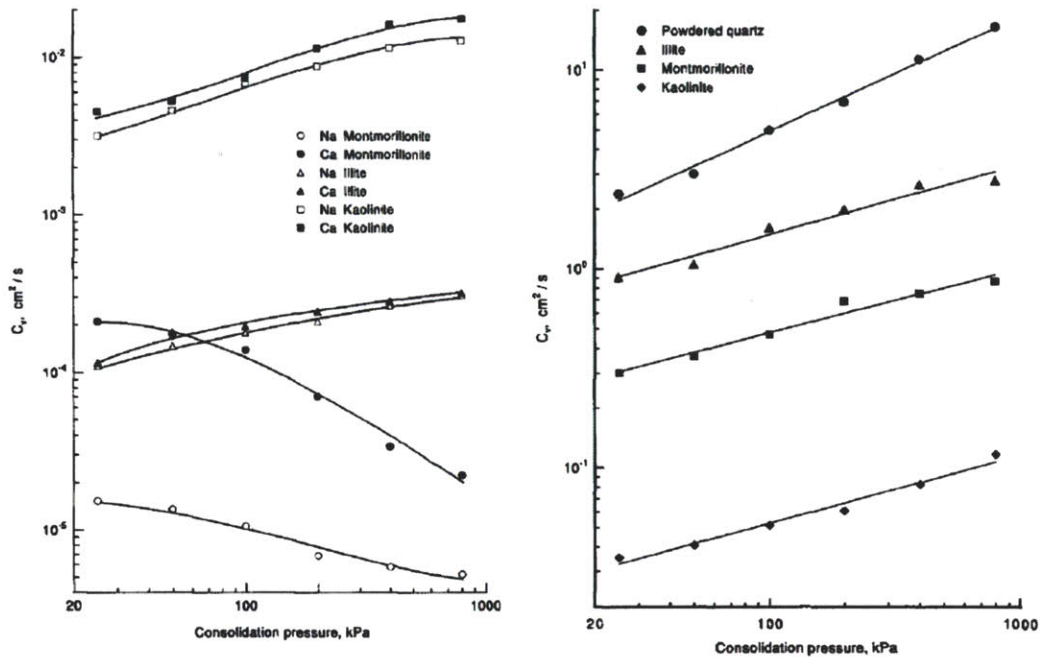


Figure 3.70 Variation in coefficient of consolidation, c_v with axial consolidation stress for clay minerals with water as the pore fluid on left, and with CCL_4 (carbon tetrachloride, which negates the double layer) on the right (Robinson & Allam, 1998)

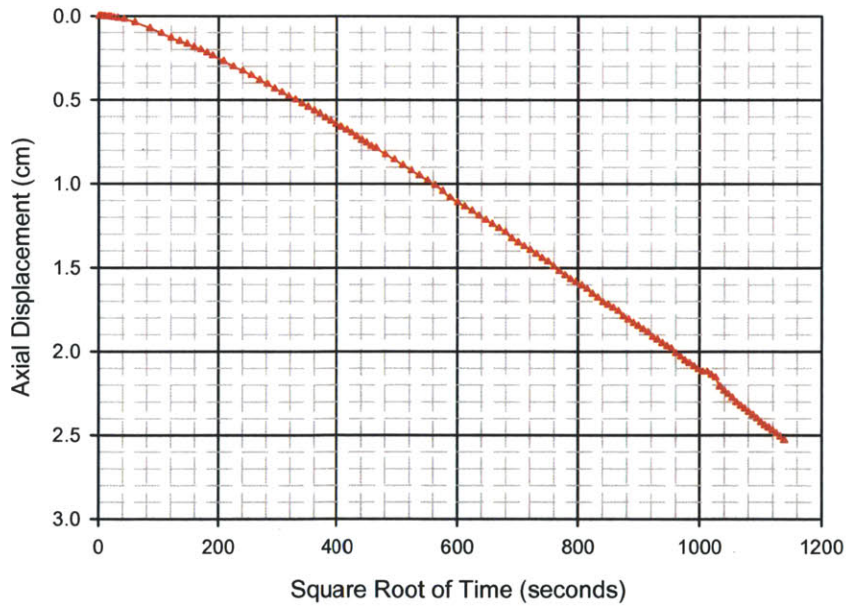


Figure 3.71 Square root of time versus axial displacement for 1 g/l montmorillonite (data from RS245 - target stress level 50 kPa)

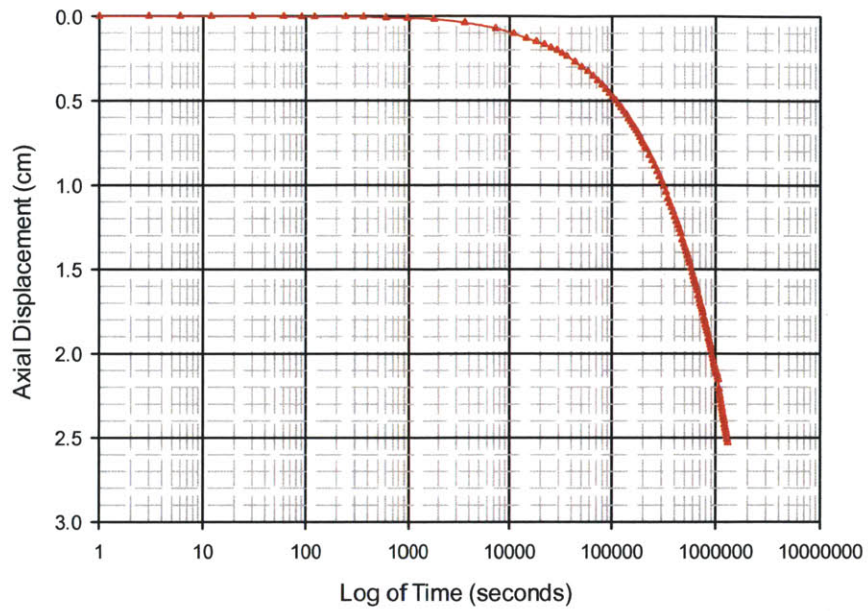


Figure 3.72 Log of time versus axial displacement for 1 g/l montmorillonite (data from RS245 - target stress level 50 kPa)

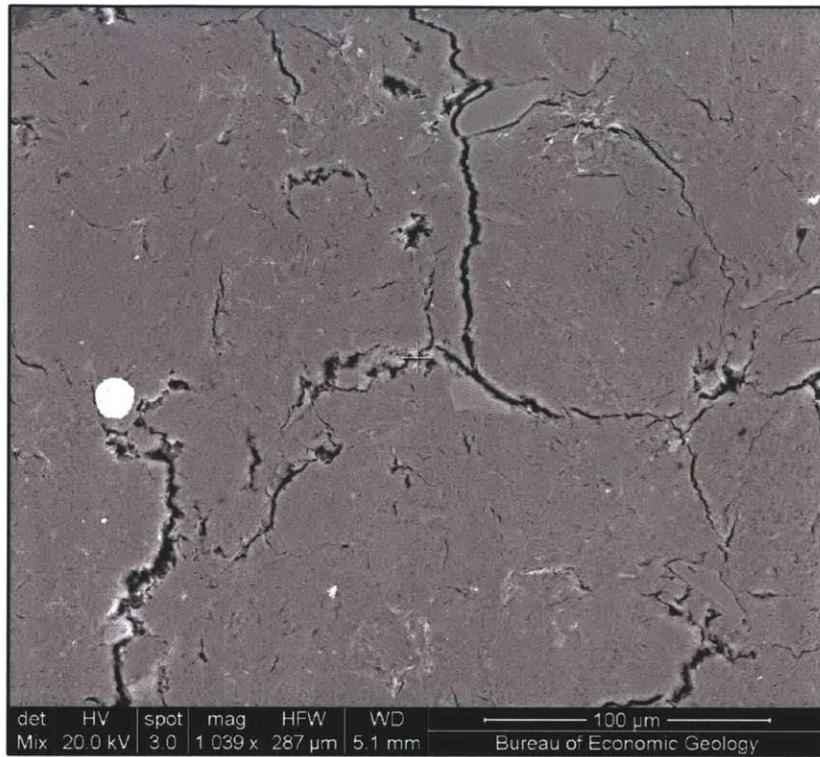


Figure 3.73 Images of sodium montmorillonite resedimented with 256 g/l pore water at a stress level of 200 kPa. Note: different magnification. (corresponding void ratio 1.58)

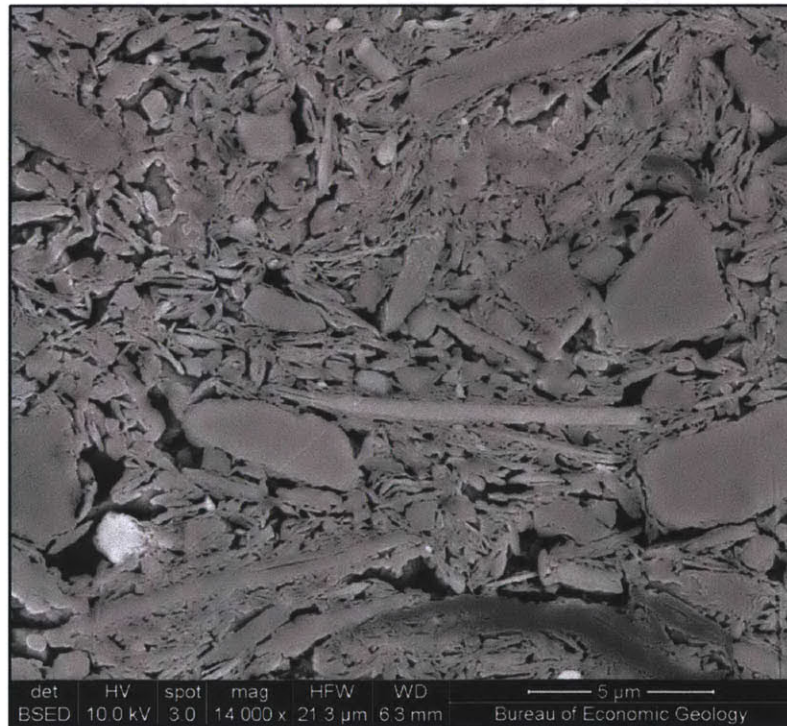
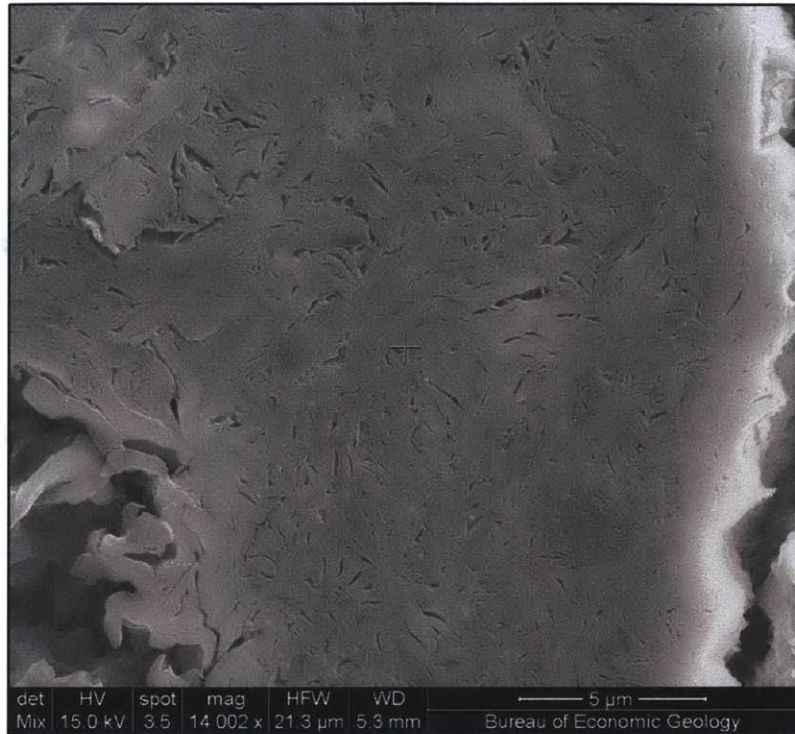


Figure 3.74 Comparison between sodium motmorillonite and natural RBBC Series IV at similar stress levels and at the same pore fluid salinity. Sodium montmorillonite (top) at 200 kPa BBC (bottom) at 100 kPa. Corresponding void ratios 1.58 (SM) and 1.16 (RBBC).

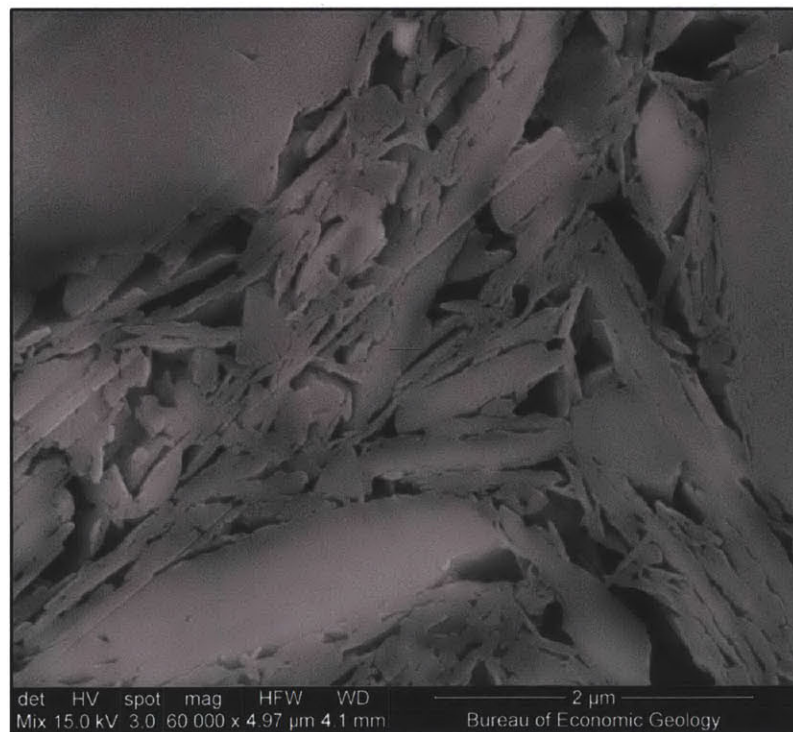
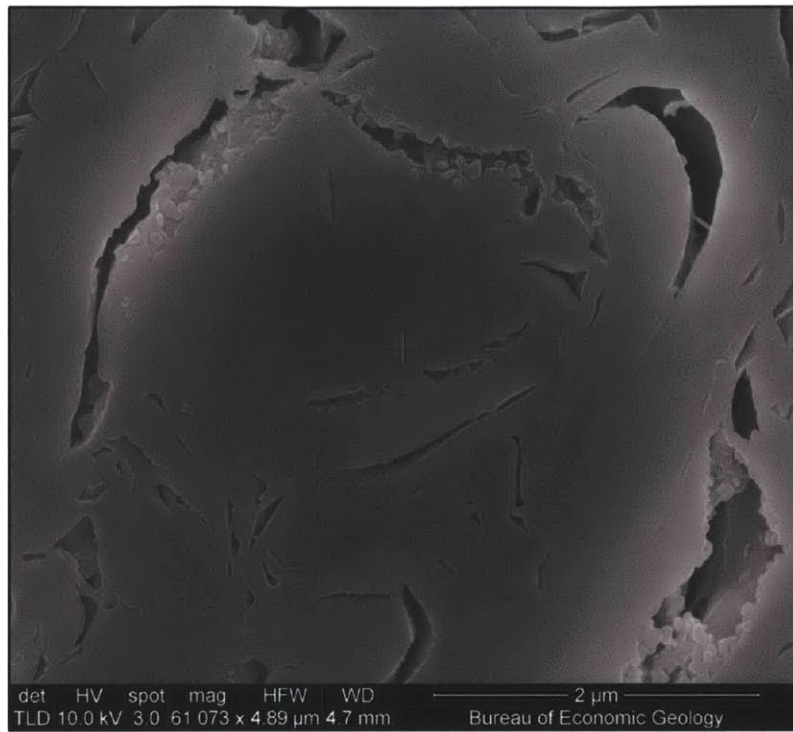


Figure 3.75 Comparison between sodium motmorillonite and sodium hex BBC at similar stress levels at the same magnification. Sodium montmorillonite (top) at 200 kPa, sodium hex BBC (bottom) at 100 kPa. Corresponding void ratios 1.58 (SM) and 0.98 (RBBC)

4 MATERIAL PROCESSING, EQUIPMENT AND TESTING PROCEDURES

4.1 INTRODUCTION

This chapter describes the equipment and procedures used in the testing program. The 1-D compression and permeability data for resedimented Boston Blue Clay Series IV, leached Boston Blue Clay, in-situ Boston Blue Clay, sodium hex Boston Blue Clay, Gulf of Mexico soil, London Clay and sodium montmorillonite were obtained using a modified Trautwein Constant Rate of Strain (CRS) cell. This CRS cell was also used to perform reverse leaching tests on leached Boston Blue Clay. This test will be described in the latter part of this chapter. Strength testing was performed on resedimented Boston Blue Clay Series IV, leached Boston Blue Clay and in-situ Killian Court Boston Blue Clay using a low pressure automated stress path triaxial apparatus originally developed in the MIT geotechnical laboratory by Sheahan (1991).

The one dimensional CRS consolidation tests were performed on small diameter specimens which were resedimented to a axial effective stress of 100 kPa and then tested in the CRS device to a axial effective stress of 10,000 kPa. Selected London Clay and Gulf of Mexico specimens were stressed to an axial effective stress of 40,000 kPa. All Boston Blue Clay specimens were consolidated at a strain rate of 2 %/hour, London Clay specimens were strained at a strain rate of 0.5 %/hour, Sodium Montmorillonite was strained at a strain rate of 1 %/hr and Gulf of Mexico-Ursa clay was strained at a strain rate of 1 %/hour. The results were interpreted using standard linear theory (Wissa et al., 1971). The strain rates were selected to produce a pore pressure ratio that is between 3 % and 15 % at the end of the loading phase and all tests were run in general accordance with the guidelines laid down in ASTM D4186. A table of the soils tested their properties and associated strain rates can be seen in Table 4-1. An overview of the CRS testing equipment employed to perform the experimental program is presented in Section 4.4.5.

Automated triaxial tests consisted of K_0 consolidated undrained shearing tests (CK_0UC). This automated system provides high quality results and eliminates many man-hours of time

which would otherwise be required. The type of triaxial cell used was a low pressure triaxial cell with a plexiglass chamber. The maximum confining pressure that the low pressure apparatus can sustain is about 1,500 kPa. The specimen dimensions for the triaxial testing program had a diameter of 3.55 cm and a height of 7.55 cm. An overview of the triaxial testing equipment employed to perform the experimental program is presented in Section 4.4.6.

4.2 MATERIAL PROCESSING

4.2.1 INTRODUCTION

This Section describes the methods used to process both London Clay and leached BBC. It was not necessary to determine the in-situ properties of London Clay as the soil which was received to MIT was only to be used for resedimentation purposes. Approximately 300 kg of London Clay was shipped to the MIT Geotechnical Laboratory in a wooden crate. The soil had been hand excavated from a tunneling project in the greater London area, and its origin has already been described in Chapter 3. The soil was subdivided in six sealed plastic bags each containing approximately 50 kg of material inside the crate. Because the bags were sealed, a water content was taken for the soil once it arrived. It was found that this water content closely resembled the in-situ water content.

Section 4.2.3 describes the processing of leached BBC. Leached BBC is a derivative of Series IV BBC and has had a portion of its in-situ salts removed by flushing through distilled water in a centrifuge. The quantities in which soil could be spun in a centrifuge were small (120 g per run). The testing program required approximately 3.5 kg (dry mass) to satisfy all planned testing.

4.2.2 PROCESSING OF LONDON CLAY

The London Clay which was received at the MIT Geotechnical Laboratory in August of 2011 was recovered from between 5-6 m deep. The soil was sealed in large durable plastic bags. In total six bags containing approximately 50 kg each were delivered. Assuming that the maximum particle size which exists in London Clay is 0.1 cm, to get to a precision of 0.1 % in the results, a dry mass of approximately 1.5 kg would be required (Germaine & Germaine, 2009). Given that the quantity delivered to MIT exceeds this quantity, representative samples

should be readily obtainable. It is worth pointing out that this rule may be violated by the grinding process described later.

Because no intact samples were taken at the development location, all the material which arrived at the MIT Geotechnical Laboratory was processed for use in resedimentation. The bulk soil consisted of 10-15 kg solid lumps of soil placed directly into the plastic bags. Each bag contained several of these chunks. A typical chunk of London Clay soil as received can be seen in Figure 4.1, and a close up shot is shown in Figure 4.2. It was decided to delay blending the soil in order to achieve a homogeneous material until after it had been processed to a powder. In order to process the soil to a state where it is suitable for resedimentation, a powder must be produced which will pass a US#100 sieve. This procedure consists of:-

- The material was received in a moist state. It was therefore necessary to remove this moisture to facilitate further processing. The soil was air dried in a large room by positioning a large fan such that it was circulating air over the top of the soil as can be seen in Figure 4.3. Larger chunks were broken into smaller and smaller pieces until they measured approximately 3 cm in their longest dimension. This 3 cm size is dictated by the opening size of the soil grinder which is used in a later stage. If the soil had been oven dried, the natural fabric and possibly even the individual soil particles may have been damaged by the high temperatures and shrinkage of the soil matrix.
- Once all moisture had been removed and all soil chunks were a manageable size, it could then be ground down to a fine powder. Traditionally when dealing with large quantities of soil which required processing, a third party external company would be employed to fulfill this task. The London Clay was to be processed in-house and therefore, a grinding machine was purchased. This machine was a GPX Disc-Style Grinder acquired from Modern Process Equipment, Chicago, IL. Several photos of the device can be seen in Figure 4.4. This grinder has the ability to grind material so that 100 % of the resultant powder will pass a US#100 sieve. The discs which perform the grinding are wear parts and once they are no longer able to reduce the soil to an appropriate size, they can be replaced. The machine also has the ability to grind the soil to different sizes via control of an adjusting screw which moves the discs closer together or further apart. For processing of the London Clay, the best results were obtained when the soil was run through once on

a coarse setting to produce a sandy type material, and then a second time on the finest setting to produce the final powder. Although this method produces an acceptable material for resedimenting, it must be acknowledged that any constituents of the soil that are naturally larger than the final powder, will be ground to a smaller size than what they exist at naturally. While processing the London Clay, dense pockets of quartz were visible to the naked eye and could easily be seen with a X2 times microscope. This quartz was sandy in size and could readily be felt between the fingers. Such an area is shown in Figure 4.5. This quartz, once processed did not alter the particle size distribution of the soil appreciably. This was demonstrated in Chapter 3. The throughput of the grinder depends on the size of the bulk material being ground. For the coarse raw soil chunks (3 cm elements), one can process approximately 15 kg/hour when the output soil is set to coarse. For the second run when the sand from the first process is being fed back into the hopper, it is important not to “choke” the grinding discs. Therefore, a slow feed rate is required. The output soil from the second run will be fine enough so that 100 % will pass a US#100 sieve. It can take approximately 1 hour to process 10 kg of fine material. Because of the vast range of soils which are tested at the MIT Geotechnical Laboratory, it is essential that the grinder be thoroughly cleaned after each use to avoid cross contamination. A combination of compressed air and soft wire brushes are found to adequately clean all areas exposed to soil.

- Blending of the soil was done in accordance with guidelines given in Germaine & Germaine (2009). Blending produces a homogeneous material which will give systematic results. The blending was performed on material which could pass a US#100 sieve, with the appropriate respect being paid to dust control. The blending process involves dividing the parent sample into four portions labeled 1, 2, 3 & 4. Each of these portions is then split into equal quarters labeled a, b, c & d. The four “a” portions are then combined together and blended in a second operation. Each of the four second blends will now be uniform and equal. A diagram of this operation is shown in Figure 4.6.
- Once a uniform material is produced via the blending operation, masses must be obtained which are easy to work with. This is done by splitting the material. Splitting of the soil is the process of reducing the sample size while maintaining uniformity and was done in

accordance with guidelines given by Germaine & Germaine (2009). Quartering is a systematic splitting process, and is the method used to split the London Clay into manageable quantities for working with. Each quartering operation reduces the sample mass by one half. The soil is placed in a pile and then split into two portions which are spread apart. These portions are then further split in half and then spread apart. Finally, opposite quarter portions are combined to provide a representative half of the original sample. This method can be repeated several times to sequentially reduce a sample to the required size. A diagram of this operation is shown in Figure 4.7.

- Once workable masses of material have been obtained, it can then be stored in sealed 10 gallon buckets while it awaits testing. A picture of the finely ground soil being prepared for storage can be seen in Figure 4.8.

4.2.3 PROCESSING OF LEACHED BOSTON BLUE CLAY

Series IV BBC contains approximately 2.65 g of salt for every 1 kg of dry soil powder. For research purposes, it was necessary to remove some of this salt from the soil fabric. In order to do this, distilled water must be flushed through the soil in a centrifuge. 3.50 kg of leached BBC was required in order to satisfy the quantity required for CRS and triaxial resedimentation. BBC was leached twice in the centrifuge in order to remove as much of the soil as possible given the effort involved in the process.

The process of leaching the in-situ salt from BBC is similar to the process used in salinity testing which is described in Section 4.5.2.5. When leaching large quantities of soil, efficiency is the key to reducing the time taken to produce the final quantity of soil. Normally, 15 g of BBC Series IV powder is mixed with 30 g of distilled water (200 % water content) in a test tube and this mixture is allowed to hydrate for 24 hours. The centrifuge in which the leaching was done, a Damon/IEC HT Centrifuge, has the ability to hold eight test tubes per run which means 120 g of soil can be processed per run. In order to increase the throughput of the centrifuge, it was necessary to develop new procedures to hydrate large quantities of slurry without occupying the test tubes for this task. Plastic containers were used to hydrate large quantities of BBC to a water content of 200 %, meaning that the custom centrifuge tubes, which were in short supply, could be used exclusively to leach soil in a repetitive manner. Once the supernatant was decanted from

the test tubes, the BBC was extracted from the base of the tube and air dried with the assistance of a standard desk fan. The end product from this stage was small “nuggets” of solidified soil.

The process used to leach soil in bulk quantities is described below:-

1. Mix 2 liters of distilled water with 1 kg of BBC Series IV and allow to hydrate for 24 hours, or any desired quantity of BBC to a water content of 200 % (assuming 1 g distilled water equals 1 cm³)
2. After 24 hours hydration time it is important to thoroughly agitate the slurry. This is necessary because any coarse material present in the soil may have settled to the bottom of the container. It is desirable to have a uniform slurry when filling the centrifuge tubes.
3. Add 45 g of uniform slurry to each of the tubes. This slurry consists of 15 g soil and 30 g of distilled water.
4. Place tubes in the centrifuge and spin for 30 minutes at between 10-15,000 rpm
5. Once the cycle is complete, remove tubes and dispose of supernatant. Carefully extract the soil from the base of the tubes and place it in an open bowl for air drying. Position the bowl under a standard desk fan and allow to dry. Note: for salinity testing which will be described later, the supernatant is of primary importance, however, in this process it is a byproduct which can be discarded.
6. Clean the centrifuge tubes using a water jet and dry them using a paper towel.
7. Repeat process from step 2 until the desired quantity of soil has been obtained. Note that there will be an amount of soil lost on every run because of the inability to extract all soil from the tube, these losses should be built into the calculations. The amount of soil lost represents approximately 5 % of the starting mass.

Because the soil had to be run through the centrifuge twice, it was necessary to reprocess these soil “nuggets”. This was necessary in order to obtain a material which could be mixed with distilled water again in order to produce a slurry for further washing in the centrifuge. Because BBC Series IV has already undergone blending and splitting, it was unnecessary to perform the same processes on the final leached material. Once the required quantity of soil had been

obtained from the first round of leaching, the soil was ground to a powder using the same method described in Section 4.2.2 for London Clay with the disc grinder. When the soil is ground to a powder which passes a US#100 sieve, it can then be leached for a second time using the same method already described. Finally, once the soil has been run through the centrifuge, extracted from the test tubes and air dried, it must again be ground to a powder once more. After grinding the soil for a second time, the soil is now ready to be used for research purposes. Although the soil was run through the centrifuge twice for this research, there is no upper limit as to how many runs will produce changes in behavior. Given time constraints, two washings in the centrifuge were deemed acceptable.

4.3 RESEDIMENTATION

4.3.1 INTRODUCTION

Numerous types of resedimented soil were used in the testing program. These included Boston Blue Clay (Series IV), London Clay, Gulf of Mexico clay, Sodium Montmorillonite and derivatives of Boston Blue Clay. These derivatives included Boston Blue Clay which has had its salt removed by leaching with distilled water, and also Boston Blue Clay which has had its fabric completely dispersed by mixing a quantity with sodium hexametaphosphate. A list of all samples prepared via the resedimentation technique is shown in Table 4-2.

The most commonly used soil in the testing program was traditional Boston Blue Clay (Series IV). BBC has been studied at MIT since 1961 and an extensive database on the engineering properties now exists. This database is for natural BBC as excavated from the ground and then processed to form the powder that passes a US#100 sieve. This powder is then tested in the laboratory as required. BBC is an excellent research material because:-

- a) a good supply exists
- b) it produces consistent and repeatable results
- c) uniform samples can be created
- d) it has typical consolidation characteristics and it is a fairly insensitive soil

Different resedimentation techniques were required for the BBC which has been altered, and therefore different results can be expected. An up to date reference on the research which has been performed on Boston Blue Clay is given in Chapter 3.

Gulf of Mexico soil, London Clay and sodium montmorillonite have higher plasticities than BBC and will therefore require modifications to the established resedimentation techniques. As London Clay had never been resedimented at MIT prior to this research, it was necessary to determine the water content at which it would exist as a stable slurry. Although Gulf of Mexico soil has been tested at MIT in recent years, (Mazzei, 2008), it was again necessary to determine the water content at which Gulf of Mexico soil should be resedimented to. This is mainly because the resedimentation which was performed for this research was done so with high salinity saltwater. When resedimenting with high salinity saltwater, the mass of fluid added to a soil powder does not resemble the mass of water available to wet the soil particles. A large fraction of the mass of fluid now comprises sea salt (up to 25 %). It is for this reason that greater masses of high salinity fluid are required to achieve the same stable slurry as with say a 16 g/l saltwater where the effect of the salt fraction in the fluid is not so pronounced.

The resedimentation procedure which was developed at MIT in the 1960's has been refined throughout the years. The most significant improvements were made by Germaine (1982) who refined the resedimentation technique to produce fully saturated and uniform samples of resedimented BBC. This process has since been extrapolated to other soils with a great deal of success.

The various types of soil which have been successfully resedimented as part of this research are described in the following Sections. These Sections detail what areas of the resedimentation procedure have to be altered to suit each individual soil type.

4.3.2 RESEDIMENTATION PROCEDURE

4.3.2.1 WORKING WITH NEW SOILS

In the process of implementing research with soils that are new to a given laboratory, it is important in terms of resedimentation, to determine the water which will produce an ideal slurry for resedimentation. This is done by placing known masses of soil in several clear test tubes with

varying water contents. It is important that the fluid used in this test is the same fluid that the soil will eventually be resedimented with. The reason for doing so is because in a high salinity resedimentation procedure, the mass of the fluid may not be the mass of water which is available to wet the soil due the large salt mass occupancy. Normally in the lab, we assume that 1 g of water is equal to 1 cm³. If we are dealing with a 200 g/l saltwater fluid and we add 1 g of fluid to a soil, only 0.833 g of water is actually being added to the soil. Although we say the saltwater is 200 g/l, which would mean we add 200 g of sea salt to 1,000 g of distilled water, the salt concentration by volume is 167 g/l after dilution.

When a stable slurry is produced in the lab, no free water appears on the surface of the slurry after being allowed to sit for a time. This is the essence of the test which is performed to determine the correct resedimenting water content. The test tubes which contain the different water contents should be left to sit for at least 24 hours (or longer for extremely plastic soils such as sodium montmorillonite), and then examined. It is important that the test tubes are not shaken because visual examination of the surface is required. Tubes in which clear water is present on top of the soil may produce slurry which can potentially segregate during consolidation. It is necessary to find the highest water content that will not produce this free water on top of the soil. This water content should then be used for resedimenting. Figure 4.9 shows the result of such a test that has been performed on leached BBC.

In order to determine a range of water contents to test, it is helpful to perform Atterberg limit tests of the soil. Once the liquid limit is determined, a good starting point will be double this value. Say for instance a soil has a liquid limit of 65 %, a good range of water contents to test initially may be 120, 125, 130, 135 and 140 %. It is useful to further refine the required water content over a smaller target range once it apparent where the water content of interest falls.

4.3.2.2 PROCEDURE

Only the procedures currently used will be covered in this Section. For details on previous resedimentation techniques, reference should be made to Ladd & Varallay (1965). The modern day techniques follow the methods set forward by Germaine (1982) and Seah (1990).

This resedimentation procedure can produce individual test specimens, or a column of soil from which multiple test specimens can be trimmed.

The tube in which the soil is resedimented in is called a consolidometer. These consolidometers retain the soil throughout all load increments from when the soil is a flowable slurry, to when it has achieved the desired resedimentation stress level. In this research, two types of consolidometers were used – one for triaxial samples and one for CRS samples. The triaxial consolidometer has an internal diameter equal to that which is required for a triaxial testing meaning that only the ends of the soil require trimming after extrusion. Consolidometers for CRS testing produce samples with diameters that are larger than the diameter required for testing. The tube diameters used for resedimenting for CRS testing were 4.15 and 4.4 cm. This is done to facilitate trimming of the soil into a cutting ring. Both consolidometers are clear plexiglass tubes. A photo of these consolidometers can be seen in Figure 4.10. This Figure also shows smaller height consolidometers were used when small quantities of soil needed to be resedimented for CRS testing.

The method of how the BBC was processed from its natural water content, or as it was excavated from the ground will not be covered here. However, a similar method has already been described for how the London Clay was processed (Section 4.2.2). For details on how BBC was processed, reference should be made to Cauble (1996). The following describes the resedimentation procedure for BBC Series IV from when a processed powder exists (at least 95 % passing a US#100 sieve).

HYDRATION

The desired quantity of dry soil powder should be carefully estimated in order to eliminate waste. This powder is then added to a predetermined quantity of saltwater and allowed to hydrate. Depending on the soil type and mineralogy, hydration can take several days. It is advantageous to allow the soil to hydrate in the desired fluid. Mechanically agitating the slurry alone may not guarantee full hydration prior to placement in the consolidometer. As a reference, it was found that natural BBC powder is hydrated fully after 24 hours while for sodium montmorillonite, hydration can take up to a week depending on the pore fluid chemistry and the quantity under consideration. For sodium montmorillonite, the quantity of soil which was added

to a low salinity pore fluid was observed to slowly expand to occupy the free water space over time. Once the montmorillonite had stopped “growing” it was deemed to be hydrated. This observation is not so evident in other soils.

MECHANICAL AGITATION

Once the slurry has fully hydrated, it is necessary to mechanically agitate it to help ensure a uniform paste. This is done in the MIT Geotechnical Laboratory with a Kitchen Aid mixer which is shown in Figure 4.11. This mixer is fitted with a flat beater attachment. The slurry is mixed for approximately 30 minutes in this manner, with the sides of the bowl being cleaned down with a soft spoon occasionally to ensure thorough mixing.

DEAIRING SLURRY

Once the slurry is adequately mixed, a partial vacuum is applied to remove any entrapped air from the slurry matrix. The setup for vacuuming is shown in Figure 4.12. A vacuum flask is connected to a vacuum pump which applies approximately 25 inches of Mercury (in Hg) vacuum to the slurry. The soil enters the flask under vacuum and is allowed to free-fall a distance inside the container as shown in Figure 4.13. This helps free any entrapped air. Once all the slurry is inside the vacuum flask, a stopper is used to isolate the soil from atmospheric pressure. The time required for vacuuming depends on the size of the vacuum flask, quantity of soil, mineralogy and atterberg limits of the soil. For small quantities of BBC (say 250 g of powder), 30 minutes of vacuuming is adequate to remove the entrapped air, while for montmorillonite (both calcium and sodium), Mesri & Olsen (1970) required a two week vacuuming period to ensure full saturation of the soil. Although montmorillonite was also resedimented as part of this research, vacuum times were in the order of 2 hours given the much smaller quantities. It is important not to leave the slurry under vacuum for too long because water will evaporate. This causes a reduction in the water content, potentially leading to thickening of the slurry which will have knock on effects when pouring the soil into the consolidometer.

POURING

When the slurry has been de-aired, it is then poured into the consolidometer. The slurry is poured directly from the vacuum flask into a funnel with a long flexible tube which discharges

into the consolidometer as shown in Figure 4.14. The tip of the funnel should be kept just above the top of the rising soil column to prevent any air being introduced to the soil.

CONSOLIDATION

The slurry can be poured into any size consolidometer. A photo of the consolidometers used in this research has already been shown in Figure 4.10. These consolidometers have rigid walls and openings at the top and bottom. A picture of a typical consolidometer setup can be seen in Figure 4.15. Once the slurry is poured, it is consolidated between two porous stones, one top and bottom. These porous stones transfer the applied stress to the soil and also provide a drainage path through which excess pore pressure can escape. The soil is loaded incrementally with a load increment ratio $\Delta\sigma_v/\sigma_v = 1$ to a prescribed maximum axial effective stress. This maximum stress level is dictated in part by the type of test the batch is being created for. For CRS testing, the soil is taken to an axial effective stress (σ'_{ac}) of 100 kPa. Soil used in triaxial testing was taken to an axial effective stress of 200 kPa. The increase in stress for triaxial specimens makes interaction with the soil easier because they require more intense handling than the CRS specimens.

Once the soil has reached its target axial effective stress, it is unloaded to a prescribed overconsolidation ratio (OCR). It was shown by Ladd (1965) that at an OCR of 4, the soil is close to hydrostatic stress conditions, meaning the lateral stress ratio K_0 is close to 1. Therefore, shear strains due to soil extrusion from the consolidometer are minimal and it can be assumed that BBC possesses no sample disturbance once extruded. This OCR value was also used for London Clay, GOM soil and sodium montmorillonite pending further research.

Given that the maximum axial effective stresses which the soils were resedimented to were small, all loading increments were done using dead weights. In the very low stress range (up to 10 kPa), weights can be placed directly on top of the consolidometer. In the higher stress range, the weights are hung from a frame as shown in Figure 4.16. Throughout each consolidation phase, the axial deformation of the slurry column is measured using an LVDT. Each load increment is maintained until the End of Primary (EOP) consolidation, which is the time taken for all excess pore pressures to dissipate and secondary compression to commence. By monitoring the axial deformation versus the square root of time, we can estimate this time to

EOP. A sample graph that is produced from a typical load increment can be seen in Figure 4.17. An exception to this rule was made when re-sedimenting montmorillonite. Given the fact that EOP for the initial increments could take months, additional axial stress was added before EOP was reached. Care should be taken not to overload the slurry when it is in a weak state. This may cause large quantities of soil to be extruded between the stone and the consolidometer wall

EXTRUSION

After consolidation is complete, the soil is ready for testing. Given that the soil is re-sedimented to a relatively low stress, extrusion can be done by applying a downward force to the plexiglass tube (usually by hand), while sitting the interior porous stones on a platform which will cause the interior soil column to move relative to the outer plexiglass tubing. A photograph of this process is shown in Figure 4.18. If it is not possible to extrude the soil in this way, a hydraulic hand-jack can be used to apply the necessary force. Once the soil is extruded, it is trimmed to the required dimensions for testing. The trimming process is covered in the respective test method (CRS & triaxial), as the techniques used are specific to the test type.

4.3.3 RESEDIMENTING BOSTON BLUE CLAY

4.3.3.1 INTRODUCTION

BBC has been re-sedimented at MIT since the 1960's (Abdulhadi 2009). Re-sedimented BBC is done using BBC powder which passes a US#100 sieve. This powder is taken as natural soil from the Boston area and processed to create a series which is then used for laboratory testing purposes. The current batch of BBC powder that is used in the MIT Geotechnical Laboratory is called Series IV and was obtained in 1992 from the base of an excavation for MIT's Biology Building (building #68). Prior to 1992, previous series of BBC were tested. Series IV BBC was used for this thesis. Chapter 3 gives an up to date summary on the research which has been performed on re-sedimented BBC since the 1960's.

4.3.3.2 RESEDIMENTING BOSTON BLUE CLAY TO DIFFERENT SALINITIES

Recent work at MIT has involved re-sedimenting BBC to 16 g/l (e.g. Adams, 2011; Abdulhadi, 2009). With the exception of Casey (2011), and Bailey (1961), very few laboratory tests had been performed on re-sedimented BBC at various pore fluid salinities. Casey (2011),

resedimented BBC with pore fluid salinities ranging from 2.65 g/l to 24 g/l, while Bailey resedimented BBC at pore fluid salinities of 2-3 g/l and 35 g/l.

Throughout this research, natural BBC Series IV was resedimented to salinities of 4, 16, 64, 128 and 256 g/l. BBC has been traditionally resedimented to a water content of 100 % with a salt concentration of 16 g/l. The natural BBC used in this research was also resedimented to a water content of 100 % for salinities of 4, 16, 64 and 128 g/l. Natural BBC which was resedimented to a salinity of 256 g/l required a water content of 110 % in order to achieve a workable slurry.

The saltwater used for resedimentation was prepared prior to use and stored in labeled plastic containers in the laboratory. Ordinary sea salt (NaCl) was used in the preparation of the saltwater and natural BBC was resedimented to 4, 16, 64, 128 & 256 g/l for CRS testing, and to 4 & 256 g/l for triaxial testing.

4.3.3.3 RESEDIMENTING LEACHED BOSTON BLUE CLAY

BBC which was leached as described in Section 4.2.3, was resedimented to salt contents of 1, 16, 64 & 256 g/l for CRS testing, and to 1 and 256 g/l for triaxial testing. One batch of leached BBC soil was also resedimented with distilled water (0 g/l) for CRS testing. One observation which was noted was that when the BBC was leached, its sensitivity to water increased. This means that each individual salt concentration now requires its own unique resedimenting water content. The lowest water content used for natural BBC Series IV (Section 4.3.3.2) was 100 %, however, the lowest water content required for leached BBC is now 62 % when using distilled water. When using 1 g/l saltwater, the water content required rises to 80 %. At the other end of the scale, a water content of 120 % is needed to resediment with 256 g/l saltwater. This is in stark contrast to resedimenting with natural BBC where all resedimentation water contents were the same except for 256 g/l batches. A list of required water contents versus pore fluid salinity can be seen in Table 4-3.

It is believed that when the natural BBC is leached of its salt, the clay fabric is deflocculated. This has already been discussed in Chapter 3.

4.3.3.4 RESEDIMENTING BOSTON BLUE CLAY WHICH HAS BEEN DISPERSED WITH SODIUM HEXAMETAPHOSPHATE

Sodium hexametaphosphate (sodium hex) is a dispersing agent which has traditionally been used in Soil Mechanics for the hydrometer test. This dispersant neutralizes the surface charge on the individual soil particles for an inorganic soil, which is a primary cause of floc formation (Germaine & Germaine, 2009). Essentially, the dispersant will de-flocculate all soil elements which were agglomerated when the soil was deposited. It breaks down the soil to its basic components. It is believed that once this dispersed soil was resedimented, similarities in fabric and mechanical behavior with traditional RBBC would no longer be evident. In effect, particles on the micro scale now have little surface charge, therefore flocculation during resedimentation is unlikely. The dispersed soil was resedimented with distilled water, and the water content required to produce a stable slurry was 56 %.

4.3.3.4.1 OBSERVATIONS

Even though the dispersed soil has the same constituents and elements as the BBC Series IV soil, a much lower water content is now required to resediment these same minerals to a similar slurry state. This lends evidence to the theory that flocs exist in the natural BBC powder which are not broken down through processing. These flocs still exist in the material which is used for laboratory testing at MIT, namely BBC Series IV. It is also here the first similarities with leached BBC are observed whereby a lower resedimentation water content was required for leached BBC particularly in the lower salinity range and especially for distilled water.

Once the dispersed soil had been resedimented with distilled water, small deflocculated particles can remain in suspension for many months (up to 9 months as witnessed by the author). Owing to the fact that sodium hex can have such a profoundly negative effect on soil behavior, this soil was among the last to be tested in the program. It is for this reason the prolonged suspension of soil particles in the water baths at the bottom of a consolidometer setup was noticed. This same effect is not evident if BBC Series IV powder is placed into distilled water.

4.3.4 RESEDIMENTING LONDON CLAY

The effect of pore fluid salinity on natural London Clay was also investigated as part of this research. The origins of this London Clay are described in Chapter 3. Resedimentation was performed on natural London Clay powder which had undergone grinding as described in Section 4.2.2. After performing sieve analysis on the ground powder, it was found that 100 % passed a US#100 sieve and was therefore deemed acceptable for resedimenting.

Given time constraints, salinities of 4, 16 & 256 g/l were investigated for natural London Clay in an attempt to determine the effect at both ends of the salinity range in question. The three salinities mentioned were successfully resedimented without any issues. As London Clay was a new material to the MIT Geotechnical Laboratory, its resedimentation water content had to be determined for all target salinities. This was done in a similar fashion to the method described in Section 4.3.2.1. For salinities of 4 & 16 g/l, the water content used for resedimentation was 130 %, while for salinities of 256 g/l, the water content was 140 %. From this research, it is apparent that London Clay is an acceptable candidate for use in resedimentation.

4.3.5 RESEDIMENTING GULF OF MEXICO SOIL

Gulf of Mexico (GOM) soil has been resedimented at MIT in recent years by Mazzei (2008), and although this research also involved resedimenting and testing GOM soil, it must be appreciated that the GOM region spans a vast area and soils obtained from different locations will almost certainly have differing mineralogy, gradation curves and mechanical behaviors. The same is true of BBC samples taken from a far smaller catchment area.

RGOM-Ursa was tested as part of this research. This RGOM-Ursa soil was resedimented with distilled water (0 g/l) and tested in the CRS device in order to compliment other work ongoing in the MIT Geotechnical Laboratory, and also to establish a bank of test results for this material. RGOM Ursa soil required a water content of 100 % when resedimented with distilled water.

4.3.6 RESEDIMENTING SODIUM MONTMORILLONITE

The effect of salt on a clay mineral is displayed excellently within the montmorillonite family of soils. This is shown in Figure 4.19. Montmorillonite forms an ideal medium for the

theoretical investigation of clay minerals. While it is not thought that pure montmorillonite has been resedimented at the MIT Geotechnical Laboratory in the past, montmorillonite has been resedimented for research purposes by others such as Mesri & Olsen (1970). Their observations were taken into account while performing this research.

Sodium montmorillonite was resedimented to 1 & 256 g/l for this research and large differences were found in the water contents required to produce a stable slurry. When resedimenting to a pore fluid salinity of 1 g/l a water content of 1050 % was required. When the pore fluid salinity was 256 g/l, a water content of 100 % was adequate. This represents more than an order of magnitude difference in required water contents, to produce the same viscosity slurry for resedimentation. This is in contrast to other soils such as BBC and London Clay where an increase in water content was required for the higher salinities.

It is important, especially when dealing with highly expansive soils such as montmorillonite, that the soil be afforded adequate time to hydrate. It was discovered that for low salinity montmorillonite such as 1 g/l, this took up to one week. For the high salinity 256 g/l soil, hydration times were very short and no volume change of the soil was observed. The standard 24 hours hydration time was given to high salinity montmorillonite.

The sodium montmorillonite slurry at 1 g/l was resedimented in the MIT Geotechnical Laboratory on the 20th of December 2011, and eventually reached end of primary consolidation on in the middle of May, 2012.

4.3.7 RESEDIMENTATION ISSUES

The saturation point for salt (NaCl) in water is approximately 360 g/l at 20° C. Early in the testing program when working with 256 g/l saltwater, it was noticed that after approximately one day, salt began to precipitate out of solution and settle to the bottom of the storage container. Although the salt content was a long way from the saturation limit, it was never discovered exactly why the salt was falling out of solution. This issue was resolved by mixing the salt into the water after it was heated to approximately 50° C. This was done on a hotplate with built in magnetic stirrer. Once this procedure was followed, further precipitation of the salt was not witnessed. It is now standard practice to mix all saltwater, regardless of salt content in this fashion.

When resedimenting with salinities above 64 g/l, a cake of salt grows on the water bath and consolidometer a few days after the slurry has been poured. This salt originated from the saltwater bath which is charged with keeping the slurry saturated at the correct salinity during resedimentation. If salt is being lost from this water, then the water will no longer be at the required salinity. A photo of this occurring while resedimenting sodium montmorillonite to 256 g/l, is shown in Figure 4.20. The salt was found mostly around the rim of the water bath. This is because the water bath has a relatively large surface area available for evaporation. Very little if any salt was found on top of the consolidometer. It can be assumed that the fluid permeates from top to bottom during the consolidation process, so because the salinity on the top reservoir is not as affected by water evaporation as the salinity on the bottom reservoir, a substantial change in target pore fluid salinity should not be expected.

When dealing with thin slurries, it is possible for large quantities of slurry to extrude under the fluids own hydrostatic pressure, through any gap between the porous stone and the consolidometer wall. This can lead to an unacceptable loss of slurry into the water bath, effectively reducing the quantity remaining in the consolidometer. This quantity may therefore fall below what is necessary to produce a test specimen. To overcome this, a method was devised to seal the gaps between the porous stone and consolidometer wall. Commercially available PolyTetraFluoroEthylene (PTFE) tape was used circumferentially around the porous stone to produce a flexible seal between the two rigid surfaces. The PTFE tape allows for small irregularities in the stones circumference to be masked and sealed. This method produced very satisfactory results when dealing with troublesome slurries and a photo of the method can be seen in Figure 4.21. Because the tape was placed circumferentially on the stone, the middle area was still available to allow fluid flow to and from the soil. The only apparent drawback to this method is that large friction forces can now be generated between the stone and the consolidometer. These friction forces can be negated by stacking weights in a methodical manner onto a piston which transfers force to the stone until movement is observed. Once axial movement of the stone has been noted, the mass causing this movement should be added to each load increment. This can prove to be a troublesome and delicate operation in the low stress range say for instance when trying to apply a force of 0.40 kg to a slurry through a porous stone which requires 1.50 kg to overcome the friction. The 0.40 kg force may also be absorbed by the friction

of the stone owing to the “stick-slip” nature of this type of movement. In the high stress range, the issue is not so pronounced.

An additional method to overcome extrusion around the base stone is shown in Figure 4.22. The bottom internal porous stone is placed flush with the base of the consolidometer, and this in turn is placed on a larger diameter porous stone with a filter screen separating the large porous stone and the consolidometer. This method reduced extrusion to zero on each instance of its use and it does not suffer from the same frictional issues as the previous method. At some stress level, the large diameter stone on the base can be removed and the floating tube consolidation process can be used as normal. This method will only work for the base of a consolidometer.

4.3.8 MEASURING PORE PRESSURES DURING RESEDIMENTATION

During the resedimentation program, an attempt was made to measure the pore pressures generated, and associated rate of dissipation throughout consolidation of a soil. This was done in response to the length of time the sodium montmorillonite was taking to consolidate. A curiosity existed as to if excess pore pressures were present in the soil a long time after loading, or if secondary compression was in fact occurring.

The transducer was not originally placed on tube when the slurry was poured, but was attached some months after consolidation was initiated. A photograph of the resultant pore pressure measuring device is shown in Figure 4.23. As can be seen from this Figure, the transducer was attached retrospectively by attaching a collar to the outside of the consolidometer. This collar was sealed to the consolidometer with an O-ring. A Swagelok fitting was attached to the collar, which would act as the connection between the collar and the transducer. A 2 mm diameter hole was then drilled through this Swagelok fitting until the consolidometer wall was pierced. In a timely manner, all connections were made between the Swagelok fitting and the transducer. Every effort was made to ensure saturation of the system prior to fixing the connections permanently. A 350 kPa pressure transducer was used. This transducer was installed prior to the application of the final stress increment to the soil (to bring the soil to a stress of 100 kPa).

Owing to the fact that the pore pressures (in the immediate vicinity of the piercing) would have instantaneously dropped to atmospheric levels once the drill penetrated the consolidometer, the tube was given two weeks for pore pressures to equilibrate and establish a zero or base reference pressure. Upon application of the next loading increment, the channel recording the pore pressure transducer was monitored in conjunction with the LVDT recording axial movement. The resulting plots from the axial deformation and normalized pore pressures can be seen in Figure 4.24, Figure 4.25 and Figure 4.26. It should be noted from Figure 4.24, when the pore pressures are approaching zero, an upward concave shape is forming in the displacement versus square root of time data. This is the first such instance of resedimentation time-displacement data for sodium montmorillonite plotting in the traditional “upward” direction. This “upward” plot usually signifies that the transition is occurring between primary consolidation and secondary compression.

Although the pore pressure measuring method employed here is primitive and crude, the technique can be built on and expanded. It is possible to apply this technique to other soils which are not as notoriously problematic as montmorillonite. Several pore pressure transducers can be used in a column to determine how the pore pressures behave at different heights in the soil column as the end of primary consolidation is reached.

4.4 EQUIPMENT

4.4.1 INTRODUCTION

This Section describes the testing equipment used for the testing program. Constant Rate of Strain (CRS) and triaxial devices were used in this research to investigate the one dimensional and undrained shear properties.

Throughout the course of this research, many types of transducers were used to collect data. These transducers measure the physical quantities which can change throughout a test such as axial movements, volume changes, pressure increases and changes in stress. Section 4.4.2 describes these transducers and indicates under what circumstances a given type would be used.

The data from these transducers is then collected in a central location in the MIT Geotechnical Laboratory. Section 4.4.3 describes the system which exists to facilitate the collection and storage of this data.

Section 4.4.4 describes the computer controlled triaxial testing system which is used at MIT and outlines the advantages of computer control over traditional methods.

The CRS equipment used is described in Section 4.4.5. Descriptions of the cell as well as the load frame are given, along with modifications to the load cell which had to be made as part of this research.

The triaxial testing equipment is covered in Section 4.4.6 and describes the triaxial cell, load frame and the Pressure Volume Actuators (PVA's) used to control the cell and pore pressures.

4.4.2 MEASUREMENT INSTRUMENTATION

4.4.2.1 INTRODUCTION

Various types of transducers are used to digitally record the physical quantities that are measurable during a test. All of these require a common excitation of approximately 5.5 volts Direct Current (DC) from a regulated power supply. Because the output voltage is dependent on the input voltage, the input voltage must also be recorded. When processing data and determining calibration factors for transducers, the output voltage must be normalized to the input voltage in order to eliminate any errors which may be present due to slight fluctuations in the input voltage. The transducers which were used in this study can be summarized into four categories: axial transducers, volume change transducers, load cells and pressure transducers. Details of the transducers used for CRS and triaxial testing are given in Table 4-4, Table 4-5, Table 4-6 and Table 4-7. These tables correspond to CRS cell TR4, and triaxial apparatus MIT01, MIT02 and MIT04 respectively. The tables also include a summary of the calibration factors as well as the achievable resolutions and stability of the output signal as measured by the central data acquisition.

4.4.2.2 AXIAL DISPLACEMENT TRANSDUCERS

Axial displacement for the CRS and triaxial tests were measured externally. CRS testing used two transducers positioned at 180° to each other, with the average of the two being taken as true displacement. Axial movement during triaxial testing depended on one transducer. Two transducers were used for the CRS test owing to the small specimen size and a belief that any lateral movement of the piston, however small, may adversely affect the results. The transducers used were Linear Variable Differential Transformers (LVDT) manufactured by Trans-Tek Inc. (series 240). Depending on the actual model number, these transducers can produce linear results over ranges of movement from as small as approximately 0.10 cm, up to 10 cm. The LVDT tube generates a magnetic field through which a ferromagnetic core moves. When the core, which is not mechanically attached to the casing in any way, displaces axially through the LVDT tube, an output voltage is produced which is directly proportional to the position of the core in the tube. A picture of two LVDT's can be seen in Figure 4.27.

4.4.2.3 VOLUME CHANGE TRANSDUCERS

Changes in volume of a specimen during a triaxial test, and determining the quantity of fluid which has passed through a specimen during a reverse leaching test are determined by measuring the displacement of a piston in a Pressure Volume Actuator (PVA). A typical PVA for the CRS test is shown in Figure 4.28 and PVA's used for triaxial testing are shown in Figure 4.29. The cross sectional area of the piston is calculated and the axial movement of this piston during a test is recorded using either an LVDT or a string pot. The LVDT used in a standard PVA is a Trans-Tek Series 240 displacement transducer with linear range of approximately 10 cm. The string pot (linear position transducer) is manufactured by Celesco (SP1 type). When axial movement occurs, the extension of the wire rope rotates an internal capstan and sensing device (precision potentiometer) to produce an electrical output signal proportional to the wire rope extension. The range of this device is approximately 30 cm.

4.4.2.4 LOAD CELLS

The load cells used for triaxial testing are data instruments JP type shear beam load cells with a 500 lb (2.2 kN) capacity. The load cell used for CRS testing was manufactured by Toledo Transducers Inc. and has a 10,000 lb (44.5 kN) capacity. All load cells used an S-shaped steel

section instrumented with strain gages. A photo of a 500 lb capacity load cell can be seen in Figure 4.27 while a picture of the 10,000 lb load cell is shown in Figure 4.30.

The load cells for triaxial testing were placed internally in the cell, while the load cell for CRS testing was mounted externally.

4.4.2.5 PRESSURE TRANSDUCERS

Pressure transducers are used in the triaxial test to monitor and control the cell pressure, and the back (pore water) pressure. They are used in the CRS test to measure the cell pressure, and record the base excess pore water pressure generated by the consolidation process. The pressure transducers in use in the MIT Geotechnical Laboratory are manufactured by Data Instruments and are of the AB/HP type. These transducers measure the absolute pressure by deflection of a thin steel diaphragm that is instrumented with strain gages. The triaxial test and the CRS test both use two 200 psi (1,400 kPa) pressure transducers. A photo of a 200 psi (1,400 kPa) pressure transducer can be seen in Figure 4.28. This Figure also shows a section through a pressure transducer for reference.

4.4.3 DATA ACQUISITION

4.4.3.1 INTRODUCTION

Modern day testing requires many readings to be taken simultaneously. These readings can include time, axial stress, axial strain, pore water pressures, radial strain and specimen volume change to name but a few. Traditionally, these readings were taken manually using timers, data sheets and dial gages which can prove to be a laborious task, particularly for lengthy tests. Here the advantages of electronic instrumentation become apparent whereby force, displacement and volumes can be converted to an electronic signal which can be then recorded automatically using a data acquisition system. This reduces the man-hours required per test and leads to an increase in quality control. For CRS, triaxial testing and soil batching performed in this study, all data was collected utilizing the central data acquisition system in the Geotechnical Laboratory.

4.4.3.2 CENTRAL DATA ACQUISITION SYSTEM

The central data acquisition system in the MIT Geotechnical Laboratory provides a single location from where multiple readings can be taken simultaneously. The method allows for complex recording schedules which will be defined by the operator. Once a set of readings are taken, they are written to a text file (.dat) and stored on a computer until the operator retrieves it. The system will continue to record data until either the number of prescribed readings specified by the operator has been reached, or the test is stopped. Abdulhadi (2009) describes the system in detail.

The Central Data Acquisition System (CDAQ) is based on a 486 microprocessor PC driven by a Windows based operating system, with an expanded channel Hewlett Packard HP3497A data acquisition unit which uses very low noise integrating analog to digital converter. The system has a 5.5 digit integrating analog to digital converter with auto-ranging amplification to four voltage scales namely 0.1, 1, 10 & 100 V. The system is configured to monitor 140 channels simultaneously while providing analog to digital conversion and data storage at rates up to 1 Hz. This high quality low noise system makes it possible to directly measure laboratory transducers without any signal amplification. The resolution and stability of transducers used in the testing program as measured by the CDAQ are given in Section 4.4.2.1.

A schematic diagram of the central data acquisition system is shown in Figure 4.31. The data acquisition system can be broken down into the following basic components:

- The laboratory device which contains the transducers, power supply, junction box, voltmeter and ground
- A switching mechanism which allows the data acquisition computer to select a particular transducer to measure
- An analog to digital converter then changes the voltages to digital word. This device is critical to the precision of the final measurement
- A computer which orchestrates the components and performs the administrative and computational tasks

4.4.4 COMPUTER CONTROL SYSTEM FOR TRIAXIAL TESTING

The modification of existing manual system components to permit automation was first conducted in the MIT Geotechnical Laboratory in the early 1990's by Sheahan (1991). He developed an automated stress path triaxial cell for testing. The addition of innovative new components to complete the system automation, increase flexibility and quality control has continued ever since. The main advantages of automation are the huge reduction in man hours and increased accuracy.

Automation is controlled by a closed feedback loop for the driving systems of the apparatus. It works under the following principles:

- The transducers measure the actual specimen stress-strain state
- The transducer signals are sent to the computer and converted to engineering units
- Software compares these engineering units with a prescheduled time history of specimen state
- A control algorithm computes what action needs to be taken by the electric motors to keep the stress-strain state on schedule
- Signals are then sent to the electric motors to carry out the required action

Sheahan (1991) describes closed loop feedback control as direct measurements in an iterative system to maintain specific time histories of the parameters being measured.

The hardware to convey electronic information along the digital feedback control loop is shown in Figure 4.32. The output from the transducers is sent to an analog to digital (A/D) converter which translates the analog signal in volts to digital signal in bit counts. Multichannel A/D converter devices (MADC) are used. They provide high precision with a minimum 18 bit resolution. The key component of the MADC is the Analog Devices AD 1170 A/D convertor. A computer processes the incoming signals and determines the new command signal to be sent to the testing device. The command signal generated is then converted back into an analog signal through a digital to analog (D/A) converter board that is located within the computer. The D/A converter is a commercial board manufactured by Strawberry Tree Inc. with a 12 bit resolution and a ± 5 volt range. The analog signals are sent via a motor driver from the D/A converter to the electric motor. The electric motor then drives the required components such as the piston of the

PVA to adjust pressures or the load frame to control axial stress. Electro-craft motors Model E286 are used in the majority of MIT load frames, while Electro-craft motors Model E372/352 drive 0.5 Tonne actuators in the PVA's.

Automated control is carried out using a control program written in the QBASIC programming language. The program allows the user to set up the system for testing and also to allow for test control. The software was originally developed for automated triaxial testing but has been constantly updated. It is now task specific, allowing functions such as initial pressure up, saturation, consolidation and shear phases. Despite this local computer control, the central data acquisition is still used for recording data.

4.4.5 CONSTANT RATE OF STRAIN TESTING EQUIPMENT

4.4.5.1 TRAUTWEIN CELL

A modified Trautwein CRS cell (known locally in the MIT Geotechnical Laboratory as TR4), was used for all CRS tests performed. This cell has been modified from a standard CRS Trautwein cell insofar as the specimen being tested is smaller than standard and two LVDT's are now used to measure axial deformation instead of one. The piston plunger also required downsizing owing to the smaller specimen size. A photo of the CRS ring used in the testing can be seen alongside a standard CRS ring in Figure 4.33. The entire CRS cell can be seen disassembled in Figure 4.34, and assembled while running a test in Figure 4.35.

An additional modification was required to the cell half during the testing program. The piston seal which isolates the cell pressure from atmospheric pressure around the seal can be seen in Figure 4.36. Occasionally, this seal would leak. Once the water passed the seal and existed on the atmospheric side of the cell, the first exit point was at the top of the opening for the piston lock through which the water would weep. Housed in this column which the cell water permeates up through are a series of roller bearings that facilitates axial movement of the piston while loading and unloading. After this occurred several times with high salinity water, rust was noticed on the piston upon retraction. Small rust particles also got wedged between the seal and the piston leading to further leakage. The saltwater had corroded the roller bearings and the piston was beginning to seize. The issue was resolved by drilling a 3 mm diameter hole at a low

level on the column to intercept any leaking water which exits the cell. This hole is shown in Figure 4.37 and eliminated any water rising through the roller bearing area.

4.4.5.2 LOAD FRAME

All constant rate of strain testing was performed in a Wykeham Farrance Model T-57, screw-driven loading frame with a 10,000 lb (44.4 kN) axial capacity. This particular load frame has 30 displacement rates ranging from 0.0037 to 46 cm/hour. The main strain rates used were 2 %/hour for BBC in all states and 0.5 %/hour for London Clay. A photo of this load frame can be seen in Figure 4.38. The rate at which data is collected using the central data acquisition system while performing a CRS test is vital. If there are too many readings, the data may be difficult to interpret and may require extensive analysis as the MIT produced QBASIC reduction program can only deal with 1,000 data points at a time. If there are too few data points, the data may be jagged when plotted, and important information such as the preconsolidation pressure may not be captured accurately. A good rule of thumb employed during this research was that when the strain rate was 2 %, readings would be taken at 2 minute intervals meaning that 33.3 hours of data could be recorded. If the strain rate was halved, the recording rate would be doubled due to the longer test time and so on. It may also be advantageous to set the data acquisition system recording at a faster rate in order to define the preconsolidation pressure very well, and then at greater intervals in the normally consolidated range where change in behavior is not as frequent.

There are two main drawbacks when using this load frame. The first is that the frame is a purely mechanical device with no electronic interaction. This requires the operator to continually check on the progress of the test and manually determine the current stress level. There is no computer readout, and no computer control to halt the device once a certain stress is achieved – it is entirely operator dependent and must be operated by an on/off switch. The second drawback is that it can only apply a constant rate of strain and not a constant level of stress. This means that it is not possible to allow secondary compression at the end of a loading phase. Once the target stress level is achieved and consolidation halted, the soil will naturally relax and the stress level drop. This is a deviation from ASTM D4186 which requires secondary compression as part of a standard test. In order to obtain an unload curve for a soil, the frame must be set to unload once a prescribed stress level is achieved.

All in all, the Wykeham Farrance load frame used was an extremely robust and user-friendly piece of equipment to work with. It provided systematic and consistent strain rates and never posed one issue throughout the some 90 CRS tests performed for this research.

4.4.6 TRIAXIAL TESTING EQUIPMENT

4.4.6.1 LOW PRESSURE TRIAXIAL CELL

The triaxial apparatus has a clear plexiglass chamber with an internal pressure capacity of 1,500 kPa. The specimen is housed inside this chamber and is seated on a base pedestal. A fixed cap confines the top of the specimen and drainage is provided to the soil via the base pedestal and the fixed top cap. A compact shear beam load cell is also located within the chamber for direct measurement of the axial deviator force. The placement of the load cell inside the chamber eliminates the effect of piston seal friction on the load measurements. The soil specimen is sealed using two thin impermeable membranes (un-lubricated latex Trojan brand condoms), and these are sealed to the base pedestal and top cap using 4 O-rings at each location (8 in total). Owing to the existence of an internal load cell in the chamber, internal connections are required to supply power to, and take readings from this load cell. These electrical connections are supplied through the base of the cell, whereby a male plug exists on the interior and exterior of the base from which connections can be made. The internal load cell is connected to the loading piston which rides through a low friction, linear bearing with an O-ring seal. Axial movement of this piston is monitored externally with an LVDT. Figure 4.39 shows a schematic of the chamber with the main items identified and Figure 4.40 shows a picture of the apparatus (MIT04). For clarity, Figure 4.41 shows the sealing arrangement between the top and bottom caps and the membranes for reference.

During triaxial testing, the chamber is filled with Dow-Corning “200 fluid”, 20 centistokes silicone oil. This silicone oil exhibits extremely low viscosity over a wide range of temperatures, is optically transparent and does not degrade the seals or the latex membranes used in the testing procedures. This oil also has the benefit of being nonconductive which is convenient when locating electronic devices inside the chamber. The alternative would be to use sealed connections in the cell.

4.4.6.2 TRIAXIAL LOAD FRAME

The system is axially loaded through the use of a 1 Tonne (9.8 kN) capacity bench top Wykeham Farrance screw driven loading frame. The load frame has been modified to respond to computer control and can be set to halt axial movement when either a prescribed stress or strain level has been achieved. A photo of the load frame can be seen in Figure 4.42.

4.4.6.3 ANCILLARY TRIAXIAL EQUIPMENT

Pressure-Volume Actuators (PVA; see Section 4.4.2.3) are used to control the cell and back (pore water) pressures. Volume changes in the specimen are computed from an LVDT monitoring the motion of the back pressure PVA which will have a piston of known area. Cell and back pressures are monitored and controlled with high performance diaphragm type (200 psi [1,400 kPa] capacity) pressure transducers that are located on the base of the cell. The enclosure and the rest of the apparatus are located inside an air-conditioned laboratory. A photo of the complete triaxial setup showing cell, load frame, both PVA's and the computer control is shown in Figure 4.43. The load frame and both PVA's have been modified so they operate under computer control. This has been described in Section 4.4.4.

4.5 TESTING PROCEDURES

4.5.1 INTRODUCTION

This section describes the various test procedures employed for CRS testing, reverse leaching tests performed in the CRS cell and triaxial compression tests. Issues which required addressing during the testing program will also be described, along with tactics employed to overcome these issues. Also covered in this section are ancillary tests such as salinity testing, index testing and organic content testing.

4.5.2 CHARACTERIZATION

4.5.2.1 INTRODUCTION

This section describes the test procedures used to characterize the various soils. Not all characterization tests mentioned below were performed on all soils, but specific tests were performed on individual soils.

4.5.2.2 GRAIN SIZE ANALYSIS

As most of the soils used throughout the testing program were predominantly clay and silt sized, the Hydrometer was used as the main method to determine the grain size distribution. All Hydrometer tests were conducted in accordance with ASTM - D422 Particle Size Analysis of Soils. The results for the tests performed can be seen in Chapter 3.

4.5.2.3 ATTERBERG LIMITS

The Atterberg Limit tests provide methods to determine in which state a soil exists, and therefore basic judgments can be made as to the likely properties the soil will display. The water contents of most importance are the Plastic Limit and the Liquid Limit. The Plastic Limit is the theoretical water content where the soil transitions between brittle and plastic behavior, while the Liquid Limit defines the theoretical water content at which the soil changes from a plastic to a liquid behavior.

The Plastic Limit test was run in accordance with ASTM D4318 using the rolling test. The Liquid Limit test was performed in accordance with BS 1377 – 2 which describes the Fall Cone method. The fall cone method was preferred over the Casagrande Cup method due to the fact that results are very repeatable and the risk of operator error is reduced. For some soils such as sodium montmorillonite, both the Casagrande Cup method and fall cone method were used to estimate the liquid limit. Both the Casagrande Cup method and Fall Cone method were used on sodium montmorillonite.

4.5.2.4 SPECIFIC GRAVITY

Specific Gravity (G_s) is the ratio of the density of a substance to the density of a water at 20° C. The test is highly dependent on ambient temperature due to the contraction and expansion

of water, and therefore careful control of the test is required in this regard. All G_s tests were performed in a polystyrene box in the MIT Geotechnical Laboratory to allow time for temperature equilibrium. Testing was performed in accordance with ASTM – D854.

4.5.2.5 SALINITY TESTING OF SOIL

Salinity is reported in grams of salt per liter of fluid. Almost all natural soils have some fraction of salt included in their pore fluid. When these soils are brought into the laboratory for testing, the natural water is removed for processing prior to resedimentation. The salt which was present in this water is now left behind as a solid in the soil. This quantity of salt which exists naturally must be determined. The rationale behind this is when a soil is resedimented, it usually do so to a certain salinity. If salt exists naturally in the processed powder, this must be allowed for when determining the quantity of salt to be added to the resedimented material in order to obtain the target salt concentration. For example if it was determined a soil had a natural salt content of 6 g/l (after allowing for the in-situ water content) and is then due to be resedimented to 16 g/l, a pore fluid containing 10 g/l would need to be added in order to get to the target value. The salinity test is used to quantify the salt existing naturally in a soil.

Measurement of the salinity was done with a trace portable conductivity meter, model 23226 – 505 from VWR International. This meter has been previously calibrated by Grennan (2009). There is no standard test method for measuring the salinity of a soil. The following procedure was adapted from Germaine & Germaine (2009), Grennan (2009), and Martin (1982).

- Before testing, create a 1 g/l saltwater reference fluid taking extreme care with the quantities used. Subsequent readings taken from soil will be normalized to the readings taken from the reference fluid
- Obtain eight centrifuge tubes, clean thoroughly and dry using paper towels. Slight impurities present in the tubes may alter the readings significantly
- Once dry, pair a tube with a lid. These will remain together for the duration of the test
- Record the mass of each centrifuge tube on its own first, and then with its cap
- Placing one centrifuge tube on a digital scale at a time (tare the scale to allow for the stand holding the tube), and add 30 g of distilled water to each tube. If too much water is added, it can be removed using a paper towel. Do this for four tubes only

- Repeat the process of placing each tube on the scale, but this time add 15 g of the desired soil.
- Fill the remaining four tubes with 40 g of the reference 1 g/l saltwater solution. There should be four tubes containing the reference solution and four tubes containing the soil to undergo testing
- Leave for one hour, then shake each tube to agitate the mixture
- Regardless of soil type, allow to hydrate for 24 hours
- Before placing tubes in the centrifuge, shake vigorously once more to ensure the soil is dispersed uniformly throughout the liquid. It is important to place similar tubes opposite each other in the centrifuge so their masses will be cancelled out due to the high centrifugal force which will be generated at high RPM e.g. soil tubes opposite soil tubes, reference tubes opposite reference tubes
- Run the centrifuge at between 10-15,000 RPM for 30 minutes. A Damon/IEC HT Centrifuge was used in this testing program
- Once the centrifuge has stopped spinning, remove the tubes and allow them to sit in a holder
- The tubes are noticeably warmer upon removal from the centrifuge. The spinning of the tubes in the centrifuge generates heat, which in turn heats the liquid in the tubes. Because the conductivity of water increases with an increase in temperature, it is highly recommended to allow the tubes to equilibrate to room temperature before pouring out the supernatant to test. 3 hours was usually allowed for this equilibration
- Each soil laden tube should be paired with a tube containing the reference saltwater
- Unpack the conductivity meter and clean all glassware to be used for testing. The probe should also be cleaned with distilled water and allowed to dry
- Decant the supernatant from a given soil laden tube into a 10 ml glass beaker and measure its conductivity. Remove the probe and wash with distilled water. Dry carefully using a paper towel. Take a total of 4 readings in this manner
- Pour the reference saltwater into a separate 10 ml glass beaker and measure its conductivity. Again, repeat the process to obtain a total of 4 readings
- It is important to move the probe through the fluid while taking readings. This helps prevent polarization, ensures the solution is well mixed and helps maintain a uniform temperature within the solution

- Clean and store the probe

Using the conversion factor generated from the calibration, the salinity of the supernatant can be estimated. The salinity of the test specimen can be then calculated by multiplying this Figure by the testing water content and dividing it by the natural water content. The equation for this is given in Equation 4.1:

$$RSS = SS \times \frac{w_c}{w_n} \quad (4.1)$$

Where:

RSS = salinity of the test specimen (g/l)

SS = Salinity of the liquid supernatant (g/l)

w_c = water content of soil after centrifuging (%)

w_n = natural water content of the specimen (%)

4.5.2.6 ORGANIC CONTENT

Organic matter exists in soil as vegetation roots, microbes and other organisms. In order to determine how much of these organics are present, the loss on ignition test is performed. This test will also evaporate any bound water from the soil at temperatures up to 440° C. The test is described in ASTM D2974 and its guidelines were followed when determining the organic content. The material to be tested was originally placed in a standard laboratory oven at 105° C until constant mass was achieved. This process removed any free moisture which may exist in the soil. The soil was then transferred to a muffle furnace whose temperature was 440° C. Again, the soil was left in this furnace until constant mass was achieved. The organic content test was performed on London Clay and BBC Series IV.

4.5.3 CONSTANT RATE OF STRAIN TESTS

4.5.3.1 INTRODUCTION

The history and development of the CRS testing method is described in Force (1998) and Gonzalez (2000). The CRS cell used in this testing program was a modified Trautwein CRS apparatus. Modifications to the standard Trautwein cell include a reduction of the normal plunger size, the custom manufacture of a smaller specimen ring to test smaller quantities of soil and the

use of two LVDT's to measure axial displacement. These modifications were necessary owing to the fact that some of the material in the testing program originated in the Gulf of Mexico, and due to high retrieval costs and limited availability of material, smaller specimens are required. The modifications also allow soil to be tested to much higher stress levels. All CRS testing was therefore performed in this reduced sized ring in order to eliminate any size effects which may exist due to different specimen sizes and also to directly compare the results from several soil types. Additional valves were also added to the pore pressure line in order to facilitate the reverse leaching tests which were performed. A schematic of the Trautwein cell is shown in Figure 4.36 with the main components identified.

The testing strain rate is of primary importance. The selected strain rate must produce pore pressure ratios, which is the base excess pressure divided by the total axial stress, between 3 and 15 %. ASTM D4186 gives guidelines on selecting a strain rate which will satisfy these requirements based on the soils Atterberg limits. They recommend a strain rate of 10 %/h for MH materials, 1 %/h for a CL material and 0.1%/h for a CH material (note material definitions based on USCS classification system, ASTM D2487).

Two types of test were performed in the CRS device: standard one dimensional CRS loading tests, and reverse leaching tests which involved replacing the pore fluid in a low salinity BBC leached soil specimen with high salinity saltwater during a test.

Given the range of salinities used throughout the testing program (1 to 256 g/l), the cell fluid for all CRS tests mimicked the pore fluid salinity. The only exception to this rule was when the reverse leaching tests occurred. In this instance, 256 g/l saltwater was used as the cell fluid for a 1 g/l leached BBC specimen.

4.5.3.2 STANDARD 1-D CONSTANT RATE OF STRAIN TESTING

4.5.3.2.1 INTRODUCTION

The standard CRS test was performed in general accordance with ASTM D4186. The specimen is incrementally back pressured using a PVA capable of maintaining and controlling the back pressure to within ± 2 % of the target back pressure throughout the test. A graph of the back pressure stability as a function of time can be seen in Figure 4.44. Both the cell pressure

and the excess pore pressure were measured using a pressure transducer, axial deformation was measured using two LVDT's with true axial deformation taken as the average of the two. The load was measured with an external load cell. Deformation of the soil specimen was corrected for apparatus compressibility.

In this test method, the specimen is constrained axially between two parallel, rigid platens and laterally such that the cross sectional area remains constant. For this series of testing, a Trautwein CRS cell was used. This device provides more flexibility in testing than the conventional incremental oedometer test. With the Trautwein apparatus, the specimens can be saturated under a back pressure, initially with drainage allowed from top and bottom, then loaded with no lateral strains, at a constant rate of strain. The main features of this equipment are presented here. For a more detailed description of CRS testing and procedures, refer to Force (1998) and Gonzalez (2000).

Drainage is provided along the top boundary and the pore pressure is measured at the bottom boundary. The specimen is deformed axially at a constant rate while measuring time, axial deformation, load required to produce the axial deformation and excess pore pressure. Strain rates are limited in the test method by specification of the pore water pressure ratio which is the base excess pressure divided by the total axial stress. This ratio must not drop below 3 % or rise above 15 % in order to produce successful results. This criterion is not always achievable when testing to high stresses. A full description of the test requirements can be found in ASTM D4186 – 06.

The Trautwein cell has a clear plexiglass chamber which fixes onto a metal base. A recess in the metal base accommodates a porous stone, which in turn provides access to a base drainage line from where excess pore pressures are measured during consolidation. A confining ring containing the test specimen sits above this porous stone. The consolidation stress is applied to the specimen via a piston which loads the soil from the top. A schematic diagram of the CRS cell is shown in Figure 4.36.

The CRS tests were performed on small diameter specimens (diameter = 3.55 cm, height = 1.264 cm). The specimen is protected top and bottom with filter screen discs and porous

stones. Once assembled, the cell pressure will be isolated from the base pressure to facilitate the measurement of the excess pore pressure.

Owing to the fact that the testing program involved testing soils to a very high stress, compressibility of the apparatus must therefore be taken into account when reducing the data to separate compression of the apparatus from axial strain in the soil. Two determinations of the apparatus compressibility were performed for the stress range up to 40,000 kPa (based on the specimen diameter) and these plots can be seen in Figure 4.45.

4.5.3.2.2 PROCEDURE

Reference should be made to Figure 4.36 while reading the following in an attempt to follow what is being described. Many different soils were tested in the CRS device throughout this testing program. These ranged from in-situ BBC Shelby tube samples taken from underneath Killian Court, MIT during the summer of 2010 to resedimented soils. Regardless of the soil to be tested, the test preparation procedure remains very similar. All mass measurements should be done on a scale which can read to 0.01 g.

1. Clean the cutter-ring so that it is free from surface dirt and any residues. Obtain the mass of the ring and one filter screen. Clean the recess tool in a similar fashion and obtain its mass. The inside of the cutter ring is then greased to aid in trimming.
2. Square the ends of the soil to be trimmed into the cutting ring using a squaring block. Take at least 2 water contents of the trimmed soil for reference. If the soil is from a Shelby Tube, obtain three Torvane readings on the freshly exposed face of the parent sample. These are to be noted on the data sheet, as well as the location the specimen was taken from along the tubes length. If the soil to be tested is taken from a consolidometer, the resedimentation number is to be noted on the data sheet, as well as the specimens location within the column i.e. 4-6 cm of soil taken from the base of the tube. It is important to keep the same datum within the tube as unlike the Shelby Tube specimens, resedimented soil is extruded from the column. Resedimented soils for CRS testing purposes was generally resedimented to a stress of 100 kPa and rebound to an Over Consolidation Ratio (OCR) of 4.

3. Place the soil to be trimmed below the cutting ring carefully so that soil occupies the entire area of the ring. This is shown in Figure 4.46. Carefully trim the specimen into the cutting ring using the trimming tool. It is important to ensure that the cutting ring is orthogonal to the turntable on which the soil being trimmed sits. A picture of this stage is shown in Figure 4.47. Continue trimming soil into the cutting ring until it contains enough soil to satisfy the requirements of the test (1.264 cm high in this study). Once this has been accomplished, remove the cutting ring from the trimming device. Trim the soil at the end of the ring initially using a wire saw, and then with a straight edge to remove any soil left behind due to the deflection of the wire. A photograph of this stage is shown in Figure 4.48. Clean the area surrounding the freshly trimmed surface and apply a filter screen to the surface of the soil. It is important that the filter screen is the exact same size as the interior of the cutting ring. The recess tool is machined so accurately that there is no room between the cutting ring and the recess tool to accommodate the folding of the filter screen. If this occurs, the recess tool may become jammed in the ring possibly leading to damage of the specimen. Once the recess tool has been pushed as far as it can go into the ring, the required height of soil now exists inside the ring by default. The soil protruding from the opposite side of the ring must now also be trimmed to form a smooth surface in a similar fashion to the method already described. This step is shown in Figure 4.49.
4. The cutting ring now contains soil with the correct dimensions for testing, a filter screen and also a recess tool. The mass of all items must now be taken as one. The mass of the soil can then be found by subtracting the masses obtained from stage 1. The soil is ready to be tested.
5. Before testing, allow all transducers at least 15 minutes to “warm up” before recording their zero values. The cell should be assembled as shown in Figure 4.36. It was noted during the testing program that a square O-ring provided a better seal between the base porous stone and the cell pressure than the previously used double O-ring system. Once the cell is assembled, lower the piston so that it rests on the soil, apply a very small pressure to the piston to ensure the soil is seated on the base porous disc but be careful not to overstress the specimen. The piston is then locked in place and the cell placed into

the load frame. Affix the bracket which holds both LVDT's to the load button and ensure the LVDT's will be in an acceptable voltage range for the duration of the test. Place the load button in contact with the load cell while monitoring the voltage of the load cell to determine when contact is made. Apply a seating load of approximately 2 kgf to the specimen. Ensure that there is pure axial load transfer from load cell to piston, and finally to the loading table. Any eccentricity introduced to the test may introduce errors in the recorded stresses.

6. The cell can now be filled with the appropriate fluid. This is dependent on the soil being tested. The cell was normally filled using a syphon through the cell pressure line. The valve on the cell pressure line which accesses the base pressure was opened for the filling sequence so as to ensure saturation of all test lines. The pore pressure transducer was not attached until the housing into which it fits was overflowing with cell fluid. This ensured saturation of the line from the base of the specimen to the pore pressure transducer. Once the cell was filled, the syphon was disconnected. The connection to the PVA was quickly made, with the pipe coming from the PVA being allowed to drip under a slight pressure while it was connected into the cell, again to ensure saturation of all lines.
7. The cell has now been filled and is connected to the external ancillary plumbing such as the PVA and water supply. Back pressure saturate the specimen in accordance with ASTM D4186 to pressures of 35, 70, 150, 300 and finally 396 kPa. All CRS tests in this research were run at a back pressure of 396 kPa. Depending on the plasticity and hydraulic conductivity of the soil, the time required between these increases in back pressure will change. Generally as the plasticity increases, so does the time between back pressure increments. Throughout this research, it was found that for BBC, a minimum of 15 minutes is required between pressure increments, while for more plastic soils such as London Clay, 40 minutes was a good equalization time. It is important that the specimen be back pressure saturated from both the cell and the base at the same time.
8. Once the specimen is back pressure saturated, the specimen is almost ready to be tested. Two very important steps must be completed prior to testing 1) the piston which is still in the locked position must be unlocked 2) the valve on the cell pressure line must now be closed, if it remains open then no excess pore pressures at the base will be produced.

Once these steps are complete, loading of the specimen can commence at the desired strain rate.

9. The maximum stress level the specimens were tested to in this research was 40,000 kPa. Given that the cross sectional area of the specimen is 9.886 cm^2 , this represents an axial force on the load frame of approximately 4,000 kg. Once the maximum stress was realized, the load frame used was unable to perform secondary compression so the test was either concluded or the specimen unloaded.
10. Once the test is completed, the cell pressure was reduced gradually. This can be done over a period of roughly 30 seconds rather than simply allowing all pressure to evacuate at once. Remove the CRS cell and extrude the soil from the confinement ring taking care to note any extrusion on the interior of the cutting ring which may have occurred. If extrusion has occurred, scrape the extruded soil into a tare in order to obtain the dry mass. With the main test specimen, obtain the final wet mass and then place in an oven at 105°C until constant mass has been reached.

4.5.3.3 REVERSE LEACHING TESTING IN THE CRS CELL

4.5.3.3.1 INTRODUCTION

For the reverse leaching test, an additional Pressure Volume Actuator similar to the one shown in Figure 4.28 was required in order to keep the base pressure of the specimen at a pressure greater than atmospheric, but less than the cell pressure in order to maintain an acceptable pressure differential across the specimen. Because of the small height of the specimen (1.26 cm), accurate control on the base pressure was required. Any increase or decrease in pressure would adversely affect the hydraulic gradient across the specimen. Too low of a gradient and flow would not take place, and too high of a gradient and risk of the soil blowing out was increased. For this test, the cell pressure was maintained with a PVA at 396 kPa, while the base pressure was maintained with a separate PVA at 386 kPa.

4.5.3.3.2 PROCEDURE

Reverse leaching tests were performed on leached BBC. This leached BBC was resedimented to a salinity of 1 g/l, an axial stress of 100 kPa. The soil was rebound to an OCR of

4. The cell fluid used in the test was 256 g/l saltwater. The procedure for setting up the test is identical to the method described in 4.1.1.1.1 up to point 8. The following procedure will continue from point 8 with the additional steps which were performed for the reverse leaching test:

- a. Consolidate the specimen until it lies on the virgin compression line. It is advantageous to stress the specimen well past the preconsolidation pressure to ensure that the recorded data will plot in a true log-linear way. It will be easier to detect any differences in behavior if this is the case.
- b. Once the conditions of “a” are satisfied, the consolidation process can be halted – the piston is not locked so that the relaxation of the soil can be measured. Figure 4.36 should be referenced while reading the following as it will help explain the process. The valve on the cell side of the pore pressure transducer can be closed so that an additional PVA can be connected to the valve on the atmospheric side of the transducer. The valve can then be opened to allow the pore pressure transducer to read the pressure which is present in the PVA. The pressure in the PVA is adjusted until the transducer records a pressure of 390 kPa. Allow the PVA to equilibrate for 1 hour before commencing leaching. Once the base pressure has stabilized at 390 kPa, record the zero value of the LVDT attached to the PVA. The valve on the cell side of the pore pressure transducer can now be opened. Flow should now occur through the specimen.
- c. Depending on the cell fluid and the hydraulic conductivity of the soil, the test may take several weeks to complete. It was found for BBC that the pore volume could be replaced 2.11 times in approximately 2.5 weeks. The volume of fluid which has passed through the soil can be monitored by recording the voltage of the LVDT attached to the PVA.
- d. Once an adequate quantity of fluid has passed through the soil (which would be a test dependent decision), the valve to the PVA is closed. The pore pressure transducer should now be given adequate time to equilibrate with the cell pressure before consolidation recommences. Given the small pressure gradient which existed initially, this takes a matter of minutes for BBC.

- e. Consolidation of the soil can now recommence to the desired stress level. It is important to note that actual consolidation of the soil will proceed at the same rate as in a standard test, the time is lost by performing the reverse leaching on the soil.

4.5.4 **TRIAXIAL TESTING**

4.5.4.1 **INTRODUCTION**

Triaxial testing was performed using the existing triaxial apparatus in the MIT Geotechnical Laboratory. The main features of this apparatus are presented here. For a more complete description of the MIT stress path triaxial apparatus, Sheahan (1991), Sheahan & Germaine (1992) and Santagata (1998) provide more detailed information.

4.5.4.2 **TRIAXIAL COMPRESSION TEST PROCEDURE**

A typical triaxial test can be broken into five stages.

- 1) cell and apparatus preparation
- 2) specimen trimming and measuring
- 3) Specimen saturation
- 4) Consolidation
- 5) Specimen shearing

In order to minimize setup time and help ensure the test runs smoothly, extra emphasis should be placed on proper setup and preparation as corners cut at this stage may show up in the form of leaks, incorrect transducer readings (or zero values) and/or poor phase relation calculations after some time has been invested in the test. Corners cut in the setup phase will be paid for one way or another. In general, procedures developed by Dr. John Germaine for the Graduate Laboratory class at MIT (class number 1.37) were followed when preparing for, and conducting triaxial testing. These notes give a step by step approach to what must be done in order to realize a successful test.

4.5.4.3 OBSERVATIONS

Although the same procedures were employed when testing all soils, some notable differences in soil behavior during testing can be identified. When back pressure saturating specimens, a B value greater than 0.98 was desired prior to advancing the test. When resedimented material had been back pressure saturated with a cell pressure of ~300 kPa and a pore pressure of 280 kPa, the required B value was achieved in the vast majority of cases. As the triaxial testing program also involved in-tact material (Killian Court BBC), differences were noted in the amount of cell pressure and pore pressure required to achieve the same degree of saturation. In-situ material usually required cell pressures of 4 - 450 kPa with corresponding pore pressure values of 380 - 430 kPa respectively.

Soil	Liquid Limit (%)	Plastic Limit (%)	Plasticity Index (%)	Clay Fraction (%)	USCS Classification	Strain Rate (%/hour)
Boston Blue Clay Series IV	48	25	23	56	CL	2
Leached BBC	48	25	23	56	CL	2
Sodium Hex BBC	48	25	23	56	CL	2
Killian Court In-Situ BBC	48*	25*	23*	56*	CL	2
London Clay	73.8	30.5	43.3	63	CH	0.5
Sodium Montmorillonite	634 ¹ 505 ²	76	558 ¹ 429 ²	100*	CH	1 ³
GOM - Ursa	51.7	23.7	28	54	CH	1
GOM - Soil 1	70	29	41	59.2	CH	0.6

Notes: *Assumed values

1 - Determined using the Casagrande cup method

2 - determined using the fall cone method

3 - The sodium montmorillonite quoted in this table was tested with 256 g/l saltwater as the pore fluid for CRS testing. The pore fluid used to obtain the atterberg limits for sodium montmorillonite was distilled water.

Table 4-1 Details of soils tested in CRS testing program

RESEDIMENTATION DATA						
#	Sample Number	Start Date (dd/mm/yyyy)	Source Material	Salinity (g/l)	Pore Fluid Content (%)	Tested via (test number)
1	RS165 *	20/2/2011	Kaolinite	0	100	CRS (1214, 1213, 1211)
2	RS174	27/2/2011	Natural BBC Series IV	64	100	CRS (1218, 1216, 1217)
3	RS175	27/2/2011	Natural BBC Series IV	16	100	CRS (1222, 1221, 1220, 1219)
4	RS178	12/4/2011	Natural BBC Series IV	4	100	CRS (1231, 1230, 1229)
5	RS179	14/4/2011	Natural BBC Series IV	128	100	CRS (1223, 1224, 1225)
6	RS184	10/5/2011	Natural BBC Series IV	256	110	CRS (1228, 1227, 1226)
7	RS190	1/6/2011	Natural BBC Series IV	4	100	CK ₀ UC (TX1068)
8	RS192	2/6/2011	RGOM - Ursa	0	100	CRS (1309, 1308, 1307)
9	RS193	2/6/2011	Natural BBC Series IV	256	110	CK ₀ UC (TX1069)
10	RS194	6/6/2011	Natural BBC Series IV	4	100	CK ₀ UC (TX1074)
11	RS195	6/6/2011	Natural BBC Series IV	4	100	CK ₀ UC (TX1078)
12	RS197	13/6/2011	Natural BBC Series IV	256	110	CK ₀ UC (TX1075)
13	RS199	17/6/2011	Natural BBC Series IV	64	100	CRS (1234, 1233, 1232)
14	RS200	20/6/2011	Natural BBC Series IV	256	110	CK ₀ UC (TX1081)
15	RS201	20/6/2011	Natural BBC Series IV	4	100	CRS (1252, 1251)
16	RS202	28/6/2011	Leached RBBC	1	80	CRS (1238, 1237, 1236, 1235)
17	RS205	6/7/2011	Leached RBBC	256	120	CRS (1239, 1240, 1241)
18	RS206	7/7/2011	Leached RBBC	64	95	CRS (1245, 1246, 1247)
19	RS207	9/7/2011	Leached RBBC	16	90	CRS (1242, 1243, 1244)
20	RS209	29/7/2011	Leached RBBC	1	80	CK ₀ UC (TX1084) / CRS (1250)
21	RS210	29/7/2011	Leached RBBC	1	80	CK ₀ UC (TX1082) / CRS (1248, 1249)
22	RS211	5/8/2011	Leached RBBC	256	120	CK ₀ UC (TX1086)
23	RS212	5/8/2011	Leached RBBC	256	120	CRS (1254, 1253)
24	RS216	16/8/2011	Sodium Hex BBC	0	56	CRS (1314, 1313)
25	RS219	8/9/2011	Leached RBBC	64	90	CRS (1290, 1271)
26	RS222	12/9/2011	London Clay	16	130	CRS (1303, 1294, 1291)
27	RS229	15/9/2011	Leached RBBC	256	120	CK ₀ UC (TX1094)
28	RS230	5/10/2011	London Clay	256	140	CRS (1306)
29	RS232	15/10/2011	London Clay	4	130	CRS (1305, 1304)
30	RS234 *	26/10/2011	Natural BBC Series IV	4	100	CK ₀ UE (TX1104-A)
31	RS237 *	29/10/2011	Natural BBC Series IV	4	100	CK ₀ UE (TX1103)
32	RS238 *	11/11/2011	Natural BBC Series IV	256	120	CK ₀ UE (TX1107)
33	RS240 *	15/11/2011	Natural BBC Series IV	256	120	CK ₀ UE (TX1104-B)
34	RS245 *	20/12/2011	Sodium Montmorillonite	1	1050	CRS
35	RS246 *	20/12/2011	Sodium Montmorillonite	1	1050	CRS
36	RS250	24/1/2012	Sodium Montmorillonite	256	100	CRS (1322, 1318, 1316)
37	RS251 *	29/1/2012	RGOM - Soil 2	100	138	CRS
38	RS252 *	2/2/2012	RGOM - Soil 1	100	138	CRS (1312)
39	RS255	25/2/2012	Leached RBBC	0	62	CRS (1328, 1327, 1324, 1323)
40	RS262 *	24/3/2012	RGOM - Soil 1	200	-	CRS (1329)
41	RS266 *	23/4/2012	RGOM - Soil 2	200	-	CRS

* indicates sample whose results are not included in this thesis
Right hand column shows how specimen was tested with the corresponding test number in parentheses

Table 4-2 List of all resedimentation batches produced for this research

Soil Type	Salt Content (g/l)	Fluid Content (%)	Comments
BBC Series IV	4	100	Not much change in required fluid content over a large range of salinity
	16	100	
	64	100	
	128	100	
	256	110	
Leached BBC	0	62	Produces a very thin slurry
	1	80	Increase in fluid content with an increase in salinity - contrast to natural BBC Series IV
	16	90	
	64	95	
	256	120	
Sodium Hex BBC	0	56	Produces a very thin slurry, required we almost half that required for BBC Series IV
London Clay	4	130	Similar observations to BBC Series IV, not much change in required fluid content over a large salinity range
	16	130	
	256	140	
Sodium Montmorillonite	1	1050	Produces a very thin slurry at low salinity. Huge variation in required water content
	256	100	
GOM Ursa	0	100	Resedimented with distilled water only
<p>Note: All soils resedimented with sea salt (NaCl). The salt concentrations shown indicate the mass of salt added to 1 litre of distilled water</p>			

Table 4-3 List of soils resedimented during the course of this research and the required mass of fluid required to bring the soil to a stable slurry at the salt concentrations indicated

Device	Data Acquisition Channel	Measurement	Device	Calibration Factor (v/v)	Range	Resolution	Stability
TR4	41	Axial Deformation	External LVDT	-2.535 cm	2.50 cm	±0.000248 % (0.1 mV)	±0.00248 % (1 mV)
	42	Specimen Volume	Volume Strain LVDT	71.19 cm ³	45 cm ³	±0.00048 % (0.1 mV)	±0.000048 % (1 mV)
	44	Input Voltage	-	-	-	-	-
	72	Axial Force	External Load Cell	14798.2 kN	44.5 kN	0.77 N (0.001 mv)	7.7 N (0.01 mV)
	73	Axial Deformation	External LVDT	2.571 cm	2.50 cm	±0.000379 % (0.1 mV)	±0.00379 % (1 mV)
	74	Cell Pressure	Pressure Transducer	69.25 MPa	1.4 MPa	0.04 kPa (0.001 mv)	0.4 kPa (0.01 mV)
	75	Pore Pressure	Pressure Transducer	68.65 MPa	1.4 MPa	0.05 kPa (0.001 mv)	0.5 kPa (0.01 mV)
	76	Input Voltage	-	-	-	-	-

Table 4-4 Characteristics of instruments used in CRS TR4 apparatus Note: Resolution and stability based on central data acquisition system, calculations based on specific dimensions

Device	Data Acquisition Channel	Measurement	Device	Calibration Factor (v/v)	Range	Resolution	Stability
MIT01	10	Specimen Volume	Volume Strain LVDT	-96.26 cm ³	45 cm ³	±0.0006 % (0.1 mV)	±0.006 % (1 mV)
	11	Pore Pressure	Pressure Transducer	68.68 MPa	1.4 MPa	0.021 kPa (0.001 mv)	0.21 kPa (0.01 mV)
	12	Axial Force	Internal Load Cell	68.44 kN	2.22 kN	0.77 N (0.001 mv)	7.7 N (0.01 mV)
	13	Cell Pressure	Pressure Transducer	68.74 MPa	1.4 MPa	0.05 kPa (0.001 mv)	0.5 kPa (0.01 mV)
	14	Axial Deformation	External LVDT	-2.08 cm	2.50 cm	±0.007 % (0.1 mV)	±0.007 % (1 mV)
	15	Input Voltage	-	-	-	-	-

Table 4-5 Characteristics of instruments used in triaxial MIT01 apparatus Note: Resolution and stability based on central data acquisition system, calculations based on specific dimensions

Device	Data Acquisition Channel	Measurement	Device	Calibration Factor (v/v)	Range	Resolution	Stability
MIT02	30	Specimen Volume	Volume Strain LVDT	23.23 cm ³	45 cm ³	±0.0003 % (0.1 mV)	±0.003 % (1 mV)
	31	Axial Deformation	External LVDT	2.48 cm	2.50 cm	±0.004 % (0.1 mV)	±0.004 % (1 mV)
	32	Input Voltage	-	-	-	-	-
	33	Cell Pressure	Pressure Transducer	-68.52 MPa	1.4 MPa	0.015 kPa (0.001 mv)	0.15 kPa (0.01 mV)
	34	Axial Force	Internal Load Cell	65.84 kN	2.22 kN	0.02 N (0.001 mv)	2 N (0.01 mV)
	137	Pore Pressure	Pressure Transducer	68.82 MPa	1.4 MPa	0.055 kPa (0.001 mv)	0.55 kPa (0.01 mV)

Table 4-6 Characteristics of instruments used in triaxial MIT02 apparatus Note: Resolution and stability based on central data acquisition system, calculations based on specific dimensions

Device	Data Acquisition Channel	Measurement	Device	Calibration Factor (v/v)	Range	Resolution	Stability
MIT04	108	Axial Deformation	External LVDT	2.08 cm	2.50 cm	±0.0018 % (0.1 mV)	±0.0018 % (1 mV)
	109	Cell Pressure	Pressure Transducer	69.1 Mpa	1.4 Mpa	0.027 kPa (0.001 mv)	0.27 kPa (0.01 mV)
	110	Axial Load	Internal Load Cell	64.49 kN	2.22 kN	0.015 N (0.001 mv)	1.5 N (0.01 mV)
	111	Pore Pressure	Pressure Transducer	68.68 Mpa	1.4 mPa	0.011 kPa (0.001 mv)	0.11 kPa (0.01 mV)
	112	Specimen Volume	Volume Strain LVDT	22.60 cm ³	45 cm ³	±0.0002 % (0.1 mV)	±0.002 % (1 mV)
	113	Input Voltage	-	-	-	-	-

Table 4-7 Characteristics of instruments used in triaxial MIT02 apparatus Note: Resolution and stability based on central data acquisition system, calculations based on specific dimensions



Figure 4.1 Bulk London Clay as received to the MIT Geotechnical Laboratory



Figure 4.2 Close up of bulk London Clay soil with blue flow channel areas and pockets of quartz visible



Figure 4.3 Air Drying of London Clay using industrial fan (performed in MIT basement, building 1)

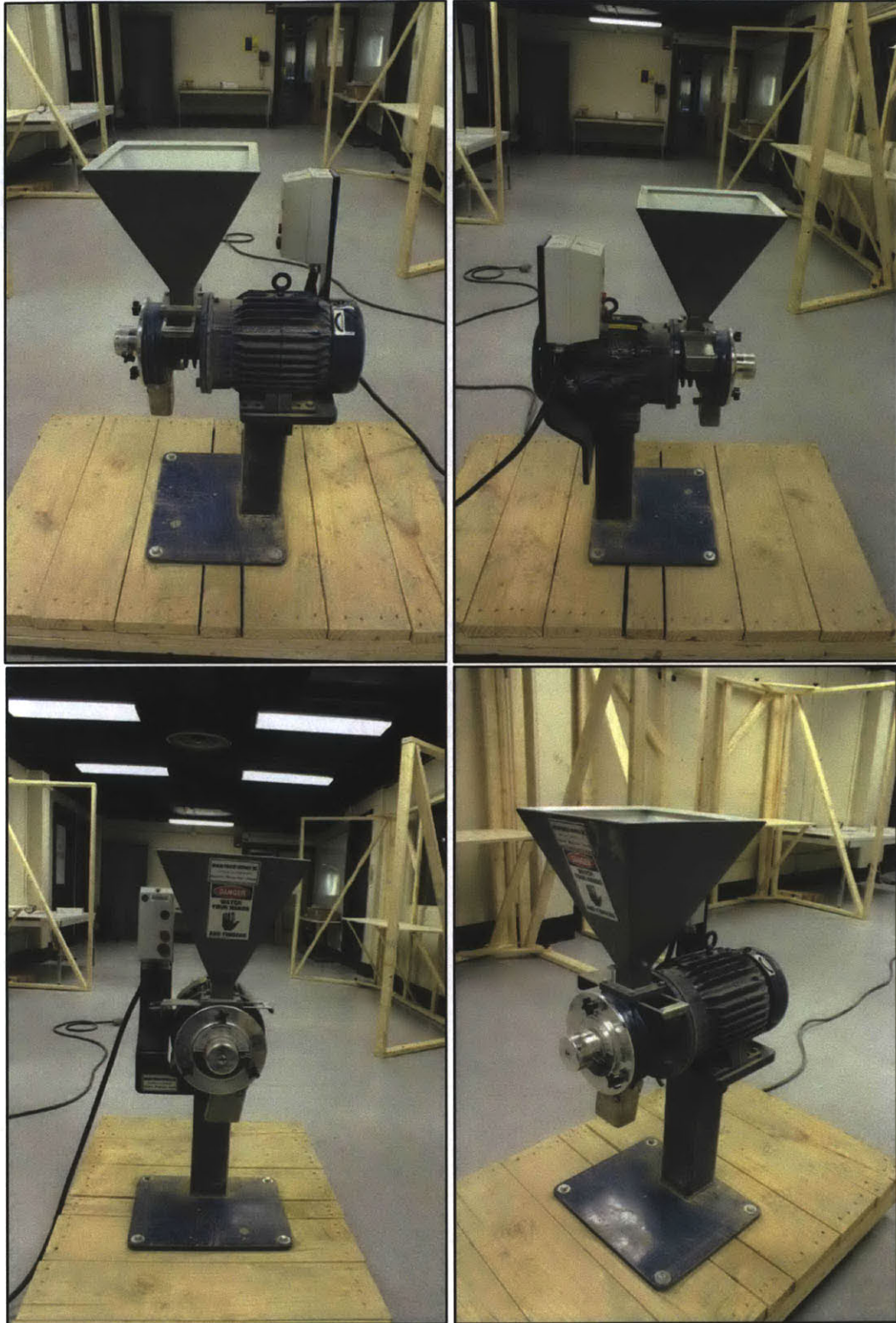


Figure 4.4 GPX Disc Grinder Used in Processing London Clay and Leached BBC

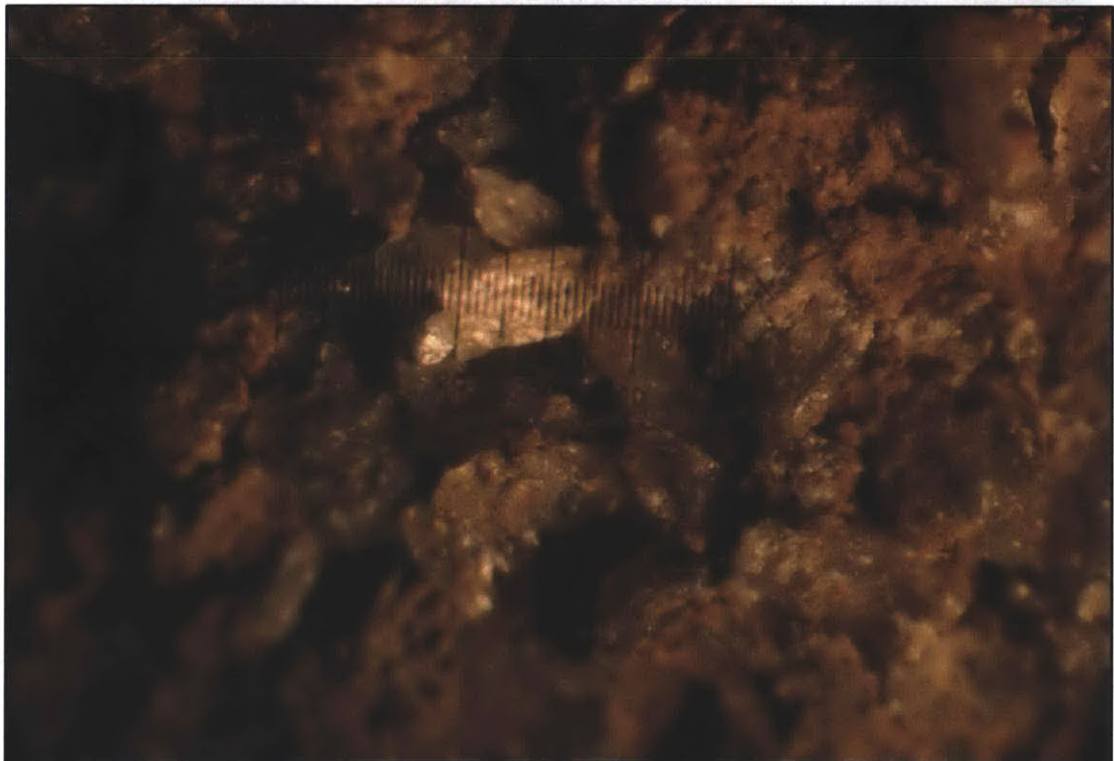
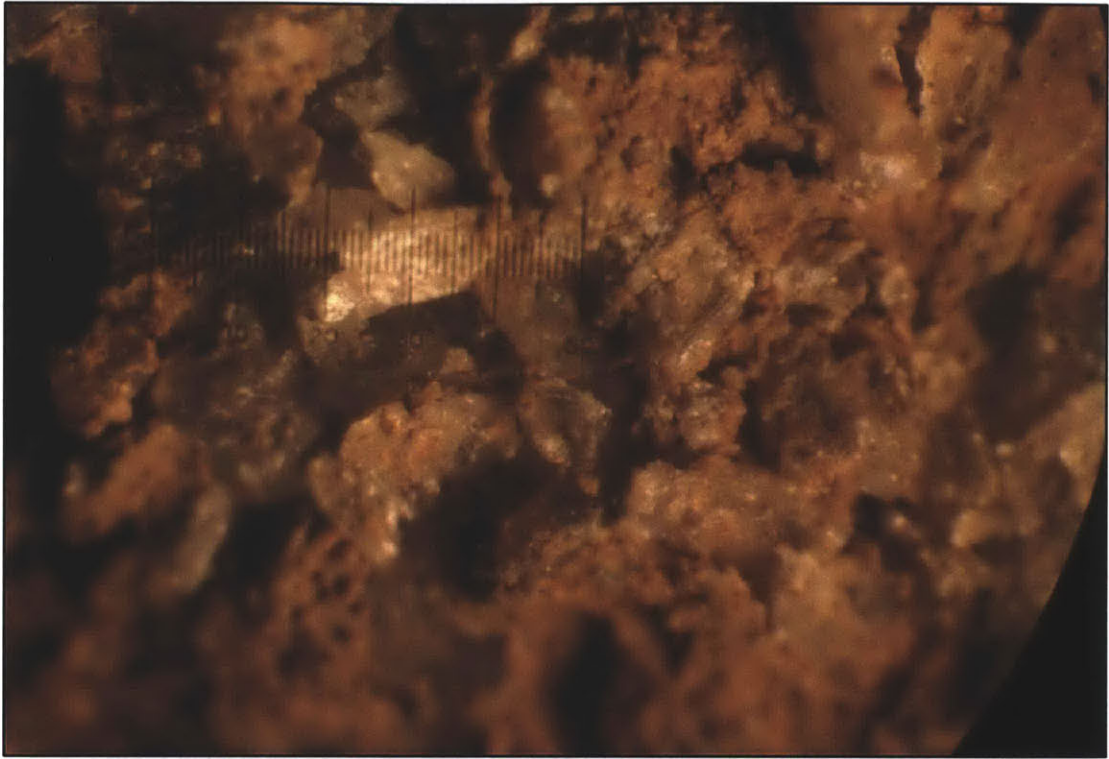


Figure 4.5 Quartz crystals visible in bulk London Clay visible at X2 magnification

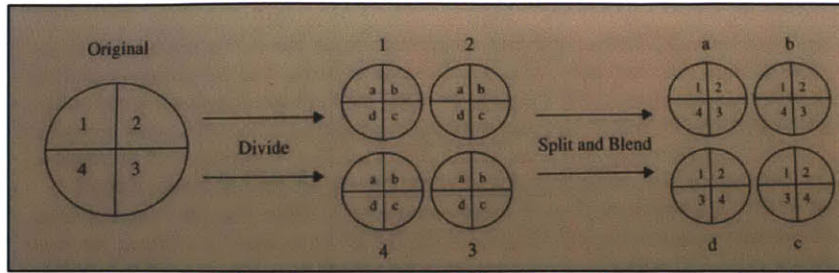


Figure 4.6 Schematic of the blending procedure for large samples (Germaine & Germaine, 2009)

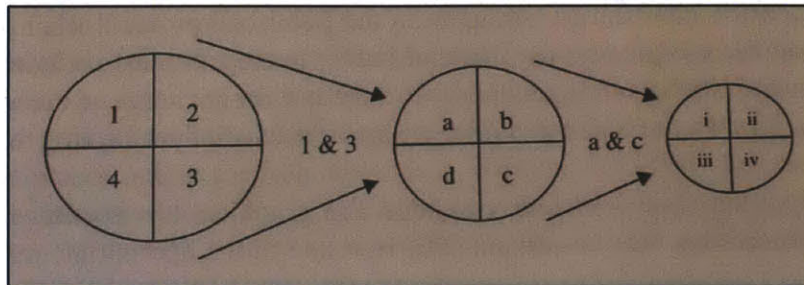


Figure 4.7 Schematic of the sequential quartering procedure (Germaine & Germaine, 2009)



Figure 4.8 Finely ground London Clay being prepared for storage in 10 gallon plastic containers

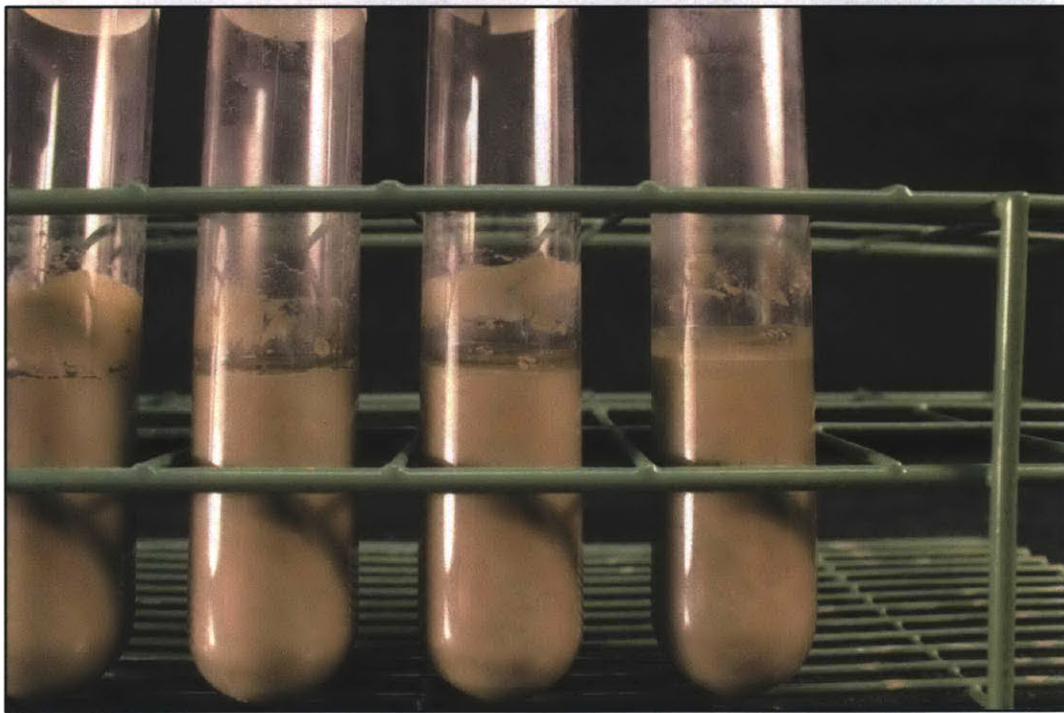
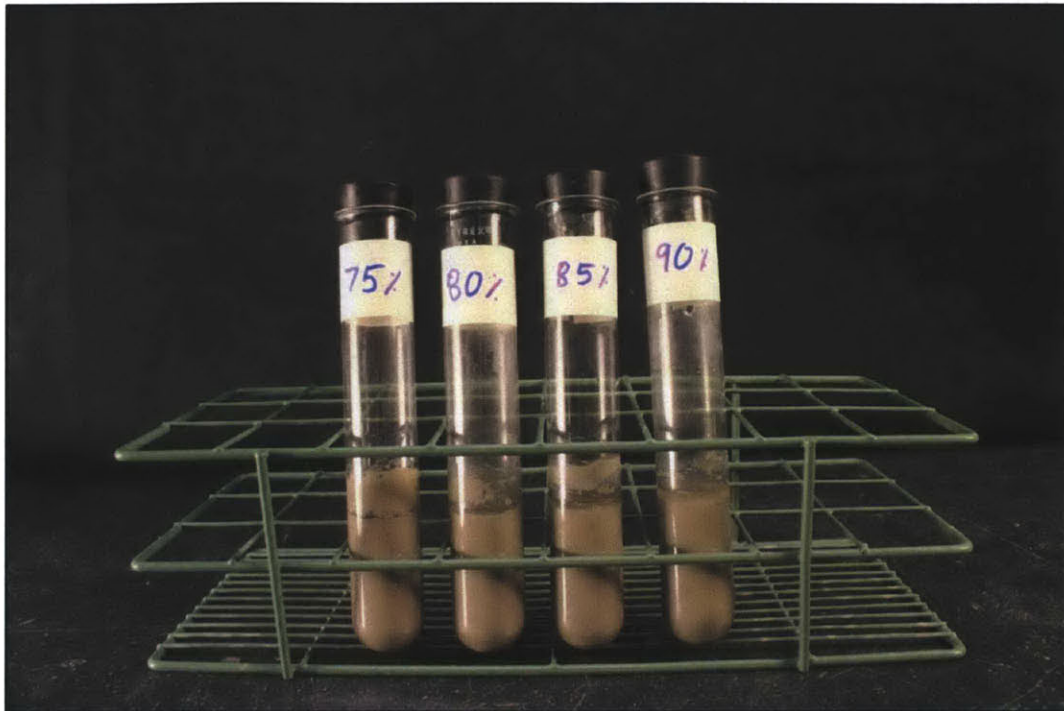


Figure 4.9 Test for determining ideal water content for resedimenting an unfamiliar soil. Top: test tubes showing water contents which were tested Bottom: close up showing free water existing on top of tubes containing too much water (soil being tested BBC which has been leached twice)

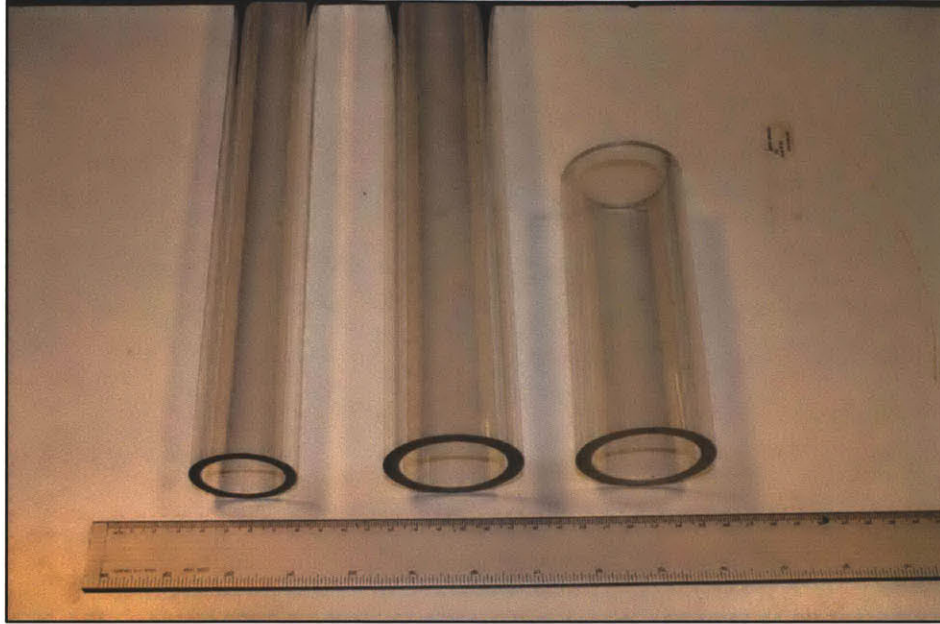


Figure 4.10 Consolidometers used for this research. Left: consolidometer for triaxial testing, Middle: consolidometer for CRS testing, Right: consolidometer for CRS testing when very small quantities of soil were resedimented



Figure 4.11 Kitchen Aid mixer which is used in the laboratory to mechanically agitate slurry

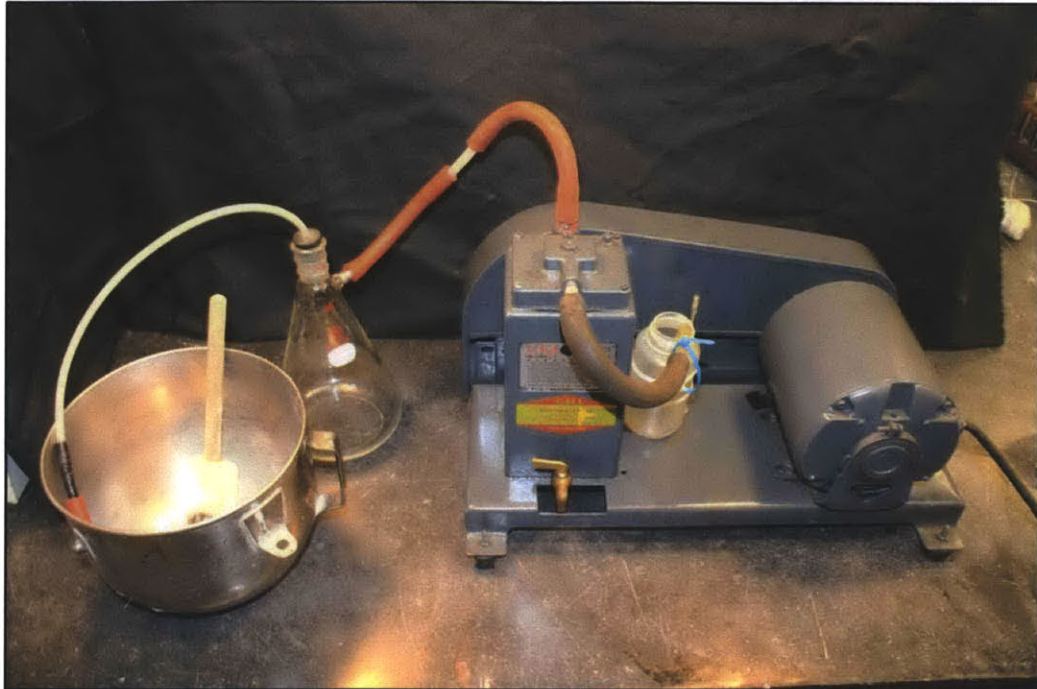


Figure 4.12 Vacuuming arrangement for slurry. Process starts on left with mixed slurry then proceeds into vacuum flask. Vacuum pump on right creates vacuum which de-airs slurry



Figure 4.13 Vacuum flask ready to de-air soil on left, and de-airing soil on right where soil is allowed to free fall into the vacuum flask

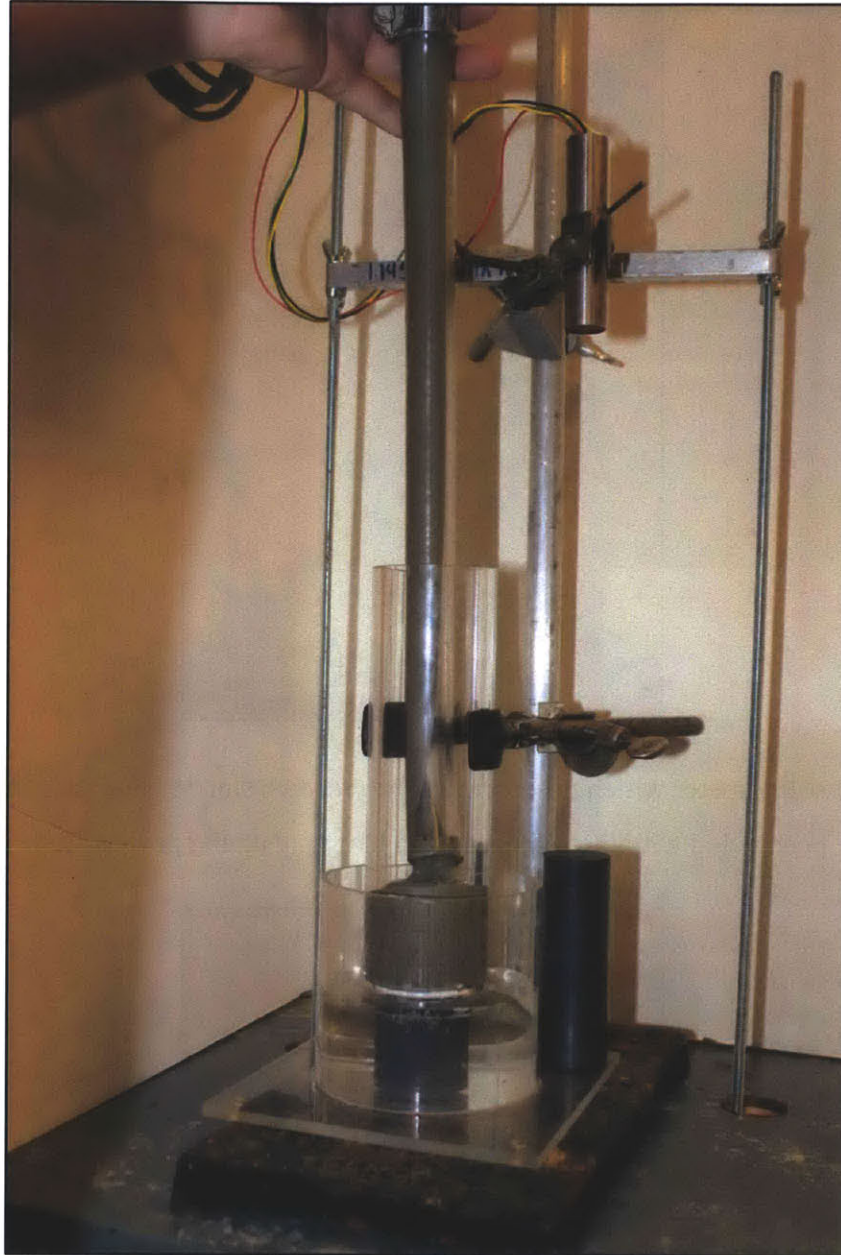


Figure 4.14 Pouring slurry into consolidometer with funnel and flexible tube. Note the discharge is kept slightly over the rising soil surface (soil being poured is BBC leached twice which was resedimented with distilled water)

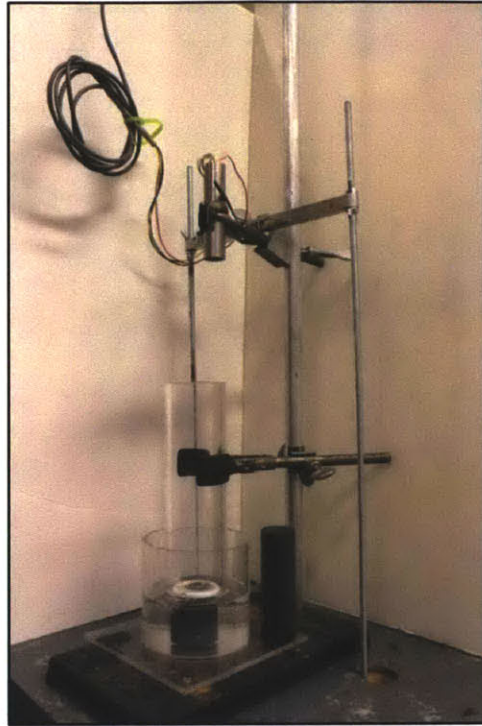
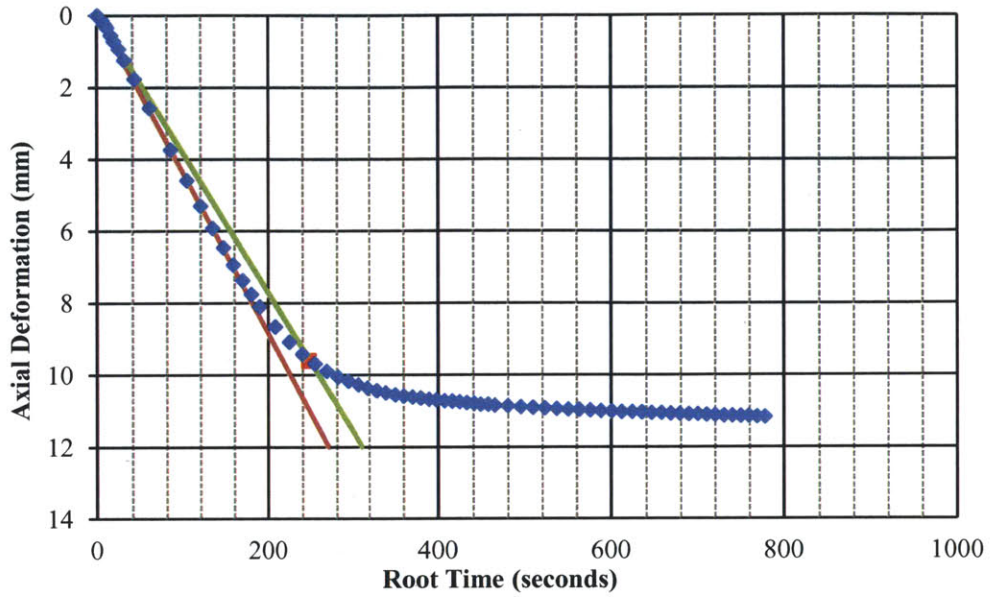


Figure 4.15 Consolidometer which is set up ready to receive slurry. Note that the water bath has been filled with the required fluid half way up the porous stone



Figure 4.16 Resedimentation set-up at high stress with hanger weights applying stress for safety

Root Time Method



Log Time Method

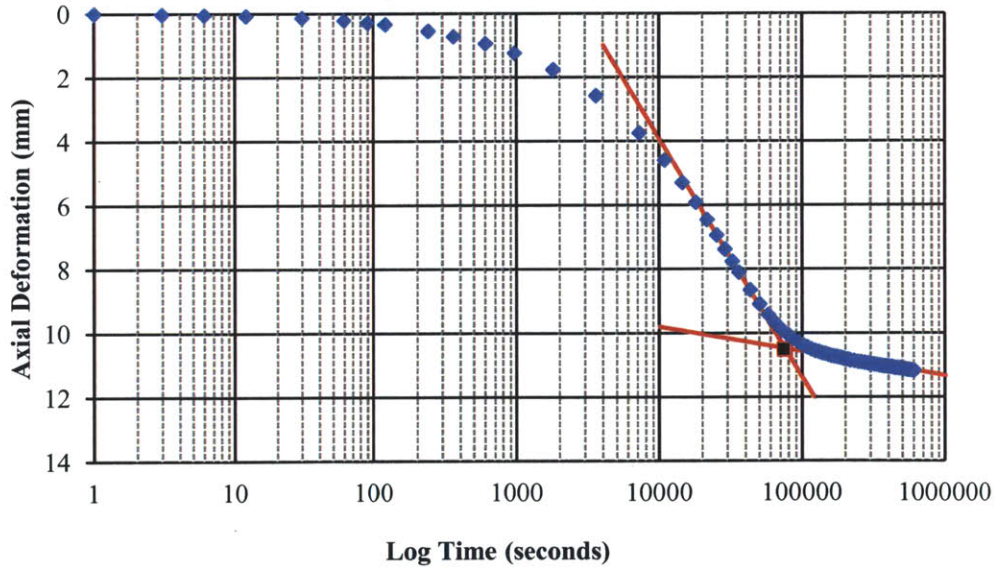


Figure 4.17 Top: Root time method for determining time to end of primary consolidation. Bottom: The same data plotted in log time to determine the time to end of primary (graph for London Clay resedimented to 4 g/l – the stress level at EOP is 100 kPa)

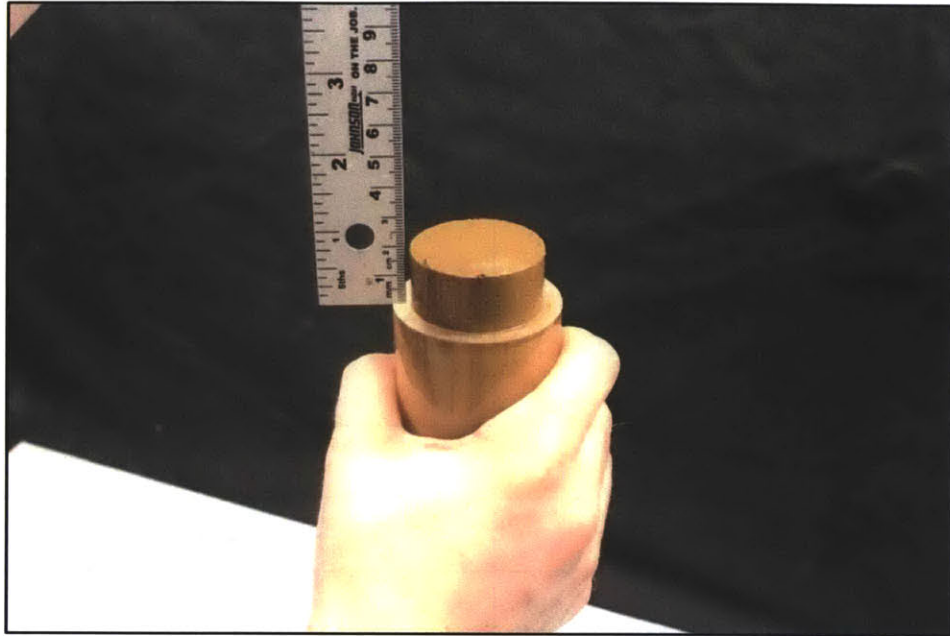


Figure 4.18 Extruding London Clay soil from consolidometer. Approximately 2 cm of soil is required per CRS test with careful trimming (soil being extruded is London Clay at 256 g/l)

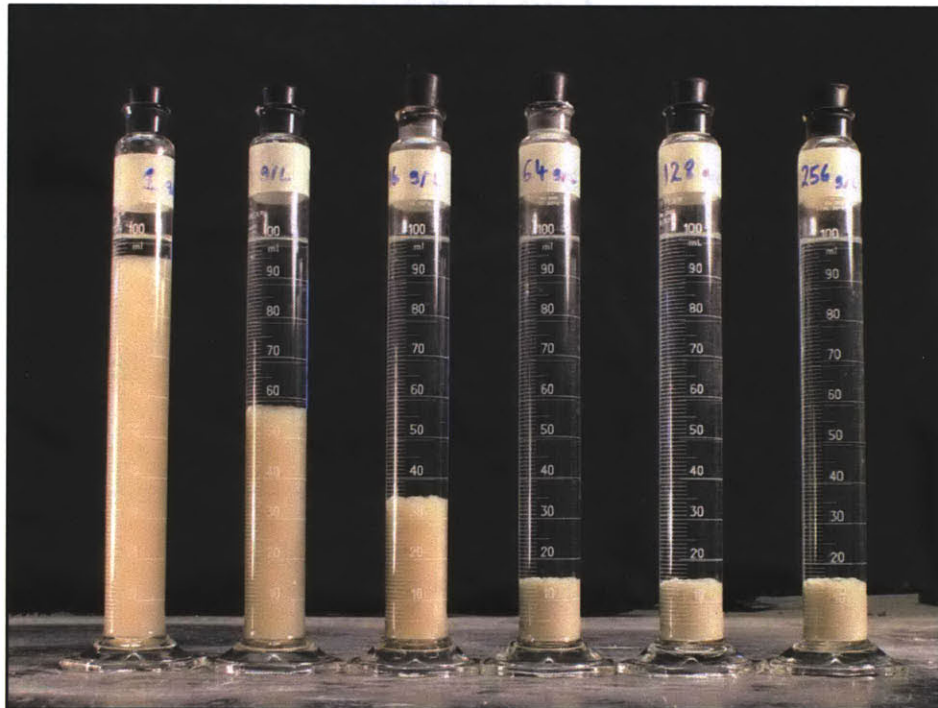


Figure 4.19 Sedimentation test showing the variation in sedimentation height with different quantities of pore fluid salinity (1 g of sodium montmorillonite in each tube. Pore fluid salinities

L-R: 1, 4, 16, 64, 128 & 256 g/l NaCl)



Figure 4.20 Issue of salt precipitating out of solution in high salinity resedimentation (soil shown is sodium montmorillonite being resedimented to 256 g/l)

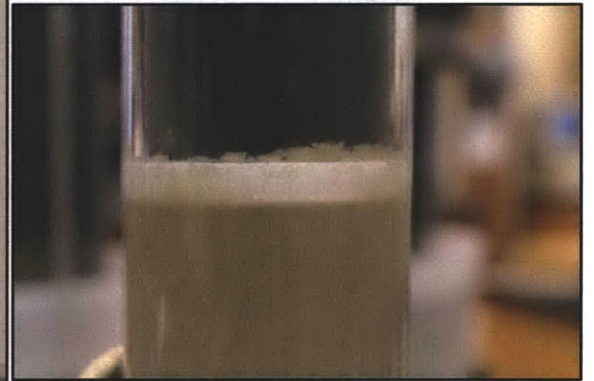
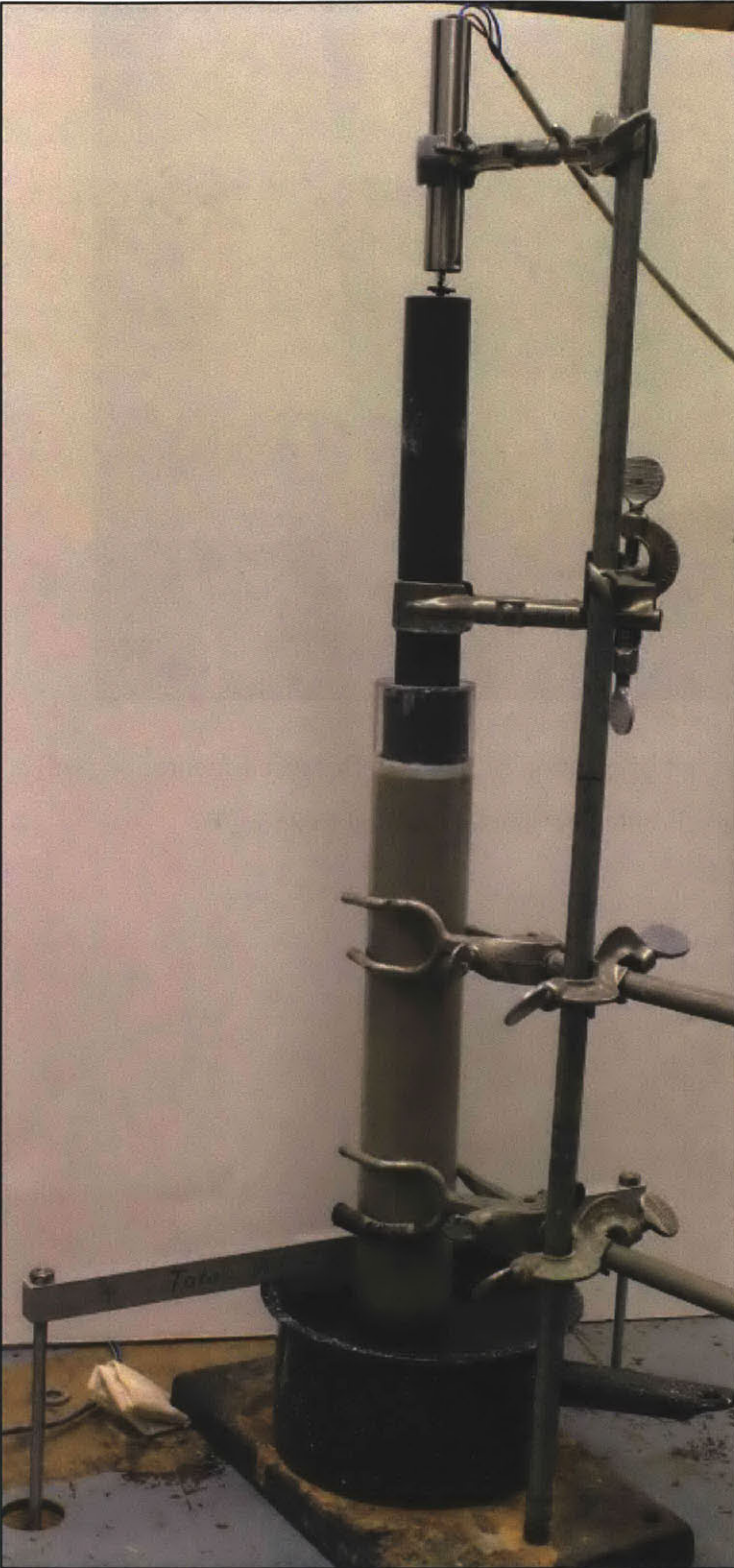


Figure 4.21 New method of wrapping porous stone in PTFE tape to help prevent extrusion, close-up shown on right (soil being consolidated is sodium montmorillonite at 1 g/l)



Figure 4.22 Method to help reduce extrusion from base stone in thin slurries (internal porous stone placed flush with the base of the consolidometer; this in turn is placed on top of a larger diameter porous stone and filter screen as shown)

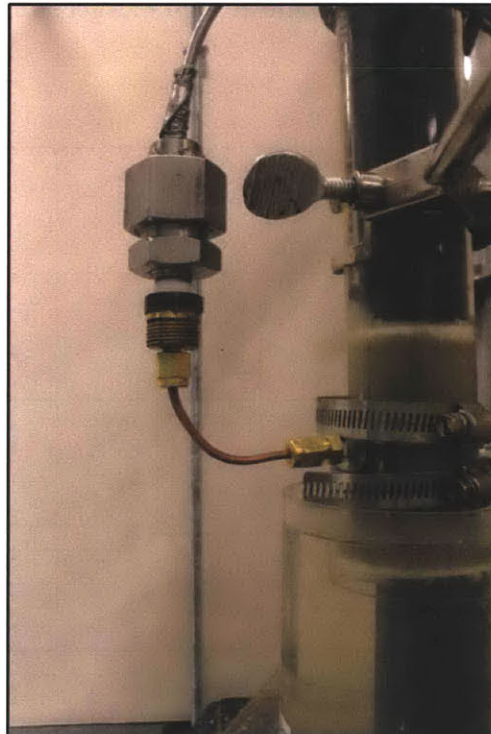


Figure 4.23 Basic method of measuring pore pressures during resedimentation (soil is sodium montmorillonite at 1 g/l)

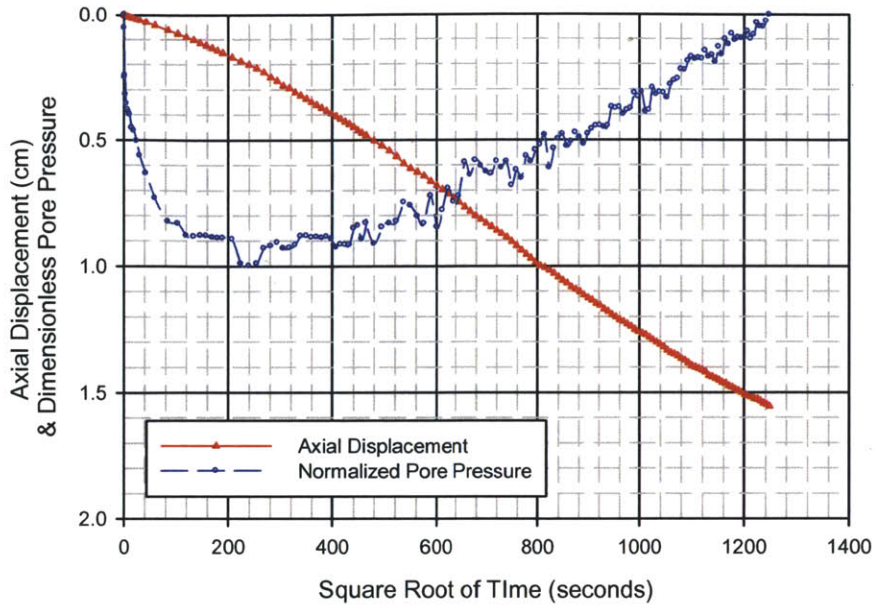


Figure 4.24 Plot of axial deformation and normalized pore pressures versus the square root of time (soil is sodium montmorillonite at 1 g/l - target stress level is 100 kPa)

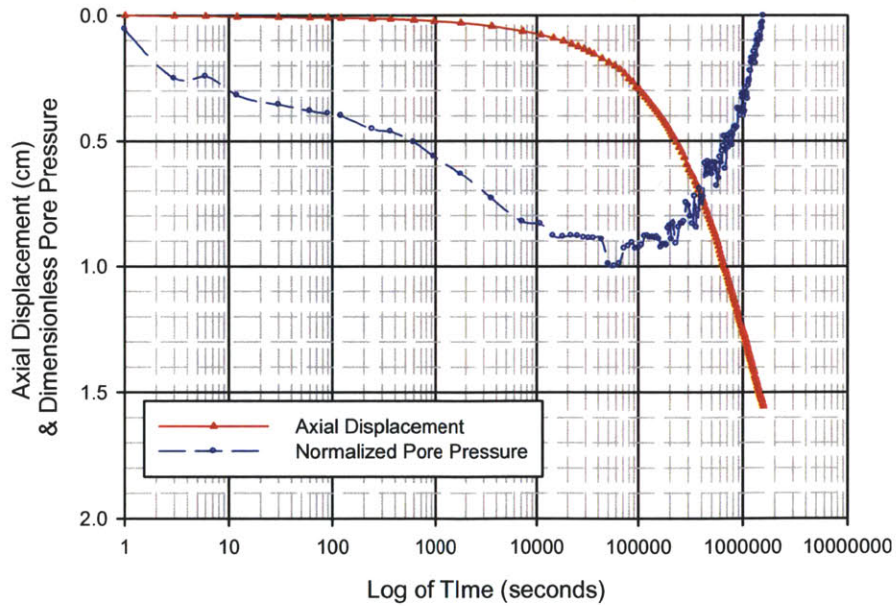


Figure 4.25 Plot of axial deformation and normalized pore pressures versus the log of time (soil is sodium montmorillonite at 1 g/l - target stress level is 100 kPa)

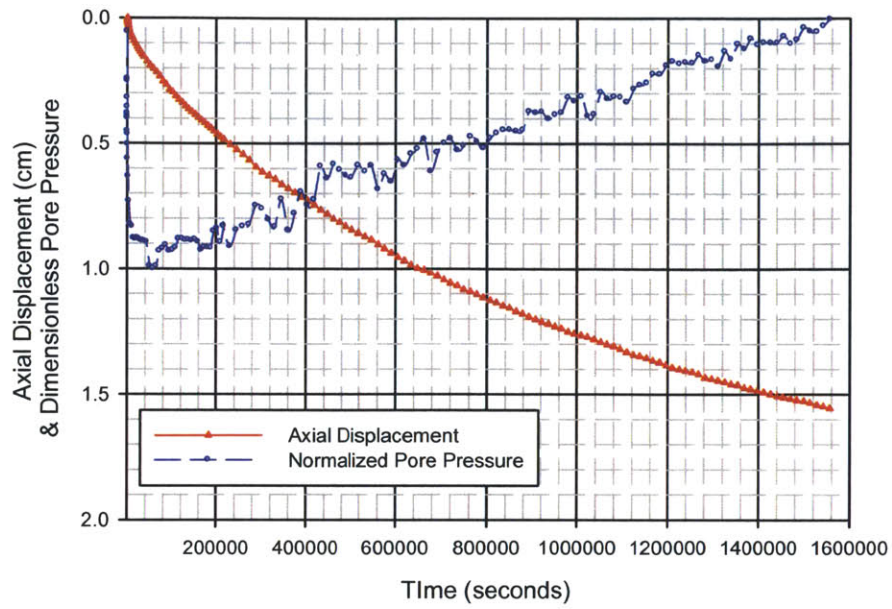


Figure 4.26 Plot of axial deformation and normalized pore pressures versus time (soil is sodium montmorillonite at 1 g/l - target stress level is 100 kPa)



Figure 4.27 Electronic transducers used throughout the testing program. Top Left: Trans-Tek LVDTs, 0243-0000 D-90 LVDT (large LVDT), 0240-0000 H-8 (small LVDT), Top Right: Pressure Transducer, Bottom Left: 500 lb Load Cell, Bottom Right: Close up of pressure transducer and also a section through a pressure transducer to help demonstrate its operation

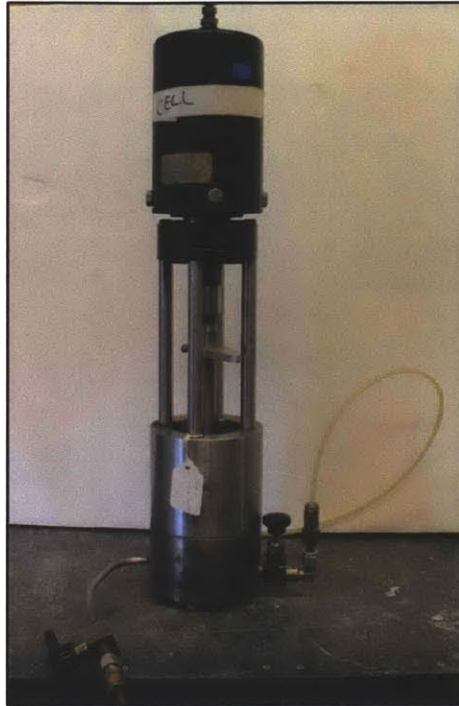


Figure 4.28 Pressure Volume Actuator for CRS testing (calibration factor on tag)

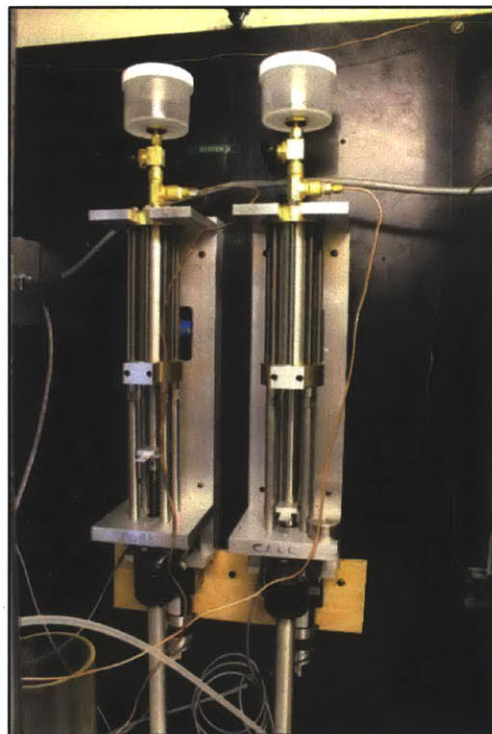


Figure 4.29 Pressure Volume Actuators for pore pressures (left), and cell pressure (right) used in triaxial testing. Copper tubing exiting from top is attached into triaxial cell



Figure 4.30 10,000 lb capacity load cell used for CRS testing

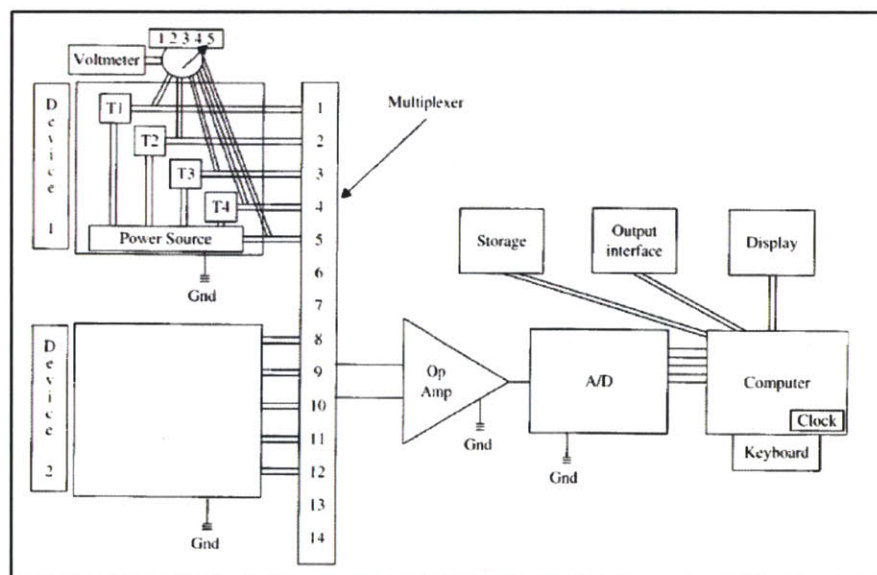


Figure 4.31 Schematic diagram of a central data acquisition system (Germaine & Germaine, 2009)

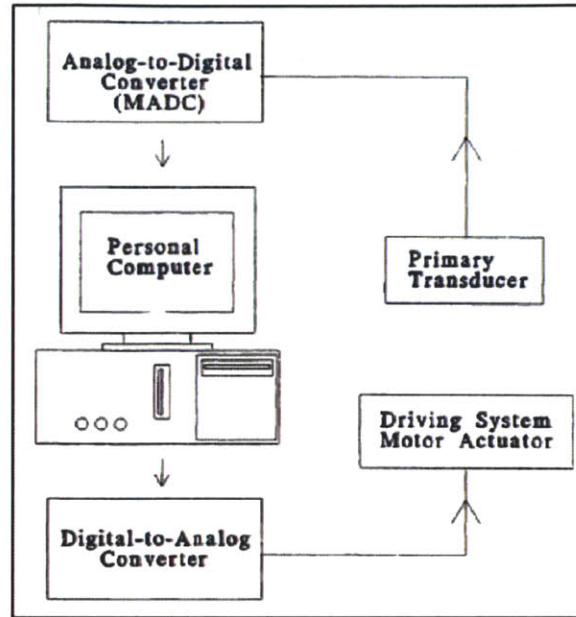


Figure 4.32 Schematic diagram of the control system hardware components



Figure 4.33 CRS trimming ring used for research on right, and standard CRS Trimming ring on left

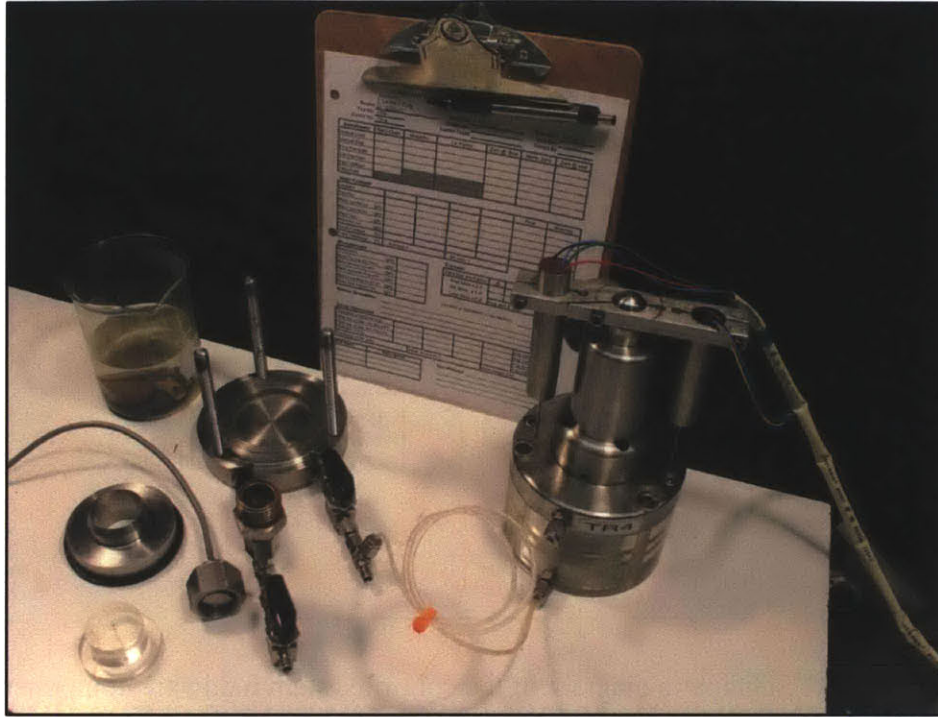


Figure 4.34 Items required for CRS testing. Items include porous stones kept saturated in distilled water, cutting ring with square seal, recess tool and data sheet

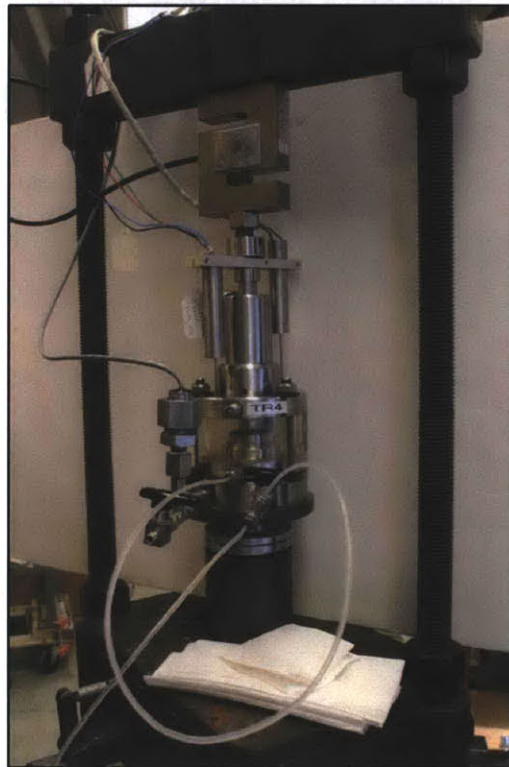


Figure 4.35 CRS Cell TR4 set-up and running a test

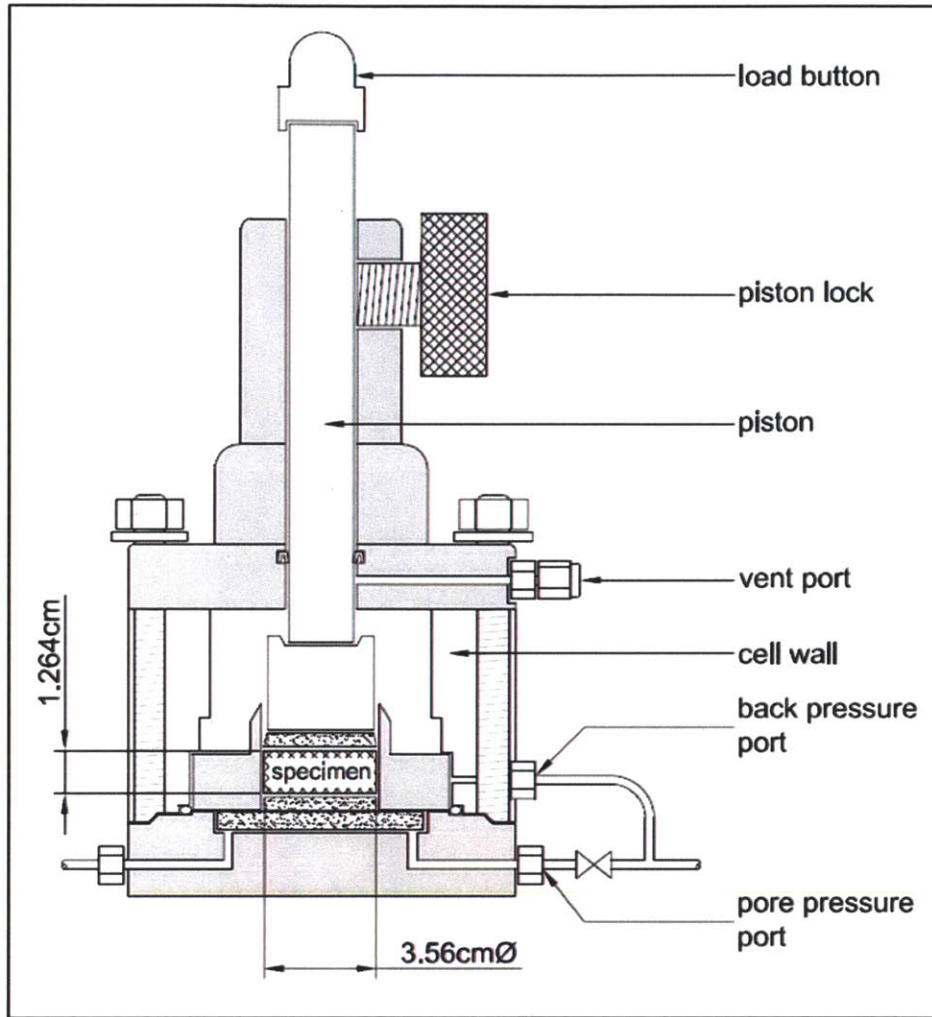


Figure 4.36 Schematic diagram of Trautwein CRS cell (TR4)



Figure 4.37 Trautwein CRS cell showing overflow hole which allows any water passing the seal to exit the apparatus before it damages the roller bearings housed higher in the column



Figure 4.38 Wykeham Farrance load frame used for CRS testing

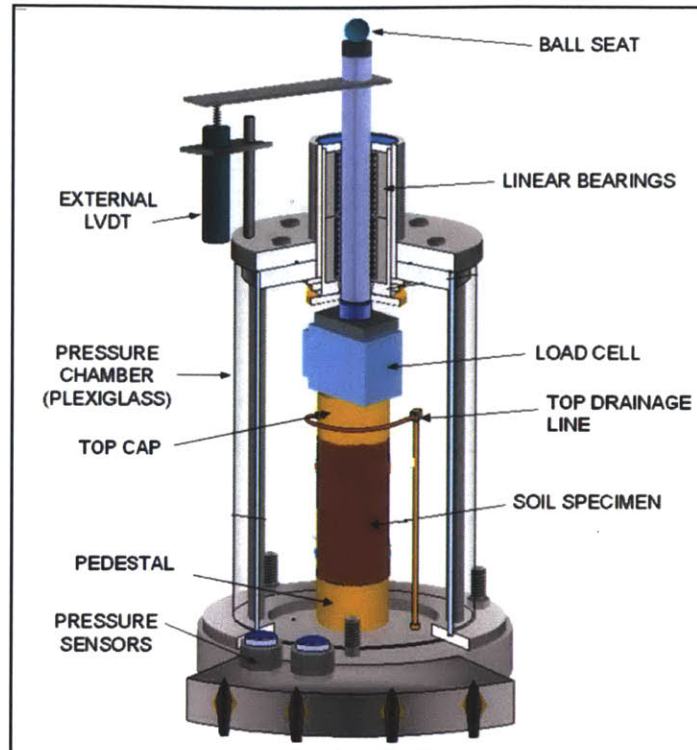


Figure 4.39 Schematic of low pressure triaxial cell (Santagata 1998)

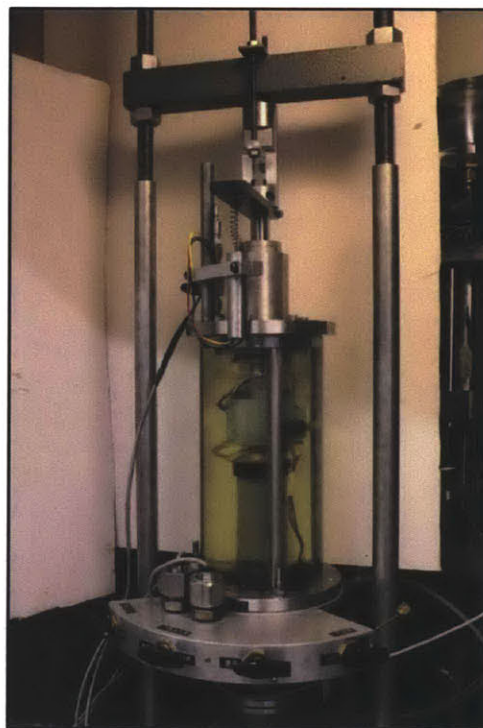


Figure 4.40 MIT04 triaxial cell

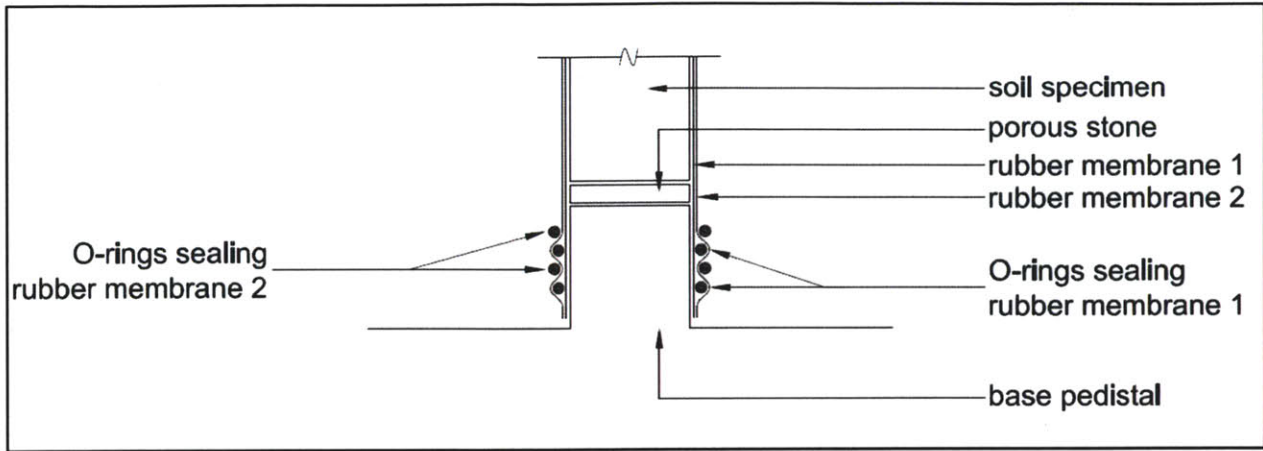


Figure 4.41 Low pressure triaxial pedestal & topcap O-ring sealing arrangement with 2 rubber membranes (spacing's exaggerated for clarity)

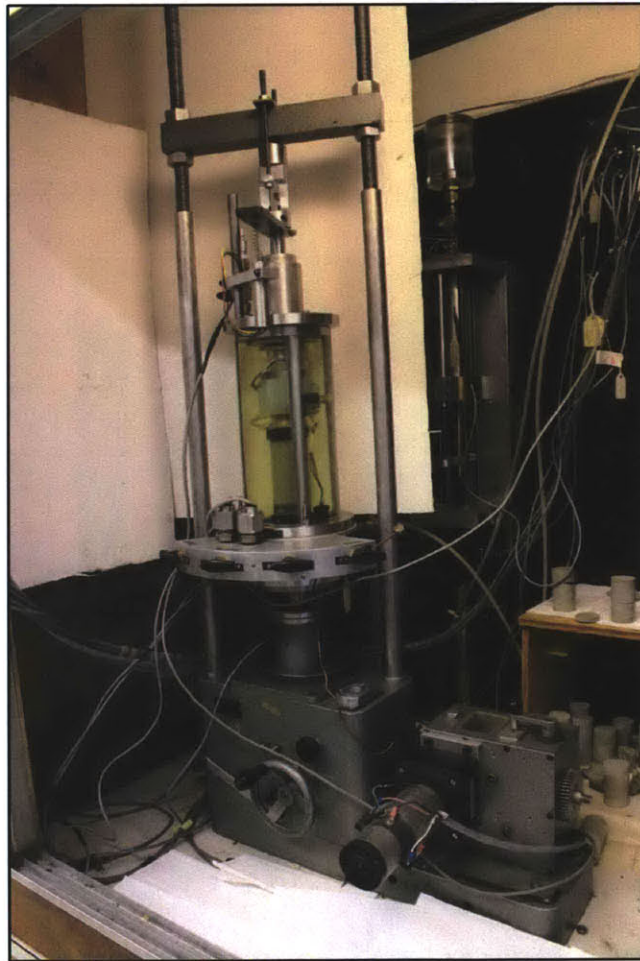


Figure 4.42 MIT04 triaxial cell in 1 Tonne (9.8 kN) Wykeham Farrance screw driven loading frame with adjustable gears

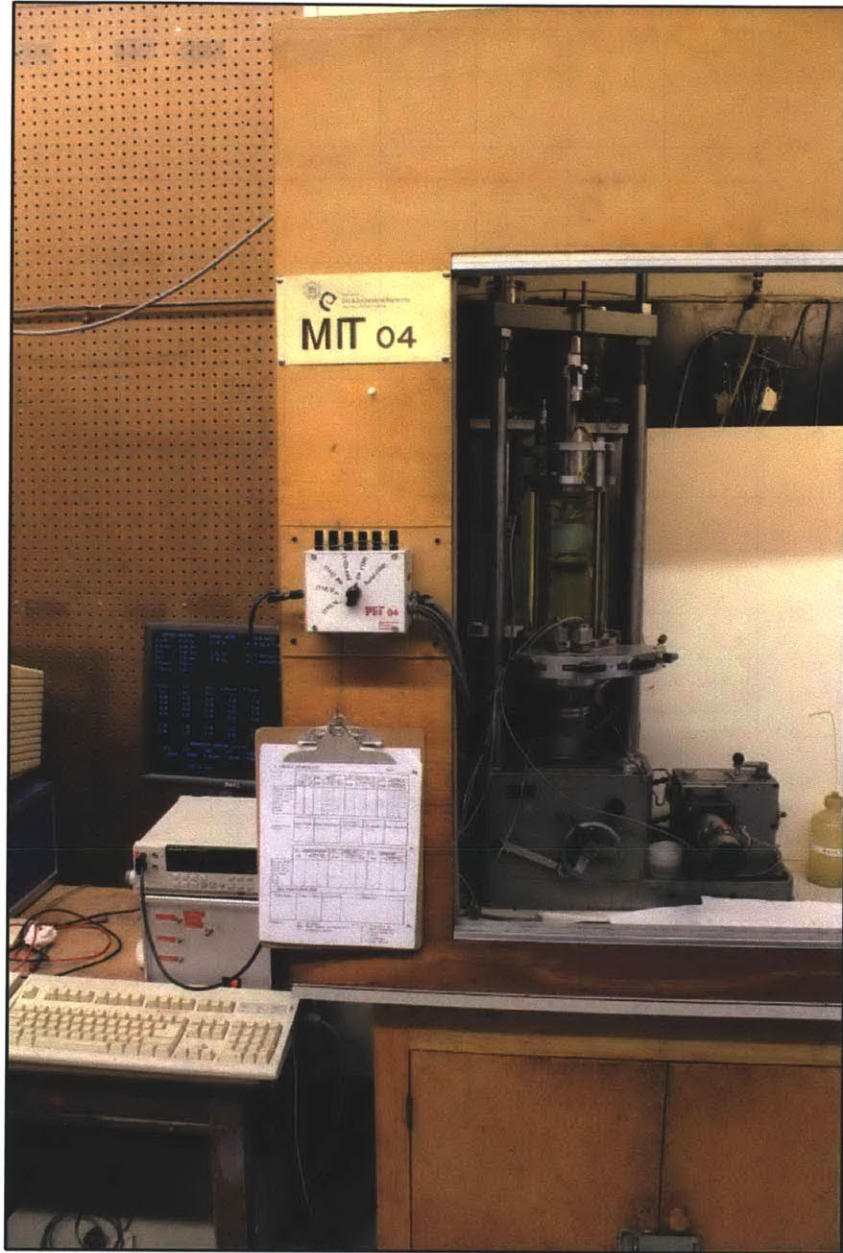


Figure 4.43 Entire triaxial testing apparatus. Cell, load frame and PVA's on right of photo; computer control on left (PVA's are masked behind cell, PC controlling testing is visible on bottom left of photo under the table)

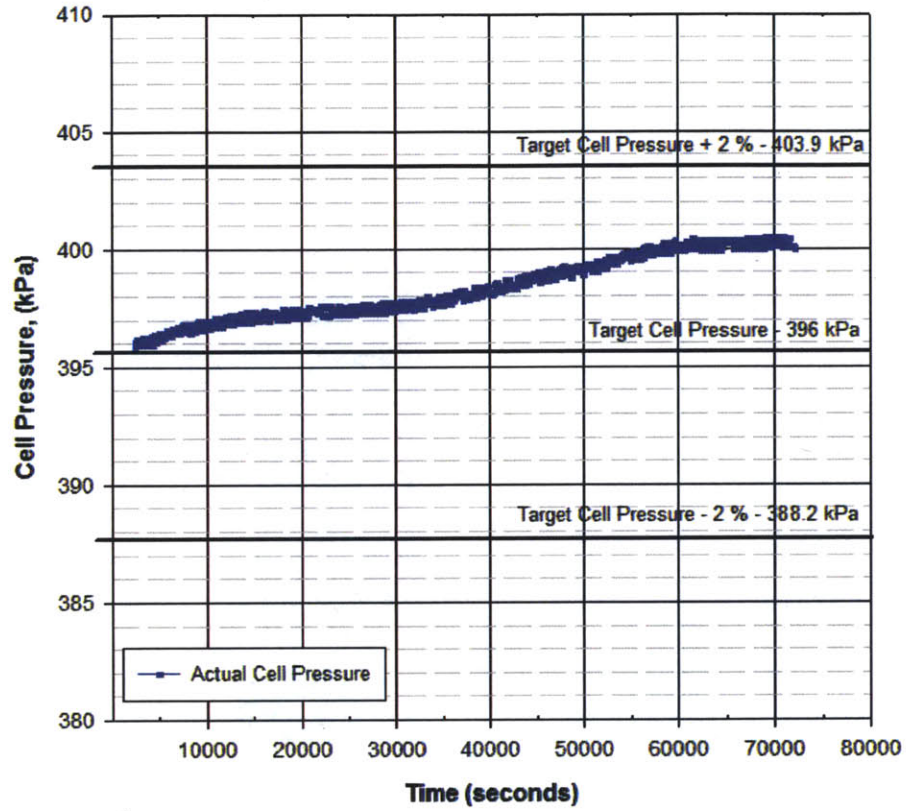


Figure 4.44 Plot of cell pressure stability for a typical CRS test

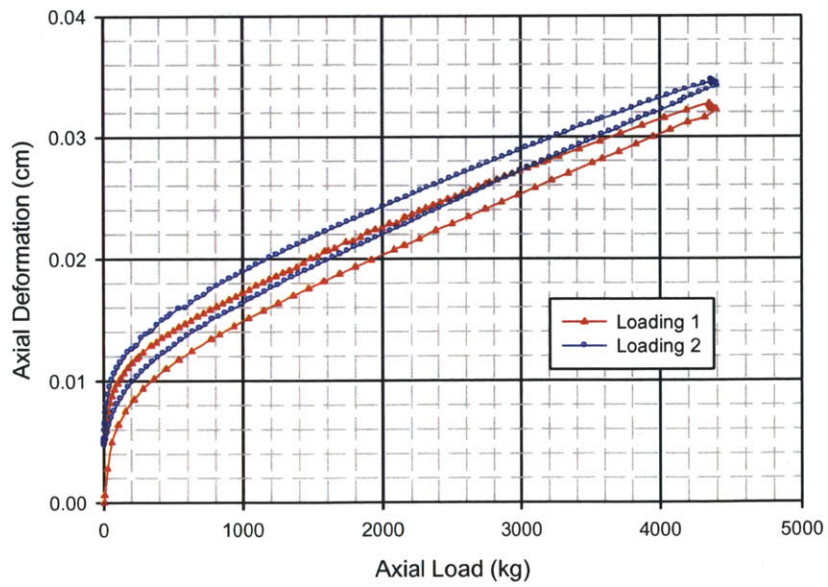


Figure 4.45 Apparatus compressibility for CRS cell TR4 - determined from 2 loadings (obtained January 2011)

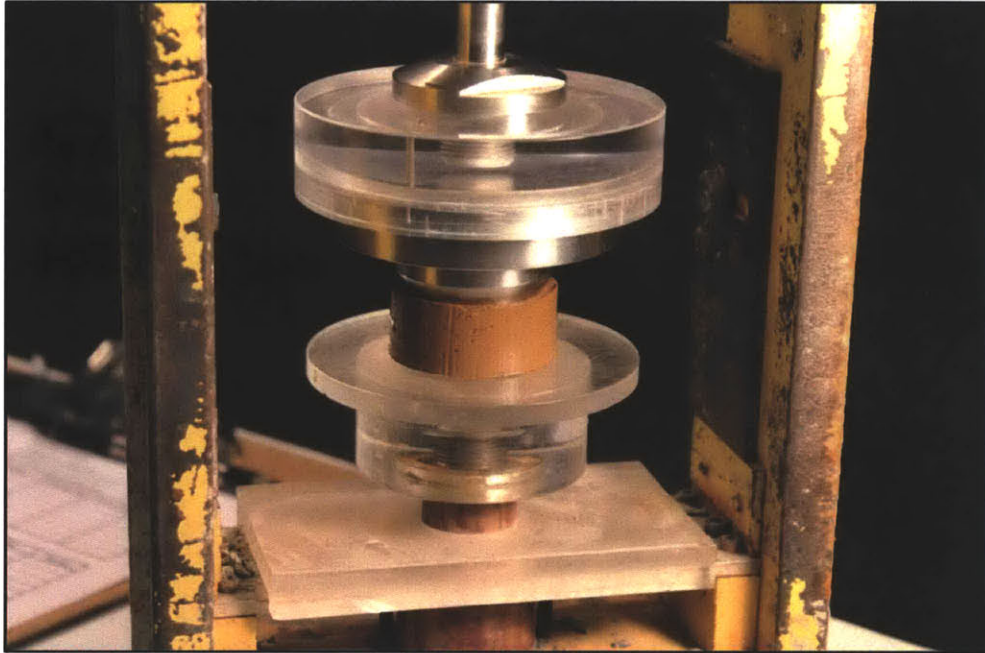


Figure 4.46 Positioning cutting edge of CRS ring onto London Clay sample taking care to ensure there is soil available to be cut all the way around (soil being trimmed is London Clay at 256 g/l)



Figure 4.47 Trimming London Clay sample into small diameter CRS ring (soil being trimmed is London Clay at 256 g/l)



Figure 4.48 Small diameter CRS ring with perfectly squared end of London Clay soil (soil being trimmed is London Clay at 256 g/l)

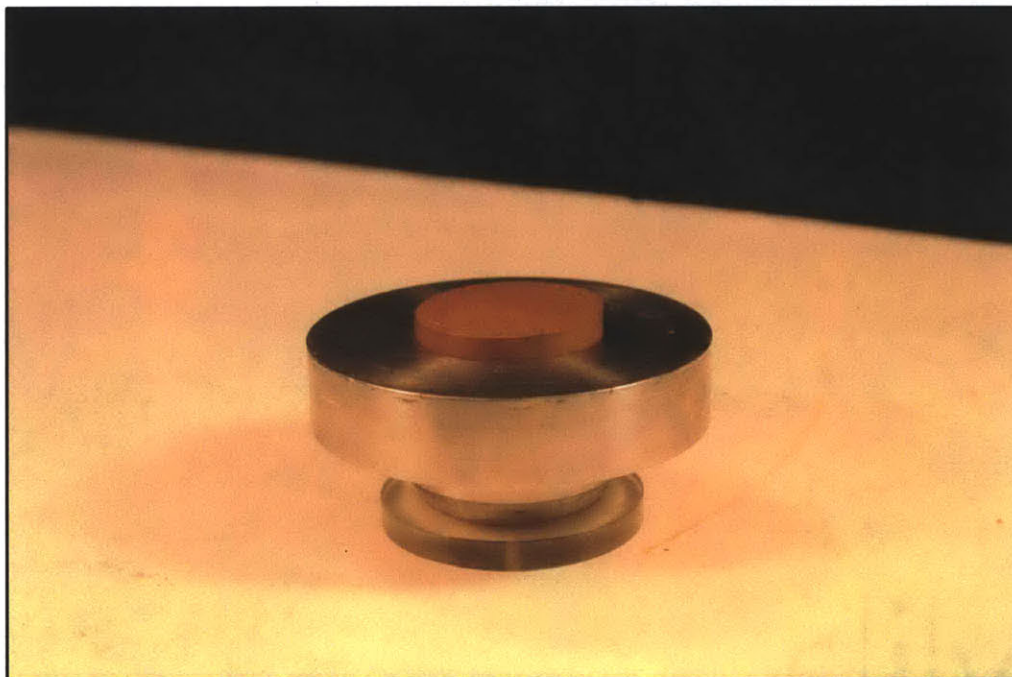


Figure 4.49 Opposite side of cutting ring to Figure 4.48 where soil has been pushed through with recess tool to leave correct height of soil inside ring for testing (soil in ring is London Clay at 256 g/l)

5 RESULTS

5.1 INTRODUCTION

The index properties of the soil have previously been discussed in Chapter 3 and will not be covered further here. The mechanical behavior of the various soils tested were evaluated using Constant Rate of Strain (CRS) tests and K_0 consolidated undrained (CK_0U) triaxial tests on resedimented and in-tact specimens. This chapter presents the one dimensional consolidation behavior, hydraulic conductivities of the soils derived from excess pore pressures generated during one dimensional consolidation behavior, as well as the normally consolidated shear behavior.

The CRS results for the various soils are presented and discussed in Section 5.2. One dimensional consolidation data as well as the hydraulic conductivity in the vertical direction are presented here. The majority of resedimented soils tested were initially consolidated to stresses of 100 kPa, then CRS tested to 10,000 kPa, with a select few tests stressing the soil to 40,000 kPa. All CRS tests were run on soil specimens that are smaller than the standard ring. This was discussed earlier in Chapter 4. A list of all tests performed on Boston Blue Clay derivatives can be seen in Table 5-1. Table 5-2 presents a list of CRS tests performed on other soils. Although results are presented here from just 25 CRS tests, these tests have been extracted from a bank of some 90 test results and can therefore be considered as representative.

An experimental triaxial testing program was performed on natural Boston Blue Clay (BBC) Series IV, Leached BBC and BBC recovered from Killian Court under the MIT campus. Natural BBC Series IV was resedimented to a stress level of 200 kPa at salt concentrations of 4 & 256 g/l. The leached BBC samples were also resedimented to a stress level of 200 kPa, but to salt concentrations of 1 & 256 g/l. The in-situ BBC was taken from Shelby Tube samples recovered from depths of 50-55 feet below ground surface. K_0 consolidated undrained triaxial compression tests (CK_0UC) were performed on all three soil types. The results from the CK_0UC tests are presented in Section 5.3.2. All the specimens were sheared in the normally consolidated range for all test types. The stress-strain and effective stress behavior are analyzed along with other testing parameters. The undrained shear strength, friction angle and axial strain at failure

are also reviewed. A list of the testing performed is given in Table 5-3 which also presents some of the important stress-strain-strength parameters.

5.2 CONSTANT RATE OF STRAIN TESTING

5.2.1 INTRODUCTION

An extensive CRS program was undertaken in order to determine the one dimensional consolidation properties and vertical hydraulic conductivities of the many soils in the testing program. In total, some 90 CRS tests were performed. An evaluation on the suitability of the new smaller sized CRS testing ring can also be drawn from this large bank of test data. The one dimensional consolidation behavior and vertical hydraulic conductivity will be examined in this Section.

Each soil type tested had a unique strain rate associated with it. The strain rates used for each respective soil are stated in their relevant subsection in this Chapter. The strain rates were chosen such that an excess base pore pressure would result from the axial consolidation loading, which in turn would provide the hydraulic conductivity information for the soil. All BBC specimens were stressed in the CRS device to an axial effective stress of 10,000 kPa while selected London Clay salt contents and every GOM soil was stressed to 40,000 kPa. At the end of consolidation, it is not possible to obtain the secondary compression characteristics with the load frame used, therefore the soil was either unloaded to obtain the unload curve, or removed from the test apparatus. The main items associated with each graph presented for every soil will be discussed in detail for natural BBC, and thereafter reference will be made to only the most important items for each soil dataset presented.

5.2.2 BOSTON BLUE CLAY

5.2.2.1 INTRODUCTION

A total of four derivatives of BBC were tested for this research. Their differences have been explained in Chapter 3. Chapter 4 described how some of these derivatives were processed. All BBC specimens were strained at a rate of 2 %/hour to a maximum axial effective stress of 10,000 kPa. All resedimented BBC specimens were stressed to a batch preconsolidation pressure of 100 kPa and then rebound to an OCR = 4 before CRS testing.

Reverse leaching tests were performed on previously leached BBC soil. This test has already been described in Chapter 4, however, the essence of the test involved flowing high salinity water through a low salinity leached BBC specimen in the CRS cell. The pore volumes of the specimen were replaced several times in an attempt to determine if the change in salinity would cause a subsequent change in the mechanical behavior. The results from two of these tests will also be presented in this Section.

5.2.2.2 NATURAL RESEDIMENTED BOSTON BLUE CLAY (SERIES IV)

A significant quantity of CRS testing was performed on resedimented natural BBC to demonstrate repeatability and consistency in the results. For clarity, only a handful of these results will be presented but they can be taken as representative of RBBC behavior. Table 5-1 gives a list of the CRS tests which will be presented for natural BBC. Results which are not presented here include the pore-pressure ratio data which will be presented in Appendix A.

Figure 5.1 shows the compression curves in ϵ_a - $\log\sigma'_{ac}$ space for five CRS tests performed on natural BBC resedimented to different pore fluid salinities. The salinities tested include 4, 16, 64, 128 and 256 g/l. Despite the major differences in salinity, the Figure is an example of the excellent repeatability which can be obtained from RBBC when meticulous testing procedures are employed. The shape of the compression curve is characterized by a well-defined break corresponding to a value below the target batch preconsolidation pressure (σ'_p for natural RBBC was 100 kPa). Up to an axial strain value of approximately 2.5 %, the soil behaves as an overconsolidated soil, this represents axial movement of 0.032 cm in the specimens. Beyond this level of axial strain, the soil is in the normally consolidated range.

The reason that the preconsolidation pressure for the resedimented specimens fall below the target batch preconsolidation pressure, is due to side-wall friction which exists between the soil and the consolidometer. As the diameter of the consolidometers employed was relatively small (~ 4 cm on average), the friction can be substantial. The preconsolidation pressure for the tests shown in Figure 5.1 falls between 70 and 80 kPa which represents a 70 – 80 % efficiency in terms of stress application during resedimentation. Even though lubrication is used internally on the consolidometer tubes prior to the placement of the slurry, the friction effect is still profound.

The same effect is seen in all soil types resedimented in small diameter consolidometers throughout this research.

All CRS tests for natural BBC were terminated at or just over 10,000 kPa which represents an average axial strain of 33 % for all specimens. This compares well with results presented in Abdulhadi, 2009. When the required axial strain to 10,000 kPa is plotted against pore fluid salinity as is done in Figure 5.6, a slight trend can be observed whereby more axial strain is required to the target axial stress level with an increase in salt content. From the data presented in Figure 5.1, it can be seen that by altering the pore fluid salinity during the resedimentation process for natural BBC, the mechanical behavior changes marginally.

Figure 5.2 shows the compression curves in e - $\log \sigma'_{ac}$ space. The initial void ratio for all tests fall between 1.24 and 1.30. There is no trend in the initial void ratio versus the salt content for natural BBC as can be seen from Figure 5.7. The discrepancies in the initial void ratio can be attributed to working with such a small specimen. Any error in recording masses will be amplified in the phase relations. Once the preconsolidation pressure is passed for all specimens, very comparable compression behavior in the normally consolidated range is observed. The compression index, c_c value for all specimens is ~ 0.32 (taken between 1,000 and 10,000 kPa). All specimens were axially stressed to 10,000 kPa where the void ratios range between 0.50 and 0.54. Figure 5.8 shows the void ratio at $\sigma'_{ac} = 10,000$ kPa and again, no trend is apparent for a given void ratio at differing pore fluid salinities. These differences in void ratio at 10,000 kPa can be attributed to the initial differences in void ratio calculation. It is worthwhile noting that the virgin consolidation line for natural RBBC is not perfectly linear in either strain or void ratio space i.e. the slope of the normally consolidated line changes slightly with stress.

Figure 5.3 presents the hydraulic conductivities for all natural RBBC Series IV specimens tested. The results are presented in void ratio space. The dataset shows the vertical hydraulic conductivity (k_v) reducing with a decrease in void ratio which represents an increase in axial consolidation stress. The hydraulic conductivities are very comparable at all stress levels and again, there is no trend in hydraulic conductivity at a given void ratio for a given salinity. The hydraulic conductivities for all soils tend to converge at a void ratio of ~ 0.76 ($k_v = 1.62 \times 10^{-8}$ cm/sec; $\sigma'_{ac} \sim 1,850$ kPa). Also, after a void ratio of 0.76, the slope of all datasets change. This kink in the hydraulic conductivity behavior has also been observed in natural RBBC Series IV by

recent researchers (Abdulhadi, 2009). The cause of this kink is not immediately apparent, however, it has also been noted that the c_v value of all soils in this dataset change at around this stress level. The c_v parameter is highly dependent on the k_v value. It was initially thought that these kinks could be attributed to temperature effects while testing. The possibility that each test suffered from temperature effects at exactly the same stress level and produced subsequently similar data is highly unlikely. A reason for this behavior is postulated in Section 5.2.2.4. All test results were corrected for the differences in viscosity of the water due to the salinity. This was done because the hydraulic conductivity in the CRS test is calculated from the base excess pore pressure, which in turn is a function of the rate at which fluid can escape through the specimen. Different viscosities will allow water to dissipate at different rates. The hydraulic conductivities range from a value of 1.45×10^{-7} cm/sec at a void ratio of 1.25 ($\sigma'_{ac} = 60$ kPa), to 1.54×10^{-9} cm/sec at a void ratio of 0.52 ($\sigma'_{ac} = 10,000$ kPa), just under two orders of magnitude.

The coefficient of consolidation in the vertical direction (c_v) lumps the hydraulic conductivity in the vertical direction (k_v) and the coefficient of compressibility in the vertical direction (m_v) into one parameter. Figure 5.4 presents coefficient of consolidation data obtained during the CRS testing of the natural BBC specimens at differing salinities. Data obtained before the preconsolidation pressure was reached produced highly erratic data points and are not shown in the plot. In general, c_v increases once the preconsolidation pressure is passed until a stress level of ~ 1950 kPa where it reaches a peak value for most soils, then gradually drops for the remainder of the test. This change in c_v value cannot be attributed to equipment issues. There is a noticeable kink in the hydraulic conductivities of the soil at around this stress level also which is visible in Figure 5.3. At no point over the stress range tested does the c_v value reach a steady number. With the exception of CRS1252, the remainder of the tests show the c_v value rise from an initial value of 3.0×10^{-3} cm²/sec just past the preconsolidation pressure, peak at a value of 4.5×10^{-3} cm²/sec at σ'_{ac} equal to around 2,000 kPa and then taper off to a value of 2.8×10^{-3} cm²/sec at σ'_{ac} equal to 10,000 kPa. The c_v value continues to fall in the tests which went past beyond this stress. This, however, is a relatively small change in c_v over such a wide range of consolidation stresses. A plot of how the hydraulic conductivity and coefficient of consolidation data changes with stress level is shown in Figure 5.5. This Figure shows that both datasets display changes in behavior at similar stress levels.

5.2.2.3 LEACHED BBC

As with natural BBC, an extensive suite of CRS tests were performed on leached BBC. For clarity, only five of them will be presented here. Table 5-1 gives a list of the CRS tests which will be presented for leached BBC. Pore pressure versus axial effective stress will be presented later in Appendix A.

Figure 5.9 presents compression data for leached BBC in ϵ_a - $\log \sigma'_{ac}$ space for four CRS tests performed on leached BBC resedimented to different pore fluid salinities. The salinities tested include 0 (distilled water), 1, 16, 64 and 256 g/l. Only five salinities were chosen for testing given that leached BBC was difficult to process large quantities of. A lower bound salinity of 0 g/l was used for the leached BBC in order to determine how the deflocculated elements would behave when full double layer growth was permitted. Given that the fabric of the soil being used has been notably altered (as shown in Chapter 3), divergences in behavior are now apparent. Again the compression curve is characterized by a well-defined break corresponding to a value below the target batch preconsolidation pressure. All leached BBC specimens were tested to a stress of 10,000 kPa. The axial strain required to reach the actual batching preconsolidation pressure is now 2 % (as opposed to 2.50 % for natural RBBC). This suggests that leached BBC is not as prone to swelling as natural BBC. After 2 % strain, the soil acts normally consolidated. A similarity which leached BBC shares with natural BBC is that the slope of the normally consolidated line is not straight for any salinity but changes with stress level. This is, however, where the similarities end. The required strain to 10,000 kPa for 0 g/l soil is 27.2 %. The virgin compression lines for 1 and 16 g/l are almost identical, but when the stress level is 10,000 kPa, the strain for these two soils is 31.3 % (as opposed to 33 % for natural BBC). The strain for 64 g/l soil is 32.8 % and for 256 g/l soil it is 35.8 %. This represents a trend of increasing compressibility at a given stress for an increase in salt content. The trend is shown in Figure 5.13 and is consistent with the findings of Stipho (1985). None of these tests suffered from extrusion issues. The 64 g/l test initially follows the 1 and 16 g/l lines up to a stress of 170 kPa, but then dips below the two lower salinities as shown in Figure 5.9. It is also interesting to point out that a similar difference in strain to a given stress is seen between salinities of 1 & 256 g/l, as is witnessed between 0 & 1 g/l.

Figure 5.10 shows the compression behavior for the leached BBC in e - $\log \sigma'_{ac}$ space. The initial void ratios cover a larger range than those observed in the natural BBC Series IV, and this time there is a trend of higher initial void ratio with an increase in salinity as shown by Figure 5.14. If it is assumed that the void ratio of 1.26 is correct and the same logic is applied to this dataset as the natural BBC Series IV insofar as there is an initial error band in the void ratio, it can be seen that both the high and low recorded initial void ratios fall outside this band and can be therefore taken as accurate representations. The 1 g/l data does not follow the same normally consolidated path as the other four tests which can be attributed to the lower salinity. It does in fact have stiffer behavior in the normally consolidated range. This is seen by the lower c_c value of 0.27 for 1 g/l as opposed to 0.32 for 256 g/l (taken between 1,000 and 10,000 kPa). The c_c value for 16 and 64 g/l soil is 0.29 and 0.30 respectively hence further proof of the increasing soil stiffness with a decrease in salt content. 0 g/l soil displays even stiffer behavior than 1 g/l soil in the normally consolidated range. This lends further evidence to the argument taken from Figure 5.9 that as the salinity increases, a more compressible soil is observed for leached BBC. Figure 5.15 shows the void ratio at an axial effective stress $\sigma'_{ac} = 10,000$ kPa for all salinities and there is no apparent trend from this data, hence all salinities converge at high stress.

Figure 5.11 shows the hydraulic conductivity data obtained from the leached BBC CRS testing. The starting hydraulic conductivities for all soils are slightly lower than those for natural BBC at 1.21×10^{-7} cm/sec at a void ratio of 1.25 (with the exception of 1 g/l which does not exist at a void ratio of 1.25). The 4 and 16 g/l data crisscross several times over the stress range, but the 1 and 256 g/l are always at different hydraulic conductivities for a given void ratio. In the void ratio range of between 0.65 and 0.75 ($\sigma'_{ac} = 1,650 - 3,400$ kPa), distinct and erratic kinks are seen in the data. Some of these kinks cause datasets to cross over one another and the data becomes chaotic past this point. These kinks occur at void ratios slightly lower (higher stress level) than the kinks observed in Figure 5.3 for natural RBBC Series IV. The kinks can therefore be attributed to actual soil behavior, however, the data past these kinks are considered variable.

Figure 5.12 shows the variation in the vertical coefficient of consolidation (c_v) obtained from the CRS tests. The same general trend is observed in leached BBC as was seen in natural RBBC whereby the c_v value rises after the preconsolidation pressure is passed, peaks at some stress level and then tapers off with a further increase in stress. The peaks in the c_v value

observed in Figure 5.12 occur at slightly different stresses for each soil as opposed to in the natural RBBC Series IV results where all the peaks were localized in a similar stress range. The peaks in c_v for leached soil range from $\sigma'_{ac} = 1,500$ kPa for 64 g/l soil to $\sigma'_{ac} = 3,500$ kPa for 256 g/l. No trend is apparent in where the peaks in c_v occur in relation to salt concentration. With the exception of the 0 & 1 g/l curve, all other tests taper to a similar c_v value at $\sigma'_{ac} = 10,000$ kPa. Assuming that the erratic differences which were seen in the hydraulic conductivity data is not so pronounced in the c_v plots, slightly lower c_v values are observed in leached BBC at $\sigma'_{ac} = 10,000$ kPa where the value is approximately 0.0021 cm²/sec as opposed to 0.0028 cm²/sec for natural RBBC.

5.2.2.4 IN-SITU BBC

Several in-tact Shelby tube samples of BBC were taken from the Killian Court area of MIT in the summer of 2010. This recovery work was supervised by Dr. Germaine of MIT and the recovery location has been described in Chapter 3. The tube samples used for CRS testing were taken from boring B10-TP2A, sample S3 and recovered from a depth of 51-53 feet below ground surface. The water table around the MIT campus is known to be 8 feet below ground surface (ground surface is +26.1 ft. relative to CCB). In-situ BBC was tested in order to provide a benchmark against which to measure the accuracy of the resedimentation process being used in this research. The specimens were extracted from their Shelby tubes in accordance with guidelines given in Germaine & Germaine, (2009) so as to minimize sample disturbance due to handling. For consistency, CRS testing was also performed on this soil in the smaller diameter ring as described in Chapter 4.

Figure 5.16 presents compression data in ϵ_a - $\log\sigma'_{ac}$ space for three CRS tests performed on Killian Court in-situ BBC. Again the compression curve is characterized by a well-defined break corresponding to the preconsolidation pressure for the recovered soil. The preconsolidation pressure was reached at 2.5 % axial strain which is the same strain needed for natural BBC Series IV to reach its preconsolidation pressure. All of the specimens were stressed to just past 10,000 kPa. Two of the specimens (CRS1269 & CRS1270) have very similar strain requirements to get to a given stress state. At 10,000 kPa the axial strain is 23 %. The third test, CRS1268 shows different behavior insofar as it is more compressible than the other two specimens. At a stress of 10,000 kPa, the strain for this test is 26 % and it also has different normally

consolidated behavior than the other two tests. One possible reason for the differences in results could be the fact that it is a natural material and specimen variability may exist. Extrusion of soil during CRS testing was not an issue for any of these tests. Also, CRS1269 & CRS1270 were taken from adjacent slices in the tube while CRS1268 was obtained from a different location in the same tube. As with all previous BBC testing, the slope of the normally consolidated line changes with stress level. Perhaps the most important fact is that the strains required to a stress of 10,000 kPa for in-situ BBC (24.5 % on average) is much less than the strain required for natural RBBC Series IV and leached BBC (33 % on average for both soils). This means that RBBC in any form is more compressible than in-situ material. One possible explanation for this could be due to the existence of both chemical and mechanical bonds which have developed over centuries in the in-situ material, which cannot be replicated in the resedimented soil. These bonds may give the in-situ extra load carrying capacity.

The same compression data in e - $\log \sigma'_{ac}$ space is shown in Figure 5.17. There are very similar initial starting void ratios for all three specimens ranging from 1.01 to 1.05. All three tests have very similar preconsolidation pressures. When the Casagrande construction was performed on these curves, the preconsolidation pressure (σ'_p) for the Killian Court BBC was found to be ~ 400 kPa for CRS1269 & CRS1270, and 320 kPa for CRS1268. The void ratios compare well to those observed in natural RBBC Series IV at similar stress levels. The c_c value for all soil tested is shown in Table 5-4. The coefficient of swelling (c_s) for CRS1268 is also greater than the other two tests meaning that more voids are opening upon unload and therefore the volume of the soil is growing. The void ratio for CRS1269 & CRS1270 are 0.55 at $\sigma'_{ac} = 10,000$ kPa while it is 0.52 for CRS1268 at the same stress level. The void ratio for natural RBBC ranged between 0.5 and 0.54 for all tests which compare well to the in-situ void ratios recorded.

Figure 5.18 presents the hydraulic conductivity for the Killian Court in-situ BBC specimens tested in the CRS device. It is shown that for a decrease in void ratio, a decrease in permeability is observed. The three tests start at different hydraulic conductivities ranging from 8×10^{-8} cm/sec to 2.2×10^{-8} cm/sec at the same void ratio of 1.06. This void ratio represents the soils when they are still in an overconsolidated state. As the void ratio decreases, meaning the stress level is increasing, a convergence of the data is observed. At a void ratio of 0.54, the

hydraulic conductivity is about 2.09×10^{-9} cm/sec. Lower hydraulic conductivities are seen in the in-situ Killian Court BBC at higher void ratios than those for natural RBBC, but the in-situ and resedimented material tend to converge to similar values at lower void ratios (higher stress levels). At a void ratio of 1.06 for natural BBC Series IV, the hydraulic conductivity is 6.7×10^{-8} cm/sec which is higher than that quoted above for Killian Court in-situ material. At a void ratio of 0.54 the corresponding hydraulic conductivity for natural RBBC Series IV is 2.1×10^{-9} cm/sec which is almost identical to that reported for Killian Court in-situ material. The kinks in the permeability curves which were observed in the natural RBBC Series IV are not visible in the in-situ test results. This indicates that the kinks are a product of either the resedimentation process or the grinding process used to obtain dry powder for use in resedimentation. A possible hypothesis which will now be proposed is that the grinding process used to obtain dry powder used in resedimentation, which was described in Chapter 4 does indeed break some but not all of the flocs at the minute scale which were naturally created during the soils formation. These broken flocs now allow more fluid flow through the soil, hence the initially higher permeability for the resedimented material. The resedimented material acts like a concrete aggregate consisting of coarse and fine particles (coarse flocs, fine flocs and individual soil particles). Upon application of stress to the soil, as in concrete, the load is distributed throughout the matrix until at some load the weakest element begins to fail whereby the large flocs remaining get “shock” loaded and begin to rearrange themselves. It is thought that this is what is being observed in Figure 5.3 and Figure 5.4 when the changes in behavior were noted in Section 5.2.2.2. These subtle changes in loading of the matrix at micro level may not be pronounced enough to show up in the recorded compression data, hence we do not see a corresponding change in the compression curves. In contrast, when an in-situ material is loaded, the entire soil matrix is continually rearranging and breaking the natural flocs once the preconsolidation pressure is passed, this is why we do not see any kink in the behavior. The reason both hydraulic conductivities are almost identical at $\sigma'_{ac} = 10,000$ kPa is because the microstructure has been broken to similar levels. Natural RBBC Series IV appears to be behaving as if it has “two soil memories”, the preconsolidation memory and the floc strength memory.

The coefficient of consolidation for Killian Court in-situ BBC is shown in Figure 5.19. In contrast to natural RBBC Series IV, the c_v of the in-situ soil drops until the preconsolidation pressure is reached and then rises with increasing stress level in the normally consolidated

region. Once the preconsolidation pressure is reached for Killian Court in-situ material, no further drop in c_v is noted as is the case for natural RBBC Series IV and leached BBC. All three tests reach minimum values of c_v ranging from 0.0032 cm²/sec to 0.0011 cm²/sec at stresses in the range of the preconsolidation pressure. The c_v values for natural RBBC Series IV initially rose until a stress level of approximately 1,950 kPa and then dropped gradually. The final c_v values for Killian Court in-situ BBC range from 0.0040 cm²/sec to 0.0026 cm²/sec. The range which natural RBBC tapered to was slightly lower at $\sigma'_{ac} = 10,000$ kPa. The lowest values observed in c_v for Killian Court BBC shown in Figure 5.19 occur when the preconsolidation pressure is passed for each soil. Therefore we can relate the known fact that the c_v changes when the soils enters a new stress state, to the passing of the preconsolidation pressure. The peaks witnessed in Figure 5.4 where the c_v value changes slope happens at 1,950 kPa which is far beyond the batch preconsolidation pressure. Given that the c_v value begins to change at this stress level, it is hypothesized that the soil fabric is changing. This further adds evidence to the theory that flocs are breaking within the matrix once a certain stress level is reached.

The process described is also visible in the leached BBC tests but the stresses at which a change in the c_v occurs, are more spread out and erratic. The reason for the higher stress is because by placing the soil in the centrifuge twice, the flocs have begun degrading and disaggregating due to the removal of the natural salt. Rather than all flocs being degraded at the same rate, some may have degraded more than others which is why we see such variations in stress levels where c_v changes. The fact that the stresses at which the c_v values change are higher than those for natural BBC may be due to a size effect – smaller flocs require a larger stress to break them.

5.2.2.5 BBC DISPERSED WITH SODIUM HEXAMETAPHOSPHATE

Sodium hexametaphosphate (sodium hex) is commonly used in laboratory Geotechnical testing in the particle size distribution by sedimentation test. It is known to completely disperse any flocs which exist in order to deflocculate the soil to its basic constituents. After a soil has been treated with sodium hex., the soil-water slurry contains only individual soil particles and no floc formations. A more accurate particle size distribution can be achieved using this method. SEM images were taken on oven dried specimens and are presented in Chapter 3.

The process mentioned above was applied to BBC that was to be resedimented and then CRS tested. This had the advantage of resedimenting a rudimentary BBC soil for the first time which contained no flocs and therefore no “memory” or stress level at which it could change behavior. The soil which was subsequently resedimented was BBC in its most basic of forms.

Figure 5.20 shows the compression curves for two tests on dispersed BBC in ϵ_a - $\log\sigma'_{ac}$ space. The preconsolidation pressure for both of these tests have exceeded the target batch preconsolidation pressure (σ'_p) of 100 kPa. This is because the soil was sitting at an overconsolidation ratio of 4 for nine months allowing secondary compression to occur in the soil. The reason the soil was idle for this amount of time is because of the presence of the sodium hex which is a detrimental chemical to soils. If this chemical was allowed to contaminate the testing equipment, it could have unfavorable implications for future tests. For this reason, testing of the dispersed BBC was left until the end of the testing program. The strain required to bring the dispersed BBC to its new preconsolidation pressure was approximately 2.4 % which is slightly less than the strain required for natural RBBC Series IV and Killian Court in-situ BBC. The behavior in the normally consolidated range differs slightly for both tests with CRS1313 taking a more linear path than CRS1314. At a stress of 10,000 kPa, the strains range from 26.4 % to 28.4 %. These strains are lower than those recorded at the same stress level for natural RBBC Series IV and leached BBC (~33 %) and are now closer to those required for Killian Court in-situ BBC (23 – 26 %). This means that even though the BBC used in these tests has been dispersed and contains no flocs, it is still more compressible than in-situ material. This further indicates that there are either mechanical or chemical bonds present in Killian Court in-situ material which have a large load carrying capacity, even at high stresses. These bonds prevent the structure being deformed to the same extent as the dispersed BBC or any of the other RBBC derivative throughout loading.

The compression data is presented in e - $\log\sigma'_{ac}$ space in Figure 5.21. The starting void ratios for both tests are similar and fall between 1.01 and 1.03 which is lower than for natural RBBC Series IV at the same stress level. This is consistent with the theory that we now have no flocs and a tighter structure at low stress. Similarly to the ϵ_a - $\log\sigma'_{ac}$ plot, the behavior for both tests differ in the normally consolidated range with CRS1313 being slightly more compressible than CRS1314. The reason for the preconsolidation pressures being larger than the target batch

preconsolidation pressure has already been explained, however, after performing the Casagrande plot on both curves, the new preconsolidation pressure was found to be 110 kPa for CRS1313 and 130 kPa for CRS1314. Despite the differences in compression behavior, the c_c value for both tests are the same at 0.28 (taken between $\sigma'_{ac} = 1,000$ and $10,000$ kPa). The most comparable c_c value for BBC that has been reported previously in this thesis was for leached BBC at 1 g/l which had a c_c value of 0.27. At a stress of $10,000$ kPa, the void ratios differ slightly between values of 0.48 and 0.46. These are the lowest void ratios recorded at $\sigma'_{ac} = 10,000$ kPa for any BBC tested indicating the most deformable structure of all BBC derivatives.

The hydraulic conductivity data versus void ratio is shown in Figure 5.22. Owing to experimental error, the hydraulic conductivity data for CRS1313 is not available. The results from CRS1314 must therefore be relied upon as being representative. The hydraulic conductivity at a void ratio of 0.95 is 2.93×10^{-8} cm/sec. The hydraulic conductivities for natural RBBC, leached BBC and in-situ BBC are 4.91×10^{-8} , 4.0×10^{-8} , and 2.45×10^{-8} cm/sec respectively at the same void ratio. This lower hydraulic conductivity at the start indicates a more compact structure. In this regard the dispersed BBC has a hydraulic conductivity closest to Killian Court in-situ material at low stress. In natural RBBC Series IV, a break in slope was observed in the data generally between void ratios of 0.70 and 0.80. A similar break in slope is observed in Figure 5.22, however, it is not so pronounced as that witnessed for natural RBBC Series IV. Traditionally for the particle size distribution test by sedimentation test, 5 g of sodium hex is used for 50 g of soil. For this research, the same quantity of sodium hex was used (5 g), but this time for 350 g of soil. The stress at which the break in slope is visible in the sodium hex plots is different than the stress where the break in slope occurs for the natural RBBC Series IV – $\sigma'_{ac} = 1,400$ kPa for the dispersed soil as opposed to $2,000$ kPa on average for the natural RBBC. Given that all other BBC soil derivatives did not achieve the same low void ratios as the dispersed soil, comparisons will be drawn in their hydraulic conductivities at a void ratio of 0.55. At this void ratio, the dispersed BBC has a hydraulic conductivity of 4.30×10^{-9} cm/sec. The hydraulic conductivities for natural RBBC Series IV, leached BBC and Killian Court in-situ BBC are 2.28×10^{-9} , 3.43×10^{-9} and 2.24×10^{-9} cm/sec respectively. The dispersed BBC therefore has a higher hydraulic conductivity than all other BBC derivatives at a void ratio of 0.55. When compared alongside the curves for natural RBBC Series IV and leached RBBC, it is obvious that

the change in slope for dispersed BBC is insignificant. This will be discussed more in Section 5.2.2.7.

The coefficient of consolidation versus axial stress for dispersed BBC is shown in Figure 5.23. A reversal in trend is now observed compared to other resedimented BBC derivatives insofar as the c_v value reaches a minimum at or close to the actual preconsolidation pressure and then gradually rises thereafter. This behavior is more closely related to Killian Court in-situ material. The one difference between the dispersed BBC c_v value and the Killian Court in-situ c_v value is that the in-situ value tends to taper off to a constant level with an increase in stress. It can be seen from Figure 5.23 that the c_v value continually rises for dispersed soil and is still rising when the test is terminated. The c_v value for the dispersed soil at high stress is not comparable with any other BBC derivative at high stress but in the low stress range (σ'_{ac} up to 2,000 kPa), the c_v value for the dispersed soil and Killian Court in-situ material are very similar. The c_v for the dispersed soil at $\sigma'_{ac} = 10,000$ kPa is $0.0056 \text{ cm}^2/\text{sec}$.

5.2.2.6 REVERSE LEACHING TESTS PERFORMED ON LEACHED BBC

Reverse leaching tests were performed on leached BBC via the procedure described in Chapter 4. The reason leached BBC was chosen is because it is more reactive to different pore fluid salinities than natural RBBC Series IV as shown by Figure 5.10. Traditional leaching tests involve flushing distilled or freshwater through a soil known to contain salts, and then loading the soil. The result of a traditional leaching test is that the void ratio drops suddenly with very little increase in stress. The soil after leaching is in a metastable form meaning it can exist at a lower energy state than it currently does. It was hypothesized that the reverse could also hold true for a sensitive soil such as leached BBC and hence the tests were undertaken.

Leached BBC resedimented to a pore fluid salinity of 1 g/l was CRS tested. The cell contained 256 g/l saltwater. A standard CRS test was performed until the soil was in the normally consolidated range and then consolidation was halted. A hydraulic gradient was placed across the specimen causing the cell fluid (256 g/l saltwater) to flow through the soil (top to bottom) until the pore volume was replaced several times.

Figure 5.24 and Figure 5.29 present the results for two such tests in $\epsilon_a\text{-log}\sigma'_{ac}$ space. As can be seen from the Figures, the soil was consolidated until it lies in the normally consolidated

region, consolidation was halted and then the pore fluid was replaced more than twice for both tests. During the hold strain portion of the test, an average stress reduction of 41.6 % was recorded on the load cell due to relaxation of the soil. This is shown by the data trace moving to the left horizontally with no change in strain but registering a change in stress. Upon recommencement of consolidation, there is a noticeable increase in the preconsolidation pressure of 28.5 % on average from where the consolidation was initially halted prior to replacement of the pore volumes. This is visible in both tests, therefore the procedure is repeatable. The increase in strength of the soil is not maintained down through the normally consolidated range of either test. The slope of the normally consolidated line after reverse leaching changes with an increase in stress level and eventually the normally consolidated line from after reverse leaching, rejoins the normally consolidated line of the initial section of the CRS test tangentially. This would indicate that the saltwater flowing through the soil has altered the chemical bond between particles thereby making them stronger. Owing to the fact that it took several weeks to replace the pore fluid in these specimens, the influence of aging of the soil cannot be ruled out as having an effect and therefore there may also be a mechanical aspect to the increase in strength. The piston on the soil was not placed on “hold stress” which would have maintained a constant total stress (similar to what happens during secondary compression) on the soil during flow through, but was simply halted. This places the soil under a constant level of strain.

Figure 5.25 and Figure 5.30 show the compressions data for both reverse leaching tests in e - $\log \sigma'_{ac}$ space. Both reverse leaching tests were taken to a maximum stress of 10,000 kPa. For CRS1248 the consolidation was halted at $\sigma'_{ac} = 640$ kPa and when consolidation was recommenced, the preconsolidation noted from performing the Casagrande construction was $\sigma'_{ac} = 820$ kPa which represents a 28 % increase in strength. During the reverse leaching procedure, the stress level relaxed to $\sigma'_{ac} = 370$ kPa (a 42.2 % decrease). For CRS1235 the axial consolidation was halted at $\sigma'_{ac} = 890$ kPa and once consolidation was restarted, the preconsolidation pressure recorded was $\sigma'_{ac} = 1,150$ kPa – a 29 % increase in strength. During the reverse leaching procedure, the stress level relaxed to $\sigma'_{ac} = 526$ kPa (a 40.9 % decrease). Both tests show very similar levels of strength gain even though they were axially loaded to different stresses. Both tests also show similar levels of stress relaxation once consolidation is halted. A very slight decrease in void ratio is also recorded in both tests once axial consolidation is halted. The void ratio for CRS1248 was 0.947 when consolidation was halted, and this void ratio

decreased to 0.942 while stress relief occurred in the soil. The void ratio for CRS1235 was 0.835 before consolidation was halted and this decreased to 0.834 during stress reduction. It is not entirely apparent at this stage what percentage of the strength increase can be attributed to chemical effects on the soil due to changing the pore fluid environment, and what percentage can be put down to mechanical effects. Figure 5.26 and Figure 5.31 show a close up of the area where axial consolidation was halted and an increase in the preconsolidation pressure was noted.

The hydraulic conductivity data versus void ratio for both tests are shown in Figure 5.27 and Figure 5.32. A noticeable change in hydraulic conductivity is visible in Figure 5.27 after the reverse leaching process. It is interesting to note that the same kink in hydraulic conductivity which was referred to in Section 5.2.2.4, is also visible in both these Figures at comparable stress levels. The hydraulic conductivity for the start and end of both tests are comparable with those shown in Figure 5.11. Although the mechanical behavior has been affected by the reverse leaching process, the hydraulic conductivity of the soil has remained comparable.

The coefficient of consolidation for both tests are shown in Figure 5.28 and Figure 5.33. There is a noticeable drop in c_v from before and after the reverse leaching process. Before reverse leaching, the c_v value is 0.0044 cm²/sec and immediately after the process the value has dropped to 0.0027 cm²/sec. This could be due to changes in the hydraulic conductivity. After this drop, the c_v value again rises gradually until it reaches a maximum of 0.0038 cm²/sec at $\sigma'_{ac} = 2,450$ kPa. After this peak, the c_v value begins to drop gradually throughout the remainder of the test and is still falling when the test is terminated. The final c_v value recorded was 0.002 cm²/sec which is very similar to c_v for leached BBC shown in Figure 5.12. The peak at $\sigma'_{ac} = 2,450$ kPa is in a similar region to where the peaks were recorded in Figure 5.12 for leached BBC. This lends further evidence to the claim in Section 5.2.2.4 that something is happening at this stress in order to cause a change in the c_v values.

5.2.2.7 SYNTHESIS ANALYSIS OF VARIOUS TYPES OF BBC

A complete picture can be presented on the behavior of several types of RBBC using Killian Court in-situ material as benchmark. In total, 3 derivatives of RBBC were tested and each displayed varying levels of behavioral change depending on what had been done to the soil prior to resedimentation.

Figure 5.34 shows the compression behavior of 4 types of BBC in ε_a - $\log\sigma'_{ac}$ space. A pore fluid salinity of 16 g/l was chosen for natural RBBC Series IV and leached BBC so as to compare them on a level playing field to the Killian Court material. A salinity of 16 g/l is the closest salinity used in the testing program to that of in-situ material (10.7 g/l). The sodium hex BBC was resedimented with distilled water. The first observation to be made from Figure 5.34 is that there is a difference of just under 10 % in the axial strain required for the specimens to reach the same stress level ($\sigma'_{ac} = 10,000$ kPa). The strongest soil is Killian Court in-situ BBC with the most compressible soil being natural RBBC Series IV resedimented to a pore fluid salinity of 16 g/l. Both the natural RBBC Series IV and the leached RBBC display similar compression behavior with the natural RBBC Series IV being slightly more compressible than the leached RBBC. The sodium hex BBC is a stronger soil than both other types of resedimented material. This stiffness can be attributed to the denser packing of the soil due to the dispersion of the flocs. Figure 5.38 presents the axial strain required for all BBC derivatives to achieve an axial effective stress of 10,000 kPa. A loose trend is observed that more strain is required for an increase in salt content. In the low salinity range, namely 0 – 1 g/l, comparatively lower strains are required to achieve maximum stress. Every resedimented BBC soil takes more strain to achieve a stress of 10,000 kPa than Killian Court in-situ material again indicating it is a stronger soil than any resedimented derivative.

The same compression data is shown in e - $\log\sigma'_{ac}$ space in Figure 5.35. A point worth bearing in mind while studying this Figure is that the natural RBBC Series IV, leached RBBC and sodium hex BBC curve are all born of the same soil powder. A large difference is seen in resedimented void ratio for the sodium hex BBC as opposed to the other resedimented material despite being composed of the same constituents. This shows that the sodium hex has performed the dispersion which it was intended for. The Killian Court in-situ BBC exists at a lower void ratio because it would have been taken to a higher stress state naturally in the ground. It also has a higher preconsolidation pressure. The normally consolidated range for all soils in this Figure show that natural RBBC Series IV is the most compressible material with a c_c value of 0.307. The leached BBC is the next most compressible with a c_c of 0.294 followed by Killian Court in-situ BBC with a c_c value of 0.285. The sodium hex BBC is the stiffest soil with a c_c value of 0.277 but it does require more axial strain to achieve a given stress. Extrusion of the soil during CRS testing was not an issue for any of these tests. Figure 5.39 shows the void ratio for all soils

at an axial stress of 10,000 kPa. There is no apparent trend from these data, however, Killian Court BBC maintains the highest void ratio on average than any other soil. The lowest void ratios are observed in the low salinity soils (0 – 1 g/l) yet these soils still took more strain to achieve this void ratio at the reference stress. Another evident fact from Figure 5.35 is that the sodium hex BBC holds far less stress at a given void ratio than all other soils. Looking at a void ratio of say 0.6, sodium hex BBC is carrying approximately 3,780 kPa, some 3,300 kPa less than Killian Court in-situ material at the same void ratio. Given that the flocs have been dispersed in the sodium hex BBC it is reasonable to assume that the load carrying capacity of the soil is mostly down to mechanical contact between grains. However, some double layer effects still exist but not enough to contribute significantly to the strength of the soil. Killian Court in-situ material on the other hand possesses its mechanical and electro-chemical bonds from nature and therefore its load carrying capacity is down to a combination of both. It is therefore postulated that this difference in load carrying abilities of both soil be attributed to the electro-chemical bond existing between adjacent soil grains in the matrix. The difference could possibly be taken as a rough first estimate for the electro-chemical contribution of a given soil to its ability to carry load. This can be a significant value.

The corresponding hydraulic conductivities for these soils can be seen in Figure 5.36. As mentioned in Sections 5.2.2.2, 5.2.2.3 and 5.2.2.4, a kink in the hydraulic conductivity curves for natural RBBC Series IV and leached RBBC can be seen at comparable void ratios and stress levels. These kinks are now more obvious when viewed against a soil displaying true log-linear hydraulic conductivity behavior such as Killian Court in-situ soil. The kink mentioned is not present in sodium hex BBC further indicating that the mechanism causing these breaks in slope is not present in the soil. This can be attributed to the presence of the sodium Hexametaphosphate. At relatively higher void ratios between 0.9 and 1.0, sodium hex BBC has a comparable hydraulic conductivity to Killian Court in-situ BBC but as the stress level increases (represented by a decrease in void ratio), divergence in the recorded conductivities can be seen. The sodium hex BBC shows higher hydraulic conductivities at any void ratio than Killian Court in-situ BBC. Despite the denser packing of sodium hex BBC (as shown by Table 5-1), more flow channels or paths exist for fluid to pass through the soil. Perhaps the pore water undergoes less tortuosity due to the dispersion of the flocs thereby creating shorter paths for water to flow through the soil. Towards the end of loading (represented at a void ratio of 0.54) for Killian

Court BBC and natural RBBC Series IV, similarities are seen in the hydraulic conductivities for both soils. It is thought that the fabric of both soils have undergone similar levels of fatigue and irrespective of their initial fabric, now have a more similar structure at high stress. This is not so for the leached RBBC as it has already undergone some induced floc breakage and dispersion from centrifuging the soil twice. The wet and dry densities for all types of BBC are shown in Figure 5.40 and Figure 5.41 respectively.

The coefficient of consolidation c_v for all BBC derivatives is presented in Figure 5.37. It should be pointed out that all RBBC soils in this Figure are born from the same natural dry powder. Similarities exist between the natural RBBC Series IV and leached BBC curves insofar as they both rise once the preconsolidation pressure is passed and then drop once more when a certain stress level is achieved. Possible reasons for this have been given in 5.2.2.4. In contrast to both curves mentioned, the c_v value for sodium hex BBC rises for the duration of the test. In fact, up to an axial stress of 3,000 kPa, sodium hex BBC displays very similar c_v values to Killian Court BBC but begins to diverge to higher values with an increase in axial stress.

The Figures presented in this Section compare the behavior of several types of RBBC to that of in-situ material. It has been shown that at some stress level, internal structural changes occur in the soil thereby affecting the coefficient of consolidation c_v and the hydraulic conductivity k_v . These changes in behavior, which were firstly thought to be anomalous, appear to represent changes in how the load is distributed throughout the soil at a micro scale. These changes are attributed to the breaking of flocs which still exist after a soil has been ground to a powder and air dried. These tiny flocs act like coarse aggregate in a set concrete whereby at some stress, the flocs will break and redistribution of the load will occur. It is therefore proposed that soil has a dual memory – that of the preconsolidation pressure and that of the floc strength. This assumption appears to be corroborated by examining data from the preceding Sections side by side.

5.2.3 NATURAL LONDON CLAY

5.2.3.1 INTRODUCTION

The origins of the London Clay used in this research have already been discussed in Chapter 3. The use of London Clay is relevant because it is also a marine clay and its

depositional regime was influenced by salinity. The time available for this research was not sufficient to subject London Clay to the same rigors as BBC insofar as leaching the soil or re-sedimenting London Clay which had been dispersed with sodium hexametaphosphate did not occur. The same terminology will be used here for the London Clay as BBC where natural London Clay which was re-sedimented as received into the lab will be termed natural RLC. This is the only derivative of London Clay which will be covered here. Natural RLC was re-sedimented to pore fluid salinities of 4, 16 and 256 g/l. Two CRS tests stressed the soil to 10,000 kPa while CRS1305 stressed the soil to 40,000 kPa. London Clay CRS tests were performed at a strain rate of 0.5 %/hr.

5.2.3.2 RESULTS FOR NATURAL RESEDIMENTED LONDON CLAY

Figure 5.42 presents the compression data in ϵ_a - $\log\sigma'_{ac}$ space. In a similar fashion to re-sedimented BBC, the preconsolidation pressure (σ'_p) for all London Clay tests fall below the target batch preconsolidation pressure of 100 kPa. Reasons for this have been given in Section 5.2.2.3. The axial strain required to bring the soil from overconsolidated to normally consolidated is approximately 2.60 %. This holds true for all salinities. The normally consolidated line for natural RLC is visibly more curved than for any type of BBC. Figure 5.47 shows the required axial strain to achieve a stress of 10,000 kPa. The strain to 40,000 kPa for CRS1305 is 48.4 %. Axial strain requirements for RLC to achieve a stress of 10,000 kPa are greater than axial strains for BBC at similar stress levels. This means that London Clay is more compressible than BBC. Given that three different strains are required to reach 10,000 kPa in Figure 5.42 for the three different salt contents, it should be noted that there is no trend in the strain requirement versus salt content. The compression behavior in the normally consolidated range is not linear and changes slope with an increase in stress level. Beyond 10,000 kPa, there is a reversal in slope change. Further tests to high stress are required in order to demonstrate that this is in fact actual soil behavior and not some anomaly which occurred for this test.

Figure 5.43 presents the compression results in e - $\log\sigma'_{ac}$ space. All three salt concentrations start at an initial void ratio of between 1.57 and 1.62. The 4 g/l soil has the lowest initial void ratio while the 16 and 256 g/l soils start at very similar initial void ratio. Again, the normally consolidated lines for all three specimens are curved and change with an increase in stress. The same slope change is seen beyond a stress of 10,000 kPa for CRS1305 that was

evident in strain space. The void ratios for all three soils range from 0.51 to 0.55 at 10,000 kPa. At an axial stress of 40,000 kPa, the void ratio for CRS1305 is 0.31. Figure 5.48 and Figure 5.49 show the initial void ratios and void ratios at 10,000 kPa as a function of pore fluid salinity. No trend is evident in the high stress Figure but for the initial void ratio, with an increase in salinity, an increase in void ratio is observed. Because the preconsolidation pressure is reached so early in loading, it is now possible to obtain the c_c value over two orders of magnitude. Starting with the 256 g/l soil, the c_c value between $\sigma'_{ac} = 100$ and 1,000 kPa is 0.52, while between $\sigma'_{ac} = 1,000$ and 10,000 kPa the c_c value is 0.39. Note that CRS1306 was not fully stressed to 10,000 kPa so the data has been extrapolated to the 10,000 kPa value and it is estimated the void ratio will be 0.55 for the soil at this stress level. Immediately upon application of stress, the 16 g/l specimen diverges from the 256 g/l line and joins the 4 g/l line just before the preconsolidation pressure. Thereafter, the 4 and 16 g/l tests have very similar compression behavior in the normally consolidated region. The c_c value for these two tests between $\sigma'_{ac} = 100$ and 1,000 kPa is 0.52. After $\sigma'_{ac} = 1,000$ kPa, the 4 g/l soil becomes stiffer than the 16 g/l soil and a change in c_c value is observed. The c_c value between $\sigma'_{ac} = 1,000$ and 10,000 kPa is 0.36 and 0.37 for the 4 and 16 g/l soils respectively. All three soils have the same compression behavior between $\sigma'_{ac} = 100$ and 1,000 kPa, but after that the 4 and 16 g/l soils become stiffer than the 256 g/l soil. This is reflected in the c_c values. None of the tests suffered from extrusion issues. All tests show a reduction in compressibility between $\sigma'_{ac} = 1,000$ and 10,000 kPa. Given that the 256 g/l curve is offset to the right of the 4 and 16 g/l tests, this indicates that the 256 g/l soil is stronger. The 256 g/l soil can hold more stress at a given void ratio than the 4 and 16 g/l soils but this difference diminishes as the stresses approach 10,000 kPa. This shows the first evidence that natural RLC is influenced by salt in terms of compression behavior at least. The fact that the 16 g/l curve starts in almost an identical location to the 256 g/l, and the jumps to the 4 g/l line would indicate that there were chemical bonds formed with the addition of more salt (in terms of the 4 g/l compared to the 16 g/l), which were not strong enough to be sustained upon the application of stress to the soil. This is why the 16 g/l bisects the 4 and 256 g/l curves in the overconsolidated range and then reverts to low salinity behavior. In general, RLC is resedimented to a much higher void ratio at 100 kPa than any BBC yet compresses to similar void ratios at $\sigma'_{ac} = 10,000$ kPa. The RLC results presented also give higher void ratios at a given stress than those previously presented for RLC in Chapter 3 by Gasparre (2005).

The hydraulic conductivity versus void ratio plots for all three RLC salinities are shown in Figure 5.44. The hydraulic conductivities span more than three orders of magnitude and start out at 2.17×10^{-7} to 3.38×10^{-8} cm/sec at a void ratio of 1.55. The curves tend to converge with the application of stress and at a void ratio of 0.5 a representative hydraulic conductivity of 7.89×10^{-11} cm/sec can be seen. There is no trend with the hydraulic conductivity at a given void ratio versus salt content. The break in slope which was observed in natural RBBC Series IV hydraulic conductivity data is not evident in RLC.

The coefficient of consolidation for all RLC tests is shown in Figure 5.45 and Figure 5.46. This Figure shows that for two of the three tests, the c_v value flattens out with an increase in stress. The only test that does not obey this is CRS1305 which has a gap in the data in the low stress range which represents a pause in the test. The c_v values for 16 and 256 g/l RLC are 1.5×10^{-4} and 1.7×10^{-4} cm²/sec respectively at 8,000 kPa. When CRS1305 reached 40,000 kPa, the c_v value is 1.4×10^{-4} cm²/sec and still dropping. Figure 5.45 shows the plot of c_v versus axial effective stress for all three tests up to 10,000 kPa while Figure 5.46 presents data up to 40,000 kPa. Interestingly, CRS1305 shows a change in c_v value at stress levels close to, or just past 10,000 kPa. After this stress level, the c_v value begins to drop and is still dropping when the test finishes. It is not certain that this is the same effect witnessed in RBBC where floc breakage was observed at certain stress levels. More tests are required to confirm that this result is representative of what happens at stress levels beyond 10,000 kPa. The hydraulic conductivity plot shown in Figure 5.44 does not indicate any change in behavior in the same way the hydraulic conductivity plots complimented the coefficient of consolidation plots for BBC in terms of behavioral change.

5.2.4 RESEDIMENTED GULF OF MEXICO – URSA CLAY

The results presented here are in general agreement with one dimensional compression curves obtained during the consolidation phase of CK₀UC testing by Brendan Casey in the MIT Geotechnical Laboratory. A comparison of these curves is shown in Figure 5.50.

RGOM – Ursa was tested to high stress as part of this research and although only one pore fluid salinity of 0 g/l (distilled water) was used, comparisons will be drawn between it and

other soils later in this Chapter. The compression data in Figure 5.51 & Figure 5.52 show that the slope of the normally consolidated region changes with an increase in stress.

The hydraulic conductivity plots shown in Figure 5.53 for RGOM-Ursa display true log-linear behavior for all three tests. The hydraulic conductivity spans roughly 2.5 orders of magnitude over the void ratio range 1.10 to 0.28. No changes in slope can be seen from these data.

The coefficient of consolidation c_v for RGOM-Ursa is shown in Figure 5.54 & Figure 5.55. All three tests show remarkably constant c_v values throughout a vast stress range. Such levels of consistency in the c_v value are only matched by London Clay. All c_v values are in good agreement throughout loading. Figure 5.54 presents the data up to 40,000 kPa while Figure 5.55 shows values up to 10,000 kPa. At a stress of $\sim 28,000$ kPa, a rise in c_v value is seen in all three tests. The cause of this rise in c_v is not yet clear but it can be taken as the true soil behavior given that it is present in all three tests. There is no apparent change in hydraulic conductivity at this stress; however, the stress range 28,000 – 40,000 kPa is responsible for reducing the void ratio only a small amount so any changes in behavior may not be obvious.

5.2.5 SODIUM MONTMORILLONITE

Given that more of a reaction to pore fluid salinity is seen in soils containing a large percentage of expanding clays, it was decided to test sodium montmorillonite at two different pore fluid salinities, namely 1 & 256 g/l. Both of these salinities were resedimented in the same manner as all other soils in the testing program. A batch of 256 g/l sodium montmorillonite was resedimented in less than 1 month and CRS tested, the results of which are presented in this Section. 1 g/l sodium montmorillonite was also resedimented in the hope of testing via CRS in order to provide data at both ends of the salinity spectrum. This 1 g/l soil batch was initiated on the 20th of December 2011 and did not reach end of primary consolidation until the middle of May 2012. It was therefore not possible to test the soil and present its results as part of this research. It is not yet a certainty that 1 g/l sodium montmorillonite can be tested via the CRS apparatus as the strain rate needed to satisfy test requirements may not be achievable. That is to say, the strain rate may be so slow that current laboratory equipment may not be able to satisfy this requirement. This is a parameter which has yet to be determined.

When the pore fluid salinity is 256 g/l for sodium montmorillonite, all double layer effect has been eliminated and the soil structure consists of predominantly mechanical contact between grains. This was shown in Chapter 3. SEM images were taken from oven dried specimens at an axial effective stress of 200 kPa.

Figure 5.56 presents the compression data for 256 g/l sodium montmorillonite in ϵ_a - $\log\sigma'_{ac}$ space. Two successful tests were performed on the soil and the results show very comparable behavior in the normally consolidated range. The normally consolidated line is non-linear and changes constantly with an increase in stress. The axial strain required to achieve a stress of 10,000 kPa is 36.2 %. CRS1322 was stressed to 2,000 kPa while CRS1318 was stressed to 27,600 kPa. The break in data at a stress of 17,300 kPa can be attributed to a relaxation test performed on the soil. Consolidation was halted at this stress, yet despite the load frame being turned off, almost 0.60 % axial strain is recorded due to relaxation of the soil over time.

The compression data from both tests is presented in e - $\log\sigma'_{ac}$ space in Figure 5.57. The initial void ratios for both tests are similar and range from 1.69 to 1.71. The c_c value obtained between 1,000 and 10,000 kPa is 0.38 indicating a very compressible soil. At an axial effective stress of 10,000 kPa, the void ratio is 0.735 – the largest void ratio at the reference stress of any soil in the testing program. The void ratio at an axial effective stress of 27,600 kPa is 0.59.

The corresponding hydraulic conductivity plots are shown in Figure 5.58 in void ratio space. The data for the specimen tested to high stress (CRS1318) does not go past a void ratio of 0.858 owing to a leak in the base excess pressure during the test. Good hydraulic conductivity data is obtained up to this point. In general, both curves agree well and the hydraulic conductivity of the soil is log-linear without any drastic changes in slope. The data covers over two orders of magnitude and would possibly cover a third were it not for the leak.

The coefficient of consolidation data is presented in Figure 5.59. Once the preconsolidation pressure is passed, the c_v value drops and continues to do so with an increase in stress level. For CRS1322 which was stressed to 2,000 kPa, the c_v value never rises. For CRS 1318, the c_v value drops, tapers off and then rises slightly until the data is cropped where the leak occurred. Further testing needs to be performed to determine if this is actually an increase in the c_v value or if it associated with the early stages of a leak in the test. At an axial effective stress of

1,000 kPa, both c_v values are comparable with an average value of 0.000429 cm²/sec. These results represent what is believed to be the first instance of sodium montmorillonite being tested in the CRS apparatus.

5.2.6 COMPARISON OF DIFFERENT SOIL TYPES

Figure 5.60 presents a synthesis plot of the compression data for all soils used in the testing program in ϵ_a - $\log\sigma'_{ac}$ space. Of these soils, all but one was resedimented. All resedimented soils were stressed to a target batch preconsolidation pressure of 100 kPa, however, the BBC sodium hex and RGOM-Ursa show preconsolidation pressures past this stress level. This is because both soils have undergone significant secondary compression while they were waiting to be tested. It can be seen from Figure 5.60 that there is a large variation in terms of required strain to reach 10,000 kPa. The soil with the lowest strain requirement to reach this stress is the only soil to possess a natural fabric, namely Killian Court in-situ BBC, hence indicating it is a much stiffer soil than the equivalent resedimented soils. This can be attributed to the natural bonds which have developed between particles over thousands of years. These bonds will also give the effect of a higher preconsolidation pressure. The axial strain required to bring the Killian Court BBC to 10,000 kPa is around 22.7 %. An analysis has already been performed on the BBC soils in Section 5.2.2.7. Of the remaining 3 soils presented, 2 are taken from different areas of the world while the last soil is a pure clay mineral. It is fortunate that there were so many soils with such differing mineralogy available for testing during this research. The London Clay is the most compressible soil of the set requiring a strain of 42.6 % 10,000 kPa. The slopes of the virgin compression line for London Clay and sodium montmorillonite change markedly more than the other soils with an increase in stress. This is shown by the distinct nonlinearity of the data. RGOM-Ursa requires a similar strain to 10,000 kPa as RBBC (Series IV & leached).

Figure 5.61 presents a synthesis plot of the compression results in e - $\log\sigma'_{ac}$ space. Even though RLC starts out a relatively high void ratio, at an axial effective stress of 10,000 kPa its void ratio is comparable to other soils tested. This is in contrast to sodium montmorillonite which also starts out at a high void ratio, and maintains its stiffness throughout loading up to 10,000 kPa. Table 5-4 shows the c_c value for all soils tested.

The hydraulic conductivity versus void ratio plots for all soils in the testing program are shown in Figure 5.62. The most striking observation to make from the Figure is that RLC and sodium montmorillonite at 256 g/l have similar hydraulic conductivities which are more than one order of magnitude smaller at a given void ratio than all other soils tested. The majority of soils display log-linear hydraulic conductivities in void ratio space, the exception being natural RBBC Series IV and leached RBBC for reasons already explained in Section 5.2.2.7. Hydraulic conductivities for the soils tested span more than three orders on magnitude.

The coefficient of consolidation versus axial consolidation stress synthesis plot is shown on two different scales in Figure 5.63 and Figure 5.64. These Figures show that the c_v value for RGOM-Ursa, sodium montmorillonite and London Clay have much lower values than any of the BBC soils tested. The soil with the lowest c_v is RLC. As RGOM-Ursa was the only soil stressed to 40,000 kPa, an additional plot showing the c_v values up to 10,000 kPa is shown in Figure 5.64. It can be seen from these plots that the c_v value for RGOM-Ursa does not change much over a large stress range, the same is true for London Clay but this is over a smaller stress window. The c_v values for all types of BBC do not show any sign of achieving constant values even at stresses up to 10,000 kPa.

5.2.7 EVALUATION OF CRS TESTING PROGRAM

The CRS test is relatively simple to perform and a great deal of useful data can be extrapolated from high quality test results. It is fortunate that so many soils were available for testing throughout the course of this research. The extensive CRS testing program employed generated a substantial bank of reference data which can now be used for future research in the area of salinity effects as well as to compliment other research ongoing in the MIT Geotechnical Laboratory.

The altering of BBC in several ways has produced a great deal of useful data on how the fabric and structure of the soil behaves and evolves with change in stress level. Some previously unknown information on how flocs break at certain stress levels is now available showing that for BBC at least, changes in mechanical behavior occur at two stress levels, namely the preconsolidation pressure and at the limit of the floc strength.

The point has also been proven that chemical and mechanical bonds can support a significant portion of the stress applied to a soil. This is demonstrated by the fact that an in-situ soil is capable of sustaining a larger stress than a completely dispersed soil comprised of the same basic minerals, which has a greater density.

5.3 TRIAXIAL TESTS

5.3.1 INTRODUCTION

A series of strength tests were performed on three BBC derivatives in order to determine the effect of the pore fluid salinity on the strength characteristics of the soil. The soils tested were natural RBBC Series IV at pore fluid salinities of 4 and 256 g/l, leached RBBC at pore fluid salinities of 1 and 256 g/l and Killian Court in-situ BBC to serve as a reference for the triaxial testing program. All tests were K_0 consolidated at a rate of 0.15 %/hr and sheared in compression (CK_0UC) in the normally consolidated range after roughly 24 hours of secondary compression was allowed on the specimen. The K_0 consolidation ensures zero lateral strain by adjusting the cell pressure to keep the axial and volume strains equal. All resedimented BBC used in the triaxial testing program were resedimented to a maximum axial stress of 200 kPa in the consolidometer. All triaxial testing was performed in a low pressure triaxial apparatus.

Data on the coefficient of earth pressure at rest (K_0) can be obtained from feedback controlled one dimensional consolidation in the triaxial cell. These K_0 values will be presented for each soil in their relevant sub Section. The general trend of K_0 decreasing during the initial loading within the overconsolidated region until the preconsolidation pressure is reached and then plateaus at some constant value is observed in all soils. Once the soil is in the normally consolidated region, the K_0 value remains relatively stable. The value of K_0 in the normally consolidated region is referred to as K_{0NC} . As was observed in Santagata (1994), the K_0 value decreases during reloading to a value lower than the K_{0NC} and then increases to a constant value once the preconsolidation pressure is passed. All triaxial specimens were K_0 consolidated so that the strain was greater than 10 % in accordance with SHANSEP recommendations. A list of all triaxial tests presented here is shown in Table 5-3.

5.3.2 TRIAXIAL RESULTS

This section presents results from triaxial tests in which NC specimens were sheared undrained in compression at a constant axial strain rate of 0.5 %/hr after K_0 consolidation to their respective final axial consolidation effective stresses. The results from 12 successful tests will be presented across all soil types. The testing of these soils was performed in three separate low pressure triaxial devices. These devices are known locally in the MIT Geotechnical Laboratory as MIT01, MIT02 and MIT04. In general, MIT01 was used for low salinity testing while MIT02 was used for high salinity testing. MIT04 was used for any salinity in order to advance the testing program in a timely manner.

Table 5-3 lists the test number and type, the apparatus, soil type and salinity, the preshear consolidation conditions and the pertinent stress-strain-strength parameters at peak shear stress and at maximum obliquity. Note that the friction angle (ϕ') represents a measure of the strain rate at peak maximum obliquity.

5.3.2.1 BEHAVIOR OF NC NATURAL RBBC

5.3.2.1.1 SHEAR STRESS-STRAIN BEHAVIOR

Figure 5.65 shows the normalized stress-strain behavior (q/σ'_{ac} versus ϵ_a , where $q = (\sigma_1 - \sigma_3)/2$) with the axial strain shown on a linear scale. The maximum axial consolidation stress (σ'_{am}) for each test is stated in the legend. This Figure illustrates that the effect of the preshear consolidation stress level has little influence on the normalized strength. In general, the peak undrained strength ratio ($USR = s_u/\sigma'_{ac}$) decreases with an increase in axial consolidation effective stress. Figure 5.75 shows the axial strain to failure as a function of pore fluid salinity while Figure 5.76 shows the relationship between axial strain to failure and the normalized shear stress as a function of pore fluid salinity. The strength ratio decreases from 0.303 at low stress to 0.283 at higher stresses. Given that range of axial consolidation effective stresses is small (920 – 452 kPa), it cannot be stated for certain that these are the effects of the stress level and not salinity. Upon further examination of Figure 5.65, it can be seen that TX1081 and TX1069 which are both 256 g/l specimens have almost identical strength ratios even though TX1069 has been consolidated to a lower stress. 4 g/l specimens which have been consolidated to similar stresses as TX1069 show higher strength ratios. It is therefore stated that the reduction in strength ratios

for the two high salinity tests are as a result of the salt content and not because of the consolidation stress level. Previous research in which the consolidation stress level effect was evident presented data over a much greater stress range, for example Abdulhadi (2009). The stress-strain data (Figure 5.65, Figure 5.66 and Figure 5.67) also show that the behavior becomes more ductile as salinity increases. Larger strains are required to mobilize the peak resistance for high salt content soil. The salinity also tends to affect the post peak portion of the stress-strain curves. Higher salinity soils tend to have more residual strength than the low salinity soils. The degree of strain softening can be represented by the brittleness, which is the ratio of the undrained strength to the large strain shear resistance of the soil. For consistency, the shear resistance at $\epsilon_a = 10\%$ was taken as the large strain resistance. Figure 5.77 summarizes the brittleness versus stress level while Figure 5.80 shows the relationship between axial strain at maximum obliquity as a function of pore fluid salinity.

5.3.2.1.2 STIFFNESS

Figure 5.68 shows curves of the undrained secant Young's modulus normalized to the axial consolidation stress (E_u/σ'_{ac}) versus axial strain on a log-log scale for the NC natural RBBC. As the measurements were performed employing external LVDT's, the estimates of the stiffness are considered reliable only above 0.01 – 0.05 % axial strain. In general, the Figure shows that the soil displays strong non linearity and that yielding occurs at small strains. The decrease in stiffness is particularly marked once the soil reaches failure due to the large amount of post peak strain softening. The maximum value of the normalized stiffness (E_{umax}/σ'_{ac}) shows no trend with salt content. The results suggest a salt level effect at larger strains as the higher salinity curves tend to require a larger strain to achieve a given modulus than the lower salinity ones. This, however, is only evident when the modulus values are extremely low.

5.3.2.1.3 EFFECTIVE STRESS BEHAVIOR

Figure 5.69 and Figure 5.70 shows the normalized effective stress paths using the MIT stress space (q/σ'_{ac} versus p'/σ'_{ac} where $q = (\sigma_1 - \sigma_3)/2$ versus $p' = (\sigma'_1 + \sigma'_3)/2$) from the triaxial compression test series on NC natural RBBC. Pore pressure measurements were made at the base of the specimen in all cases. The Figures show the change in pore pressure development during the test where there is little pore pressure generation up to a yield point followed by much

greater development thereafter. Peak shear conditions coincide with a yield condition but the peak point moves further down the stress path as the consolidation stress increases. The peak strength is linked in this case to the salt content of the soil. At large strains there is little difference in the stress obliquity (q/p') and a common linear failure envelope is reached. Table 5-3 lists the values of effective stress parameters at peak and maximum obliquity.

The corresponding variation in friction angle versus axial strain is shown in Figure 5.71. Except for TX1068, all tests reach maximum obliquity (ϕ'_{mo}) at strains of approximately 11 %. TX1068 reached ϕ'_{mo} at much smaller strains for reasons which are not apparent. The friction angle ranges from ϕ'_{mo} 31.4 to 32.5° along the failure envelope. The results suggest that a larger friction angle is observed at maximum obliquity for higher salinity soils. Figure 5.78 & Figure 5.79 show the friction angle as a function of pore fluid salinity at peak shear stress and at maximum obliquity respectively.

Figure 5.72 shows the excess pore pressure ($u_e = \Delta u - \Delta \sigma_3$) generated during undrained shear normalized to the axial effective consolidation stress (σ'_{ac}). The results show that the pore pressures rise continuously to some axial strain and then taper off. Some of the data presented in Figure 5.72 show pore pressures continually rising throughout the entire test. Both high salinity tests demonstrate similar behavior insofar as a plateau value of excess pore pressure ratio is achieved, and then they both begin to rise at high strains for reasons which are not yet apparent.

The corresponding normalized shear induced pore pressures ($u_s = \Delta u - \Delta \sigma_{oct}$, where $\Delta \sigma_{oct} = (\sigma_1 + \sigma_2)/3$). The method isolates the pore pressure change due to shear stress alone, removing the effect of the total stress path. The shear induced pore pressures versus axial strain are shown in Figure 5.73. The plot essentially removes the effect of the starting K_0 value. The results differ from the excess pore pressures presented in Figure 5.72 whereby there is no distinct plateau in pore pressures, they are continually rising throughout the test. The positive pore pressures generated throughout shearing indicate a contractive behavior. This continues for the entire shearing process and the values are still rising when the test is terminated. The magnitude of the shear induced pore pressures are similar to the excess pore pressures towards the end of shearing.

The Skempton parameter $A = ((\Delta u - \Delta \sigma_3)/(\Delta \sigma_1 - \Delta \sigma))$ versus strain is shown in Figure 5.74. The results are plotted for the small strain region up to 2 % axial strain. All tests show a starting

A parameter value of about 0.50. There is no trend in the pore pressures generated versus salinity of the soil. No peak is observed in the A parameter as it will continually rise and approach infinity at some strain. Figure 5.81 shows the A parameter at peak shear stress as a function of pore fluid salinity.

5.3.2.2 BEHAVIOR OF LEACHED RBBC

5.3.2.2.1 SHEAR STRESS-STRAIN BEHAVIOR

Figure 5.82 shows the normalized stress-strain behavior (q/σ'_{ac} versus ϵ_a , where $q = (\sigma_1 - \sigma_3)/2$) with the axial strain shown on a linear scale. The maximum axial consolidation stress (σ'_{am}) for each test is stated in the legend. The effect of preshear consolidation stress will not be evident in this Figure because all tests have been consolidated to similar stress levels. The strength ratio for leached RBBC ranges from 0.30 to 0.319 and there is no trend in strength ratio versus salt content. Figure 5.92 shows the axial strain to failure as a function of pore fluid salinity while Figure 5.93 shows the required axial strain to peak shear stress as a function of pore fluid salinity. TX1084 which is a 1 g/l soil, has its maximum undrained strength ratio fall between the two high salinity tests thereby removing any trend from the dataset. Figure 5.83 and Figure 5.84 show the stress-strain data in a close up view (up to 3 % strain) and in log space respectively. Figure 5.84 shows that the ductility of the soil is not affected with the level of salinity. Similar strains are required to mobilize the peak resistance for all salt contents. From Figure 5.82 it can be seen that the high salinity soils retain more residual load carrying capacity once the peak strength is passed. This is similar to what was observed for natural RBBC Series IV. The degree of strain softening is again represented by the brittleness, which is the ratio of the undrained strength to the large strain shear resistance of the soil. For consistency, the shear resistance at $\epsilon_a = 10\%$ was taken as the large strain resistance. Figure 5.94 summarizes the brittleness versus stress level for leached RBBC.

5.3.2.2.2 STIFFNESS

Figure 5.85 shows curves of the undrained secant Young's modulus normalized to the axial consolidation stress (E_u/σ'_{am}) versus axial strain on a log-log scale for leached RBBC. In general, the Figure shows that the soil displays strong non linearity and that yielding occurs at small strains. The decrease in stiffness is particularly marked once the soil reaches failure due to

the large amount of post peak strain softening. The maximum value of the normalized stiffness (E_{umax}/σ'_{ac}) shows no trend with salt content at any strain level.

5.3.2.2.3 EFFECTIVE STRESS BEHAVIOR

Figure 5.86 and Figure 5.87 show the normalized effective stress paths using the MIT stress space (q/σ'_{ac} versus p/σ'_{ac} where $q = (\sigma_1 - \sigma_3)/2$ versus $p' = (\sigma'_1 - \sigma'_3)/2$) from the triaxial compression test series on NC leached RBBC. Pore pressure measurements were made at the base of the specimen in all cases. The Figures show the change in pore pressure development during the test where there is little pore pressure generation up to a yield point followed by much greater development thereafter of pore pressures. Peak shear conditions coincide with a yield condition but the peak point moves further down the stress path as the consolidation stress increases. At large strains there is more of a difference in the stress obliquity (q/p') than was observed with the natural RBBC and a common linear failure envelope is not reached. Table 5-3 lists the values of the effective stress parameters at peak and maximum obliquity.

The corresponding variation in friction angle versus axial strain is shown in Figure 5.88. The low salinity tests show very similar variations in friction angle versus axial strain, however, the high salinity results differ by over 2° at maximum obliquity (ϕ'_{mo}). Nonetheless there is a definite trend insofar as a higher friction angle is observed with a higher salinity soil than for a low salinity soil. Figure 5.95 & Figure 5.96 give the friction angle at failure and maximum obliquity respectively as a function of pore fluid salinity. Similarly to the natural RBBC, the maximum obliquity is reached at strains of approximately 11 % for all tests. Figure 5.97 gives the axial strain required to maximum obliquity. The friction angle ranges from $\phi'_{mo} 29.2^\circ$ for the low salinity BBC to 33.8° for the high salinity soil along the failure envelope. This represents a maximum difference of 4.60° between the two salinities as opposed to a difference of 1.10° for natural RBBC at different salinities. The results suggest that the soil has become more sensitive with the removal of natural salts and this is reflected in the low friction angle observed in the 1 g/l tests. Even the high salinity test which produced the lowest friction angle values (TX1094) still has a ϕ'_{mo} equal to 31.7° which is still 2.50° greater than the 1 g/l tests.

Figure 5.89 shows the excess pore pressure ($u_e = \Delta u - \Delta \sigma_3$) generated during undrained shear normalized to the axial effective consolidation stress (σ'_{am}). The results show that the pore

pressures rise continuously to some axial strain and then taper off. There is no trend in the magnitude of pore pressures generated versus the pore fluid salinity. The 1 g/l tests show more similar behavior to each other than the high salinity tests.

The corresponding normalized shear induced pore pressures ($u_s = \Delta u - \Delta \sigma_{oct}$, where $\Delta \sigma_{oct} = (\sigma_1 + \sigma_2)/3$) are shown in Figure 5.90. The method isolates the pore pressure change due to shear stress alone, removing the effect of the total stress path. The plot essentially removes the effect of the starting K_0 value. The results differ from the excess pore pressures presented in Figure 5.89 whereby there is no distinct plateau in pore pressures, they are continually rising throughout the test. The positive pore pressures generated throughout shearing indicate a contractive behavior. This continues for the entire shearing process. The values are still rising when the test is terminated. The magnitude of the shear induced pore pressures are similar to the excess pore pressures towards the end of shearing.

The Skempton parameter $A = ((\Delta u - \Delta \sigma_3)/(\Delta \sigma_1 - \Delta \sigma))$ versus strain is shown in Figure 5.91. The results are plotted for the small strain region up to 2 % axial strain. All but one of the specimens show a starting A value of around 0.30 with the remaining test starting at 0.44. These values are lower than those recorded for natural RBBC Series IV and there is no trend in the pore pressures generated versus salinity of the soil. A plot of the A parameter at failure as a function of pore fluid salinity is shown in Figure 5.98.

5.3.2.3 BEHAVIOR OF KILLIAN COURT IN-SITU BBC

5.3.2.3.1 SHEAR STRESS-STRAIN BEHAVIOR

Figure 5.99, Figure 5.100 and Figure 5.101 show the normalized stress strain behavior of Killian Court BBC. The maximum consolidation stress for each test is stated in the legend and in general, Killian Court material had to be consolidated to a higher stress state than resedimented material. This is partly because when the material was being back pressure saturated in the triaxial cell, it took higher pressures to achieve a B value greater than 0.98 for in-tact material than for resedimented soil. The K_0 consolidation process therefore started from a higher total state of stress. The range of consolidation stresses to bring the soil to the normally consolidated region varied for in-situ material between $\sigma'_{ac} = 1,000$ and 1,950 kPa. It is important to note that for the shearing portion of TX1110, the drain line valves were open but because the back

pressure system is stiff enough to prevent appreciable volume change, the test is effectively an undrained one. The strength ratio for Killian Court BBC ranges from 0.293 to 0.307. These peak strength ratios are achieved at strains of approximately 0.66 % for TX1091 and TX1108 while TX1110 reaches its peak strength ratio at a strain of 0.71 %. The peak strength ratio of natural RBBC Series IV were achieved at strains of between 0.22 % and 0.34 % while for leached RBBC they were between 0.13 and 0.16 %. It is therefore obvious that strains required to fail resedimented specimens are at least half those required to fail in-tact material. The undrained strength ratio for all BBC derivatives are comparable lying generally between values of 0.282 and 0.32. It can be seen that the post-shear behavior of TX1108 and TX1091 are very similar while for TX1110, more residual strength is available. This may be because TX1108 and TX1091 were obtained from the same Shelby tube while TX1110 was taken from a different tube meaning natural soil variation may play a part in the results.

5.3.2.3.2 STIFFNESS

Figure 5.102 shows curves of the undrained secant Young's modulus normalized to the axial consolidation stress (E_u/σ'_{am}) versus axial strain on a log-log scale for the Killian Court BBC. In general, the Figure shows that the soil displays strong non linearity and that yielding occurs at small strains. The decrease in stiffness is particularly marked once the soil reaches failure due to the large amount of post peak strain softening. The moduli observed compare well with those observed for resedimented material.

5.3.2.3.3 EFFECTIVE STRESS BEHAVIOR

Figure 5.103 and Figure 5.104 show the normalized effective stress path using the MIT stress space from the triaxial compression test series on NC Killian Court in-situ BBC. The Figures show the change in pore pressure development during the test where there is little pore pressure generation up to a yield point followed by much greater development thereafter of pore pressures. Peak shear conditions coincide with a yield condition but the peak point moves further down the stress path as the shear stress increases. The peak shear stress for Killian Court BBC is not as well defined as it is for resedimented material. At large strains there is a difference in the stress obliquity (q/p') and a common linear failure envelope is not reached for all tests. Table 5-3 lists the values of the effective stress parameters at peak and maximum obliquity.

The corresponding variation in friction angle versus axial strain is shown in Figure 5.105. There is a 1.4° variation in friction angle at ϕ'_{mo} . TX1110 does not reach maximum obliquity as the test was terminated before this stage. For Killian Court material, maximum obliquity is reached at strains of about 9.5 % which are smaller strains than that required for resedimented material to reach maximum obliquity. The friction angle ranges from ϕ'_{mo} 30.4° to 31.8° along the failure envelope. Although TX1110 did not reach ϕ'_{mo} , the results are broadly similar to TX1108. It is therefore assumed that TX1108 is representative of both tests in terms of friction angle values at least.

Figure 5.106 shows the excess pore pressure generated during undrained shear normalized to the axial effective consolidation stress. The results show that the excess pore pressures continually rise throughout the test. This observation is different to resedimented material insofar as the excess pore pressures taper off to some constant value at a given strain.

The corresponding normalized shear induced pore pressures are shown in Figure 5.107. Again it is seen that the shear induced pore pressures continually rise throughout the test in a similar fashion to what was observed in resedimented material and that the shear induced pore pressures are of a similar magnitude as the excess pore pressures. The shear induces pore pressure curves rise with a steeper slope than the excess pore pressure curves. The positive pore pressures generated throughout shearing indicate a contractive behavior.

The Skempton parameter $A = ((\Delta u - \Delta \sigma_3) / (\Delta \sigma_1 - \Delta \sigma))$ versus strain is shown in Figure 5.108. The results are plotted for the small strain region up to 2 % axial strain. The starting A value for the tests range from 0.28 to 0.5. These values are in general agreement with those observed for natural RBBC.

5.3.2.4 SYNTHESIS PLOT OF BBC CK_0UC TRIAXIAL RESULTS

Only when all results are appraised side by side can true similarities and differences in soil behavior be seen. The purpose of this Section is to see where similarities lie between tests run on resedimented material, and those run on in-situ material. Results from a total of 12 triaxial tests (CK_0UC) will be plotted alongside each other and these consist of 3 Killian Court in-situ BBC tests, 5 tests on natural RBBC Series IV and 4 tests on leached RBBC. The K_0 values for all soils from the consolidation phase at shown plotted against the normalized shear stress of the

soil in Figure 5.120. A slight decrease in K_0 value can be observed with an increase in normalized shear stress.

5.3.2.4.1 SHEAR STRESS-STRAIN BEHAVIOR

Figure 5.109, Figure 5.110 and Figure 5.111 show synthesis plots of the normalized stress strain behavior for all types of BBC used in the testing program. The maximum consolidation stress for each test is stated in the legend. One of the main differences to note from these Figures is that the Killian Court in-situ material has different strains to failure than resedimented soil. For all three Killian Court tests, the post peak behavior is much more linear insofar as it drops with a constant slope with an increase in strain as opposed to the resedimented BBC. With an increase in strain, RBBC tends to taper off and the slope of the stress-strain curve flattens out. From Figure 5.110, it can be seen that the undrained strength ratio for all tests range from 0.282 to 0.32. It also evident from the same Figure that the Killian Court tests require larger strains to failure, but this point is better demonstrated in Figure 5.111. On a log scale, the differences in strain to failure for all tests are clearly shown. In general, all RBBC tests fail at strains ranging from 0.12 to 0.34 % while Killian Court BBC specimens fail at strains ranging from 0.66 to 0.71 %. It can be stated that lower strains are required to fail resedimented material as opposed to in-tact soil. Despite the lower strain requirement for failure, the stress ratios are all very comparable.

5.3.2.4.2 STIFFNESS

Figure 5.112 shows a synthesis plot of the undrained secant Young's modulus normalized to the axial consolidation stress (E_u/σ'_{am}) versus axial strain on a log-log scale for all types of BBC. In general, the Figure shows that all BBC soil derivatives display strong non linearity and that yielding occurs at small strains. The decrease in stiffness is particularly marked once the soil reaches failure due to the large amount of post peak strain softening. The moduli observed compare well with those observed for resedimented material. The E_u/σ'_{am} values at a strain of 0.01 % range from 257 to 420 and these values rapidly diminish with an increase in strain.

5.3.2.4.3 EFFECTIVE STRESS BEHAVIOR

Figure 5.113 and Figure 5.113 show the normalized effective stress path using the MIT stress space. These Figures present synthesis plots from the triaxial compression test series on NC BBC of all types. The Figures show the change in pore pressure development during the test where there is little pore pressure generation up to a yield point followed by much greater development thereafter of pore pressures. Peak shear conditions coincide with a yield condition but the peak point moves further down the stress path as the consolidation stress increases. As previously mentioned in Section 5.3.2.3.3, the occurrence of the peak for Killian Court BBC is not as well defined as it is for resedimented material. At large strains it can be argued that for some tests a common failure envelope is reached. This was true for natural RBBC Series IV, but now that all tests have been plotted together it is clear that more curves fall on the common failure envelope. Table 5-3 lists the values of the effective stress parameters at peak and maximum obliquity for all BBC derivatives.

The corresponding variation in friction angle versus axial strain is shown in Figure 5.115. There is a 4.50° variation in friction angle at ϕ'_{mo} and maximum obliquity occurs for different soils at different strains. Figure 5.121 shows the axial strain to failure versus the normalized shear stress. The friction angles at failure and maximum obliquity are shown in Figure 5.122 & Figure 5.123 respectively. The maximum friction angle observed was $\phi'_{mo} = 33.8^\circ$ and the minimum ϕ'_{mo} was 29.2° . It has been shown already that maximum obliquity for resedimented material is achieved around a strain of 11 % while for in-situ material it is achieved at a strain of 9.5 %. Abdulhadi (2009) presented data showing a correlation of reducing friction angle with increasing axial consolidation stress. This correlation is shown in Figure 5.116. For the stress range in which all the results in the synthesis plot were sheared ($\sigma'_{ac} = 452 - 1,950$ kPa), the expected friction angle at maximum obliquity is in the range of 30.9° to 33° . All but four tests fall within this range, the outliers consisting of high and low salinity soils. It has not yet been established if this observed trend is true for in-situ material as the correlation was derived from resedimented BBC.

Figure 5.117 shows the synthesis plot for the excess pore pressure generated during undrained shear normalized to the axial effective consolidation stress. The results show that the excess pore pressures continually rise throughout the test for some soils while for others, a

plateau is reached at a given strain level which is maintained until a higher strain is reached, and then an increase in excess pore pressure is recorded once more. Killian Court in-situ material shows a constant rise in excess pore pressure throughout a test while some RBBC specimens have the described plateau effect.

The corresponding normalized shear induced pore pressures are shown in Figure 5.118. The shear induced pore pressures continually rise throughout the test for all BBC derivatives and are of a similar magnitude as the excess pore pressures. The shear induced pore pressure curves rise with a steeper slope than the excess pore pressure curves. The positive pore pressures generated throughout shearing indicate a contractive behavior for all soils in the testing program.

The Skempton parameter $A = ((\Delta u - \Delta \sigma_3) / (\Delta \sigma_1 - \Delta \sigma))$ versus strain is shown in Figure 5.119. The results are plotted for the small strain region up to 1 % axial strain. The A parameter is shown in a linear scale and axial strains are shown on a log scale for clarity. Two distinct clusters of initial A value are now visible from the data and these clusters have average A values of 0.32 and 0.46. The three Killian Court in-situ tests fall into the lower initial A value band. The upper initial A value cluster is composed entirely of resedimented material. The A value for all BBC derivatives changes abruptly once the strain corresponding to the peak stress is achieved. In this plot, there is no trend with how the A values evolve for a given salt content in the small strain region.

Test No.	Soil Type	Salt (g/l)	Initial Conditions				At $\sigma'_{ac} = 10$ MPa			@ Max Stress			
			w_o (%)	e_o	γ_d (g/cm ³)	γ_w (g/cm ³)	ϵ_a (%)	e	c_v (cm ² /sec)	σ'_{am} (MPa)	ϵ_a (%)	e	c_v (cm ² /sec)
CRS1252	RBBC Series IV	4	46.71	1.267	1.225	1.799	32.5	0.54	5.07x10 ⁻³	10.65	32.8	0.534	4.96x10 ⁻³
CRS1219	RBBC Series IV	16	45.42	1.261	1.232	1.798	32.9	0.516	2.73x10 ⁻³	10.5	33.2	0.509	NA
CRS1252	RBBC Series IV	64	45.04	1.237	1.259	1.854	32.9	0.499	2.72x10 ⁻³	10.6	33.3	0.492	NA
CRS1252	RBBC Series IV	128	43.3	1.299	1.243	1.836	33.9	0.521	2.64x10 ⁻³	10.6	34.3	0.512	NA
CRS1252	RBBC Series IV	256	39.27	1.304	1.269	1.304	1.269	1.884	2.81x10 ⁻³	11.3	34.2	0.517	2.34x10 ⁻³
CRS1323	Leached BBC	0	38.72	1.075	1.337	1.855	27.1	0.513	3.16x10 ⁻³	12.2	28.3	0.489	2.66x10 ⁻³
CRS1236	Leached BBC	1	44.67	1.177	1.275	1.845	31.3	0.495	3.48x10 ⁻³	10.5	31.8	0.485	NA
CRS1242	Leached BBC	16	46.04	1.259	1.233	1.807	31.6	0.545	2.50x10 ⁻³	11.05	32.2	0.532	2.15x10 ⁻³
CRS1246	Leached BBC	64	44.08	1.264	1.245	1.819	32.6	0.525	1.93x10 ⁻³	10	32.6	0.525	1.93x10 ⁻³
CRS1239	Leached BBC	256	39.52	1.332	1.251	1.865	35.6	0.5	2.07x10 ⁻³	11.4	36.5	0.481	2.07x10 ⁻³
CRS1313	Sodium Hex BBC	0	37.19	1.037	1.362	1.869	28.4	0.46	NA	11.15	29	0.446	NA
CRS1239	Sodium Hex BBC	0	36.42	1.017	1.376	1.877	26.5	0.483	5.62x10 ⁻³	11.7	27.4	0.464	5.87x10 ⁻³
CRS1248	BBC Reverse Leaching	Varies	35.45	1.021	1.374	1.861	27.6	0.576	2.03x10 ⁻³	10.5	28	0.567	NA
CRS1235	BBC Reverse Leaching	Varies	36.58	1.034	1.364	1.864	30.8	0.514	2.26x10 ⁻³	10.8	31.3	0.502	NA
CRS1269	Killian Court in-situ BBC	11.3	35.95	1.001	1.388	1.888	22.8	0.555	3.77x10 ⁻³	11.9	23.9	0.534	3.75x10 ⁻³
CRS1270	Killian Court in-situ BBC	11.3	37.02	1.013	1.38	1.892	23.3	0.554	3.93x10 ⁻³	14.76	26	0.5	4.02x10 ⁻³
CRS1268	Killian Court in-situ BBC	11.3	37.61	1.032	1.367	1.882	25.8	0.517	.58x10 ⁻³	12.35	27.3	0.387	2.21x10 ⁻³

Table 5-1 List of Constant Rate of Strain (CRS) tests performed on several derivatives of Boston Blue Clay

Test No.	Soil Type	Salt (g/l)	Initial Conditions				At $\sigma'_{ac} = 10$ MPa			@ Max Stress			
			w_o (%)	e_o	γ_d (g/cm ³)	γ_w (g/cm ³)	ϵ_a (%)	e	c_v (cm ² /sec)	σ'_{am} (MPa)	ϵ_a (%)	e	c_v (cm ² /sec)
CRS1305	R.London Clay	4	55.5	1.55	1.096	1.706	39.7	0.54	2.61x10 ⁻⁴	41	48.4	0.316	1.44x10 ⁻⁴
CRS1303	R.London Clay	16	57.01	1.613	1.074	1.695	42.6	0.507	1.52x10 ⁻⁴	10.3	42.8	0.503	1.51x10 ⁻⁴
CRS1306	R.London Clay	256	45.57	1.62	1.125	1.779	40.4	0.56	1.77x10 ⁻⁴	10	40.4	0.56	1.77x10 ⁻⁴
CRS1318	Sodium Montmorillonite	256	50.49	1.719	1.041	1.729	36.2	0.735	NA	27.1	41.3	0.595	1.77x10 ⁻⁴
CRS1322	Sodium Montmorillonite	256	49.22	1.682	1.088	1.732	NA	NA	NA	2	27.8	0.949	2.11x10 ⁻⁴
CRS1307	RGOM - Ursa	0	35.52	1.025	1.335	1.85	29.5	0.427	6.19x10 ⁻⁴	40.7	38.6	0.244	9.43x10 ⁻⁴
CRS1308	RGOM - Ursa	0	38.42	1.102	1.302	1.826	31.7	0.436	7.48x10 ⁻⁴	41.5	39.9	0.264	9.6x10 ⁻⁴
CRS1309	RGOM - Ursa	0	37.88	1.102	1.285	1.817	32.5	0.419	6.81x10 ⁻⁴	41.9	40.9	0.242	9.44x10 ⁻⁴

Table 5-2 List of Constant Rate of Strain (CRS) tests performed on other soils in testing program

Test No.	Test Type	Device	Salinity (g/l)	Conditions			At Peak Shear Stress					At Maximum Obliquity			Comments	
				σ'_{ac} (kpa)	OCR	K_o	ϵ_a (%)	q/σ'_{ac}	p'/σ'_{ac}	A_f	Φ'_p	ϵ_a (%)	q/σ'_{ac}	p'/σ'_{ac}		Φ'_{mo}
TX1081	CK ₀ UC	MIT02	256	920	1	0.566	0.4	0.28	0.72	0.95	23	11	0.246	0.464	31.96	Natural BBC IV
TX1069	CK ₀ UC	MIT02	256	622	1	0.534	0.35	0.28	0.718	0.99	23.2	10.9	0.252	0.47	32.4	Natural BBC IV
TX1078	CK ₀ UC	MIT01	4	523	1	0.52	0.19	0.29	0.75	0.61	23		NA	NA		Natural BBC IV
TX1074	CK ₀ UC	MIT01	4	655	1	0.534	0.26	0.3	0.74	0.68	23.6	11.3	0.233	0.446	31.5	Natural BBC IV
TX1068	CK ₀ UC	MIT01	4	452	1		0.23	0.3	0.735	0.63	24.2	8.8	0.252	0.473	32.2	Natural BBC IV
TX1086	CK ₀ UC	MIT02	256	584	1	NA	0.18	0.31	0.74	0.665	24.9	9.3	0.265	0.477	33.7	Leached BBC
TX1094	CK ₀ UC	MIT01	256	479	1	0.475	0.14	0.319	0.741	0.396	25.5	9.1	0.26	0.494	31.7	Leached BBC
TX1082	CK ₀ UC	MIT01	1	485	1	0.519	0.17	0.3	0.762	0.475	23.2	11.4	0.225	0.462	29.2	Leached BBC
TX1084	CK ₀ UC	MIT01	1	565	1	0.524	0.196	0.315	0.778	0.41	23.9	10.1	0.232	0.474	29.3	Leached BBC
TX1108	CK ₀ UC	MIT01	11.3	1950	1	0.543	0.63	0.293	0.702	0.998	20.6	9.37	0.243	0.461	31.8	Killian Court BBC
TX1091	CK ₀ UC	MIT01	11.3	1000	1	NA	0.63	0.294	0.748	0.818	23.1	9.35	0.238	0.472	30.3	Killian Court BBC
TX1110	CK ₀ UC	MIT01	11.3	1575	1	0.537	0.7	0.308	0.722	1	24.1	NA	NA	NA	NA	Killian Court BBC

Table 5-3 List of triaxial tests (CK₀UC) performed on Boston Blue Clay soils in the testing program

Soil Type	Stress Range (kPa)	c_c Value
Killian Court in-situ BBC	1,000 - 10,000	0.285
Natural RBBC Series IV	1,000 - 10,000	0.307
Leached RBBC	1,000 - 10,000	0.294
Sodium Hex BBC	1,000 - 10,000	0.277
Sodium Montmorillonite	1,000 - 10,000	0.38
RGOM - Ursa	1,000 - 10,000	0.316
London Clay	100 - 1,000	0.52
London Clay	1,000 - 10,000	0.365

Table 5-4 List of c_c values for all soils tested in the CRS device

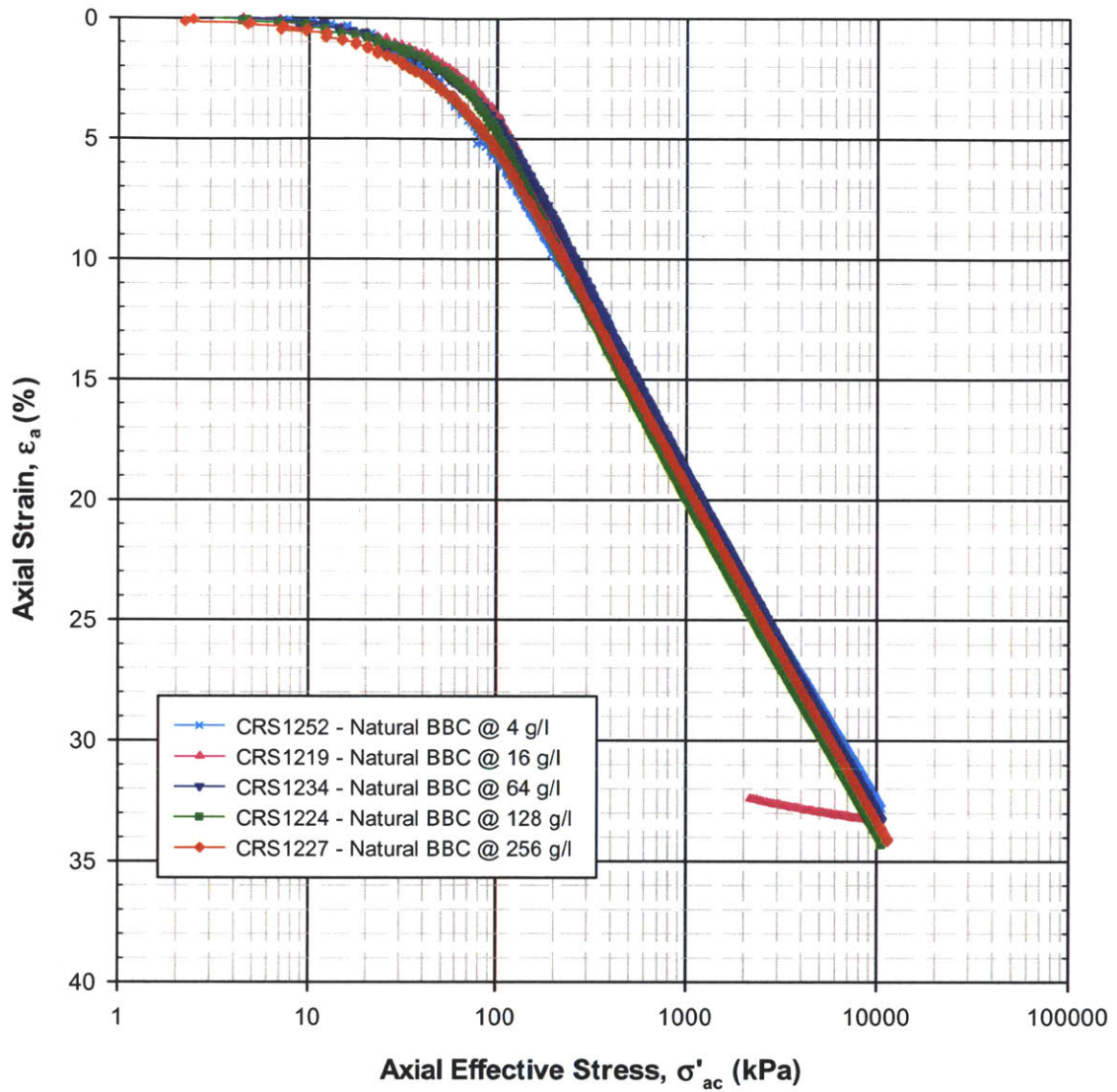


Figure 5.1 Compression behavior in ϵ_a - $\log\sigma'_{ac}$ space for RBBC Series IV at various pore fluid salt concentrations

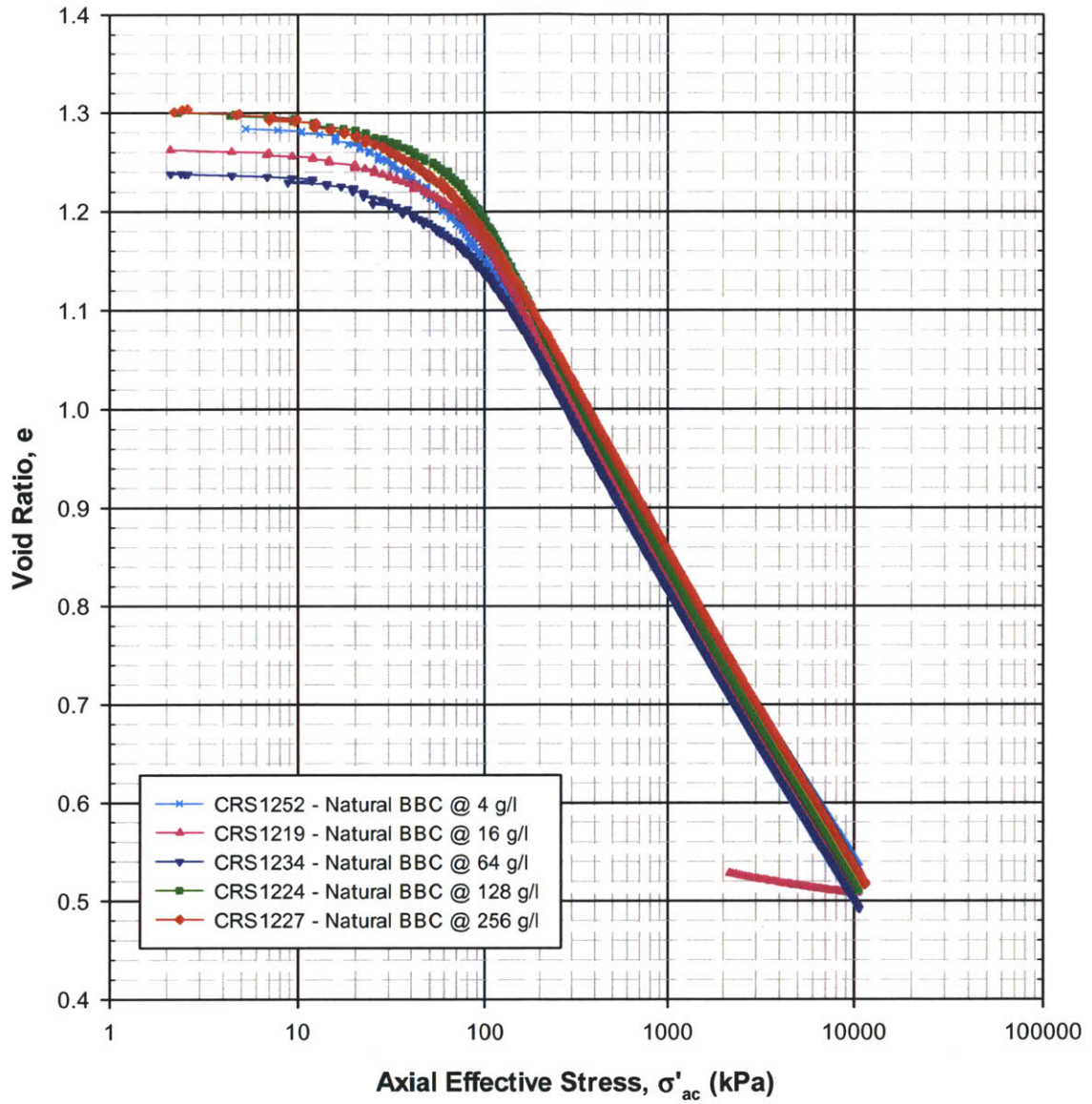


Figure 5.2 Compression behavior in e - $\log \sigma'_{ac}$ space for RBBC Series IV at various pore fluid salt concentrations

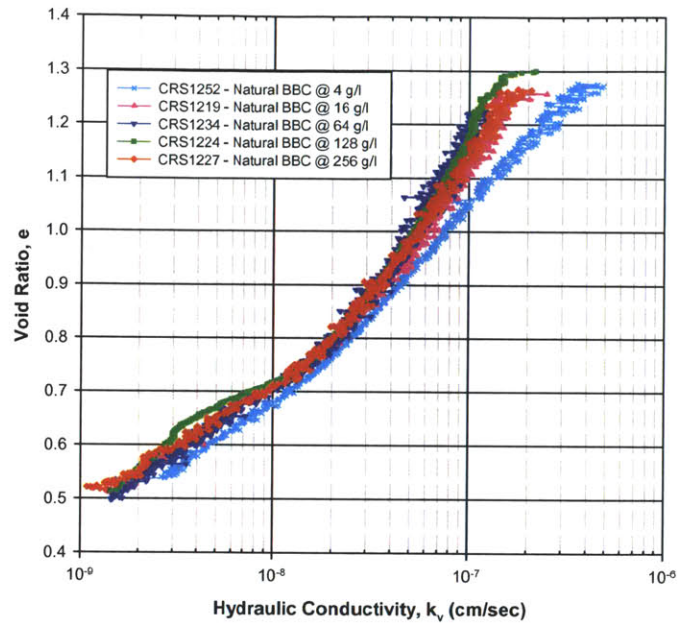


Figure 5.3 Hydraulic conductivity in void ratio space for RBBC Series IV at various pore fluid salt concentrations

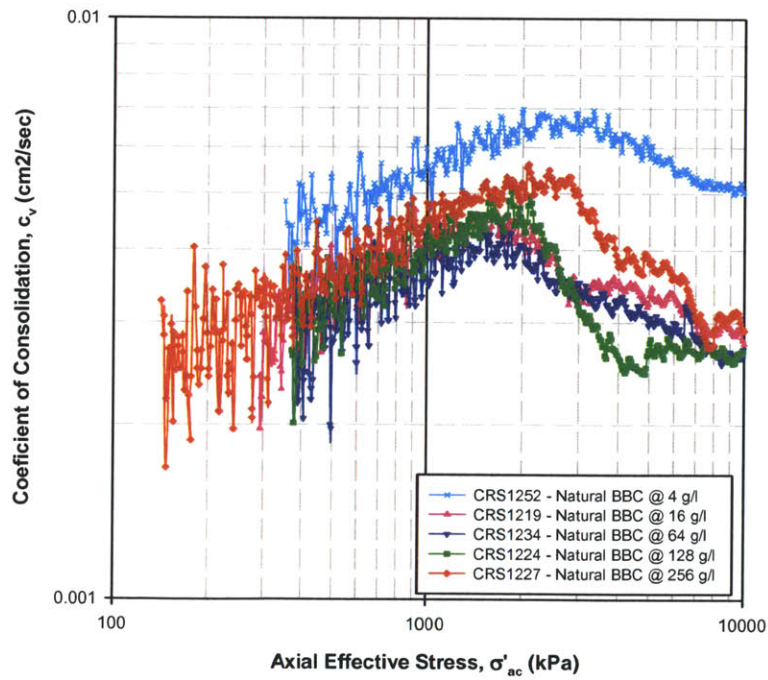


Figure 5.4 Coefficient of consolidation versus axial effective stress for RBBC Series IV at various pore fluid salinities

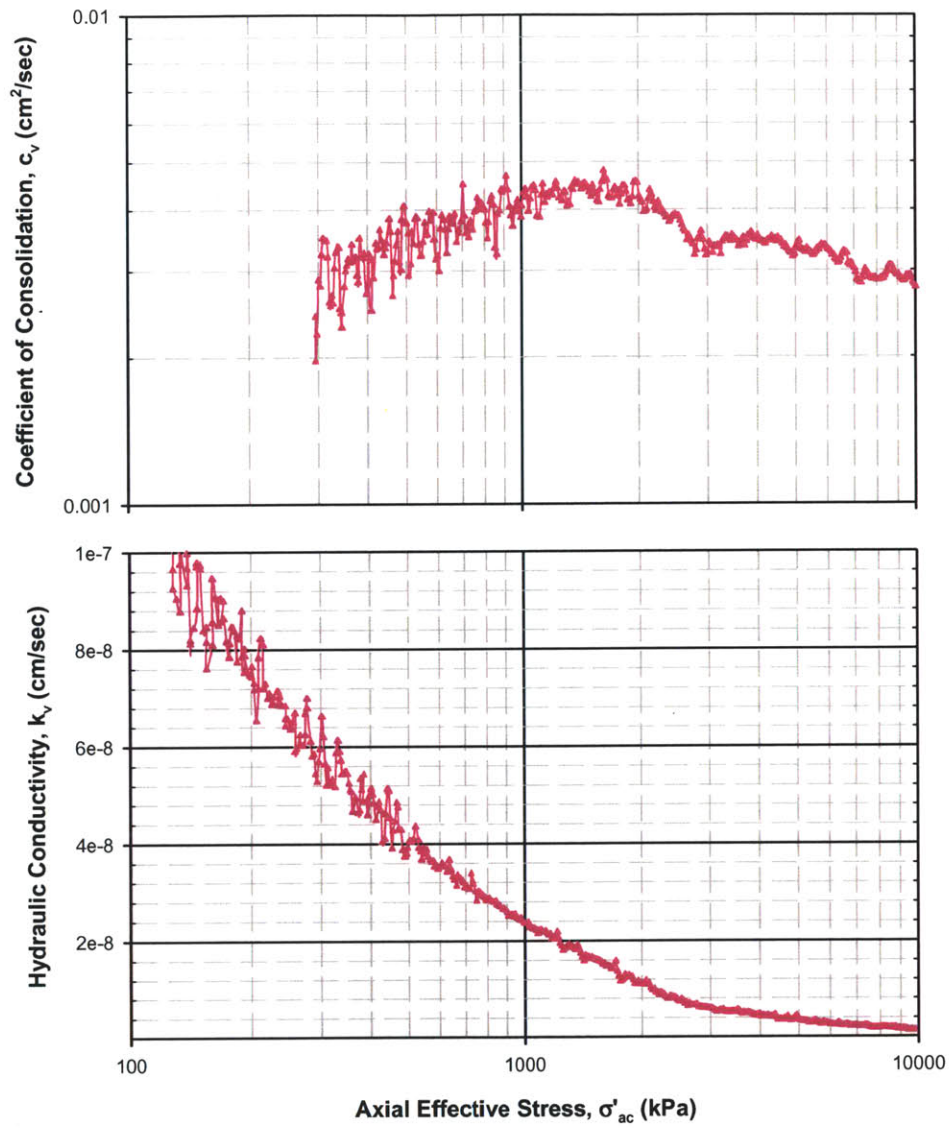


Figure 5.5 Plot of hydraulic conductivity and coefficient of consolidation data versus stress level for CRS1219 (RBBC Series IV @ 16 g/l). Note that changes in behavior for both datasets occur at same stress levels

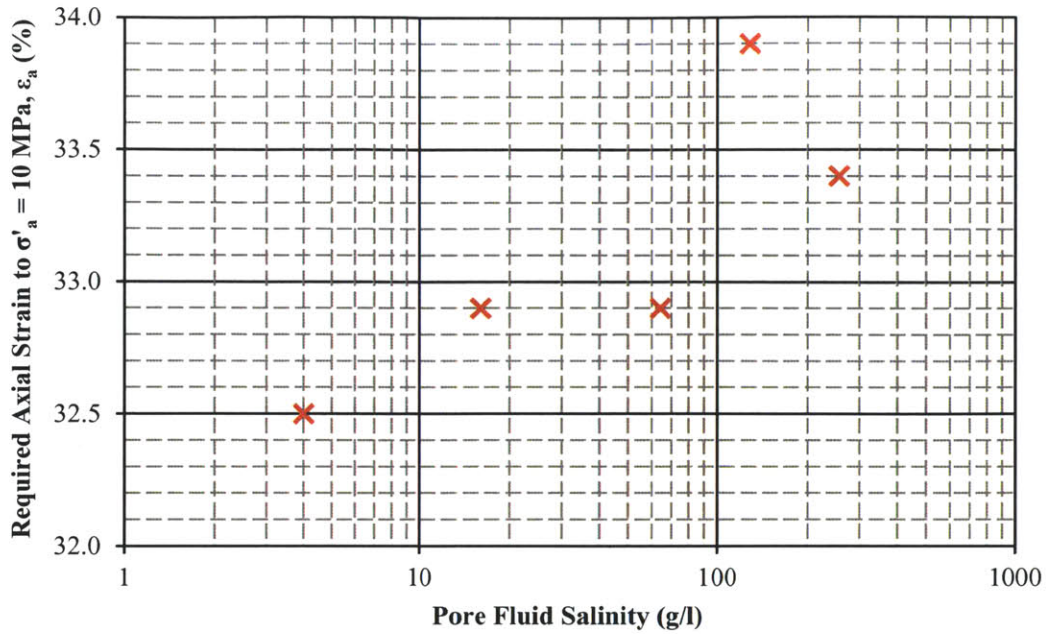


Figure 5.6 Relationship between pore fluid salinity and required axial strain to achieve an axial effective stress (σ'_a) of 10 MPa for RBBC Series IV

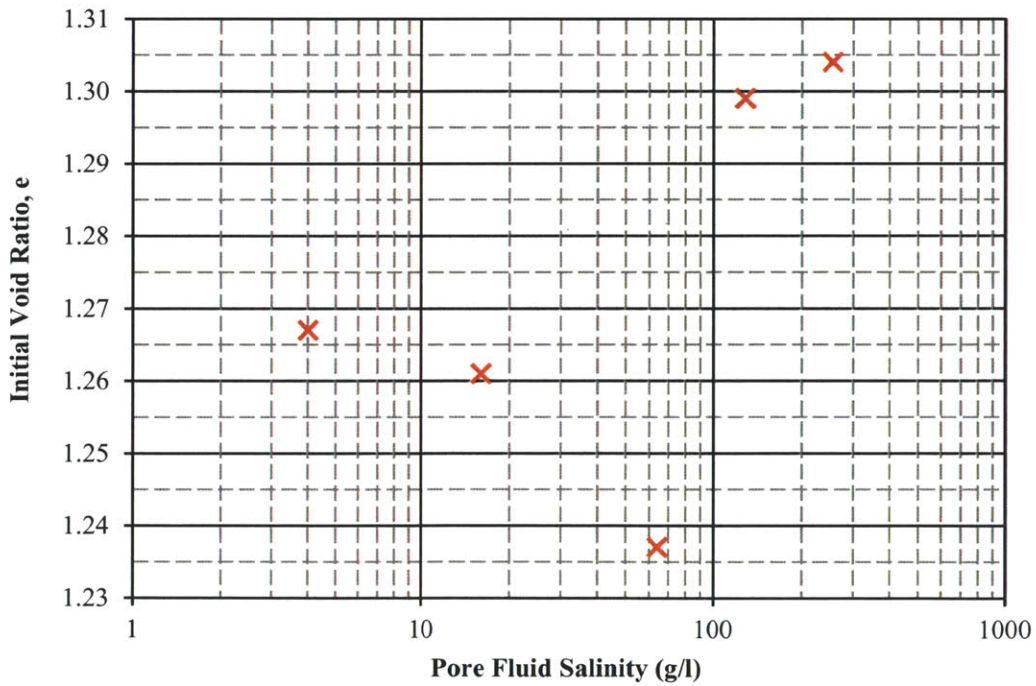


Figure 5.7 Relationship between pore fluid salinity and initial void ratio for RBBC Series IV

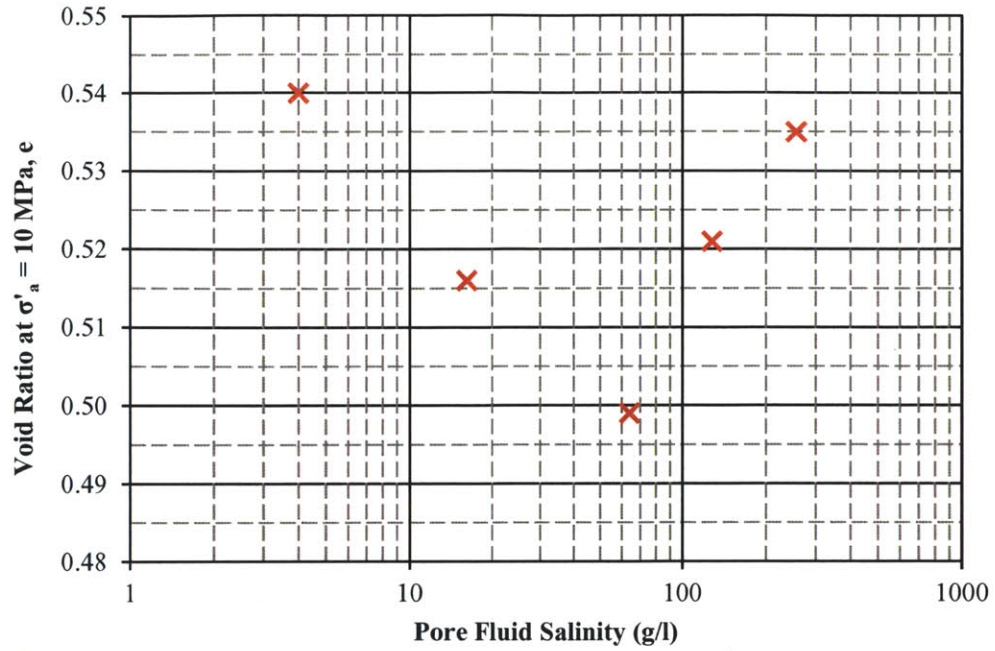


Figure 5.8 Relationship between pore fluid salinity and void ratio at an axial effective stress (σ'_a) of 10 MPa for RBBC Series IV

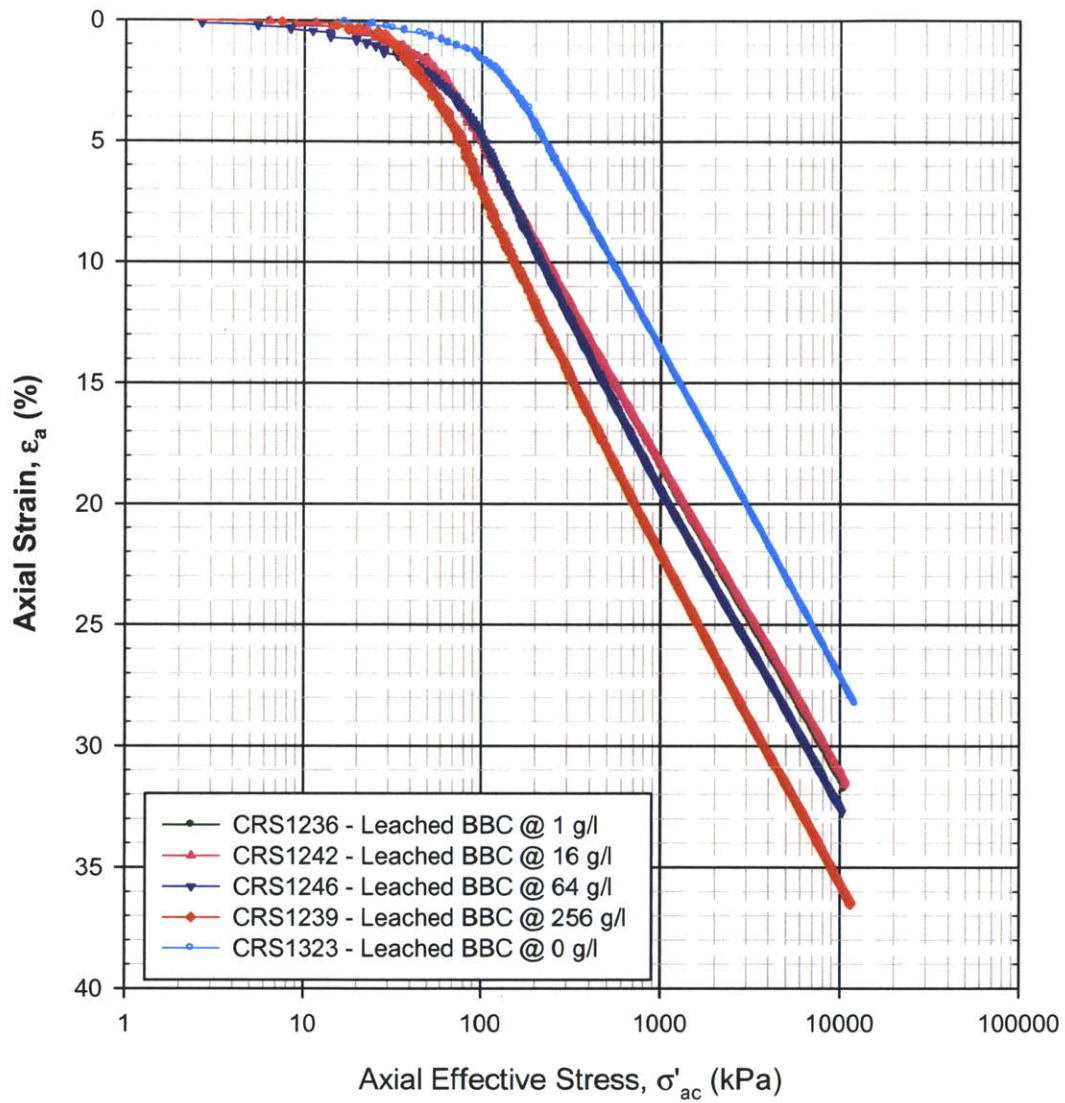


Figure 5.9 Compression behavior in ϵ_a - $\log\sigma'_{ac}$ space for leached BBC at various pore fluid salt concentrations

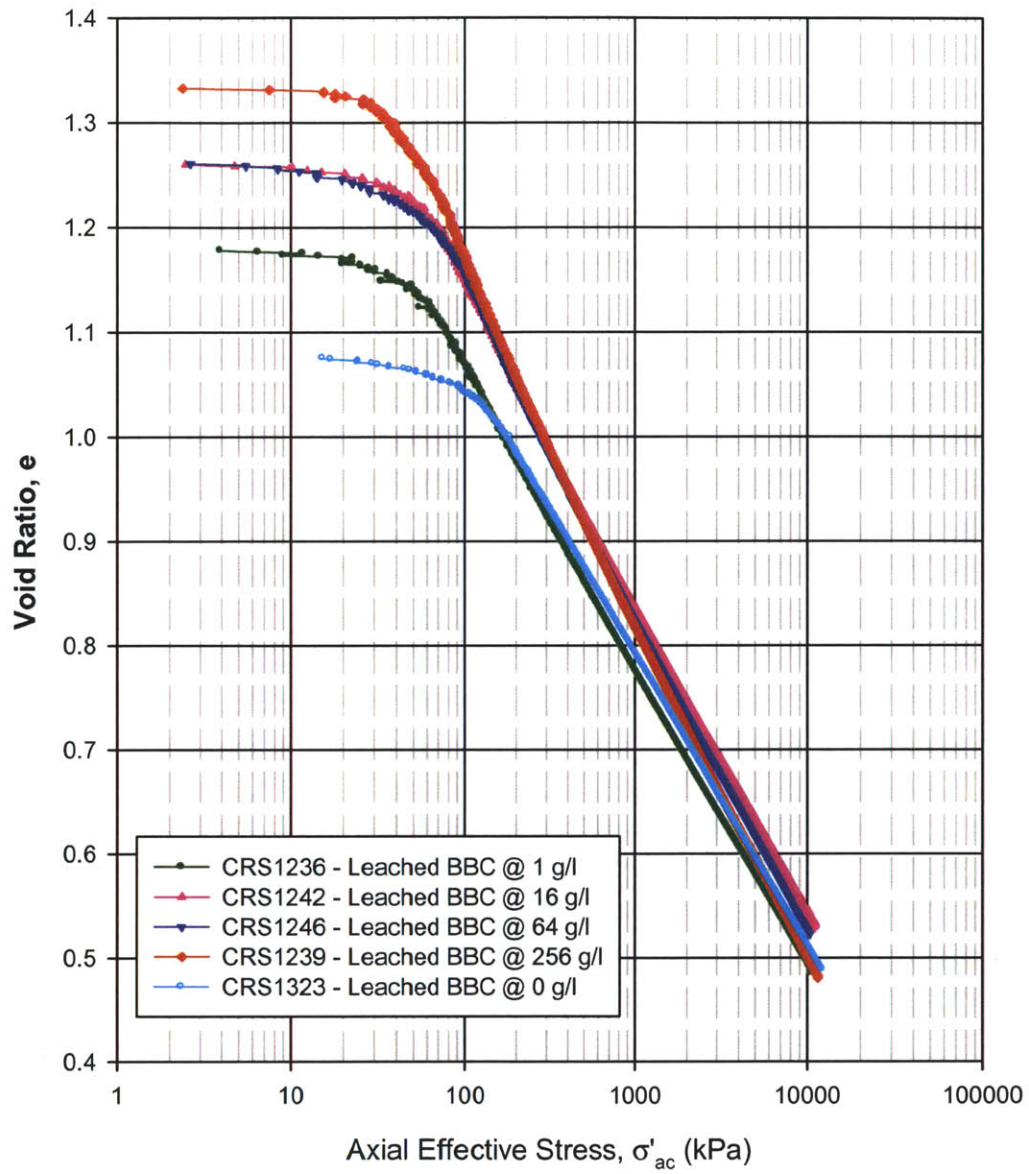


Figure 5.10 Compression behavior in e - $\log \sigma'_{ac}$ space for leached BBC at various pore fluid salt concentrations

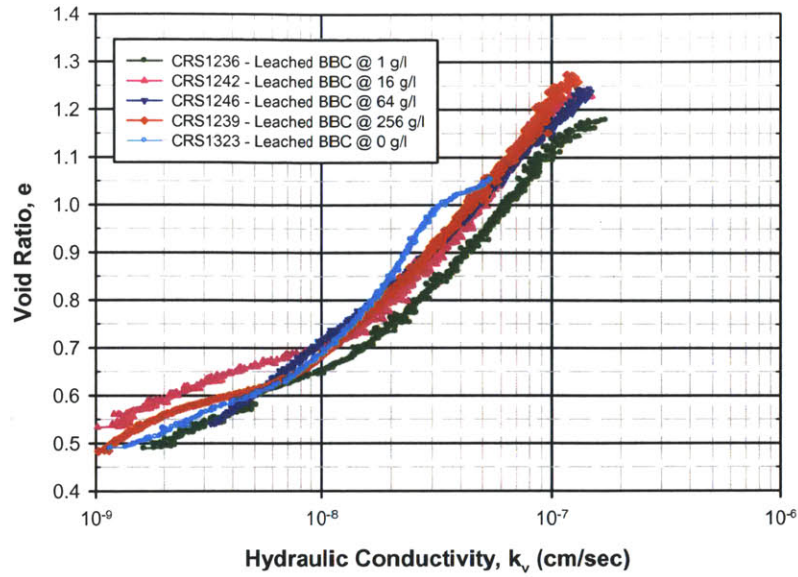


Figure 5.11 Hydraulic conductivity in void ratio space for leached BBC at various pore fluid salt concentrations

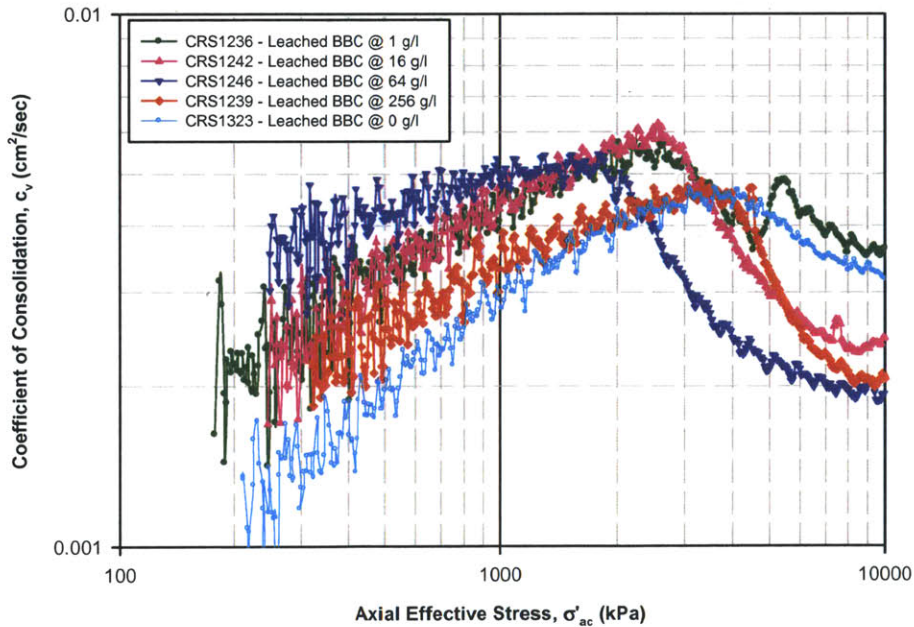


Figure 5.12 Coefficient of consolidation versus axial effective stress for leached BBC at various pore fluid salinities

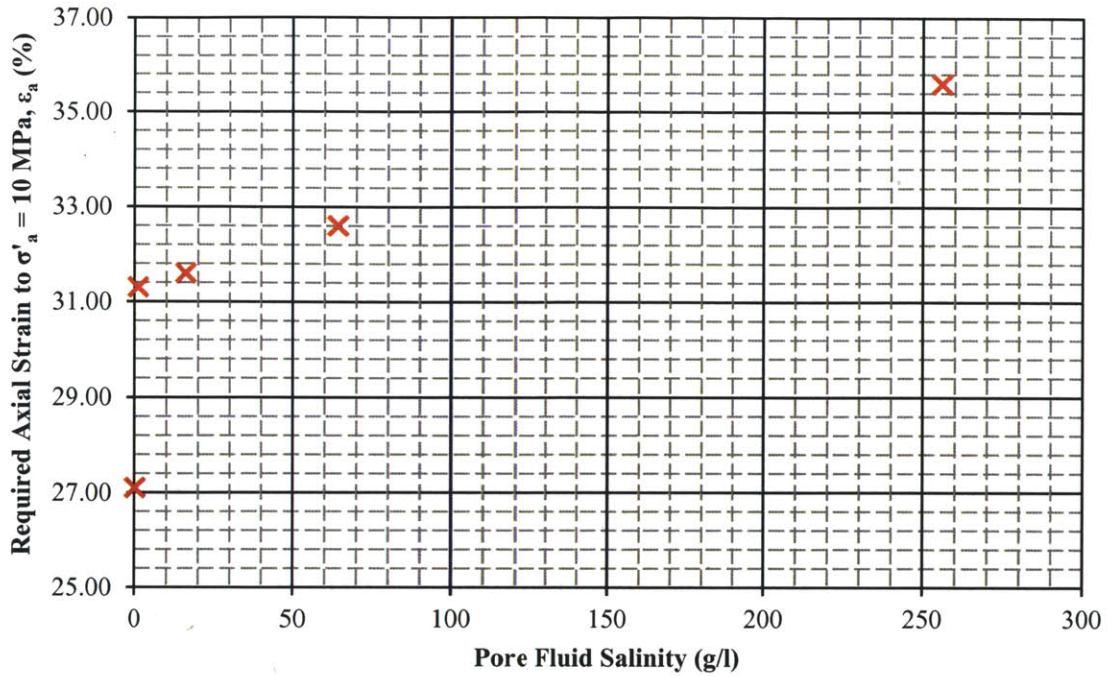


Figure 5.13 Relationship between pore fluid salinity and required axial strain to achieve an axial effective stress (σ'_a) of 10 MPa for leached RBBC

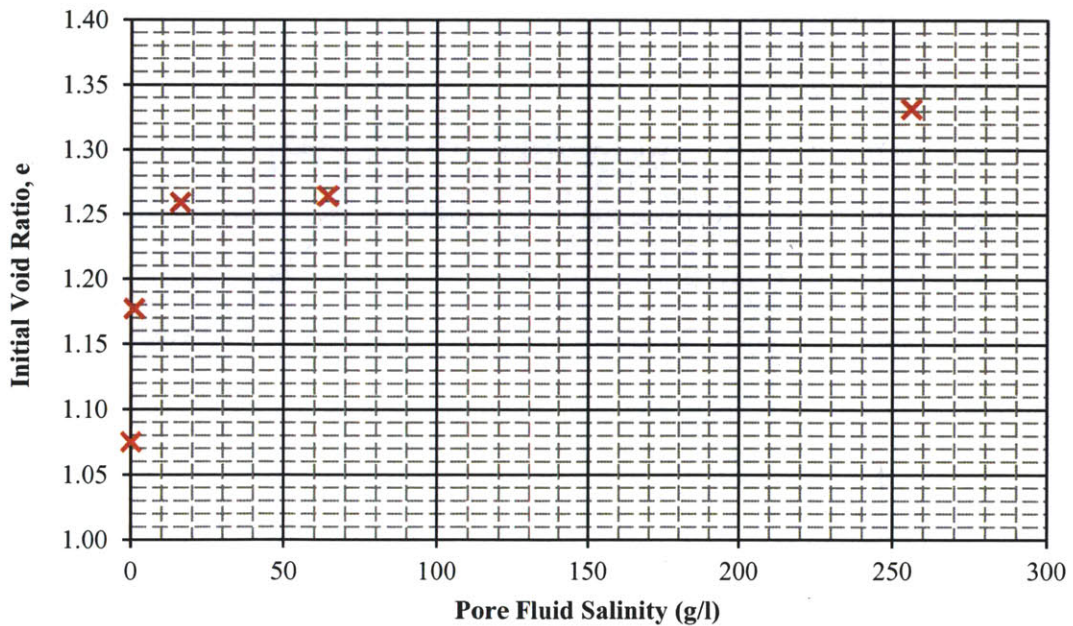


Figure 5.14 Relationship between pore fluid salinity and initial void ratio for leached RBBC

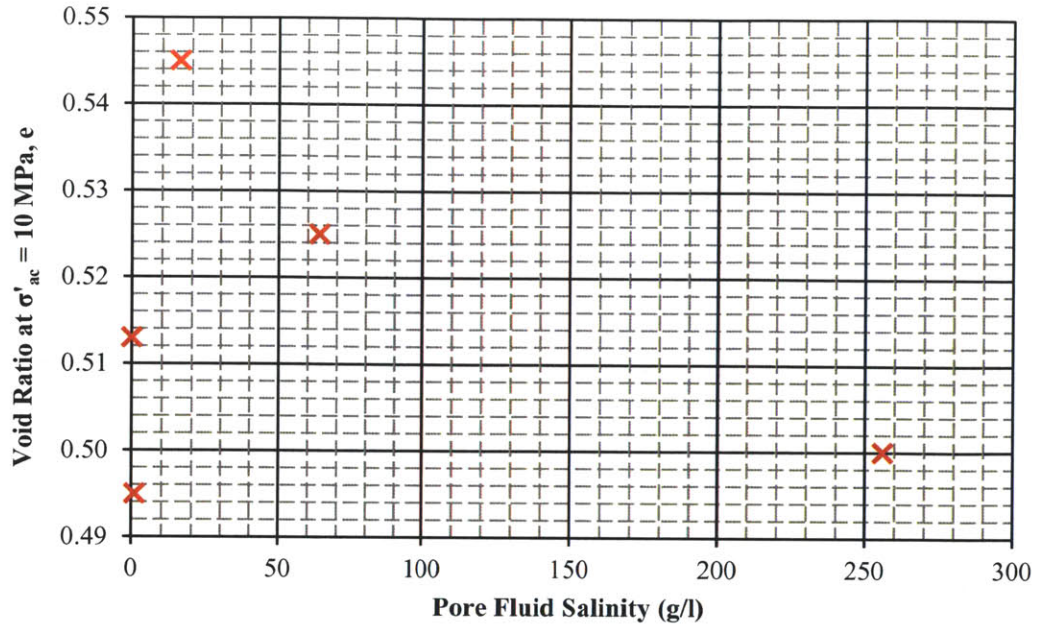


Figure 5.15 Relationship between pore fluid salinity and void ratio at an axial effective stress (σ'_a) of 10 MPa for leached RBBC

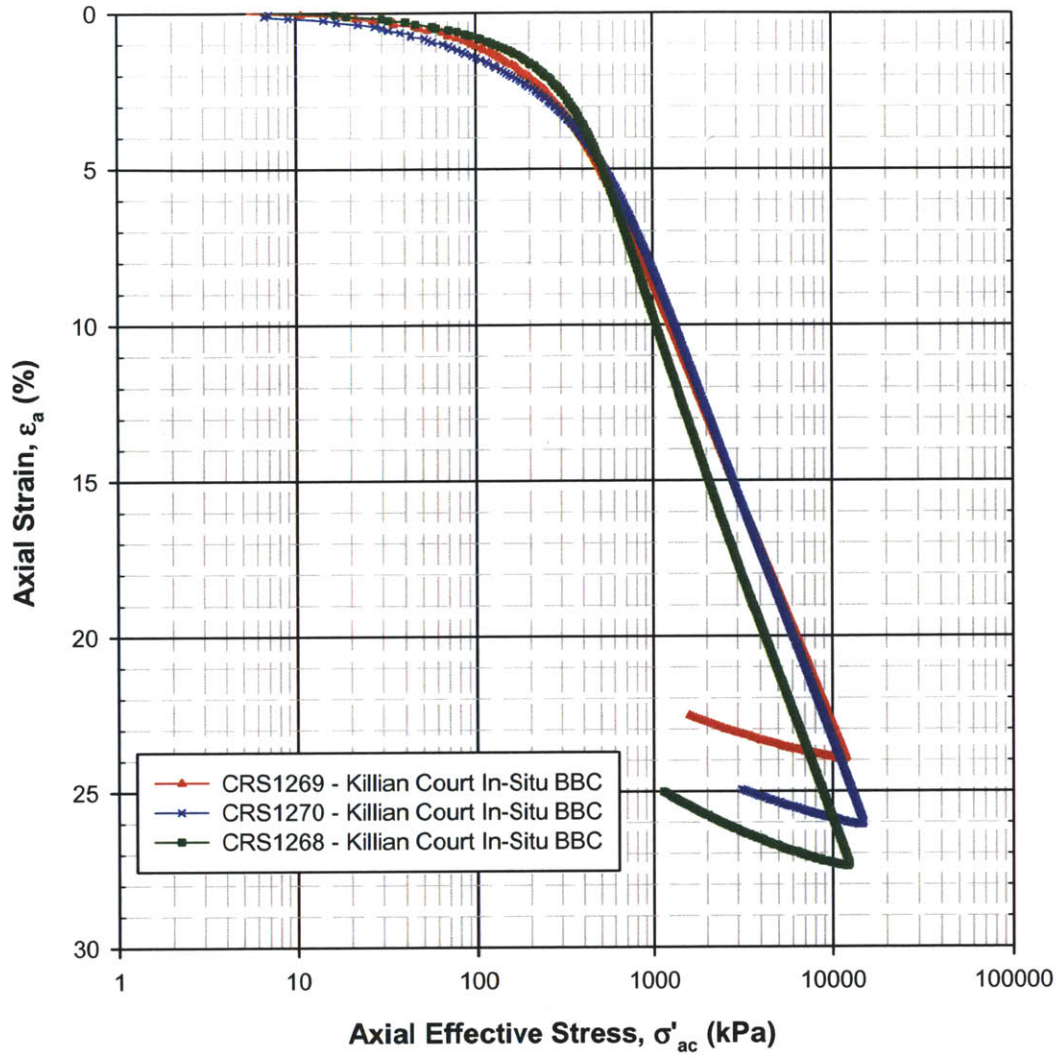


Figure 5.16 Compression behavior in ϵ_a - $\log\sigma'_{ac}$ space for Killian Court in-situ BBC

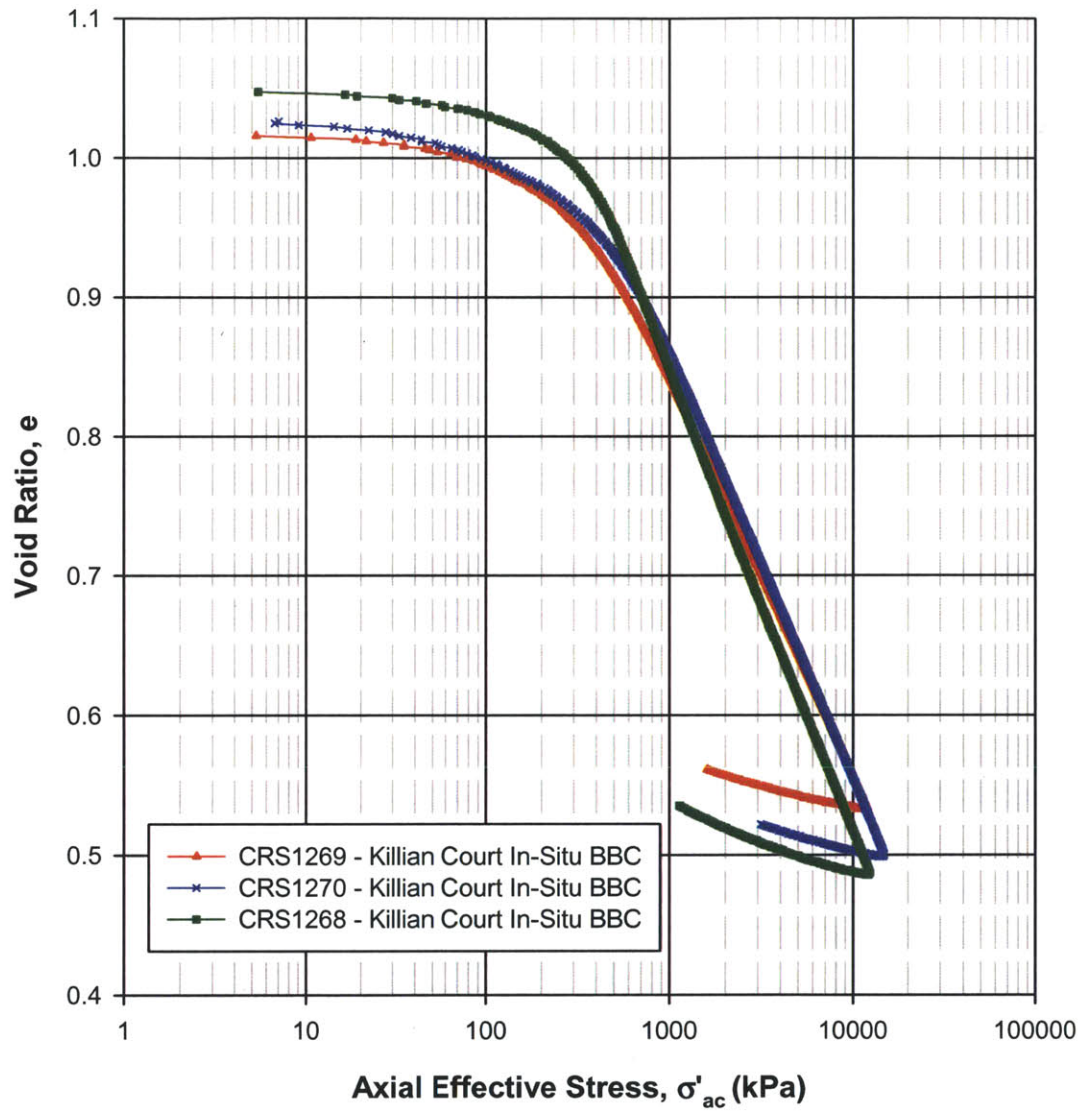


Figure 5.17 Compression behavior in e - $\log \sigma'_{ac}$ space for Killian Court in-situ BBC

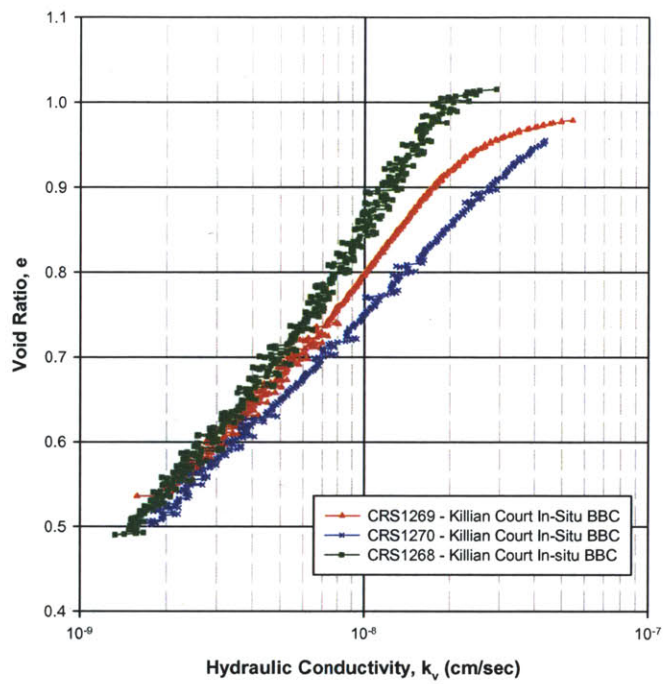


Figure 5.18 Hydraulic conductivity in void ratio space for Killian Court in-situ BBC

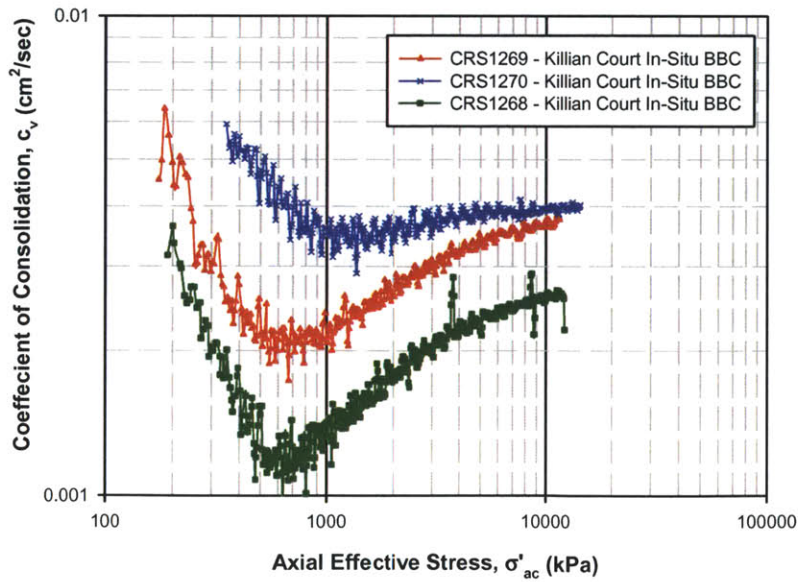


Figure 5.19 Coefficient of consolidation versus axial effective stress for Killian Court in-situ BBC

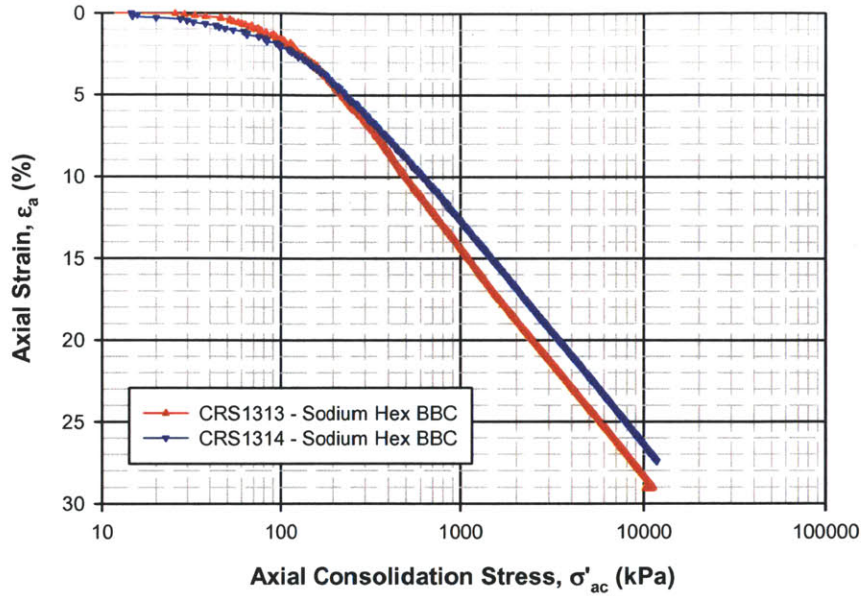


Figure 5.20 Compression behavior in ϵ_a - $\log\sigma'_{ac}$ space for BBC dispersed with sodium hexametaphosphate

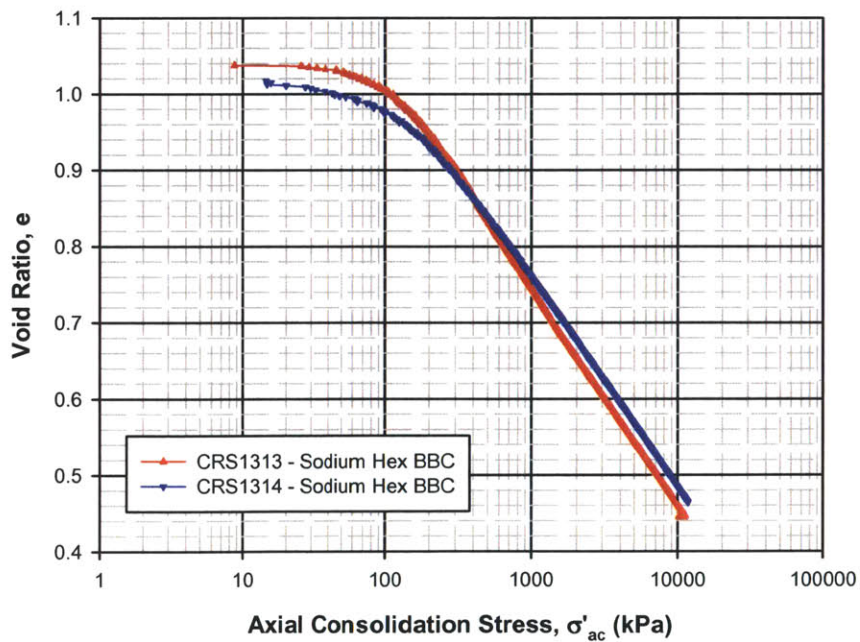


Figure 5.21 Compression behavior in e - $\log\sigma'_{ac}$ space for BBC dispersed with sodium hexametaphosphate

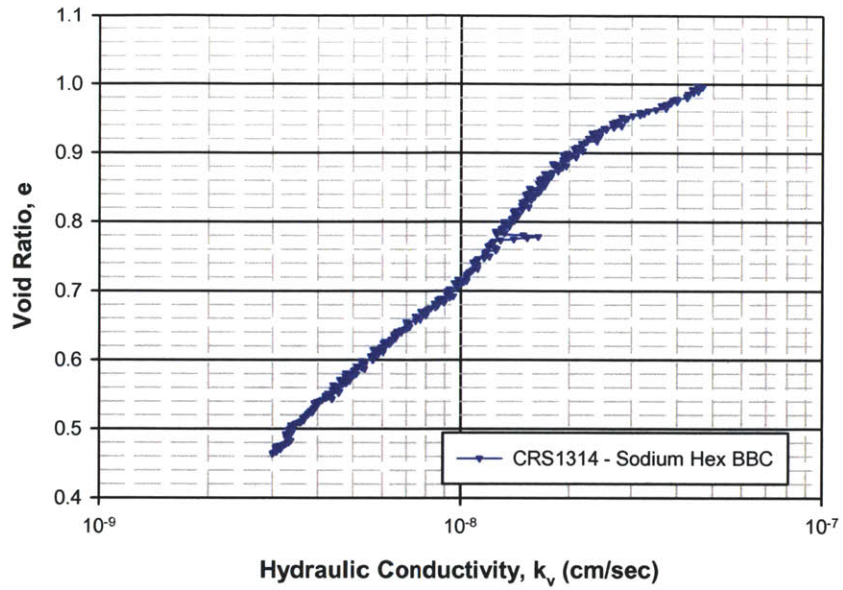


Figure 5.22 Hydraulic conductivity in void ratio space for BBC dispersed with sodium hexametaphosphate

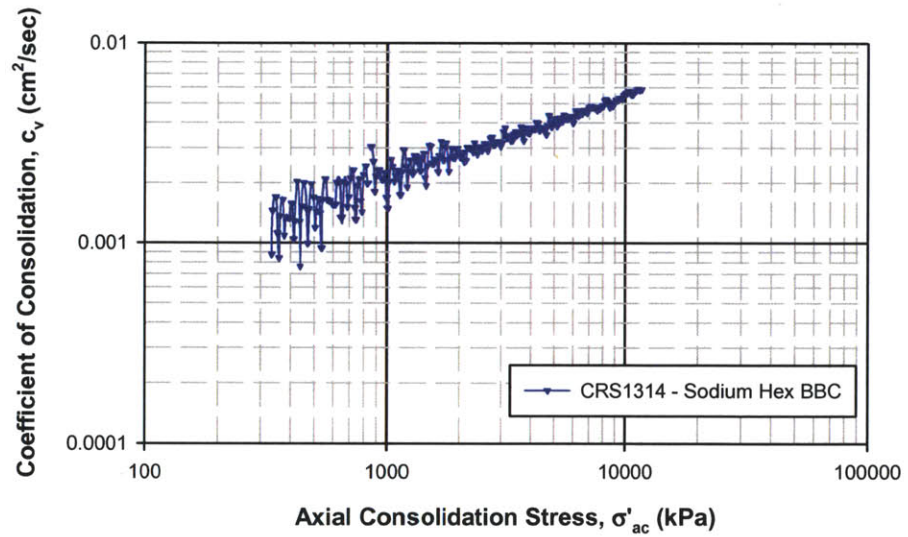


Figure 5.23 Coefficient of consolidation versus axial effective stress for BBC dispersed with sodium hexametaphosphate

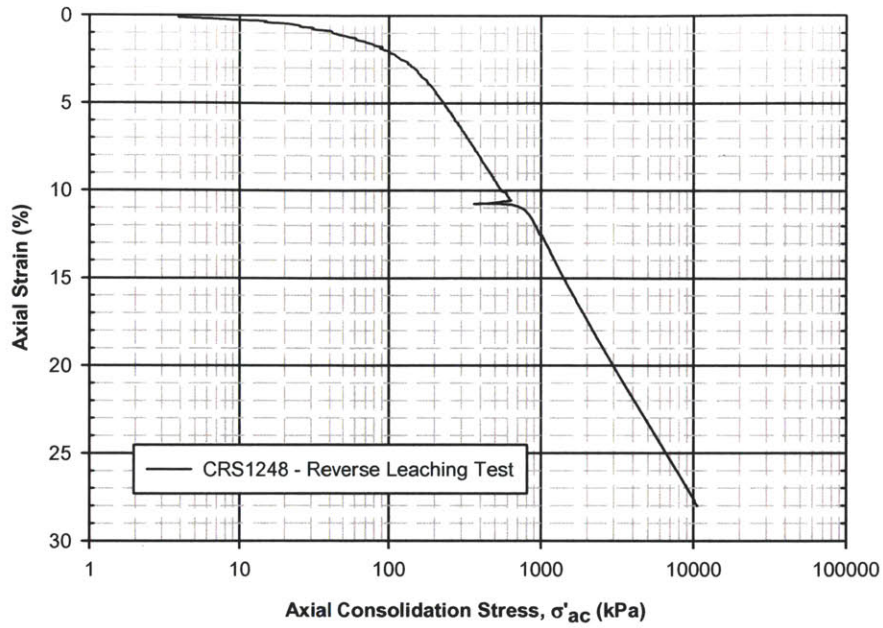


Figure 5.24 Compression behavior in ϵ_a - $\log\sigma'_{ac}$ space reverse leaching test performed on previously leached BBC

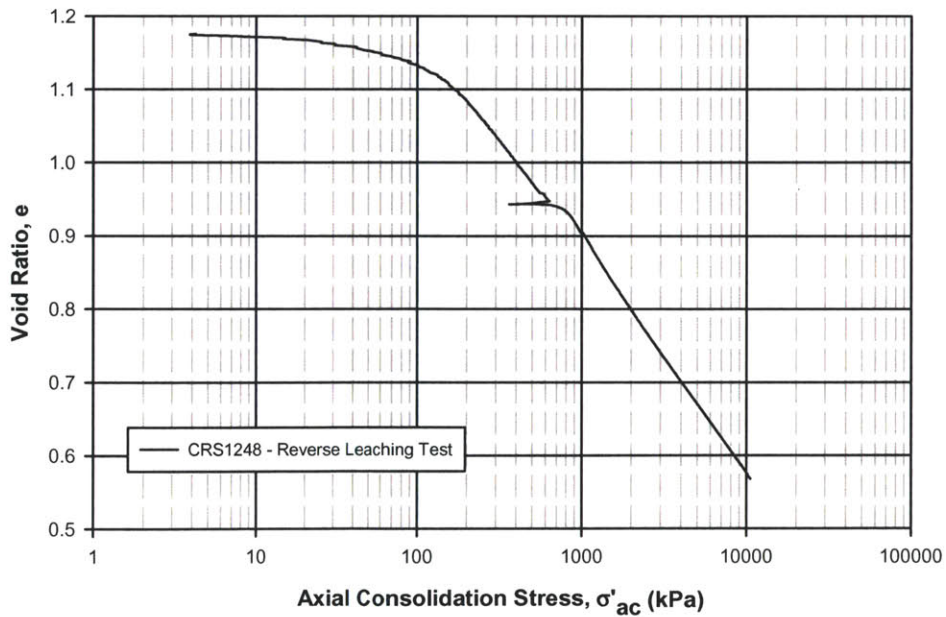


Figure 5.25 Compression behavior in e - $\log\sigma'_{ac}$ space for reverse leaching test performed on previously leached BBC

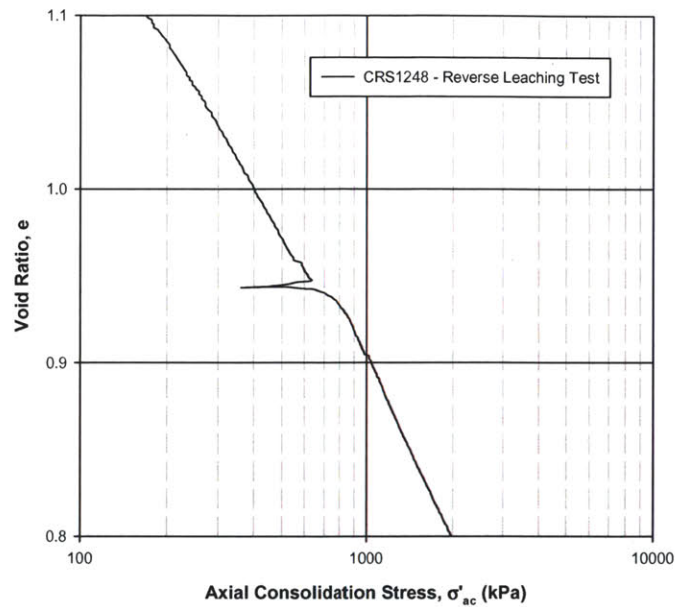


Figure 5.26 Compression behavior in e - $\log \sigma'_{ac}$ space for reverse leaching test performed on previously leached BBC, close up of point where preconsolidation pressure increases

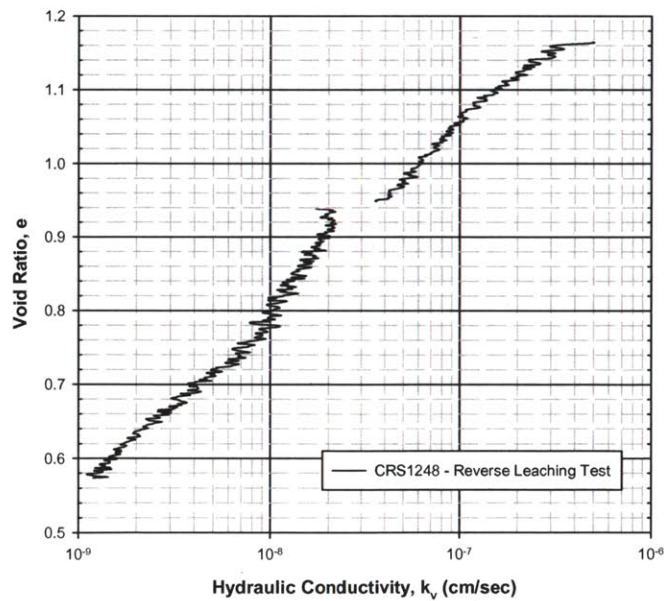


Figure 5.27 Hydraulic conductivity in void ratio space for reverse leaching test performed on previously leached BBC

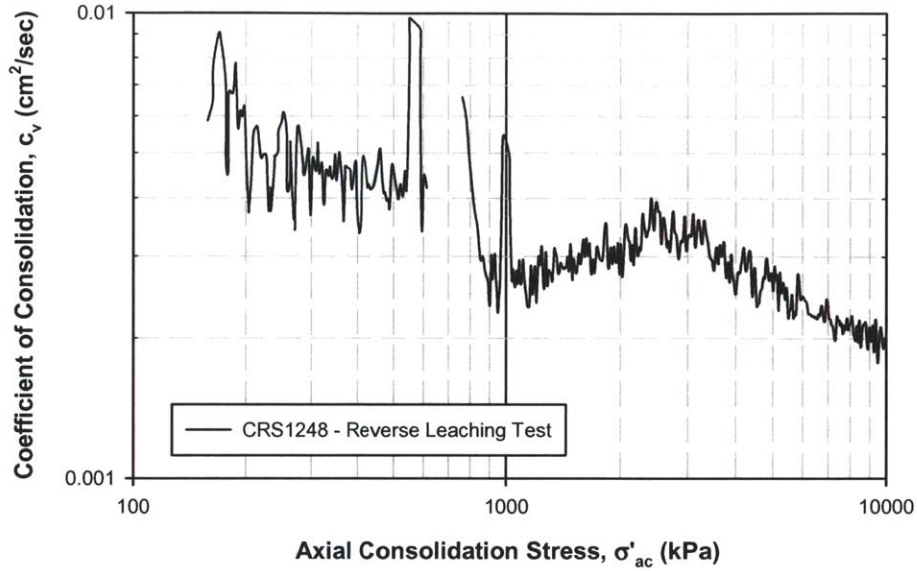


Figure 5.28 Coefficient of consolidation versus axial effective stress for reverse leaching test performed on previously leached BBC

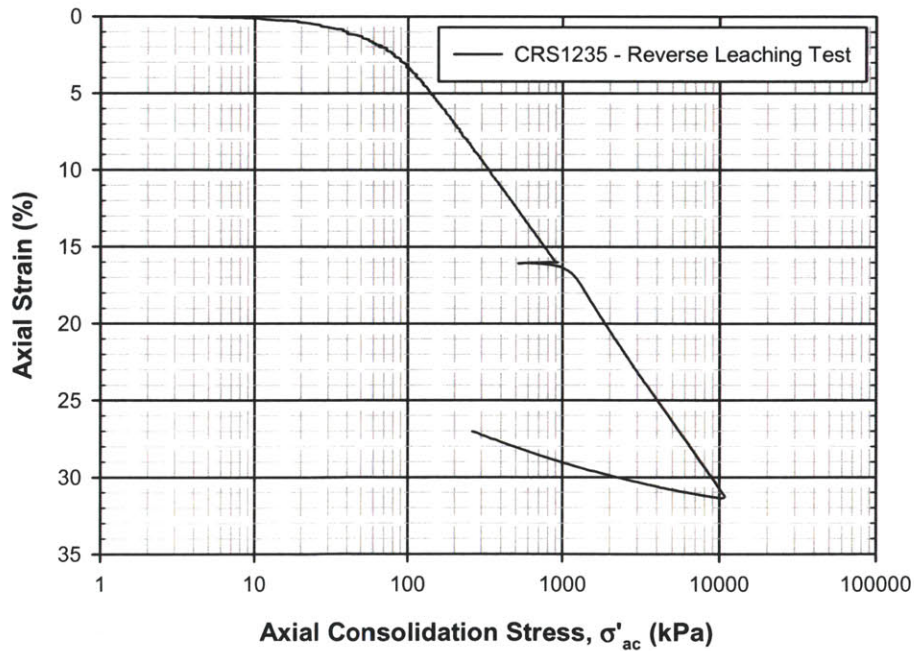


Figure 5.29 Compression behavior in ϵ_a - $\log \sigma'_{ac}$ space reverse leaching test performed on previously leached BBC

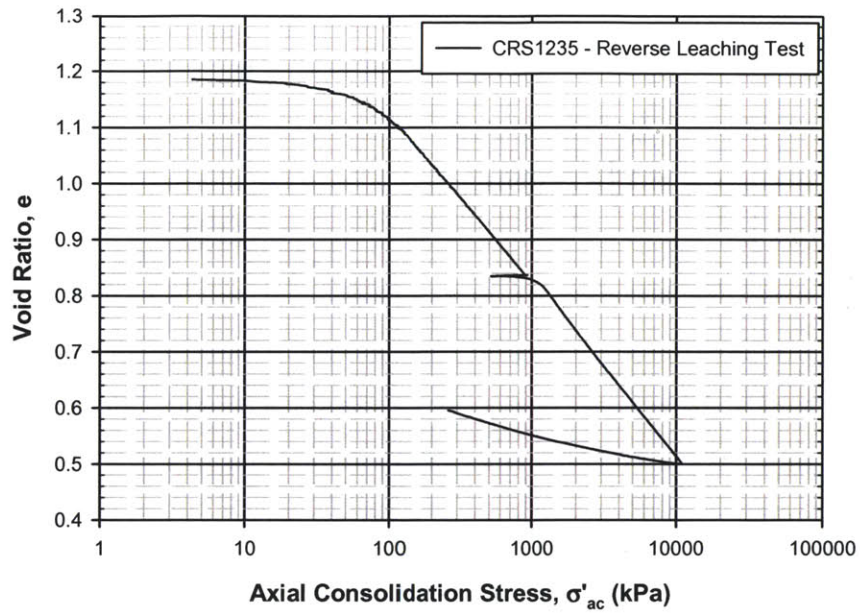


Figure 5.30 Compression behavior in $e\text{-log}\sigma'_{ac}$ space for reverse leaching test performed on previously leached BBC

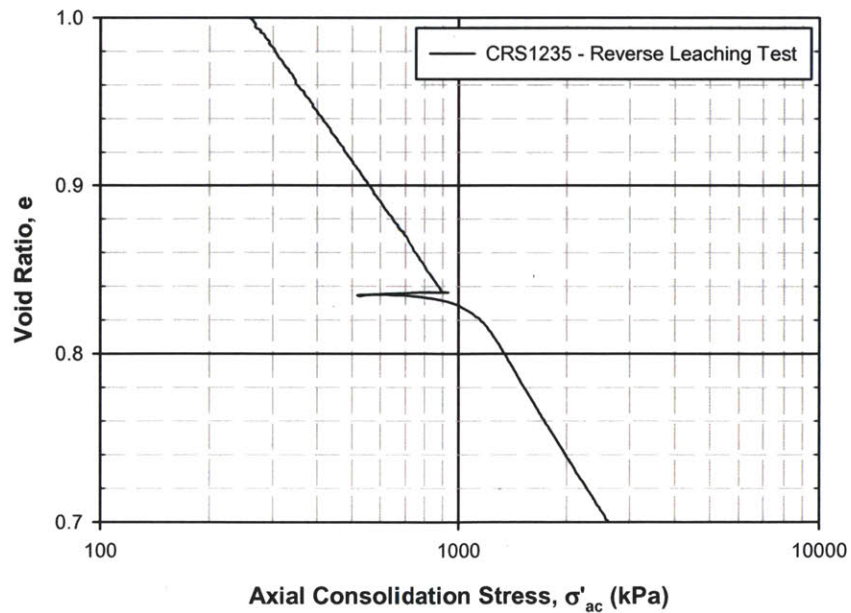


Figure 5.31 Compression behavior in $e\text{-log}\sigma'_{ac}$ space for reverse leaching test performed on previously leached BBC, close up of point where preconsolidation pressure increases

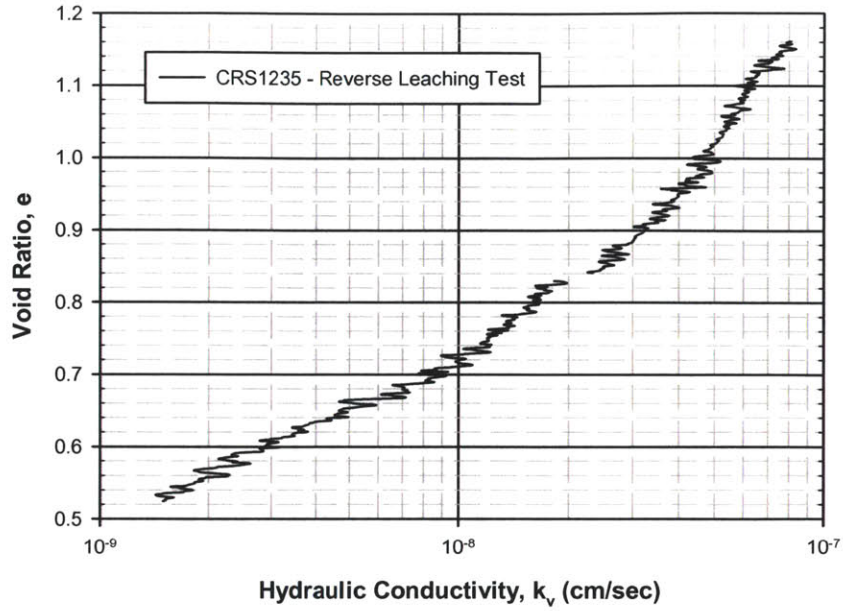


Figure 5.32 Hydraulic conductivity in void ratio space for reverse leaching test performed on previously leached BBC

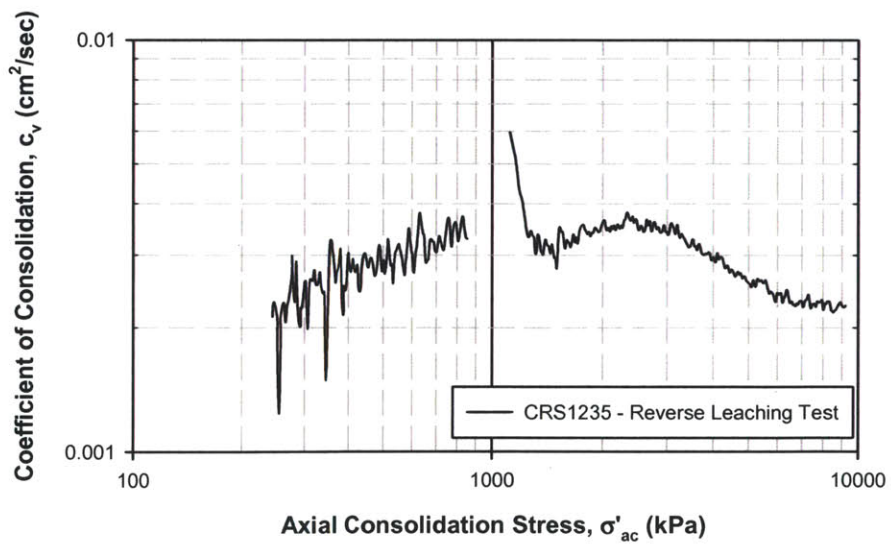


Figure 5.33 Coefficient of consolidation versus axial effective stress for reverse leaching test performed on previously leached BBC

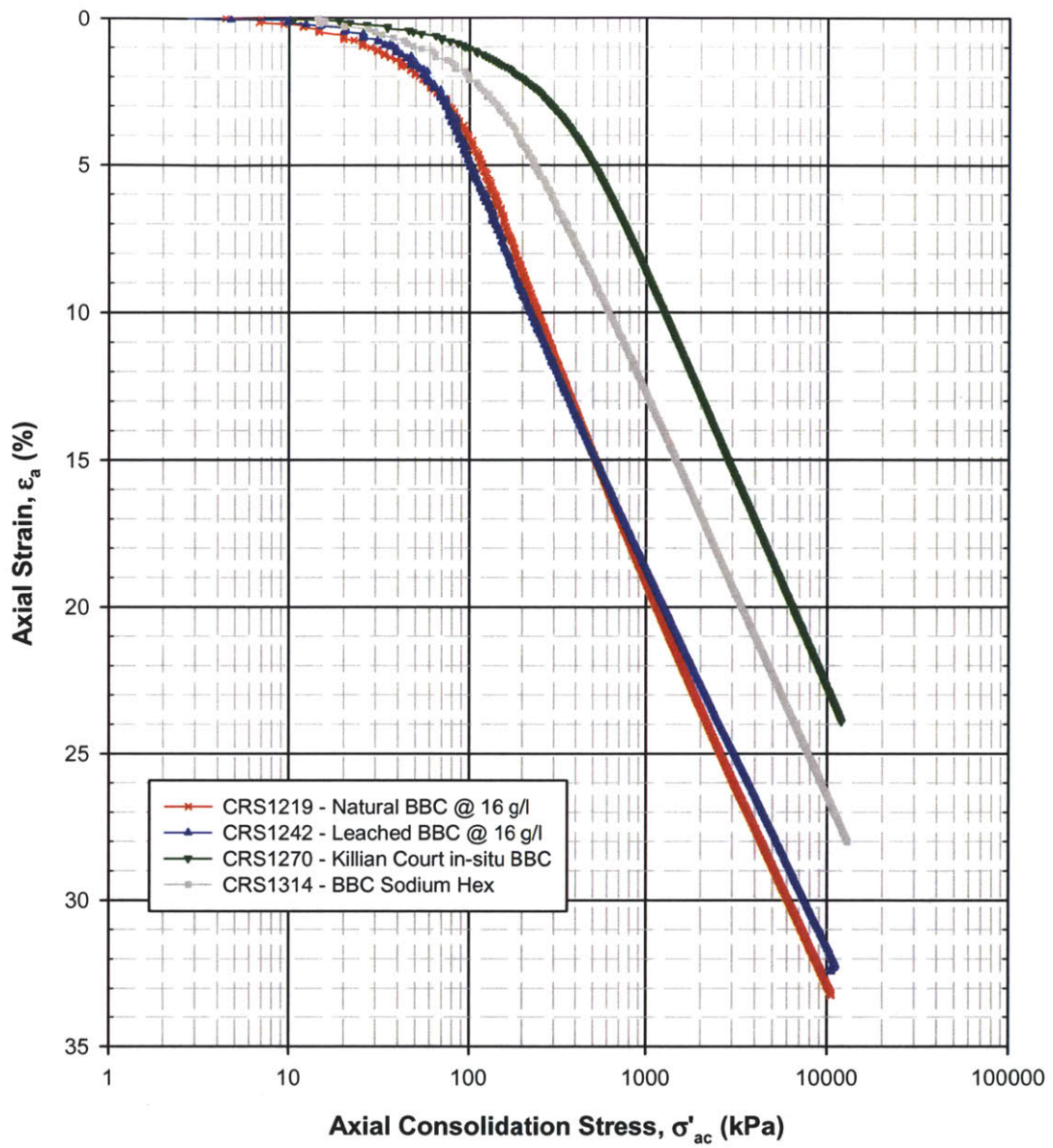


Figure 5.34 Compression behavior synthesis plot in ϵ_a - $\log\sigma'_{ac}$ space for all Boston Blue Clay derivatives in the testing program

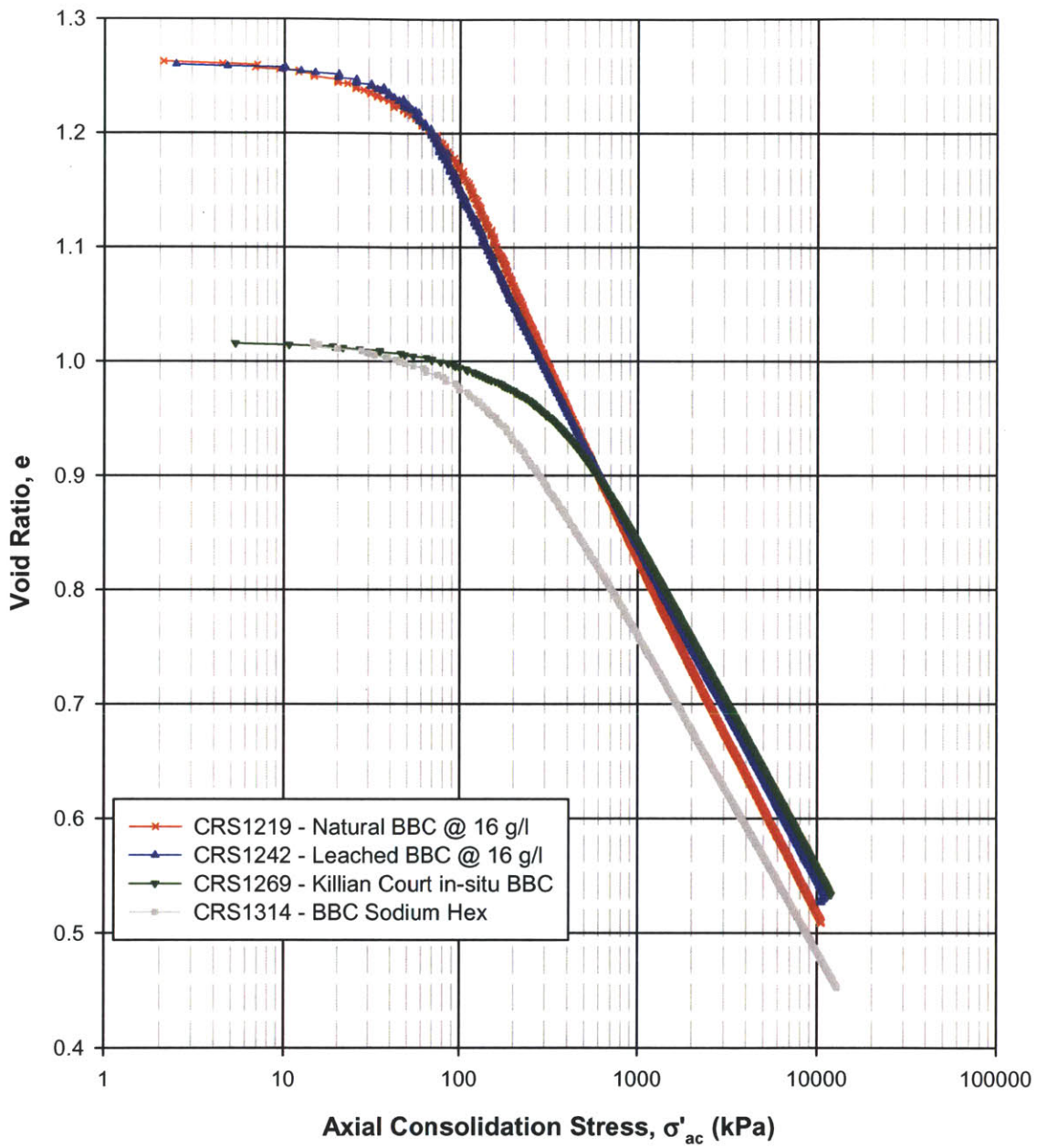


Figure 5.35 Compression behavior synthesis plot in e - $\log\sigma'_{ac}$ space for all Boston Blue Clay derivatives in the testing program

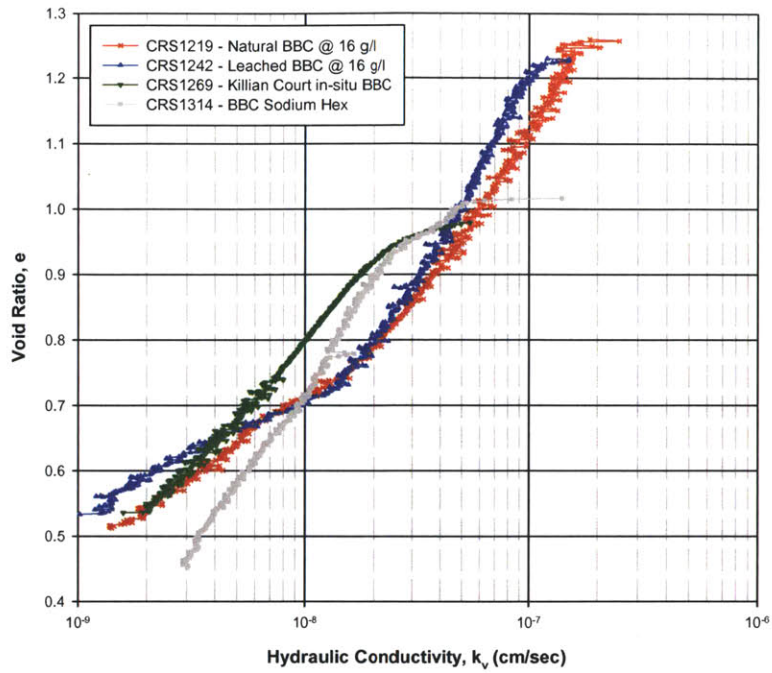


Figure 5.36 Hydraulic conductivity synthesis plot in void ratio space for all soils in testing program

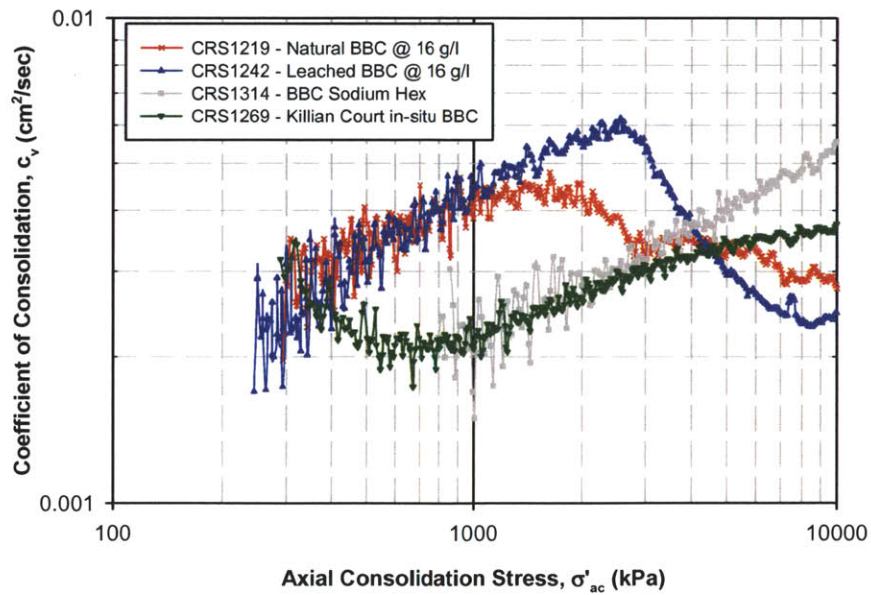


Figure 5.37 Coefficient of consolidation versus axial effective stress synthesis plot for Boston Blue Clay derivatives in the testing program

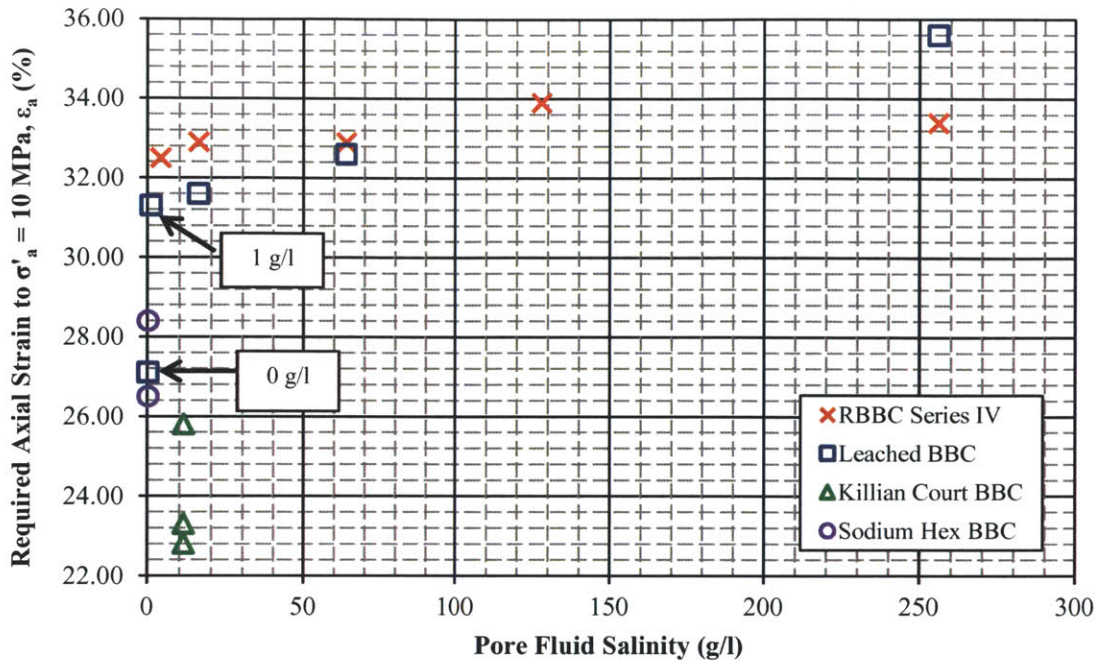


Figure 5.38 Relationship between pore fluid salinity and required axial strain to achieve an axial effective stress (σ'_a) of 10 MPa for RBBC (3 types) and in-situ Killian Court BBC

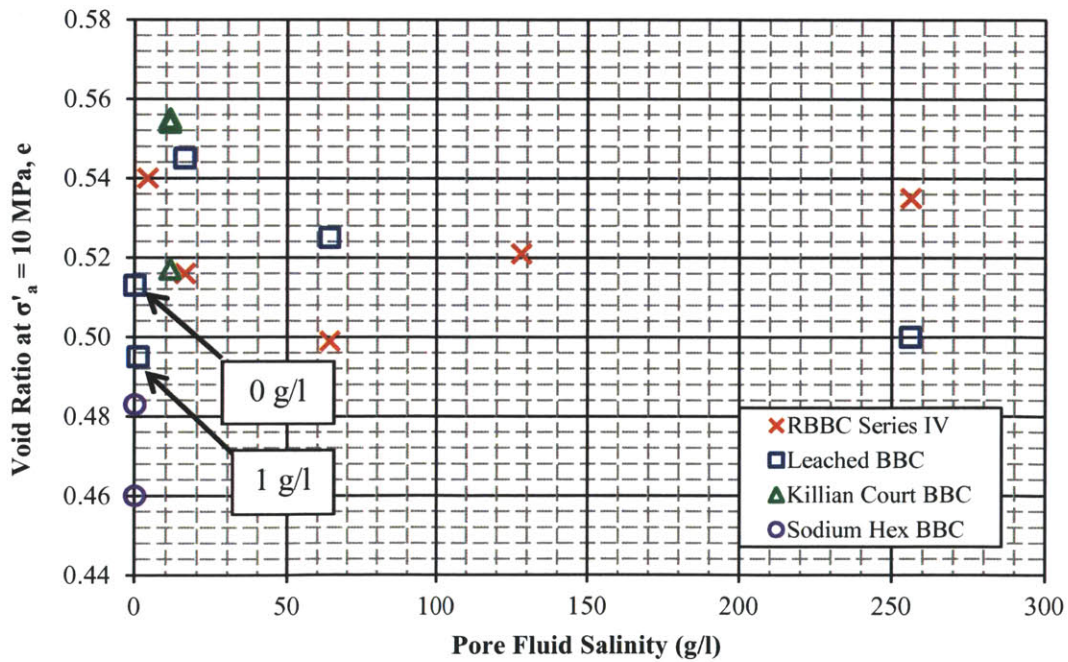


Figure 5.39 Relationship between pore fluid salinity and void ratio at an axial effective stress (σ'_a) of 10 MPa for RBBC (3 types) and in-situ Killian Court BBC

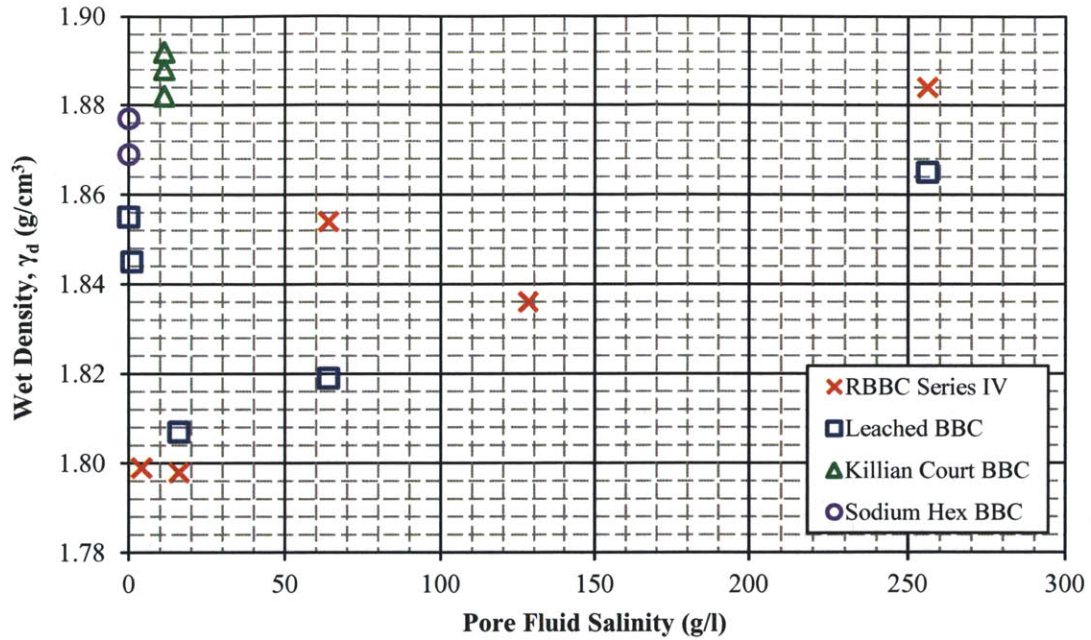


Figure 5.40 Relationship between pore fluid salinity and wet density for RBBC (3 types) and in-situ Killian Court BBC

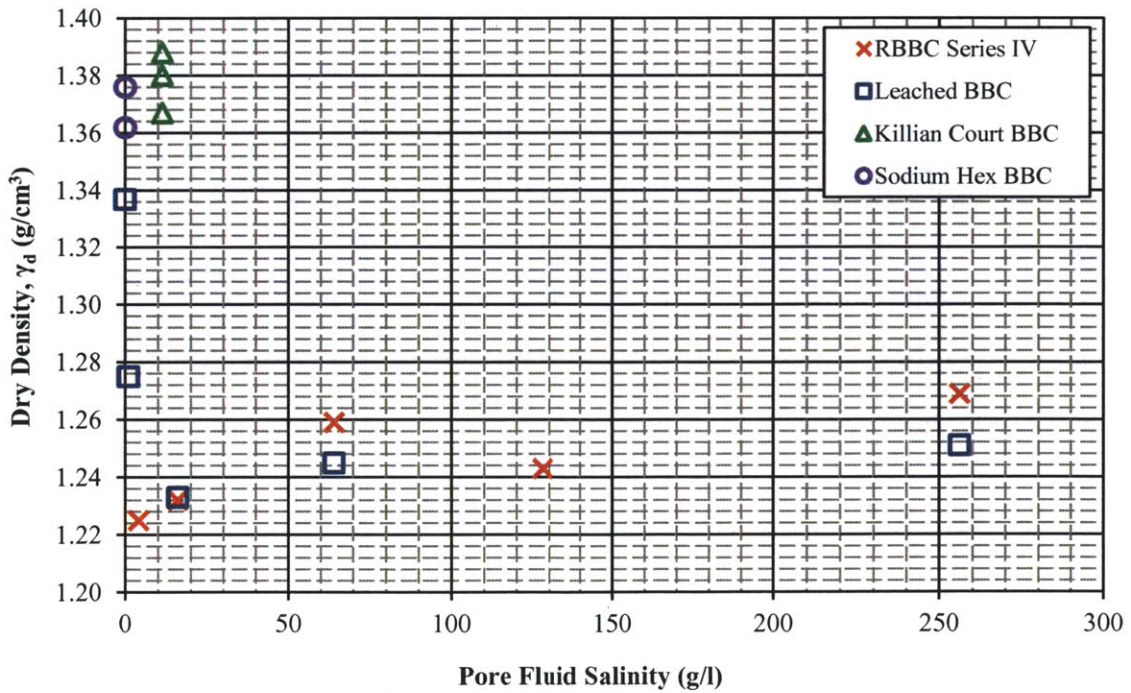


Figure 5.41 Relationship between pore fluid salinity and dry density for RBBC (3 types) and in-situ Killian Court BBC

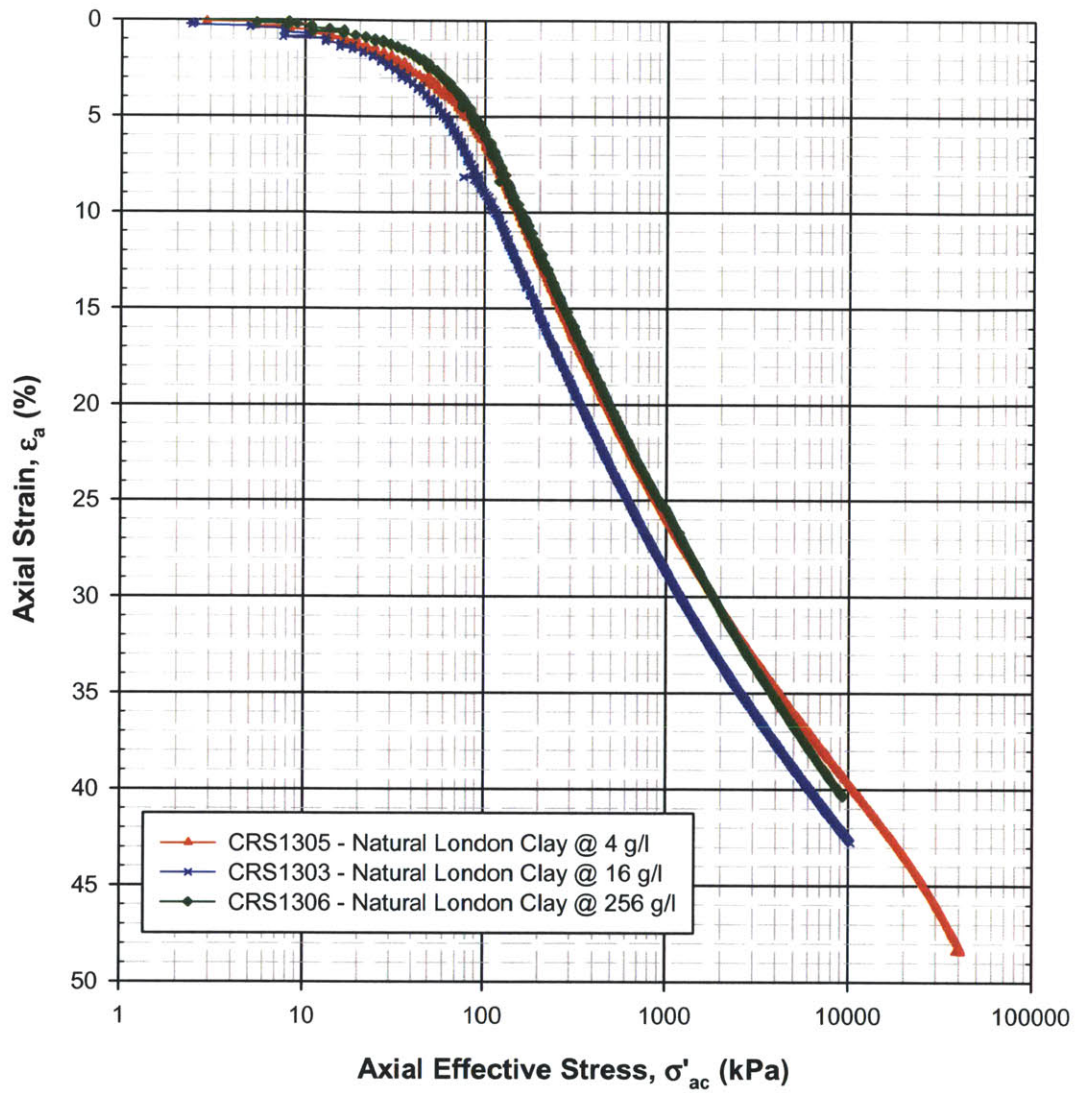


Figure 5.42 Compression behavior in ϵ_a - $\log \sigma'_{ac}$ space for R.London Clay at various pore fluid salinities

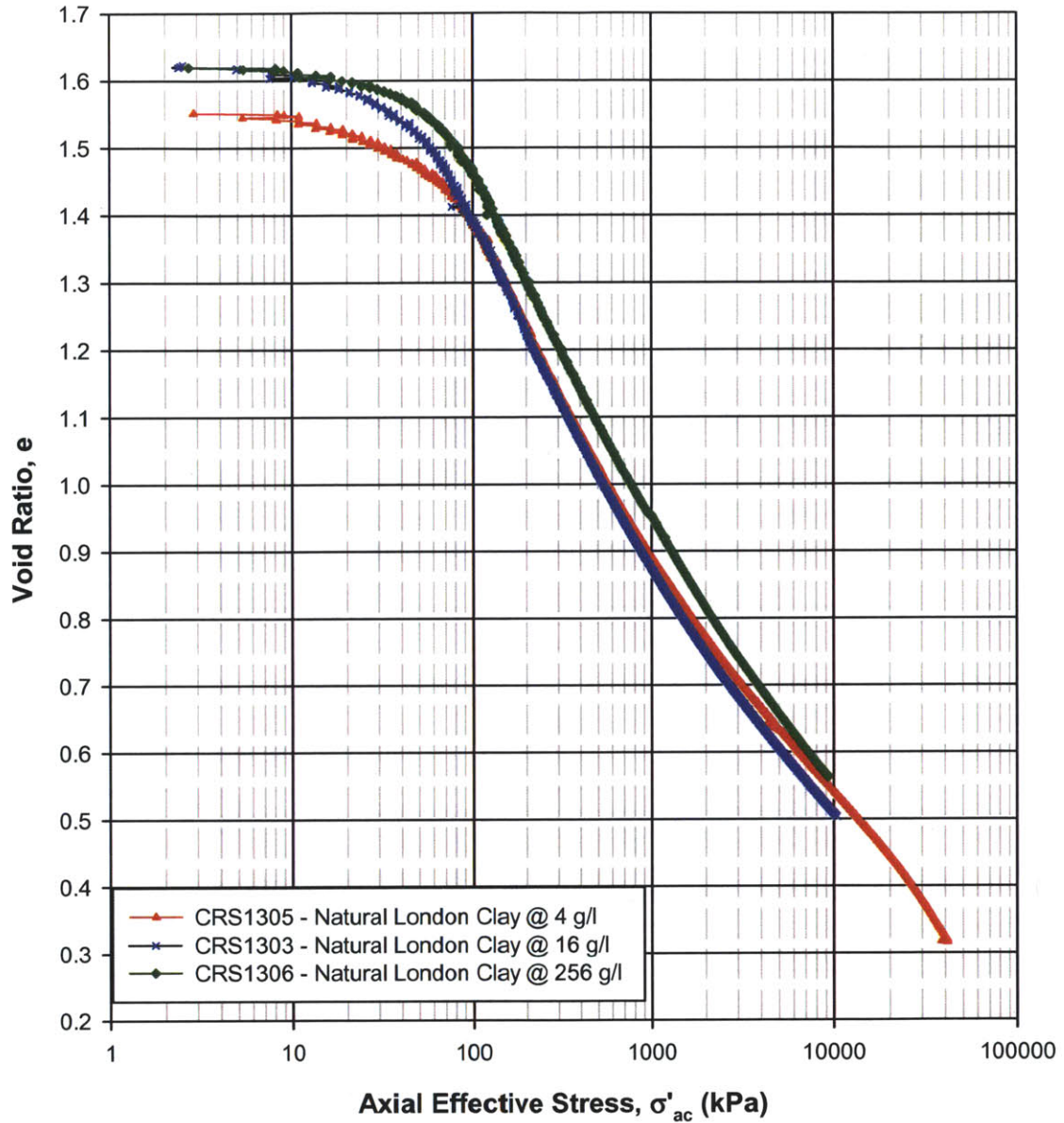


Figure 5.43 Compression behavior in e - $\log \sigma'_{ac}$ space for R.London Clay at various pore fluid salinities

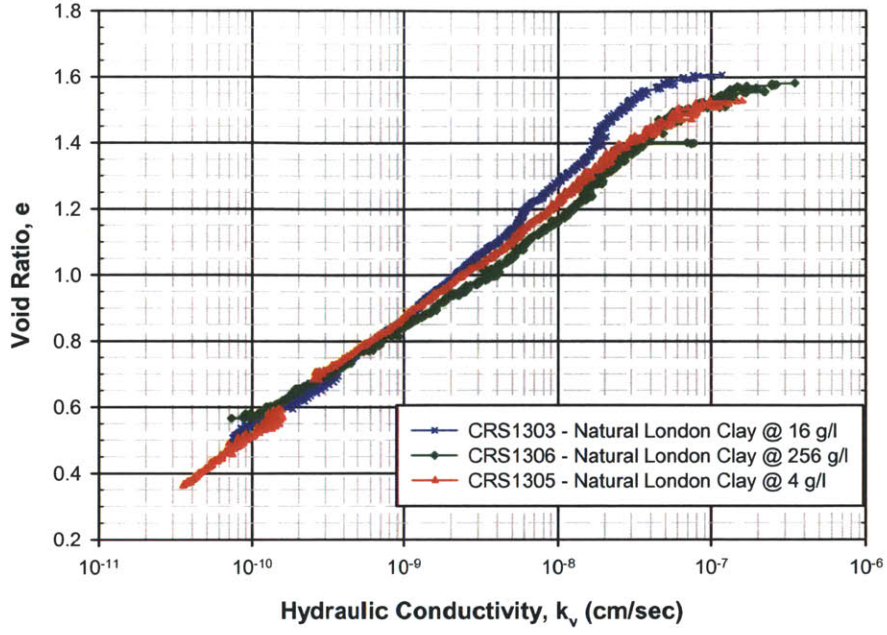


Figure 5.44 Hydraulic conductivity in void ratio space for R.London Clay at various pore fluid salinities

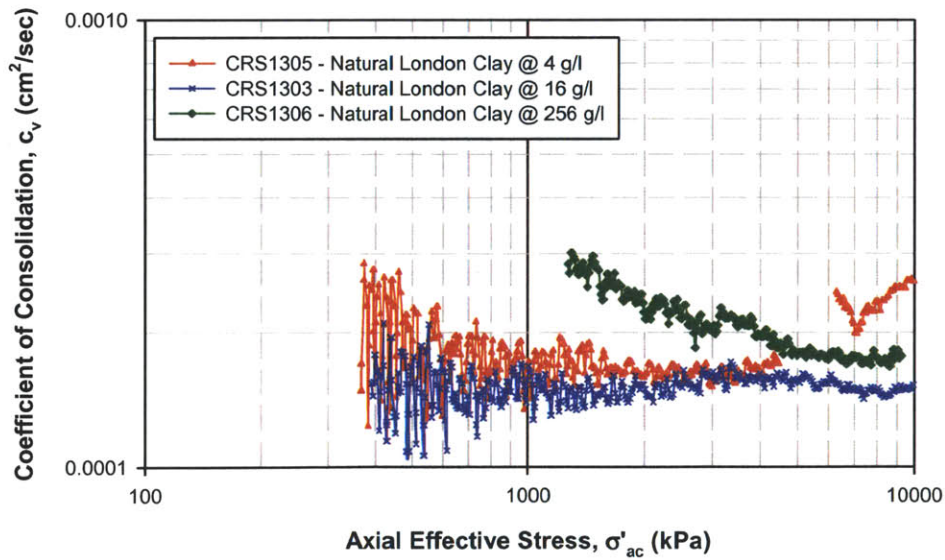


Figure 5.45 Coefficient of consolidation versus axial effective stress (up to 10,000 kPa) for R.London Clay at various pore fluid salinities

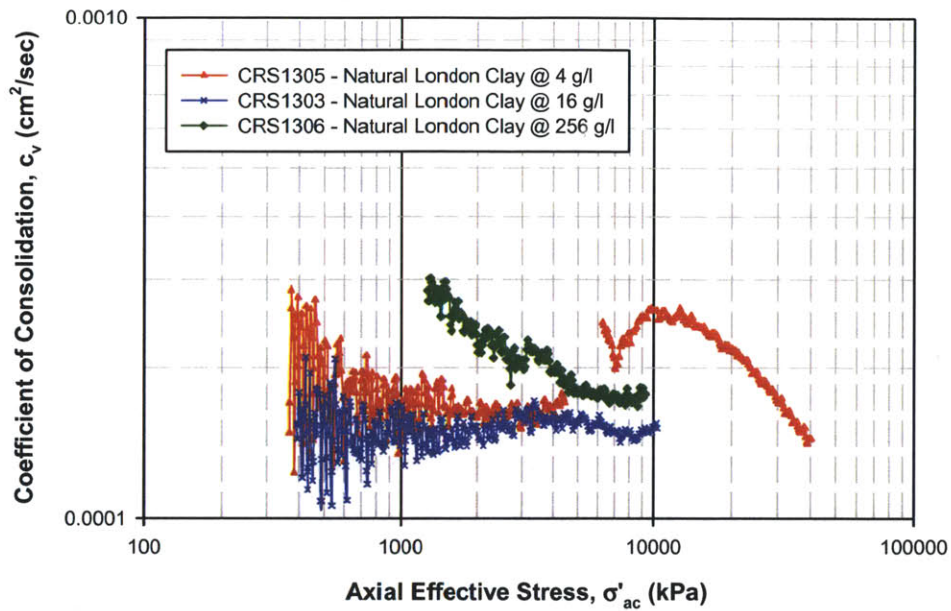


Figure 5.46 Coefficient of consolidation versus axial effective stress (up to 40,000 kPa) for R.London Clay at various pore fluid salinities

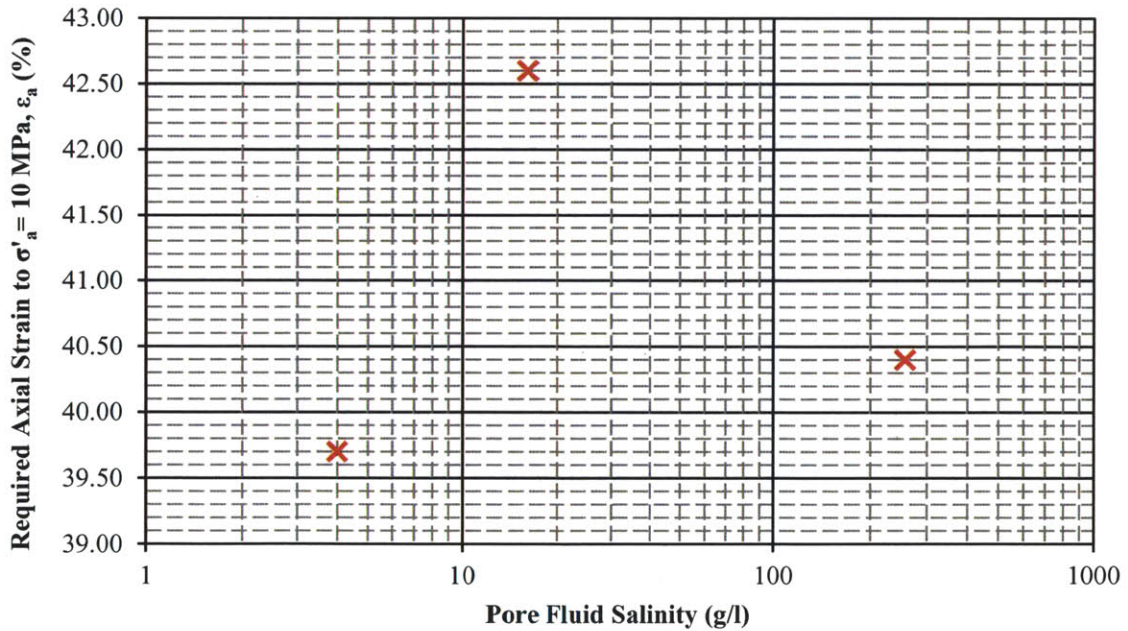


Figure 5.47 Required Axial Strain to $\sigma'_a = 10$ MPa, ϵ_a (%) for R.London Clay

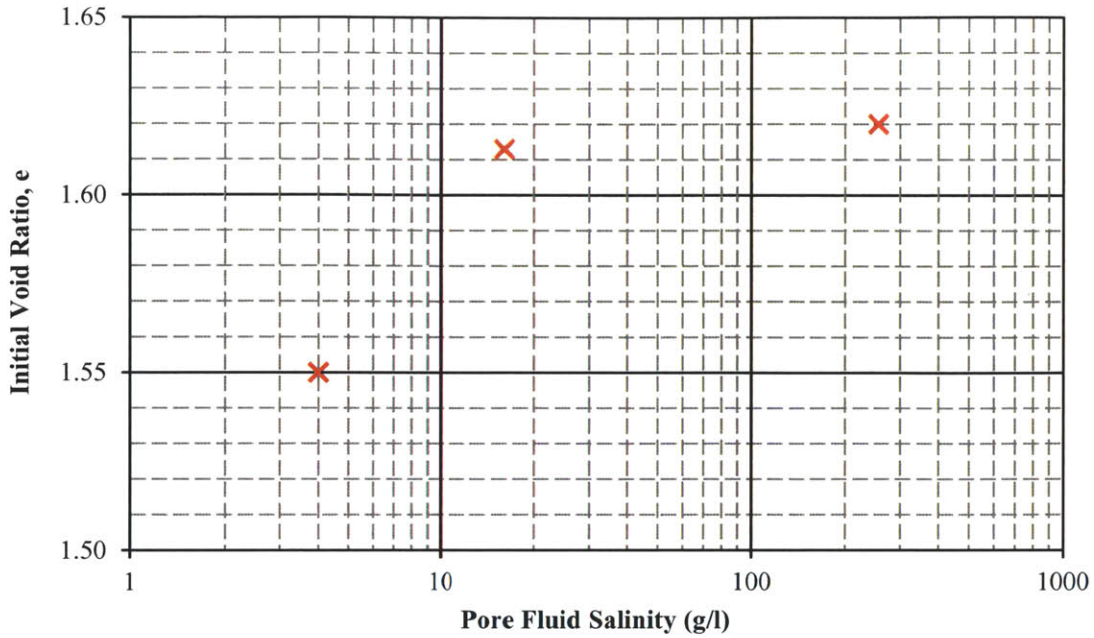


Figure 5.48 Relationship between pore fluid salinity and initial void ratio for R.London Clay

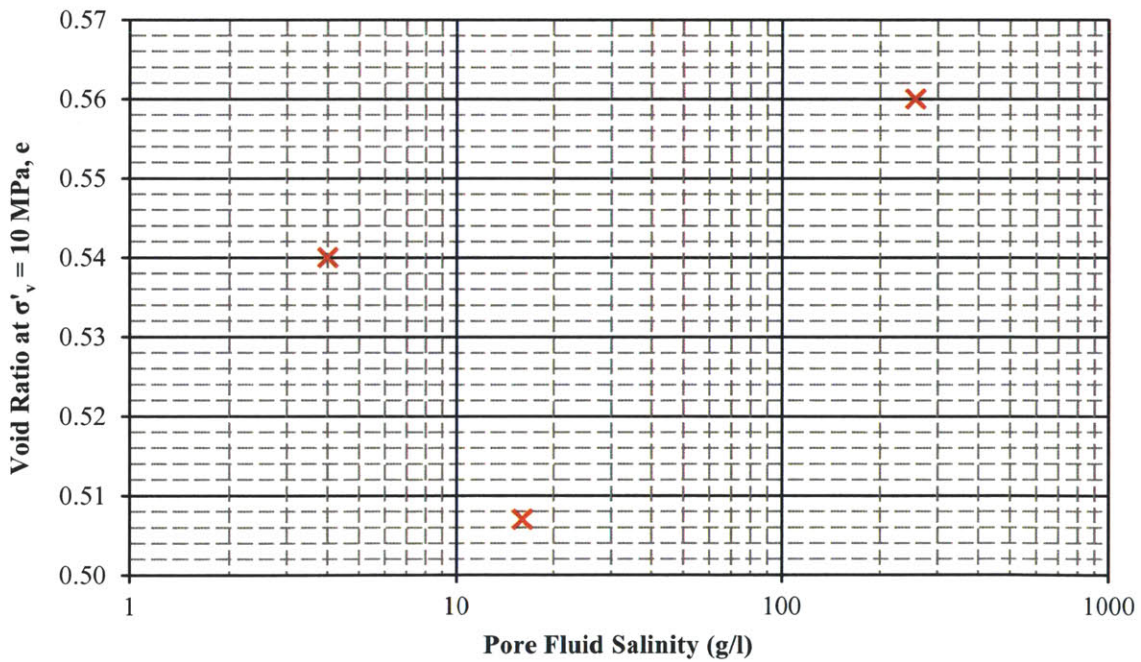


Figure 5.49 Relationship between pore fluid salinity and void ratio at an axial effective stress (σ'_a) of 10 MPa for R.London Clay

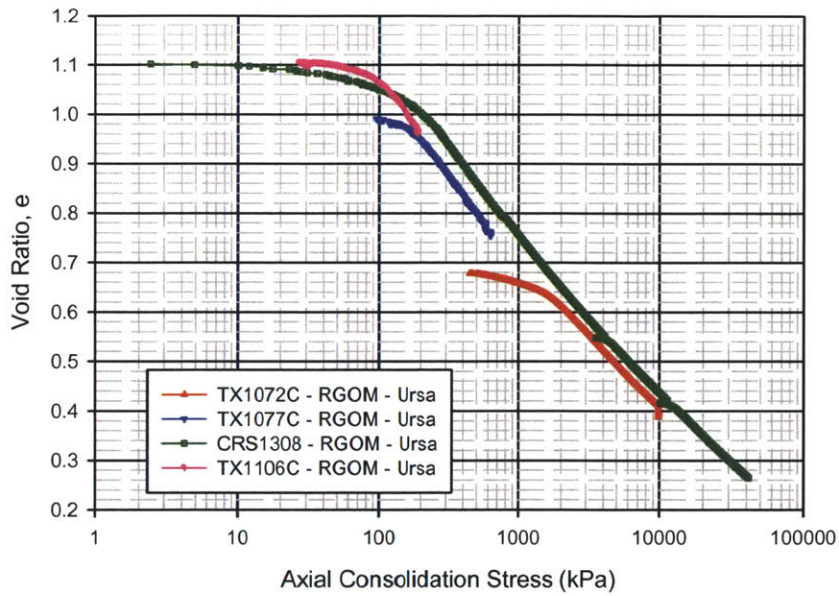


Figure 5.50 One dimensional test from consolidation phase of triaxial testing on RGOM-Ursa soil performed by Brendan Casey

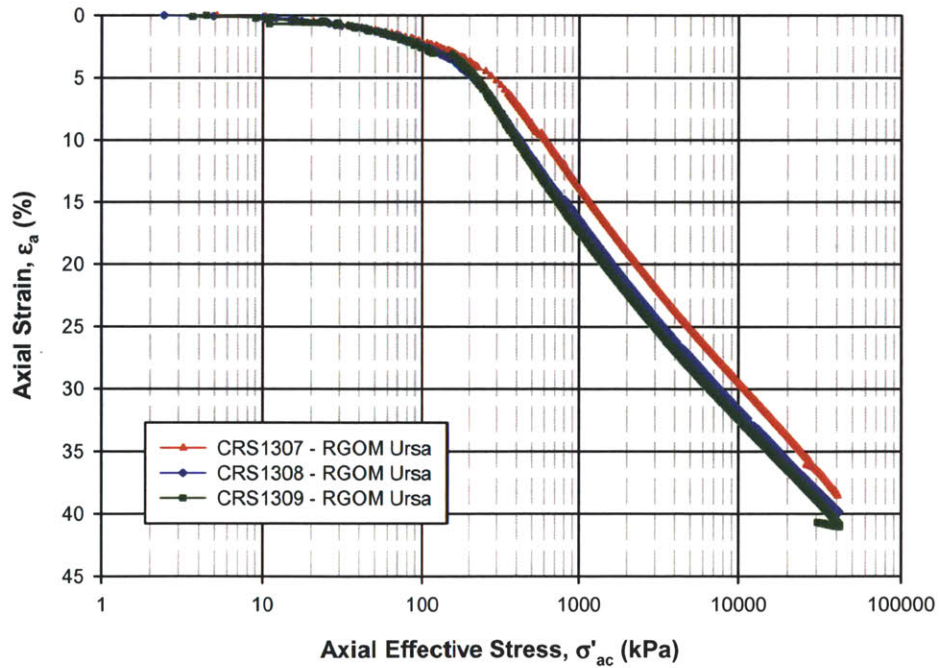


Figure 5.51 Compression behavior in ϵ_a - $\log \sigma'_{ac}$ space for RGOM-Ursa

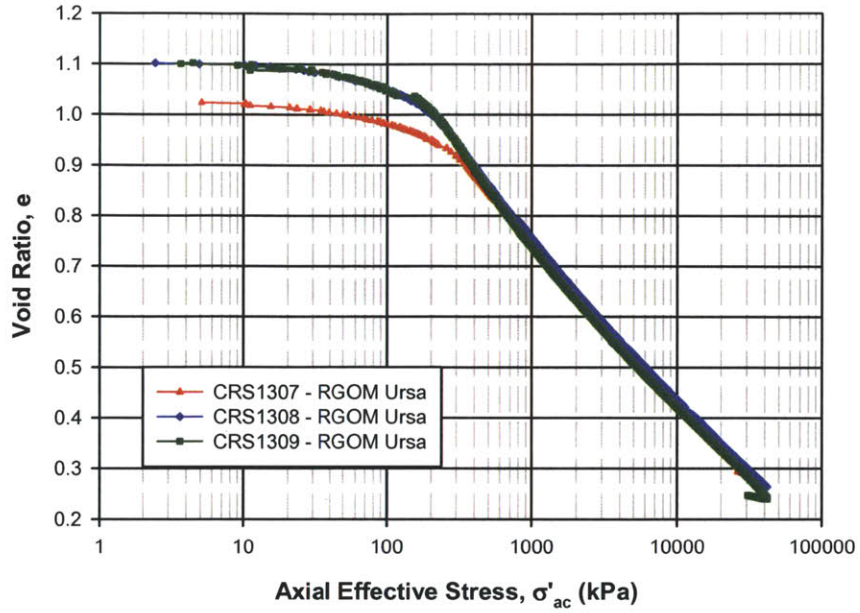


Figure 5.52 Compression behavior in e - $\log \sigma'_{ac}$ space for RGOM-Ursa

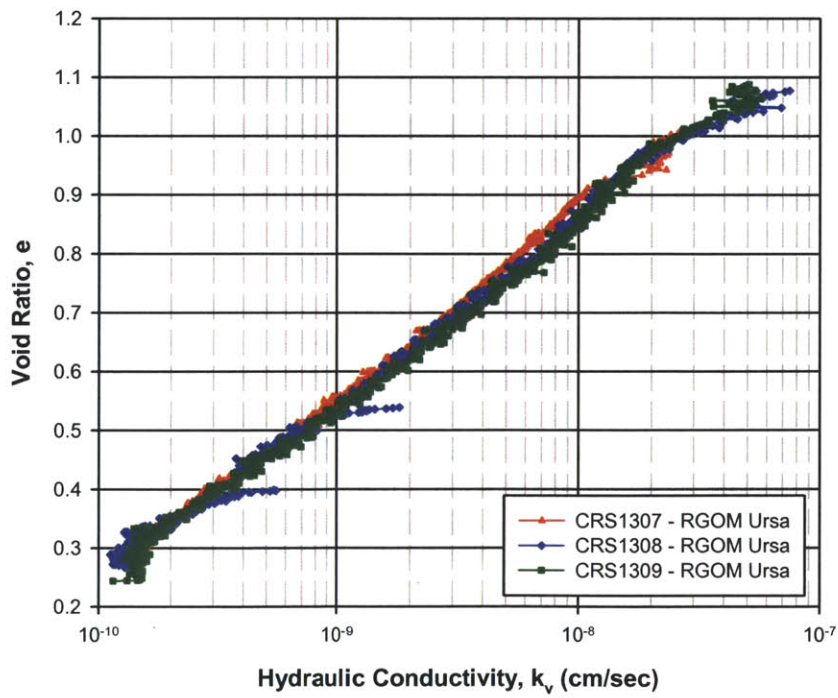


Figure 5.53 Hydraulic conductivity in void ratio space for RGOM-Ursa

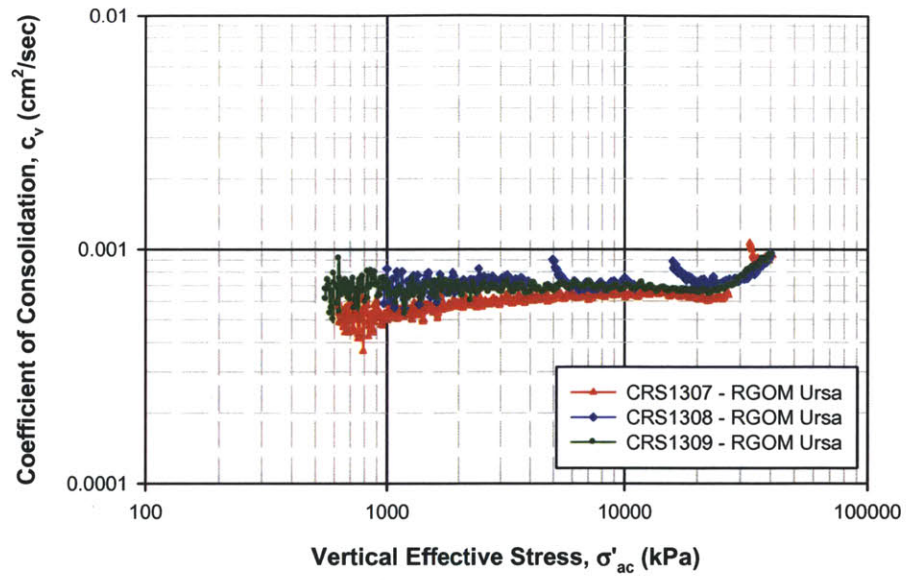


Figure 5.54 Coefficient of consolidation versus axial effective stress (up to 40,000 kPa) for RGOM-Ursa

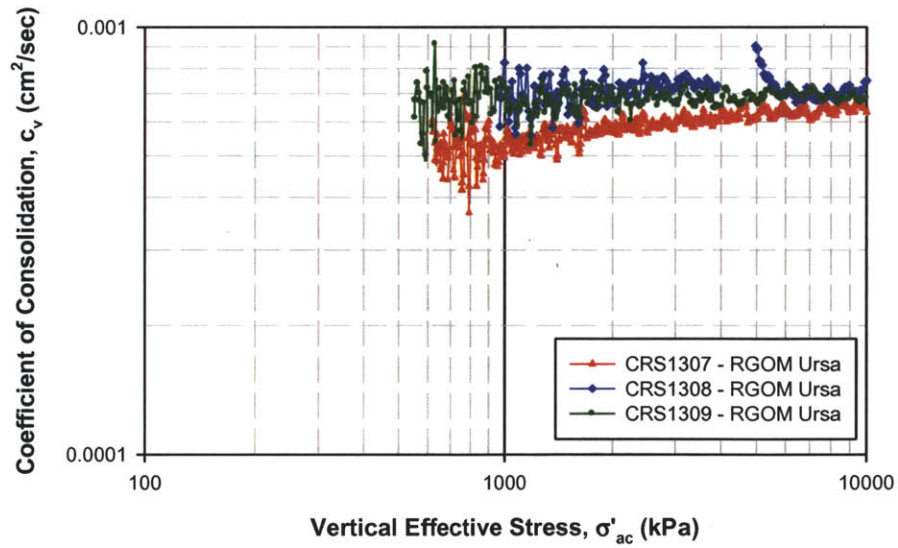


Figure 5.55 Coefficient of consolidation versus axial effective stress (up to 10,000 kPa) for RGOM-Ursa

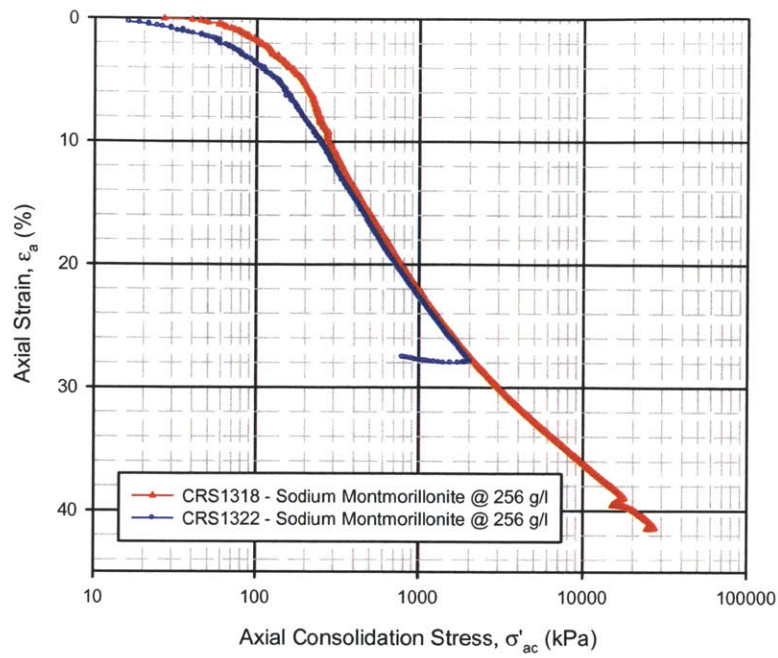


Figure 5.56 Compression behavior in ϵ_a - $\log\sigma'_{ac}$ space for sodium montmorillonite with 256 g/l pore fluid

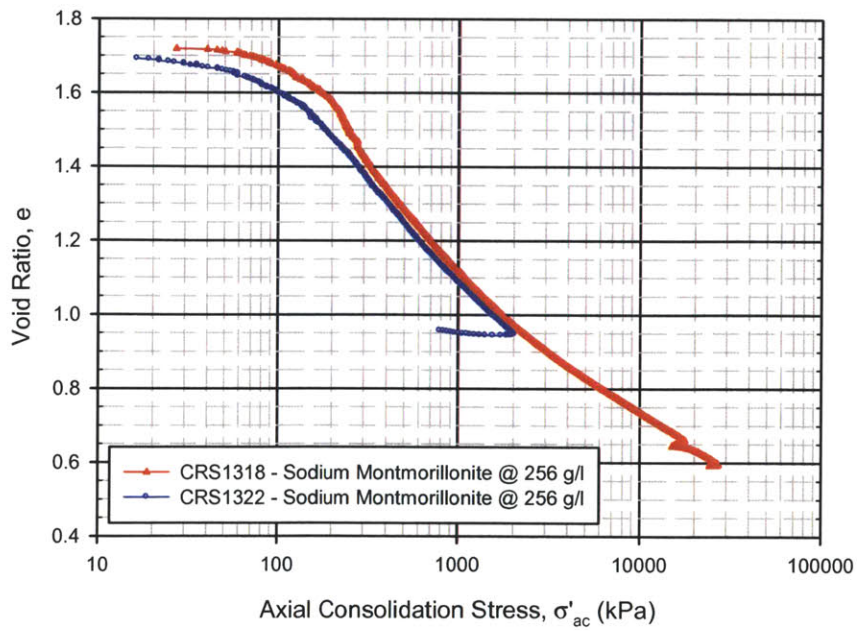


Figure 5.57 Compression behavior in e - $\log\sigma'_{ac}$ space for sodium montmorillonite with 256 g/l pore fluid

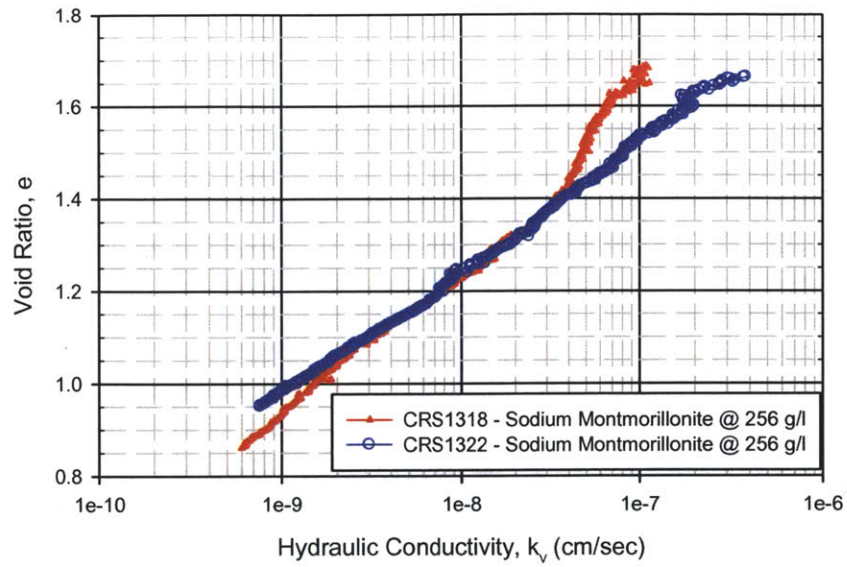


Figure 5.58 Hydraulic conductivity in void ratio space for sodium montmorillonite with 256 g/l pore fluid

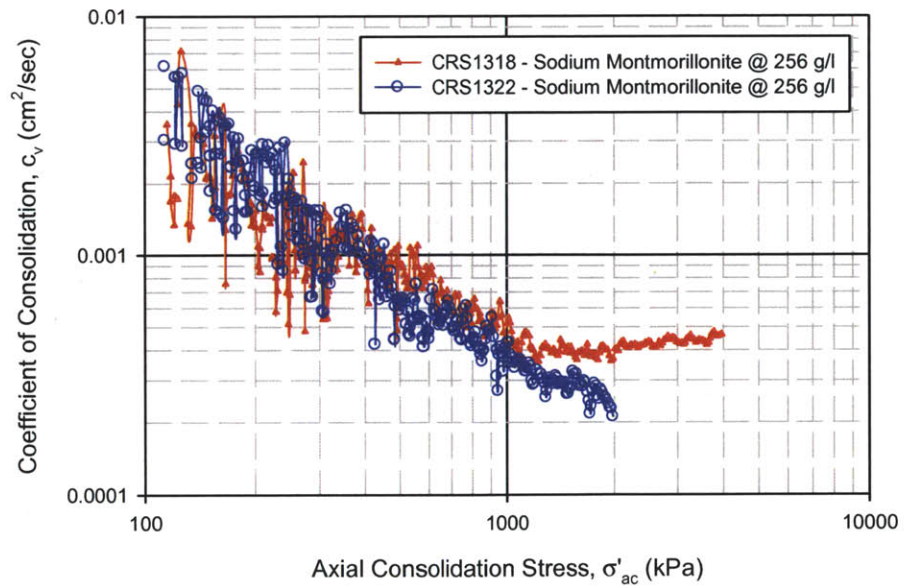


Figure 5.59 Coefficient of consolidation versus axial effective stress for sodium montmorillonite with 256 g/l pore fluid

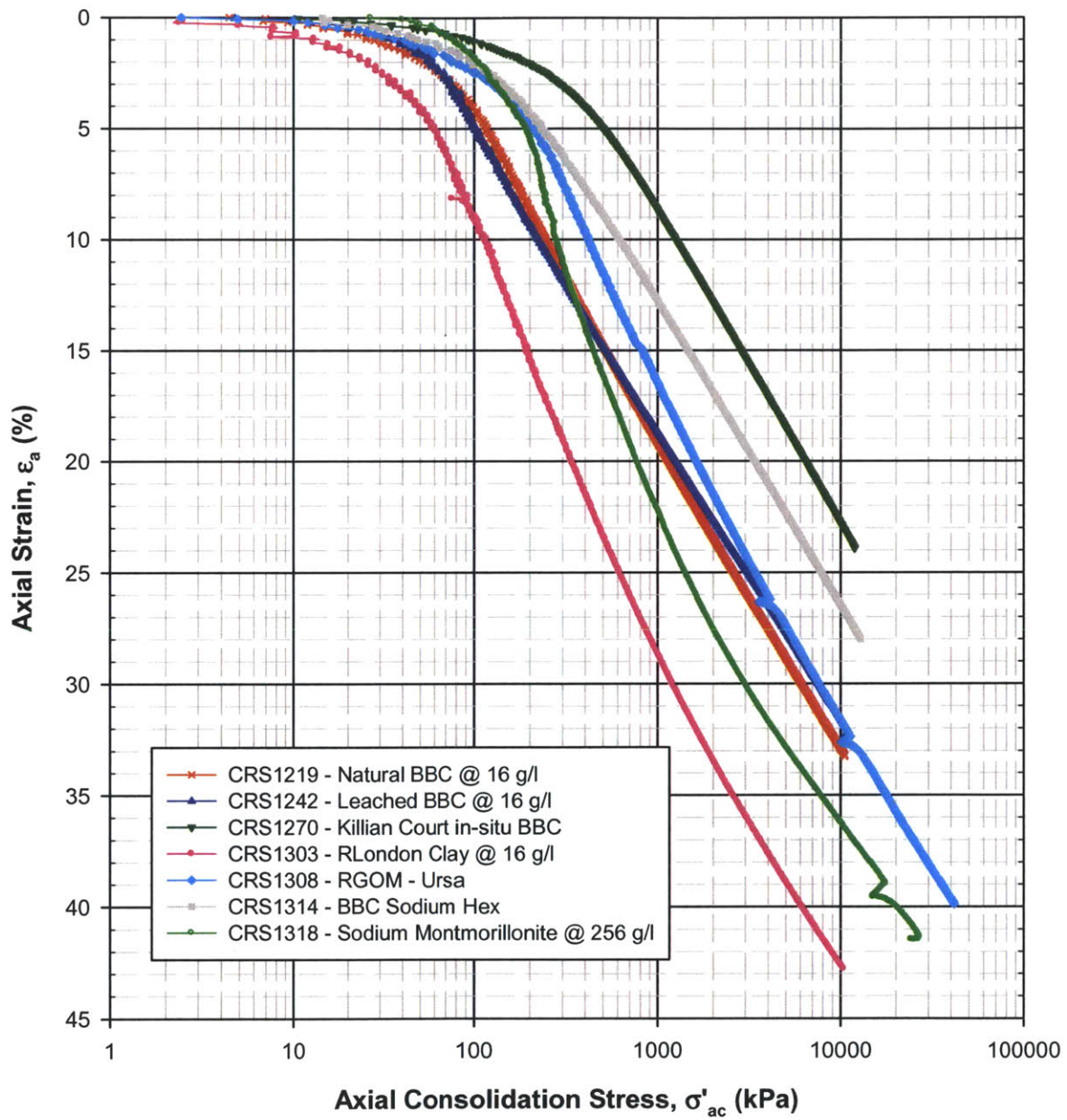


Figure 5.60 Compression behavior synthesis plot in ϵ_a - $\log\sigma'_{ac}$ space for all soils in testing program

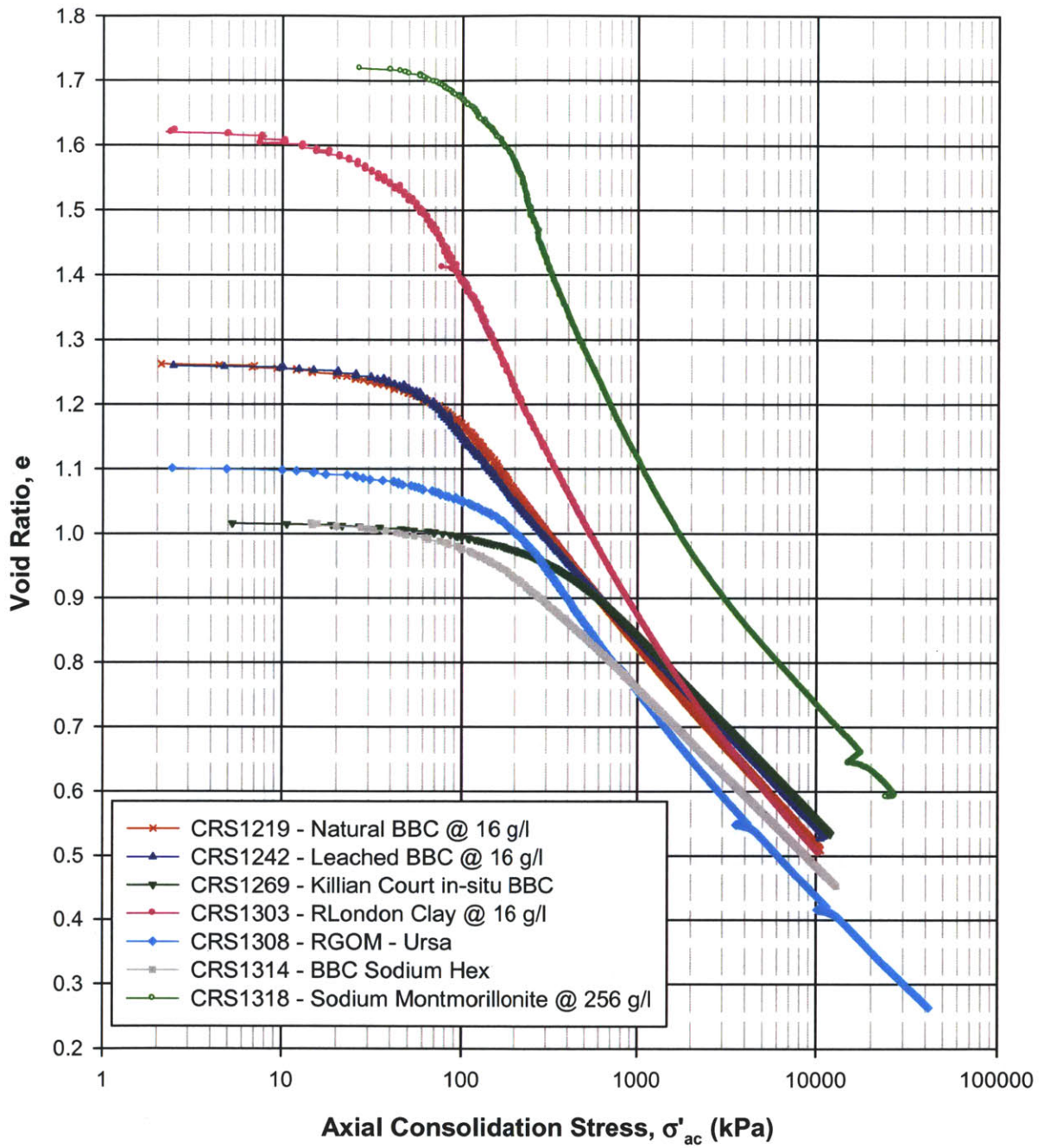


Figure 5.61 Compression behavior synthesis plot in e - $\log \sigma'_{ac}$ space for all soils in testing program

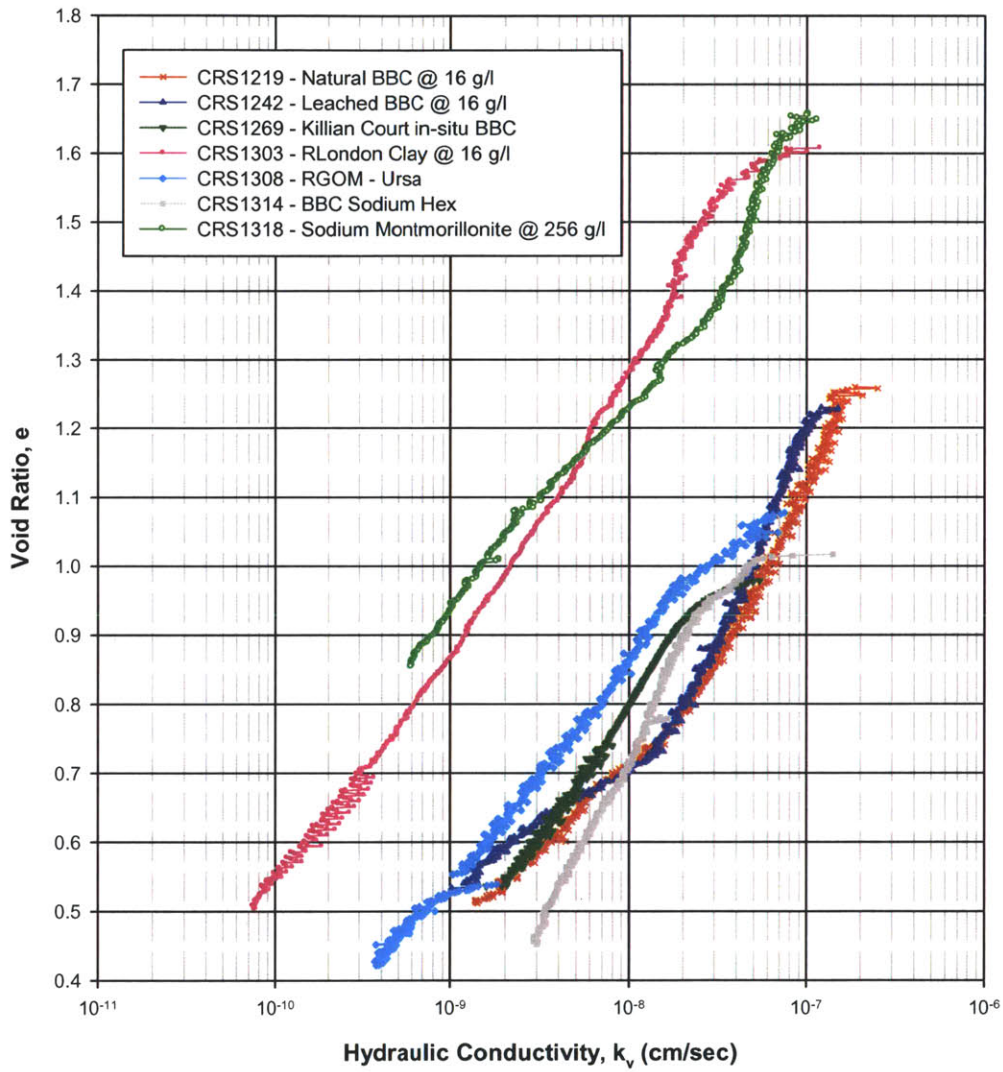


Figure 5.62 Hydraulic conductivity synthesis plot in void ratio space for all soils in testing program

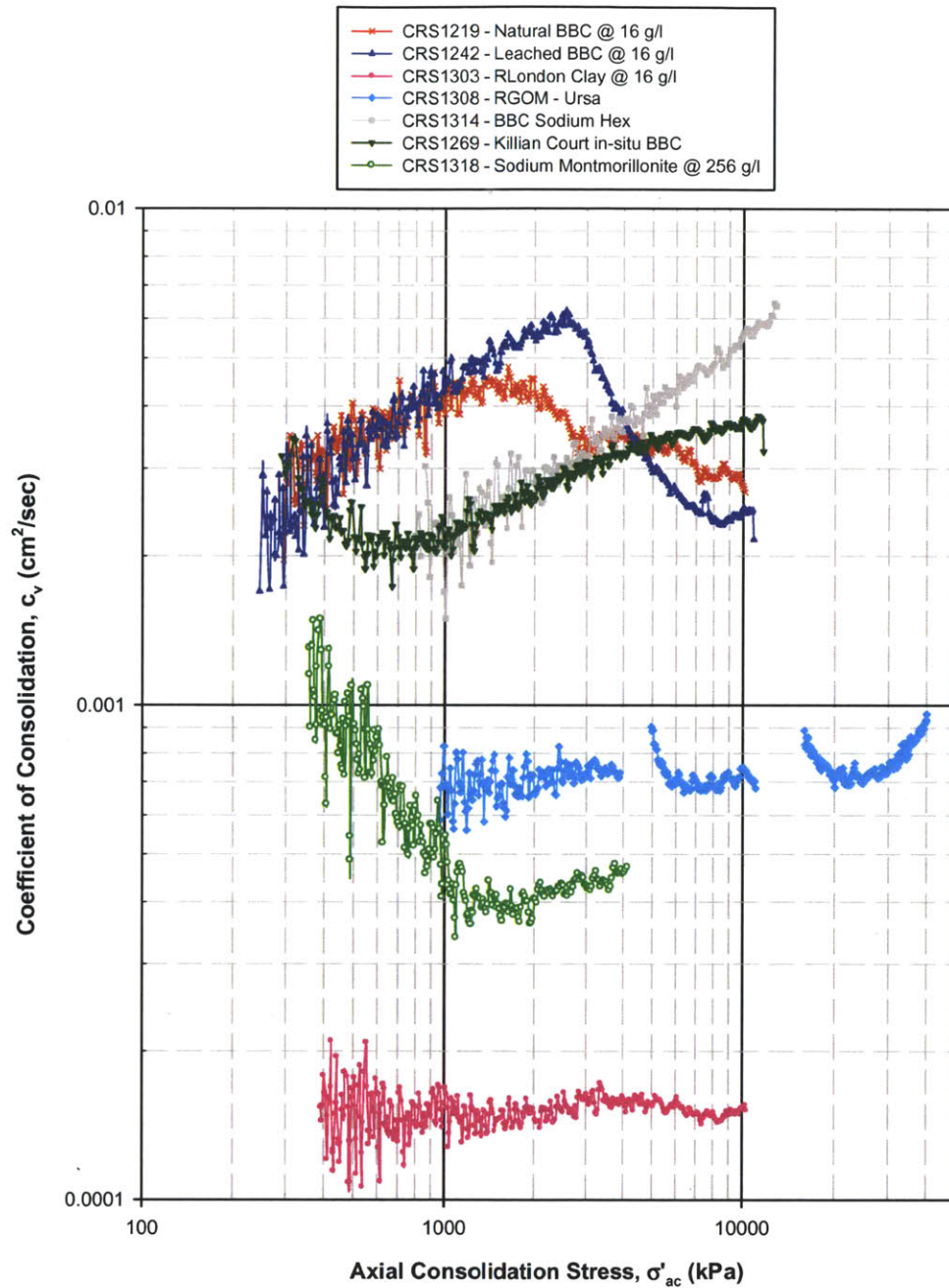


Figure 5.63 Coefficient of consolidation versus axial effective stress synthesis plot (up to 40,000 kPa) for all soils in testing program

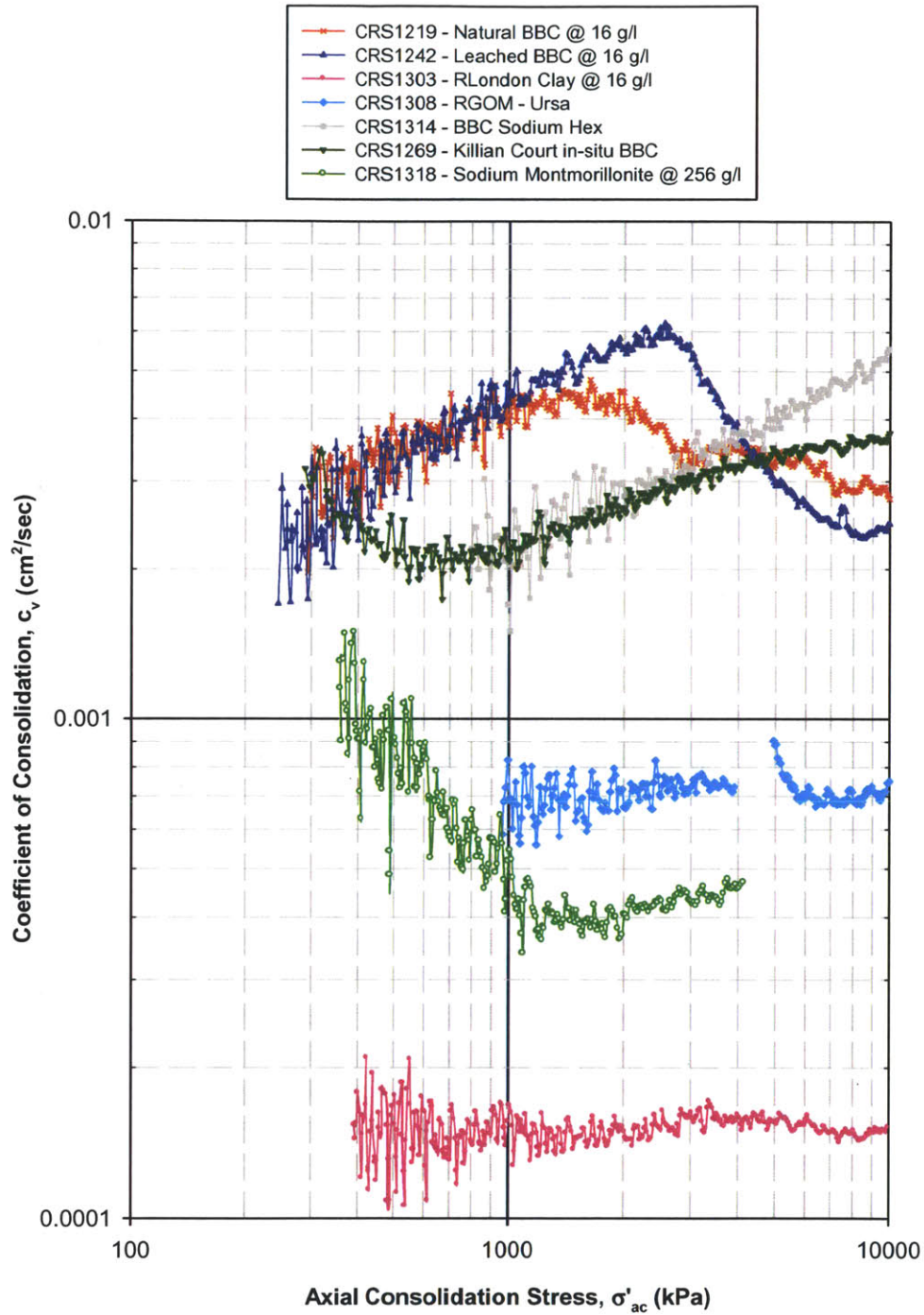


Figure 5.64 Coefficient of consolidation versus axial effective stress synthesis plot (up to 10,000 kPa) for all soils in testing program

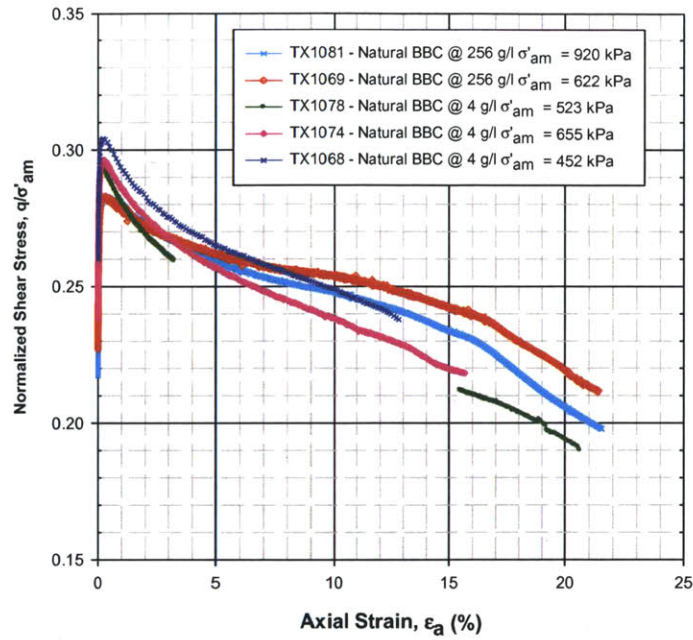


Figure 5.65 Normalized stress-strain curve for NC natural RBBC Series IV at different pore fluid salinities from CK₀UC triaxial tests

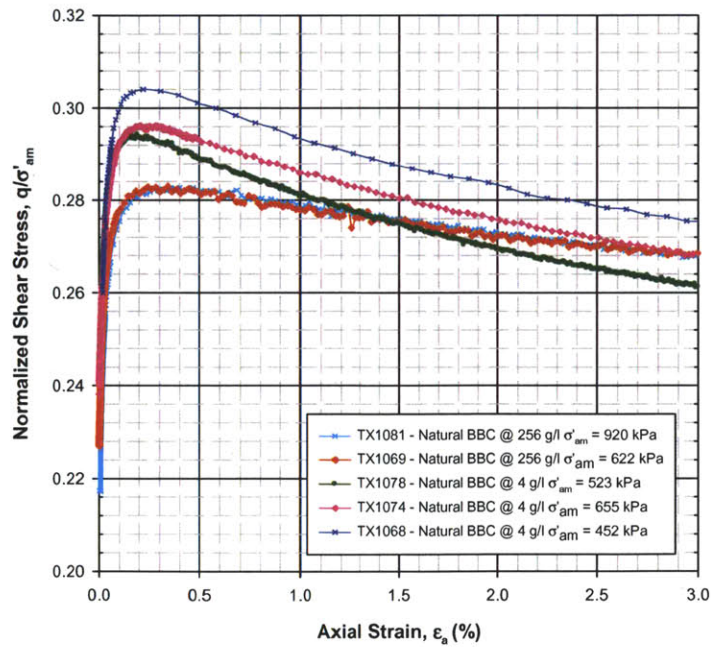


Figure 5.66 Normalized stress-strain curves (small strains) for NC RBBC Series IV at different pore fluid salinities from CK₀UC triaxial tests

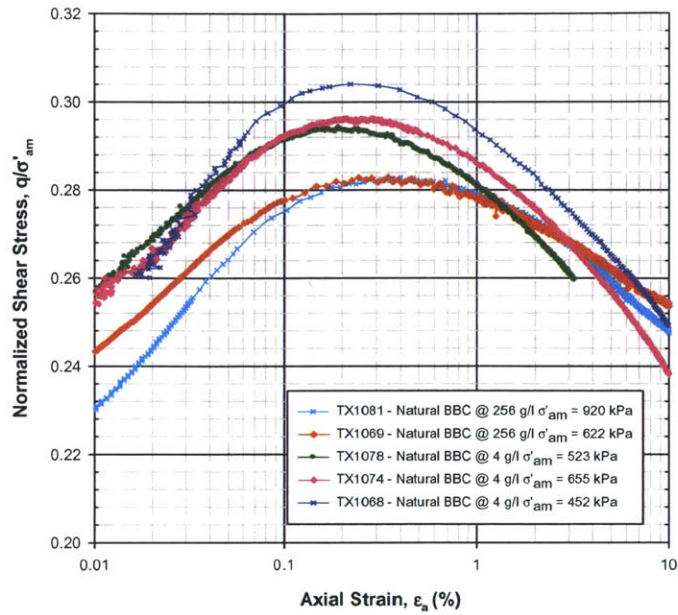


Figure 5.67 Normalized stress-(log) strain curves for NC natural RBBC Series IV from CK₀UC triaxial tests

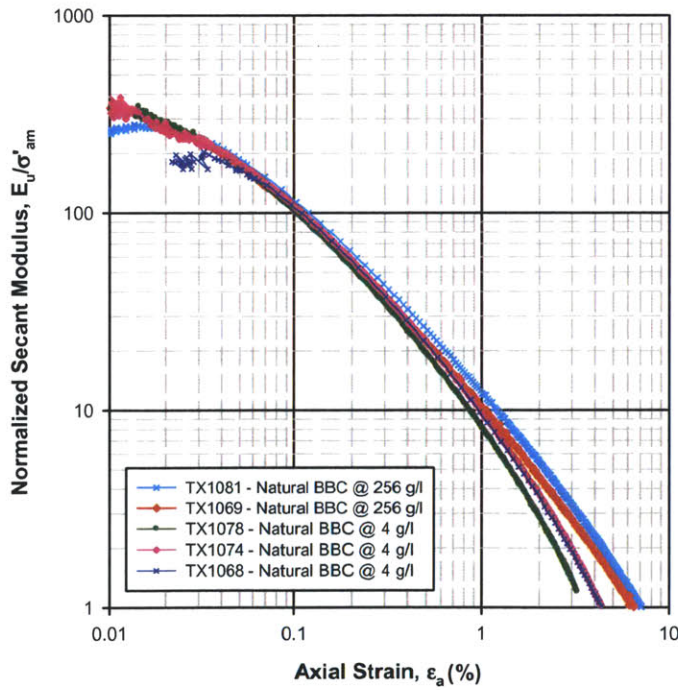


Figure 5.68 Normalized undrained secant modulus versus axial strain for NC RBBC Series IV at different pore fluid salinities from CK₀UC triaxial tests

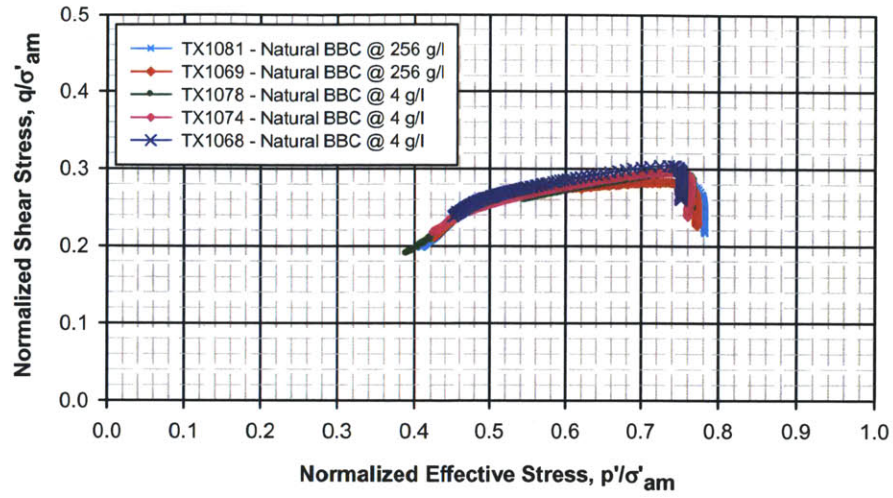


Figure 5.69 Normalized effective stress path for NC natural RBBC Series IV at different pore fluid salinities from CK₀UC triaxial testing

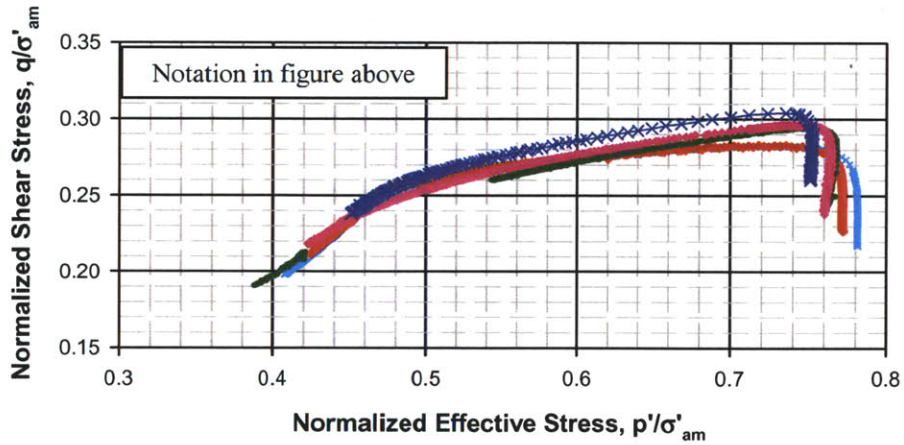


Figure 5.70 Normalized effective stress path (close up view) for NC natural RBBC Series IV at different pore fluid salinities from CK₀UC triaxial testing

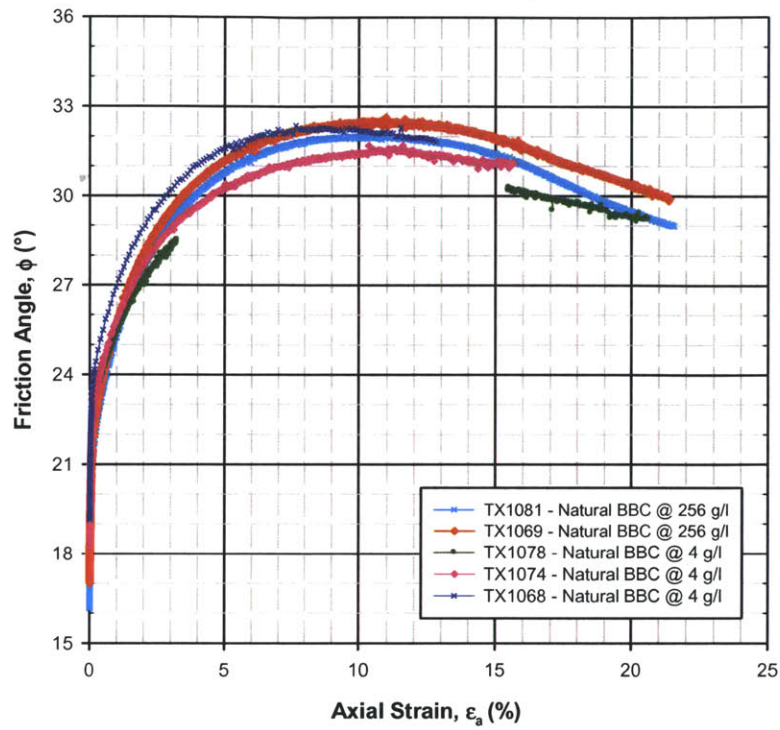


Figure 5.71 Friction angle versus axial strain for NC RBBC Series IV at different pore fluid salinities from CK₀UC triaxial tests

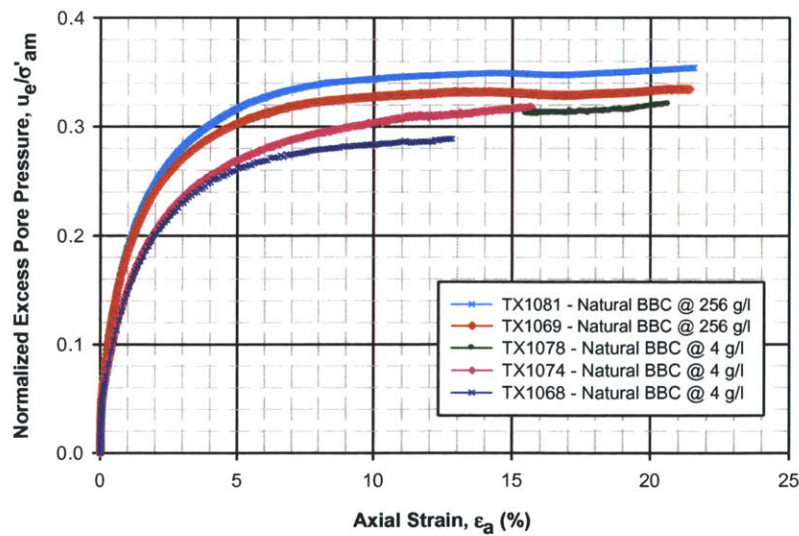


Figure 5.72 Normalized excess pore pressure versus axial strain for NC natural RBBC Series IV from CK₀UC triaxial tests

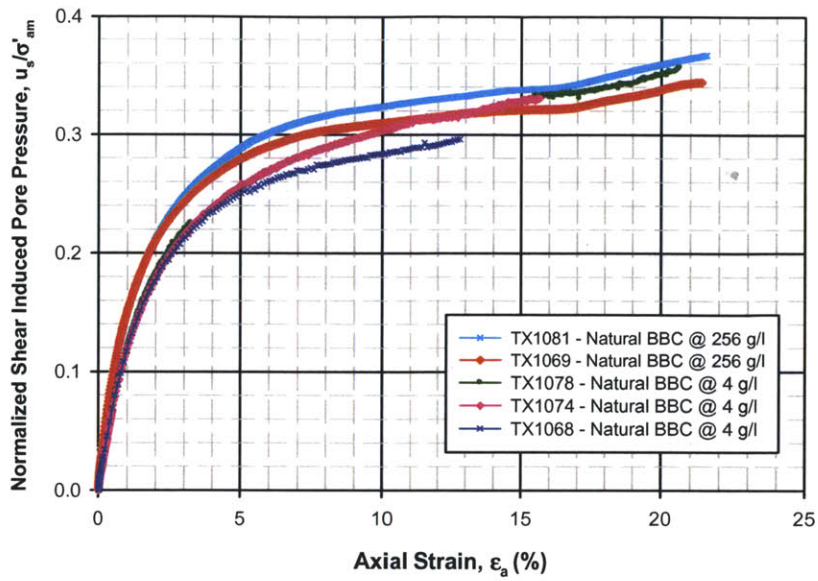


Figure 5.73 Normalized shear induced pore pressure versus axial strain for NC natural RBBC Series IV from CK_0UC triaxial tests

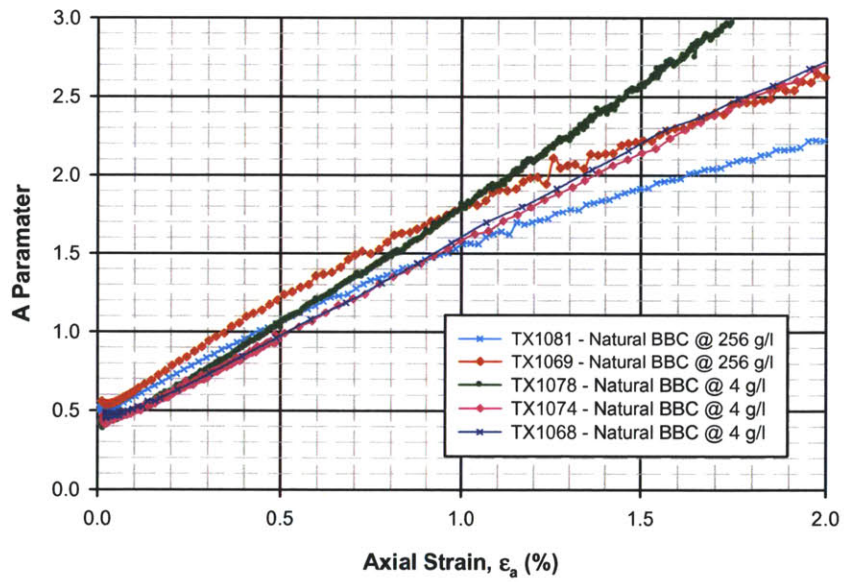


Figure 5.74 A parameter versus axial strain (small strains) for NC RBBC Series IV at different pore fluid salinities from CK_0UC triaxial testing

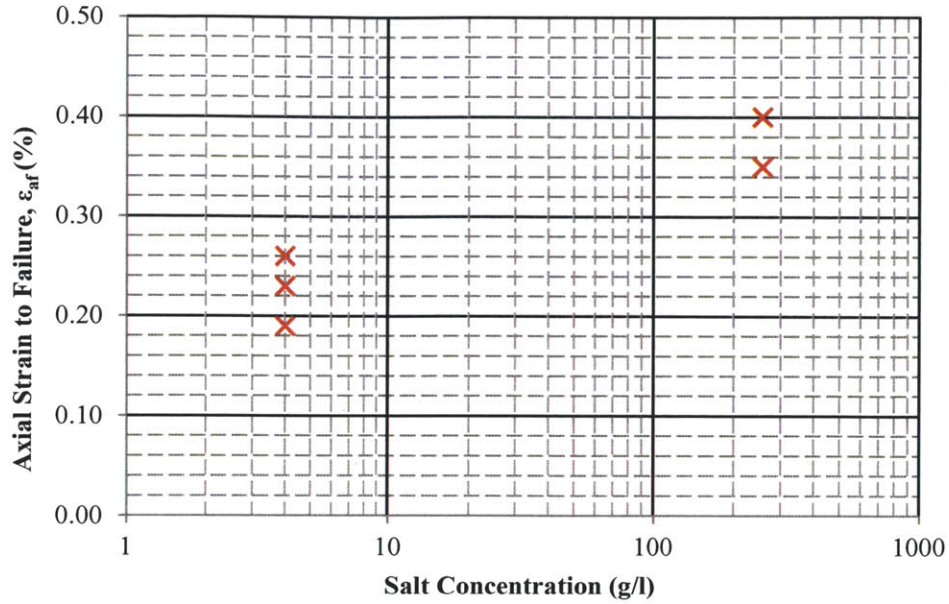


Figure 5.75 Relationship between axial strain to failure and salt concentration for natural RBBC Series IV from CK_0UC triaxial testing

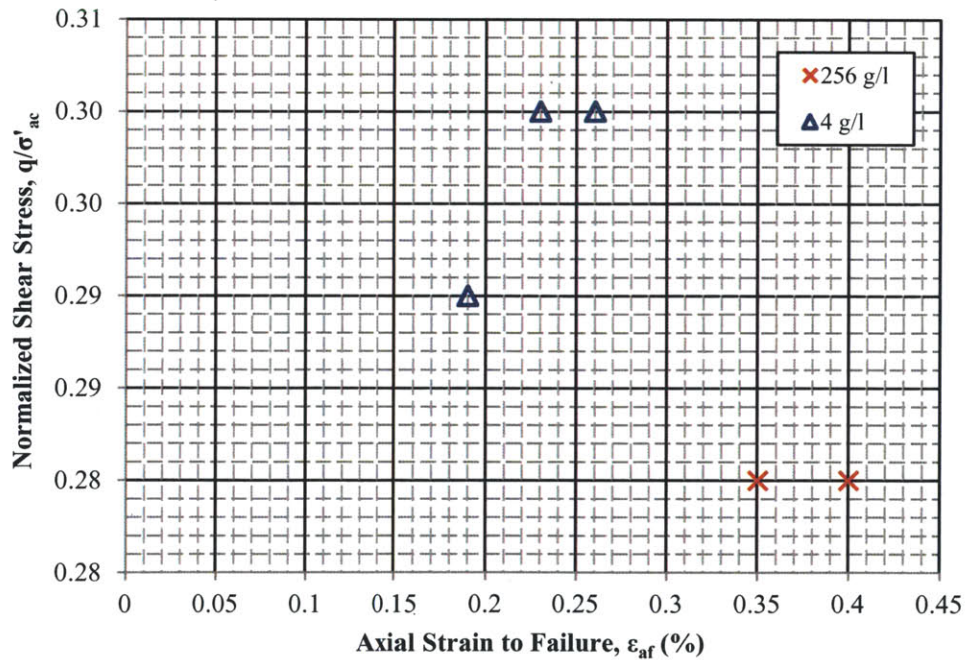


Figure 5.76 Relationship between normalized shear stress and axial strain failure for natural RBBC Series IV from CK_0UC triaxial testing

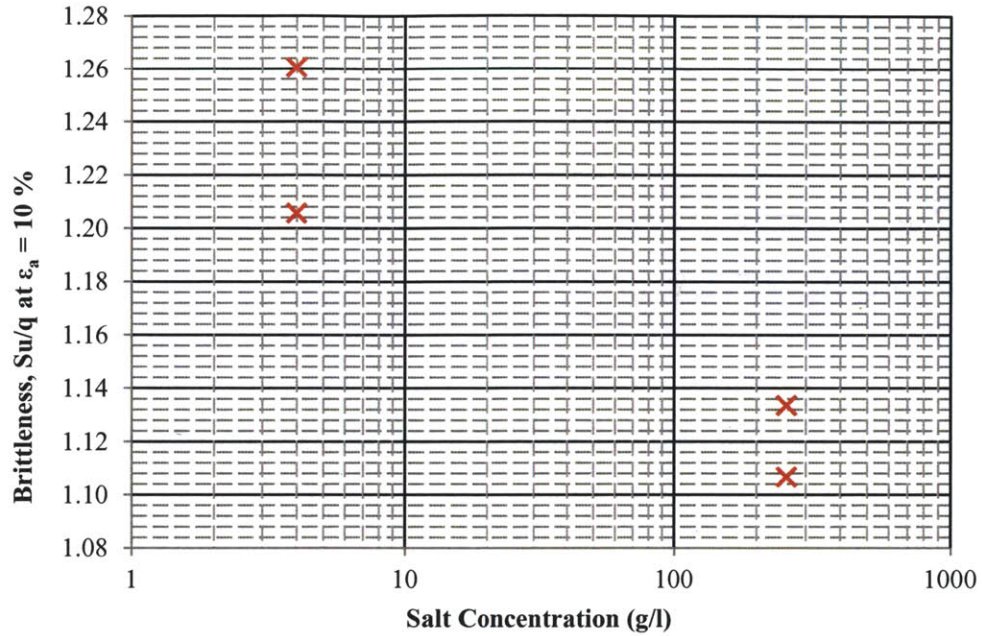


Figure 5.77 Plot of soil brittleness at an axial strain of 10 % as a function of pore fluid salinity for natural RBBC Series IV

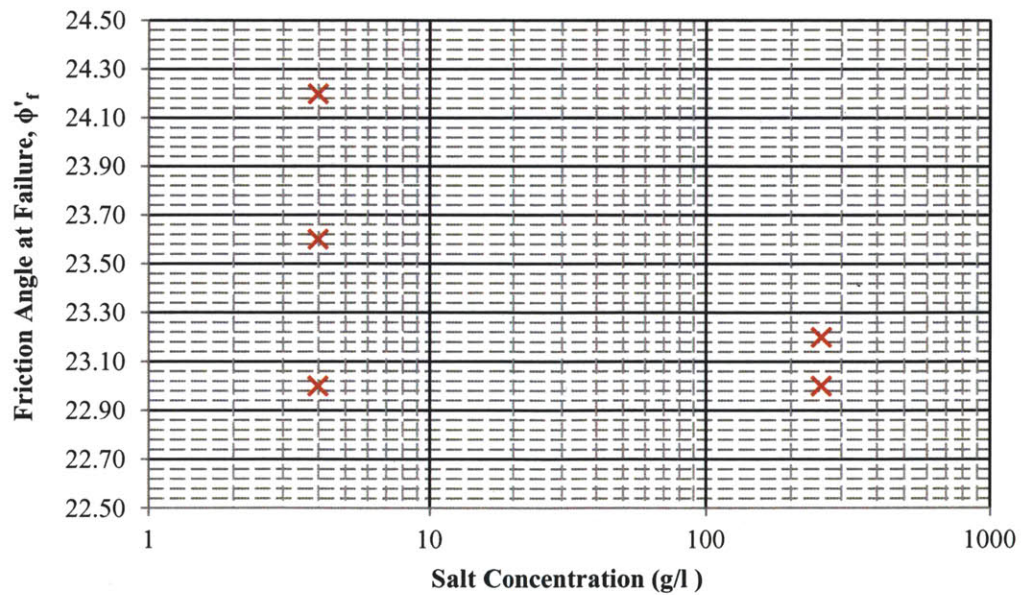


Figure 5.78 Relationship between salinity and friction angle at failure for RBBC Series IV from CK_0UC triaxial testing

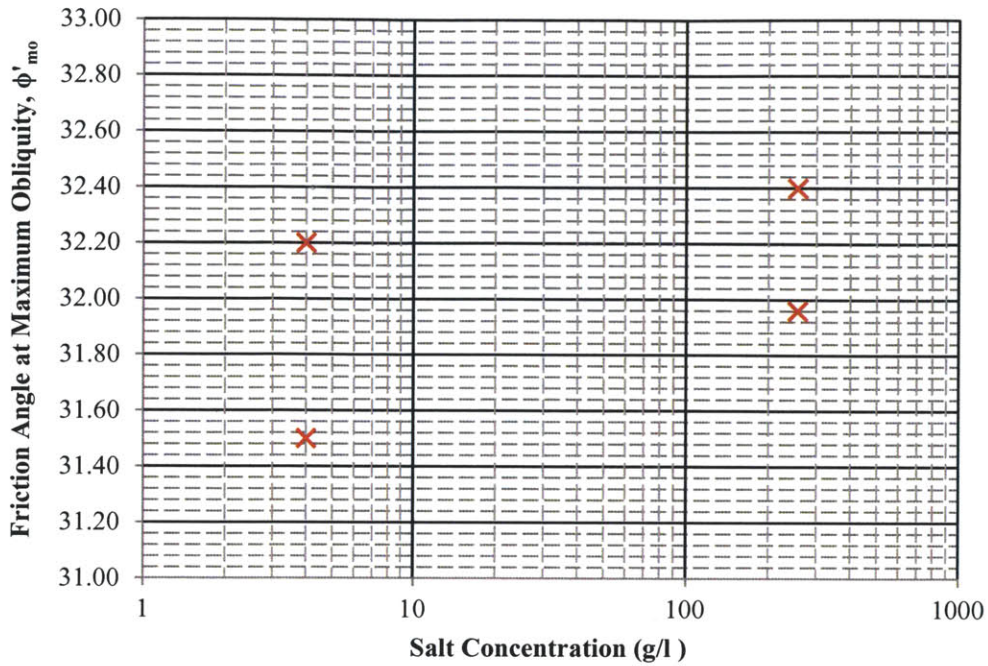


Figure 5.79 Relationship between salinity and friction angle at maximum obliquity for RBBC Series IV from CK_0UC triaxial testing

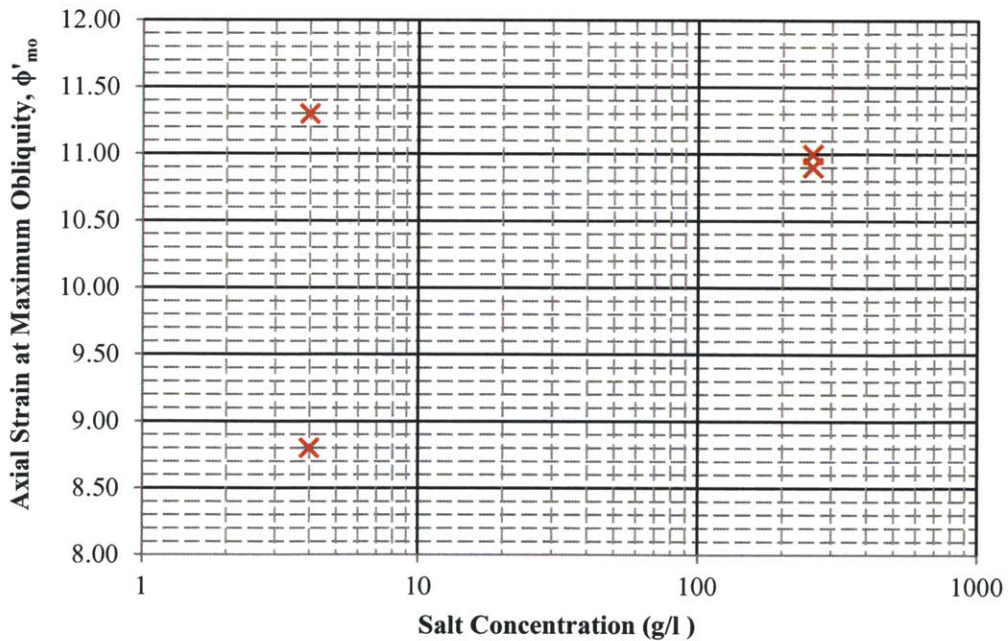


Figure 5.80 Relationship between salinity and axial strain at maximum obliquity for RBBC Series IV from CK_0UC triaxial testing

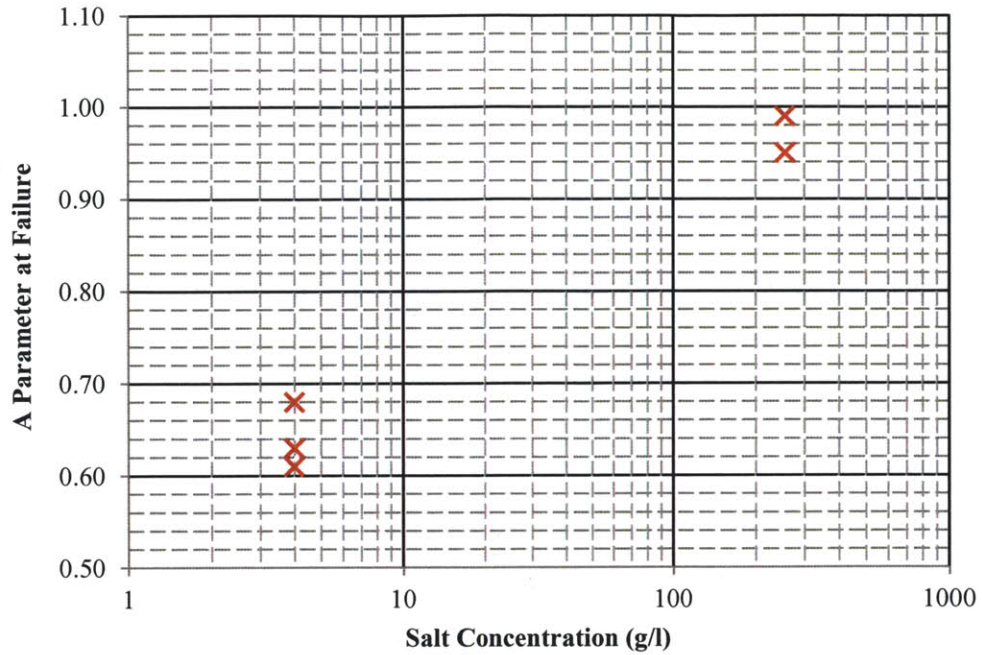


Figure 5.81 Relationship between A parameter at failure and salt concentration for natural RBBC Series IV from CK_0UC testing

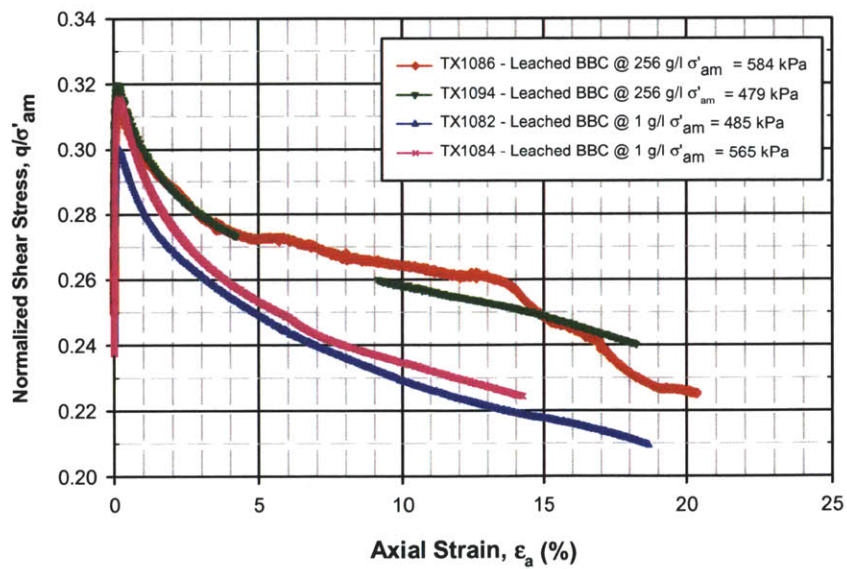


Figure 5.82 Normalized stress-strain curve for NC leached BBC at different pore fluid salinities from CK_0UC triaxial tests

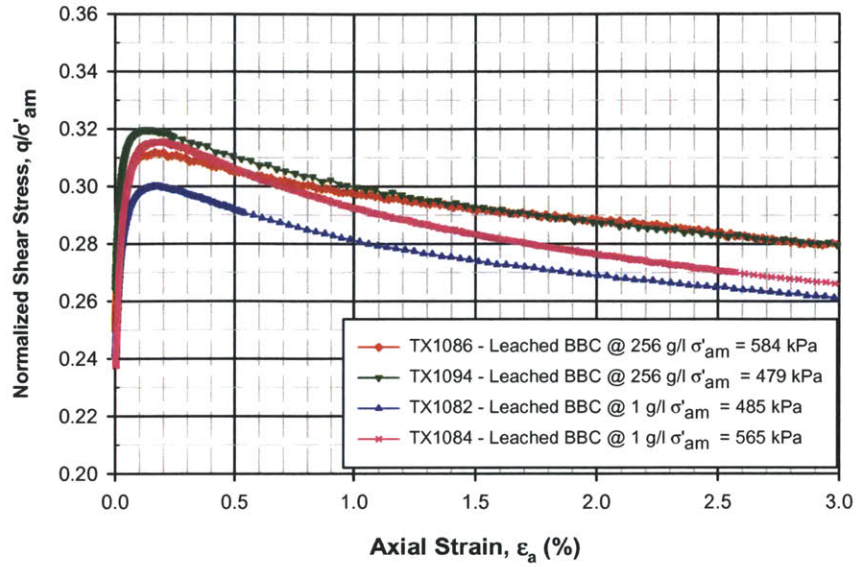


Figure 5.83 Normalized stress-strain curves (small strains) for NC leached BBC at different pore fluid salinities from CK₀UC triaxial tests

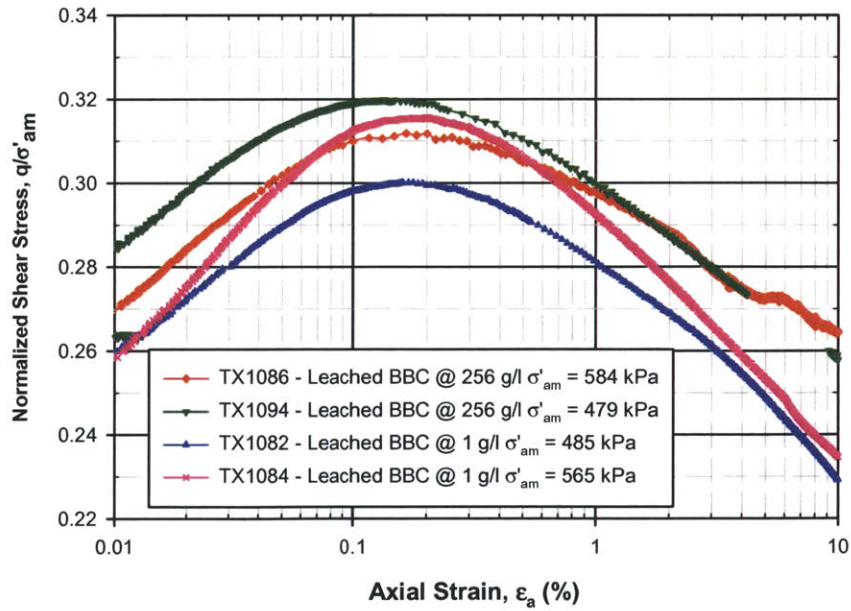


Figure 5.84 Normalized stress-(log)strain curves for NC leached BBC at different pore fluid salinities from CK₀UC triaxial tests

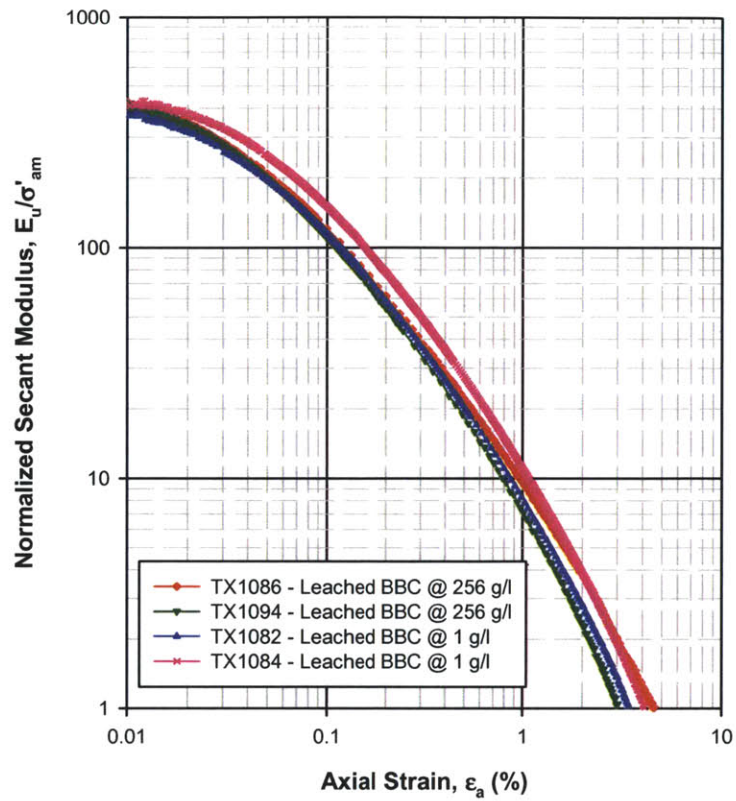


Figure 5.85 Normalized undrained secant modulus versus axial strain for NC leached BBC at different pore fluid salinities from CK₀UC triaxial tests

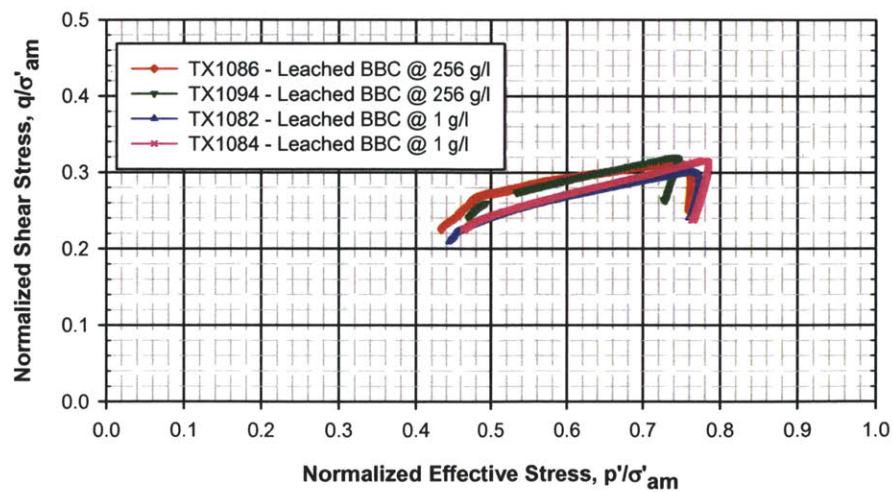


Figure 5.86 Normalized effective stress path for NC leached BBC at different pore fluid salinities from CK₀UC triaxial testing

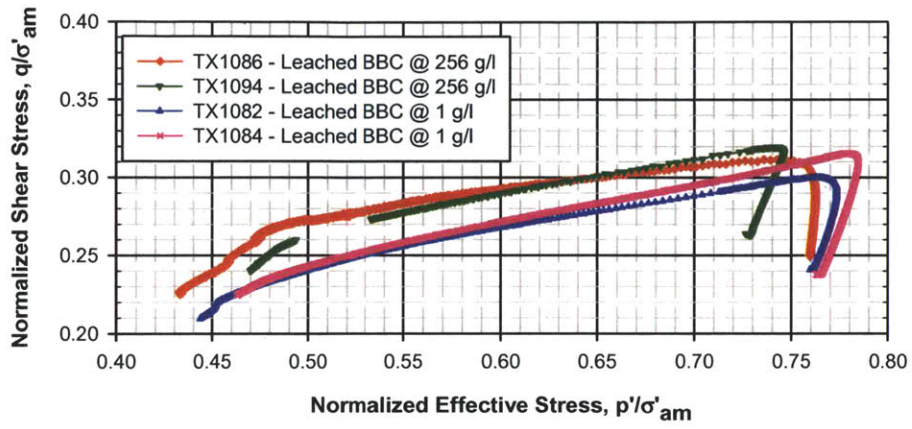


Figure 5.87 Normalized effective stress path (close up view) for NC leached BBC at different pore fluid salinities from CK₀UC triaxial testing

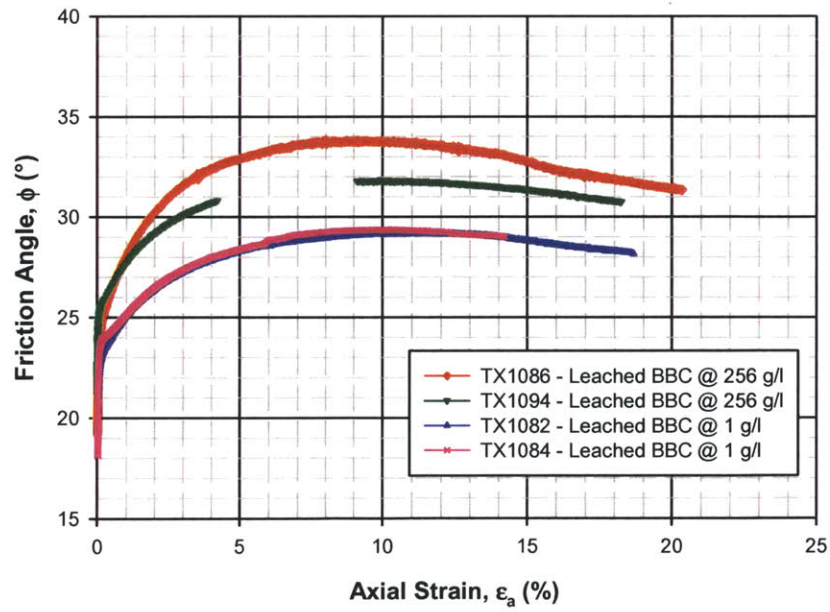


Figure 5.88 Friction angle versus axial strain for NC leached BBC at different pore fluid salinities from CK₀UC triaxial tests

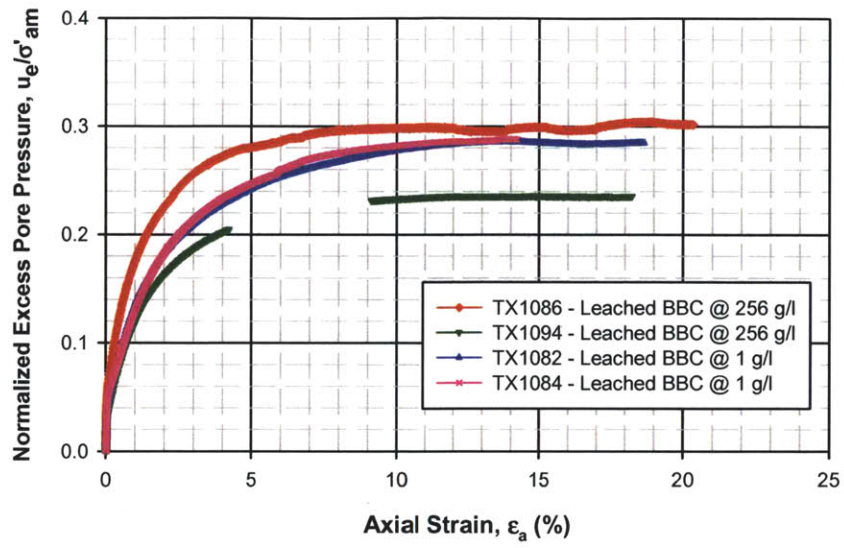


Figure 5.89 Normalized excess pore pressure versus axial strain for NC leached RBBC from CK₀UC triaxial tests

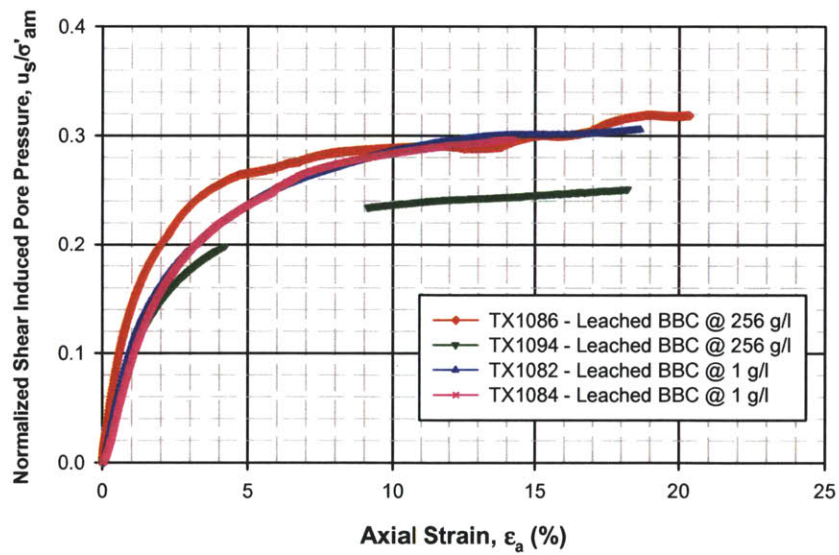


Figure 5.90 Normalized shear induced pore pressure versus axial strain for NC leached RBBC from CK₀UC triaxial tests

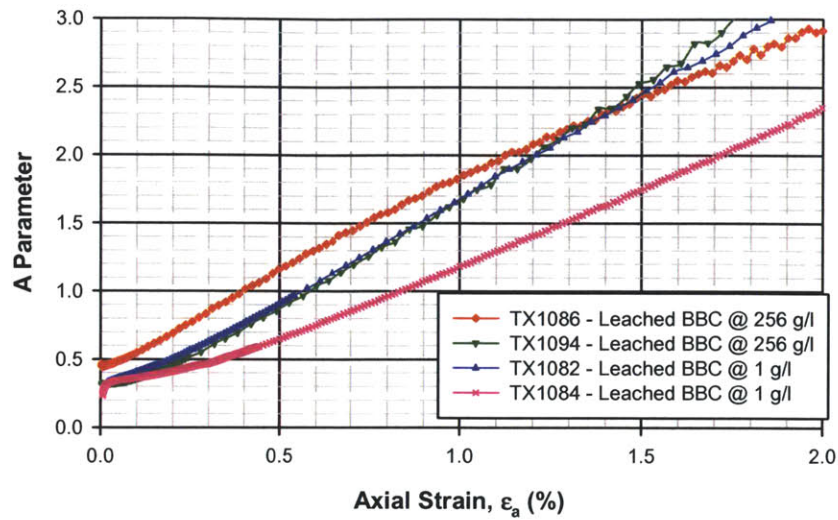


Figure 5.91 A parameter versus axial strain (small strains) for NC leached BBC at different pore fluid salinities from CK₀UC triaxial testing

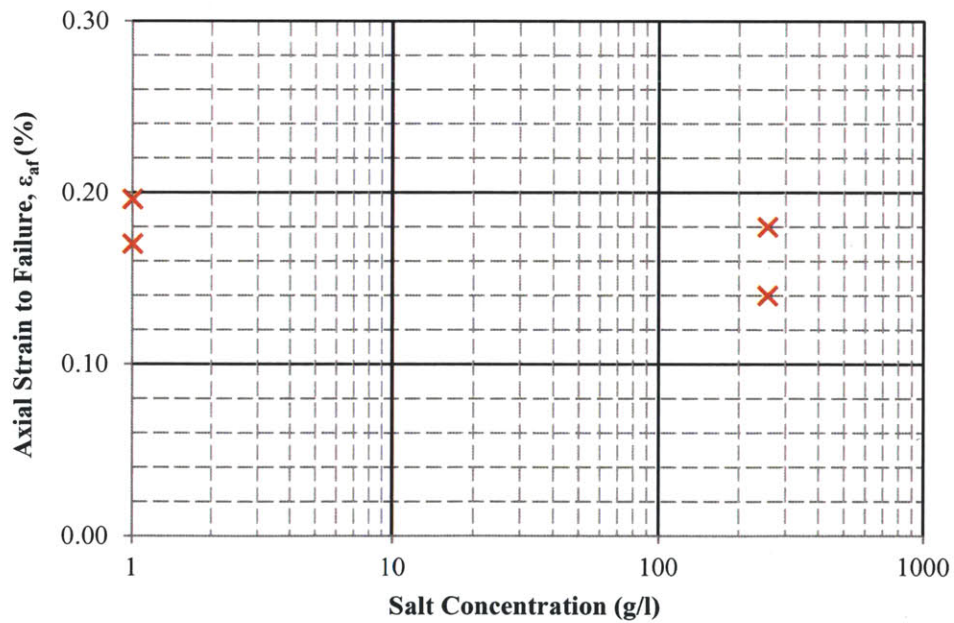


Figure 5.92 Relationship between axial strain to failure and salt concentration for natural leached BBC from CK₀UC triaxial testing

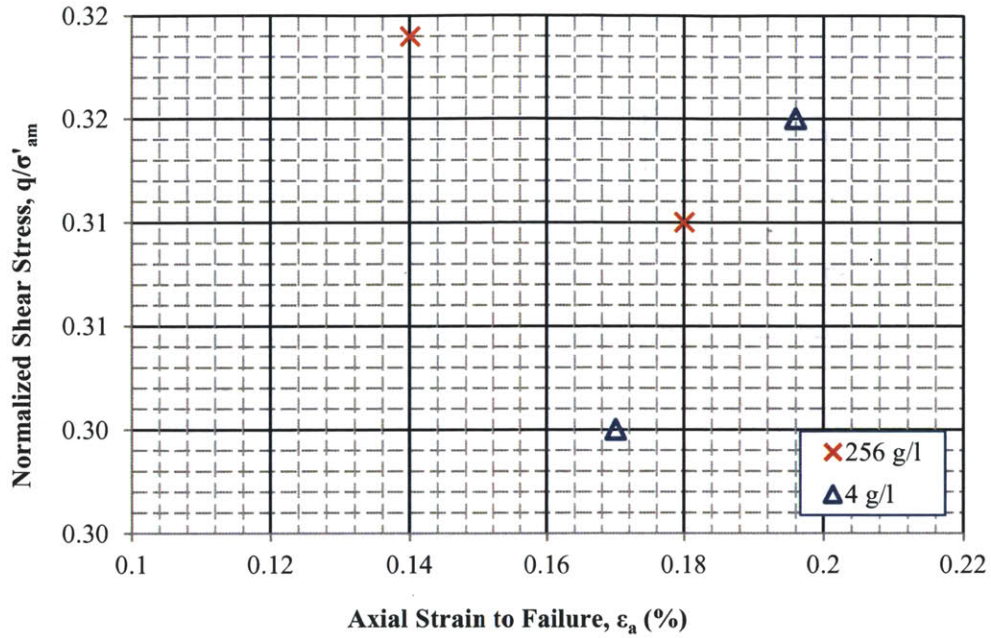


Figure 5.93 Relationship between normalized shear stress and axial strain failure for leached BBC from CK_0UC triaxial testing

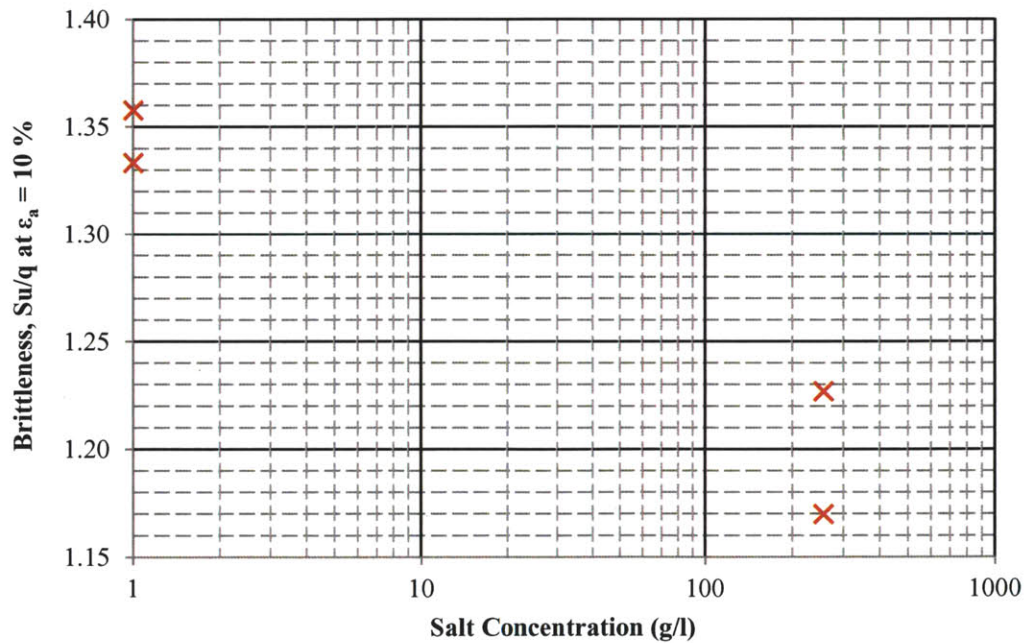


Figure 5.94 Plot of soil brittleness at an axial strain of 10 % as a function of pore fluid salinity for leached RBBC

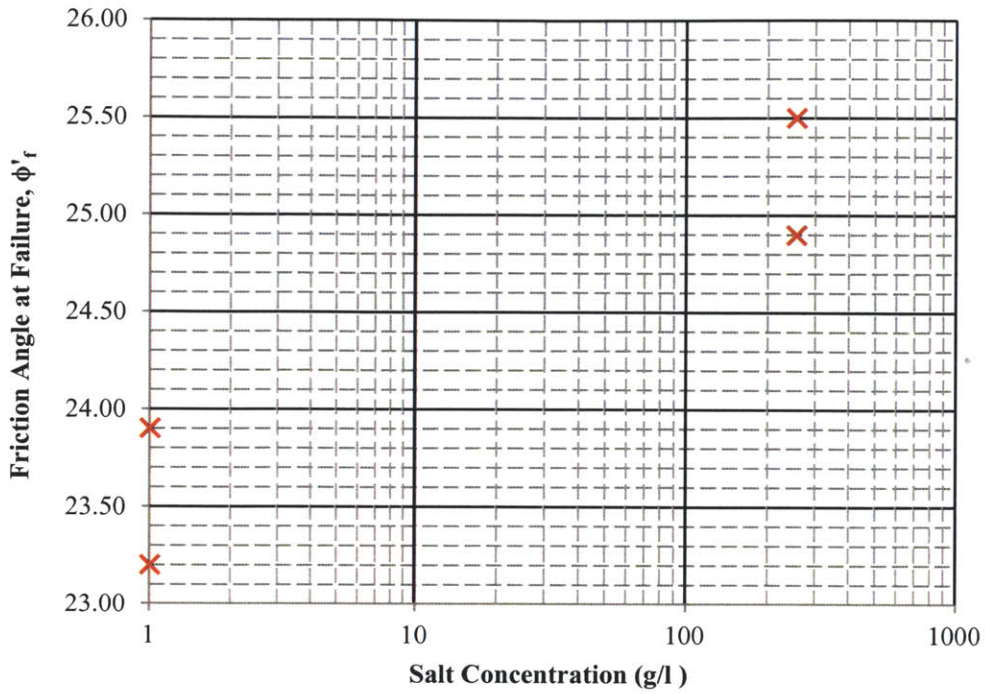


Figure 5.95 Relationship between salinity and friction angle at failure for leached BBC from CK₀UC triaxial testing

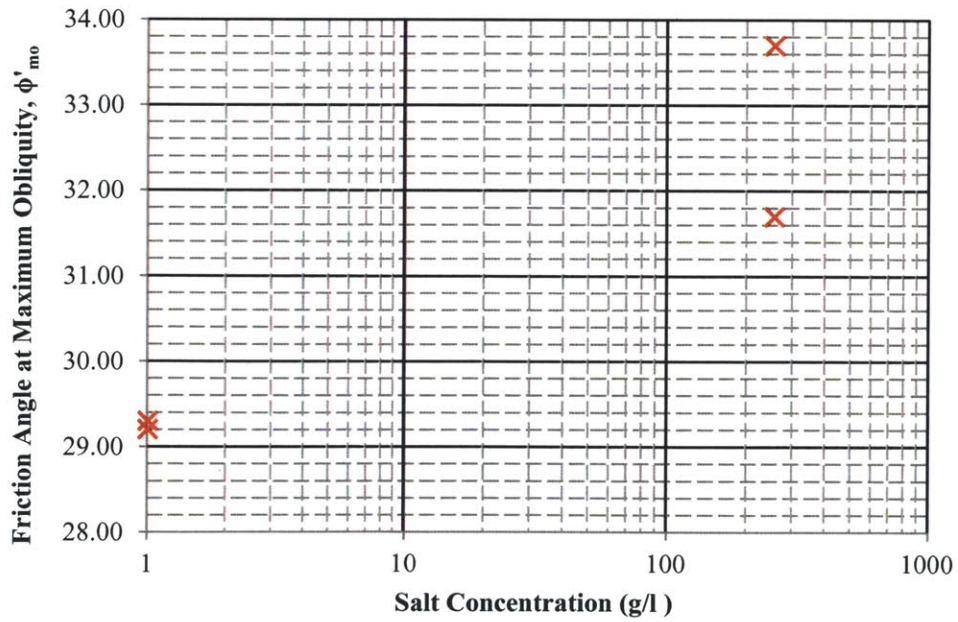


Figure 5.96 Relationship between salinity and friction angle at maximum obliquity for leached BBC from CK₀UC triaxial testing

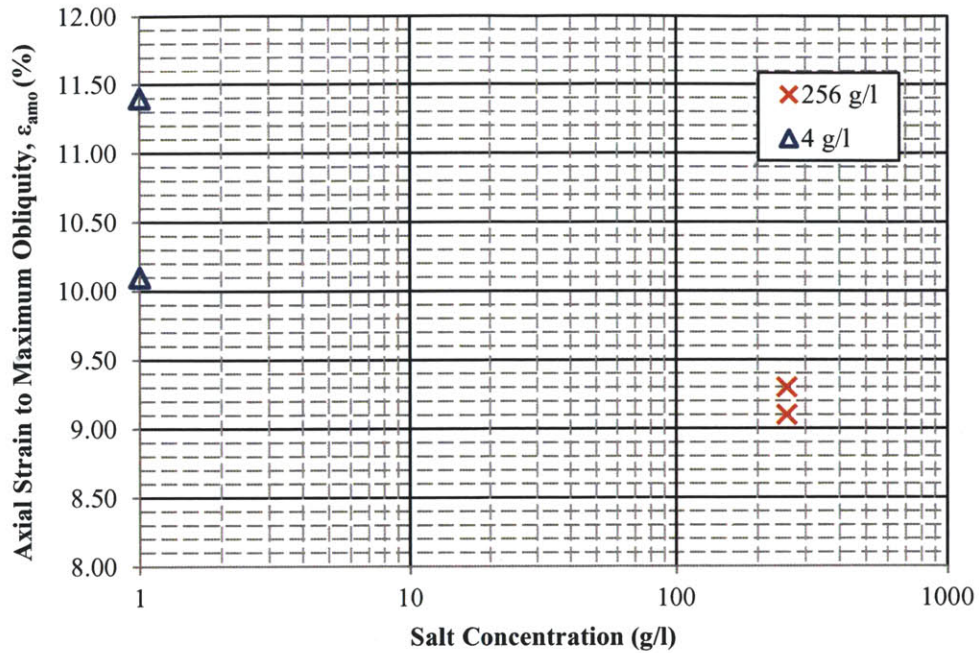


Figure 5.97 Relationship between salinity and axial strain at maximum obliquity for leached BBC from CK₀UC triaxial testing

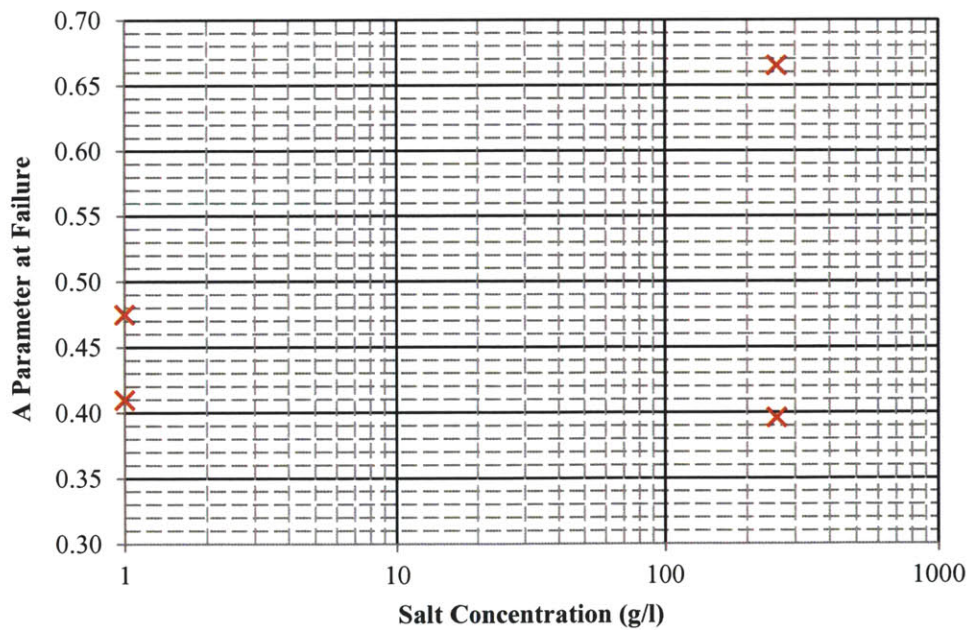


Figure 5.98 Relationship between A parameter at failure and salt concentration for leached BBC from CK₀UC testing

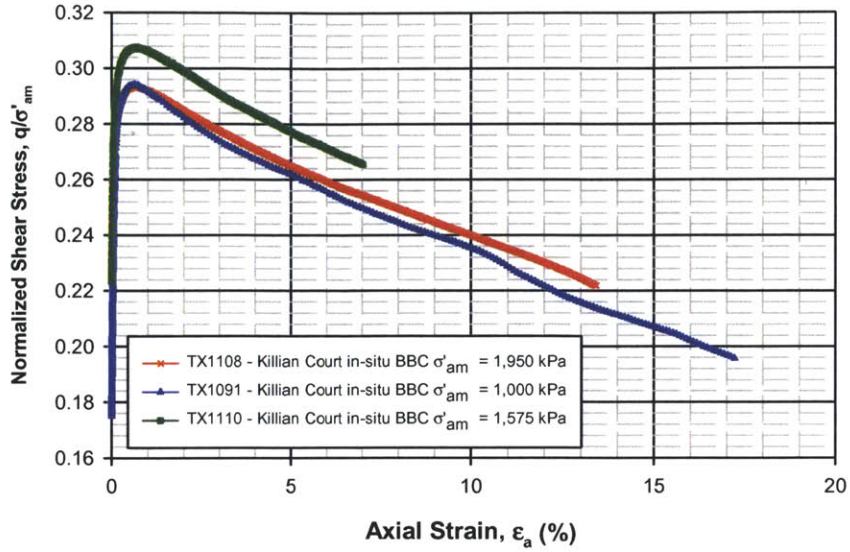


Figure 5.99 Normalized stress-strain curve for NC Killian Court in-situ BBC from CK₀UC triaxial tests

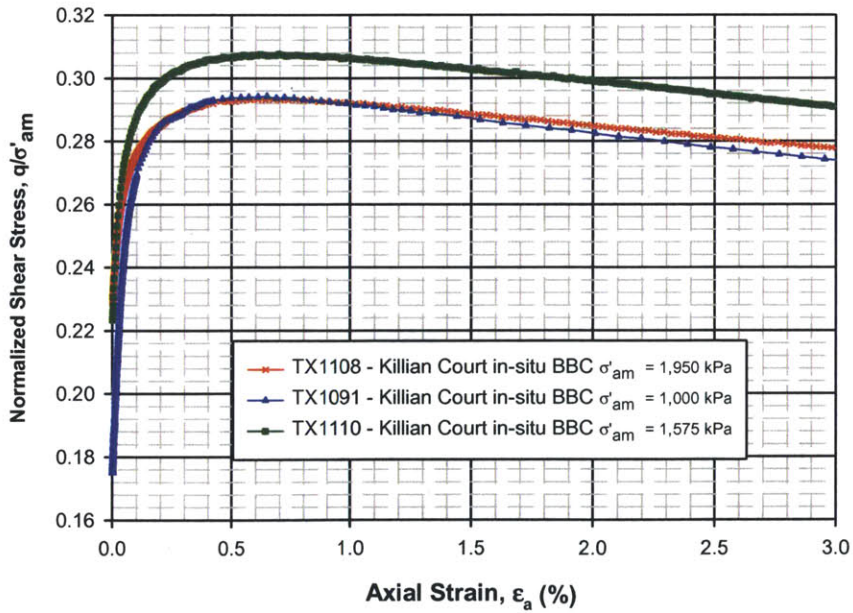


Figure 5.100 Normalized stress-strain curves (small strains) for NC Killian Court in-situ BBC from CK₀UC triaxial tests

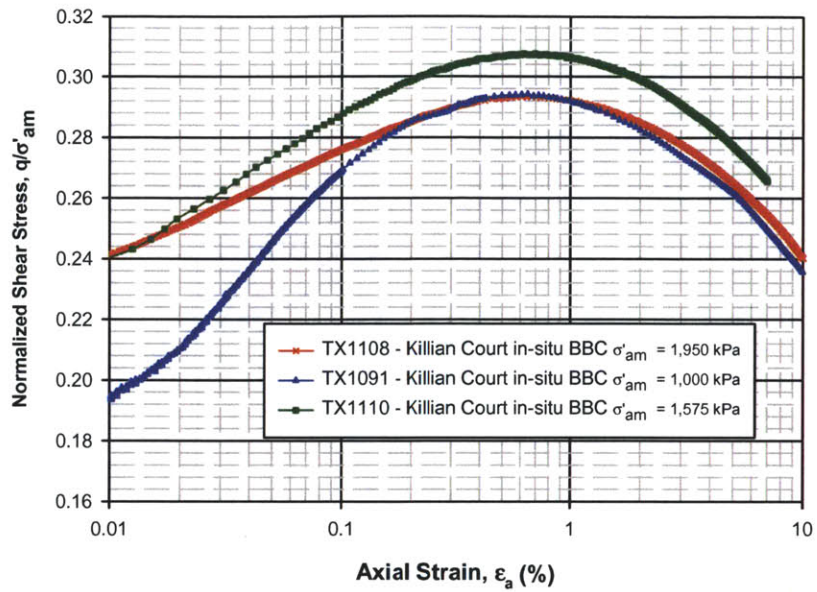


Figure 5.101 Normalized stress-strain curves (log strain) for NC Killian Court in-situ BBC from CK₀UC triaxial tests

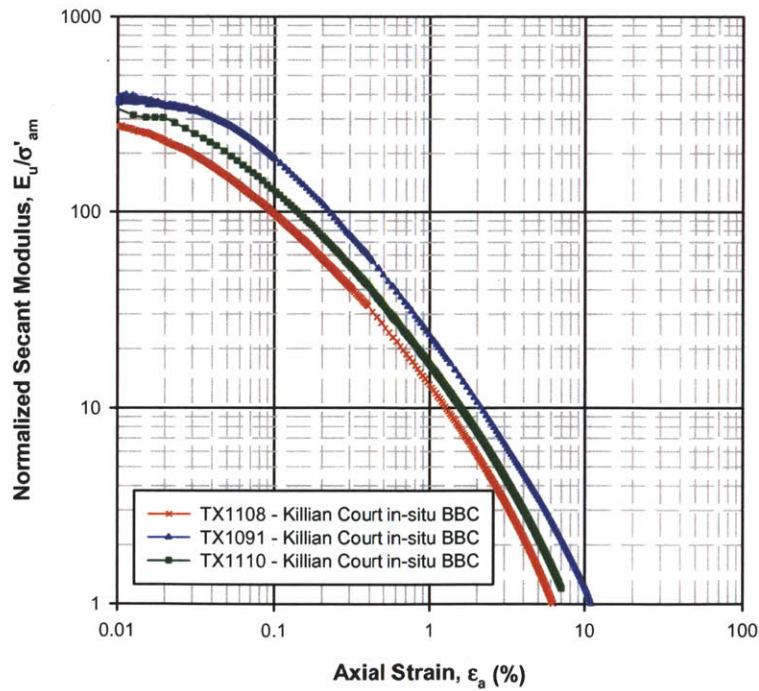


Figure 5.102 Normalized undrained secant modulus versus axial strain for NC Killian Court in-situ BBC from CK₀UC triaxial tests

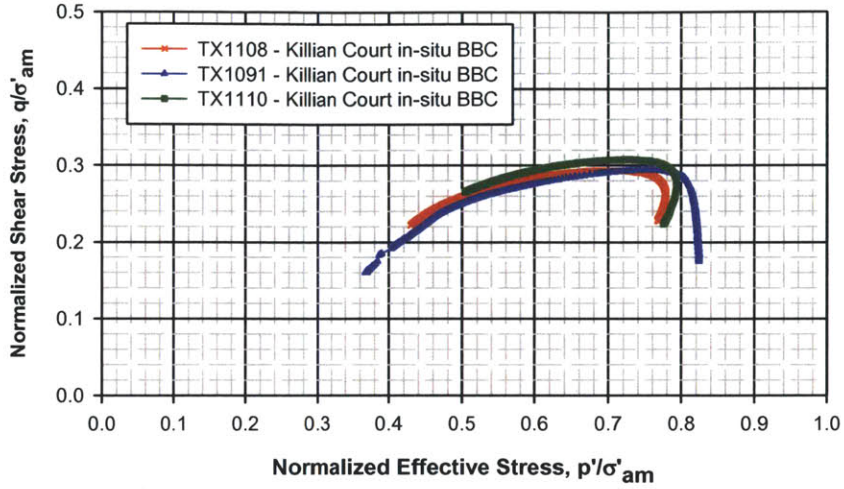


Figure 5.103 Normalized effective stress path for NC Killian Court in-situ BBC from CK_0UC triaxial testing

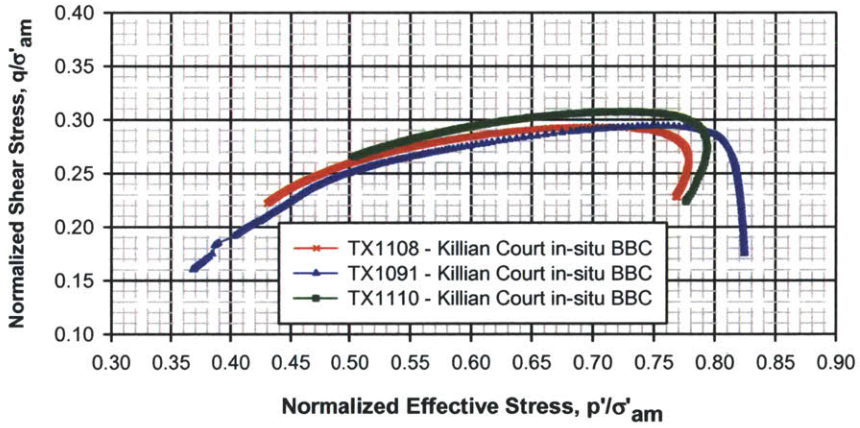


Figure 5.104 Normalized effective stress path (close up view) for Killian Court in-situ BBC from CK_0UC triaxial testing

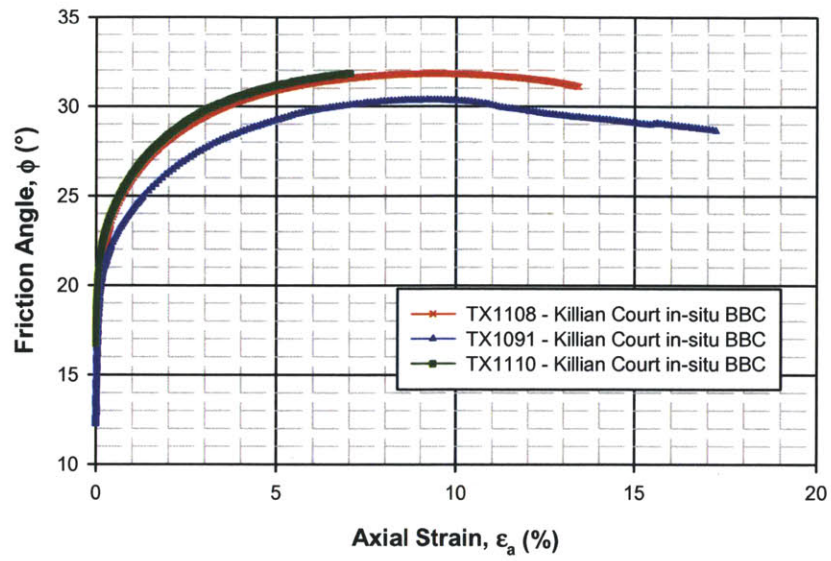


Figure 5.105 Friction angle versus axial strain for NC Killian Court in-situ BBC from CK₀UC triaxial tests

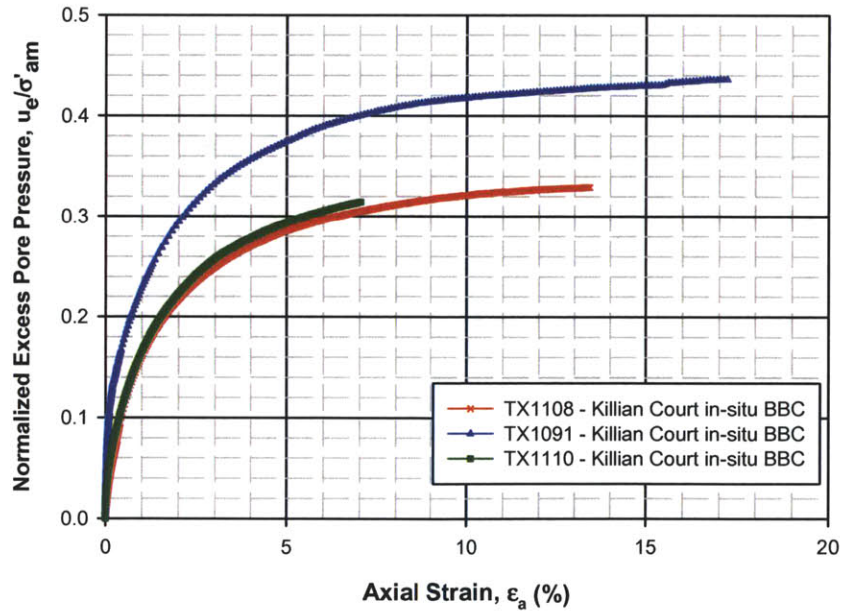


Figure 5.106 Normalized excess pore pressure versus axial strain for Killian Court in-situ BBC from CK₀UC triaxial tests

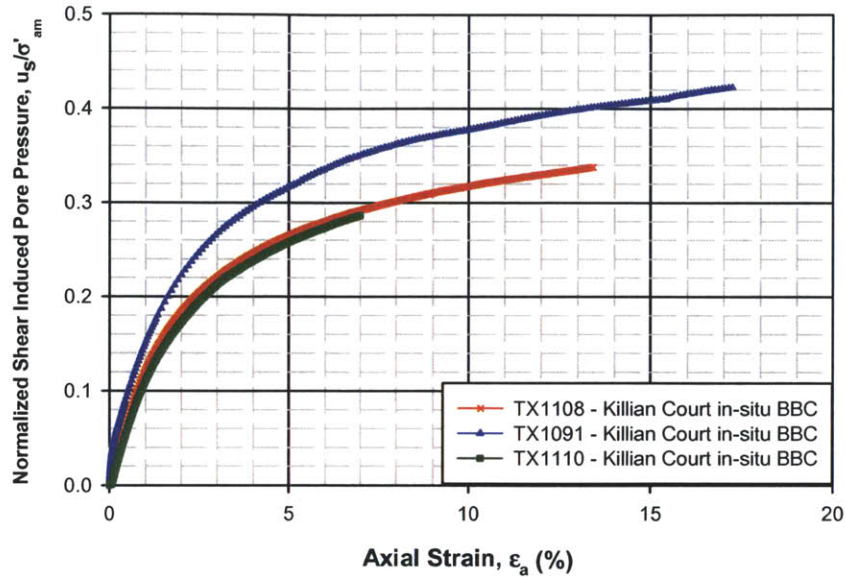


Figure 5.107 Normalized shear induced pore pressure versus axial strain for Killian Court in-situ BBC from CK₀UC triaxial tests

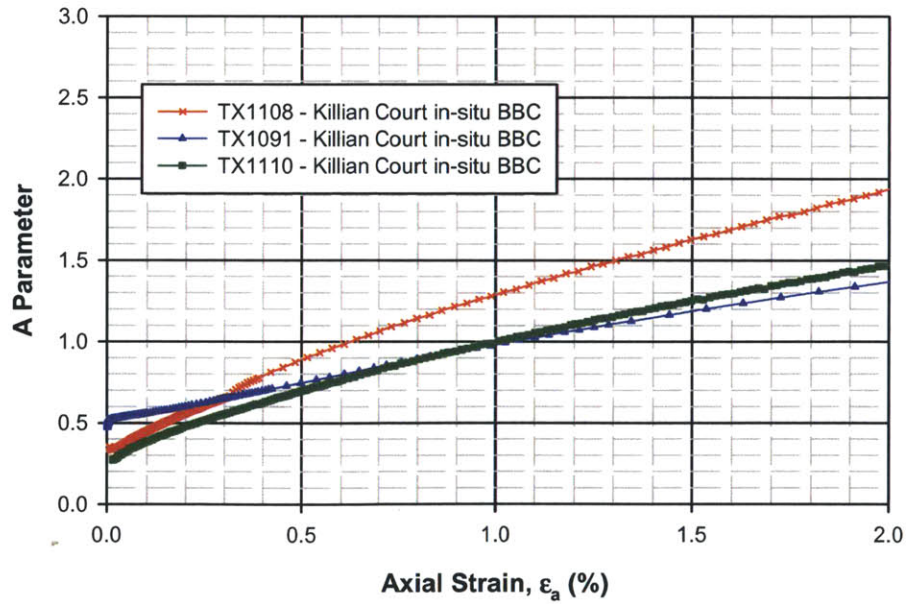


Figure 5.108 A parameter versus axial strain (small strains) for NC Killian Court in-situ BBC from CK₀UC triaxial testing

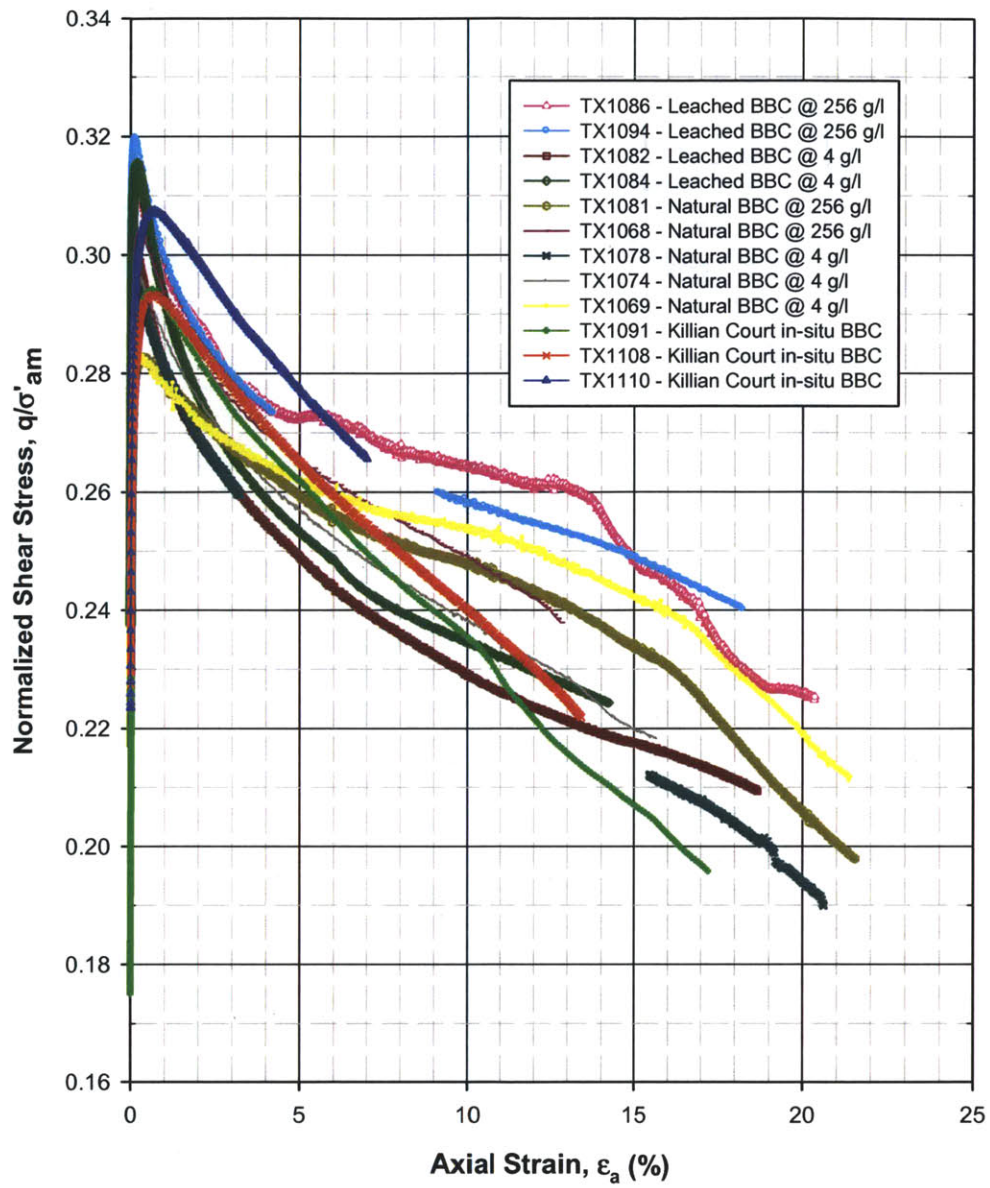


Figure 5.109 Normalized stress-strain curve synthesis plot for all types of NC BBC from CK₀UC triaxial tests

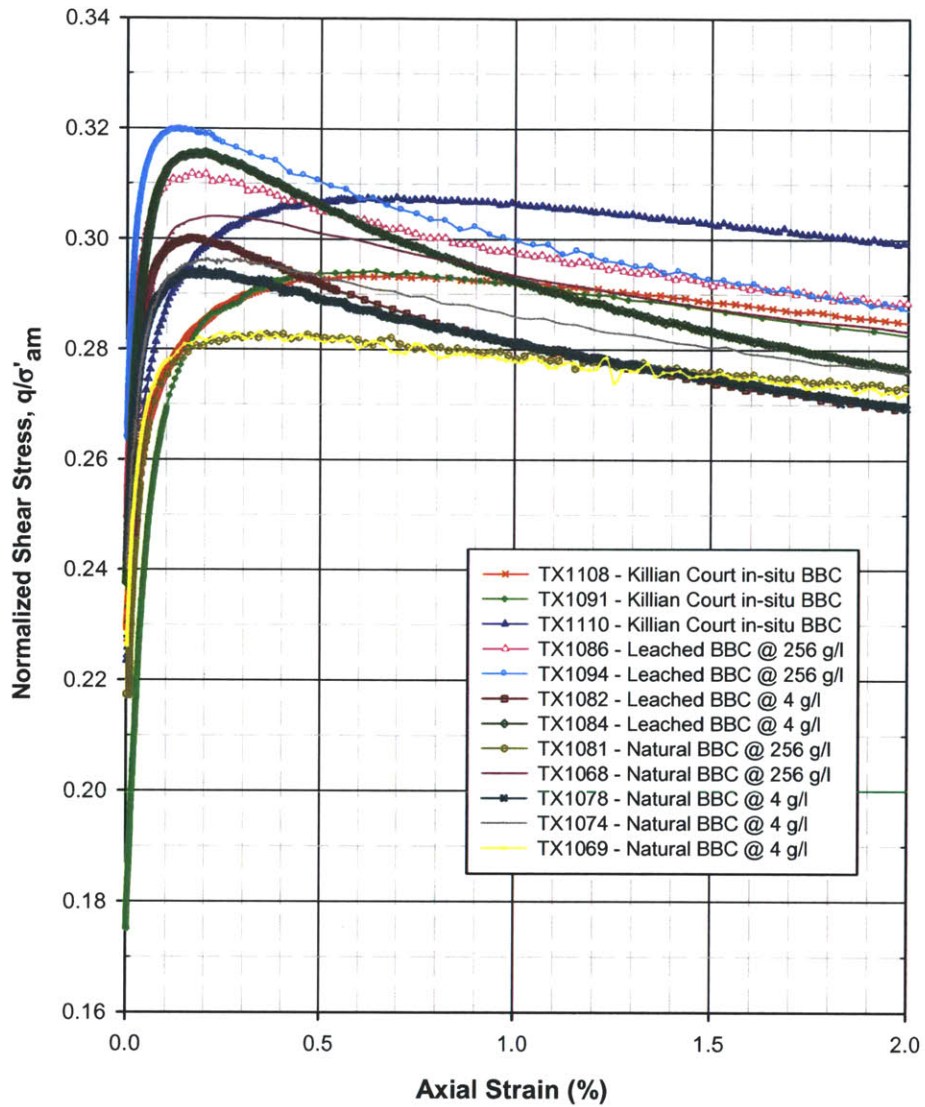


Figure 5.110 Normalized stress-strain curves (small strains) synthesis plot all types of NC BBC from CK_0UC triaxial tests

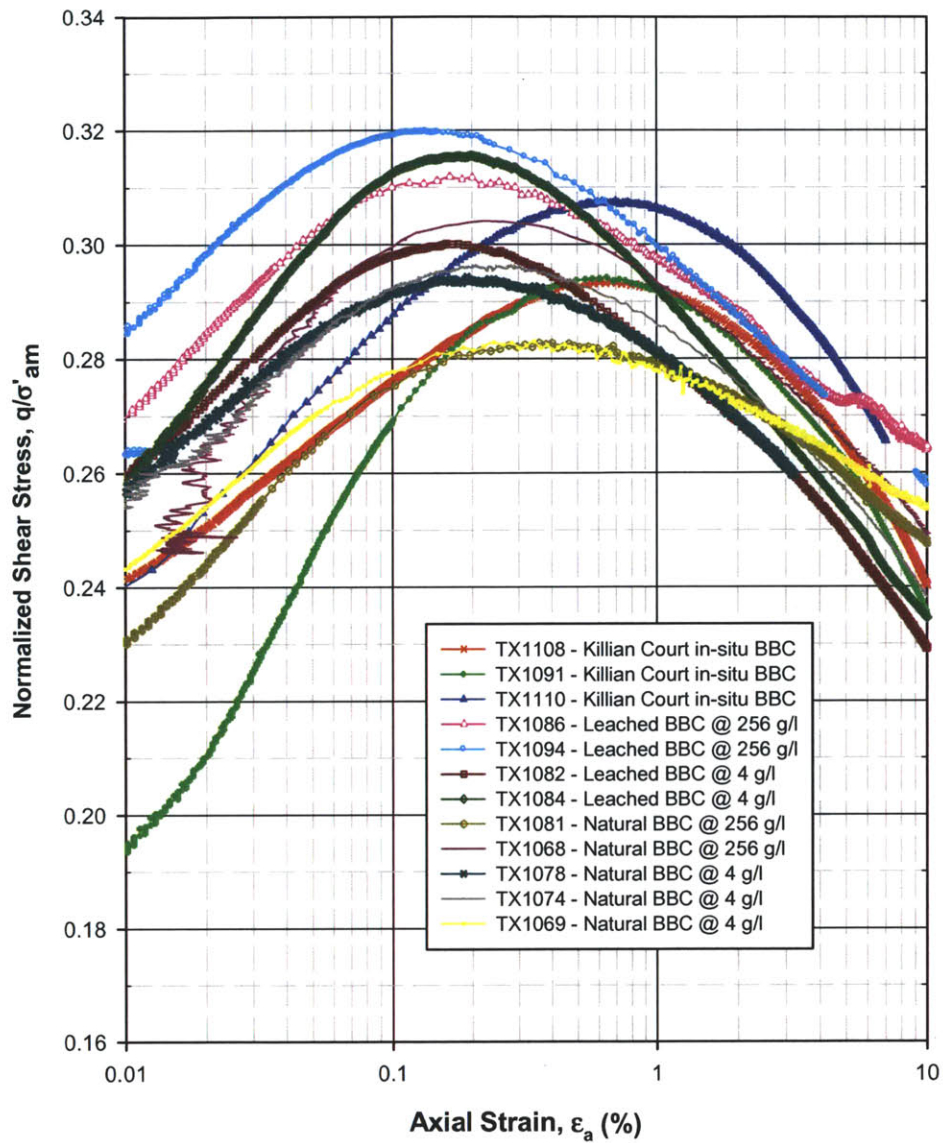


Figure 5.111 Normalized stress-strain curves (log strains) synthesis plot all types of NC BBC from CK_0UC triaxial tests

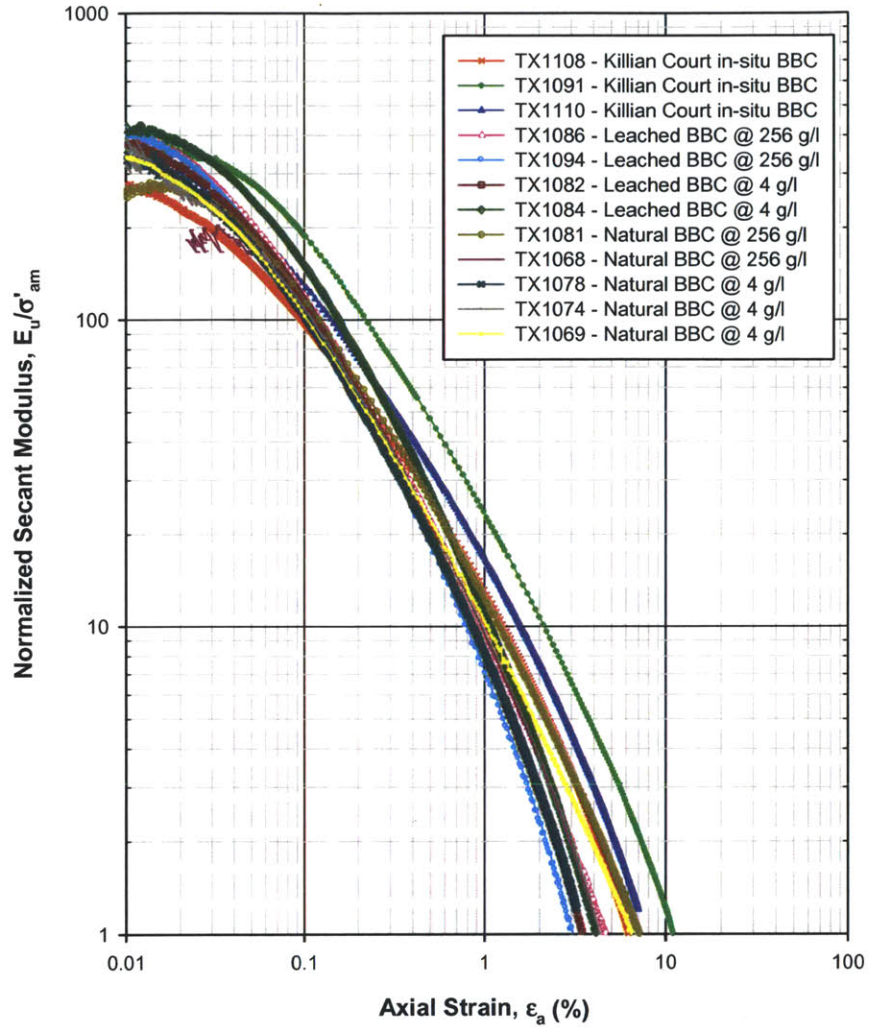


Figure 5.112 Normalized undrained secant modulus versus axial strain synthesis plot for all types of NC BBC from CK_0UC triaxial tests

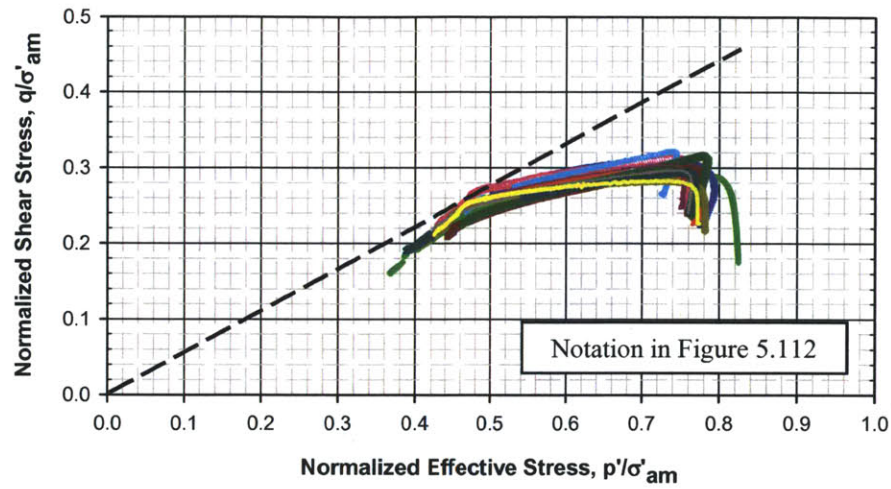


Figure 5.113 Normalized effective stress path synthesis plot for all types of NC BBC from CK₀UC triaxial testing (legend can be seen in Figure 5.111)

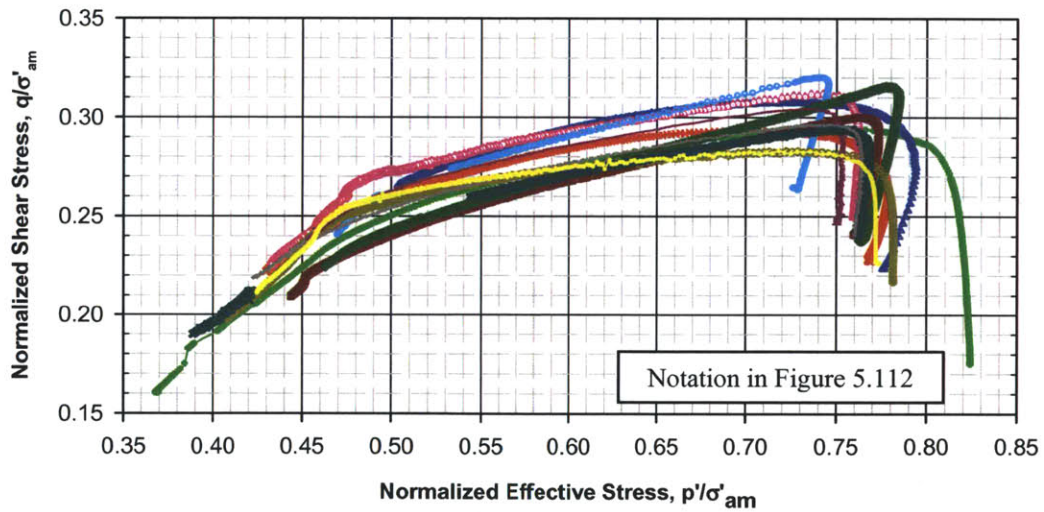


Figure 5.114 Normalized effective stress path synthesis plot (close up view) for all types of NC BBC from CK₀UC triaxial testing (legend can be seen in Figure 5.111)

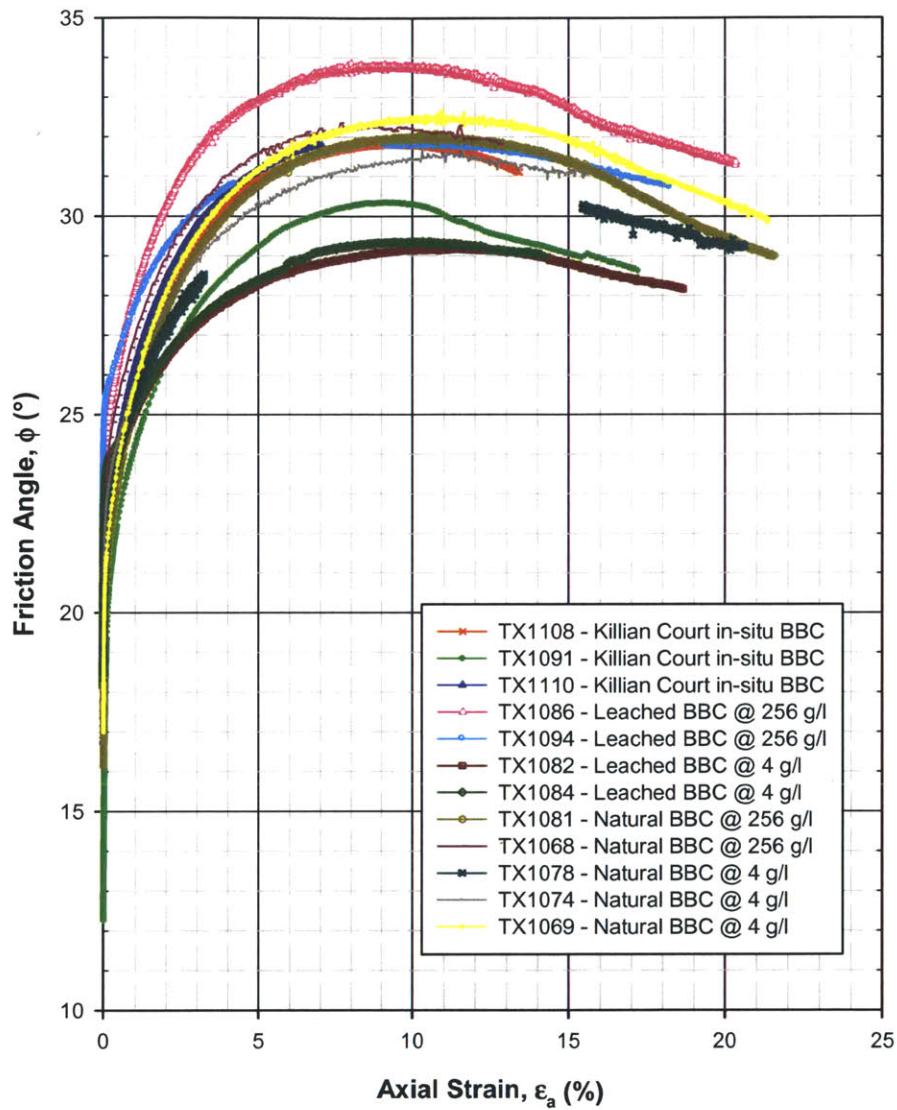


Figure 5.115 Friction angle versus axial strain synthesis plot for all types of NC BBC from CK_0UC triaxial tests

Figure 5.116 Friction angle at peak and maximum obliquity versus stress level for NC RBBC from CK₀UC triaxial tests (Abdulhadi, 2009)

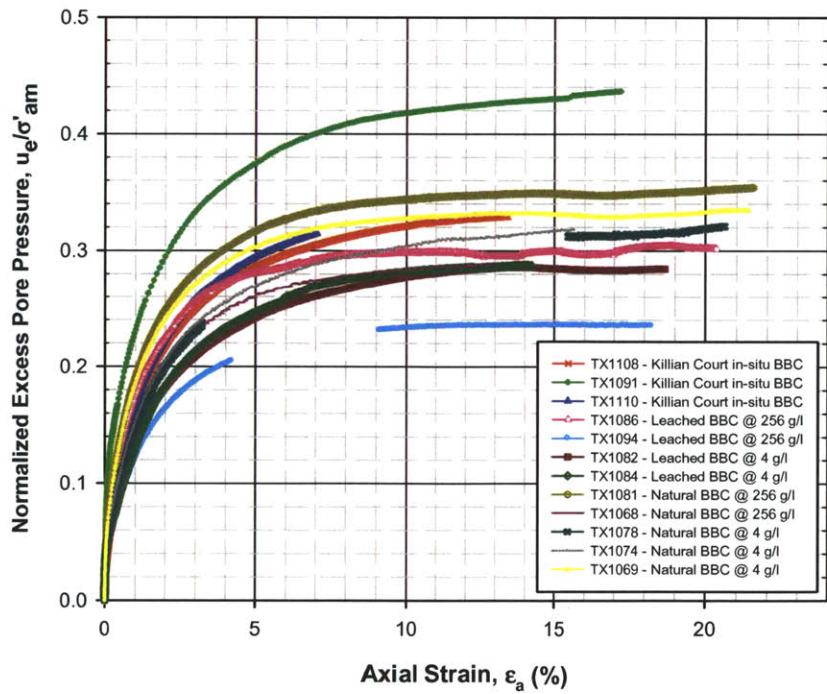


Figure 5.117 Normalized excess pore pressure versus axial strain synthesis plot for all types of NC BBC from CK₀UC triaxial tests

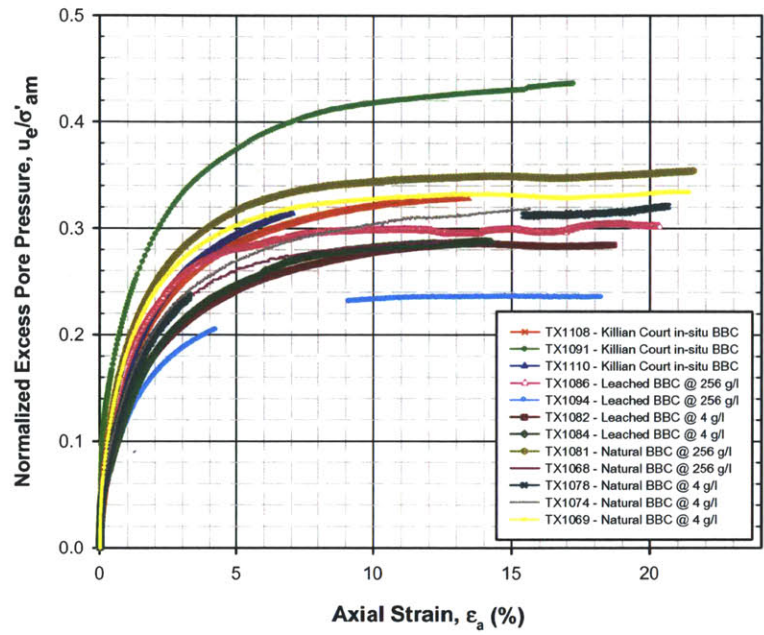


Figure 5.118 Normalized shear induced pore pressure versus axial strain synthesis plot for all types of NC BBC from CK_0UC triaxial tests

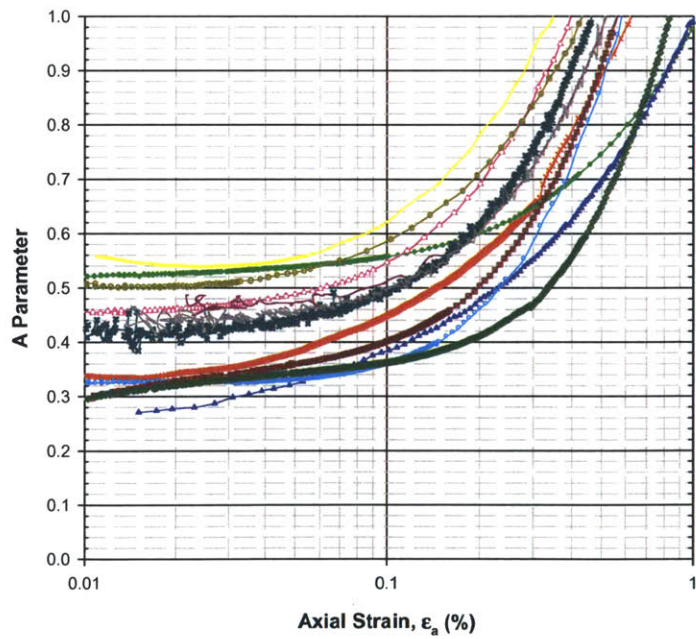


Figure 5.119 A parameter versus axial strain synthesis plot for all types of NC BBC from CK_0UC triaxial tests

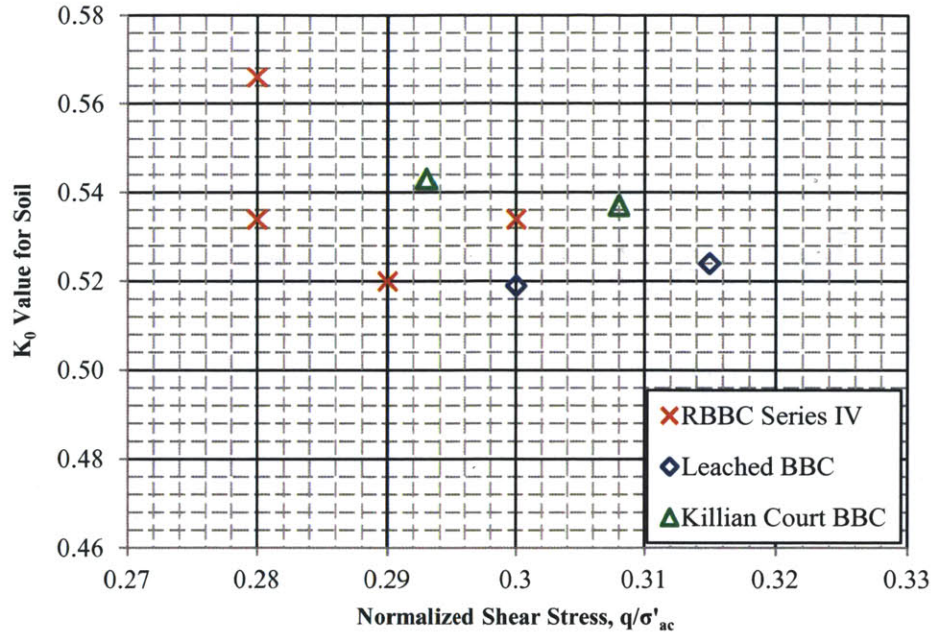


Figure 5.120 Relationship between K_0 value and normalized shear stress for all types of BBC in testing program from CK_0UC triaxial testing

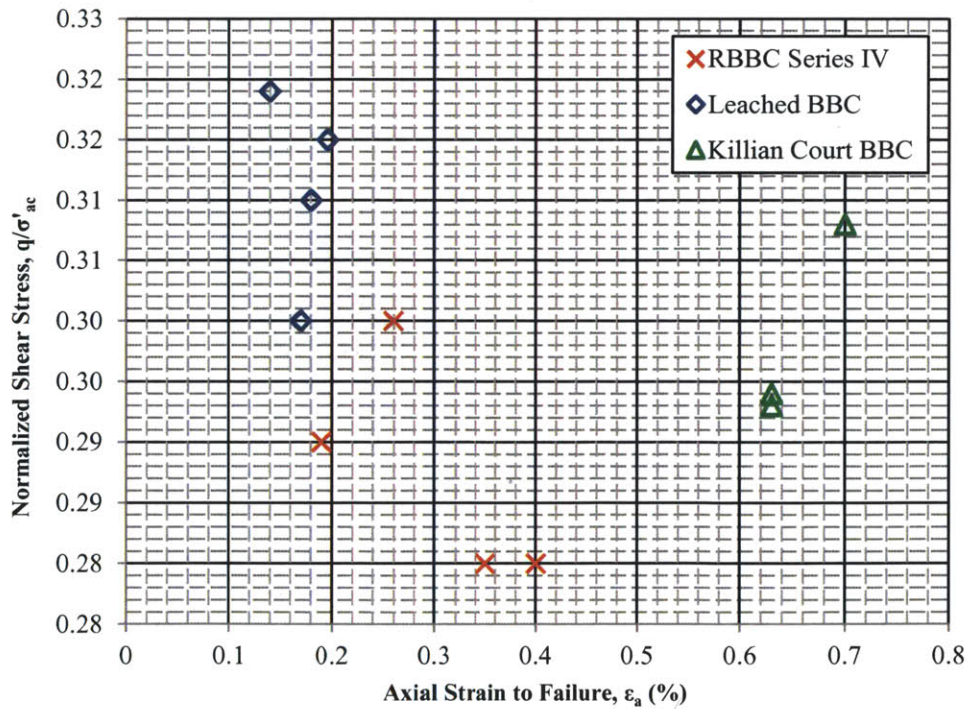


Figure 5.121 Relationship between axial strain to failure and normalized shear stress for all types of BBC in the testing program from CK_0UC triaxial testing

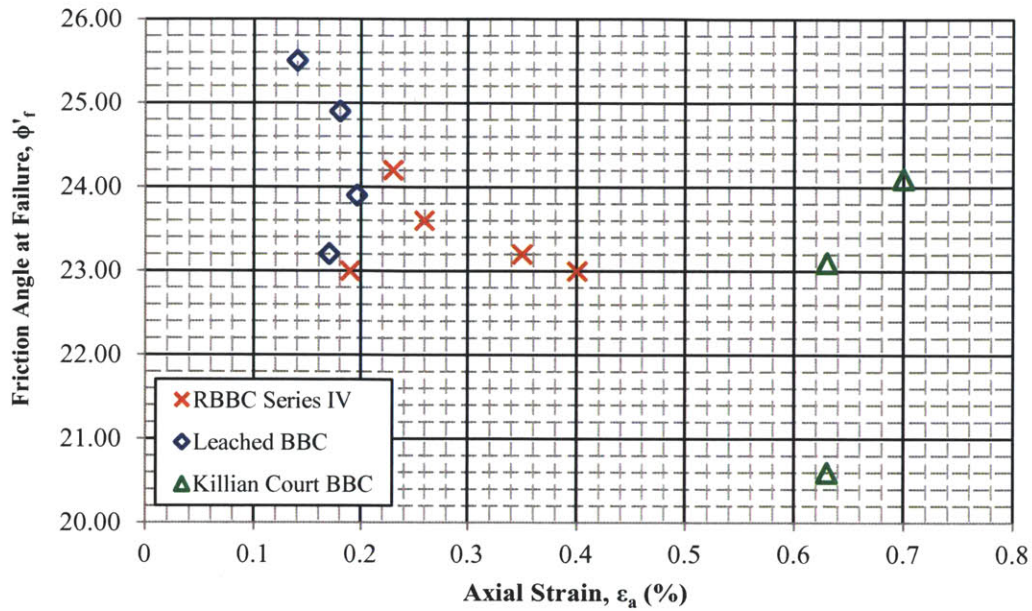


Figure 5.122 Relationship between friction angle at failure and axial strain for all types of BBC in testing program from CK₀UC triaxial testing

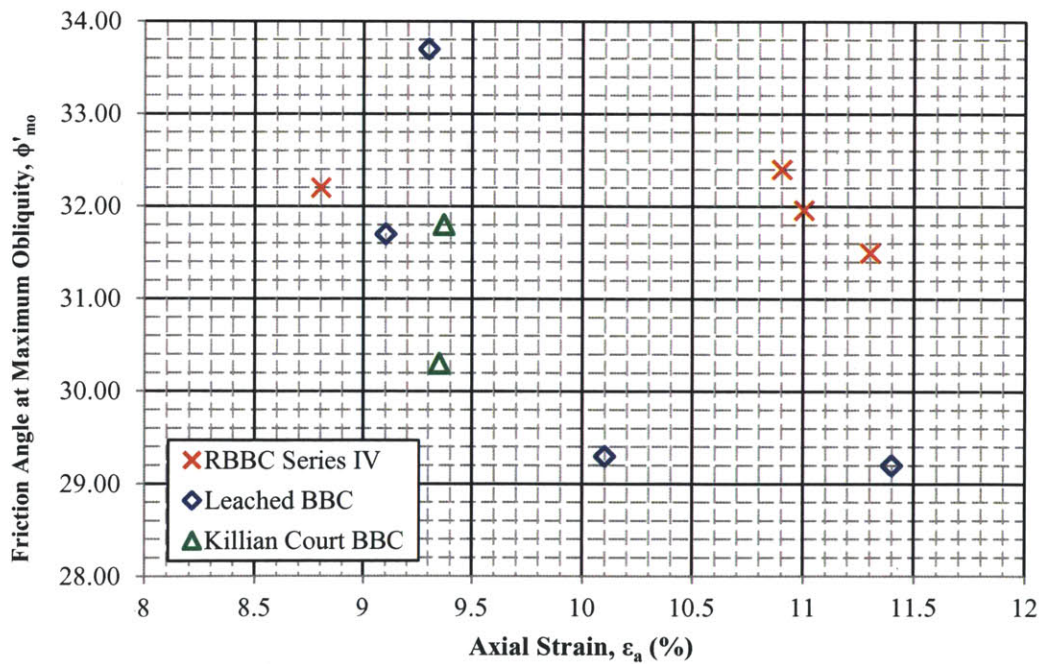


Figure 5.123 Relationship between friction angle at maximum obliquity and axial strain for all types of BBC in testing program from CK₀UC triaxial testing

6 REVIEW & CONCLUSIONS

6.1 INTRODUCTION

Pore fluid salinities in the Gulf of Mexico region can reach levels of 250 g/l after a soil has been deposited in a less saline environment. It was uncertain what effect, if any, this increase in salinity would have on the mechanical behavior of the soils which were subjected to it. Research in this area was therefore performed in order to determine what changes should be anticipated. The research involved analyzing a large bank of results obtained from several experimental procedures as well as images taken of the fabric at different stress and salinity levels, and drawing conclusions.

6.2 REVIEW OF RESEARCH UNDERTAKEN

The research involved varying the pore fluid salinity of several types of natural soils, as well as a pure clay mineral in order to determine the resulting effects on the mechanical behavior. In addition to varying the salinity, the fabric of Boston Blue Clay was also altered in an attempt to enhance the observed effects. This fabric was altered by leaching some of the natural salt from the batch of BBC Series IV, and also by deflocculating the existing fabric with sodium hexametaphosphate. In total, four derivatives of Boston Blue Clay were used in the testing program. Intact Killian Court BBC was also tested as part of the research in order to provide a benchmark against which other BBC derivatives would be measured. The majority of the testing was performed on BBC for this thesis.

Other soils tested include resedimented London Clay, Gulf of Mexico soil from the Ursa Basin and sodium montmorillonite. London Clay and sodium montmorillonite were resedimented with different pore fluid salinities ranging from 1-256 g/l. RGOM-Ursa soil was resedimented with 0 g/l pore fluid (distilled water).

An extensive testing program was undertaken whereby the one dimensional consolidation behavior of all soils was tested using a modified Constant Rate of Strain (CRS) device. These tests also produced hydraulic conductivity (k_v) and coefficient of consolidation (c_v) data for the

given soils. An analysis was then performed comparing the behavior of all soils given different pore fluid environments. Triaxial testing (CK_0UC) was also performed on three derivatives of BBC in order to determine the strength characteristics of the soil and how they changed with a corresponding change in salinity. The soils tested were natural RBBC Series IV, leached RBBC and Killian Court in-situ material.

Scanning Electron Microscope (SEM) images were taken from several oven dried specimens in the vertical plane. These images represent different soil types resedimented to different pore fluid salinities and taken at different stress levels. An extensive analysis was performed on these images and conclusions were drawn as to how the fabric of the soil evolves as the stress level changes.

6.3 RESULTS AND CONCLUSIONS

Although the primary focus of this research was based on the effects of pore fluid salinity on the mechanical behavior of normally consolidated soils, interesting side observations have been recorded in relation to how the fabric of a given soil evolves as the stress level changes.

6.3.1 OBSERVED EFFECTS ON MECHANICAL PROPERTIES

6.3.1.1 ONE DIMENSIONAL CONSOLIDATION BEHAVIOR

It was shown for natural RBBC Series IV, pore fluid salinity is not a factor when it comes to the one dimensional consolidation behavior and hydraulic conductivity. Similar strains to a given axial effective stress are required. Very comparable void ratios are also produced at given axial effective stress state for all salinities tested. In the pore fluid salinity range 4-256 g/l, very little change was observed in the behavior of resedimented BBC Series IV. Any change which was recorded cannot be correlated to the changing salinity. It was noted that at some stress level for RBBC Series IV, a change in the slope of the hydraulic conductivity line in void ratio space can be correlated to a change in the coefficient of consolidation value. This behavior was observed across all salinities and the change was noted at an axial effective stress level of $\sim 2,000$ kPa. It was postulated that this behavior is in fact breaking of reminiscent flocs in the soil fabric which have begun collapsing, therefore rearranging the soil fabric at the micro level.

When some of the natural salt was leached from RBBC Series IV and the resultant powder resedimented to different pore fluid salinities, changes in behavior were recorded. It was shown that when working with resedimented leached BBC, a larger void ratio was observed for an increase in pore fluid salinity. The leaching process increased the sensitivity of the resultant BBC powder to the presence of salt. It was observed in the compression behavior that with an increase in salinity, an increase in strain was required to a given axial effective stress. Despite the differences in initial void ratio for the different salinities, all soils tested had similar compression behavior in void ratio space. In the lower stress region ($\sigma'_{ac} = 1,000$ kPa), the lower salinity specimens give a lower void ratio at a given axial effective stress, however, given the more compressible nature of the high salinity soils, this trend shows signs of reversal at an axial effective stress of 10,000 kPa. Similar “kinks” to those observed in the natural RBBC Series IV are seen in the c_v and k_v data for leached soil, but this time at higher stress levels indicating that flocs still exist in the matrix after the leaching process.

In an attempt to disperse flocs in the soil, sodium Hexametaphosphate was used on a quantity of natural BBC Series IV powder. The resultant powder was resedimented to a pore fluid salinity of 0 g/l and then CRS tested. The results show that although the sodium hex BBC is born of the same “raw materials” as both natural RBBC Series IV and leached RBBC, a much lower initial void ratio (~20 % lower) is seen. It is further postulated that the difference in load carrying capacity of sodium hex BBC as opposed to Killian Court in-situ BBC at a given void ratio be taken as a crude first estimate as to the electro-chemical forces which exist in the soil and aid stress transfer through the matrix. Sodium hex BBC is the stiffest derivative of all BBC soils tested with the lowest c_c value. This demonstrates that the sodium hex derivative is a more-dense soil than other BBC types as less of a reduction in void ratio is recorded for a given increase in axial effective stress. Unlike the prior two RBBC derivatives, the c_v and k_v curves for sodium hex do not display the same changes in behavior. The c_v curve now resembles what would be considered a more traditional path with an increase in stress level. Once the preconsolidation pressure is passed, a gradual and continuous rise in c_v is noted throughout the test. This shows that the cause of the change in behavior at a given stress level for natural RBBC Series IV and leached RBBC has been eliminated by dispersing the flocs with sodium hex therefore lending weight to the theory that floc breakage is responsible for changes in c_v and k_v .

The effectiveness of the resedimentation procedure was analyzed against tests performed on intact BBC recovered from the Killian Court area on the MIT campus. The results show that Killian Court in-situ material requires much less axial strain to a given axial effective stress (up to 10,000 kPa). This suggests that intact material is stronger and has a greater load carrying capacity than any derivative of RBBC presented for analysis. Even the sodium hex BBC which was the densest material tested, required more axial strain to a given stress level than Killian Court BBC. The void ratios in the normally consolidated region for natural RBBC Series IV and leached RBBC compare well to those for Killian Court in-situ material up to an axial effective stress of 10,000 kPa. Given that both natural RBBC Series IV and leached BBC are more compressible, it is anticipated the behaviors may diverge further from Killian Court in-situ BBC beyond this stress level. The k_v data for three Killian Court BBC tests presented show log-linear behavior with no visible changes in slope. In a similar fashion to sodium hex BBC, once the preconsolidation pressure is passed, the c_v value rises continually and gradually throughout the test.

This is the first instance of London Clay being resedimented at MIT. The soils suitability as a candidate for the resedimentation procedure has been proven. Resedimented London Clay was tested at three pore fluid salinities in order to gauge its reactivity to changes in salinity. The results show a weak trend whereby an increase in pore fluid salinity gives a slight increase in initial void ratio. All three tests presented show different strains to a given stress level, however, these differences cannot be correlated to a corresponding change in salinity. Log-linear k_v data was recorded for all tests and the c_v value shows relatively stable behavior. RLC gives by far the lowest c_v value of all soils tested. It is therefore assumed that; a) either the same floc breaking mechanism witnessed in RBBC is not occurring; b) high enough stresses have not been achieved to break any remaining flocs; c) continuous breakage of the flocs is ongoing through the test.

Gulf of Mexico soil recovered from the Ursa Basin was tested to a high axial effective stress. The soil was only resedimented with one pore fluid derivative of 0 g/l (distilled water). The slope of the normally consolidated line changes with an increase in stress level. The k_v data displays log-linear behavior up to very high stress levels for all tests, however, a rise in c_v is noted in the data around a stress of 27,000 kPa. It is unclear at this time whether this is due to structural changes in the soil fabric or some other anomaly.

Resedimented sodium montmorillonite was successfully tested in the CRS device as part of this research. Batches with pore fluid salinities of 1 & 256 g/l were prepared for testing and although good data was obtained from the 256 g/l batch, the 1 g/l soil was unavailable for testing and inclusion in this thesis due to the amount of time taken to resediment the soil at low salinities. The 256 g/l batch produced high initial void ratios, the highest of all soils in the testing program despite the belief that in the presence of 256 g/l pore fluid, particle to particle contact dominates the fabric makeup. In a similar fashion to other soils, the slope of the normally consolidated line changes with an increase in stress. This is true in both strain and void ratio space. Log-linear k_v data was obtained, but not over void ratios representing the entire stress range. The c_v value recorded in the normally consolidated stress range drops with an increase in stress which is in contrast to all other soils tested. Sodium montmorillonite gives the lowest hydraulic conductivity recorded for this work, however, its c_v value is four times greater than the lowest c_v value recorded for London Clay.

Scanning Electron Microscope (SEM) images of different types of BBC were analyzed at different pore fluid salinities and at various stress levels in tandem with laboratory results in order to compare the findings. It was shown that not much change in fabric is visible in the stress range 100-1,000 kPa or with large variations in pore fluid salinity which would support the theory that flocs in the soil start to break at an axial stress of around 2,000 kPa. A persistent arrangement of particles can be seen at various stress levels across a number of images analyzed. It is only when the fabric of the soil is altered in some fashion that changes in particle orientation and structure are evident. It is thought the complex fabric of BBC provides a “truss” like support mechanism for the applied stress which will break at a given load.

6.3.1.2 STRENGTH CHARACTERISTICS

Natural RBBC Series IV, leached RBBC and Killian Court in-situ material were tested in order to determine the effect, if any, the pore fluid salinity would play on the strength of the soil. For a salinity increase in Natural RBBC Series IV (from 4 & 256 g/l), larger axial strains to failure are seen, but a lower shear stresses is required to produce this failure. A less brittle soil is evident at high strains ($\epsilon_a = 10\%$) for high salinity natural RBBC Series IV. A non-linear decrease in shear strength is seen with an increase in axial strain. A weak trend exists whereby a

lower friction angle at failure is seen in high salinity soil, however this trend is reversed for the friction angle at maximum obliquity. The A Parameter at failure for both soils also differs whereby a lower A Parameter is seen in the lower salinity soil than in the high salinity soil.

The salinities for leached RBBC are slightly different (1 & 256 g/l). Similar strains to failure are seen for both salinities and no trend is evident in the required stress to produce failure of the soil. A less brittle soil is evident at high strains ($\epsilon_a = 10\%$) for high salinity leached RBBC in a similar fashion to natural RBBC Series IV, however, the brittleness of both salt concentrations increases in the leached soil. A non-linear decrease in shear strength is seen with an increase in axial strain. The trends in the friction angle at failure are now more pronounced. A higher friction angle at failure is seen in the high salinity soil, and this trend holds true for maximum obliquity. Higher axial strains are required in the low salinity soils to achieve maximum obliquity. No trend is apparent in the A Parameter to failure for both salinities.

In a similar fashion to the compression data, the RBBC data was compared to tests run on Killian Court in-situ material. For intact material, a linear decrease in shear strength is seen with an increase in axial strain. This is in contrast to the resedimented material. Approximately twice the axial strain is required to fail Killian Court in-situ material as opposed to both RBBC types. This indicates a much stronger matrix in the in-situ material than can be replicated in the resedimentation process. The friction angles at failure are comparable across all material types and the friction angles at maximum obliquity demonstrate very comparable results. In general, the A Parameter at failure is closer to unity than most other soils with the exception of natural RBBC Series IV at 256 g/l which also gives values close to unity.

The resedimented material compares well with the Killian Court in-situ soil in most areas examined. The main differences between resedimented and intact material from a triaxial testing point of view are the required strains to failure and the A Parameter at failure.

6.4 RECOMMENDATIONS FOR FUTURE RESEARCH

Given that differences in mechanical behavior can be extracted from a relatively insensitive soil such as Boston Blue Clay, it is believed that these differences will be amplified

further when other more reactive soils such as Gulf of Mexico clay are used as the testing medium.

Throughout the course of this research, just as much of a difference in behavior was seen between salinities of 0-1 g/l as was observed between 1-256 g/l. It would be of academic interest to perform a testing program on soils between 0 & 1 g/l with differences in salinities in the range of orders of magnitude. Although the leached BBC used was run through the centrifuge twice, a quantity of salt still existed in the matrix. With more and more salt being removed, a greater reaction to pore fluid salinity will be observed. Leaching of the BBC powder should take place until no changes in the behavior of c_v or k_v are noted. Another option is to create several batches of soil which are all leached a different number of times say 4, 6 & 8 times. These soils can be then resedimented and tested in order to trace how the structural changes occur in relation to the degree of leaching. It is anticipated that the peak in the c_v value would move to higher stresses as the amount of leaching increases, this would correspond the “kink” in k_v moving to lower void ratios. Interesting observations could be made in relation to how the flocs control the behavior of the soil, such as what degree of leaching is required in order for changes in c_v & k_v to extend beyond the range of testing, or eliminate them completely.

The observation of floc breakage during testing was an interesting one. It is not yet clear if this behavior is limited to BBC or will exist in other soil types, and if so, at what stress is floc breakage mobilized. Reports from other researchers have indicated that the behavior outlined in this thesis has been observed in soils from other parts of the world. The idea that soils can have a dual memory is relevant to geologic stress levels only. The stress level at which floc breakage was recorded for natural RBBC Series IV represents ~100 m burial under hydrostatic conditions. Soils which undergo much deeper burial than this should be tested to see if similar changes in behavior are noted as there would be practical implications in terms of changing k_v & c_v . This would be relevant to the energy industry as energy reserves often have sediments in the order of km's overlaying them.

Using sodium Hexametaphosphate to disperse the fabric of a soil, resediment it and then test it provided an interesting twist to the research. It was proposed that the difference in stress at a given void ratio between sodium hex BBC and Killian Court in-situ BBC be attributed to the

electro-chemical forces which have developed in the Killian Court material. This is an interesting theory which may for the first time give a quantifiable value as to the load carrying capacity of the electro-chemical bonds in a soil. A possible future standard practice for soils of interest may include testing in-situ material to identify the compression behavior, process some of this in-situ material with sodium hex and resediment it. Tests can then be run on the resedimented material in order to determine the load carrying ability of the soil with no electro-chemical forces present. The difference in stress at a given void ratio could possibly be taken as the contribution of the electro-chemical forces in the intact soil. Further research should be conducted on this simple method in order to ascertain its true value in determining forces other than mechanical ones which serve to distribute stress through a soil matrix.

A final recommendation would be to revisit one of the testing criteria laid out in the current ASTM standard on CRS testing (ASTM D4186). The standard requires a pore pressure ratio of between 3 & 15 % for the test to be considered valid. Given that higher axial effective stresses are now achievable when testing (up to 40,000 kPa for this research), it is difficult to fulfill the requirement in the high stress range. Pore pressure ratios of between 1 – 2 % were normal beyond stress levels of ~ 4,000 kPa for tests run during this research. Pore pressure ratios as low as 0.0023 % were recorded on some tests while still producing excellent hydraulic conductivity and coefficient of consolidation information. Perhaps a dual system of pore pressure ratio requirements could be proposed whereby the required pore pressure ratio up to a certain effective stress level would be X, and beyond that stress level it would be Y. An alternative method would be to specify a minimum requirement for pore pressure transducer resolution so that very small excess base pressures can be accurately measured.

REFERENCES

- Abdulhadi, N.O. (2009). "An Experimental Investigation into the Stress-Dependent Mechanical Behavior of Cohesive Soil with Application to Wellbore Instability", Ph.D. Thesis, MIT, Cambridge, MA
- Adams, A.L., (2011) "Laboratory Evaluation of the Constant Rate of Strain and Constant Head Permeability Head Techniques for Measurement of the Hydraulic Conductivity of Fine Grained Soil" SM Thesis, MIT, Cambridge, MA
- Allen, L. S. & Matijevic, E., "Surface and Colloid Chemistry of Clays" Chemical Reviews, ACS, 74 (3), 385-400
- ASTM D2974 – 07a Standard Test Methods Standard Test Methods for Moisture, Ash, and Organic Matter of Peat and Other Organic Soils
- ASTM D4186 – 06 Standard Test Method for One-Dimensional Consolidation Properties of Saturated Cohesive Soils Using Controlled Strain Loading
- ASTM D4318 - 10 Standard Test Methods for Liquid Limit, Plastic Limit, and Plasticity Index of Soils
- Bailey, W.A. (1961) "Effects of Salt on the Shear Strength of Boston Blue Clay," SM Thesis, MIT, Cambridge, MA
- Berman, D.R. (1993) "Characterization of the Engineering Properties of Boston Blue Clay at the MIT Campus," SM Thesis, MIT, Cambridge, MA
- Bjerrum, L. & Rosenqvist T.H., (1956) "Some Experiments With Artificially Sedimented Clays" *Géotechnique*, 6 (3), 124-136
- Bolt, G.H., (1956) "Physico-Chemical Analysis of the Compressibility of Pure Clays" *Géotechnique*, 6 (2), 86-93
- Burland, J.B. (1990) "On the Compressibility and Shear Strength of Natural Soils," *Géotechnique*, 40 (3), 329-378
- Casey, B., (2011) "The Significance of Specimen End Restraint in High Pressure Triaxial Testing of Cohesive Soil" SM Thesis, MIT, Cambridge, MA
- Cable, D.F. (1993) "The Behavior of Resedimented Boston Blue Clay at OCR4 in Cyclic and Post-Cyclic Undrained Direct Simple Shear," SM Thesis, MIT, Cambridge, MA

- Cauble, D.F. (1993) "An Experimental Investigation of the Behavior of a Model Suction Caisson in a Cohesive Soil," PhD Thesis, MIT, Cambridge, MA
- Cooling, L.F. & Skempton, A.W. (1942) "A Laboratory Study of London Clay" *Journal of the Institution of Civil Engineers*, Vol. 17 (3), 251-276
- Cripps, J.C. & Taylor, R.K. (1981) "The Engineering Properties of Mudrocks" *Quarterly Journal of Engineering Geology*, Vol. 14, 315-346
- Force, E.A. (1998) "Factors Controlling Pore-Pressure Generation during K0-Consolidation of Laboratory Tests," SM Thesis, MIT, Cambridge, MA
- Flemings, P.B., Behrmann, J.H. & John, C.M. (2006) "IODP Expedition 308 Report – Site U1322" *Proceedings of the Integrated Ocean Drilling Program*, Volume 308
- Germaine, J.T. (1982) "Development of the Directional Shear Cell for Measuring Cross-Anisotropic Clay Properties," ScD Thesis, MIT, Cambridge, MA
- Germaine, J.T. & Germaine, A.V. (2009) *Geotechnical Laboratory Measurements for Engineers*, John Wiley and Sons, Inc.
- Gonzalez, J.H. (2000) "Experimental and Theoretical Investigation of Constant Rate of Strain Consolidation," SM Thesis, MIT, Cambridge, MA
- Grennan, J.T. (2010). "Characterization of a Low Plasticity Silt", SM Thesis, MIT, Cambridge, MA
- Hight, D.W., Gasparre, A., Nishimura, S., Minh, A., Jardine, R.J. & Coop, M.R. (2007) "Characteristics of the London Clay from the Terminal 5 Site at Heathrow Airport" *Géotechnique*, 57 (1), 3-18
- Ismael, N. F., "Laboratory and Field Leaching Tests on Coastal Salt-Bearing Soils", *Journal of the Geotechnical Engineering Division, ASCE* 119 (3), 453-470
- Kenny, T.C. (1964) "Sea-Level Movements and the Geologic Histories of the Postglacial Marine Soils at Boston, Nicolet, Ottawa and Oslo," *Géotechnique*, 14 (3), 203-230
- Kestin J., Ezzat Khalifa H. & Correia R. J., (1981) "Tables of the Dynamic and Kinematic Viscosity of Aqueous NaCl Solutions in the Temperature Range 20-150° C and the Pressure Range 0.1-35 MPa" *Journal of Physical Chemistry, National Standard Reference Data System*, Vol. 10, No. 1, 71-87
- King C. (1981), "The stratigraphy of the London Basin and associated deposits" *Tertiary Research Special Paper*, Vol. 6, Backhuys, Rotterdam

- Koutsoftas, D.C. & Ladd, C.C. (1985) "Design Strengths for an Offshore Clay," ASCE, Journal of Geotechnical Engineering Division, 111 (3), 337-355
- Ladd, C.C. (1960) "Stress-Strain Behavior of Saturated Clay and Basic Strength Principles," Research Report R64-17, Research on Earth Physics, Department of Civil Engineering, MIT, Cambridge, MA
- Ladd, C.C. & Varallyay, J. (1965) "The Influence of Stress System on the Behavior of Saturated Clays during Undrained Shear," Research Report R65-11, Soil Publication No. 177, Department of Civil Engineering, MIT, Cambridge, MA
- Ladd, C.C. & Kinner, E., (1967) "The Strength of Clays at Low Effective Stress." Research in Earth Physics, Research Report R67-4, Phase Report 8
- Ladd, C.C. & Foott, R. (1974) "New Design Procedure for Stability of Soft Clays," Journal of the Geotechnical Engineering Division, ASCE, 100 (7), 763-786
- Ladd, C.C. (1991) "Stability Evaluation during Staged Construction," ASCE, Journal of Geotechnical Engineering, 117 (4), 540-615
- Lambe, T.W. (1951) Soil Testing for Engineers, John Wiley and Sons, New York
- Lambe, T.W. & Whitman, R.V. (1969) Soil Mechanics, John Wiley and Sons, New York
- Man, A. & Graham, J., (2010) "Pore Fluid Chemistry, Stress-Strain Behavior, and Yielding in Reconstituted Highly Plastic Clay" Journal of Engineering Geology, Vol. 116, 296-310
- Marsland, A. & Randolph, M.F., (1976) "Comparisons of the Results from Pressuremeter Tests and Large in-situ Plate Tests in London Clay" Géotechnique, 27 (2), 217-243
- Marsland, A. (1974) "Comparisons of the Results from Static Penetration Tests and Large in-situ Plate Tests in London Clay" Building Research Establishment Current Paper, CP 87/74
- Martin, R.T. (1970) "Suggested Method of Test for Determination of Soluble Salts in Soil," ASTM STP 476, 288-290
- Mazzei, D.P., (2007) "Normalized Mechanical Properties of Resedimented Gulf of Mexico Clay from Integrated Ocean Drilling Program Expedition Leg 308" SM Thesis, MIT, Cambridge, MA
- Mesri, G. & Olson, R.E., (1970) "Shear Strength of Montmorillonite" Géotechnique, 20 (3), 261-270

- Mesri, G. & Olson, R.E., (1971) "Consolidation Characteristics of Montmorillonite" *Géotechnique*, 21 (4), 341-352
- Mesri, G. & Olson, R.E., (1971) "Mechanisms Controlling the Permeability of Clays" *Clays and Clay Minerals*, Vol 19, 151-158
- Pantelidou, H. & Simpson, B. (2007) "Geotechnical Variation of London Clay Across Central London" *Géotechnique*, 57 (1), 101-112
- Pusch, R. & Arnold, M., (1969) "The Sensitivity of Artificially Sedimented Organic-Free Illitic Clay" *Journal of Engineering Geology*, Vol. 3 135-148
- Robinson, R.G. & Allam, M.M., (1998) "Effect of Clay Mineralogy on the Coefficient of Consolidation" *Clays and Clay Minerals*, 46 (5), 596-600
- Roscoe, K.H. & Burland, J.B. (1968) "On the Generalized Stress-Strain Behavior of 'Wet' Clay," in *Engineering Plasticity*, Cambridge University Press, 535-609
- Rosenqvist, T.H., (1966) "Norwegian Research into the Properties of Quick Clay – A Review" *Journal of Engineering Geology*, Vol. 1 (6), 445-450
- Santagata, M.C. (1994), "Investigation of Sample Disturbance in Soft Clays Using Triaxial Element Tests," SM Thesis, MIT, Cambridge, MA
- Santagata, M.C. (1998), "Factors Affecting the Initial Stiffness and Stiffness Degradation of Cohesive Soils," PhD Thesis, MIT, Cambridge, MA
- Schofield, A.N. & Wroth, C.P. (1968) *Critical State Soil Mechanics*, McGraw-Hill
- Seah, T.H. (1990) "Anisotropy of Resedimented Boston Blue Clay," ScD Thesis, MIT, Cambridge, MA
- Souli, H., Fluereau, M., Ayadi, M. T. & Kbir-Arigoib, N., (2010) "A Mineralogical Identification of a Tunisian Clayey Soil and Fabric Changes During Wetting" *Clay Minerals*, The Mineralogical Society, 45, 315-326
- Sheahan, T.C. (1988) "Modification and Implementation of a Computer Controlled Triaxial Apparatus," SM Thesis, MIT, Cambridge, MA
- Sheahan, T.C. (1991) "An Experimental Study of the Time-Dependent Undrained Shear Behavior of Resedimented Clay Using Automated Stress-Path Triaxial Equipment," ScD Thesis, MIT, Cambridge, MA

Sheahan, T.C. & Germaine, J.T. (1992) "Computer Automation of Conventional Triaxial Equipment," *Geotechnical Testing Journal*, 15 (4), 311-322

Sheahan, T.C., Ladd, C.C., & Germaine, J.T. (1996) "Rate-Dependent Undrained Shear Behavior of Saturated Clay," *Journal of Geotechnical Engineering, ACSE*, 122 (2), February, 99-108

Sinfield, J.V. (1994) "An Experimental Investigation of Sampling Disturbance Effects in Resedimented Boston Blue Clay," SM Thesis, MIT, Cambridge, MA

Sorensen, K.K., Baudet, B.A. & Simpson, B., (2007) "Influence of Structure on the Time-Dependent Behavior of a Stiff Sedimentary Clay" *Géotechnique*, 57 (1), 113-124

Skempton, A.W. & Northey, R.D., (1952) "The Sensitivity of Clays" *Géotechnique*, Vol 3 (1), 30-53

Skempton, A.W., (1953) "The Colloidal "Activity" of Clays" *Proceedings from the 3rd International Conference of Soil Mechanics, Zurich*, 57-61

Skempton, A.W. (1977) "Slope Stability of Cuttings in Brown London Clay" *Proceedings from the 9th International Conference of Soil Mechanics, Tokyo, 1977*, 3, 261-270

Skempton, A.W., (1959) "Cast in-situ Bored Piles in London Clay" *Géotechnique*, 9 (4), 153-173

Stipho, A.S., (1985) "On the Engineering Properties of Salina Soil" *Quarterly Journal of Engineering Geology*, 18, 129-137

Tchalenko, J.S., (1968) "The Microstructure of London Clay" *Quarterly Journal of Engineering Geology and Hydrogeology*, Vol. 1, 155-168

Terzaghi, K. & Peck, R.B. (1948) *Soil Mechanics in Engineering Practice*, John Wiley and Sons, Inc.

Tiwari, B., Tuladhar, G.R. & Mariu H., (2005) "Variation in Residual Shear Strength of the Soil with the Salinity of Pore Fluid" *Journal of Geotechnical and Geoenvironmental Engineering, ASCE*, Vol. 131 (12), 1445-1457

U.T. Austin Publication, "The T2P Project: Land Deployment in Boston, MA" Jackson School of Geosciences

Van Olphen, H., (1977) "An Introduction to Clay Colloid Chemistry" Krieger Publishing Company

- Van Paassen. L.A. & Gareau L. F., (2004) "Effect of Pore Fluid Salinity on Compressibility and Shear Strength Development of Clayey Soils" *Engineering Geology for Infrastructure Planning in Europe*, Vol. 104, 327-340
- Varallyay, J. (1964) "The Influence of Stress System Variables on the Undrained Strength of Boston Blue Clay," SM Thesis, MIT, Cambridge, MA
- Velde. B., (1996) "Compaction Trends of Clay-Rich Deep Sea Sediments" *Journal of Marine Geology*, Vol. 133, 193-201
- Ward, W.H., Marsland, A. & Samuels, S.G., (1965) "Properties of the London Clay at the Ashford Common Shaft: In-Situ and Undrained Strength Tests" *Géotechnique*, 15 (4), 321-344
- Ward, W.H., Samuels, S.G. & Butler, E. (1959) "Further Studies of the Properties of London Clay" *Géotechnique*, 9 (2), 33-58
- Whittle, A.J. & Kavvadas, M. (1994) "Formulation of the MIT-E3 Constitutive Model for Overconsolidated Clays," *ASCE Journal of Geotechnical Engineering*, 120 (1), 173-198
- Wissa, A.E.Z. (1961) "A Study of the Effects of Environmental Changes on the Stress-Strain Properties of Kaolinite," SM Thesis, MIT, Cambridge, MA
- Wissa, A.E.Z., Christian, J.T., Davis, E.H., & Heiberg, S. (1971) "Consolidation at Constant Rate of Strain," *Journal of Soil Mechanics and Foundation*, ASCE, Vol. 97, No. SM10, 1393-1413
- Yong, R.N. & Warkentin, B.P., (1975) "Soil Properties and Behavior" Elsevier Publication
- Zreik, D.A. (1994) "Behavior of Cohesive Soils and their Drained, Undrained, and Erosional Strengths at Ultra-Low Stresses," PhD Thesis, MIT, Cambridge, MA

APPENDIX A

PORE PRESSURE RATIOS FOR SOILS TESTED

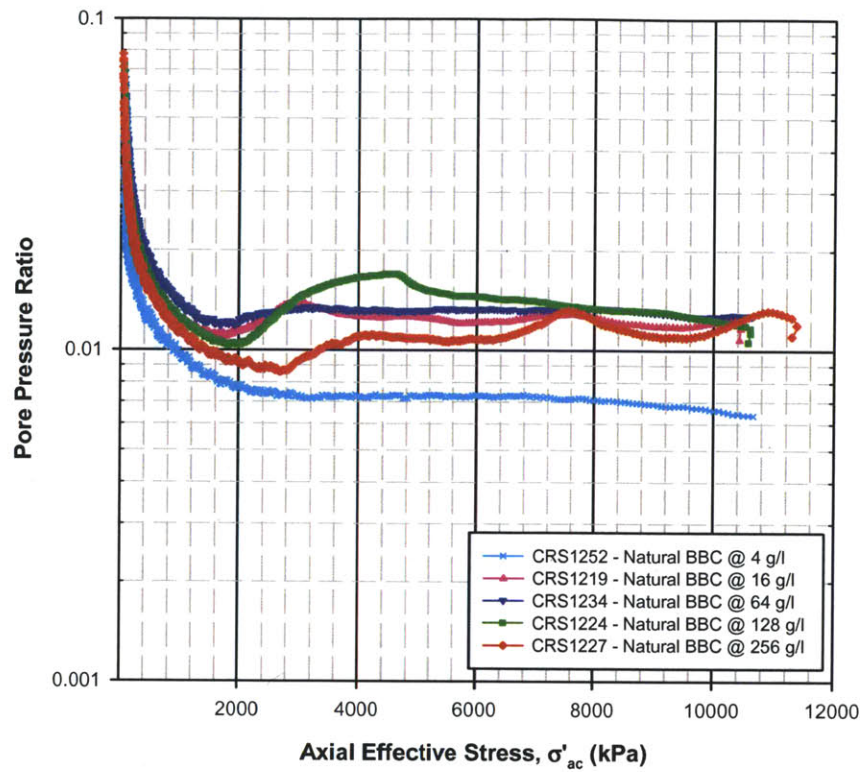


Figure 1 Pore pressure ratio for natural RBBC Series IV from CRS testing

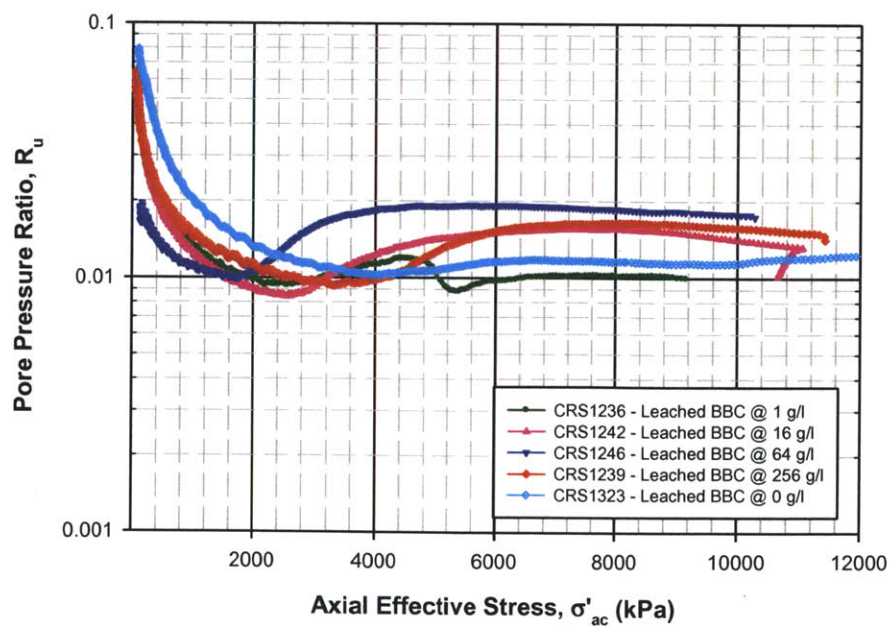


Figure 2 Pore pressure ratio for leached RBBC from CRS testing

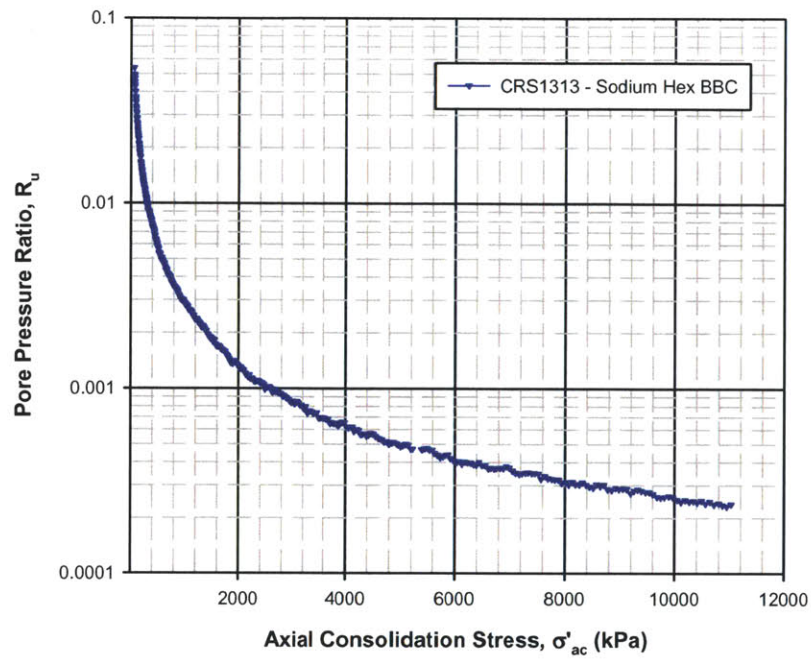


Figure 3 Pore pressure ratio for sodium Hexametaphosphate RBBC from CRS testing

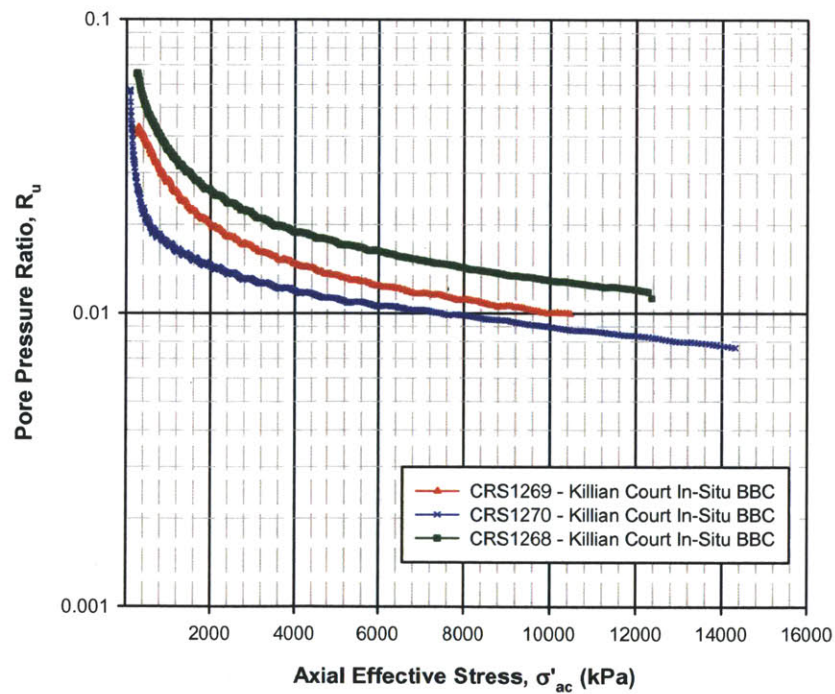


Figure 4 Pore pressure ratio for Killian Court in-situ BBC from CRS testing

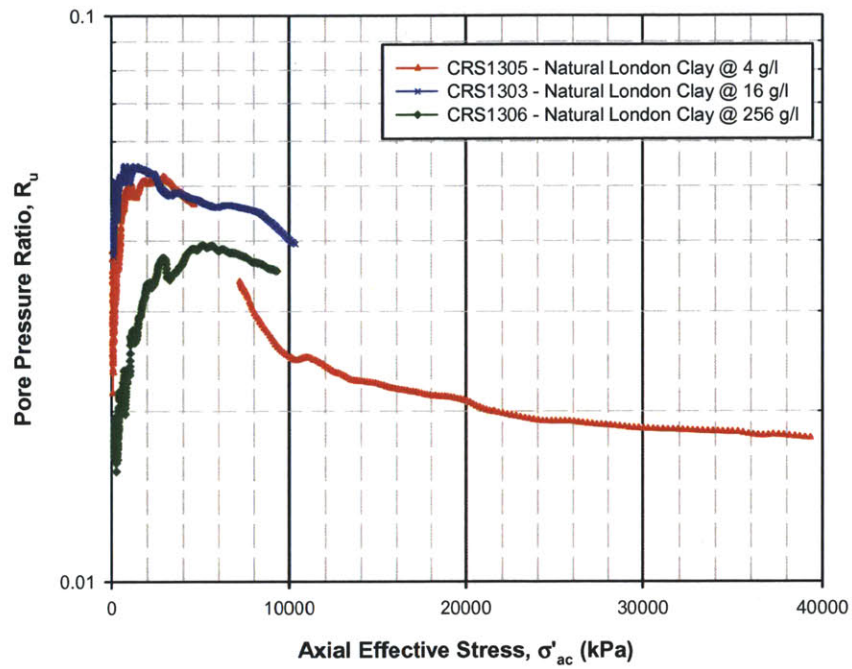


Figure 5 Pore pressure ratio for natural RLC up to 40,000 kPa from CRS testing

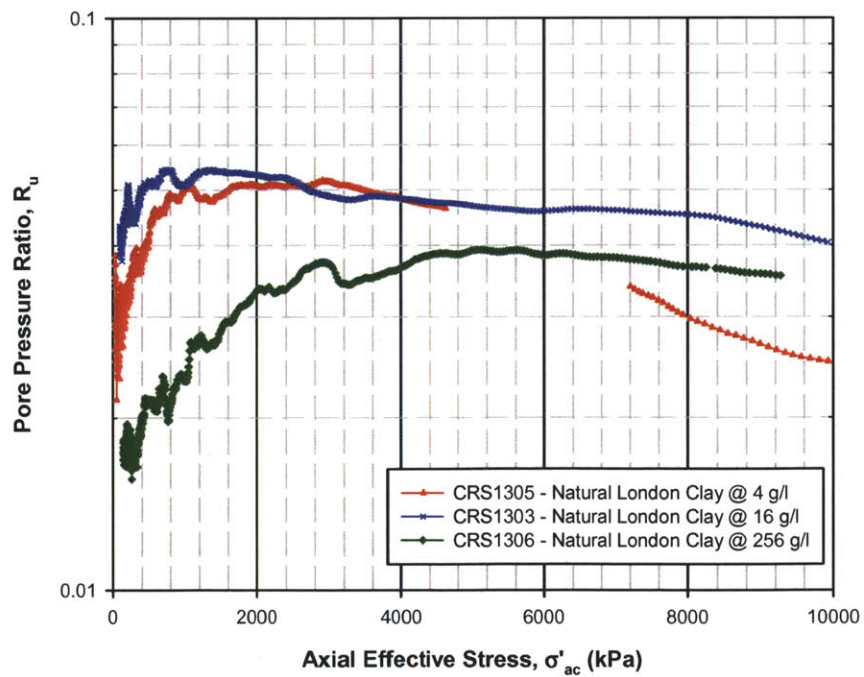


Figure 6 Pore pressure ratio for natural RLC up to 10,000 kPa from CRS testing

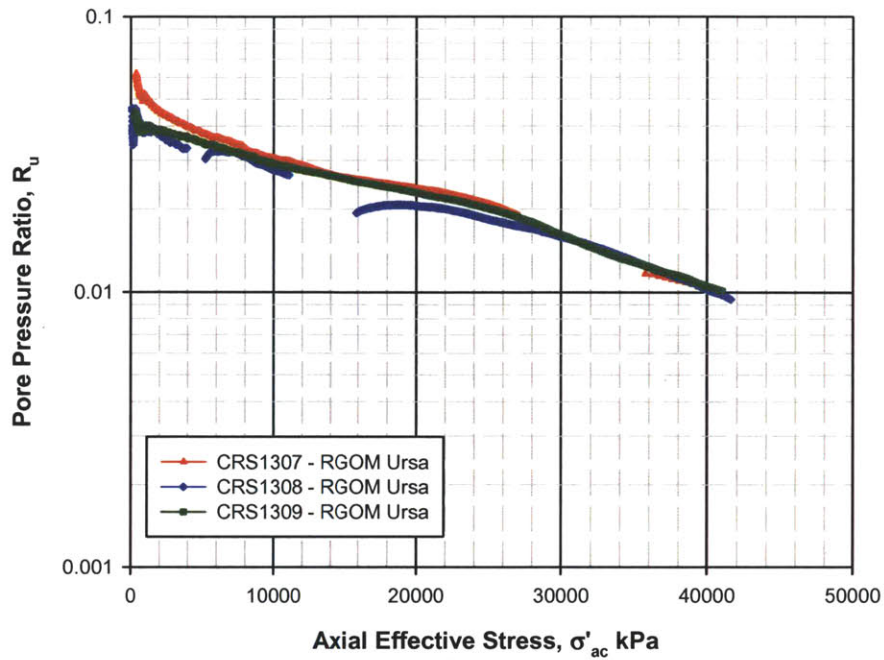


Figure 7 Pore pressure ratio for natural RGOM – Ursa Soil up to 40,000 kPa from CRS testing

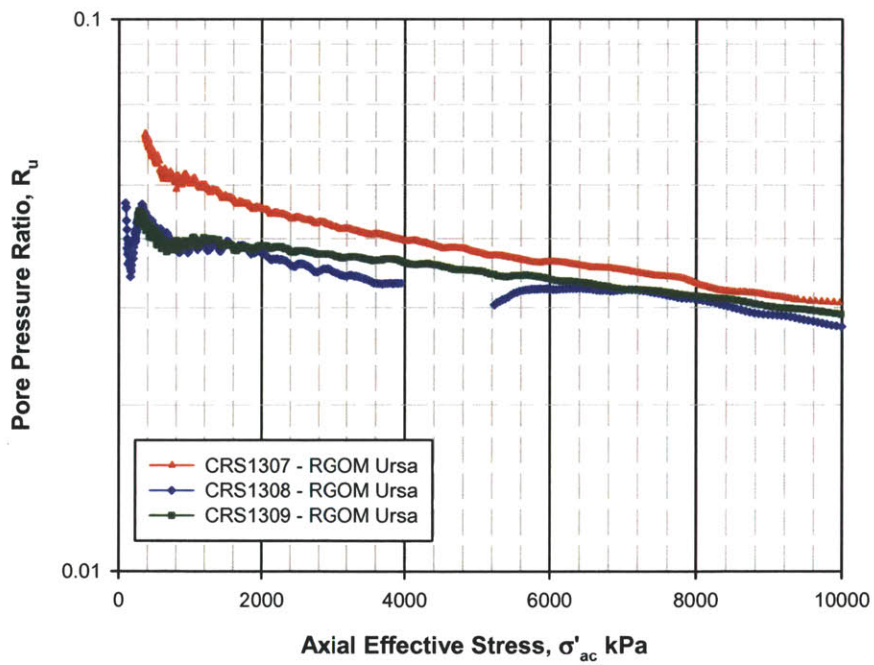


Figure 8 Pore pressure ratio for natural RGOM – Ursa Soil up to 10,000 kPa from CRS testing

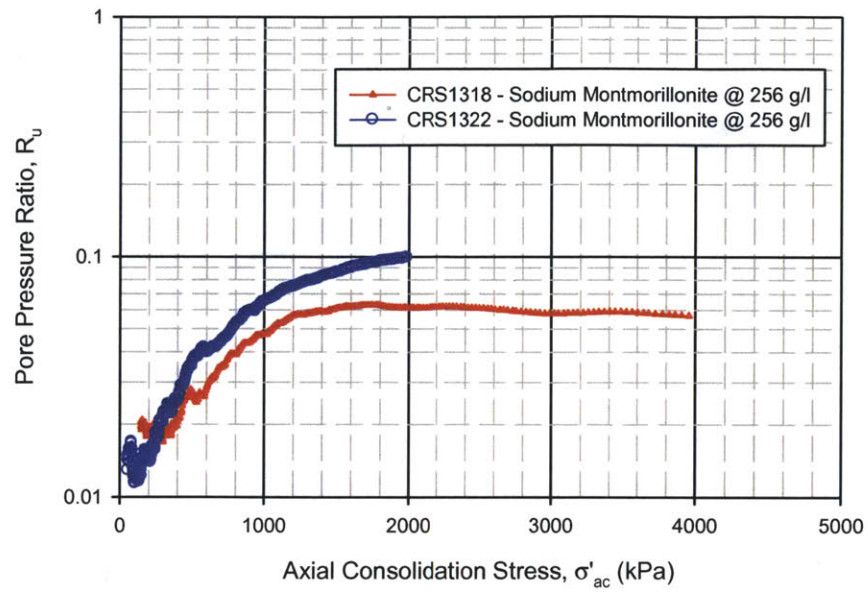


Figure 9 Pore pressure ratio for sodium montmorillonite up to 4,000 kPa from CRS testing

APPENDIX B

EXAMPLE PHASE RELATION CALCULATIONS ALLOWING FOR PORE FLUID SALINITY

EXAMPLE 1

The following data was taken from CRS1306 – London Clay tested with a pore fluid salinity of 256 g/l.

Initial wet mass	22.23 g
Initial volume	12.495 cm ³
Wet mass of final specimen	17.39 g
Dry mass of final specimen	13.86 g
Specigic gravity of solids	2.80
Mass density of water at 20 ° C	0.9982 g/cm ³
Mass density of 256 g/l saltwater	1.1742 g/cm ³

CALCULATIONS

$$\text{Final water content} = \frac{3.54}{13.86} \times 100 = 25.54 \%$$

$$\text{Final fluid volume} = \frac{\left(\frac{(13.86 \times 25.54)}{100}\right)}{1.1742} = 3.015 \text{ cm}^3$$

$$\text{Final mass of Salt} = \left(\frac{(3.015 \times 256)}{1000}\right) = 0.7718 \text{ g}$$

$$\text{Final mass of soil grains} = 13.86 - 0.7718 = 13.088 \text{ g}$$

$$\text{Volume of soils} = \frac{13.088}{0.9982} \div 2.80 = 4.6827 \text{ cm}^3$$

$$\text{Initial fluid mass} = 22.23 - 13.088 = 9.142 \text{ g}$$

$$\text{Initial fluid volume} = \frac{9.142}{1.1742} = 7.786 \text{ cm}^3$$

$$\text{Initial mass of salt} = \frac{(7.786 \times 256)}{100} = 1.993 \text{ g}$$

$$\text{Initial water content} = \frac{(22.23 - 13.088 - 1.993)}{(13.09 + 1.993)} \times 100 = 47.40 \%$$

$$\text{Initial void ratio} = \frac{(12.495 - 4.6827)}{4.6827} = 1.668$$

$$\text{Initial degree of saturation} = \frac{(7.786)}{(12.495 - 4.6827)} \times 100 = 99.66 \%$$

$$\text{Wet density} = \frac{22.23}{12.495} = 1.779 \text{ g/cm}^3$$

$$\text{Dry density} = \frac{13.86}{12.495} = 1.109 \text{ g/cm}^3$$

EXAMPLE 2

The following data was taken from CRS1331 – Killian Court in-situ material which has a natural pore fluid salinity of 11.3 g/l.

Initial wet mass	23.32 g
Initial volume	12.495 cm ³
Wet mass of final specimen	21.33 g
Dry mass of final specimen	17.04 g
Specific gravity of solids	2.78
Mass density of water at 20 ° C	0.9982 g/cm ³
Mass density of 11.3 g/l saltwater	1.00291 g/cm ³

CALCULATIONS

$$\text{Final water content} = \frac{4.29}{17.04} \times 100 = 25.17 \%$$

$$\text{Final fluid volume} = \frac{\left(\frac{17.04 \times 25.17}{100}\right)}{1.00291} = 4.277 \text{ cm}^3$$

$$\text{Final mass of Salt} = \left(\frac{4.277 \times 11.3}{1000}\right) = 0.0483 \text{ g}$$

$$\text{Final mass of soil grains} = 17.04 - 0.0483 = 16.99 \text{ g}$$

$$\text{Volume of solids} = \frac{16.99}{0.9982 / 2.78} = 6.1225 \text{ cm}^3$$

$$\text{Initial fluid mass} = 23.32 - 16.99 = 6.33 \text{ g}$$

$$\text{Initial fluid volume} = \frac{6.33}{1.00291} = 6.3116 \text{ cm}^3$$

$$\text{Initial mass of salt} = \frac{(6.3116 \times 11.3)}{1000} = 0.0713 \text{ g}$$

$$\text{Initial water content} = \frac{(23.32 - 16.99 - 0.0713)}{(16.99 + 0.0713)} \times 100 = 36.68 \%$$

$$\text{Initial void ratio} = \frac{(12.495 - 6.1225)}{6.1225} = 1.041$$

$$\text{Initial degree of saturation} = \frac{(6.3116)}{(12.495 - 6.1225)} \times 100 = 99.04 \%$$

$$\text{Wet density} = \frac{23.32}{12.495} = 1.866 \text{ g/cm}^3$$

$$\text{Dry density} = \frac{17.04}{12.495} = 1.364 \text{ g/cm}^3$$

EXAMPLE 3

Allowance of salt in calculation of Atterberg Limits

Data will be given for 1 determination from the Liquid Limit test via the Fall Cone method:

Pore Fluid Salinity:	256 grams of NaCl per liter of water (g/l)	
Penetration (mm):	30/29.8	
Mass Tare & wet soil (g):	26.91	
Mass Tare & Dry soil (g):	21.47	
Mass of Tare (g):	10.62	
Mass of Dry Solids (g):	10.85	(21.47 – 10.62)
Mass of Water (g):	5.44	(26.91 – 21.47)
Mass of Salt (g):	1.393	(5.44 x 0.256)
Volume of Salt (cm ₃):	0.6055	(1.393/2.3)
Total Mass of Water (g):	6.045	(5.44 + 0.6055)
Water Content (%):	55.7	(6.045/10.85) x 100